TRANSPORTATION RESEARCH

RECORD

No. 1288

Soils, Geology, and Foundations

Geotechnical Engineering 1990

A peer-reviewed publication of the Transportation Research Board

TRANSPORTATION RESEARCH BOARD
NATIONAL RESEARCH COUNCIL
WASHINGTON, D.C. 1990

Transportation Research Record 1288
Price: $31.00

Subscriber Category
IIIA soils, geology, and foundations

Modes
1 highway transportation
3 rail transportation

Subject Areas
21 facilities design
24 pavement design and performance
25 structures design and performance
33 construction
34 general materials
61 soil exploration and classification
62 soil foundations
63 soil and rock mechanics
64 soil science

TRB Publications Staff
Director of Publications: Nancy A. Ackerman
Senior Editor: Naomi C. Kassabian
Associate Editor: Alison G. Tobias
Assistant Editors: Luanne Crayton, Kathleen Solomon, Norman Solomon
Production Coordinator: Karen S. Waugh
Graphics Coordinator: Diane L. Ross
Office Manager: Phyllis D. Barber
Production Assistant: Betty L. Hawkins

Printed in the United States of America

Library of Congress Cataloging-in-Publication Data
National Research Council. Transportation Research Board.

Geotechnical engineering 1990.
p. cm. — (Transportation research record ; 1288)
ISBN 0-309-05064-2
1. Roads—Foundations. 2. Soil mechanics. 3. Waste products as road materials. I. National Research Council (U.S.). Transportation Research Board. II. Series.
TE7.H5 no. 1288
[TE210]
388 s—dc20 90-26445
[625.7'33] CIP

Sponsorship of Transportation Research Record 1288

GROUP 2—GENERAL DESIGN
Chairman: Raymond A. Forsyth, Sacramento, California

Stabilization Section
Chairman: J. M. Hoover, Iowa State University

Committee on Soil-Portland Cement Stabilization
Chairman: Lynne H. Irwin, Cornell University
Secretary: Dallas N. Little, Texas A & M University
Ara Arman, Henry H. Duval Jr., Donald G. Fohs, K. P. George, Amir N. Hanna, J. M. Hoover, Robert W. Israel, Raymond K. Moore, Robert G. Packard, Thomas M. Petry, Lutfi Raad, Daniel R. Turner, Mumtaz A. Usmen, Anwar E. Z. Wissa

Soil Mechanics Section
Chairman: Michael G. Katona, Tyndall AFB

Committee on Foundations of Bridges and Other Structures
Chairman: Richard S. Cheney, Federal Highway Administration
Francois J. Baguelin, Jean-Louis Briaud, Bernard F. Butler, Murty S. Devata, Albert F. Dimillio, Victor Elias, Richard L. Engel, Bengt H. Fellenius, George G. Goble, Richard J. Goettle III, James S. Graham, Robert C. Houghton, Alan P. Kilian, Hugh S. Lacy, Robert M. Leary, John F. Ledbetter, Jr., Larry Lockett, Randolph W. Losch, Lyle K. Moulton, Peter J. Nicholson, Michael Wayne O'Neill, Harvey E. Wahls, John L. Walkinshaw, Gdalyah Wiseman

Committee on Subsurface Soil-Structure Interaction
Chairman: J. Michael Duncan
George Abdel-Sayed, Baidar Bakht, Sangchul Bang, Timothy J. Beach, Mike Bealey, Lester H. Gabriel, James B. Goddard, John Owen Hurd, Michael G. Katona, Kenneth K. Kienow, Richard W. Lautensleger, L. R. Lawrence, Donald Ray McNeal, Samuel C. Musser, Thomas D. O'Rourke, Raymond B. Seed, Ernest T. Selig, H. J. Siriwardane, Mehdi S. Zarghamee

Committee on Geosynthetics
Chairman: Verne C. McGuffey, New York State Department of Transportation
Richard D. Barksdale, Robert K. Barrett, Laurinda T. Bedingfield, John A. Bove, Calvin G. Burgess, Robert G. Carroll, Jr., Jerome A. Dimaggio, James B. Farris, Graham Ford, S. S. Dave Guram, Neil F. Hawks, Gary L. Hoffman, Robert D. Holtz, Thomas C. Kinney, Robert M. Koerner, Larry Lockett, James H. Long, R. Gordon McKeen, Bernard Myles, Malcolm L. Steinberg, John E. Steward, Harry H. Ulery, Jr., Dennis B. Wedding, David C. Wyant

Geology and Properties of Earth Materials Section
Chairman: William Lovell, Purdue University

Committee on Exploration and Classification of Earth Materials
Chairman: J. Allan Tice, Law Engineering Testing Company
Robert K. Barrett, P. J. Beaven, John A. Bischoff, Martin C. Everitt, H. Allen Gruen, Neil F. Hawks, Robert K. H. Ho, C. William Lovell, B. Sen Mathur, M. Dewayne Mays, R. L. Nanda, Zvi Ofer, Harold T. Rib, Lawrence C. Rude, Surendra K. Saxena, Edward Stuart, Berke L. Thompson, Sam I. Thornton, A. Keith Turner, Gilbert Wilson, Duncan C. Wyllie

Committee on Physicochemical Phenomena in Soils
Chairman: Thomas F. Zimmie, National Science Foundation
John J. Bowders Jr., Myron L. Hayden, John B. Heagler Jr., Richard H. Howe, Robert Johnson, Joakim G. Laguros, Milton W. Meyer, Anwar E. Z. Wissa

Committee on Engineering Geology
Chairman: A. Keith Turner, Colorado School of Mines
Robert K. Barrett, William D. Bingham, Scott F. Burns, Jerome V. Degraff, Carol J. Hammond, C. William Lovell, Steve M. Lowell, Stanely M. Miller, Stephen F. Obermeier, Rodney W. Prellwitz, Berke L. Thompson, J. Allan Tice, Duncan C. Wyllie

Committee on Environmental Factors Except Frost
Chairman: Robert L. Lytton, Texas A & M University
Warren T. Bennett, Michael L. Bunting, Samuel H. Carpenter, Fu Hua Chen, Koon Meng Chua, Judith B. Corley, Barry J. Dempsey, Gary L. Fitts, Donald G. Fohs, Donald J. Janssen, Lawrence D. Johnson, Amos Komornik, C. William Lovell, Joseph Massucco, Said Ossama Mazen, R. Gordon McKeen, Thomas M. Petry, Miguel Picornell, Rogel H. Prysock, Albert C. Ruckman, Larry A. Scofield, Malcolm L. Steinberg, Jacob Uzan, Gdalyah Wiseman

Railway Systems Section
Chairman: Robert E. Kleist, Ft. Washington, Maryland

Committee on Railroad Track Structure System Design
Chairman: James W. Winger, P'Sumit Engineering Incorporated
Secretary: Charles L. Stanford, New York City Transit Authority
Dale K. Beachy, Earl E. Frank, Crew S. Heimer, Thomas B. Hutcheson, Ben J. Johnson, Mohammad S. Longi, W. Scott Lovelace, Jerry R. Masters, Philip J. McQueen, Howard G. Moody, Myles E. Paisley, Gerald P. Raymond, Alfred E. Shaw Jr., W. S. Stokely, Daniel H. Stone, Marshall R. Thompson, John G. White

G. P. Jayaprakash and Elaine King, Transportation Research Board staff

Sponsorship is indicated by a footnote at the end of each paper. The organizational units, officers, and members are as of December 31, 1989.

Transportation Research Record 1288

Contents

Foreword

The twenty-two papers included in this record have been arranged in three groups. The first group contains six papers on effects of natural and applied electrokinetic processes on contaminated soils. The second group has three papers on the use of waste materials in construction. The information presented is useful in minimizing environmental impacts. The remaining 13 papers comprise the third group and deal with different aspects of geotechnical engineering.

Landfills and impoundments will continue to play a major role in environmental protection in spite of the intense efforts at waste minimization, recycling, and alternate forms of waste disposal. Therefore, geotechnical engineers are interested in the application of electrokinetic phenomena as electrochemical processing techniques. The first six papers included in this record deal with the theoretical, experimental, and field investigation of electrokinetic phenomena in soils. Mitchell and Yeung describe results of theoretical analyses and experimental evaluation of electrokinetic flow barriers to contaminant transport through compacted clay and propose an electrokinetically induced counter flow to stop the migration of contaminants. Gray and Outcalt report on measurements of soil water potential and temperature made in the field during a freeze event to support the concept of variations in electrical potentials during freezing and thawing caused by soil electrolyte concentration changes resulting from phase transformations and advection. Olsen et al. review laboratory evidence for mechanisms of groundwater movement related to chemico-osmosis and diffusion-osmosis and provide data on loosely compacted kaolinite and an undisturbed sample of claystone. Acar et al. review an analytical model and present the results of laboratory tests conducted to predict electrical, hydraulic, and chemical gradients across saturated strata generated by application of an electro-osmosis process. Korfiatis et al. describe an experimental approach to assess relative magnitudes of hydraulic and electro-osmotic permeabilities under the application of hydraulic or electric gradients or both and the extent of pH changes during the electro-osmotic process. Pamucku et al. report on investigation of the feasibility of using electro-osmosis to remove zinc from contaminated soil.

Information on engineering behavior and on economic and environmental assessments is essential in considering the use of waste materials in transportation-related constructions. The next three papers detail the use of waste materials in highway construction. The paper by Ormsby and Fohs has a wealth of information on industrial, municipal, domestic, and mining wastes, and the papers by Usmen and Bowders and Bowders et al. provide results of tests conducted with Class F fly ash.

The third group of papers discuss various geotechnical aspects of highway engineering. George reports on structural characteristics relevant to the design of cement-treated bases, design criteria, and distress modeling. Ismael et al. describe expansive behavior of crushed cemented-sand used as road base material in arid areas and appropriate remedial measures. Berg et al. report on the economics of using reinforced soil slopes, particularly steepened highway embankment slopes. Bathurst and Benjamin describe the results of tests conducted on a large-scale reinforced soil wall built within the Royal Military College of Canada's Retaining Wall Test Facility. Pfeiffer and Higgins give the basic theory behind the Colorado Rockfall Simulation Program (CRSP) and data on experimental verification and calibration of CRSP. Katona describes the requirements for corrugated high-density polyethylene plastic pipe to withstand vehicular loading when used as a culvert under roadways. Abdel-Karim et al. examine load dispersion through soil and distribution of load through rigid pavements and concrete box culvert top slab. Bang and Yeon report on a quasi-three-dimensional method of analyzing earth-retaining structures with skew reinforcement (such as bridge abutments). Boghrat describes four design methods for drilled piles used as foundation for sound barrier walls on roadways in residential areas. Keaton and Eckhoff provide data to evaluate in comparable terms all geologic hazards at a site and a method of intelligent decision making

on the basis of the evaluation. Akinyede et al. report on application of probabilistic analysis methods during the preengineering phase to predict construction and maintenance costs. Roberds describes potential problems associated with subjective probability assessments related to geotechnical investigations, ways of mitigating those problems, and methods of selecting appropriate techniques. Sattler et al. report on implementation of a bearing-capacity design procedure and describe a computer program that computes the stresses involved.

Electro-Kinetic Flow Barriers in Compacted Clay

JAMES K. MITCHELL AND ALBERT T. YEUNG

Double liner systems are now required for new hazardous waste landfills and impoundments to prevent groundwater contamination caused by leachate. However, uncertainty always exists about the longevity of the synthetic flexible membrane liner, and the compacted clay components of the liner system may release some seepage in time under a sustained hydraulic head. The mechanisms of contaminant retention by clay minerals are not fully understood, and the attenuation capacity of any containment system is finite. In addition, diffusion through the clay liner under a concentration gradient may increase the rate of contaminant migration into the environment above that owing to advection alone. Electro-kinetic counterflow may be an effective measure to stop the migration of contaminants under a hydraulic gradient. An electro-kinetic fluid flow barrier can be created by the continuous or periodic application of an electrical gradient across a compacted clay liner. A coupled flow theory to describe the simultaneous flows of water, electricity, and contaminant ions under the influences of hydraulic, electrical, and chemical gradients has been developed by using the formalism of the thermodynamics of irreversible processes. An experimental testing program demonstrated the existence of electro-osmotic flow in partly saturated compacted clay and provided a basis to evaluate the validity of the theoretical predictions. An electrical gradient may move some inorganic species in soils much more effectively than hydraulic gradient. An electro-kinetic flow barrier halted the migration of the cation but accelerated that of the anion under laboratory testing conditions.

In spite of intense efforts at waste minimization, recycling, and alternative forms of waste disposal, landfills and impoundments will continue to play a major role in environmental protection.

The U.S. EPA issued regulations and performance standards for liner systems as a part of the 1984 RCRA Amendments. Guidelines for the design, construction and operation of liner systems were promulgated in 1985 (*1*) to control groundwater contamination caused by those disposal facilities. A composite double liner system with leachate collection systems above and between liners is required for most disposal facilities. Those liners contain both synthetic flexible membrane layers (FML) and compacted clay layers. A recently published Technical Resource document (*2*) provides extensive information and data about clays and their role in the system.

Unfortunately, the longevity of the FML is uncertain, and the FML, and the compacted clay component of the liner, may ultimately release some seepage under the influence of a sustained hydraulic head. The mechanisms for retention of contaminants by clay minerals are not fully understood, and the attenuation capacity of the liner is finite. In addition, diffusion through the clay liner under the influence of a concentration gradient may increase the rate of contaminant migration into the environment. An electro-kinetically induced counterflow has been proposed as a means to stop the migration of contaminants.

Electro-kinetic phenomena in clay are reviewed in this paper to establish the fundamental principles of electro-kinetic flow barriers. Theoretical analysis and experimental evaluation of electro-kinetic flow barriers to contaminant transport through compacted clay are described. Other potential applications of electro-kinetics for hazardous waste site remediation are also noted in the hope that they may stimulate future research.

J. K. Mitchell, Department of Civil Engineering, 439 Davis Hall, University of California, Berkeley, Calif. 94720. A. T. Yeung, Department of Civil Engineering, Texas A & M University, College Station, Tex., 77843-3136.

ELECTRO-KINETIC PHENOMENA IN CLAY

The surfaces of clay particles are normally negative charged because of isomorphous substitutions and the presence of broken bonds. Adsorbed cations for electrical neutrality form diffuse double layers on the surfaces of clay particles when they are placed in water (*3,4*). The electro-kinetic properties of clay are determined principally by the structure of the diffuse double layer on the wet clay surfaces.

Several electro-kinetic phenomena arise in clay when there are couplings between hydraulic and direct current electrical driving forces and flows. Those phenomena can broadly be classified into two pairs by the driving forces causing the relative movement between the liquid and the solid phases. The first pair consists of electro-osmosis and electrophoresis, where the liquid or the solid phase moves relative to the other under the influence of an imposed electrical potential. The second pair consists of streaming potential and migration or sedimentation potential, where the liquid or the solid phase moves relative to the other under the influence of hydraulic or gravity force and thus inducing an electrical potential. Those four electro-kinetic phenomena in clay are presented in Figure 1. Detailed descriptions of these phenomena are given by Mitchell (*3*) and van Olphen (*4*).

POTENTIAL USES OF ELECTRO-KINETICS FOR HAZARDOUS WASTE SITE REMEDIATION

Electro-kinetics may be useful for hazardous waste containment or site remediation or both in several ways. Each of these ways is briefly described next.

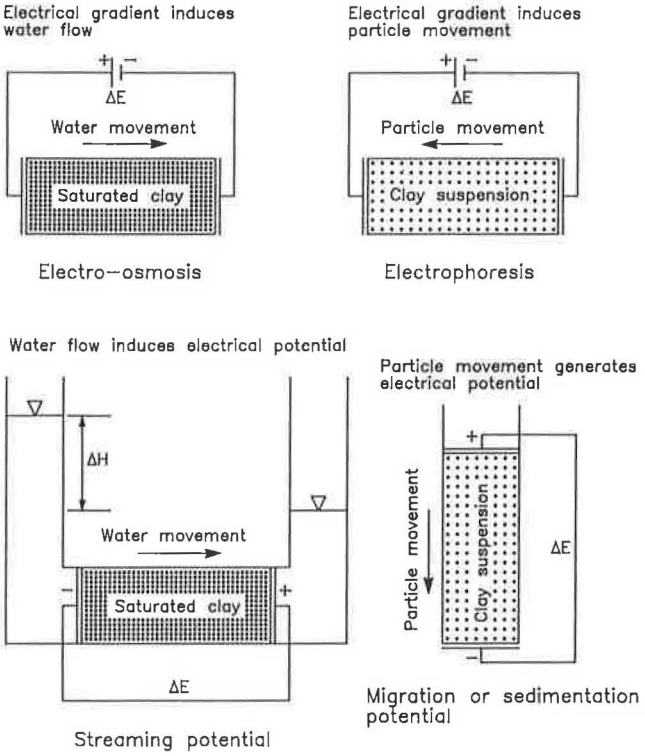

FIGURE 1 Electro-kinetic phenomena in clay. [Adapted from Mitchell (*3*).]

Electro-Kinetic Flow Barrier to Contaminant Transport

The periodic or continuous application of an electrical gradient across a low permeability compacted clay liner of a hazardous waste landfill in the direction indicated in Figure 2 to inhibit any outward migration of hazardous constituents is denoted as electro-kinetic flow barrier. The contaminant migration is opposed by the combined effects of electro-osmosis and the effective ionic mobility of contaminant ions in compacted clay under the influence of the imposed electric field.

The in-place saturated hydraulic conductivity k_h of the compacted clay component of a liner system for a hazardous waste landfill must be 1×10^{-7} cm/sec or less to fulfill the requirements of the Hazardous and Solid Waste Amendments (HSWA) of 1984 (*1*). The coefficient of electro-osmotic permeability, k_e, is a soil property that indicates the hydraulic flow velocity through soil under a unit electrical gradient (i.e. 1 V/cm) and is generally in the range of 1×10^{-5} cm²/V sec to 10×10^{-5} cm²/V sec for most soils and is relatively independent of soil type (*3*). Hydraulic flow induced by a small electrical gradient in such a system should be able to balance that induced by a large hydraulic gradient. Hence, a small DC electrical gradient applied continuously or periodically in the direction indicated in Figure 2 may stop the advection component of contaminant migration.

The movement of contaminants by hydrodynamic dispersion and advection also may be resisted by an electrical gradient. Molecular diffusion in fine-grained soils, which are the soil types in which electro-kinetics are most likely to be effective, can be expected to be the dominant component of hydrodynamic dispersion. Ionic contaminants will move relative to the hydraulic flow under the influence of the imposed electrical gradient. However, the directions and velocities of the ionic migrations depend on the charges and the ionic mobilities of the cation and the anion. Figure 3 illustrates the movements of the cations and the anions under the influence of hydraulic, electrical, and chemical gradients in terms of concentration against distance at a certain time t. The hydraulic

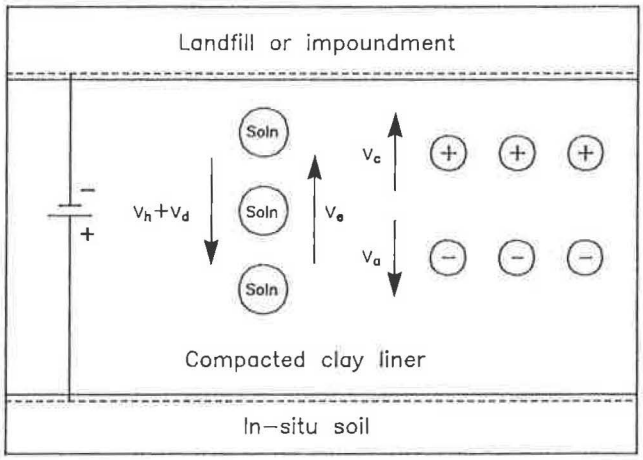

FIGURE 2 Concept of electro-kinetic flow barrier.

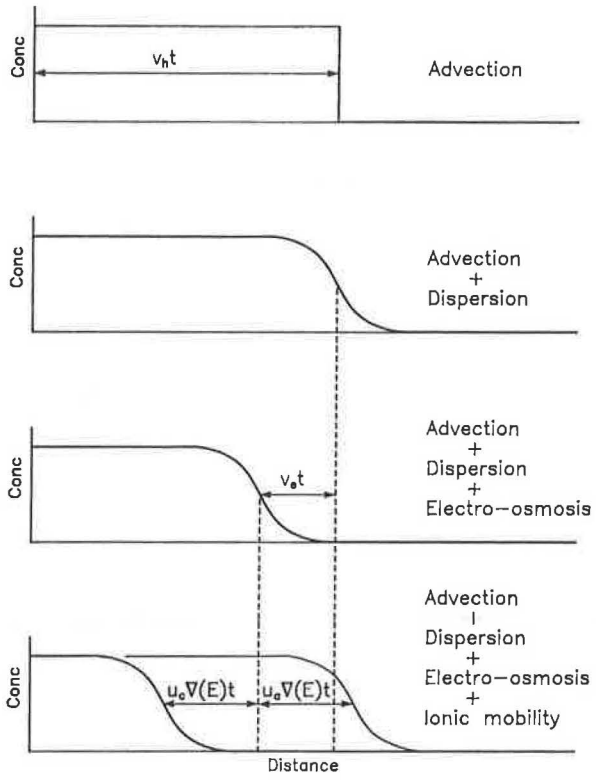

FIGURE 3 Movements of cations and anions under the influences of hydraulic, electrical, and chemical gradients.

flow velocities are v_h and v_e owing to the imposed hydraulic and electrical gradients, respectively. The effective ionic mobilities of the cation and the anion in soil (i.e., the velocities of the ions under the influence of a unit electric field) are u_c and u_a. The applied electrical potential across the soil is E. The theoretical analysis and experimental evaluation of the viability of the electro-kinetic flow barrier to contaminant transport through compacted clay are the main subjects of this paper.

Concentration, Dewatering, and Consolidation

It takes a long time for waste sludges, slimes, coal washeries, mine tailings, or polluted dredged materials to settle by gravity and to consolidate. The shortage of long-term disposal sites and the increasing demand for reuse of dump sites for some other purposes shortly after being filled necessitate techniques to accelerate the concentration, dewatering, and consolidation processes.

Electrophoresis and electro-osmosis may provide means to concentrate and dewater those fine-grained slurries. When an electric field is imposed on a slurry, suspended particles carrying negative charges will migrate toward the anode under the influence of the electric field (Figure 4). The densified sediments at the anode can be removed periodically for further treatment or ultimate disposal without much difficulty. After the sediment has been densified sufficiently and the particle mobility has been reduced, further dewatering and consolidation can be achieved by electro-osmosis. Different procedures of applying those electro-kinetic techniques to densify and dewater coal waste slurry were outlined by Sprute and Kelsh (*5*), whose laboratory and field test results also indicated that a 100-acre by 110-ft-deep impoundment of coal waste sludge can be effectively consolidated by these electro-kinetic techniques. Moreover, the successes of electro-osmosis in dewatering polluted dredged materials and coal washery slimes were demonstrated in small scale experiments (*6–8*). However, attempts to dewater phosphate slimes in Florida have been only moderately successful.

Electro-Kinetic Injection

Electro-osmosis was successfully applied in lieu of injection pressure to cause bentonite suspension to move in controlled direction at an accelerated velocity through fine-grained soils (*9*). The bentonite suspension was injected from perforated steel tubular anodes into the soils toward the cathodes to seal off a building substructure from water percolation. Similarly, it may be possible to inject other chemical grouts to form a barrier in situ to mitigate contaminant migration and thus confine the contaminants within known boundaries.

Electro-kinetic injection might be used to inject cleanup chemicals into contaminated soils to release adsorbed hazardous materials from the surfaces of soil particles, thus facilitating subsequent removal by an appropriate method. Other chemicals may react with the toxics in situ to form harmless compounds or to fix the toxics on the surfaces of soil particles and render them immobile.

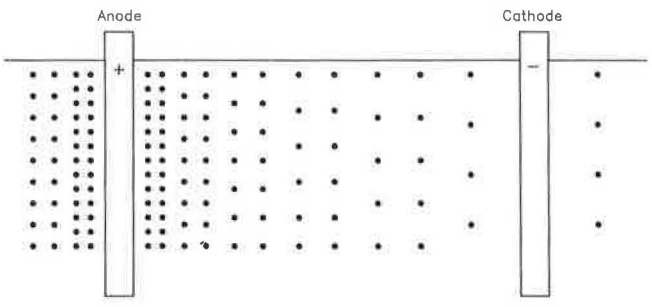

FIGURE 4 Densification of negatively charged particles from dilute suspension by electrophoresis.

Electro-Kinetic Extraction

When an electric field is imposed on a wet soil mass, ionic migrations take place in directions dictated by the charges of the ions. The anions move toward the anode and the cations move toward the cathode (Figure 5). The soil pore fluid moves toward the cathode because of electro-osmosis. The combined effects of electro-osmosis and ionic migration under the influence of an imposed electric field may provide an effective means for removing contaminants from soils.

Some factors affecting the effectiveness of electro-kinetics in contaminant removal were studied by Hamnett (*10*), whose experimental results on silica sand and by using carbon electrodes indicate the high potential for removing inorganic contaminants from soils by electro-kinetics. The possibility for movement of nonpolar organics through soil by electro-osmosis remains essentially unexplored.

Electrochemical Effects in In Situ Cleanup

A number of electrochemical effects other than electro-osmosis, electrophoresis, and ionic migration may develop when an electric field is imposed on a wet soil mass or clay suspension, such as ion diffusion, ion exchange, development of osmotic and *p*H gradients, desiccation owing to heat generation at the electrodes, mineral decomposition, precipitation of salts and secondary mineral, electrolysis, hydrolysis, oxidation, reduction, physical and chemical adsorption, and soil fabric changes.

Contaminants may be transformed into inert forms by precipitation of salts and secondary minerals and by chelation and may be removed from the soil by electrolysis, hydrolysis, or redox reactions. Hamnett (*10*) reported that the chloride

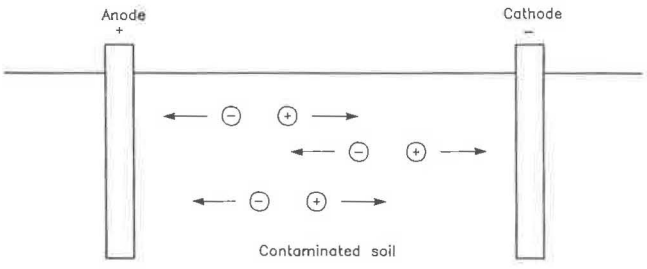

FIGURE 5 Electro-kinetic extraction of ionic pollutants.

ions in silica sand evolved as chlorine gas at the anode as a result of electrolysis. The *p*H at the cathode becomes higher and that at the anode becomes lower owing to the electrolysis of water at the electrodes. Segall et al. (*11*) reported that the highly alkaline water at the cathode could desorb organics, pesticides, and heavy metals from the surfaces of soil particles and thus facilitated removal from soil by electro-osmosis.

THEORETICAL ANALYSIS OF ELECTRO-KINETIC FLOW BARRIERS

The theoretical formulation is only outlined here. The complete development is given by Yeung (*12*). Contaminant migration through a compacted clay liner equipped with an electro-kinetic flow barrier involves several coupled simultaneous flows (i.e., water, electricity, and ions under the influences of hydraulic, electrical, and chemical gradients). Those transport processes are formulated by the formalism of the thermodynamics of irreversible processes to give a quantitative description of the phenomenological coefficients (*13–16*).

By the assumptions of the thermodynamics of irreversible processes, the flows or fluxes J_i are linear and homogeneous functions of the gradients or driving forces X_i. That is, any flux or flow J_i is related to the gradients or driving forces by

$$J_i = \sum_{j=1}^{n} L_{ij} X_j \qquad (i = 1, 2, \cdots, n) \tag{1}$$

where the phenomenological coefficients L_{ij} are independent of the driving forces. The L_{ii} are the conductivity coefficients for direct flows, and the L_{ij} $(i \neq j)$ are called coupling coefficients, which quantify the cross phenomena (*3*). The coupled flows that can occur under the influences of hydraulic, thermal, electrical, and chemical gradients are given in Table 1. Moreover, the matrix of phenomenological coefficients L_{ij} is symmetric; that is,

$$L_{ij} = L_{ji} \qquad (i, j = 1, 2, \cdots, n) \tag{2}$$

provided a proper choice is made for the fluxes J_i and driving forces X_i (*13*). Those identities are called the Onsager reciprocal relations (*14,15*). The proper choice has to be formulated from the local balance equations of mass, energy, and momentum (*16*).

Assuming the contaminant consists of an ionic salt that dissociates into one cation and one anion, the driving forces are identified to be the hydraulic gradient $\nabla(-P)$, the electrical gradient $\nabla(-E)$, the concentration dependent parts of the chemical gradients of the cation $\nabla(\mu_c^c)$, and of the anion $\nabla(\mu_a^c)$. The fluxes are the volume flow rate of the solution per unit area J_v, the electric current density I, the diffusional flow rate of the cation J_c^d, and of the anion J_a^d per unit area relative to the flow of water. The diffusional flows are related to the absolute flows by

$$J_i = J_i^d + \frac{c_i}{c_w} J_w \tag{3}$$

TABLE 1 COUPLED AND DIRECT-FLOW PHENOMENA
[adapted from Mitchell (*3*)]

Flow J	Gradient X			
	Hydraulic	Thermal	Electrical	Chemical
Fluid	Hydraulic conduction *(Darcy's Law)*	Thermo-osmosis	Electro-osmosis	Normal osmosis
Heat	Isothermal heat transfer	Thermal conduction *(Fourier's law)*	Peltier effect	Dufour effect
Electric current	Streaming potential	Thermo-electricity	Electric conduction *(Ohm's law)*	Diffusion and membrane potentials
Ion	Streaming current	Soret effect	Electrophoresis	Diffusion *(Fick's law)*

where c_i is the concentration of ion i and c_w is the concentration of water. Hence, the set of phenomenological equations relating the four flows and the four driving forces is

$$J_v = L_{11}\nabla(-P) + L_{12}\nabla(-E) + L_{13}\nabla(-\mu_c^c) + L_{14}\nabla(-\mu_a^c) \quad (4a)$$

$$I = L_{21}\nabla(-P) + L_{22}\nabla(-E) + L_{23}\nabla(-\mu_c^c) + L_{24}\nabla(-\mu_a^c) \quad (4b)$$

$$J_c^d = L_{31}\nabla(-P) + L_{32}\nabla(-E) + L_{33}\nabla(-\mu_c^c) + L_{34}\nabla(-\mu_a^c) \quad (4c)$$

$$J_a^d = L_{41}\nabla(-P) + L_{42}\nabla(-E) + L_{43}\nabla(-\mu_c^c) + L_{44}\nabla(-\mu_a^c) \quad (4d)$$

Those equations contain four conductivity coefficients, L_{ii} as defined next, and 12 coupling coefficients. Those phenomenological coefficients are not independent. As a result of the Onsager reciprocal relations,

$$L_{12} = L_{21} \quad (5a)$$

$$L_{13} = L_{31} \quad (5b)$$

$$L_{14} = L_{41} \quad (5c)$$

$$L_{23} = L_{32} \quad (5d)$$

$$L_{24} = L_{42} \quad (5e)$$

$$L_{34} = L_{43} \quad (5f)$$

Hence, there are only 10 independent coefficients characterizing the system. If any three of the driving forces can be set to zero in different experiments, then the quantities of flows are determined by a single driving force. The ratios of the measured quantities of flows to this force give the L_{ij}. However, it is not always possible or convenient to perform experiments with only one driving force. Instead, it is often more convenient to set two forces and one flow to zero and to evaluate the appropriate L_{ij} by solution of the simultaneous equations that represent the actual test conditions.

Considering the testing conditions used for the measurements of hydraulic conductivity, electro-osmotic permeability, electrical conductivity, osmotic efficiency, effective diffusivities, and the effective ionic mobilities, and assuming the solution is dilute with no interaction between the cation and the anion, the L_{ij}s were determined to be (*12*)

$$L_{11} = \frac{k_h}{\gamma_w n} + \frac{L_{12}L_{21}}{L_{22}} \quad (6a)$$

$$L_{12} = L_{21} = \frac{k_e}{n} \quad (6b)$$

$$L_{13} = L_{31} = \frac{-\omega c_c k_h}{\gamma_w n} + \frac{L_{12}L_{23}}{L_{22}} \quad (6c)$$

$$L_{14} = L_{41} = \frac{-\omega c_a k_h}{\gamma_w n} + \frac{L_{12}L_{24}}{L_{22}} \quad (6d)$$

$$L_{22} = \frac{\kappa}{n} \quad (6e)$$

$$L_{23} = L_{32} = c_c u_c \quad (6f)$$

$$L_{24} = L_{42} = -c_a u_a \quad (6g)$$

$$L_{33} = \frac{D_c c_c}{RT} \quad (6g)$$

$$L_{34} = L_{43} = 0 \quad (6h)$$

$$L_{44} = \frac{D_a c_a}{RT} \quad (6i)$$

where

k_h = the hydraulic conductivity,
k_e = the electro-osmotic permeability,
κ = the bulk electrical conductivity of soil,
ω = the reflection coefficient (the ratio of the measured osmotic pressure to the theoretical value),
γ_w = the unit weight of water,
c_c = the concentration of cation,
c_a = the concentration of anion,
u_c = the effective ionic mobility of cation,
u_a = the effective ionic mobility of anion,
D_c = the effective diffusivity of cation,
D_a = the effective diffusivity of anion,
n = the porosity of soil,
R = the universal gas constant, and
T = the absolute temperature.

The contaminant flows relative to the soil are of more significance than the diffusional flows relative to water. Combining Equations 3 and 4 gives the flow equations for cations and anions under the influences of hydraulic, electrical, and chemical gradients:

$$J_c = (L_{31} + c_c L_{11})\gamma_w\nabla(-h) + (L_{32} + c_c L_{12})\nabla(-E) + (L_{33} + c_c L_{13})\frac{RT}{c_c}\nabla(-c_c) + (L_{34} + c_c L_{14})\frac{RT}{c_a}\nabla(-c_a) \quad (7a)$$

$$J_a = (L_{41} + c_a L_{11})\gamma_w\nabla(-h) + (L_{42} + c_a L_{12})\nabla(-E) + (L_{43} + c_a L_{13})\frac{RT}{c_c}\nabla(-c_c) + (L_{44} + c_a L_{14})\frac{RT}{c_a}\nabla(-c_a) \quad (7b)$$

where $\nabla(-h)$ is the hydraulic gradient (dimensionless). Applying the principle of conservation of mass for steady flow, the governing equation for the concentration of species i is

$$\frac{\partial c_i}{\partial t} = -\nabla\cdot J_i - G_i \quad (8)$$

where G_i is a source-sink term denoting the removal rate of species i per unit volume. Solution of this equation gives concentration of species i as a function of time and position.

Special cases of the general coupled flow theory were compared with existing solutions describing the phenomena for consistency (*12*), such as the diffusion potential equation, the advection dispersion equation, the van't Hoff equation, and the chemical osmosis and ultrafiltration equations. Those comparisons indicate that the developed theory is general and incorporates all flow phenomena as special cases.

A one-dimensional computer model was developed to solve Equation 8 by finite differences as a function of time and position. The electrical and hydraulic gradients are assumed constant. However, the time and position dependencies of the chemical gradients are taken into account. The program allows input of all the required parameters and the application of periodic or continuous electrical gradients. When no externally applied electric field exists, the computer simulation converges to the analytical solution given by Ogata and Banks (*17*) for contaminant transport by advection and dispersion.

EXPERIMENTAL EVALUATION OF THE THEORY

A laboratory testing program was developed to establish the effectiveness of electro-osmosis in driving water through both partially saturated and fully saturated compacted clay, to evaluate the validity of the theoretically developed equations, and to establish the viability of the electro-kinetic flow barrier concept.

Because the experimental apparatus required for this laboratory testing program could not be adapted from conventional soil testing equipment, a new apparatus was designed, fabricated, and assembled and contains two sets of fixed wall permeameters with five identical permeameters in each set. One set of permeameters is equipped with electrodes, and the other serves as controls to compare the efficiency of the electro-kinetic flow barrier. The schematic diagram of the experimental apparatus is depicted in Figure 6. The compacted clay samples are 1.4 in. in diameter and 4 in. in length. All samples are permeated under identical hydraulic gradients. Each permeameter is equipped with independent measuring devices for inflow and outflow volumes. The voltage across each sample and the electric current passing through can be monitored independently. The voltage measurement electrodes are separated from the electric current supply electrodes so that any adverse effects on voltage measurements arising from electrode reactions during the electro-kinetic process are eliminated. The current anodes are made of platinum mesh to minimize electrode reactions, and the other electrodes are made of stainless steel mesh for economic reasons.

The soil used in this laboratory test program is a gray brown silty clay of moderate plasticity (Unified Soil Classification CH), comes from Livermore, California, and has been used to construct the compacted clay liner of a landfill at Altamont (it is referred to as Altamont soil throughout this paper). The maximum dry density is 110 pcf, and the optimum water content is 17.4 percent as determined by the modified Proctor compaction test. The liquid limit, plastic limit and plasticity index of the soil are 52, 27 and 25 percent, respectively.

Five samples were prepared to establish the effectiveness of electro-osmosis as a means of water transport by kneading compaction at different moisture contents into the permeameters equipped with electrodes. The samples were saturated to different degrees of saturations using back pressures of 1 kg/cm^2 up to 5 kg/cm^2 applied in five steps. Different electrical gradients were applied to the samples at each saturation stage, and the respective volume flow rates of water were measured to determine the coefficients of electro-osmotic permeability.

Ten uniform replicate samples were compacted to evaluate the viability of an electro-kinetic flow barrier. All the samples were fully saturated with tap water and then were permeated with sodium chloride solution under identical hydraulic gradients. A periodic electrical gradient of 1 V/cm was applied for 1 hr/day to the group of permeameters equipped with electrodes. One sample from each group was dismantled from the system at an interval of 5 days. Each sample was then sectioned into eight pieces, and complete chemical analyses were performed on the pore fluid extracted from each piece.

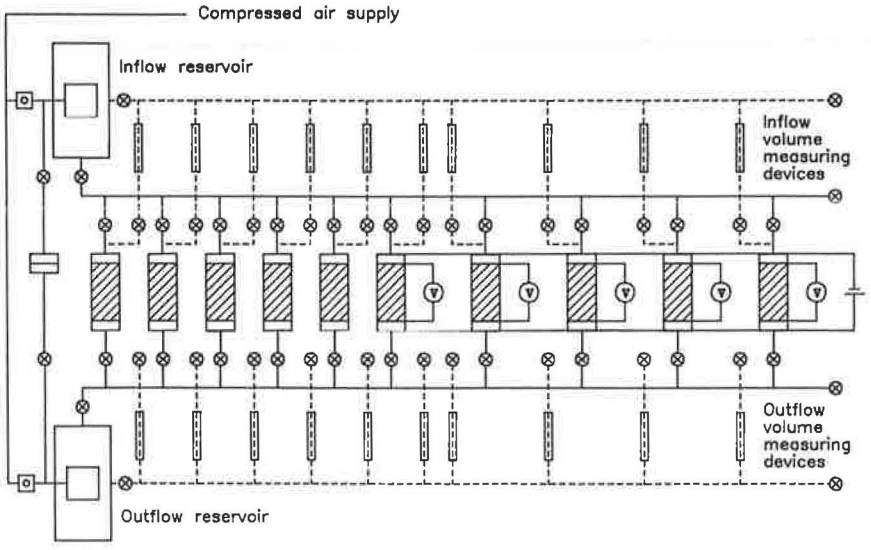

FIGURE 6 Schematic diagram of the experimental apparatus.

RESULTS AND DISCUSSION

The measured coefficients of electro-osmotic permeability of Altamont clay at different stages of back-pressure saturation are plotted against compacted dry densities and compaction moisture contents in Figures 7 and 8, respectively. Here, k_e is within the range of 1×10^{-5} cm²/V sec to 7×10^{-5} cm²/V sec. The decrease in measured k_e at later stages of back-pressure saturation may be due to the growth of micro-organisms that block flow channels through the samples after prolonged permeation. The measured hydraulic conductivities k_h are in the range of 1×10^{-7} cm/sec to 1×10^{-10} cm/sec, depending on the compaction water content and density, and are decreased with time even though the degrees of saturation were increased by the increase of back pressure. The growth of micro-organisms in the samples was evident after careful examination of the samples at the end of the test. Nonetheless, the experimental results demonstrate the existence of electro-osmotic flow in both partially saturated and fully saturated compacted clay. The k_e measured is in the range of that for most saturated soils studied in earlier investigations (i.e., 1×10^{-5} cm²/V sec to 10×10^{-5} cm²/V sec).

The replicate samples for the electro-kinetic flow barrier study were compacted wet of optimum to 90 percent relative compaction. The hydraulic conductivities of those samples were measured to be on the order of 1×10^{-9} cm/sec. The coefficients of electro-osmotic permeability were measured to be 2×10^{-5} cm²/V sec. The diffusion coefficient of NaCl was measured in a separate experiment on similar samples to be 3×10^{-6} cm²/sec under conditions of standard temperature and pressure. The periodic application of an electro-kinetic flow barrier to the compacted clay samples indicated that the

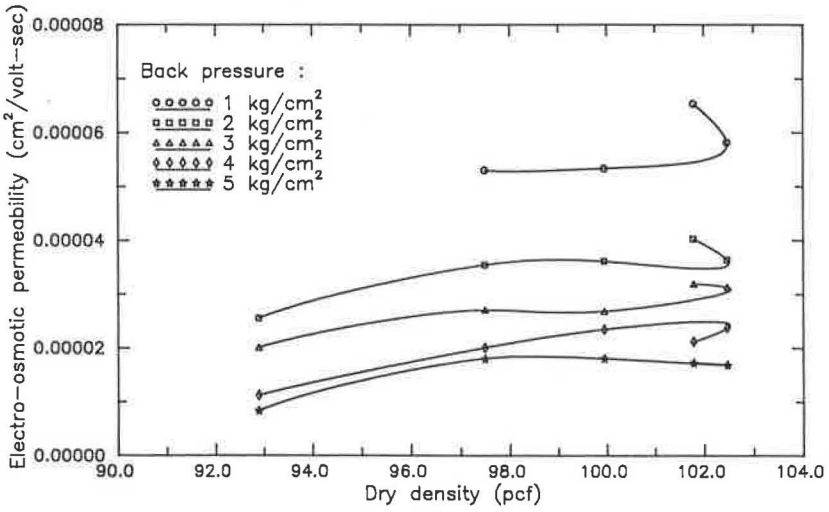

FIGURE 7 The relationship between electro-osmotic permeability and dry density for compacted Altamont clay.

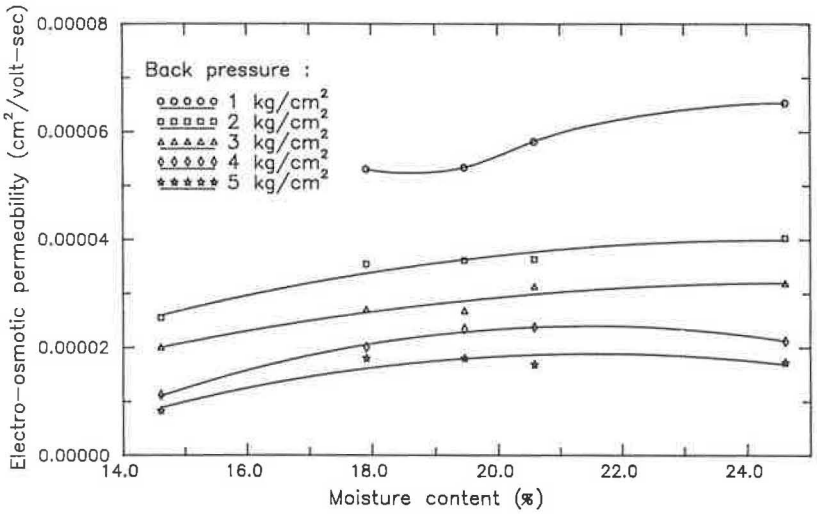

FIGURE 8 The relationship between electro-osmotic permeability and compaction moisture content for Altamont clay.

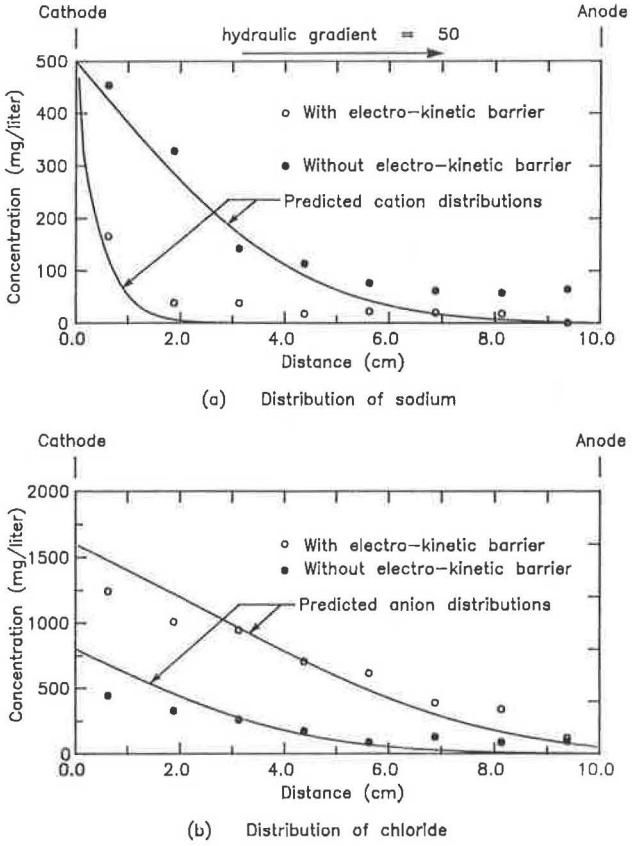

FIGURE 9 Distributions of contaminants after 20 days. Continuous application of hydraulic gradient and periodic (1 hr/day) application of electrical gradient.

migration of sodium ions was halted and the migration of chloride ions was accelerated. In this case, the ionic mobility of the chloride ions exceeded the electro-osmotic counterflow and resulted in a net migration of chloride ions toward the anode. However, the electrical gradient provided a very effective flow barrier to the migration of the cation.

The distributions of contaminants (NaCl) after 20 days of permeation is presented in Figure 9. The curves give the computer model predictions by using the measured parameters as input. The measured concentration profiles are observed to be in good agreement with the predicted profiles given by the theory.

PRACTICAL APPLICATION

The results from this continuing research indicate that electro-osmosis can stop advective and dispersive flows through compacted clay. The cathode would be installed on the landfill side of a clay liner when applied to a landfill. Transport of contaminants by those mechanisms would be prevented by maintaining a small net inward flow (i.e., a greater inward electro-osmotic flow than outward hydraulic flow).

However, the results also show that ionic transport in the electric field would cause migration of anions to the anode underneath the liner. Should those anions pose a risk to the environment, then a collection system would be required for their removal.

Analysis indicates that for values of hydraulic conductivity and electro-osmotic permeability typical of those for compacted clay liner materials (i.e., $k_h \leq 1 \times 10^{-7}$ cm/sec and $k_e \approx 5 \times 10^{-5}$ cm²/V sec) the required sustained DC voltage across a liner of typical thickness (i.e., 3 ft) would be quite low (of the order of a few tenths of a volt). Thus, problems resulting from gas and heat generation and cracking often associated with electro-osmosis when used for clay consolidation may be minor. Because both the voltage and the current density would be low, the power costs would be low.

CONCLUSIONS

1. The existence of electro-osmotic flow in partially saturated and fully saturated compacted clay of the type used in waste landfill liner systems was demonstrated experimentally.
2. The coefficients of electro-osmotic permeability of compacted Altamont clay were measured to be in the range of 1 $\times 10^{-5}$ cm²/V sec to 7 $\times 10^{-5}$ cm²/V sec. Those values are in the range of values for most of soils (*3*).
3. An electro-kinetic flow barrier such as the one depicted in Figure 2 halted the migration of the cation but accelerated that of the anion under laboratory testing conditions.
4. The developed coupled flow theory reasonably predicted the migration of the contaminant ions under the influences of the hydraulic, electrical, and chemical gradients.
5. An electrical gradient may move some inorganic species in soils much more effectively than a hydraulic gradient.

ACKNOWLEDGMENTS

This research was supported by the University of California Water Resources Center under Project W-699, *Waste Containment and Cleanup Using Electro-Osmosis*; by the Environmental Institute for Waste Management Studies of the University of Alabama; and by The Earth Technology Corporation, Long Beach, California, which selected the second author as The Earth Technology Corporation Fellow 1987–1989. The support is gratefully acknowledged. This paper has not been subjected to the peer and administrative review of those organizations and therefore does not necessarily reflect their views and no official endorsement should be inferred.

REFERENCES

1. *Draft Minimum Technology Guidance on Double Liner Systems for Landfills and Surface Impoundments: Design, Construction, and Operation*, 2nd version. Report EPA/530/SW-85/014, EPA Cincinnati, 1985.
2. L. J. Goldman, L. I. Greenfield, A. S. Damle, G. L. Kingsbury, C. M. Northeim, and R. S. Truesdale. *Design, Construction and Evaluation of Clay Liners for Waste Management Facilities*. Report EPA/530/SW-86/007F, EPA, Washington, D.C., 1988.
3. J. K. Mitchell. *Fundamentals of Soil Behavior*, John Wiley, New York, 1976.
4. H. van Olphen. *An Introduction to Clay Colloid Chemistry*, 2nd edition, John Wiley, New York, 1977.
5. R. H. Sprute and R. H. Kelsh. *Electrokinetic Densification of Solids in a Coal Mine Sediment Pond: A Feasibility Study*: 1, Laboratory and Field Tests. Report of Investigations 8666, Bureau of Mines, U.S. Department of the Interior, Washington, D.C., 1982.

6. R. J. Krizek, F. B. Gularte, and P. L. Hummel. Stabilization of Polluted Dredgings by Electro-Osmosis. *Proc., ASCE National Water Resources and Ocean Engineering Convention*, San Diego, 1976.
7. N. C. Lockhart. Sedimentation and Electro-Osmotic Dewatering of Coal-Washery Slimes. *Fuel*, Vol. 60, No. 10, 1981, pp. 919–923.
8. N. C. Lockhart and R. E. Stickland. Dewatering Coal-Washery Tailings Ponds by Electro-Osmosis. *Powder Technology*, Vol. 40, No. 1–3, 1984, pp. 215–221.
9. W. J. Holmes. Electro-Osmosis and the Civil Engineer. *Civil Engineering Public Works Review*, Vol. 58, No. 682, 1963, pp. 624–626.
10. R. Hamnett. *A Study of the Processes Involved in the Electro-Reclamation of Contaminated Soils*. M.Sc. dissertation, University of Manchester, 1980.
11. B. A. Segall, C. E. O'Bannon, and J. A. Mathias. Electro-Osmosis Chemistry and Water Quality. *Journal of the Geotechnical Division, ASCE*, Vol. 106, No. GT10, 1980, pp. 1148–1152.
12. A. T. Yeung. *Electro-Kinetic Barrier to Contaminant Transport Through Compacted Clay*. Ph.D. dissertation, University of California, Berkeley, 1990.
13. S. R. de Groot and P. Mazur. *Non-Equilibrium Thermodynamics*, North-Holland, Amsterdam, 1962.
14. L. Onsager. Reciprocal relations in irreversible process, 1. *Physical Review*, Vol. 37, No. 4, 1931, pp. 405–426.
15. L. Onsager. Reciprocal Relations in Irreversible Process, 2. *Physical Review*, Vol. 38, No. 12, 1931, pp. 2265–2279.
16. D. D. Fitts. *Nonequilibrium Thermodynamics*, McGraw-Hill, New York, 1962.
17. A. Ogata and R. B. Banks. *A Solution of the Differential Equation of Longitudinal Dispersion in Porous Media*. Professional Paper 411-A, U.S. Geological Survey, 1961.

Publication of this paper sponsored by Committee on Physicochemical Phenomena in Soils.

Thermally Driven Electrical Coupling Effects and Pore Water Advection in Soils

DONALD H. GRAY AND SAMUEL I. OUTCALT

Measurements of near-surface temperature fluctuations during a period of night frost were used in conjunction with a surrogate measure of soil water ion concentration to attempt to trace inflections in these time series to soil water advection effects. Major inflections in the ion concentration time series were traceable to water and water vapor processes as a freeze-thaw front propagated vertically through a soil profile at shallow depths. Relative ion concentration was related to the electrical potential measured between a probe at different depths of interest and a ground spike. The field probe electric circuit was modeled as an electrolytic cell without transference. Field time series data illustrated that effects of water migration toward near-surface evaporation/freezing fronts, solute expulsion from a freezing region, internal evaporation, and clean melt water release could be detected by variations in the electric potential or its surrogate, the relative ion concentration index. The spatial/temporal pattern of temperature and relative ion concentration helps to explain interactions or coupling between induced hydraulic, osmotic, and electrical gradients during the propagation of a thermal disturbance through a soil.

Electro-osmosis and streaming potential are manifestations of isothermal coupling of flows of water and electricity in a soil. Coupling effects become more complex when a thermal gradient or disturbance (e.g., freezing and thawing) are present. Passive generation of electrical potential gradients in soils by thermal gradients has been reported in a number of laboratory experiments (*1–3*). Measurements of electric potential variation across the freezing isotherm have been reported from permafrost regions in recent years (*4–6*). Those measurements demonstrated significant changes in electric potential near the freezing front. Outcalt et al. (*7*) propose that those electrical potential variations during soil freezing and thawing events may be interpreted as the product of soil electrolyte concentration variations resulting from phase changes and advection.

A primary purpose of this paper is to present additional evidence in support of this hypothesis based on soil-water potential and temperature measurements during a night frost event in the field. Another objective is to test the significance of electrical potentials associated with soil freezing and thawing. For example, Kelsh and Taylor (*8*) have claimed that freezing potentials depend in complex ways on so many different variables that it is hard to sort out their individual effects. Accordingly, they assert that although freezing of water may indeed influence water migration and modify pore water ion concentrations freezing potential is not a useful measure of such effects.

An opposite view is that thermally induced concentration changes appear to explain best the gross features of the measured electrical potentials, which does not preclude, however, the presence of other coupling effects similar to those noted by Elrick et al. (*9*). Several types of coupling effects could conceptually manifest themselves during freeze-thaw events in a soil-water-electrolyte system as a result of complex interactions between the flows of matter and energy. If present, those effects would tend to modulate but not dominate concentration-induced potentials associated with freezing and thawing.

As an example of a secondary coupling effect, freezing of soil water can give rise to a large soil-water suction with a strong advective flow of water into the freezing region. This advective flow in turn can produce an electrokinetic streaming potential. However, the "electrokinetic potentials" cannot account for the magnitude and pattern of the observed electric potentials associated with frost-thaw events. Gray and Mitchell (*10*) measured streaming potential by using reversible Ag-AgCl electrodes on either side of homoionic clays and silty clays saturated with sodium chloride solutions varying from 10^{-3} to 10^{-4} N in concentration. The measured streaming potentials varied from 1 to 60 mV/atm with potentials decreasing sharply as either the concentration of the pore water electrolyte or the exchange capacity of the clay soil increased. Those potentials are an order-of-magnitude lower than the electric potentials measured between our near-surface probes and reference ground spike.

Other types of induced electrical potentials associated with freeze-thaw events (diffusion potentials, phase boundary potentials, and freezing potentials) have also been cited from time to time in the technical literature. So-called "freezing" potentials in the range of 1 to 25 mV have been reported by Drost-Hansen (*11*) in dilute aqueous solutions (10^{-4} – 10^{-3} N KCl) between the advancing ice front (negatively charged) and unfrozen water (positively charged). This potential is alleged to arise as the result of the incorporation of ions into ice and the crystallographic rearrangement of water molecules as freezing occurs. However, gentle stirring obliterated this potential. Stirring would also have eliminated ion concentration differences and suggests that the "freezing" potential is caused in large part by ionic concentration differences near the ice interface.

D. H. Gray, Department of Civil Engineering, University of Michigan, Ann Arbor, Mich. 48109. S. I. Outcalt, Department of Geological Sciences, University of Michigan, Ann Arbor, Mich. 48109.

EXPERIMENTAL PROGRAM

A field study was conducted in a grass lawn area at the University of Michigan Matthaei Botanical Gardens northeast of Ann Arbor, Michigan. The soil at the site is a pebble-rich upland sandy loam of glacial origin with a plow zone approximately 10 cm deep. A mixture of loess and sandy loam is present in the disturbed plow zone.

The data were collected by using copper probes (electrodes), each with an enclosed thermistor, and were installed in a vertical array or stack at shallow depths (0, 3, 6, and 9 cm) in the sandy loam. The surface probe was placed at the base of the grass mat, or organic-mineral soil interface, and the deeper probes were centered at the indicated level. The electric potential measurements were made relative to a 2-m-long copper-plated ground spike driven vertically into the soil and separated horizontally from the probe array by a distance of 2 m. A detailed description of the field installation, data system, and derivation of the C-index (a linear surrogate measure of relative ion concentration) is presented in an earlier publication (*7*).

Because the use of the C-index is critical, the derivation will be repeated here. The electrical potential developed by an electrolytic cell without transference is given by Equation 1. The basis for this equation may by found in Glasstone (*12*).

$$\Delta E = -2K \log C_p/C_s \quad (1)$$

where the electric potential (ΔE) in mV is measured and used to calculate the natural logarithm of the ratio of the probe/ground spike soil water ion concentrations (C_p/C_s). The parameter (K) is the product of the gas constant and absolute temperature divided by the Faraday constant and has a value of approximately 23.5 mV near the ice point. The mid-range value of potentials was 500 mV at the experimental site. By using 500 mV, the (C_s/C_p) ratio is 4.17×10^4. Substituting 4.17×10^4 for (C_s) in Equation 1 and solving for the probe concentration (C_p) yields a relative index of soil water concentration on a linear scale (Equation 2).

$$\text{C-index} = 4.17 \times 10^4 \exp(-\Delta E/47) \quad (2)$$

The C-index is normalized to unity at 500 mV and corresponds to a (C_s/C_p) ratio of 4.17×10^4. The C-index calculation assumes that the ion concentration at the ground spike is quasi-constant during a single data acquisition period. This assumption appears valid, because all data sets show a rapid attenuation in C-index variation with depth at the shallow near-surface probes. During the summer drought of 1988, in the U.S. middle west, the C-index of the surface probes increased nine orders-of-magnitude and returned to near mid-range values with drought-terminating rains. No attempt is made to update the quasi-constants in Equation 2, because only relative change is of interest.

A table-top analog of the field probe electric circuit is two glass jars filled with a low concentration brine (probe) and high concentration brine (ground spike) "jumped" by a copper wire and connected to a voltmeter by copper electrodes in the two jars. Brine solutions need not be in physical contact because the electric potential is generated only by the concentration contrast. In the soil the "jump wire" is the soil water. Use of the electrolytic cell model without transference is based on the rapid response of the probes to ice nucleation and thaw. However, all models of electrolyte cells are based on the same general algebraic expression where the electrode potential is a function of the logarithm of the concentration ratio regardless of the absence or presence of transference. Therefore, in a strict sense, this model is equally applicable to both conditions. Reservations have been expressed (*13*) concerning the application of equilibrium thermodynamics to electrolyte cells. However, after the C-index transfer has been applied to the electric potential data, a lengthy series of soil frost and thaw events can be interpreted in terms of well-known processes (*14*).

The laboratory data described by Kelsh and Taylor (*8*) were collected by using methods that differed significantly from those employed here. Those differences are summarized:

1. Kelsh and Taylor reported electric potential across the freezing isotherm, and the system used in the present study yielded probe potential relative to a ground spike.
2. The Kelsh and Taylor test cell appears to be a closed hydraulic system, and the configuration used in the present study was open. Measurement in a closed cell may generate masking effects in the freezing region where pore water is mobile and tends to circulate as the freezing front advances.
3. Kelsh and Taylor reported their data as electric potential rather than converting to a relative measure of ion concentration, which was possible with the configuration in the present study.

EXPERIMENTAL RESULTS

Temperature and electric potential readings were collected at 10-min intervals by using an automatic acquisition system during a 1-day period from 14:00 EST on March 12, 1987, to 14:00 EST March 13, 1987. Figure 1 is a time series record

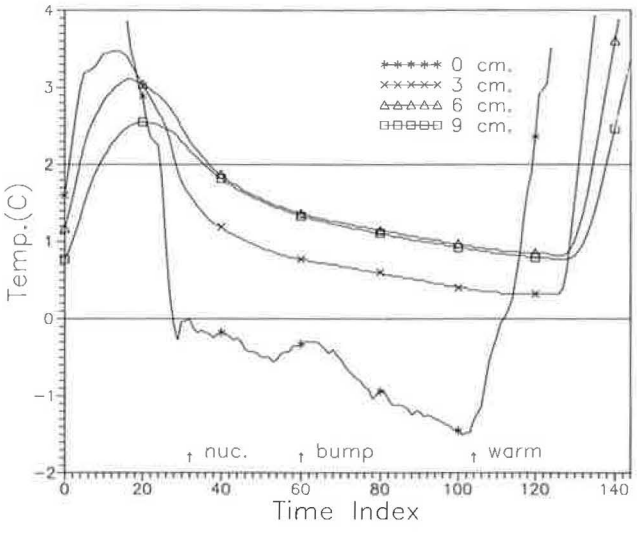

FIGURE 1 Temperature plotted on a linear scale. Time index divisions represent observations at 10-min intervals for a 24-hr period. The labels "nuc.," "bump," and "warm" indicate ice nucleation, warm water advection, and the onset of warming.

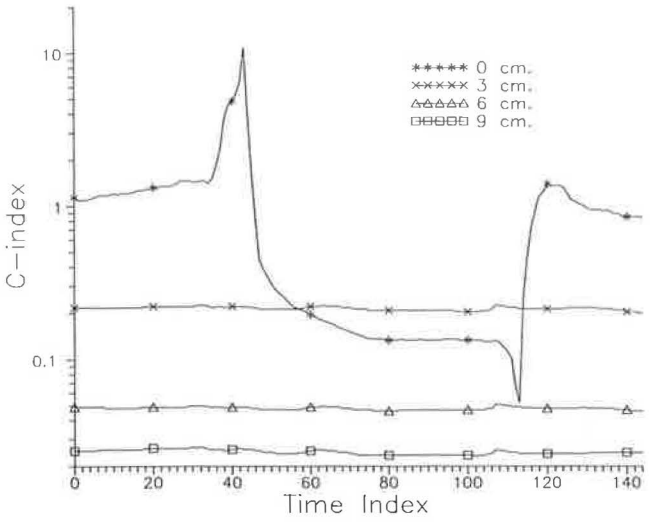

FIGURE 2 C-index plotted on logarithmic scale.

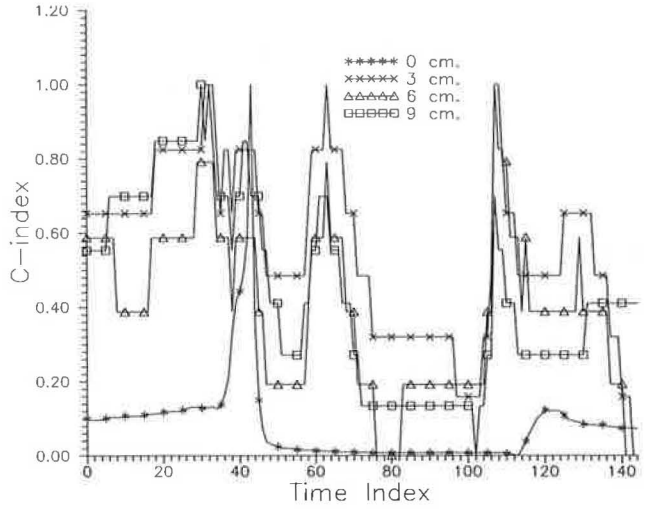

FIGURE 3 C-index plotted on a linear scale after adjustment to 0–1 range.

of the temperature at different probe depths. Figure 2 is a time series record of the C-index plotted on a logarithmic scale. Figure 3 is a time series plot of C-index values that have been normalized to a 0–1 scale to provide a more detailed perspective of fluctuations over time.

Interpretation of Time Series

The interpretation of events in the temperature and C-index plots is given in Table 1. Different events and their manifestations in either the thermal or C-index record at the 0-cm probe are referenced by their corresponding 10-min time observation index. Each of those events will be discussed in turn.

Hallet (*15*) described the expulsion of solute toward the warm side of the freezing region. Accordingly, as the temperature of the 0-cm probe declines while the freezing isotherm moves downward, the typical undercooling-nucleation pattern in the temperature record and steep increase in the C-index followed by a purification decline would be expected (see Figures 2 and 3 at time index 41). This pattern appears after ice nucleation (labeled "nuc." in Figure 1).

As the surface temperature declines, an increase in temperature at 0 cm exists that interrupts the smooth parabolic decline curve. This region near time index 60 is labeled "bump" in Figure 1 and can be interpreted as a consequence of a sudden and steep increase and decline in solute concentration from 3 to 9 cm. The increased ion concentration in the pore water can only be produced by two mechanisms in the absence of frost or a local solute source/sink. Those mechanisms are the advection of relatively solute rich soil water or, alternatively, the evaporation of water, both of which produce a concentration increase. Water advection or vapor condensation or both also can produce a decrease in ion concentration in an analogous manner.

The 0-cm level begins to warm near time index 108 (marked "warm" in Figure 1). The solute concentration or its surrogate, the C-index, increases after the thaw is completed at time index 113 after a slight drop owing to melt water dilution (see Figures 2 and 3). Strongly correlated ion concentration variations at the 3-, 6-, and 9-cm levels are evident as well when the C-index values are normalized to a 0–1 scale (as indicated in Figure 3). Because of the rapid propagation of

TABLE 1 EVENTS AT THE 0-cm PROBE BY TIME INDEX NUMBER

Event	Time Index	Record Manifestation
Undercooling-Nucleation	30	Temp. trough (-0.25°C)
Pre-Freezing Upturn	35	C-index upturn
Solute Expulsion Start	44	C-index peak
Warm Water Advection	54-79	Temp. convex "bump"
Melt Start	102	Temp. upturn
Thaw Downturn	108	C-index downturn
Melt End	113	Temp. > 0°C
Post-Thaw Upturn	114	C-index upturn

those disturbances, they may be produced by internal evaporation and distillation processes strongly modulated by both the total (matric and osmotic) potential-vapor pressure variations near the surface [as discussed by Henry (*16*)].

In the case of those field measurements, relatively slow soil water migration toward the freezing-thawing or evaporating regions or both near the surface would bring relatively pure soil water into the near-surface zone as the solute concentration decreases downward below the freezing-thawing region. The tendency for local dilution by soil-water advection from 3 cm downward is countered by evaporation concentration events. Those events are initiated by changes in the near-surface water vapor pressure gradient, which in turn is modulated by the water potential. The C-index at the lower levels increases when there is strong evaporation below the surface. At times, when the vapor flux toward the surface is reduced the lower levels are diluted by the upward movement of relatively pure liquid water. As was observed previously by Outcalt (*17*), the vertical velocity of liquid water flow reaches maximum values of about 2 cm/hr under night-frost conditions. Therefore, the rapid propagation of surface disturbances downward must occur in the vapor phase.

A final demonstration of the detail available in C-index records is provided by a logarithmic plot of the 0-cm probe presented in Figure 2. Interpretation of this record indicates that thaw is complete at the level of this probe at time index 113. An initial release of melt water exists that lowers the C-index. As melting begins at the 0-cm probe, the solute-rich water below the lower boundary of the freezing isotherm is hydraulically separated by a subfreezing ice-rich zone. Because this cold zone warms toward the ice point and thaws the water (thereby increasing the hydraulic conductivity in the subfreezing zone), a solute-rich "pool" is advected toward the evaporating organic mat surface and thus reduces the C-index at the probe.

Role of Water Advection

If the position is accepted that the C-index is a good surrogate for solute concentration, then observations indicate that the solute concentration of the near-surface layers is strongly modulated by both liquid water and water vapor advection. The strongly correlated and rapid solute concentration fluctuations (C-index readings) in the upper 9 cm of the mineral soil must be initiated by changes in the water system state owing to phase transitions and meteorological variation near the surface. Those rapid fluctuations are transmitted to depth by fluctuations in the water vapor pressure gradient and alter the magnitude of internal evaporation/condensation. Evaporation increases the local solute concentration, and condensation reduces solute concentration. In those data there may have been a continuous liquid water migration toward the surface that varied in magnitude but not direction.

Pressure on both the liquid and the vapor phases of water is decreased with increased solute concentration [as pointed out by Henry (*14*)]. The soil water potential is composed of both the gravitational, the matric, and the osmotic potentials. The osmotic potential, produced by solute concentration gradients, is usually neglected. However, Hallet (*13*) indicated that osmotic effects may be significant near an advancing frost front owing to the high solute concentration of the soil water on the warm side of the freezing region. An advancing freezing front will increase both the water and the vapor pressure gradients, which in turn favor liquid and vapor advection from depth toward the freezing region.

CONCLUSION

The preceding interpretation of these data demonstrates that Kelsh and Taylor (*8*) are to some degree correct, because the time series variations they measured are indeed the products of several interacting natural processes. However, the predictable response of the probe at the organic-mineral soil interface to the passage of the freezing isotherm (during both freezing and thawing) and the strong correlation of the solute concentration (C-index) patterns between the 3- and 9-cm levels indicates that electric potential variations follow the concentration cell model.

Variations of the vertical electric potential gradient in the near-surface soil is traceable to a finite group of well-documented physical-chemical processes that increase or decrease the local solute concentration. The spatial-temporal variations in soil electric potential are produced by variations in solute concentration and can be interpreted by the calculation of a relative index of solute concentration called the C-index.

Constrained horizontal dimensions of typical laboratory test cells can complicate the analysis of electric potential data because frost-expelled water may tend to migrate vertically along cell walls. Therefore, it may be prudent to carry out future laboratory tests in cells where the cell horizontal diameter/vertical depth ratio is much greater than unity.

ACKNOWLEDGMENTS

The initial funds to purchase the instrumentation were provided by the Office of Vice President for Research, University of Michigan. Scott Baird, Electronics Technician, Department of Geological Sciences, constructed the probes and data acquisition system essential to the project. The authors thank Stanley J. Bolsenga, Great Lakes Environmental Research Laboratory, NOAA, who reviewed the manuscript and made numerous editorial suggestions.

REFERENCES

1. T. O. Hanley and S. Ramachandra Rao. Freezing Potential Studies in Wet Clays, 1, Early Results, 2, Specific Systems. *Cold Regions Science and Technology*, Vol. 3, 1981, pp. 165–175.
2. D. H. Gray. Thermo-Osmotic and Thermoelectric Coupling in Saturated Soils. In TRB Special Report 103: *Proc. International Conference on Effects of Temperature and Heat on Engineering Behavior of Soils*, TRB, National Research Council, Washington, D.C., 1969, pp. 66–77.
3. I. G. Yarkin. *Natural Electrical Potentials That Arise When Soils Freeze*. CRREL Special Report 86-12, U.S. Army Corps of Engineers, 1986.
4. V. R. Parameswaram and J. R. Mackay. Field Measurements of Electrical Freezing Potentials in Permafrost Areas. In *Proceedings, 4th International Conference on Permafrost*, National Academy Press, Washington, D.C., 1984, pp. 962–967.

5. V. R. Parameswaram, G. H. Johnson, and J. R. Mackay. Electrical Potentials Developed During Thawing of Frozen Ground. *Proc., 4th International Symposium on Ground Freezing*, Sapporo, Japan, 1985, pp. 9–15.
6. V. P. Borovitskii. The Development of Inherent Electric Fields During the Freezing of Rocks in the Active Layer and Their Role in the Migration of Trace Elements. *Journal of Geochemical Exploration*, Vol. 5, 1976, pp. 65–70.
7. S. I. Outcalt, D. H. Gray, and W. S. Benninghoff. Soil Temperature and Electric Potential During Diurnal and Seasonal Frost. *Cold Regions Science and Technology*, Vol. 16, 1989, pp. 37–43.
8. D. J. Kelsh and S. Taylor. *Measurement and Interpretation of Electric Freezing Potential of Soils*. CRREL Report 88-10, U.S. Army Corps of Engineers, Hanover, 1988.
9. D. E. Elrick, D. E. Smiles, N. Baumgartner, and P. H. Groenvelt. Coupling phenomena in saturated homoionic montmorillonite, 1, Experimental. *Soil Science Society of America Proceedings*, Vol. 40, 1976, pp. 490–491.
10. D. H. Gray and J. K. Mitchell. Fundamental Aspects of Electro-Osmosis in Soils. *Journal of the Soil Mechanics and Foundations Division, ASCE*, Vol. 93, 1967, pp. 209–236.
11. W. Drost-Hansen. Freezing Potentials in Dilute Aqueous Solutions. *Journal of Colloid and Interface Science*, Vol. 25, 1967, pp. 131–160.
12. S. Glasstone. *Textbook of Physical Chemistry*, 2nd. ed., Van Nostrand Reinhold, New York, 1946.
13. D. Miller. Application of Irreversible Thermodynamics in Electrolyte Solutions, I, Determination of Ionic Transport Coefficients. *Journal of Physical Chemistry*, Vol. 70, 1966, pp. 2638–2659.
14. D. H. Gray and S. I. Outcalt. Two Electric Potential Signatures of Serial Diurnal Frost. *Physical Geography*, Vol. 9, 1988, pp. 354–360.
15. B. Hallet. Solute Redistribution in Freezing Ground. *Proc., Third International Conference on Permafrost*, National Research Council of Canada, Ottawa, 1978, pp. 86–89.
16. K. Henry. *Chemical Aspects of Soil Freezing*. CRREL Report 88-17, U.S. Army Corps of Engineers, Hanover, 1988.
17. S. I. Outcalt. The Climatology of a Needle Ice Event: An Experiment in Simulation Climatology. *Arch. Met. Geoph. Biokl.* Ser. B., Vol. 19, 1971, pp. 325–338.

Publication of this paper sponsored by Committee on Physicochemical Phenomena in Soils.

Chemico-Osmosis Versus Diffusion-Osmosis

HAROLD W. OLSEN, ELLIOT N. YEARSLEY, AND KARL R. NELSON

During the 1960s it became widely recognized that chemico-osmosis is a mechanism by which chemical gradients cause groundwater to move from dilute to more concentrated pore-fluid solutions and is most effective in densely compacted materials of high exchange capacity. Evidence has been accumulating since about 1970 that an additional mechanism may cause groundwater movement in response to chemical gradients and reactions. Some data show that the direction of soil-pore-fluid movement in response to a concentration gradient is opposite to that of chemico-osmosis. Other data suggest that chemically induced groundwater movement may be significant not only in densely compacted materials of high exchange capacity but also in poorly consolidated materials of low exchange capacity. Laboratory evidence is reviewed for the additional mechanism and include recent data on loosely compacted kaolinite and an undisturbed sample of claystone. The additional mechanism appears to be diffusion-osmosis (i.e., the convection, or drag, of bulk pore fluid by the diffusion of solute species). It is suggested that electro-osmosis is a special case of diffusion-osmosis where pore fluid moves in response to the migration of solute species caused by an externally imposed electrical potential gradient.

The term "osmosis" refers to nonhydraulic components of groundwater movement that arise from thermal, electrical, and chemical causes. This paper is concerned with osmosis having chemical causes and, more specifically, with the mechanisms by which chemical gradients cause groundwater movement.

Osmosis generated by naturally occurring chemical causes is referred to in the literature by different names, including osmosis (*1–5*), chemical osmosis (*6*), normal osmosis and chemico-osmosis (*7*), and natural electro-osmosis (*8*), suggesting that more than one mechanism is involved and that the characteristics of and differences among those mechanisms have yet to be clarified adequately.

One of those mechanisms, referred to as chemico-osmosis in this paper, became widely recognized during the 1960s as a possible source of anomalous pore-fluid pressures and a cause of groundwater movement from dilute to more concentrated pore-fluid solutions. Evidence has been accumulating since about 1970 that an additional mechanism, denoted here as "diffusion-osmosis," may cause groundwater movement in response to chemical gradients and reactions and that this mechanism drives soil-pore-fluid movement in the direction of decreasing solute concentrations, which is opposite to that for chemico-osmosis. This paper reviews laboratory evidence for those mechanisms, including recent data on loosely compacted kaolinite and an undisturbed sample of claystone.

H. W. Olsen, Branch of Geologic Risk Assessment, U.S. Geological Survey, Box 25046, Mail Stop 966, Denver, Colo. 80225. E. N. Yearsley, Colog Inc., 1019 8th Street, Golden, Colo. 80401. K. R. Nelson, Department of Engineering, Colorado School of Mines, Golden, Colo. 80401.

CHEMICO-OSMOSIS

Here, chemico-osmosis is used to describe water movement from less concentrated to more concentrated solutions separated by a semipermeable membrane, which restricts solute flows but allows water flow. The driving force for chemico-osmosis is the chemical potential difference of the water phase between the two solutions, the more concentrated solution having the lower potential. In a perfect semipermeable membrane (i.e., a membrane that totally excludes the flow of solutes), the driving force equals the pressure difference that must be applied to the concentrated side to stop water flow. This chemico-osmotic pressure for a perfect semipermeable membrane is given by the well-known thermodynamic relation

$$\Delta\pi = \frac{RT}{V_w} \ln \frac{a_1}{a_2} \tag{1}$$

where

$\Delta\pi$ = chemical potential difference of water across membrane,
R = gas constant,
T = absolute temperature,
V_w = molar volume of water,
a_1 = activity of water on the less concentrated side, and
a_2 = activity of water on the more concentrated side.

Flow of water through a perfect semipermeable membrane is governed by both the hydraulic pressure difference and the chemical potential difference in the water phase across the membrane.

$$q = k[\Delta P + \Delta\pi]\left[\frac{1}{\gamma_w}\right] \tag{2}$$

where

q = flow rate per unit cross-sectional area,
k = hydraulic conductivity,
ΔP = hydraulic pressure difference across membrane,
$\Delta\pi$ = chemical potential difference of water across membrane, and
γ_w = unit weight of water.

The so-called "membrane properties" of clays result from charge deficiencies on the surfaces of clay particles balanced by a deficiency of anions compared with cations in the pore fluid adjacent to the particle surfaces. Because of this deficiency of anions, which is commonly referred to as "anion exclusion," the flow of solute is restricted relative to the flow of water. In consequence, clays behave, to some degree, like a semipermeable membrane and are commonly called imperfect or leaky membranes. Therefore, chemico-osmotic pressures and flows in argillaceous materials are generally some fraction of those predicted from Equations 1 and 2.

The degree to which clays exhibit membrane behavior has been characterized by terms such as "ideality" and "membrane efficiency" and is generally quantified by a parameter Staverman (*9*) introduced and named the "reflection coefficient." Some investigators of membrane behavior in geologic materials adopted both Staverman's parameter and the term reflection coefficient to describe it (*5,10*). Others, such as Kemper and Rollins (*11*), adopted Staverman's parameter but describe it with a different name, "osmotic efficiency coefficient." Staverman (*9*) defined this parameter σ as presented in Equation 3. Comparison with Equation 2 indicates that the reflection coefficient σ modifies the chemico-osmotic driving force for water flow through a perfect membrane $\Delta\pi$. Here, σ varies from zero to unity for membranes having efficiencies that vary from zero to 100 percent.

$$q = k[\Delta P + \sigma\Delta\pi]\left[\frac{1}{\gamma_w}\right] \tag{3}$$

Similarly, the chemico-osmotic pressure difference that develops when flow is prevented is

$$\Delta P_{q=0} = \sigma\Delta\pi \tag{4}$$

where $\Delta\pi$ is given by Equation 1.

A more useful form of Equation 3 is obtained for this paper by separating the osmotic and hydraulic components of flow and then by defining separate hydraulic and chemico-osmotic conductivities, as follows.

$$q_t = q_h + q_{co} \tag{5}$$

$$q_h = k_h\Delta P\left[\frac{1}{\gamma_w}\right] \tag{6}$$

$$q_{co} = k_{co}\Delta\pi\left[\frac{1}{\gamma_w}\right] \tag{7}$$

$$\sigma = -\frac{k_{co}}{k_h} \tag{8}$$

where

q_t = total flow rate per unit cross-sectional area,
q_h = hydraulic flow rate per unit cross-sectional area,
q_{co} = chemico-osmotic flow rate per unit cross-sectional area,
k_h = hydraulic conductivity, and
k_{co} = chemico-osmotic conductivity.

Figure 1 illustrates the experimental system used by Kemper (*12*) and data he obtained to demonstrate chemico-osmotic pressures across compacted clay specimens in response to a 5.4 N NaCl solution above the specimen and distilled water below the specimen. Figure 2 illustrates the experimental system used by Young and Low (*13*) and the data they obtained to demonstrate chemico-osmotic flow of water in two siltstone samples (A and B in Figure 2) composed of 8 to 12 percent of clay-size material of which 40 to 50 percent was illite, 30 to 40 percent kaolinite, and the remainder was montmorillonite or mixed-layer clays. The Kemper and the Young and Low studies are two of the earliest studies that demonstrate chemico-osmotic pressures and flow in argillaceous earth materials.

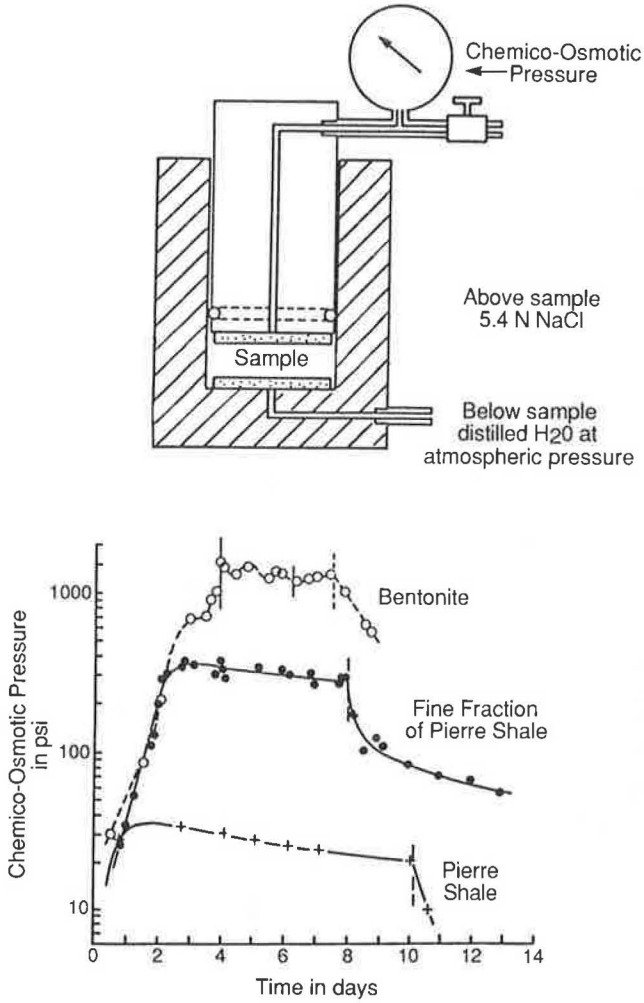

FIGURE 1 Kemper's test cell and data (*12*).

Various investigators have demonstrated that the chemico-osmotic efficiency coefficient σ increases with the cation exchange capacity of an argillaceous material, increases with its degree of compaction, and decreases with increasing concentration of dissolved solutes in the pore fluid of the material (*5,11,14*). Figure 3 illustrates the Kemper and Rollins (*11*) test cell and some of the classic data they obtained on bentonite that illustrate the variation of chemico-osmotic efficiency with the degree of compaction, as reflected in the moisture content of the clay, and with pore-fluid solute concentration, which is reflected in the average normality of the solutions on either side of the clay specimen.

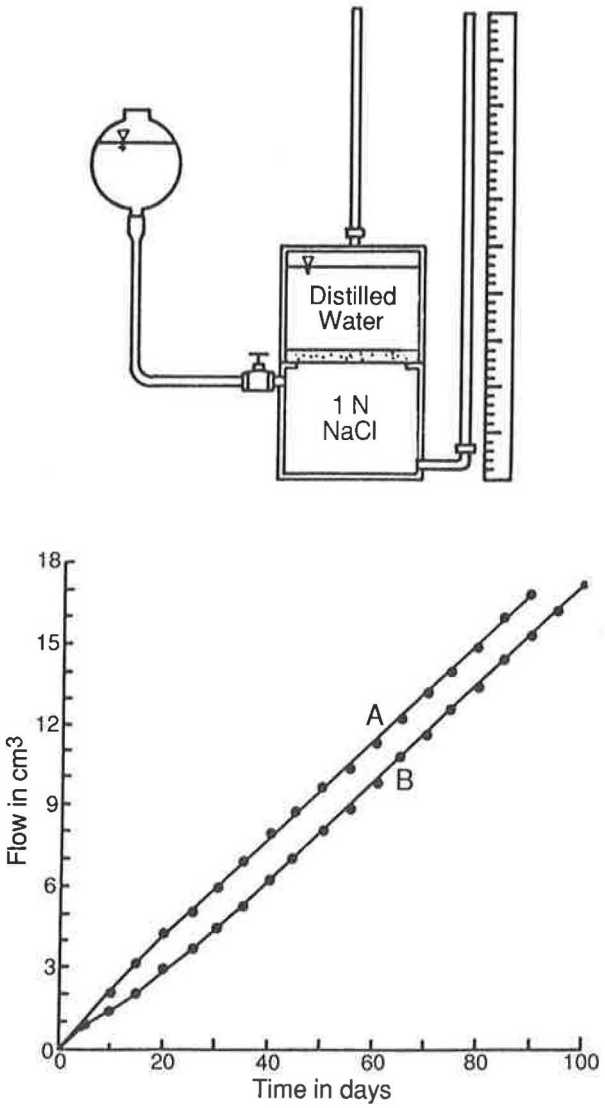

FIGURE 2 Young and Low's experimental system and data (*13*) on two siltstone samples.

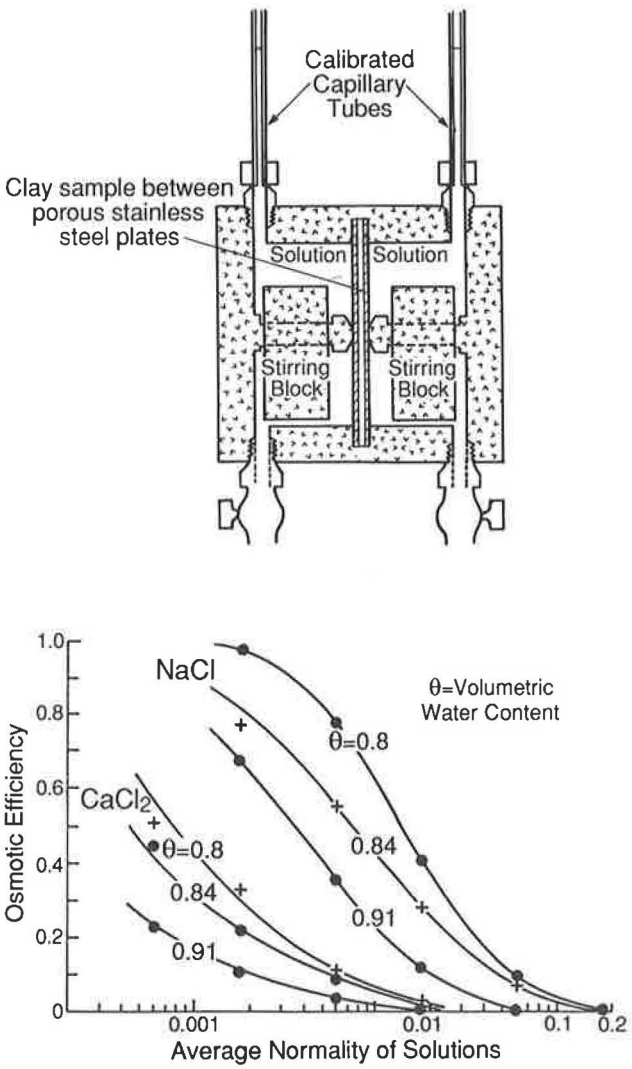

FIGURE 3 Kemper and Rollins' test cell and data on bentonite (*11*).

DISCREPANCIES FROM CHEMICO-OSMOSIS

In 1972, Kemper and Quirk (*15*) published the data in Figures 4 to 6 that expanded the scope of Kemper and Rollins' (*11*) 1966 investigation (illustrated in Figure 3) in three ways: (a) Ag-AgCl electrodes were used to measure the electric potential differences induced by solute concentration differences across the clay sample, (b) data were obtained over a larger range of average solute concentrations, and (c) data were obtained not only on bentonite but also on illite and kaolinite.

Those data show that the direction of soil-pore-fluid movement in response to solute concentration gradients is often opposite to that for chemico-osmosis. This is reflected in osmotic efficiency coefficients having negative values. Kemper and Quirk describe this discrepancy from chemico-osmosis as "negative osmosis," and they suggest the mechanism to be electro-osmosis, as follows: "The osmotic flow was often from the high salt to low salt concentration side and was generally in the direction of more negative [electric] potential, indicating electro-osmosis as the mechanism involved in osmotic flow." Negative osmosis occurred primarily where the average solute concentrations were very high and became increasingly pronounced in illite and kaolinite when compared with bentonite. Under such conditions the chemico-osmotic efficiency of the clay samples is low because anion exclusion and, hence, the degree of restriction to the solute flux, is low, as is noted previously.

In 1976, Elrick et al. (*16*) reported data on osmotic pressures and electrical potentials caused by concentration gradients across homo-ionic montmorillonite by using the test cell illustrated in Figure 7 (top). Their data, also in Figure 7 (bottom), show dramatic changes can be caused by short circuiting the reversible Ag-AgCl electrodes on either side of the clay specimen. The rate of transfer of salt increases, and the direction of the osmotic pressure is reversed.

The explanation given by Elrick et al. for those changes is illustrated in Figure 8. The top half of Figure 8 illustrates the

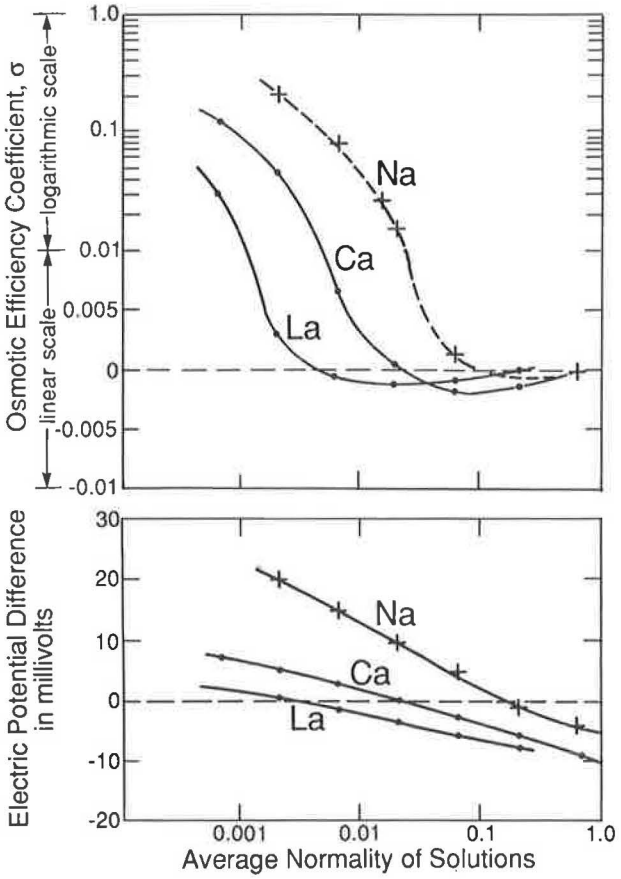

FIGURE 4 Kemper and Quirk's (*15*) data presenting variations in osmotic efficiency and chemically induced electrical potential differences across bentonite with average normality of external solutions and exchangeable cations.

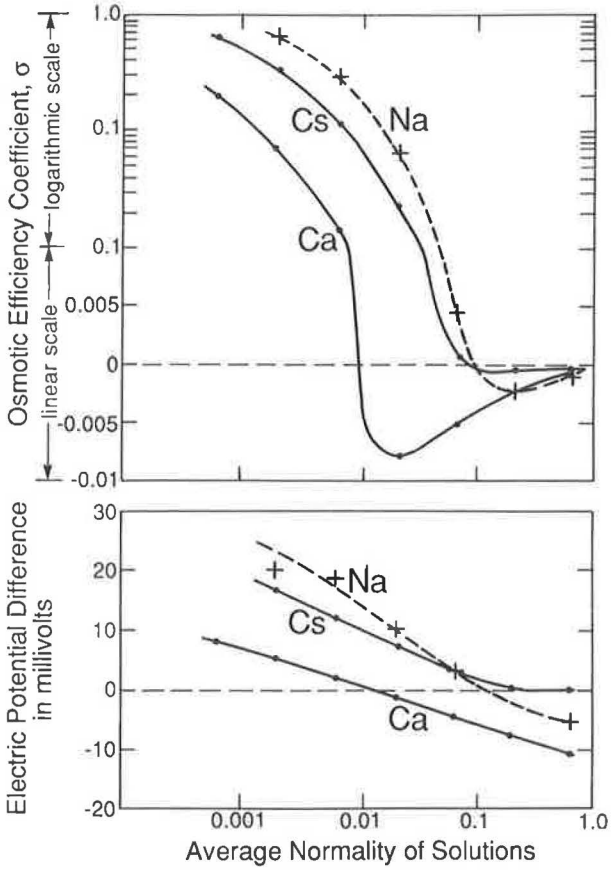

FIGURE 5 Kemper and Quirk's (*15*) data presenting variations in osmotic efficiency and chemically induced electrical potential differences across Fithian illite with average normality of external solutions and exchangeable cations.

case when the potential difference between the electrodes is being measured with a high-impedance voltmeter, or potentiometer. The clay sample behaves like a membrane because anions are excluded from the pore space and thus are prevented from migrating across the clay. Electroneutrality restrains the cations, and, hence, the flux of solute through the clay is prevented. Water migrates toward the chamber having the high solute concentration and thus generates a chemico-osmotic pressure gradient needed to stop water movement.

In contrast, the bottom half of Figure 8 illustrates the case when the electrodes are short circuited. The Ag-AgCl electrodes provide a mechanism for chlorine ions in the left chamber to become attached to the electrode in the left chamber and release their electrons to the interconnecting wire. Those electrons can flow through the wire and combine with chlorine atoms attached to the electrode in the right chamber, which converts the chlorine atoms into ions and releases them from the electrode into the adjacent solution. Electroneutrality allows cations to flow through the clay, consistent with the rate at which anions are adsorbed and released at the electrodes in the left and right chambers, respectively. The cation flow exerts drag on the water in the direction opposite to the direction of flow in chemico-osmosis. Because short circuiting reversed the direction of the osmotic pressure, the tendency for water flow induced by cation diffusion was considerably greater than that induced by chemico-osmosis.

The discrepancies from chemico-osmosis in the Kemper and Quirk (Figures 4 to 6) data are identical to those in the Elrick et al. data (Figure 7) in that the discrepancies appear when solutes are able to migrate through the clay pores in response to externally imposed solute concentration gradients. There are two differences between the systems. One difference is that cations and anions migrate together through the Kemper and Quirk samples whereas only cations migrate through the Elrick et al. sample. The other difference is that solute migration rates in the Kemper and Quirk data vary with the composition of the samples and their pore fluids whereas in the Elrick et al. sample the solute migration rate is externally controlled with reversible Ag-AgCl electrodes. Nevertheless, the fundamental mechanism causing discrepancies from chemico-osmosis appears to be the same in both studies (i.e., solute migration). In other words, solute diffusion in response to a concentration gradient imposes drag on, or momentum transfer to, the pore fluid and thus tends to move the pore fluid in the direction of decreasing solute concentration, which is opposite to the direction of pore-fluid movement in chemico-osmosis.

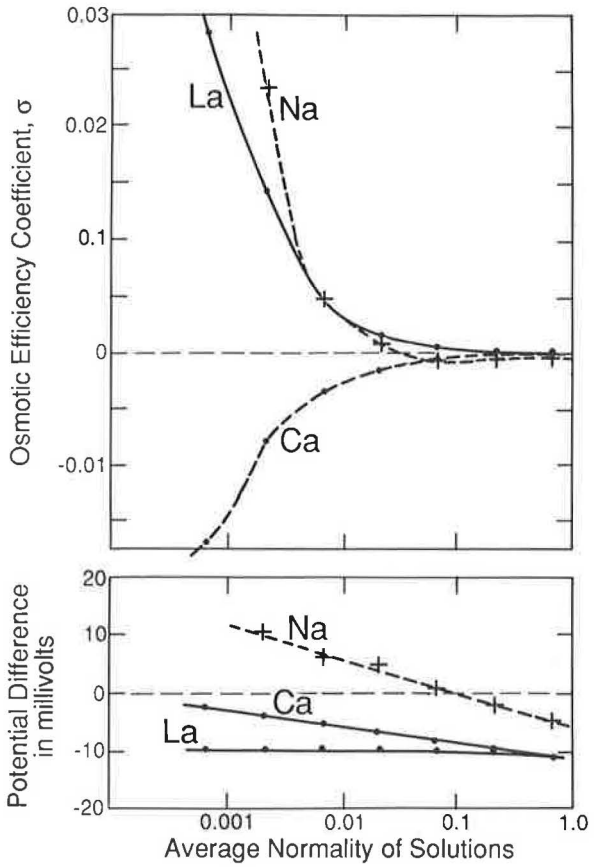

FIGURE 6 Kemper and Quirk's (*15*) data presenting variations in osmotic efficiency and chemically induced electrical potential differences across kaolinite with average normality of external solutions and exchangeable cations.

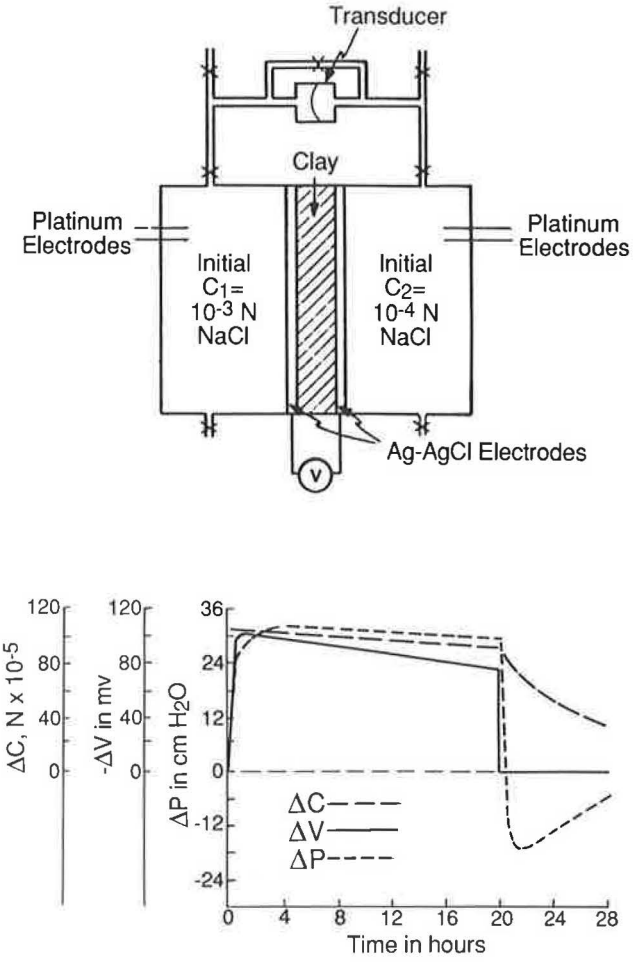

FIGURE 7 Elrick et al.'s test cell and data (*16*).

DIFFUSION-OSMOSIS

Olsen et al. (*17*) introduced the term "diffusion-osmosis" to describe the transport of water in response to diffusion of dissolved solutes. They demonstrated this process on a loosely compacted specimen of kaolinite mounted in a triaxial system.

The triaxial system, illustrated in Figure 9, consists of a triaxial cell (A), two differential pressure transducers (C and D), a single-syringe flow pump (E), and a dual-syringe flow pump (F). The differential pressure transducers monitor the effective stress in, and the pressure difference across, the specimen (B). The single-syringe flow pump controls the volume of the specimen. The dual-syringe flow pump controls pore-fluid movement in either direction through the specimen without changing its volume and provides a means to exchange the permeant solution at either end of the specimen without changing its volume or its effective stress.

Figure 10 illustrates diffusion-osmotic pressures measured on a 5.08-cm diameter by 2.55-cm high specimen at a void ratio of 1.03 after having been consolidated to 90 psi and subsequently rebounded to 20 psi. The graph shows head difference (Δh) values across the specimen when flow through the specimen is prevented. Positive values (values above the zero axis) indicate higher pore pressure at the top of the sample than at its base.

During the initial period, while distilled water was circulated through porous discs in the top cap and base pedestal, no head difference or osmotic pressure developed across the specimen. However, when 1 M NaCl was circulated through the porous disc in the base pedestal, an osmotic pressure of a few centimeters of water developed, which is on the order of the 2.55-cm height of the specimen. In this case, the higher pore pressure was at the top of the sample. Hence, the solute concentration difference tends to drive pore-fluid movement from a high concentration to a low concentration. This is consistent with diffusion-osmosis but inconsistent with chemico-osmosis.

Subsequently, as the 1 M NaCl solution leached upward through the specimen, the magnitude of the osmotic pressure diminished substantially after leaching about 50 to 75 cm^3 upward through the sample. Because this quantity of flow is equivalent to 2 to 3 pore volumes of the specimen, solute should have migrated upward through the specimen and into the porous stone in the top cap. In consequence, a decrease in the solute concentration difference across the specimen, and a corresponding decrease in osmotic pressure, are to be expected.

In the next period, distilled water was alternately circulated through the porous disc in the base pedestal and leached upward through the specimen. The higher pressure is now at

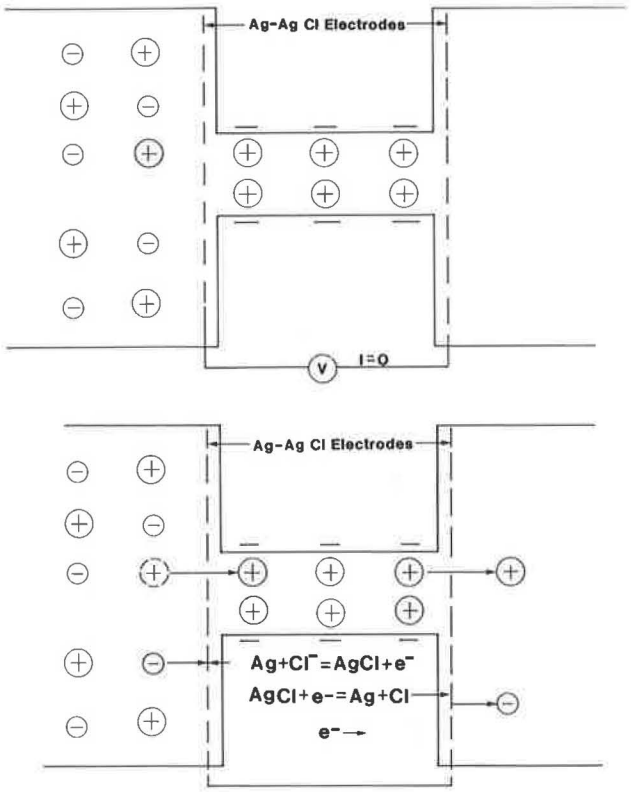

FIGURE 8 Models of the mechanisms involved in Elrick et al.'s (*16*) experimental data (Figure 7) when the electrodes were connected to a high-impedance voltmeter (top) and when they were short circuited (bottom).

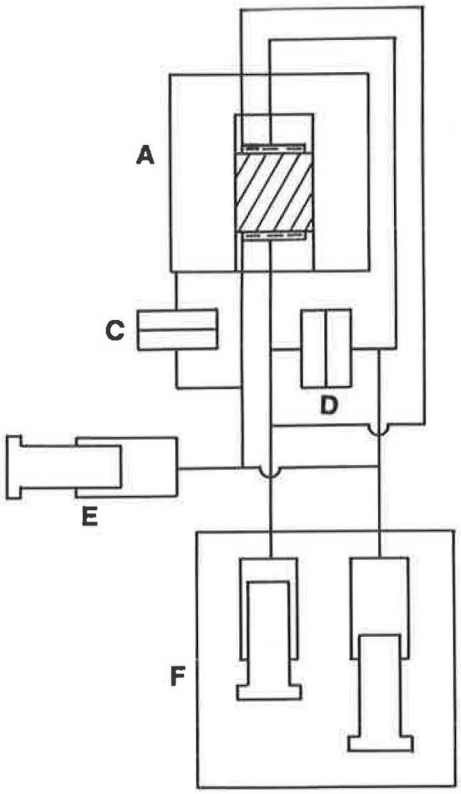

FIGURE 9 Scheme of triaxial cell (A) and permeant system.

the base, because the higher solute concentration is at the top, and the direction of solute diffusion is downward through the sample. While leaching takes place, the osmotic pressure decreases as the solute concentration in the porous disc in the top cap is diluted.

In the final period, 0.5 M $CaCl_2$ was first circulated through the porous disc of the base pedestal. The ensuing osmotic pressure is similar qualitatively in both direction and magnitude to that generated by the 1 M NaCl solution. Subsequently, the osmotic pressure was eliminated by circulating the same 0.5 M $CaCl_2$ solution through the porous disc in the top cap.

More recently, Yearsley (*18*) measured osmotic pressures in response to solute concentration gradients on undisturbed core samples from the Salton Sea Geothermal System in southern California. Those measurements were conducted in a one-dimensional consolidation test cell illustrated in Figure 11. The cylindrical sample (S) is epoxied within the sample holder (H) and confined axially by pistons (P) and laterally by a cylindrical sleeve (CS). Axial load is applied to the sample through the pistons by means of a hydraulic press (not shown). A dual-syringe flow pump (DFP) provides a means to exchange the pore fluid at either end of the specimen and to generate pore-fluid movement in either direction through the specimen. A differential pressure transducer (DPT) monitors the pressure difference across the specimen.

Figure 12 illustrates data Yearsley obtained on a light gray-green silty shale sample from a depth of 6,037 ft, having a

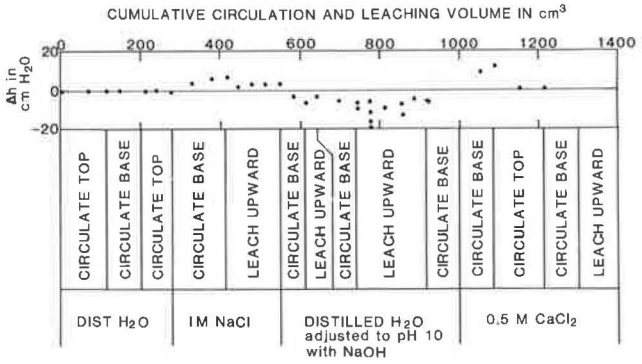

FIGURE 10 Data illustrating diffusion-osmosis in a kaolinite specimen obtained with the triaxial system illustrated in Figure 9.

porosity of 2 percent, where the dominant clay minerals were illite and chlorite. The sample was saturated and tested with solutions that have a range of solute concentrations but the same chemical composition, which was designed to simulate the chemistry of the in situ interstitial fluids. The pore-fluid solute concentration is shown on the horizontal axis in terms of weight percent of total dissolved solids (TDS). The vertical axis shows the head difference (Δh) across the specimen while flow through the specimen is prevented. Positive values designate cases where the direction of the head difference is

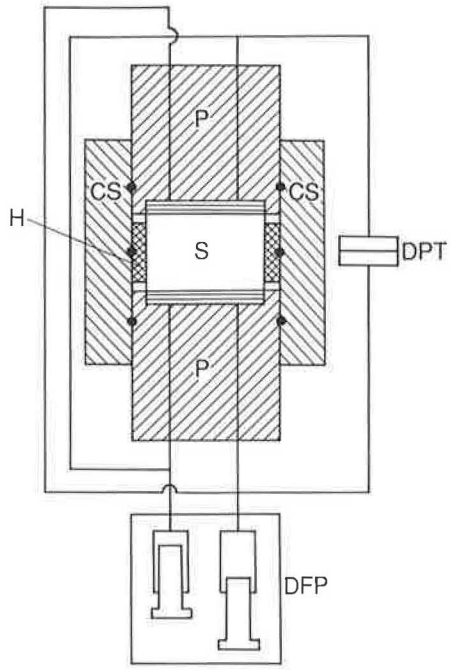

FIGURE 11 Scheme of a one-dimensional consolidation test cell and permeant system (*11*).

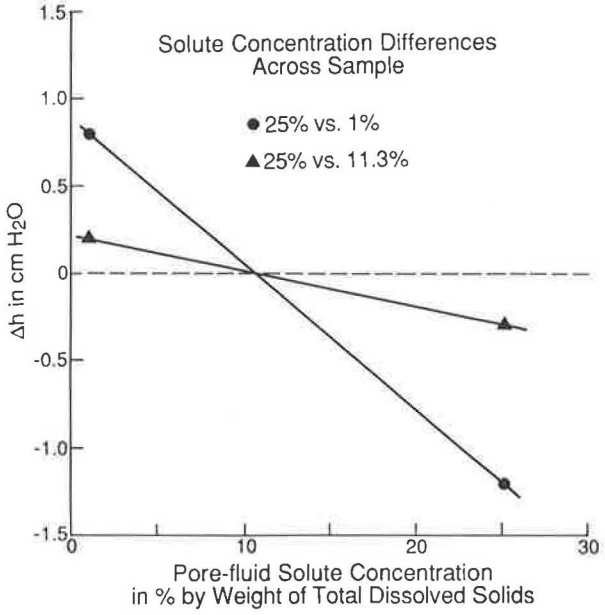

FIGURE 12 Hydraulic head differences (Δh) induced by solute concentration differences across a silty shale specimen.

consistent with chemico-osmosis. Conversely, negative values designate cases consistent with diffusion-osmosis.

The sample was initially saturated by elevating the pressure in the permeant system and by leaching with a permeant having a 1 percent concentration of dissolved solutes (1 percent by weight of TDS). Then, the 1 percent solution in the upper porous disc was replaced sequentially with 11.3 percent and 25 percent solutions, which induced osmotic head differences of 0.2 and 0.8 cm H_2O, consistent with chemico-osmosis. Next, the pore fluid solute concentration was increased by leaching to 25 percent. Thereafter, the 25 percent solution in the upper porous disc was replaced sequentially with 11.3 percent and 1 percent solutions, which induced osmotic head differences of 0.3 and 1.2 cm H_2O, consistent with diffusion-osmosis.

Finally, the lines connecting measurements with solute concentration differences of 25 percent versus 1 percent and 25 percent versus 11.3 percent both intersect the $\Delta h = 0$ line at the same pore-fluid solute concentration. Those data indicate that chemico-osmosis and diffusion-osmosis progress simultaneously in the specimen, that their relative magnitudes vary with pore-fluid solute concentration, and that their magnitudes may be equal and opposite for a pore-fluid solute concentration of approximately 10 percent (by weight of TDS).

DISCUSSION OF RESULTS

The question arises whether electro-osmosis is an additional mechanism involved in chemically driven groundwater movement. Kemper and Quirk (*15*) suggested that electro-osmosis was the mechanism involved in the osmotic flows they observed in the direction of decreasing solute concentration because the flow was generally in the direction of more negative potential. Also, Veder (*8*) uses the term "natural electro-osmosis" to describe his view that the pore water in argillaceous materials migrates in response to electrical potentials generated by weathering reactions.

To examine this question, it needs to be recognized that the term "electro-osmosis" is commonly used from a phenomenological point of view to describe soil-pore-fluid movement in response to an electric potential gradient that is externally imposed through electrodes. The potential gradient generates a current between the electrodes, and the current causes movement of the bulk pore fluid. The mechanisms involved include chemical reactions that transfer charge between the electrodes and the soil pore fluid. The mechanisms also include fluxes of, and interactions among, charged solute species and water. The number and complexity of the mechanisms involved vary with the magnitude of the electric potential imposed and the composition of the electrodes, the soil, and its pore fluid.

In contrast, Kemper and Quirk (*15*) refer to "electro-osmosis" as a specific mechanism that can be driven by externally imposed chemical gradients and reactions. This use of the term differs from the other in that this use focuses on a single mechanism (i.e., the coupling of an electrical gradient or current with bulk pore-fluid movement). In the simplest case, consistent with Kemper and Quirk's experimental system, the electrical gradient generates a current by driving positive ions to the cathode and negative ions to the anode. Ion fluxes are coupled with bulk fluid through viscous drag. Because of the relative sizes and distributions of cations and anions in soil pores, the amount of fluid carried by cations toward the cathode generally exceeds the amount of fluid carried toward the anode.

A fundamental problem with Kemper and Quirk's definition of "electro-osmosis" is that no current flows through the clay specimen. Another difficulty is that the measured elec-

trical potentials are not generating a current. Rather, they are well-known consequences of the diffusion of charged solutes through porous media in response to solute concentration gradients. The potentials are induced to counteract the tendency for ions of one charge to diffuse more rapidly than do ions of the opposite charge. In other words, the induced potentials equalize the fluxes of oppositely charged species and thus prevent current flow through the specimen.

Therefore, Kemper and Quirk's (*15*) use of the term "electroosmosis" may be inappropriate and that "diffusion-osmosis" is both adequate and more appropriate to describe the mechanism involved in the osmotic flows they observed in the direction of decreasing solute concentration gradients. In addition, electro-osmosis can be understood more clearly as a special case of diffusion-osmosis. In both mechanisms, bulk fluid movement is driven by the diffusion of solute species. Electro-osmosis differs from diffusion-osmosis only in that an externally applied electrical gradient controls the fluxes of the solute species.

The forgoing also has implications concerning the mechanism Veder (*8*) introduced and described with the term "natural electro-osmosis." In Veder's mechanism, geochemical weathering reactions generate electric potentials that drive electro-osmosis. One unknown is whether such electrical potentials cause currents by driving fluxes of cations and anions or whether they are induced for a different reason, such as the potentials that arise from diffusion in response to concentration gradients. Another unknown is whether chemical reactions in nature can drive diffusion-osmosis without the aid of electric potentials and currents. Those questions have yet to be clarified.

CONCLUSIONS

A review of laboratory evidence demonstrates two mechanisms by which chemical gradients cause groundwater movement. Chemico-osmosis, widely recognized since the 1960s, causes soil-pore-fluid movement from dilute to more concentrated solutions and is most effective in densely compacted clays of high exchange capacity and low soil-pore-fluid solute concentration. Evidence has been accumulating since about 1970 for an additional mechanism for which the term "diffusion-osmosis" was recently introduced. In contrast with chemico-osmosis, diffusion-osmosis causes soil-pore-fluid movement from concentrated to dilute solutions, and it has been observed in argillaceous materials of low exchange capacity and high soil-pore-fluid solute concentrations. It is suggested that electro-osmosis is a special case of diffusion-osmosis where soil pore fluid moves in response to the migration of solute species when an externally imposed electrical gradient controls the migration of the solute species.

REFERENCES

1. B. B. Hanshaw and E-an Zen. Osmotic Equilibrium and Overthrust Faulting. *Geological Society of America Bulletin*, Vol. 76, 1965, pp. 1379–1386.
2. I. W. Marine. Geohydrology of Buried Triassic Basin at Savannah River Plant, South Carolina, *American Association of Petroleum Geologists Bulletin*, Vol. 58, 1974, pp. 1825–1837.
3. I. W. Marine and S. J. Fritz. Osmotic Model to Explain Anomalous Hydrostatic Heads. *Geological Society of America Abstracts with Program*, Vol. 10, No. 7, 1978.
4. I. W. Marine and S. J. Fritz. Osmotic Model to Explain Anomalous Hydrostatic Heads. *Water Resources Research*, Vol. 17, 1981, pp. 73–82.
5. S. J. Fritz. Ideality of Clay Membranes in Osmotic Processes: A Review. *Clays and Clay Minerals*, Vol. 34, No. 2, 1986, pp. 214–223.
6. D. F. Graf. Chemical Osmosis, Reverse Chemical Osmosis, and the Origin of Subsurface Brines. *Geochimica et Cosmochimica Acta*, Vol. 46, 1982, pp. 1431–1448.
7. J. K. Mitchell. *Fundamentals of Soil Behavior*. John Wiley, New York, 1976.
8. C. Veder. *Landslides and Their Stabilization*. (With contributions by Fritz Hilbert), translated by Erika Jahn, Springer-Verlag, New York, 1981.
9. A. J. Staverman. Non-Equilibrium Thermodynamics of Membrane Processes. *Transactions of the Faraday Society*, Vol. 48, 1952, pp. 176–185.
10. P. H. Groenveldt and D. E. Elrick. Coupling Phenomena in Saturated Homo-Ionic Montmorillonite, 2, Theoretical. *Soil Science Society of America Proceedings*, Vol. 40, 1976, pp. 820–823.
11. W. D. Kemper and J. B. Rollins. Osmotic Efficiency Coefficients Across Compacted Clays. *Soil Science Society of America Proceedings*, Vol. 36, 1966, pp. 426–433.
12. W. D. Kemper. Movement of Water as Affected by Free Energy and Pressure Gradients, 2, Experimental Analysis of Porous Systems In Which Free Energy and Pressure Gradients Act in Opposite Directions. *Soil Science Society of America Proceedings*, Vol. 25, 1961, pp. 260–265.
13. A. Young and P. F. Low. Osmosis in Argillaceous Rocks. *American Association of Petroleum Geologists Bulletin*, Vol. 49, No. 7, 1965, pp. 1004–1008.
14. S. J. Fritz and I. W. Marine. Experimental Support for a Predictive Osmotic Model of Clay Membranes. *Geochimica et Cosmochimica Acta*, Vol. 47, 1983, pp. 1515–1522.
15. W. D. Kemper and J. P. Quirk. Ion Mobilities and Electric Charge of External Clay Surfaces Inferred From Potential Differences and Osmotic Flow. *Soil Society of America Proceedings*, Vol. 36, 1972, pp. 426–433.
16. D. E. Elrick, D. E. Smiles, N. Baumgartner, and P. H. Groenvelt. Coupling Phenomena in Saturated Homo-Ionic Montmorillonite, 1, Experimental. *Soil Science Society of America Proceedings*, Vol. 40, 1976, pp. 490–491.
17. H. W. Olsen, E. N. Yearsley, and K. R. Nelson, Chemical Causes of Groundwater Movement. In *Groundwater Contamination*, (L. M. Abriola, ed.) Publication 185, IAHS, 1989, pp. 65–72.
18. E. N. Yearsley. Transport Properties and Coupled Flow Phenomena in Salton Sea Scientific Drilling Program Cores. M. S. thesis, Department of Engineering, Colorado School of Mines, Golden, 1989.

Publication of this paper sponsored by Committee on Physicochemical Phenomena in Soils.

Acid/Base Distributions in Electrokinetic Soil Processing

YALCIN B. ACAR, ROBERT J. GALE, JIHAD HAMED, AND GREGG PUTNAM

The development of pH gradients in the electrokinetic processing of soils is investigated. An analytical model, based on the Nernst-Planck equations, is presented to evaluate the acid/base distributions and the flow patterns generated in electro-osmotic flow. One-dimensional laboratory experiments with Georgia kaolinite demonstrated the validity of the predictions of the analytical model. Effects of the pH gradients on the efficiency of the process and soil properties are discussed. Results of studies are reviewed based on this new understanding of the acid/base distributions.

Electro-osmosis has been of interest to geotechnical engineers for 50 years as an electrochemical processing technique initiated by applying an electrical gradient across a soil mass to generate water flow. The technology has been used successfully to improve the geotechnical properties of fine-grained deposits by dewatering and consolidating (*1–4*). Studies are being conducted at Louisiana State University to investigate the feasibility of using electrokinetic processing to decontaminate soils from organic and inorganic contaminants. It is essential to investigate the theoretical basis of electrochemically generated material gradients and any subsequent chemistry that may occur in the medium for the practical use of such methods in the decontamination of soils.

Electrokinetic processing of soils or similar porous media by use of a low DC current results in development of electrical, hydraulic, and chemical gradients across the saturated strata. If a uniform concentration of ions is assumed to initially exist throughout a specimen, the application of an electrical potential will create a uniform electric field gradient. Subsequently, the process will result in the movement of ions and associated water molecules under the direct influence of and also because of coupling effects generated by those gradients. Figure 1 presents a schematic diagram of the process and development of those gradients in time. Initially, a constant current and constant hydraulic potential difference are assumed to be applied across a saturated, homogeneous specimen.

Presently available theoretical descriptions of electro-osmosis disregard the existence of any chemical gradients and reactions. However, the existence of a current in the soil implicitly necessitates faradaic reactions at the electrode boundaries. A review of previous studies indicate that those electrochemical effects may significantly affect the results of the process (*5*). Formation of chemical gradients will depend on the extent of electrolysis and the coupled chemical reactions between the soil and electrolyte products. The importance of pH gradients in electro-osmosis has been noted by several investigators who have recorded the time rate of changes in pH of the pore fluid and mostly at the electrodes (*6–12*). The general trend is that the pore fluid gets acidic (pH = 1–4) at the anode and basic at the cathode (pH = 10–13). In assessing the chemistry of the medium (e.g., the adsorption and desorption of species on soil substrate), prediction of the development of pH gradients therefore becomes essential.

This paper reviews an analytical model and presents results of subsequent laboratory tests conducted to predict those gradients. Results of studies are reviewed based on this understanding of pH gradients.

ELECTROCHEMICAL REACTIONS AT ELECTRODES

In the absence of all but traces of electrolyzable solutes in the pore fluid (i.e., metal ions, Cl^-, organic matter or pollutants, dissolved oxygen) and for the case of inert electrodes, the approximation of 100 percent faradaic efficiency may be taken for water electrolysis. The primary electrode reactions would then be, at the anode,

$$2H_2O - 4e^- \rightarrow O_2 \uparrow + 4H^+ \quad (1)$$

and, at the cathode,

$$4H_2O + 4e^- \rightarrow 2H_2 \uparrow + 4OH^- \quad (2)$$

The production of H^+ ions at the anode decreases the pH at this electrode by Reaction 1, and the OH^- ion concentration at the cathode leads to a rise of pH. Twice as many water molecules are electrolyzed at the cathode than at the anode for the same quantity of electricity, leading to a chemical gradient of molecular water insignificant at current densities used in experiments. Two supplemental ionic species are generated as a consequence of Reactions 1 and 2 and in addition to migration of existing anions and cations in the pore fluid of the specimen. Those species can complicate further the net transfer of hydrated water or followup chemical gradients during the process or both. In other words, the ions generated in the medium by electrolysis, together with the ionic species available in the pore fluid, may carry a portion of the current depending on concentrations and types.

A variety of theories and models has been proposed to explain the electro-osmotic flow of water (e.g., Hemholz-Smoluchowski, Schmid, and Spiegler friction models), but

Y. B. Acar, J. Hamed, and G. Putnam, Department of Civil Engineering, Louisiana State University, Baton Rouge, La. 70803. R. J. Gale, Department of Chemistry, Louisiana State University, Baton Rouge, La. 70803.

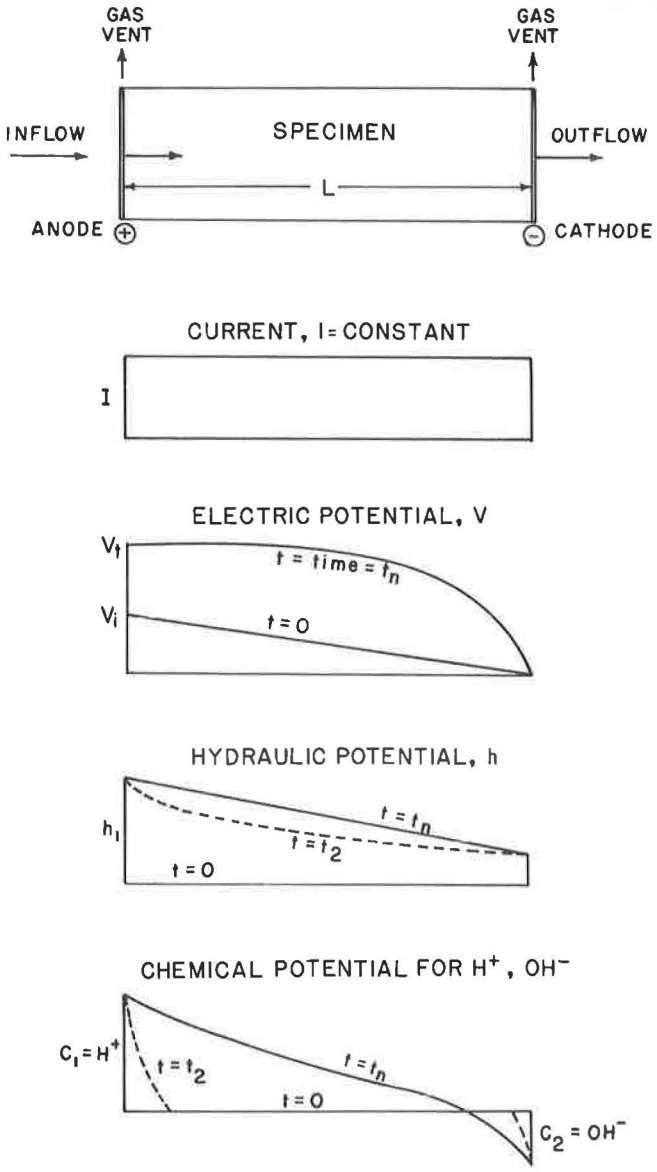

FIGURE 1 Schematic diagram of potential gradients in electro-osmosis (*5*).

none of those appears to have sufficient generality to account for the full range of behavior found in clay-water-electrolyte systems (*13*). Those models also largely disregard the electrode product chemistry in the medium and attempt to explain how the electro-osmotic coefficient of permeability, k_e, empirically relating the total flow of water, Q_t, to the electrical potential gradient in the system i_e could be predicted from the characteristics of the clay mineral, the pore fluid, and the pore sizes in the medium. The physical basis for the water transport can be summarized as follows:

1. Cations that transport their hydrated water sheath toward the cathode (less the transport of the solvated water by the anions to the anode);
2. Moving cations impart a dragging force on the solvent molecules as they move toward the cathode;
3. Displacement of water molecules by colloidal particles that move toward the anode by electrophosesis; and
4. Miscellaneous chemico-osmotic effects as a consequence of electrolysis.

Thus, as a result of electro-osmosis and prevailing electrode reactions, as is illustrated in Figure 2, there will be a movement of cations to the cathode and anions to the anode. Figure 2 depicts qualitatively the amount of water molecules carried by each species depending on their hydration numbers. Hence, the rate of movement, v_i, of each species will depend on the ionic current carried by the species, on the chemical gradients of species produced or removed, and on any local hydraulic and electrical potential gradients present in the system. The hydraulic gradients are either externally imposed on the system or may be internally generated owing to chemical/electrical interactions of the species present or produced with the porous media.

Experimental evidence indicates that the water flow is orders of magnitude (100 to 4,000 moles/Faraday) greater than that possible from transport of the waters of hydration (possibly 1 to 15 moles/Faraday). In addition, physical chemistry models for ionic motion through solvents do not support the existence of any sustained or appreciable drag beyond the immediate hydration sphere for homogeneous systems (open space). Therefore, it is difficult to understand how the large quantity of water flow in porous systems can be explained by basis 1. The analytical model developed by Acar et al. (*14*) and detailed next does not require a complete quantification of all the contributory factors to electro-osmosis because the Nernst-Planck equations are able to account for all the components of species of transport regardless of the actual phenomenology that produce them.

ANALYTICAL MODEL

It is assumed that constant current and hydraulic potential difference are applied across a water-saturated and homogeneous specimen of clay. It is necessary to assess the product distributions generated by the electrolysis to estimate the boundary conditions generated by the electrode reactions. Acar et al. (*5*) demonstrated that for currents of the order of milliamperes used in electro-osmosis there will be an ample amount of H_2O flow to sustain the electrolysis and that local convection will be present at electrodes producing gases.

In electro-osmosis the water flow rate q_e is related empirically to the current by (*13*)

$$q_e = k_e(\text{cm}^2/\text{V sec})i_e(\text{V/cm})A(\text{cm}^2)$$
$$= k_i(\text{cm}^3/\text{amp sec})I(\text{amp})$$
$$= \frac{k_e}{\sigma} I \qquad (3)$$

where σ is the conductivity of the pore fluid in mhos/cm, k_i is given in L/amp sec, I in amp, and k_e is the electro-osmotic

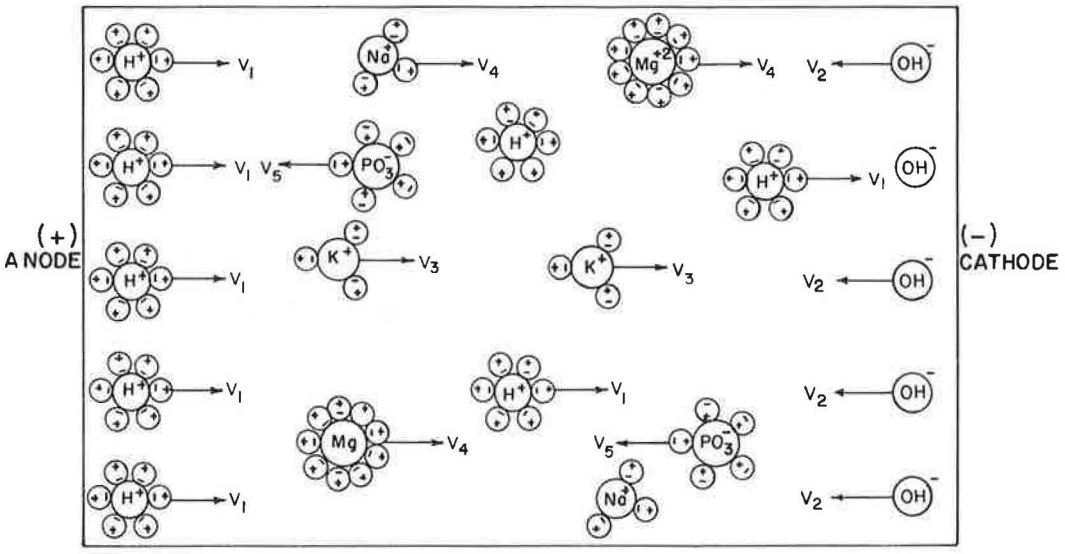

FIGURE 2 Movement of cations and anions in an electric field.

coefficient of permeability. Here, k_i values range between 0 to 1.0×10^{-3} L/amp sec for soils.

If the applied current is I, 2 moles of H_2O needs 4F coulombs at anode (Equation 1), and then the rate at which H_2O is lost

$$R_{H_2O}(\text{mole/sec}) = \frac{I(\text{amp})}{(2)(96485(\text{amp sec/mole}))}$$
$$= I \times (5.18 \times 10^{-6})\text{moles/sec} \quad (4)$$

Considering an incremental element at the anode, the instantaneous steady state pH will be estimated as follows:

$$Q_{H^+} = \text{rate of } H^+ \text{ production} = 2 \times R_{H_2O}$$
$$= (1.036 \times 10^{-5})I(\text{moles/sec}) \quad (5)$$

The net steady state concentration will then be

$$\text{molar concentration} = \frac{Q_{H^+}(\text{moles/sec})}{q_e(\text{L/sec})}$$
$$= \frac{(1.036 \times 10^{-5})(\text{moles/amp/sec})}{k_i(\text{L/amp/sec})}$$
$$= \frac{1.036 \times 10^{-5}\text{M}}{k_i} \quad (6)$$

For maximum k_i of 1.0×10^{-3} L/amp sec, Equation 6 renders a maximum pH of 2.0 at the anode, which is in conformity with recorded values in previous studies. Interestingly, as the efficiency of the process decreases (smaller k_i values), the pH at the anode will also decrease. Similarly, at the cathode (Equation 2), 4 moles of H_2O need 4F coulombs of electrical charge to produce 4 moles of OH^- ion, and, hence, the $[OH^-]$ ion concentration of the solution at the electrode will have a pH of 12.0.

This deliberation is for an aqueous solution where the decomposition of water is the primary result and thus for an anode that does not decompose. Several types of electrodes (aluminum, steel, iron, graphite, bronze, copper, platinum, gold) are used in processing studies. The electrolyzed products of some of those electrodes will introduce other ions in conjunction with the H^+ and OH^- ions and thus can change the chemistry generated at the boundaries. Those ions will complicate the chemistry further by diffusion into the specimen or precipitating or both, depending on the pH of the pore fluid.

MASS TRANSFER IN THE SYSTEM

The total material flux into an incremental element of thickness dx, q_{tc}, is composed of three components:

$$q_{tc} = q_{cc} + q_{ch} + q_{ce} \quad (7)$$

where

q_{cc} = material influx due to chemical gradients,
q_{ch} = material influx due to hydraulic gradients, and
q_{ce} = material influx due to electrical gradients.

The concentration of the material (solute), C_J, is defined as the mass of solute per unit volume of solution. The mass of solute per unit volume of porous media is, therefore, (nC_J), where n is the porosity of the medium (the volume of voids over the total volume of the element). The total mass transfer caused by electrical and material gradients in an electrochemical system, in general, is described by the Nernst-Planck equations (*15*)

$$q_{tc} = \left[-D_J \frac{\partial C_J}{\partial x} + V_x C_J - \frac{zF}{RT'} D_J C_J \frac{\partial \phi}{\partial x} \right] n \quad (8)$$

where

z = charge on the ion,
F = Faraday's constant (96,485 coulombs),
R = universal gas constant,
T' = temperature (°K),
ϕ = electrical potential,
D_J = diffusion coefficient,
x = the flow direction,
V_x = average seepage velocity = v/n, and
v = discharge velocity.

The material (solute) flux owing to chemical gradients is given by Fick's First Law:

$$q_{cc} = -D_x \frac{\partial C_J}{\partial x} n \tag{9}$$

where D_x is called the longitudinal dispersion coefficient in a saturated porous media and is composed to two components (*16*):

$$D_x = \alpha_x V_x + D^* \tag{10}$$

The first term represents the dispersion of the species caused by the average linear seepage velocity in the pores of the medium, and the second term describes the diffusion of the chemical in the pores. Here, α_x is the longitudinal dispersivity dependent on the size and frequency of the pores in the medium (fabric). In finc-grained soils, the contribution of the first term is negligible because of very low seepage velocities, and, hence, the longitudinal dispersion coefficient may be taken equal to the diffusion coefficient (*16*). The molecular diffusion coefficient D^* in the pore fluid is related to the diffusion coefficient in the free solution by

$$D^* = \rho D_0 \tag{11}$$

where ρ depends on porosity and tortuosity of the medium and varies between 0.13 to 0.49 (*17*).

The solute flux caused by hydraulic gradients (convection) is directly related to the seepage velocity and, hence, Darcy's law:

$$q_{ch} = \left(k_x \frac{\partial h}{\partial x}\right) n C_J \tag{12}$$

where k_x is the hydraulic conductivity of the medium and h is the hydraulic potential.

Those expressions show that the material flux depends on the diffusion gradients, the convective flow conditions, and the migration contributions of species, respectively. The average seepage velocity of species will be taken as linear, uniform, and equal to the average macroscopic fluid velocity. The migration contribution presented in Equation 8 represents all the ionic species in the medium. For conditions where a dilute aqueous electrolyte is slowly passed through an electro-osmotic cell at a small but constant electrical current, the migration term will be nonlinear in concentration if the electric field $\partial\phi/\partial x$ is not constant or if the species in question carry a significant but varying fraction of the current anywhere in the bulk solution. Migration effects are usually avoided in electrochemical cells by providing an excess of an inert and supporting electrolyte.

One further simplifying assumption will be made in the following derivation. The electrical field ($\partial\phi/\partial x$) is assumed to be constant in time across the specimen. This assumption may not entirely be valid, because the electrical field in electro-osmotic experiments depends on the concentration gradients imposed by the generated H^+ and OH^- ions and, hence, the specific conductance of the pore fluid in time and space. However, this assumption will be considered valid to provide a first-order approximation to chemical gradients.

These conditions will simplify the total material flux as

$$q_{tc} = \left[kC_J - D^* \frac{\partial C_J}{\partial x}\right] n \tag{13a}$$

$$k = -\frac{zF}{RT} D^* \frac{\partial \phi}{\partial x} + k_x \frac{\partial h}{\partial x} = -k_m + k_h \tag{13b}$$

where k is a constant with units of $[L/T]$ representing the velocity of the pore fluid. The first term represents the contribution to the flow of water molecules caused by, for example, the migration of H^+ ion and its hydrated water molecules under an electric potential gradient, and the second term K_h depicts the contribution to flow caused by the induced or applied hydraulic gradients as a consequence of the electro-osmosis phenomena.

The mass balance across the element requires

$$\nabla q_{tc} = -R \frac{\partial C}{\partial t} n \tag{14}$$

where $(\partial C/\partial t)$ is the rate of mass change, A is the area, and R is called the retardation coefficient, a term representing the adsorption and desorption of different species on clay surfaces or any interactions between the different species leading to precipitation or other chemical reactions or both,

$$R = 1 + \rho_d k_p / n \tag{15}$$

where ρ_d is the dry bulk density of the soil and k_p is the partition coefficient.

The gradient operator ∇ in one-dimensional conditions renders

$$\left(\frac{\partial q_{tc}}{\partial x}\right) = -R\left(\frac{\partial C}{\partial t}\right) \tag{16}$$

When Equations 8–10 and 13 are substituted in Equation 16,

$$D_x C_{,xx} - k C_{,x} = R C_{,t} \tag{17}$$

where $C_{,xx}$, $C_{,x}$, $C_{,t}$ represent partial derivatives in space and time. If the experiments were conducted with a constant hydraulic potential gradient across the specimen, or if it were assumed that the total flow caused by water molecules being transported through the migration of H^+ ions is constant throughout the system, then k simplifies to V_x,

$$D_x C_{,xx} - V_x C_{,x} = R C_{,t} \tag{18}$$

Equation 18 can be further nondimensionalized by taking

$$X = x/L \tag{19a}$$

$$C^* = 1 - \frac{C}{C_i} \tag{19b}$$

$$P = V_x L/D_x \tag{19c}$$

$$T = D_x t/RL^2 \tag{19d}$$

where L is the length of the specimen and C_i is the initial concentration of the specific species in the bulk solution. In solute transport, P is often called the Peclet number and T is the nondimensional time. When Equations 19 are substituted in Equation 18, the nondimensional form is obtained:

$$C^*_{,xx} - PC^*_{,x} = C_{,T} \tag{20}$$

Equation 20 must be solved with appropriate boundary conditions for the initial conditions and process rate to have a first estimate of the pH gradients in electrochemical processing of soils.

The species generated at the inlet and the outlet is different. A constraint exists at the boundary; therefore, when they meet at a location, the following neutralization reaction occurs:

$$H^+ + OH^- \leftrightarrows H_2O \tag{21}$$

A computer program (DIFFUSE) has been written in FORTRAN based on the given formalism (*14*).

PREDICTIONS OF THE ANALYTICAL MODEL

Figure 3 presents different pH gradients predicted by the model. Figure 3a presents the case when the pH at the anode and cathode are 2.0 and 12.0, respectively, and when the initial pH of the porous medium is 7.0. The front presented is for diffusion only, and, hence, the acid-base front meets in the middle. A neutralization reaction will occur when those fronts meet. Figure 3b depicts the case when the specimen is initially acidic with a pH of 5.0. Here, the OH^- ion front moves through the specimen. Figure 3c presents the case when the convective flux provides a P value of 30. The acid front moves farther toward the cathode in time and is expected to flush the specimen eventually. The three cases presented indicate that the pH gradient would be a function of

1. The pH values established at the electrodes by the rate of electrolysis: extreme values occur at low k_i (see Equation 6) and, hence, high electrolyte concentrations of productions (see Equation 3);
2. The initial pH of the porous medium;
3. Whether the flows would be governed by solely diffusion of the chemical or by the advection of the bulk fluid flow (P value); and
4. Any adsorption/desorption and precipitation of H^+ and OH^- ions: the effects are included in the retardation coefficient R given in Equation 15.

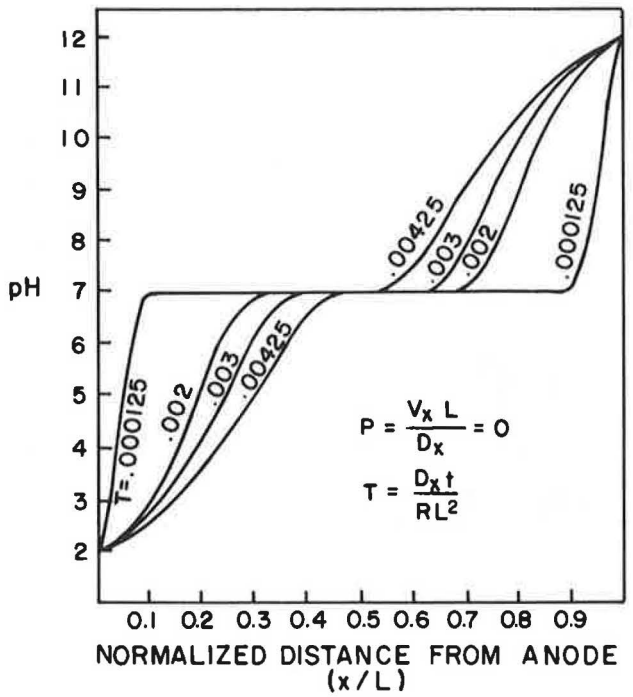

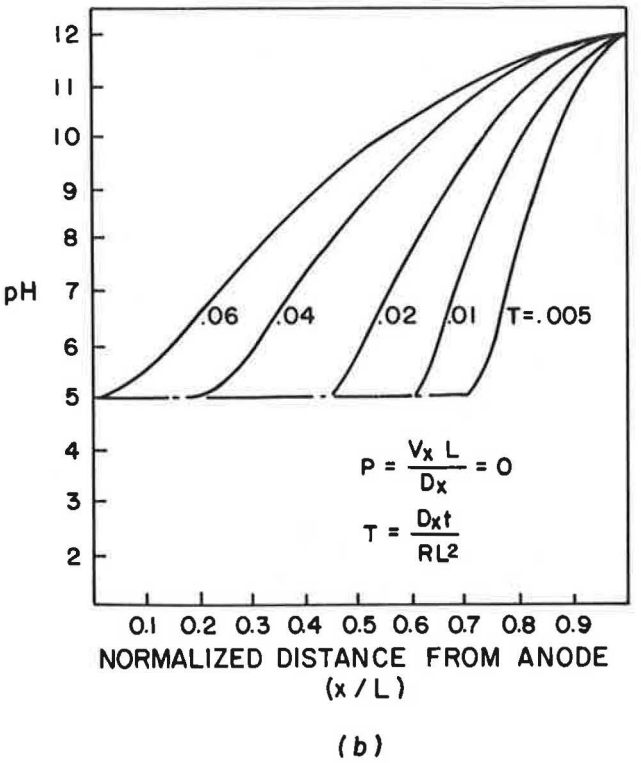

FIGURE 3 pH gradients predicted by the model (*5*). (a) Diffusive flux only: pH_i (initial) = 7.0, pH_{inl} = 2.0, pH_{out} = 12; (b) diffusive flux only: pH_i = 5.0, pH_{inl} = 5.0, pH_{out} = 12; and (c) diffusive and convective flux: P = 30, pH_{inl} = 2.0, pH_{out} = 12.

FIGURE 3 (*continued on next page*)

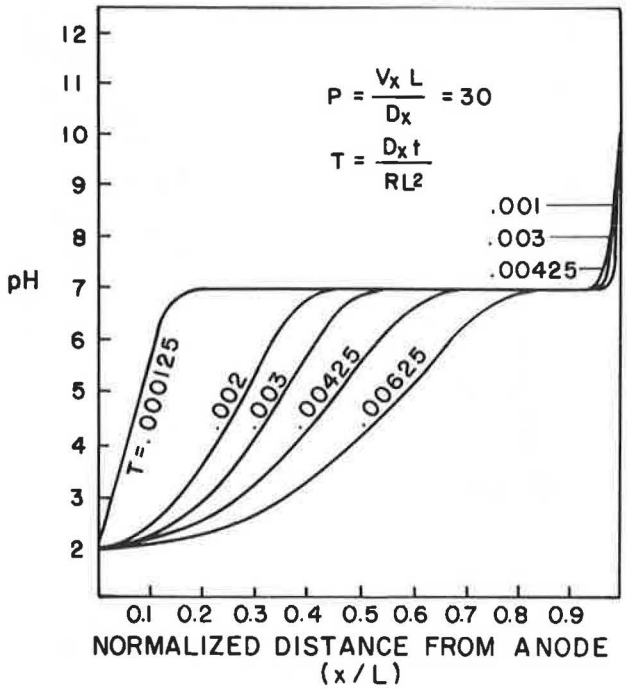

(c)

FIGURE 3 (*continued*)

EXPERIMENTAL METHODOLOGY AND PROCEDURE

Soil Description

The soil used in this study was an air-floated kaolinite clay RC-32 lot number G-237 from the Thiele Kaolin Company in Wrens, Georgia. The Atterberg limits and the other soil characteristics determined in conjunction with this study are presented in Table 1.

Pore Fluid Description

Distilled and deionized water was added to the dry kaolinite at about 2,000 percent water content, and the slurry was allowed to settle 24 hr. The procedure was repeated three times, and the supernatant collected on top of the clay during each washing was removed to be used as the pore fluid in the electro-osmosis tests. The supernatant from the clay washing was assumed to represent the actual pore fluid in the clay during testing because it contained the mineral salts and other soluble material on the dry clay surfaces. The clay washing removed excess ions on the clay surfaces to increase the electrolyte concentration of the pore fluid and thus to have the effect of reducing the efficiency of electro-osmosis.

The pH of the supernatant ranged between 6.5 to 8.5. Three separate chemical analyses were performed to determine the ions in the pore fluid by using both a Dionex ion chromatograph and an Atomic Absorption (AA) spectrometer. The pore fluid was filtered through a 0.2-micron filter prior to all tests to remove any particles present in the sample.

Results are summarized for some of the ionic species in Table 2. The predominant cations and anions are Na^+ and SO_4^{2-}, respectively. The normality of the supernatant was in the order of magnitude of 10^{-4} equivalents/l (*18*).

Procedure

The washed clay was allowed to consolidate under its own weight to a water content about 1.5 times the liquid limit of the kaolinite and then was consolidated. The glass sleeve containing the clay specimen (2.54 cm diameter and 10.2 cm

TABLE 1 COMPOSITION AND CHARACTERISTICS OF GEORGIA KAOLINITE

Characteristic	K[a]
Mineralogical Composition (% by weight)	
Kaolinite	98
Illite	2
Na-montmorillonite	--
Index Properties (ASTM D 4318)[b]	
Liquid Limit (%)	64
Plastic Limit (%)	34
Plasticity Index	30
Specific Gravity (ASTM D 854)[c]	2.65
% Finer than -2 μm Size	90
Activity	0.32
Proctor Compaction Parameters	
Maximum Dry Density, tons/m^3	1.37
Optimum Water Content, %	31.0
Initial pH of Soil[d]	4.7-5.0
Initial Water Content (Air Dry) (%)	1.75
Compression Index (C_c)	0.25
Recompression Index (C_r)	0.035
Permeability of Specimens Compacted at the Wet of Standard Proctor Optimum (x 10^{-7} cm/sec)[e]	6-8

[a] K = Georgia Kaolinite

[b] ASTM Method for Liquid Limit, Plastic Limit, and Plasticity Index of Soils (D 4318-83)

[c] ASTM Method for Specific Gravity of Soils [D854-58 (1979)]

[d] pH Measured at 50% Water Content

[e] Flexible wall permeability at full saturation

TABLE 2 SUMMARY OF CHEMICAL ANALYSES OF THE SUPERNATANT

Ion	Molecular Weight	Concentration* (mg/L)
Anion		
SO_4^{-2}	96.1	14.8
Cl^{-1}	35.5	1.6
F^-	19.0	0.2
Cation		
Na^+	23.0	12.7
K^+	39.0	0.4
Mg^{+2}	24.3	0.1
Ca^{+2}	40.0	3.8

*All the ionic species in the system were not analyzed.

length) was removed after consolidation. The sleeve was cleaned, trimmed, and weighed to determine the percent of saturation. The "average water content" in the clay prior to testing was determined by averaging three samples from the top and bottom trimmings.

A schematic diagram of the electro-osmosis cell and the test setup is presented in Figure 4. The glass sleeve containing the consolidated specimens was directly placed in the electro-osmosis cell. Filter paper was placed at the ends of the clay. Carbon electrodes were used for electro-osmosis. To allow flow, 30 to 40 3-mm holes were drilled in those electrodes. Constant current tests were conducted. The current, voltage, effluent pH, and flow were continuously monitored.

The current was turned off at the end of the test, and the glass sleeve was removed. The clay was extruded from the cell and dissected into ten 1-cm-wide sections. A water content sample was taken from each section, and the pH of the soil and the pore fluid was determined.

Determination of pH in Soil

The pH measurements were made by using combination pH electrodes and a pH meter. The meters were calibrated with pH buffers in the range of the measurements to be made.

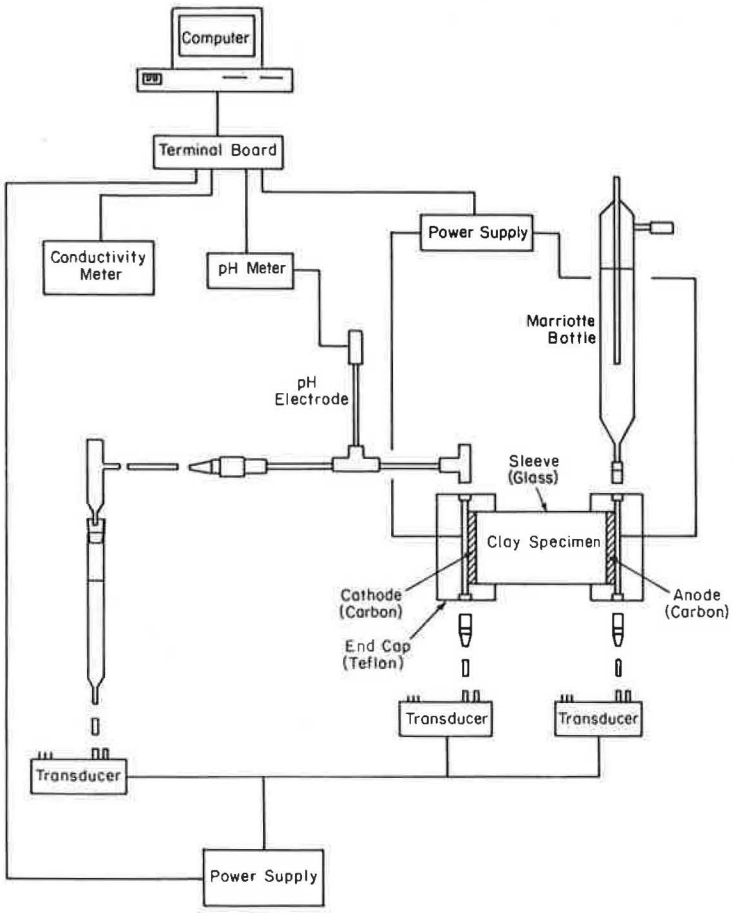

FIGURE 4 Schematic diagram of the test setup.

The pH was determined by two methods: (a) direct measurement of the pore fluid pH after its extraction from the clay by applying hydrostatic pressures to samples from each section by using compressed nitrogen gas and (b) direct measurement of the pH in the specimen. The clay specimen was dissected, as in the first method, and water content samples were taken. The combination pH electrode was immediately inserted directly into the wet clay slices. Putnam (*18*) demonstrated that in situ pH values thus recorded did not significantly vary for a wide range of water contents. Variations were recorded only at water contents more than 200 percent for the kaolinite used in this study.

ANALYSIS OF RESULTS

Coefficient of Electro-Osmotic Permeability, k_e

The coefficient of electro-osmotic permeability, k_e, varied between 0.80×10^{-5} to 3.0×10^{-5} cm²/V sec in tests conducted in this study. The flow and, hence, k_e, decreased with time of processing.

Coefficient of Water Transport Efficiency, k_i

Figure 5 compares the range of k_i values obtained in this study with previous studies. The initial k_i values were generally within the values obtained in previous studies, and a significant variation was observed in time. Figure 6 presents the change of k_i with time in selected tests. All tests indicated that water transport efficiency decreases in time after the initial increase (*18*).

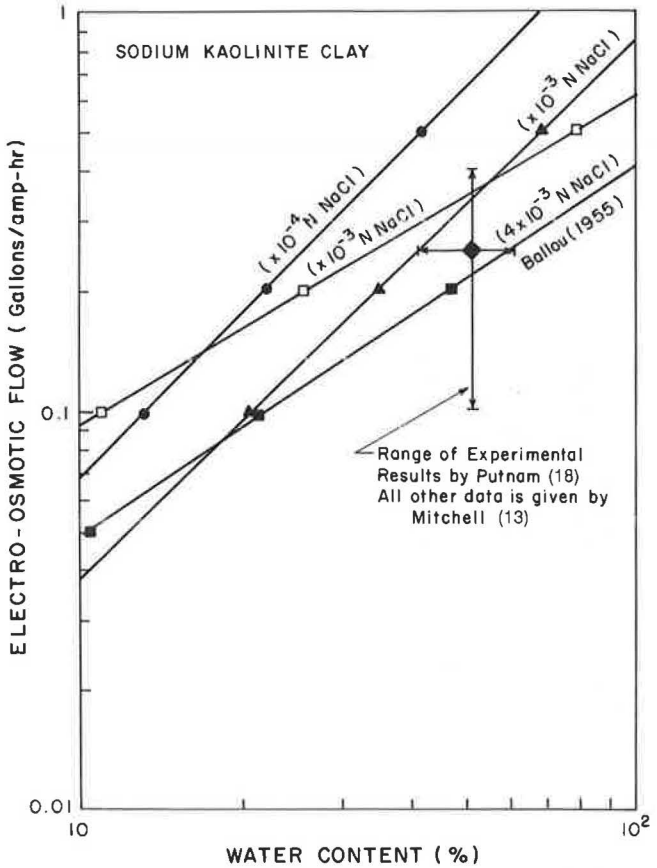

FIGURE 5 Comparison of k_i with previous studies.

Electrical Potential

Figure 7 presents an example of the voltages measured across the electrodes. The voltage steadily increases in each test and implies an increase in total "apparent" resistance and a decrease in "apparent" conductivity of the system.

The change in all voltages is a consequence of several phenomena. First, H^+ and OH^- ion concentration will steadily increase in the cell owing to the migration of the material fronts and will independently increase the pore fluid conductivity (lower resistance). Separately, any polarization at the electrodes owing to generation of gas bubbles, the decrease in porosity owing to any changes in water content across the cell, and depletion of ionic species will increase those "apparent" resistances. Further, the neutralization reaction at the front where H^+ and OH^- ions meet will result in forming of H_2O molecules decreasing the conductivity of the pore fluid. Figure 7 indicates that factors affecting the increase in resistance are more predominant.

pH Gradient Distributions

Figure 8 depicts a summary of some of the results of pH gradients determined for the 1.0 mA constant current tests

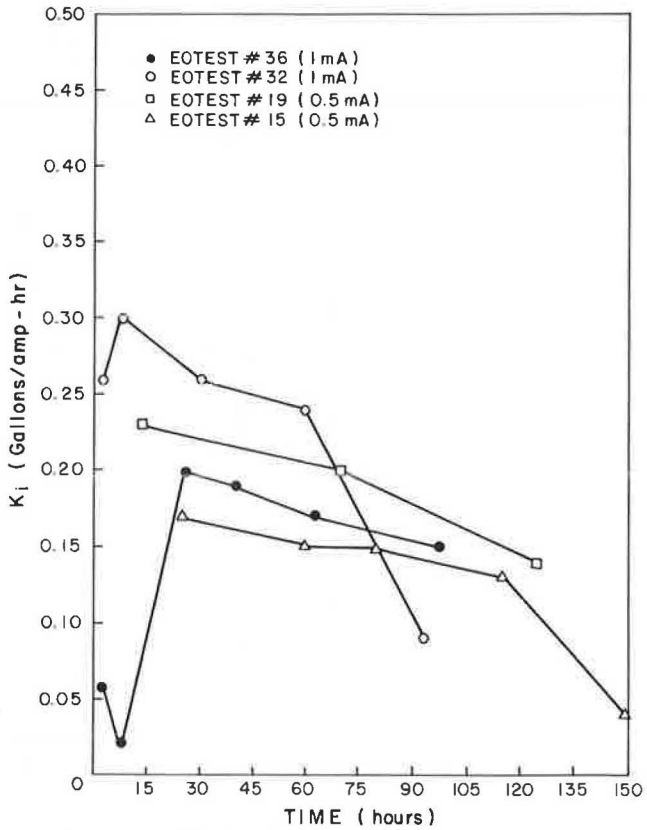

FIGURE 6 Change of k_i in time.

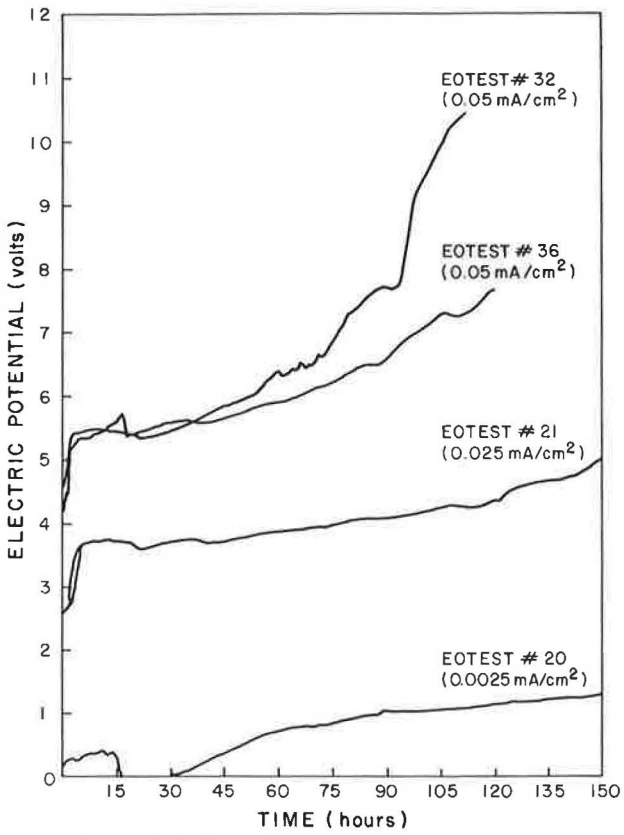

FIGURE 7 Change of voltage in time.

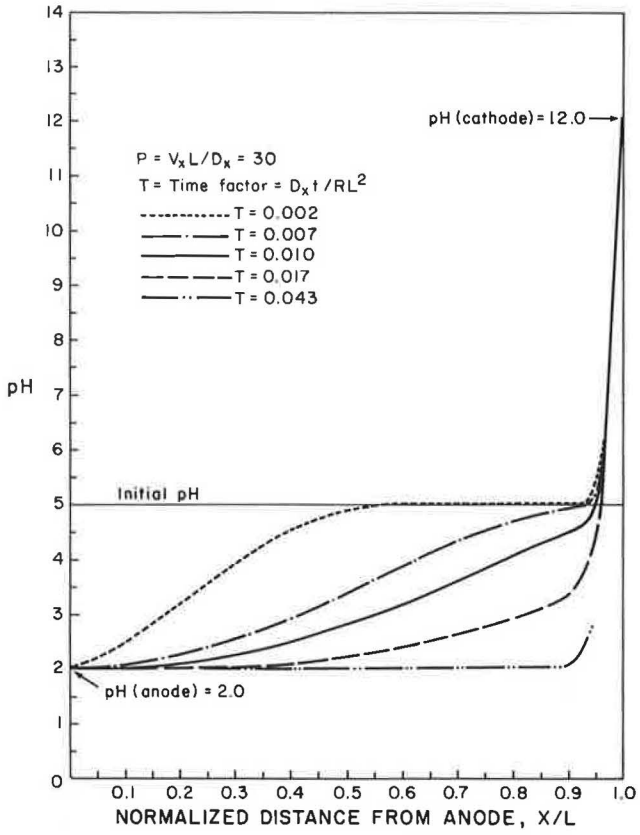

by using the in situ method of pH measurement. The acid front flushes over 75 to 85 percent of the clay specimen in a few hours, and the specimen becomes more acidic with time. The pH profiles obtained in those experiments conform with the predictions of analytical model. The change in pH becomes more pronounced at the discontinuity layer as the treatment time increases.

The movement of the hydrogen ion front through the specimen by diffusion is augmented by the transport of hydrogen ions owing to convection. In addition, water flow at the outlet will help remove some of the hydroxide ions generated from the cathode reaction.

Pore Fluid pH versus In Situ pH

Figure 9 presents a comparison of in situ and pore fluid pH values measured. The pore fluid pH is generally higher than the in situ pH. The difference was predominant in the case when the in situ pH was acidic. Identical values were obtained by both methods (*18*) in the case when the in situ value was basic. Those results demonstrate that the clay surfaces hold a major portion of H^+ ions by ion exchange equilibria.

Water Content Across the Cell

Figure 10 summarizes the changes in water content across the cell. The average water content line was determined by aver-

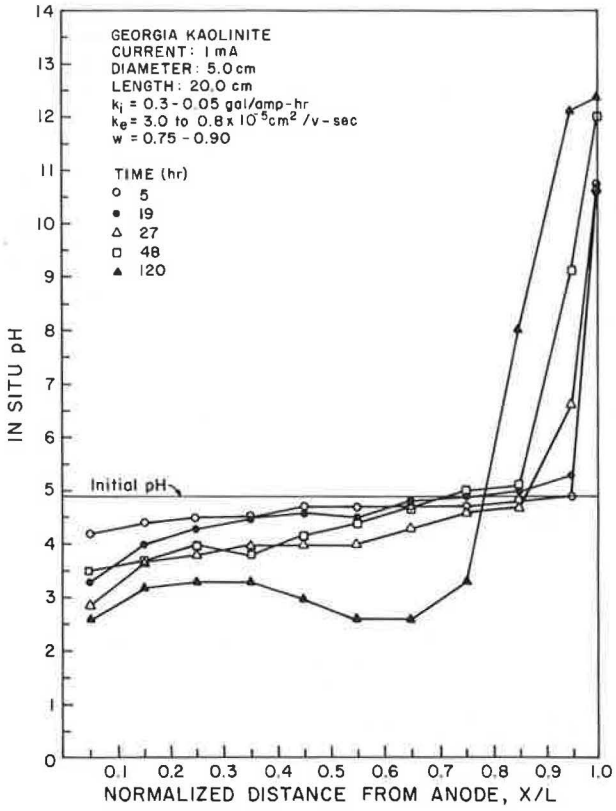

FIGURE 8 pH gradients across the cell.

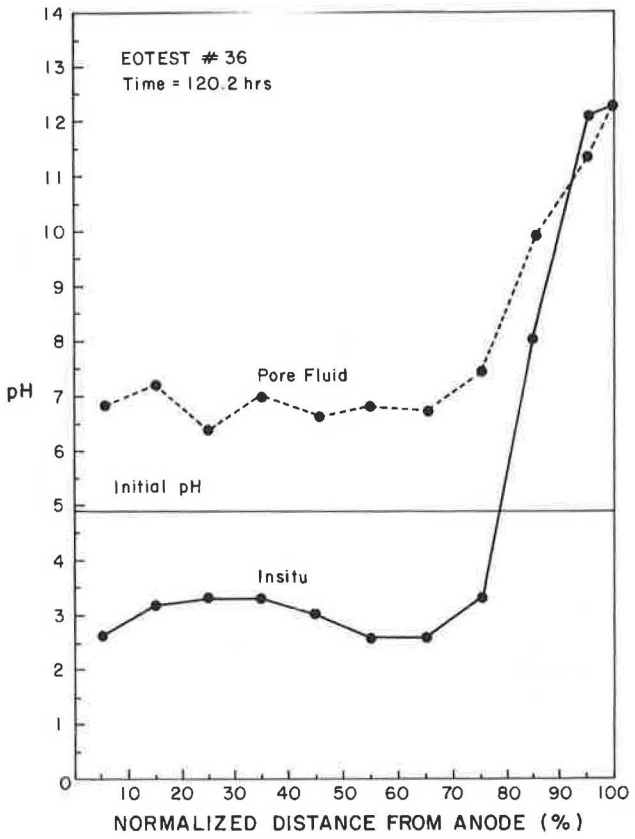

FIGURE 9 Comparison of in situ and pore fluid pH across the cell.

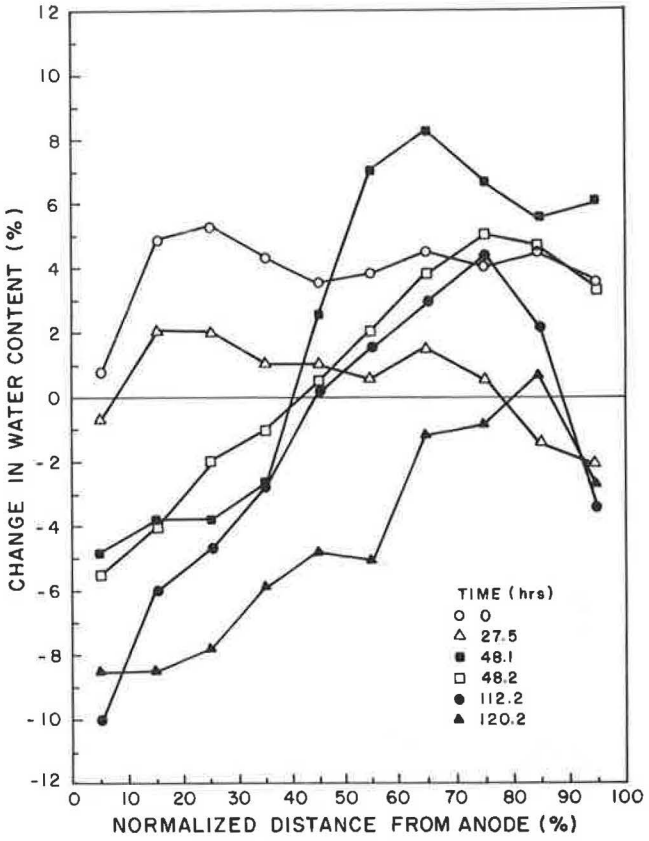

FIGURE 10 Change in water content across the cell.

aging three water content samples from the top and bottom trimmings of the specimens after consolidation but before testing. The zero water content line represents a straight-line approximation of the water contents obtained from those trimmings. The zero hour curve indicates that variation in water content exists across the specimen after consolidation and is due to incomplete consolidation under the specified load.

Interestingly, a substantial decrease exists in the water content close to the anode, although open boundary conditions for pore fluid ingress prevail during testing. This decrease in water content implies either an increase in hydraulic potentials or consolidation. Hydraulic potentials may increase across the cell owing to an increase in the osmotic potential by soil chemistry caused by electrolysis products.

DISCUSSION

The interactions of the ions in the pore fluid and the ions generated at the electrodes with the minerals of the porous medium result in physicochemical changes leading to variations in engineering characteristics and mechanical behavior. On the basis of the current state of knowledge (*13*), the following physicochemical interactions would be expected owing to changes in pH:

1. Dissolution of the minerals beyond a pH range of 7–9;
2. Replacement of H^+ and OH^- ions by exchangeable ions on the clay surface;
3. Precipitation of salts and metal ions in high pH environments leading to cementitious products or dissolution of such products at very low and very high pH environments;
4. Changes in the structure of the soil owing to variations in repulsive forces on clay surfaces; and
5. Complications of physicochemical interactions owing to the corrosion products produced at the electrodes.

A review of the previous studies indicates that all those phenomena have been observed in electrochemical processing (*5*). Esrig and Gemeinhardt (*8*) and Gray and Schlocker (*19*) are the only previous studies where pH measurements were reported across the cell in tests conducted with open electrodes at both ends. Esrig and Gemeinhardt conducted experiments that studied the rate at which electrokinetic stabilization takes place in an illitic soil with a pH of about 2.0. The cathode compartment was kept dry during testing. Gray and Schlocker studied electrochemical alteration of clays. In those tests the cathode compartment also was buffered to a maximum pH of 8.0. The original pH of the soil was about 6.0, and the cathode compartment contained a large volume of pore fluid. The results of those studies are summarized in Figure 11. In those tests the base front advances gradually into the cell, similar to the predictions presented in Figure 3b.

The model and experimental studies presented here indicate that different flow and boundary conditions employed in experiments will result in different pH gradients across the cell, leading to significantly different interactions. Therefore, it is essential to monitor and specify the flow conditions and the electrochemical products formed at the boundaries in electrochemical processing of soils.

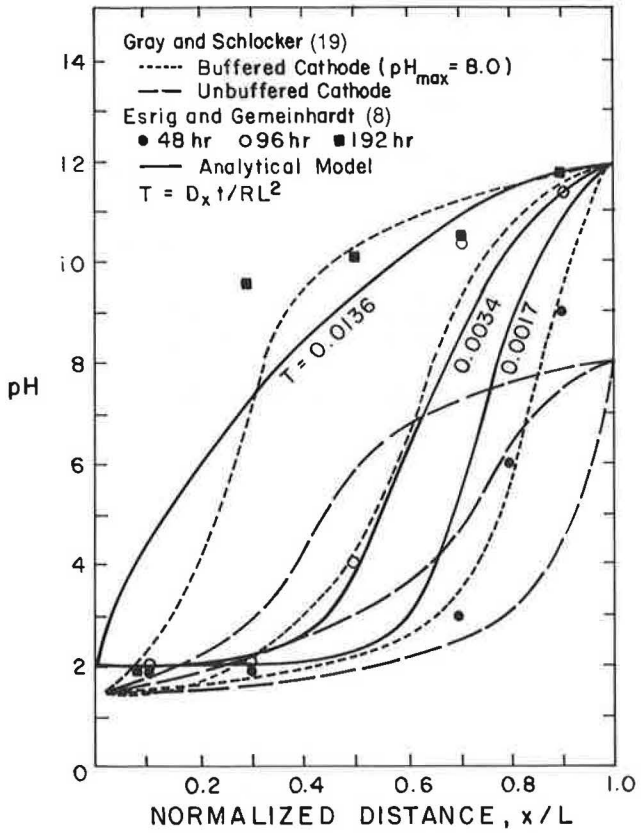

FIGURE 11 Comparison of pH gradients reported in previous studies.

The limitations of the assumptions used in present theories and models in electrochemical processing of soils are that they fail to explain all of the physicochemical effects. It is not yet well established how the chemistry relates to the mechanical behavior, although the studies indicate a strong influence exists on the water flow and soil-pore fluid interactions. An understanding of the chemical interactions in the pore fluid and perception of how diffusion, convection, and migration effects can be better quantified are needed. Further, the acid-base front generated at the electrodes will meet in the specimen accompanying a neutralization reaction, releasing an energy of 10 to 15 kcal/mole. It is yet to be understood how this energy release might affect the observed electro-osmotic flow.

Recent studies by Lockhart (*12*) indicate that the efficiency of processing is a function of the pH generated at the anode. The most interesting conclusion is that k_i is not usually proportional to the concentrations of ions present, nor to the zeta potential. Those results further substantiate that, as postulated in the analytical model presented here, the electro-osmotic dewatering is a direct current process where the water flow is only a consequence of transport by hydrated metal ions (mechanism a) or drag forces (mechanism b).

CONCLUSIONS

The following conclusions are made:

1. Electrochemical processing of soils has the potential to be used as a method of decontamination, an efficient pumping mechanism, or as an opposing gradient to flows from storage facilities.
2. The theory and model presented provide the rational basis in developing a better understanding of the electrochemistry associated with the process.
3. pH gradients lead to the physicochemical interactions in the soil and dominate the ion flow associated with the applied current in a low ionic strength media.
4. The presented analytical model and experimental results indicate that different flow and boundary conditions in electrochemical processing will result in different pH gradients, leading to different soil-pore fluid interactions.
5. Acid generated at the anode moves into the specimen by both diffusion and convection in open flow conditions.
6. Tests indicate that the efficiency of the process and water flow decrease with time of processing. Specimens consolidate under open flow arrangements in electro-osmosis.

The relationship of the chemistry generated by the electrodes, and the observed mechanical behavior, flow, and physicochemical changes, are not yet well understood. The potential use of electrokinetic processing of soils can be enhanced if the fundamental understanding of those issues is developed.

ACKNOWLEDGMENTS

This study is funded by the Board of Regents of the State of Louisiana under the Research Enhancement and Development Program by Grant LEQSF-RD-B-10(86-89). The funds provided by this agency are gratefully acknowledged. Harold Olsen is acknowledged for his valuable suggestions in this study.

REFERENCES

1. L. Casagrande. Review of Past and Current Work on Electro-Osmotic Stabilization of Soils. *Harvard Soil Mechanics Series 38*, 1952 (supplement 1957).
2. D. H. Gray and J. K. Mitchell. Fundamental Aspects of Electroosmosis in Soils. *Journal of Soil Mechanics and Foundation Division*, ASCE, Vol. 93, No. SM6, 1967, pp. 209–236.
3. L. Bjerrum, J. Moum, and O. Eide. Application of Electro-Osmosis on a Foundation Problem in a Norwegian Quick Clay. *Geotechnique*, Vol. 17, No. 3, 1967, pp. 214–235.
4. J. K. Mitchell. In-Place Treatment of Foundation Soils. *Journal of Soil Mechanics and Foundations Division*, ASCE, Vol. 96, No. SM1, 1970, pp. 73–109.
5. Y. B. Acar, R. J. Gale, G. Putnam, and J. Hamed. Electrochemical Processing of Soils: Potential Use in Environmental Geotechnology and Significance of pH Gradients. In *2nd International Symposium on Environmental Geotechnology*, Envotech, Bethlehem, Pa., 1989, pp. 25–38.
6. N. I. Titkov, V. P. Petrov, and A. Y. Neretina. *Mineral Formation and Structure in the Electrochemical Induration of Weak Rocks* (transl.), Consultants Bureau, New York, 1965.
7. T. Mise. Electro-Osmotic Dewatering of Soil and Distribution of the Pore Water Pressure. *Proc., 5th ICSMFE*, 1961, pp. 255–258.
8. M. I. Esrig and J. P. Gemeinhardt. Electrokinetic Stabilization of an Illitic Clay. *Journal of Soil Mechanics and Foundations Division*, ASCE, Vol. 93, No. SM3, 1967, pp. 109–128 (Discussion by D. Edwards and R. Lewis, Vol. 94, No. SM1, 1968, pp. 332–334).

9. D. H. Gray. Electrochemical Hardening of Clay Soils. *Geotechnique*, Vol. 20, No. 1, 1970, pp. 81–93.
10. R. J. Krizek, F. B. Gularte, and P. B. Hummel. Stabilization of Polluted Dredgings by Electro-osmosis. Presented at ASCE National Water Resources and Ocean Engineering Convention, San Diego, Calif., April 5–8, 1976.
11. B. A. Segall, C. E. O'Bannon, and J. A. Matthias. Electro-Osmosis Chemistry and Water Quality. *Journal of the Geotechnical Division*, ASCE, Vol. 106, No. GT10, 1980, pp. 1143–1147.
12. N. C. Lockhart. Electroosmotic Dewatering of Clays, 3, Influence of Clay Type, Exchangeable Cations and Electrode Materials. *Colloids and Surfaces*, Vol. 6, 1983, pp. 243–269.
13. J. K. Mitchell. *Fundamentals of Soil Behavior*, John Wiley, New York, 1976, pp. 113, 117.
14. Y. B. Acar, R. Gale, G. Putnam, J. Hamed, and I. Juran. Development of pH Gradients in Electrochemical Processing of Soils. Report presented to the Board of Regents of Louisiana, July, 1988.
15. N. Ibl. Comprehensive Treatise of Electrochemistry. In *Electrodics: Transport*, Vol. 6, (E. Yeager, J. O'M. Bockris, B. E. Conway, and S. Sarangapani, eds.), Chap. 1, Plenum, New York, 1983.
16. R. W. Gillham and J. A. Cherry. *Contaminant Migration in Saturated Unconsolidated Geological Deposits*. Special Paper 189, Geological Society of America, 1982, pp. 31–62.
17. K. R. Rowe. Pollutant Transport Through Barriers. In *Geotechnical Practice for Waste Disposal*, Geotechnical Special Publication 13, (R. D. Woods, ed.), ASCE, 1987, pp. 159–189.
18. G. Putnam. Determination of pH Gradients in the Electrochemical Processing of Kaolinite. M.S. thesis, Louisiana State University, Baton Rouge, 1988.
19. D. H. Gray and J. Schlocker. Electrochemical Alteration of Clay Soils. *Clays and Clay Minerals*, Vol. 17, 1969, pp. 309–322.

Publication of this paper sponsored by Committee on Physicochemical Phenomena in Soils.

A Study of Coupled Electric/Hydraulic Flow in Kaolinite

GEORGE P. KORFIATIS, LAKSHMI N. REDDI, AND VINCENT MONTANTI

Results of a laboratory investigation on the effects of electro-osmosis on the permeability of kaolinite clay are presented. Application of an electric potential to the kaolinite clay increased the permeability of the clay and created a pH gradient across the sample. With application of combined electric and hydraulic gradients, electric gradients were found to contribute significantly to discharges across the sample at low hydraulic gradients. Results presented will enhance understanding as to the feasibility of using electro-osmosis to decontaminate fine-grained soils.

Electro-osmosis is the process by which water flows through a soil mass in response to the application of an electric potential and is the result of the exchangeable nature of the adsorbed cations in clay particles and the dipolar nature of the water molecules. Although the principles of electro-osmosis are more than a century old (*1*), the applications of the process are quite recent. Since its first application for soil stabilization (*2*), electro-osmosis has been successfully employed in tasks such as dewatering (*3*), consolidation (*4*), and as an aid in pile driving (*5*).

In principle, soil stabilization or dewatering is accomplished by applying electric current to electrodes driven in the soil mass. As a result of electric treatment, inhomogeneities of ionic concentration develop, and pH changes, and lead to the development of nonuniform voltage gradients and resulting pore water pressures. Esrig (*4*) studied the effects of electrode geometry on pore water pressures and found that the pore water pressure at a certain point is related to the voltage at that point. Similar studies by other investigators (*5–7*) indicate a linear relationship between electro-osmotic flow and electric gradients and significant variations of coefficient of electro-osmotic permeability and variations in water content. Olsen (*8*) found that with increasing overburden pressures in clayey soils, osmotic and electro-osmotic permeabilities play a greater role in controlling flow than does hydraulic permeability. Subsequent studies concentrated on numerical solutions of the governing differential equation for combined electrokinetic and hydrodynamic flow (*9,10*).

Recent studies focused on electrochemical effects associated with the process of electro-osmosis. Nemec (*11*), in a study of pH changes in electrochemical cells, found that electrochemical effects in soils are enhanced and controlled by the strong pH gradients developed in the electric potential field and primarily is due to the electrolysis of water. Possible electrochemical effects include ion exchange, alteration of soil minerals, changes in soil fabric, electrolytic introduction of new species from the electrode decomposition products or external injections, and development of chemical gradients in soil. The pH gradients developed by electro-osmosis affect the solubility of metallic ions (such as in iron, magnesium, calcium, and aluminum) and, therefore, control the extent and rate of electrolytic transfer of ions into the soil. Renaud and Probstein (*12*), in their numerical simulations by using double-layer theory, clearly showed the strength of electro-osmosis in diverting groundwater flow from a potentially hazardous waste site by development of pore water pressure gradients in the soil. The potential use of electro-osmosis to decontaminate fine-grained soils is indicated in those studies.

In light of those developments, an experimental approach was used in the present study to assess relative magnitudes of hydraulic and electro-osmotic permeabilities under application of hydraulic or electric gradients or both and to study the extent of pH changes during the electro-osmotic process. Results are believed to aid in evaluating the feasibility of using electro-osmosis to decontaminate fine-grained soils.

EXPERIMENTAL SETUP

The electro-osmotic cell (Figure 1) used in the experiment consisted of three 6-in.-diameter chambers made of Plexiglas. The center chamber, 6 in. long, was used to house the soil sample. Each of the two 4-in.-long end chambers contained an opening for pH electrodes with calomel reference and a drainage valve and external burette for measuring the hydraulic gradient. The voids in the two end chambers were filled with crushed stone to exert a confining pressure on the ends of the sample. End plates (8 in. × 8 in. × ½ in.) were used to seal the outside chambers and to house the circular graphite plates (6 in. × ¼ in.), which were used as electrodes.

An LA 300 LAMBDA power supply was used, and Fluke 75 multimeters were also used to measure both voltage and current across the sample. An Expandable Ion-Analyzer EA 940 by Orion Research was used in conjunction with the pH electrodes to determine pH values throughout the experiment.

Tests were conducted on a kaolinite sample, because kaolinite is the least active of the clay minerals with a low colloidal activity; therefore, kaolinite provides a conservative indication of the importance of electro-osmosis in soils. The slurry was prepared, poured into the Plexiglas mold, and then dynamically compacted at its optimum moisture content. [The optimum moisture content and the maximum dry density as

G. P. Korfiatis and L. N. Reddi, Department of Civil, Environmental, and Coastal Engineering, Stevens Institute of Technology, Hoboken, N.J. 07030. V. Montanti, Robert C. Bogart and Associates, Flemington, N.J. 08822.

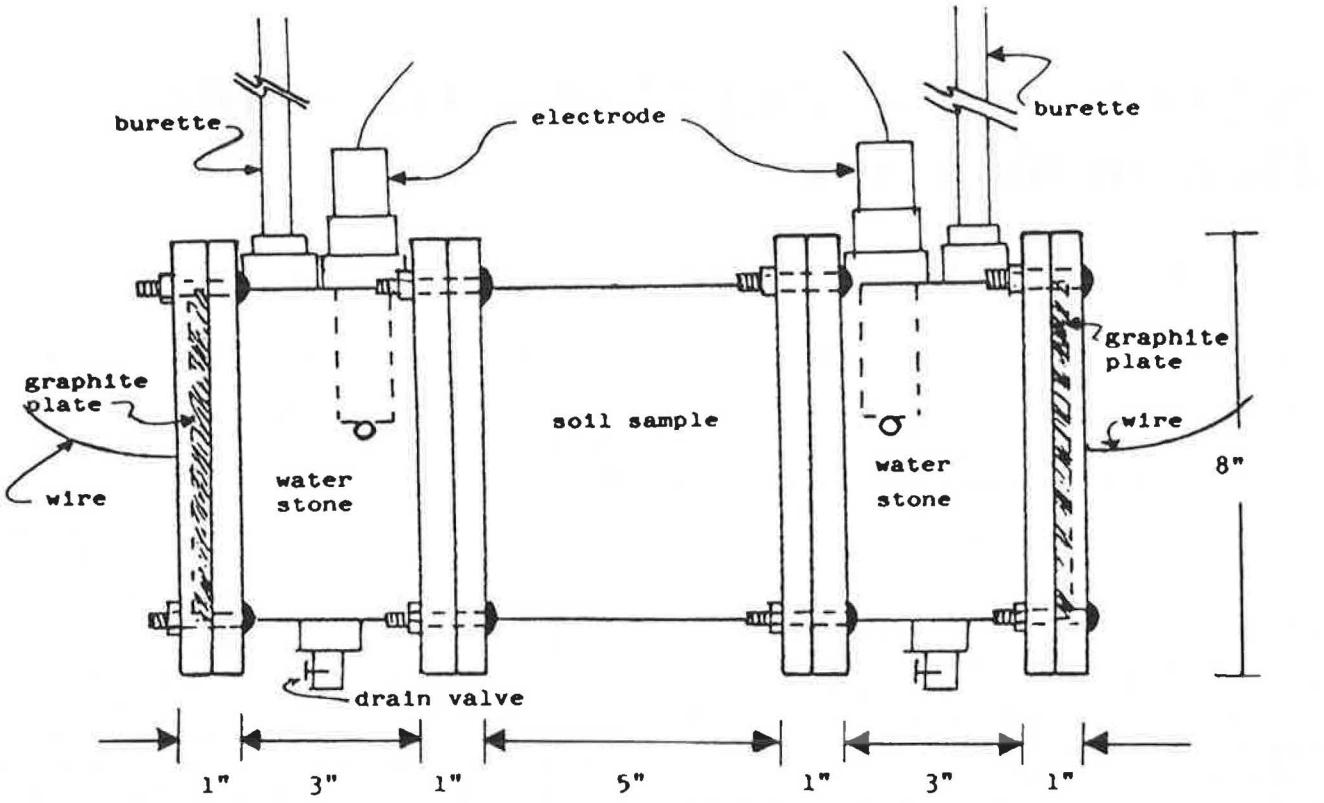

FIGURE 1 Experimental setup (cell description).

determined by the modified Proctor test (ASTM D1557-78) were found to be 23.5 percent and 93.6 pcf, respectively.] The sample was saturated with a back pressure of 3 psi and a hydraulic head of 40 cm. Permeability of the sample was computed to be 2×10^{-7} cm/sec, using the Falling Head method. A flexible wall permeability test was conducted on another kaolinite sample with the same moisture content and dry density to establish the permeability value further and resulted in values of conductivity equal to 5×10^{-7} cm/sec. Those values agree closely with those reported in the literature for kaolinite.

With hydraulic conductivity values established, an electric potential of 20 V was directed to the graphite plates. As a result of hydrolysis, hydrogen bubbles began to appear almost immediately at the cathode. Even at a potential of 5 V, hydrolysis remained a problem and thus made burette readings less reliable. Consequently, volume flux was measured at the anode side of the sample where electrolysis reactions were less significant. The electrical conductivity of the soil is given by the equation

$$K_e = q/(i_e \times A)$$

where

- q = flow passing through the sample as measured at the anode side,
- i_e = electrical gradient equal to the voltage across the sample divided by its length, and
- A = cross-sectional area of the sample.

Further testing of the sample included application of combined hydraulic and electric gradients. Electric potential created electric gradient, and burette levels were manipulated to create hydraulic gradient. The pH/reference electrodes in conjunction with the ion analyzer were used to monitor the pH of the cathode and anode cell waters periodically.

DISCUSSION OF RESULTS

Hydraulic Gradient Versus Permeability

The hydraulic permeability was first monitored as the hydraulic gradient was allowed to change. To validate those results, flexible wall tests were conducted at various gradients. Figure 2 presents the results of both testing methods. It can be noticed in Figure 2 that a linear extrapolation of flexible wall test results agrees fairly well with the results obtained from the cell test and that a linear relationship between hydraulic gradient and permeability within the hydraulic gradient ranges tested in flexible wall tests is implied. The permeability, however, remained constant under lower gradients.

Individual Application of Electric and Hydraulic Gradients

The kaolinite soil specimen was monitored for changes in discharge across the sample in response to time of application of electric and hydraulic gradients. Figure 3 presents discharges versus time when the sample was subjected individ-

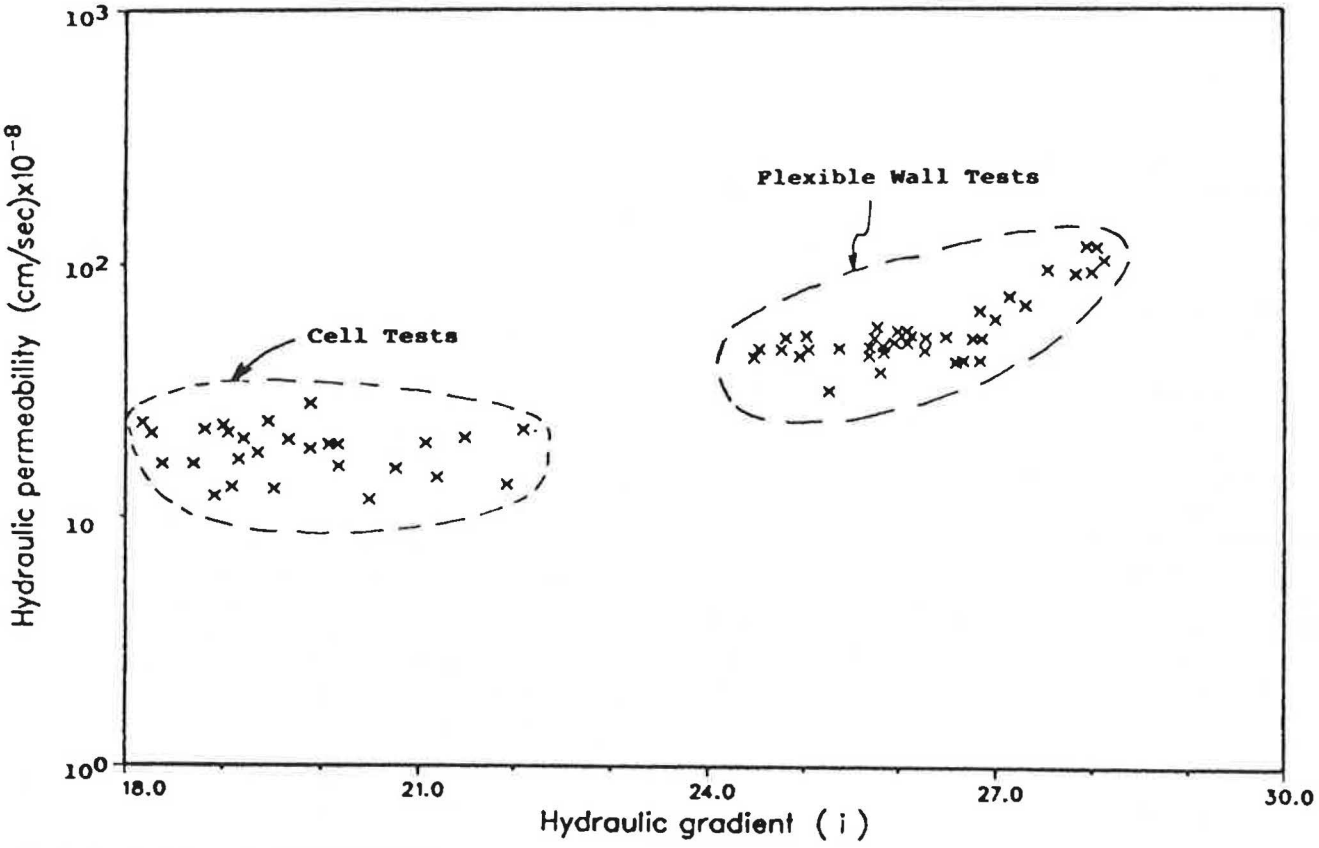

FIGURE 2 Variation of hydraulic permeability with hydraulic gradient.

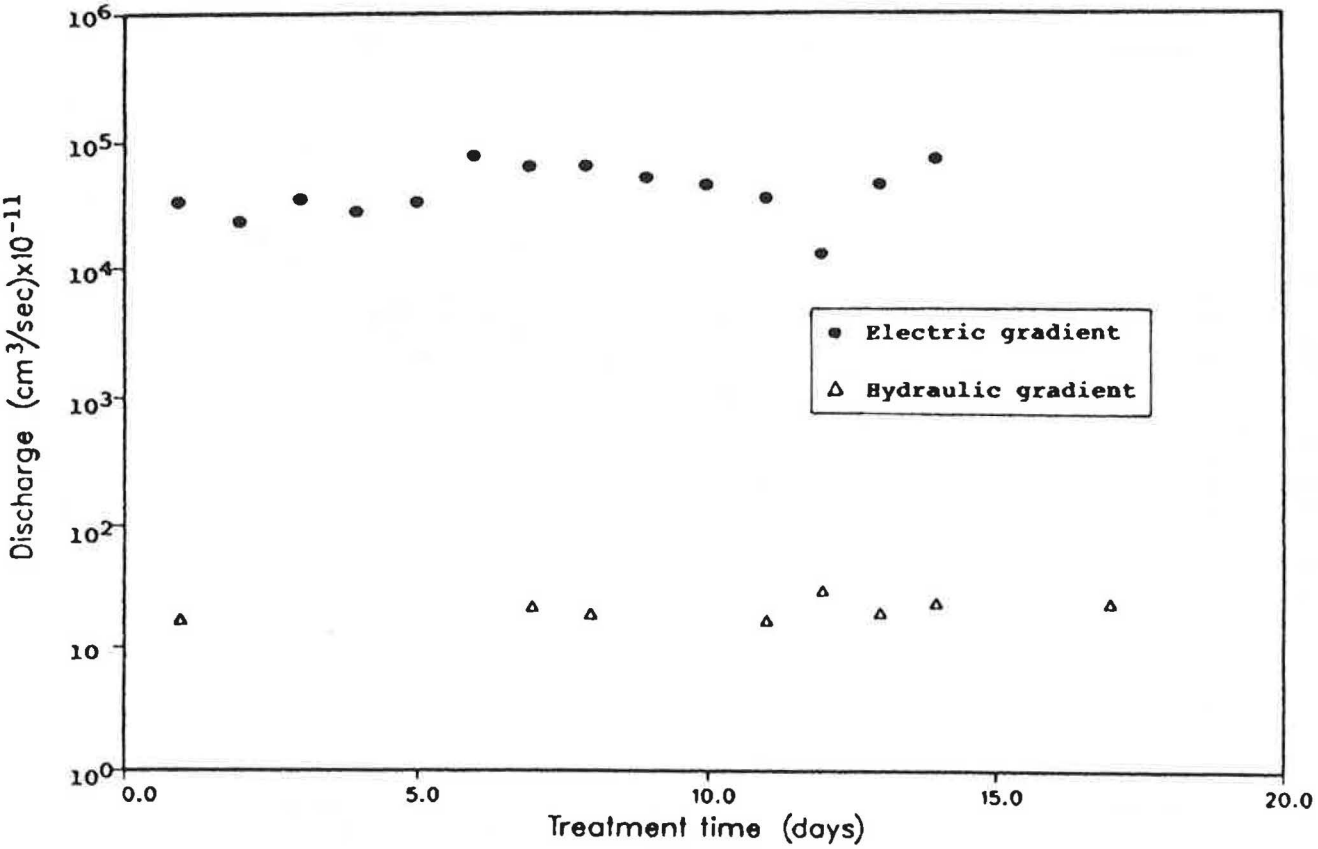

FIGURE 3 Time-dependent discharges caused by electric gradient (0.0025 volts/cm) and hydraulic gradient (20).

ually to hydraulic and electric gradients. As can be seen, an average hydraulic gradient of 20 resulted in discharges on the order of 10^{-10} cm³/sec, and an electric gradient of 0.0025 V/cm yielded discharges on the order of 10^{-7} cm³/sec. Discharges owing to hydraulic gradient did not indicate any significant fluctuations with time. However, noticeable fluctuations existed in discharges caused by electric gradients and are attributed to nonuniform spatial orientation of moisture gradients in the soil sample. Similar observations were made by Nemec (*11*), who noticed that in the initial phases of treatment moisture minima develop near anode and cathode and moisture maxima develop near the center of the sample. With elapsing treatment time, Nemec observed the moisture gradients becoming much sharper and their spatial orientation tending to be more uniform. Figure 3 also indicates sudden increases in discharges because of electric gradient at the end of 6 days and 12 days. Those increases with the progression of electro-osmotic treatment may be attributed to the cation exchange capacity of the clay. Clay particles immersed in a liquid partially dissociate the ions adsorbed to the clay and thus make them available for ionic conductivity. Therefore, the increase in discharge may be a result of the time necessary for ions to dissociate from clay particles and enhance conductivity.

Combined Application of Electric and Hydraulic Gradients

Figure 4 presents discharges resulting from the combined application of hydraulic gradients and an electric gradient of 0.0025 V/cm. There is a significant increase in discharges, from 7×10^{-7} cm³/sec to 6×10^{-6} cm³/sec as the hydraulic gradient is increased from 0 to 4. Assuming the increase in discharges is purely due to hydraulic gradients, application of a constant electric potential increased the discharges across the sample by 7×10^{-7} cm/sec. The contribution to discharge by electric gradient is computed to be 70 percent at a hydraulic gradient of 1 and 14 percent at a hydraulic gradient of 4, which undermines the significant contribution of electro-osmosis to the permeability characteristics of soils at low hydraulic gradients.

pH Changes During Electro-Osmosis

The pH at the anode and cathode were monitored throughout the experiment. As was expected, the pH of the distilled water decreased at the anode and increased at the cathode. Figures 5 and 6 demonstrate pH changes under two scenarios. Figure 5 represents when the cells were filled with distilled water and an electric field was applied immediately. The pH at the anode decreased from 7 to values close to 5, and the pH at the cathode increased to values approaching 10. Figure 6 represents when the pH of the distilled water was allowed to reach that of kaolinite, which was found to be 5.2, and then the electric potential was applied. The pH at the cathode approached a value of 10, and the pH at the anode increased to approximately 7.

It is worthy to study those results in light of Nemec's observations (*11*). Nemec noticed a highly nonuniform nature of pH gradients between anode and cathode. His experiments

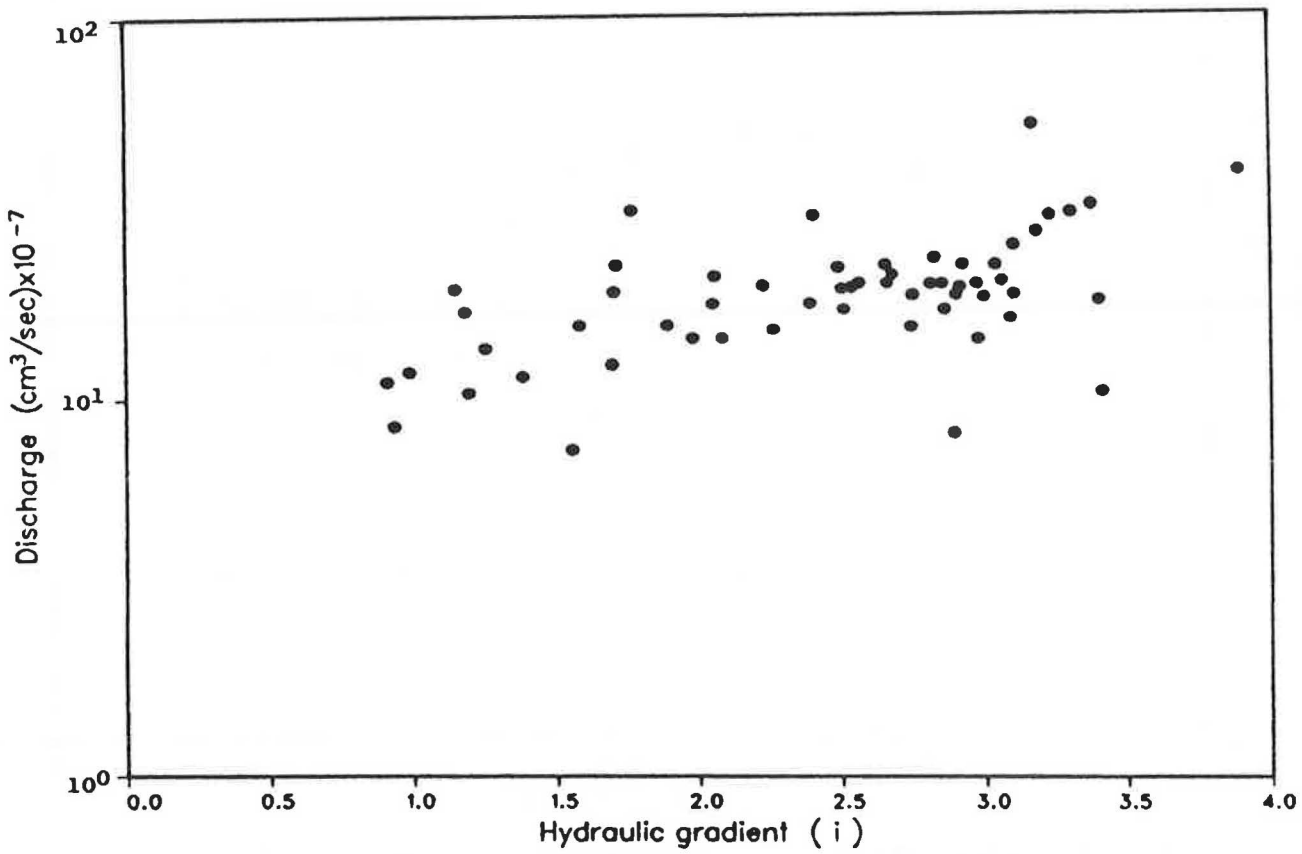

FIGURE 4 Variation of discharges with hydraulic gradient combined with an electric gradient of 0.0025 volts/cm.

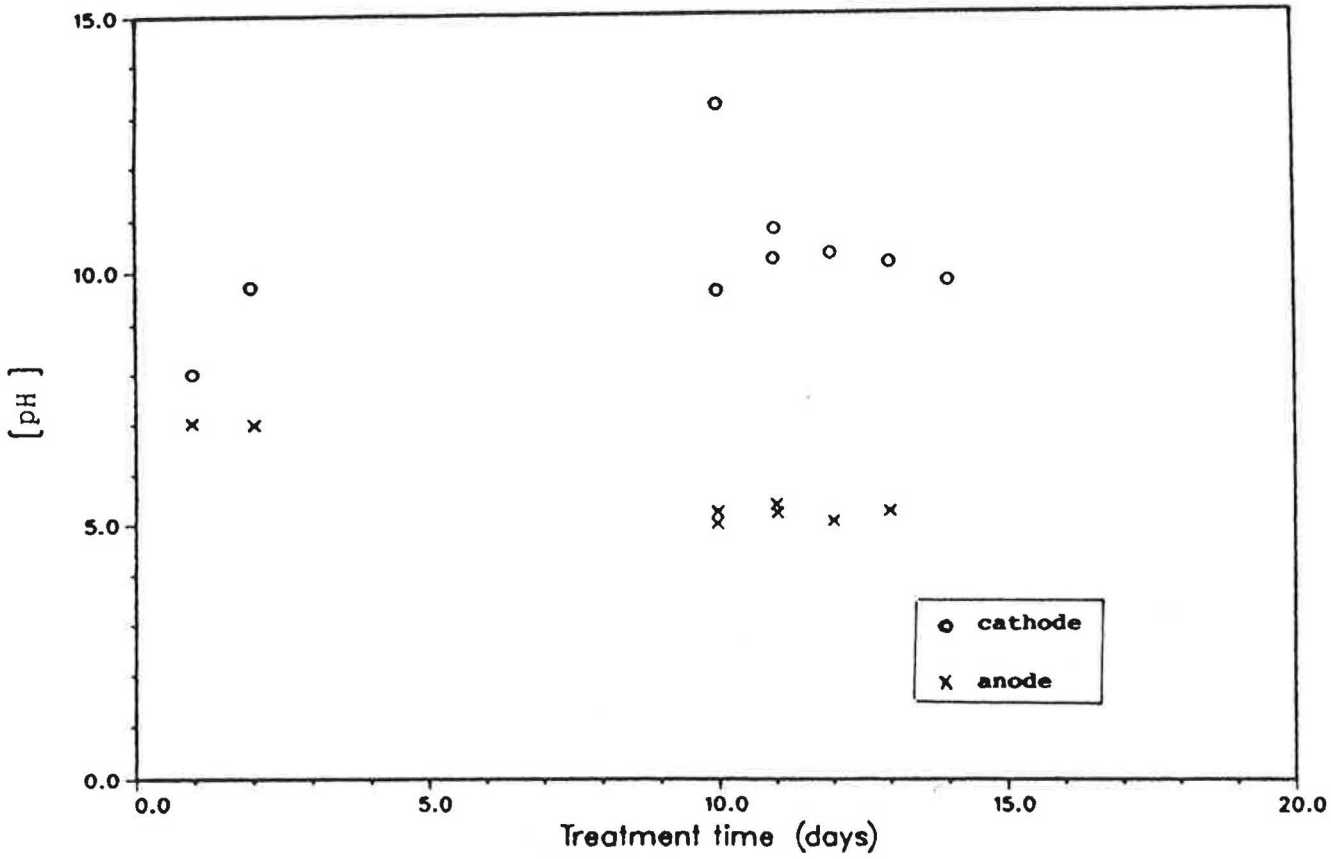

FIGURE 5 Time-dependent variation of pH caused by instantaneous application of electric potential.

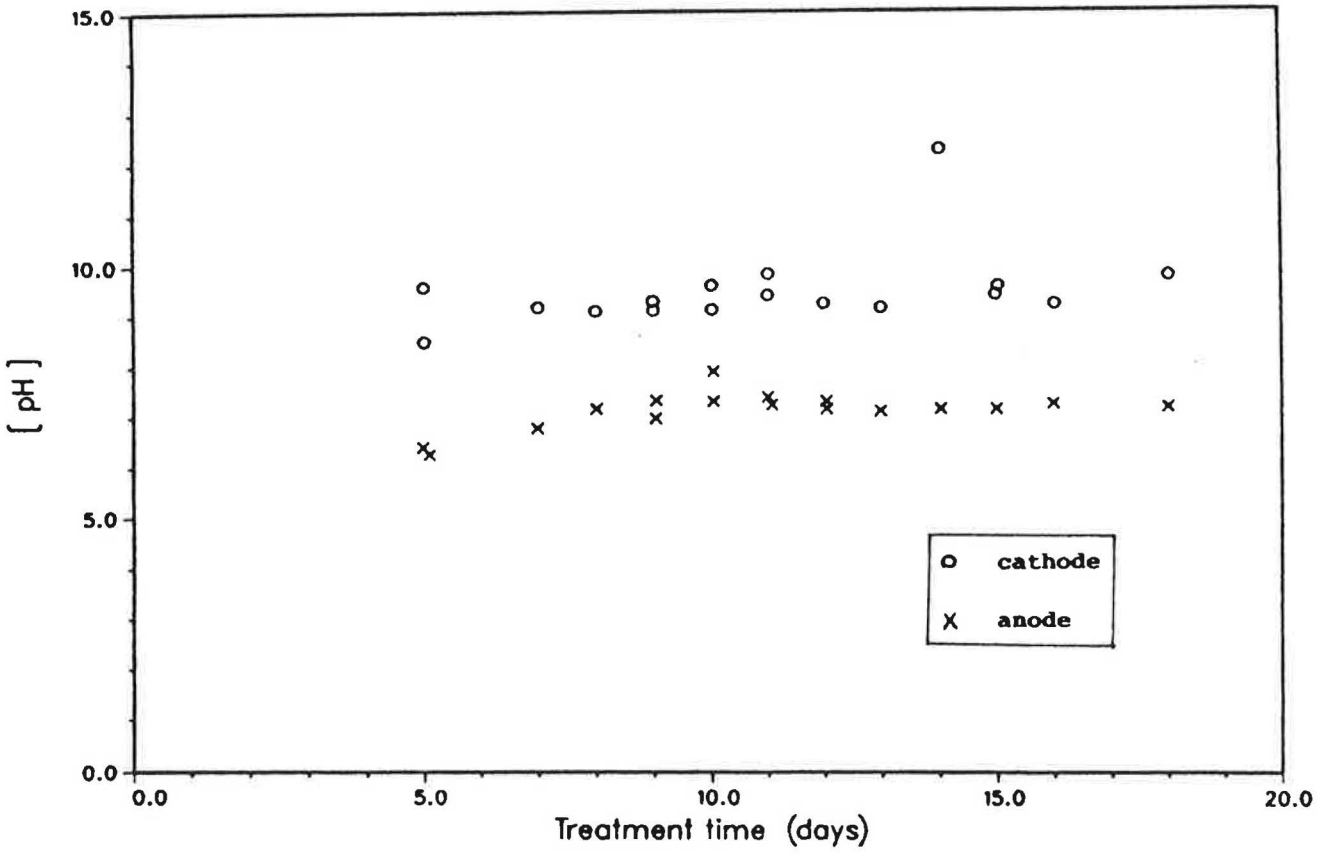

FIGURE 6 Time-dependent variation of pH caused by delayed application of electric potential.

indicated that in a period of 168 hr the pH at the cathode increased consistently from an initial value of 5.23 to 8.99 and the pH at the anode decreased oscillatorily to 4.83. The pH behavior at cathode is generally accepted to be governed by clay deflocculation and hydrogen ion adsorption, but pH behavior at anode is controlled by many electrochemical factors. Kaolinite displays anion-adsorption capacity in acid (anodic) environment. Dissolution of iron at the anode and also presence of amorphous noncrystalline compounds in the soil suspension enhance the anion-exchange capacity of acid soils. All those factors, together with the electrode processes (such as formation of gas bubbles), are thought to produce the changing pattern of pH behavior at anode in Nemec's experiments and in the present experiments.

Results suggest that additional observations in various soils are required for a general interpretation of pH changes during electro-osmotic treatment. Further research is needed to understand fully electrolysis reactions at the electrodes and the degree of transport of the ions caused by their size, mobility, and exchange capacities. The success of electro-osmosis in the decontamination effort of any soil is dependent on the electrochemical nature of the soil and its constituents. Whether or not contaminated soils would release adsorbed pollutants to electro-osmotically driven water is a subject of potential importance.

ACKNOWLEDGMENTS

This research was partially supported by the Hazardous Substance Management Research Center. The center is a consortium of five New Jersey universities and an advanced technology center of the New Jersey Commission on Science and Technology.

REFERENCES

1. F. F. Reuss. *Memoires Society Imp Naturalistes*, Moscou 2, 1809, pp. 327.
2. L. Casagrande. *Review of Past and Current Work on Electroosmotic Stabilization of Soils*. Harvard Soil Mechanics Series 45, Cambridge, Mass., 1957.
3. C. A. Fetzer. Electro-Osmotic Stabilization of West Branch Dam. *Journal of Soil Mechanics and Foundations Division*, ASCE, 1967, pp. 85–106.
4. M. I. Esrig. Pore Pressures, Consolidation, and Electrokinetics. *Journal of Soil Mechanics and Foundations Division*, ASCE, 1968, pp. 899–920.
5. J. K. Mitchell. In-Place Treatment of Foundation Soils. *Journal of Soil Mechanics and Foundations Division*, ASCE, 1970, pp. 73–107.
6. M. Grey. Fundamental Aspects of Electro-Osmosis in Soils. *Journal of Soil Mechanics and Foundations Division*, ASCE, Vol. 93, No. SM6, 1967, pp. 209–230.
7. D. V. Morris, S. F. Hillis, and J. A. Caldwell. Improvement of Sensitive Silty Clay by Electro-Osmosis. *Canadian Geotechnical Journal*, Vol. 22, 1985, pp. 17–24.
8. H. W. Olsen. Liquid Movement Through Kaolinite Under Hydraulic, Electric, and Osmotic Gradients. *American Association of Petroleum Geologists*, Vol. 56, 1972, pp. 2022–2028.
9. R. W. Lewis, C. Humpheson, and J. C. Bruch. Applications of Electro-Osmosis to Ground-Water Flow Problems. *Journal of Ground Water*, Vol. 13, 1975, pp. 484–491.
10. J. Bruch. *Electroosmosis in Ground-Water Pollution Control*. Technical Report N.S.F., University of California, Santa Barbara, 1976.
11. H. T. Nemec. Environmental pH Changes in Electrochemical Cell During Electro-Osmotic Stabilization of Soils. *Studia Geotechnica et Mechanica*, Vol. 5, 1983, pp. 13–38.
12. P. C. Renaud and R. F. Probstein. Electro-Osmotic Control of Hazardous Wastes. *Journal of Physicochemical Hydrology*, Vol. 9, 1987, pp. 345–360.

Publication of this paper sponsored by Committee on Physicochemical Phenomena in Soils.

Zinc Detoxification of Soils by Electro-Osmosis

SIBEL PAMUKCU, LUTFUL I. KHAN, AND HSAI-YANG FANG

The feasibility is determined of applying electro-osmosis to selective removal of zinc, a moderately toxic metal, from groundwater in low permeability soils. A laboratory study was conducted to increase the basic understanding of the effect of electro-kinetic phenomena on this chemical species and, subsequently, develop the methodology and technology for large-scale utilization. Equipment was constructed to simulate a system composed of electrode/solvant/membrane/solvant/electrode, where the soil represented the membrane. Experiments were conducted by applying an electrical gradient to the zinc-contaminated soil, which was placed between an anode and a cathode. Removal of metallic zinc from the soil pores to the anode and cathode cells was measured. Diffusion was also allowed between two experiments. Application of electricity appeared to enhance diffusion of zinc into the anode chamber. At the completion of the experiment the concentration of total Zn in the anode chamber increased from 275 mg/l to 745 mg/l and in the cathode chamber from 200 mg/l to 440 mg/l. The experiment consisted of 8 days of diffusion followed by 100 min of electro-osmosis and then 6 days of diffusion followed by 140 min of electro-osmosis. Thirty volts of electricity were applied across the soil specimen in electro-osmosis experiments. Influence of using ligands such as ammonia and hydroxyl ion on removal of zinc was also investigated.

Hazardous waste sites threaten the environment and pose a hazard to the public as potential sources of contamination of groundwater. The migration of contaminants from hazardous waste facilities and spills sites often results in contamination of a large volume of soil. Among the more difficult situations in remediation of such sites are when: the contaminants are strongly adsorbed onto the surface of colloidal soil constituents and when the soil possesses very low permeability. Those situations make it difficult to remove the contaminant by a treatment process or to accomplish in situ remediation.

A potential technology applicable to in situ treatment of hazardous waste sites is electro-osmosis (E-O) (*1–4*). E-O is the transport of water under the influence of an electric current between a cathode and an anode and has been applied successfully in large-scale projects to improve geotechnical properties of fine-grained soils by dewatering and consolidation (*5–8*). The effectiveness of E-O in moving chemicals from anode to cathode has been utilized in grouting fine-grained soils in situations where chemical grouts cannot be transported through the soils by hydraulic pressure. Use of E-O in void-filling practices with colloidal chemicals or gels (e.g., silicates, bentonite, aluminum hydroxide) also has been reported (*9*).

Segall et al. (*10*) applied E-O to dewatering of dredged material. The concentrations of chemical constituents in the leachate generated by gravity forces and in the leachate generated electro-osmotically were compared. The study showed a significant increase in heavy metals and organic materials in E-O-generated leachate when compared with the leachate generated by hydraulic pressure. This is a promising indication that the method may be used effectively for removal of toxic substances typically found at waste sites or in contaminated groundwater.

The study presented in this paper is an attempt to investigate the feasibility of using electro-osmosis to remove zinc from soil. Zinc is an element found abundantly in many industrial wastes. Examples include waste from brass and bronze alloy productions, galvanizing metals, and byproducts of insecticides, glues, rubber, inks, and glass production. Zinc is listed among the 129 priority pollutants by EPA and is known to possess moderate noncarcinogenic toxicity (*11*) and is found frequently in the soil in contaminated sites.

BACKGROUND

On the Concept of Electro-Osmosis

Electro-osmosis is an electro-kinetic phenomena. An electro-kinetic process occurs when two phases move with respect to each other while the interface is the location of an electric double layer. In the motion, for example, between a solid and a liquid phase, a thin layer of liquid adheres to the solid surface, and the shearing plane between liquid and solid is located in the liquid at some unknown distance from the solid surface. Part of the counter ion atmosphere therefore stays with the solid, and part moves with the liquid. The electric double-layer potential at this shearing plane is called electro-kinetic potential or zeta-potential. This potential was shown by Helmholtz in 1879 to be a function of dielectric constant of the liquid medium, thickness of electric double layer, and electrical charge per unit area of particles. According to the Helmholtz-Smoluchowski theory (1914), the electro-osmotic flow rate is directly proportional to zeta-potential, which is directly related to the specific surface of the solid. In clays, total wetted particle surface is very large. Therefore, the rate of electro-osmotic flow should be comparatively large in clay soils.

Some of the important factors that have been identified to influence electro-osmosis follow: electrical potential, current density, solvation of ions, change in the viscosity and dielectric constant of the fluid, *p*H of the system and *p*H gradients, temperature of the system and temperature gradients, surface conductance, and cation exchange capacity of the soil (*12*).

Department of Civil Engineering, Lehigh University, Fritz Engineering Laboratory, Bethlehem, Pa. 18015.

An extension of the Helmholtz-Smoluchowski theory incorporates the surface conductance of a solid in the following equation to calculate the volume rate of electro-osmotic flow (*13*):

$$V = \frac{\varepsilon \cdot i \cdot \zeta}{4\pi\eta\,(\lambda + L\,\lambda_s/s)} \quad (1)$$

where

V = volume rate of E-O flow,
ε = dielectric constant of water,
i = electric current,
η = viscosity of the solvent,
λ = specific conductance of the liquid,
L = circumference of the capillary,
λ_s = specific surface conductance,
s = cross-sectional area of E-O flow, and
ζ = zeta potential.

Previous Investigations

E-O tests were conducted on artificially prepared pure clay specimens in the laboratory to investigate the effects of some of the experimental parameters and procedures on the efficiency of E-O flow. The results and implications of those experiments are reported elsewhere (*14*,*15*). Only a short review will be presented here. The experiments were conducted on Georgia kaolinite clay consolidated from a slurry to about its liquid limit by using tap water as the pore fluid. Prototype equipment (Figure 1) was used to conduct the experiments. (Details of this equipment and the procedure are given in the next section.) Basically, the amount of water flow from the anode chamber into the cathode chamber was measured under an electric current applied through the soil sample. The following results were obtained:

1. E-O permeability of the kaolinite clay used was measured to be 3.3×10^{-5} cm/sec V.
2. E-O flow increased with increasing voltage and attained a maximum value at around 70 V and decreased at higher voltage applications and suggested that there may be an optimum operating voltage for the process for a given soil/electrolyte combination.

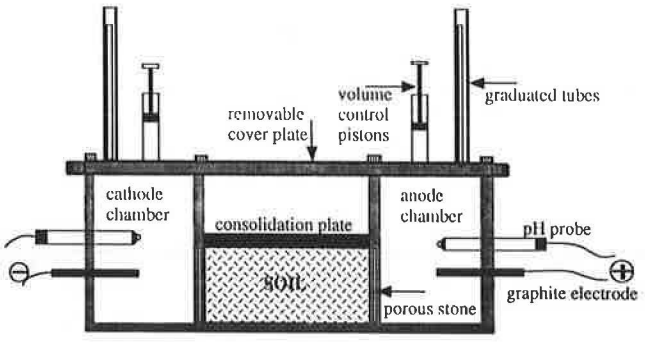

FIGURE 1 Schematic diagram of the electro-osmosis cell.

3. Increased flow was observed when an electrolyte (NaCl) was injected in the anode chamber. Flow increased even more when NaCl was injected in both chambers rather than in the anode chamber only.
4. When Li^+ was used instead of Na^+, the E-O flow increased, possibly owing to the larger hydrated radius of the Li^+ ion.
5. The *p*H values measured after 40 min of application of 30 V across the soil were approximately 9.4 on the cathode side and 4.4 on the anode side.
6. Current reversal experiments resulted in reduced E-O flow in the reverse direction. When cell water was replaced with neutral (*p*H 7) water before the current was reversed, no significant change in the amount of flow was observed. Therefore, *p*H gradients between anode and cathode chambers were suggested to influence the E-O flow.

INVESTIGATION

Experimental Setup

A prototype E-O apparatus was constructed (see Figure 1). The apparatus is rectangular with a 25.2-cm × 6.6-cm base area and 9.6-cm height and is made of transparent acrylic 0.5 cm thick. The box is divided into three chambers separated by acrylic walls, which are fitted with circular porous stones to allow liquid passage. Permeability of the porous stones to water is 10^{-3} cm/sec. The end chambers are the same, each with a volume of 265 cc. The middle chamber is about twice as large as each end chamber, and its length is 15.2 cm.

A graphite electrode and a *p*H-measuring probe are inserted horizontally in each end chamber. One of the chambers contains a heating coil, which was not utilized in this particular set of experiments. The electrodes are connected to a DC power source, and the *p*H probes are connected to a *p*H meter. The middle chamber houses the soil specimen, which is covered by what is called in this paper a "consolidating plate," which was originally intended to consolidate the soil sample in the chamber by applying vertical pressure to a soil slurry and measure deformation by a dial gauge. However, because preconsolidated specimens were used in this study, the consolidating plate was initially used to push and conform the soil pad into the chamber and then was transfixed on to the walls of the chamber with silicon glue just above the soil, which served to confine the specimen and also render the middle chamber water tight at the top. A cover plate is affixed on top of each of the side chambers. A volume control piston (a plastic syringe) and a graduated tube are fitted on each cover plate. The volume control pistons are used to expel gas, agitate water, and collect samples from the chambers. The graduated tubes are used to measure the volume of electro-osmotic flow. The volume of samples withdrawn (2 to 3 cc) is insignificant when compared with the volume of the chambers.

Sample Preparation

Georgia kaolinite clay was used as the soil medium. The liquid limit of this clay was measured to be 60 percent. It was thoroughly mixed with heptahydrate zinc sulfate salt ($ZnSO_4 \cdot 7H_2O$)

in dry form and was made into a slurry by using distilled water. The amount of zinc salt added was 54 gr for every 900 gr of dry clay and resulted in the calculated value of 13,578 mg Zn/kg dry clay.

The slurry was poured into a large one-dimensional consolidation cell and consolidated to 20 KPa vertical pressure. The water content of the soil was 58 percent following consolidation, which was near its liquid limit. The specimen was extracted and trimmed to size to fit the middle chamber of the E-O cell and was gently pushed into the chamber by the consolidating plate. Some degree of compaction might have occurred during this process while the soil was being conformed to the inner walls of the chamber. The final height of the specimen in the chamber was measured to be 5.5 cm.

Measurements and Sample Calculations

A sample of the soil placed in the E-O cell was tested to determine the initial zinc concentration in pore water. A small amount of wet soil sample (4.8 gr dry clay) was diluted to 100 ml of volume with distilled water and then acidified to ensure dissolution of zinc. The concentration of the zinc was measured in an Atomic Absorption Spectrophometer and revealed an initial concentration of 10,166 mg Zn/kg of dry clay, which is lower than the calculated value of 13,578 mg Zn/kg dry clay. Apparently, during consolidation, some of the zinc moved out of the sample with the water. Heptahydrate zinc sulfate is a water-soluble salt. Therefore, it may be relevant to assume that most, if not all, of it dissolved in the initial slurry mixture. With this assumption, the approximate concentration of zinc in the pore fluid of the soil sample can be calculated as follows:

Zinc in 900 gr of soil

$$10{,}166 \text{ mg/kg} \times 0.9 \text{ kg} = 9149 \text{ mg}$$

Water in 900 gr of soil

$$900 \text{ gr} \times 0.58 = 522 \text{ cc}$$

Concentration of zinc in pore water

$$9149 \text{ mg}/0.522 \text{ l} = 17{,}527 \text{ mg/l}$$

Subsequent concentration measurements can be verified easily through a simple calculation by using this initial concentration. As an example, if 5 cc E-O water flows into one of the chambers containing 265 cc distilled water, then,

Zinc in 5 cc E-O water

$$17{,}527 \text{ mg/l} \times 5 \text{ cc} \times 1 \text{ l}/1000 \text{ cc} = 87.6 \text{ mg of Zn}$$

Concentration of Zn in chamber

$$(87.6 \text{ mg}/270 \text{ cc}) \times (1000 \text{ cc}/1 \text{ l}) = 324.6 \text{ mg/l}$$

The actual Zn concentration measurements by using the Atomic Absorption AA Spectrophotometer gave results similar to the ones just calculated.

Progress of the Experiment and Results

Figure 2 illustrates the progress of the experiment over a period of 14 days, which includes two periods of diffusion between two short periods of E-O application. Initially, the anode and the cathode chambers were filled with distilled water with *p*H 7. The zinc was allowed to diffuse from the soil pores into those chambers for 3 days. At the end of this period, the *p*H in both of the cell waters was found to be 5.7. A potential difference of 30 V was applied across the soil sample for approximately 5 min and produced a *p*H difference of 0.4 between the anode and cathode chambers, with the *p*H at the anode of 5.4 and at the cathode of 5.8. Water samples were retrieved from the chambers, and total zinc concentrations were measured. The initial concentrations were 275 mg/l at the anode and 200 mg/l at the cathode.

The first period of diffusion following the start up E-O application of 5 min was 8 days. At the end of this diffusion period, the zinc concentration at the anode had increased to 385 mg/l, and at the cathode it increased slightly to 210 mg/l. Following diffusion, 30 V was applied across the soil for 100 min. Water samples were collected at intervals during this time. Figure 3 indicates the total and aqueous zinc concentration variations with increasing E-O time in the anode and cathode chambers. Total zinc concentration in the cathode cell at end of the 100 min of voltage application increased from 210 mg/l to 475 mg/l and changed little in the anode cell (from 385 mg/l to 405 mg/l). The soluble zinc in those chambers showed similar trends to that of total zinc. After 70 min of voltage application, 0.5 percent NaCl was injected into the anode cell to determine if the contribution of enhanced E-O flow to zinc removal was significant. As is observed from Figure 2, the total and aqueous zinc concentrations increased at a higher rate than before in the cathode cell. Zinc removal rate in the anode chamber was unaffected.

The second period of diffusion of 6 days took place after the 100 min of electro-osmosis. As is observed from Figure 2, the total zinc concentration in the anode chamber increased during this time and remained more or less unchanged in the cathode cell. The rate of diffusion of zinc into the anode chamber in the 8–14-day stretch was observed to be higher

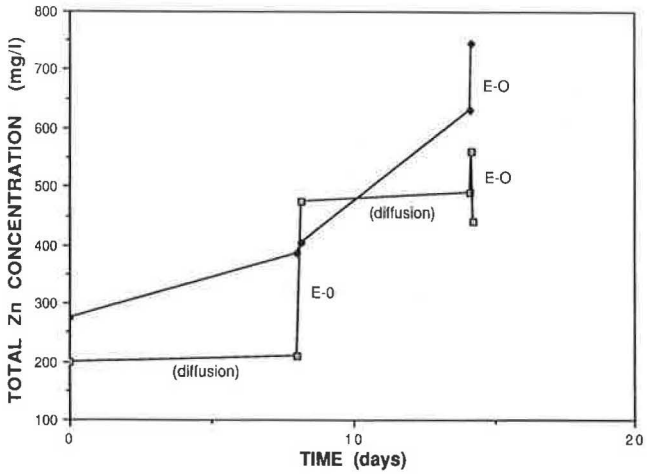

FIGURE 2 Variation of total zinc concentration with time in the anode and cathode chambers during electro-osmosis.

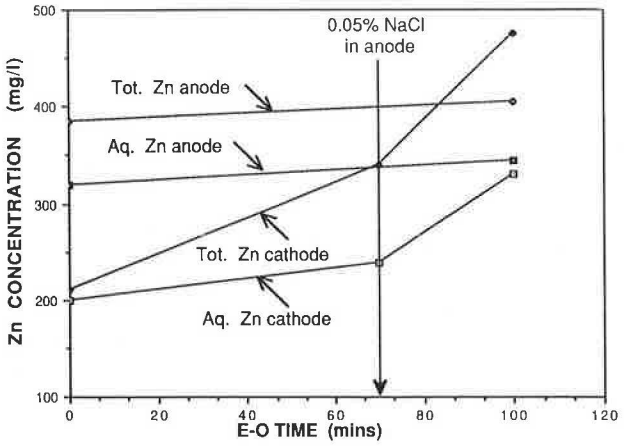

FIGURE 3 Variation of total and aqueous zinc concentration in the anode and cathode chambers during electro-osmosis following the first period of diffusion (8 days).

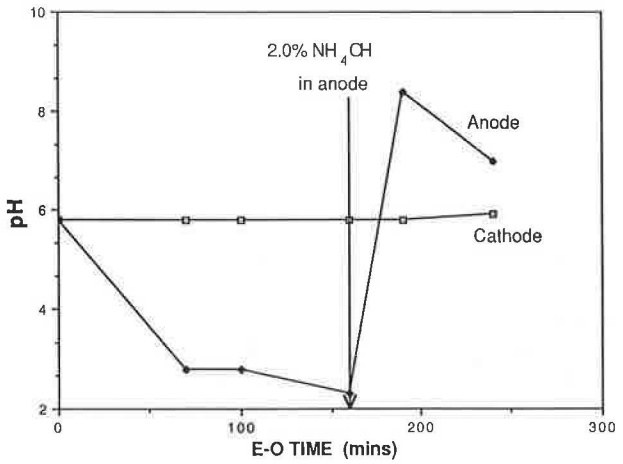

FIGURE 5 Variation of *p*H in the anode and cathode cells with electro-osmosis time.

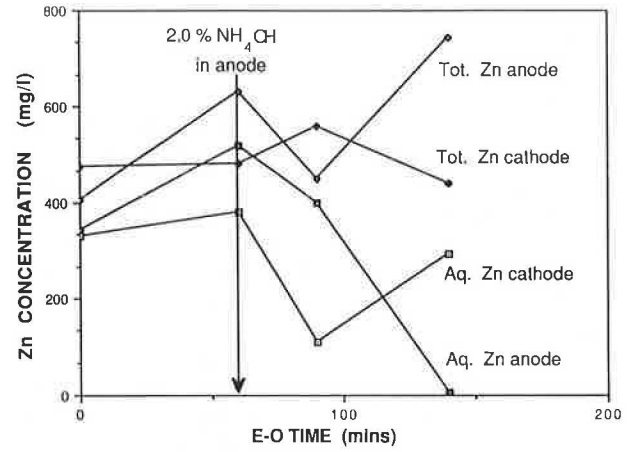

FIGURE 4 Variation of total and aqueous zinc concentration in the anode and cathode chambers during electro-osmosis following the second period of diffusion (6 days).

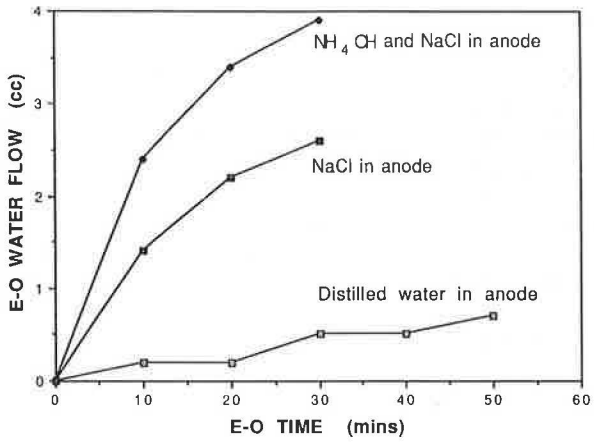

FIGURE 6 Electro-osmotic flow with NaCl and NH_3 as ligand.

than that of the 0–8 day stretch. Following this diffusion period, 30 V was again applied across the soil specimen for a duration of 140 min. Figure 4 indicates the variation of total and aqueous zinc concentrations in the anode and cathode chambers throughout this period of E-O. This time, the concentrations in the anode cell increased but remained more or less unchanged in the cathode chamber for the first 60 min of application of electricity. After 60 min, 2 percent NH_4OH was injected into the anode cell. NH_4OH disassociates in water and forms ammonia, which acts as a ligand with zinc. The ligand was added to determine its net effect on zinc removal and efficiency of E-O flow. The ligand would also release any insoluble zinc by forming positively charged complexes such as $Zn(NH_3)^{2+}(aq)$, $Zn(NH_3)_2^{2+}(aq)$, and $Zn(NH_3)_3^{2+}(aq)$, which would then flow toward the cathode. Addition of NH_3 initially resulted in a slight increase in the total zinc concentration in the cathode chamber but with extended application of electricity the zinc decreased to the final value of 440 mg/l. Total zinc first decreased and then increased to the final value of 745 mg/l in the anode chamber.

The *p*H variation in the cathode and the anode cells during E-O time only is presented in Figure 5. Some of the phenomena observed in Figures 2, 3, and 4 can be explained readily by examining this *p*H variation with E-O. E-O flow to cathode cell was also measured. Both NaCl and NH_4OH influenced E-O flow (see Figure 6). Rate and the total quantity of flow to the cathode cell was enhanced by the addition of those agents when compared with distilled water as pore fluid.

Discussion of Results

In Figure 2, the initial higher diffusion rate of zinc into the anode chamber may be due to the drop in *p*H from 5.7 to 5.4 in this chamber with the initial application electricity of 5 min. This change in *p*H would increase the solubility of zinc com-

pound in the soil adjacent to the anode cell and, in turn, would increase diffusion rate to the anode cell. It is also possible for zinc to form polynuclear complexes containing two or more atoms once it reaches the anode cell and hence increases the concentration of both total and aqueous zinc. The lower rate of diffusion of zinc into the cathode chamber may be explained in part as the effect of the slight *p*H increase from 5.7 to 5.8. Probably, this prevented any zinc dissolution from adjacent soil and migration into the cathode cell. In the second stretch of the diffusion from 8 to 14 days, the rate of zinc diffusion into the anode chamber increased even more. This, again, can be explained by the low *p*H (2.4) of the water in the anode chamber.

Addition of 0.5 percent NaCl in the anode cell increased E-O flow to the cathode cell (Figure 6) and elevated the aqueous and total zinc concentrations at the cathode cell (Figure 2). This indicates that E-O flow is capable of increasing zinc transport from soil pores to the cathode cell.

Previous E-O studies indicate that *p*H at anode and cathode decrease and increase, respectively, during E-O experiments (*14–16*). The cell water at anode becomes acidic with *p*H about 4, and the cell water at the cathode becomes basic with *p*H about 9. It may be noted from observing Figure 4 that the *p*H at the anode reaches the expected acid range with a value of 2.4. However, the cathode cell did not show any appreciable change in the *p*H value. In fact, *p*H remained in the acidic range rather than attaining alkaline values, which may be explained as follows: The anode cell has excess H^+ owing to electrolysis of water and Zn^{++} and SO_4^{--} ions. Because SO_4^{--} is an anion of strong acid, it remains dissociated from H^+ and contributes to lowering the *p*H and, hence, the measure of the *p*H value of 2.4. The chemical species predominant in cathode chamber are Zn^{++}, SO_4^{--}, and excess OH^- from electrolysis of water. If the excess OH^- forms complexes with zinc, such as $Zn(OH)_3^-(aq)$ and $Zn(OH)_4^{--}(aq)$, then it may arrest the increase of *p*H and, hence, little or no change in *p*H. Some zinc might also have precipitated in the form of $Zn(OH)_2$. The water in the cathode cell was observed to take an opaque form, which did indicate some precipitation. The presence of SO_4^{--} also would have contributed to the observed low *p*H.

Addition of NH_4OH into the anode cell neutralized the acid increasing the pH to 8.4. This immediately produced precipitation in the cell. Zinc was removed from aqueous phase, and at *p*H 7 the aqueous concentration of zinc was found to be almost zero. At this time the total zinc in the anode cell remained as precipitate. The total zinc increased in the cathode cell initially, following the addition of NH_4OH. It is not known if this is the result of the removal effect of ammonia forming positively charged complexes in the soil that would move toward cathode or the result of its enhancement of E-O flow. The subsequent drop in total zinc in the cathode cell suggests reverse flow or loss of zinc back into the soil pores. The increased zinc migration toward anode could have taken place if zinc had formed negatively charged complexes in the soil pores, which then would migrate toward the anode. Because hydroxyl ion can act as a ligand, it is likely that negatively charged complexes such as $Zn(OH)_3^-(aq)$ and $Zn(OH)_4^{--}(aq)$ would form and then would move toward anode.

CONCLUSIONS

Zinc migrated to the cathode chamber under the influence of electrical potential, as was expected during the initial part of the experiments. However, total zinc removal was found to be greater at the anode chamber at the completion of the experiment because of the combined effect of higher rate of diffusion of zinc into the anode chamber and also the actions of NH_3 and OH^-, which acted as ligands with zinc. The following observations were made:

1. E-O increases zinc movement to anode cell by increasing dissolution and diffusion. This is attributed to the decrease of *p*H in the anode cell.
2. E-O increases zinc movement to cathode cell by enhancement of transportation of water through the contaminated soil mass. Addition of NaCl and NH_4OH into the anode chamber increased the rate and amount of flow into the cathode chamber.
3. It is potentially possible to apply E-O to zinc detoxification of soils efficiently. However, a number of complex reactions exist that may occur between various chemical species within the soil pores that may hinder or enhance removal or create preferential paths of removal at different stages of the process. Careful examination of those reactions in site-specific situations is needed to understand the process better and to develop the technology for large-scale applications.

REFERENCES

1. I. Demir. *Electrokinetic and Chemical Aspects of Transport of Chloride Brines Through Compacted Smectite Layers at Elevated Pressures.* Ph.D. dissertation, University of Illinois at Urbana-Champaign, 1984.
2. J. F. Ferguson and P. Nelson. Migration of Inorganic Contaminants in Groundwater Under the Influence of an Electric Field. Presented at the USEPA-University of Washington Workshop on Elektrokinetic Treatment for Hazardous Waste Remediation, Seattle, Wash., 1986.
3. J. K. Mitchell. Potential Uses of Electro-Kinetics for Hazardous Waste Site Remediation. Presented at the USEPA-University of Washington Workshop on Electrokinetic Treatment for Hazardous Waste Remediation, Seattle, Wash., 1986.
4. R. F. Probstein and P. C. Renauld. Quantification of Fluid and Chemical Flow in Electrokinetics. Presented at the USEPA-University of Washington Workshop on Electrokinetic Treatment for Hazardous Waste Remediation, Seattle, Wash., 1986.
5. L. Bjerrum, J. Moum, and O. Eide. Application of Electro-Osmosis on a Foundation Problem in Norwegian Quick Clay. *Geotechnique*, Vol. 17, No. 3, 1967, pp. 214–235.
6. L. Cassagrande. *Review of Past and Current Work on Electro-Osmotic Stabilization of Soils.* Harvard Soil Mechanics Series 45, Harvard University, Cambridge, Mass., 1959.
7. D. H. Gray and J. K. Mitchell. Fundamental Aspects of Electro-Osmosis in Soils. *Journal of Soil Mechanics and Foundations Engineering Division*, ASCE, Vol. 93, No. SM6, 1967, pp. 209–236.
8. J. K. Mitchell. In-Place Treatment of Foundation Soils. *Journal of Soil Mechanics and Foundations Engineering Division*, ASCE, Vol. 96, No. SM1, 1970, pp. 73–109.
9. J. K. Mitchell. Soil Improvement: State-of-Art-Report. *Proc., Tenth International Conference on Soil Mechanics and Foundation Engineering*, Stockholm, Vol. 4, 1981, pp. 509–565.
10. B. A. Segall, C. E. O'Bannon, and J. A. Matthias. Electro-Osmosis Chemistry and Water Quality. *Journal of Geological Engineering*, ASCE, Vol. 106, No. GT10, 1980, pp. 1148–1152.

11. *Report 600/2-87/035*, U.S. Environmental Protection Agency, Washington, D.C., June 1987.
12. H. W. Olsen. Osmosis and Geomechanical Processes. Presented at Clay Minerals Society Annual Meeting, Baton Rouge, La., 1984.
13. A. Kitahara and W. Akira. *Electrical Phenomena at Interfaces*. Vol. 15, Mercel Dekker, New York, 1984.
14. L. I. Khan and S. Pamukcu. Validity of Electro-Osmosis for Groundwater Decontamination. *Proc., 1989 Specialty Conference*, ASCE, Austin, Texas, 1989, pp. 563–570.
15. L. I. Khan, S. Pamukcu, and I. J. Kugelman. Electro-Kinetic Mechanism in Saturated Contaminated Fine Grained Soil. In *Environmental Geotechnology*, Vol. 1, Envo, Allentown, Pa., 1989, pp. 39–47.
16. Y. B. Acar, R. W. Gale, G. Putnam, and J. Hamed. Electro-Chemical Processing of Soils: Its Potential Use in Environmental Geotechnology and Significance of pH Gradients. In *Environmental Geotechnology*, Vol. 1, Envo, Allentown, Pa., 1989, pp. 25–38.

Publication of this paper sponsored by Committee on Physicochemical Phenomena in Soils.

Use of Waste and By-Products in Highway Construction

W. C. Ormsby and D. G. Fohs

The technologies for using many waste materials including industrial, domestic, and mining/metallurgical wastes were developed by the Federal Highway Administration during the 1970s. Studies on fly ash, bottom ash, incinerator residue, sulfate wastes, digested sewage sludge, coal mine refuse, waste rubber, and cement manufacturing wastes have been completed. Materials investigated were stabilized with various binders including lime, lime-fly ash, asphalt cement, and portland cement. Both laboratory evaluations and field tests were performed. Many of the systems evaluated developed strength and other physical properties adequate for use in embankments, subbases, and bases. Some materials (e.g., fused incinerator residue) were technically adequate for use in bituminous concrete-wearing surfaces. While the emphasis of the research was on engineering behavior, assessments of economic and environmental factors were made in some cases. Information generated should be of interest and of use today when more and more emphasis is being placed on saving the environment from further desecration.

The FHWA has had an interest in waste and by-product utilization since the mid 1950s. Early work concentrated on the properties and utilization of various fly ashes and fly ash-containing systems (*1*,*2*). In the early 1970s, several events gave impetus to the development of a comprehensive research program on waste and by-product utilization in highway construction. First, the president, in his 1970 Environmental Message, stated the need to encourage more recycling and requested the Council on Environmental Quality to develop proposals in this area. Second, the Oil Embargo of 1973 demonstrated the need to conserve energy and to develop alternative materials to supplement or replace asphalt cement. Finally, a large by-product utilization demonstration project at Dulles International Airport was sponsored by FHWA (*3*,*4*) that demonstrated that many by-product materials had potential for use as paving binder and aggregate supplements or replacements. On the basis of those and other events (e.g., the Clean Air Act of 1970) the FHWA developed a research program entitled "Use of Waste Materials for Highways."

FHWA's research program was designed to evaluate a wide spectrum of by-products that, in general, were technically promising as aggregate or binder supplements or replacements. Economics and environmental concerns were also considered. In some cases, materials with little or no potential for use as a highway material (e.g., sewage sludge) were evaluated to address an immediate, critical, and specific highway problem.

Federal Highway Administration, U.S. Department of Transportation, Turner-Fairbank Highway Research Center, 6300 Georgetown Pike, McLean, Va. 22101.

This paper will describe research and development efforts undertaken by FHWA and others to develop the technologies needed to utilize wastes and by-products in highway construction. A tabulation of various materials investigated is given in Table 1 (recycled asphalt cement and portland cement concrete pavements are outside the scope of this paper).

INDUSTRIAL WASTES

Sulfate Wastes

Transpo 72

A large-scale waste utilization project was constructed in connection with Transpo 72, an International Transportation Exposition held at Dulles International Airport in 1972. Approximately 90,700 tonnes of primarily waste products were used in constructing a 40.5 hectare parking lot. The basic composition used consisted of fly ash, dolomitic lime, sulfate wastes [acid mine drainage (AMD), flue gas desulfurization sludge (FG), and fluorogyp (FLG)], limestone aggregate, and water. The dry ingredients were formulated as follows: 80.5 percent fly ash, 15 percent limestone aggregate, 2.5 percent dolomitic lime, and 2 percent sulfate waste. In addition to the fly ash-lime-sulfate-aggregate-water system, other materials tested included crushed glass, shredded tires, incinerator residue, and crushed storage batteries. Figures 1 and 2 present the plant layout for the production of the lime-fly ash-sulfate-aggregate material and the paving operation, respectively. The demonstration project indicated that satisfactory mixtures of the waste materials could be produced in a portable plant and that a suitable pavement could be constructed. However, localized failures indicated that further study was needed to develop the optimum conditions for compaction and strength development in the field. Additional studies involving multiple waste utilization follow.

Lime-Fly Ash-Sulfate Technology

On the basis of the Transpo 72 demonstration and the work of Minnick (*5*), the FHWA sponsored a comprehensive laboratory study of lime-fly ash-sulfate mixtures. This study, conducted by the Gillette Research Institute, developed the technology required for the use of sulfate wastes in highway construction, primarily in base courses and embankments. A comprehensive evaluation was made of the pertinent properties of mixtures composed of a variety of sulfates, fly ashes,

TABLE 1 MATERIALS EVALUATED IN FHWA RESEARCH AND DEVELOPMENT PROGRAM ON WASTE AND BY-PRODUCT UTILIZATION

Industrial	Municipal/Domestic	Mining
Sulfate Wastes	Incinerator Residue	Coal Mine Refuse
Cellulosic Wastes	Sewage Sludge	
Wood Lignins	Scrap Rubber	
Bottom Ash		
Fly Ash		

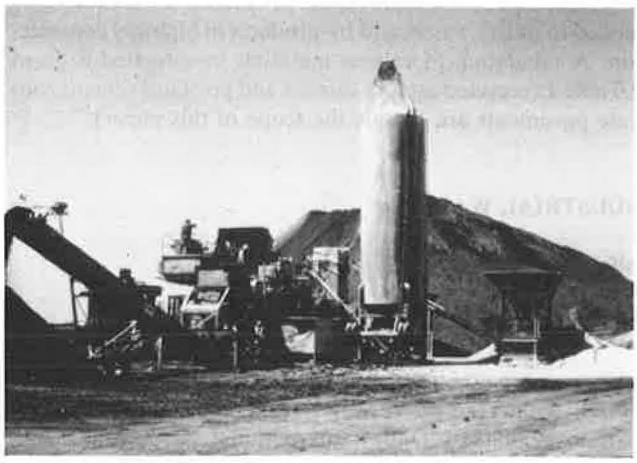

FIGURE 1 Transpo 72 plant layout for lime-fly ash-sulfate waste-aggregate pavement mixture preparation.

FIGURE 2 Transpo 72 paving operation (compaction).

and limes. Properties of sulfate wastes are given in Tables 2 and 3. Compositions and properties of the mixtures studied are given in Tables 4 and 5, respectively.

One of the more significant observations, in keeping with some of Minnick's findings (*5*), was that sulfate waste can serve to enhance the strength characteristics of lime-fly ash mixtures. Specifically, modest additions of sulfate will increase the rate of strength gain and will also increase the final strength. Increased early strengths are due to the formation of ettringite. Figure 3 illustrates the effect of gypsum on strength development in a lime-fly ash mixture moist cured for 7 and 28 days. Mixtures of the type represented in this figure, in addition to having acceptable strength properties, had high California Bearing Ratios, low permeabilities, and slightly less than adequate durability properties.

The following conclusions were reached:

1. Properly proportioned, compacted and cured mixtures produce a strong, rigid material that may be used in applications such as embankments, subbases, and bases.
2. Compacted lime-fly ash-sulfate formulations are normally lighter in weight than most compacted soils and would be a real advantage on soft, compressible ground.
3. Mixtures studied were quite impervious, indicating that selected formulations can be employed in dikes, lagoons, and levees.
4. Durability of the mixtures, as was measured by freeze-thaw and wet-dry tests, was poor for 7 days curing at 23°C. Durability of compacted mixtures for pavement components must be considered in cold climate applications.

The study delineated the range of formulations that could be prepared with acceptable strength, permeability, and leachability properties (*6–8*). Later research on fly ash-lime-phosphogypsum mixtures confirms and amplifies the results obtained by the Gillette Research Institute. Laboratory studies indicated the following composition as being highly satisfactory for subbase construction: 91 percent fly ash, 4 percent quicklime, and 5 percent industrial gypsum (phosphogypsum) (*9*). This mixture, prepared in a continuous mixing plant, has been successfully used in road installations in several locations in France, the earliest in 1969, and has performed well for several years.

Remedial Treatment of Soils

Research by Midwest Research Institute was performed to evaluate the feasibility of disposing sulfate waste in soils and the use of various power plant and other sulfate wastes for soil stabilization. This research consisted of a laboratory study to evaluate the effects of sulfate (sulfite) wastes on the engineering properties of fine-grained soils. The various sulfates studied included (a) phosphogypsum (PG) derived from treating phosphate rock with sulfuric acid to produce phosphoric

TABLE 2 PROPERTIES OF SULFATE WASTES

	Waste Source						
	Acid Mine Drainage	Rutile Mfgre	HF By-Product	FGD(1)[a]	Spent Pickle Liquor[b]	FGD(2) Lime-stone	FGD(3) Lime
Physical form and color	reddish brown slurry	grey solid dispersed in green soln.	white lumpy solid	thick grey slurry	reddish brown	--[c]	--
sulfate form	$CaSO_4 \cdot 2H_2O$	$CaSO_4 \cdot 2H_2O$	$CaSO_4 \cdot 2H_2O$+ $CaSO_4$	$CaSO_4$+ $CaSO_3$	$CaSO_4 \cdot 2H_2O$	$CaSO_4$+ $CaSO_3$	$CaSO_4$+ $CaSO_3$
"Impurities"	$Al(OH)_3$ $Fe(OH)_3$ $CaCO_3$	TiO_2	CaF_2	Fly Ash SiO_2 Al_2O_3	$CaCO_3$	Fly Ash SiO_2 Al_2O_3	Fly Ash SiO_2 Al_2O_3
pH	9.6	2.5	9.0	11.3	8.7	--	--
Free H_2O %[d]	57	41	0	24	63	--	--

[a] FGD: flue gas desulfurization waste.
[b] Pickle liquor: a waste product resulting from the cleaning of metals with acid.
[c] data unavailable.
[d] Free water: any water which is not combined as water of hydration.

TABLE 3 PARTIAL CHEMICAL ANALYSIS OF SULFATE WASTES (OXIDES, PERCENT BY WEIGHT)

	Waste Source							
	Acid Mine Drainage	Rutile Mfgre	HF By-Product	FGD(1)	Spent Pickle Liquor	FGD(2) Lime	FGD(3) Lime-stone	Phosphogypsum
SiO_2	1	17	12	19	1	4.9	1.8	0.3
FeO_3+Al_2O_3	7	4	2	18	9	4.0	2.0	0.7
CaO	7	20	54	28	16	43.2	25.0	40.4
SO_3	4	13	43	5	1	5.9	6.4	54.3
SO_2	--[a]	--	--	--	--	33.0	11.6	--

[a] data unavailable

acid, (b) sulfates from flue gas desulfurization, (c) acid mine drainage wastes, and (d) spent bed material from the fluidized bed combustion of coal (SBM). The wastes were evaluated for their effects on the strengths, consistency limits, freeze-thaw durability, and volumetric stability of 30 soil samples representing the predominant soil series indigenous to various waste sources.

Analysis of the results indicated that PG, FG, and AMD had little effect on mixture properties. However, when those wastes were used in combination with lime, lime-fly ash, or cement kiln dust, higher strengths were achieved than when lime was used with the test soils. The higher the sulfate content of the waste, the stronger the mixture. In summary, the results demonstrated that PG, FG, and AMD can be used to enhance

TABLE 4 FORMULATIONS USED IN EVALUATING PROPERTIES OF WASTE SULFATE: FLY ASH-LIME MIXTURES

Waste Type	Calcitic Lime, percent	Waste, percent	Fly Ash, percent
Pure Gypsum	4.7	9.3	86.0
Acid Mine Drainage	5.0	15.0	80.0
HF By-product	4.0[a]	11.0	85.0
Titangypsum	5.0	12.0	83.0
FGD (2)	5.0	19.0	76.0
FGD (3)	5.6	32.8	61.6

TABLE 5 PROPERTIES OF WASTE SULFATE: FLY ASH-FLY ASH MIXTURES

	Compressive Strength kN/m^2			Tensile Strength kN/m^2			Permeability, x 10^{6}cm/sec at 20 °C		CBR percent	
	7days	28days	91days	7days	28days	91days	7days	28days	7days	28days
Pure Gypsum	3651	13918	15813	782	1654	3583	3.79	9.45	346	617
Acid Mine Drainage	2756	5030	7648	482	1171	1275	2.51	7.72	208	381
HF By-product	3307	7269	7992	586	1033	689	7.19	4.27	300	487
Titangypsum	2170	7889	7820	379	1344	1550	5.02	0.82	350	-- [a]
FGD (2)	2790	4237	9715	482	872	1137	16.5	17.0	226	335
FGD (3)	1240	5202	7407	139	1102	1447	36.1	5.91	126	376

Samples moist cured at 23 °C.
[a] Data unavailable.

the rate and magnitude of strength development of soil-lime mixtures. Results with SBM indicated that it is equally effective as lime for soils treated in this study. Results of the research are given in three reports (*10–12*).

Lime and Cement Kiln Dusts

Waste material from lime and cement manufacture accumulates at a rate in excess of 18 million tonnes a year. Some of those materials are recycled, used for acid effluent neutralization, used in landfill stabilization, or used in soil stabilization, but most (approximately 70 percent) of the material is landfilled. To promote more widespread utilization of those materials, the FHWA conducted a study to determine the effectiveness of substituting kiln dusts for hydrated lime in lime-fly ash-aggregate (LFA) road bases (*13*).

A large selection of lime and cement kiln dusts (KD) and fly ashes (both class F and class C) was obtained and characterized chemically and mineralogically. Optimum kiln dust/fly ash ratios were established, and engineering properties were evaluated. Engineering properties of kiln dust-fly ash-

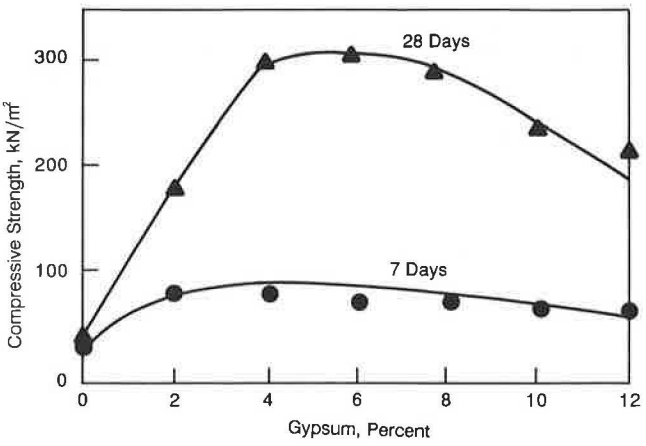

FIGURE 3 Variation in strength of lime-fly ash mixtures with varying gypsum content for 7 and 28 days curing.

aggregate (KDA) mixtures evaluated included compressive strength, durability, dimensional stability, autogenous healing, and resilient modulus.

Conclusions of the study are as follows:

1. KD are generally capable of being substituted for hydrated lime in LFA road base compositions. The possible exceptions are cement KD with high sulfate or alkali content or lime KD with very high levels of free lime.
2. KDA mixes generally develop higher early strength than do conventional LFA mixes and provide equal or better durability and volume stability characteristics. KDA mixtures are capable of autogenous healing although not as strongly as in LFA mixtures.
3. Generally, concentrations of KD required are higher than lime, meaning that greater quantities of KD are needed to react with fly ash.

The final report for the study provides detailed recommendations with regard to KD and KDA evaluation and mixture design procedures. Included in the recommendations are KD screening tests, KD-fly ash-aggregate mixture design, logistical considerations, and mixing and placement considerations.

Cellulosic Wastes

The possibility of using cellulosic wastes as a pavement binder material was investigated in a contract with SUNTECH, Inc., of Marcus Hook, Penn. (*14*) to develop and evaluate processes for converting cellulosic and related wastes into road binder materials and to evaluate the performance of such materials alone and in mixtures with aggregates.

A detailed evaluation of the supply, availability and geographic distribution of cellulosic wastes was made. Various wastes evaluated included agricultural wastes (crop residues, animal manure, foresting wastes), manufacturing wastes (food processing and wood and paper industry), and urban refuse (municipal solid waste and manufacturing plant trash). Following this evaluation, a consideration of process feasibility (e.g., pyrolysis, liquefaction, and hydrolysis) was made. Secondary processes such as distillation, extraction, air blowing, hydrotreating, and blending (with asphalts) were also considered. Finally, a study of product performance was made and involved previously reported results plus extensive experimental studies needed to complete the evaluation. After completing the survey, process feasibility study, and product performance evaluation, the following conclusions were drawn:

1. An estimated 74 $\times$ 10^9 kg/year of cellulosic waste is available for processing.
2. Pyrolysis is the preferred method for converting cellulosic waste to substitute binder material.
3. Pyrolysis products are not suitable for direct use in highway binder applications. Rheological properties do not meet performance criteria, and the products are not compatible with asphalt.
4. Hydrogenation of wood pyrolysis products improves their compatibility with petroleum asphalt.
5. A pyrolysis-hydrogenation procedure could be cost effective in a 909 tonnes/day waste-processing facility.
6. Hydrogenated pyrolysis oil is suitable for use as an extender of asphalt in paving operations.
7. The durability of a wearing surface mixture containing hydrogenated pyrolysis oil was not significantly different from that containing the reference asphalt cement.

Wood Lignins

Wood lignin is high-volume waste produced in the manufacture of paper products. An examination of the feasibility of converting lignin to a highway binder material was investigated in a study entitled, "Evaluation of Wood Lignin as a Substitute or Extender of Asphalt" (*15*). The study evaluated the use of lignin in three different applications: (a) alone as a substitute for asphalt, (b) as an extender for asphalt in hot mixes, and (c) as an extender of emulsified asphalt in conjunction with rubber in cold mixtures.

Principal conclusions of the study follow:

1. The utilization of wood lignin alone as a substitute paving binder is not feasible, and the conclusion was reached after an extensive program of chemical and physical treatments ("formulations").
2. Using lignin material to extend asphalt seems feasible with a 30 percent replacement possible with no sacrifice in physical properties. Paving mixtures prepared with lignin-asphalt material require a slightly higher binder content than does conventional asphalt cement concrete.
3. Suitable lignin-asphalt binder formulations were prepared from lignins from both major manufacturing processes (i.e., kraft and sulfite processes).
4. Because lignin-asphalt binders are somewhat stiffer than asphalt alone, precoating of the coarse aggregate is recommended, and also permits a reduction in binder content.
5. Coal tar, coal, kraft liquor, or carbon black generally enhance the reaction between lignin and asphalt and allow a lower binder content.
6. Kraft lignin appears to be suitable as a partial replacement of asphalt in emulsified asphalt paving mixtures.

7. Kraft lignin appears to be insoluble in asphalt.
8. Lignins are environmentally stable from a leaching standpoint.
9. On the basis of laboratory mixture characterization, on a comparison of expected behavior by using elastic layer theory, and on the predictive computer program, VESYS IIM, it appears that pavement mixtures using lignin-asphalt materials can be designed to match those from conventional materials.

Bottom Ash

Problems associated with using various power plant bottom ashes in pavement construction were comprehensively investigated in the laboratory to evaluate the feasibility of using bottom ashes as a partial or full substitute for natural aggregate in bituminous mixtures and to develop detailed guidelines for implementation of the findings.

Detailed results of the study and recommended guidelines for the selection of materials, testing, mixture design, evaluation of performance parameters, and quality control are summarized in two publications (*16*,*17*). The principal conclusions follow:

1. Bottom ash-asphalt mixture properties are dependent on ash content. In general, as the ash content is increased, the optimum asphalt content is increased, the mixture density is decreased, and the voids and voids in mineral aggregate are increased.
2. In bituminous mixtures the mixture stability of ash-containing compositions decreases up to an ash content of about 30 percent, and further additions do not effect significant changes in the stability.
3. Resilient moduli for ash-aggregate-asphalt mixtures are low and Poisson ratios are approximately equal when compared with standard asphalt mixtures.
4. Fatigue life and fracture toughness of ash-aggregate-asphalt mixtures increase with ash and asphalt content, and rutting susceptibility and plastic deformation also increased with higher ash and asphalt content.
5. Ash-aggregate-asphalt mixtures have a high resistance to moisture damage (immersion-compression) and environmental conditioning (samples were tested dry, saturated, and after freeze-thaw cycles).
6. It was concluded from the data and test results presented that the properties of most wet and dry bottom ashes can meet performance specifications for conventional aggregates and that those materials can be used successfully in pavement construction.

Fly Ash

As was mentioned previously, FHWA has had a long-standing interest in fly ash and fly ash–containing systems. The use of fly ash alone or in combination with, for instance, lime, sulfate wastes, or soils, has been described in many FHWA publications based on staff, Highway Planning and Research (HP&R), contract, and NCHRP studies.

Guidelines designed to promote the use of fly ash in highway construction and maintenance were developed for FHWA by General Analytics, Inc. (*18*). The guidelines provide details and examples of the use of fly ash in various highway applications such as pavements, embankments, backfills, and grouts.

FHWA's Demonstration Projects Division in 1981 initiated Demonstration Project No. 59, "The Use of Fly Ash in Highway Construction" (*19*), to promote the use of fly ash in various applicable types of highway construction processes. This project offered technical assistance and financial incentives to states willing to construct and evaluate pilot demonstration projects. As part of the technical assistance, an informative booklet, *Fly Ash Facts for Highway Engineers*, was prepared and given distribution (*20*). To date, approximately 20 projects have been constructed.

In response to Congressional requirements and incentives (*21–23*) and an Environmental Protection Agency Guideline (*24*), discriminatory clauses against the use of fly ash in portland cement concrete (PCC) have been removed. All states now allow the use of fly ash in PCC on federal-aid projects. Instructions to effect implementation of Section 117(f) of the Surface Transportation and Relocation Act of 1987 (*23*), which provides for increase in the federal-aid matching ratio for highway projects using significant amounts of fly ash or bottom ash, are given in FHWA Notice N 5080.109 (*25*). Also, guidelines and recommendations for the use of fly ash and bottom ash in bases and embankments are given in FHWA Technical Advisory 5080.9, *Use of Coal Ash in Embankments and Bases* (*26*).

In 1982, FHWA's Eastern Direct Federal Division administered a $19 million road building project for the Federal Aviation Administration and involved a 6.0-km extension of the Dulles Access Highway from its terminus at Route 123 to its intersection with I-66. Special features of the project included the use of 37,000 m^2 of 15-cm lime-fly ash base and the use of fly ash–modified concrete for the substructure of the eastbound bridge of Old Chain Bridge and Route 123. Details of the project are given in the literature (*27*).

From those examples it is apparent that FHWA's involvement in fly ash use has been continuous and comprehensive, encompassing research, implementation, demonstration, and significant construction projects. This interest will continue, especially with the recent groundswell of concern for increased use of by-products and recovered materials.

MUNICIPAL/DOMESTIC WASTES

Incinerator Residue

Several studies were performed and demonstration projects built to evaluate the technical merits of using incinerator residue as a total or partial aggregate replacement in paving mixtures. (ASTM Committee E-38 defines incinerator residue as all of the solid material collected after an incineration process is completed, comprising ash, metal, glass, ceramics, and unburned organic substances. Residue is the solid material remaining after burning.) Additionally, a process was developed for fusing incinerator residue to produce a high quality aggregate material (*28*,*29*). Material produced by using this process performed well in a bituminous surface course installation in Harrisburg, Penn. (*30*).

A comprehensive effort addressing the potential for using incinerator residue in various highway applications was completed in December 1976 (*31,32*). In this study a nationwide survey of incinerator locations and types was made, samples of residues were collected and were characterized physically and chemically, bituminous mixture designs were developed for base and surface course application, and field test installations were made. Those installations were experimental wearing surfaces composed of a 50-50 blend of residue and natural aggregate. The installations were placed in Philadelphia, Penn.; Delaware County, Penn.; and Harrisburg, Penn. (Table 5). The first two installations performed satisfactorily during the monitoring period (1 year), and the Harrisburg installation suffered considerable stripping of asphalt from the residue. None of the test installations was subjected to heavy traffic. Evaluation of those demonstration test results, along with literature and test evaluations of other possible applications, including portland cement mixes, lime- and cement-stabilized incinerator residue for base course applications, controlled fill, and subgrade use, resulted in the following recommendations:

1. Incinerator residue compositions can be mixed, placed, and compacted by using conventional bituminous construction apparatus and procedures.
2. Residues should be well burned out (less than 10 percent loss on ignition).
3. Bituminous paving mixtures for base course applications composed of approximately 50 percent natural aggregate and 2 percent lime hold the most promise for residue use.
4. Incinerator residue can be used in lime- or cement-stabilized base course mixtures.
5. The use of incinerator residue in portland cement mixtures is not recommended (excessive volume changes result from the reaction of aluminum to produce hydrogen).

Several installations using incinerator residue as an aggregate were made (Table 6) before, and subsequent to, this study. Details of those installations are given in the literature (*33–38*). Figure 4 presents the paving operation at the Washington, D.C., site.

Sewage Sludge

Sewage sludge, after some form of primary treatment including digestion, consists of a low solids content dispersion of variable viscosity, depending on the moisture content. It is generally dark brown or black in color, and, although it may contain up to 10 weight percent of twigs, cigarette butts, and rubber, it frequently has the appearance of a fairly homogeneous suspension. Sewage sludge generally has a solids content between 5 and 10 percent by weight, although some lagooned sludges may have over 40 percent solids. Table 7 presents data obtained from lagooned sewage sludge from southwest Philadelphia lagoons. This material was of interest

TABLE 6 INCINERATOR RESIDUE TEST INSTALLATIONS

Project	Date	Residue Percent	Asphalt Cement Percent	Lime Percent	Length Meters	Thickness Centimeters	Performance
Houston, TX	1974	100	9.0	2.0	61	15 base	excellent
Phila., PA	1975	50	7.4	2.5	30	3.8 surface	acceptable
Delaware Co., PA	1975	50	7.0	2.5	18	3.8 surface	acceptable
Harrisburg, PA	1975	50	7.0	2.5	73	3.8 surface	poor
Harrisburg, PA fused residue	1976	100	6.7	0.0	55	3.8 surface	excellent
Washington,D.C.	1977	70	9.0	2.0	122	11.4 base	good
Lynn, MA	1979	50	6.5	2.0	approx. 1610	3.8 binder and surface	excellent

(a)

(c)

(b)

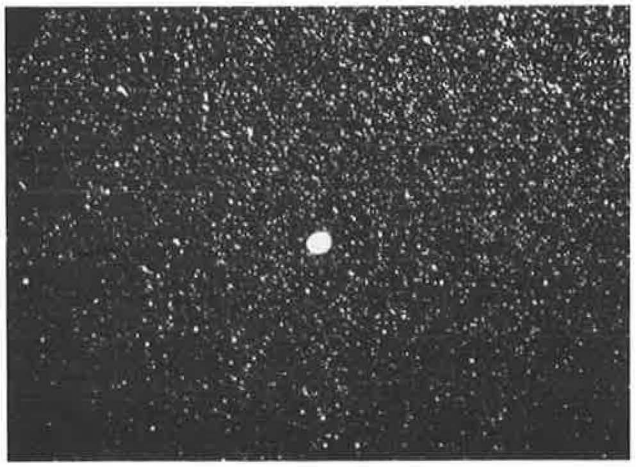

(d)

FIGURE 4 Paving with municipal incinerator residue, Washington, D.C. (a) Paver. (b) Placement. (c) Compaction. (d) Finished base (close up).

TABLE 7 TYPICAL ANALYSIS OF SEWAGE SLUDGE FROM PHILADELPHIA LAGOONS

Solids, percent	23.45
Ash, percent	13.58
Volatile solid, percent	41.61
Heat of Combustion, cal/gm	1995
Oil and Grease, g/kg	55.38
Zn, ppm Zn^{2+}	2637
Cu, ppm Cu^{2+}	809
Cr, ppm Cr(VI)	1458
Pb, ppm Pb^{2+}	1713
Cd, ppm Cd^{2+}	22
Hg, ppm Hg^{2+}	196

because a proposed roadway was to be built across the lagoon and it was theorized that the sewage sludge might have some use as a highway construction material. Laboratory tests incorporating digested sewage sludge in lime-fly ash sulfate mixtures were performed first by I.U. Conversion Systems, Inc. (*39*) of Plymouth Meeting, Penn., and later by the FHWA. Compositions were developed that had strengths adequate for embankment construction, low permeabilities, and, after suitable curing periods, acceptable leaching characteristics.

To explore the possibility of using digested sewage sludge in road embankment construction, I.U. Conversion Systems, Inc., constructed a demonstration embankment at Bridgeport, Penn. (Figure 5) that was composed of a mixture of sewage sludge, fly ash, soil, lime, and waste sulfate. The embankment was approximately 45 m long by 2.4 m wide by 0.9 m high. The embankment was placed in five lifts, each

(a)

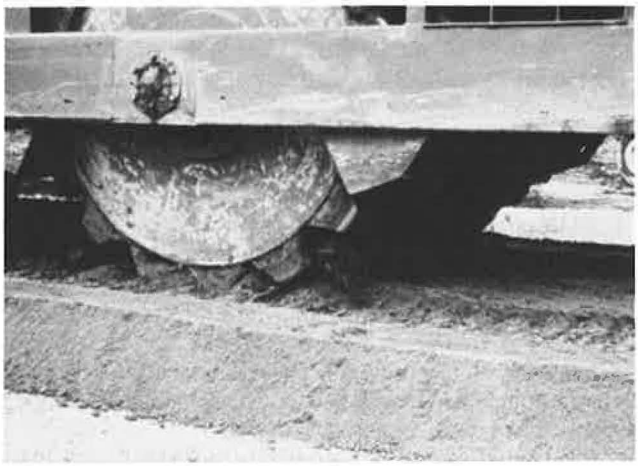

(b)

FIGURE 5 Test embankment construction, using sewage sludge. (a) Compaction. (b) Compaction (close up).

lift separately compacted. Cores were taken from the embankment after 90 days of curing for unconfined compressive strength, wet-dry stability, and freeze-thaw durability tests. Additional cores were taken and tested for leaching characteristics. Results of those tests showed the material to have acceptable properties with the exception of freeze-thaw resistance.

Additional detailed laboratory experiments on lime-fly ash-soil-sulfate-sewage sludge mixtures were performed by the Gillette Research Institute (*40*) and tests substantiated and amplified the information just summarized. The following conclusions were drawn:

1. Generally speaking, small but significant amounts of digested sewage sludge (e.g., 10 percent by dry weight of the mix) incorporated in lime-fly ash (or soil)-sulfate formulations and properly cured will result in products with strengths suitable for embankment construction.
2. The embankment material produced has acceptable permeability and leaching characteristics.
3. Freeze-thaw resistance and wet-dry stability of the embankment material are marginal, and, therefore, embankments constructed by using the material should be capped with approximately 1 m of soil.
4. The possible large-scale utilization of digested sewage sludge in embankments construction should be based on tests performed by using materials indigenous to the embankment test site.

Scrap Rubber

The FHWA has had an interest in the reuse of waste rubber for a number of years. Initially, assessments suggested that the small amounts, remote locations, and excessive collecting and processing costs would preclude any possible benefits that could be accrued in using waste rubber. Therefore, in the early and middle 1970s, research and demonstration studies were limited to HP&R efforts. Most of those studies were performed by the Arizona Department of Transportation and were given impetus by the pioneering work of C. H. McDonald (*41*).

In the late 1970s a demonstration project, "Discarded Tires in Highway Construction" (*42*), was initiated. By 1980, several test sections using asphalt-rubber had been constructed and included projects in which asphalt-rubber was used in chip seals, interlayers, and bridge deck sealing. Discarded tires were also evaluated for use in embankments and it was concluded in 1981 that asphalt-rubber membranes offer viable alternatives to conventional materials for rehabilitation of some asphaltic concrete pavements and that, in many cases, asphalt-rubber chip seals or interlayers can be advantageously used to ameliorate fatigue-type cracking in bituminous pavements (*43*).

A recent critical evaluation of asphalt-rubber systems was performed under a national pooled fund study (*44*). Over 200 experimental rubber-modified pavements were evaluated relative to their performance compared with control sections. The following pavement applications were evaluated:

1. Asphalt-rubber seal coats,
2. Asphalt-rubber interlayers,
3. Rubber-filled asphalt concrete,
4. Asphalt-rubber friction course,
5. Asphalt-rubber concrete, and
6. Rubber-filled friction course.

Those systems are outlined in Figure 6.

The results of the study are summarized graphically in Figure 7 (*45*). In the first two applications the experimental sections performed the same or worse in approximately 80 percent of the sections. In the third application, the experimental sections performed the same or better in approximately 95 percent of the sections. Too few sections were evaluated to permit definite conclusions in the remaining applications.

In summary, no conclusive evidence exists that asphalt-rubber systems are generally superior to conventional asphalt cement materials. It is important to note that the study was conducted on a nationwide basis. The generally favorable performance of rubber-asphalt systems in tests in Arizona is in contrast to the pooled-fund study results, suggesting that

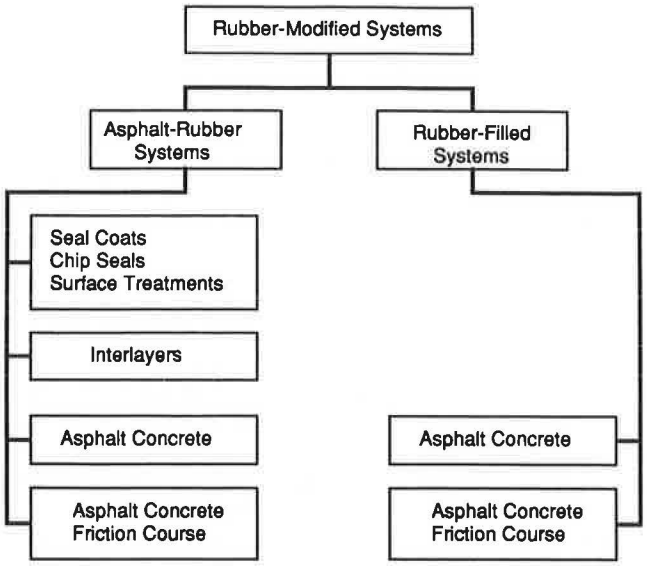

FIGURE 6 Classification of rubber-modified asphalt paving materials.

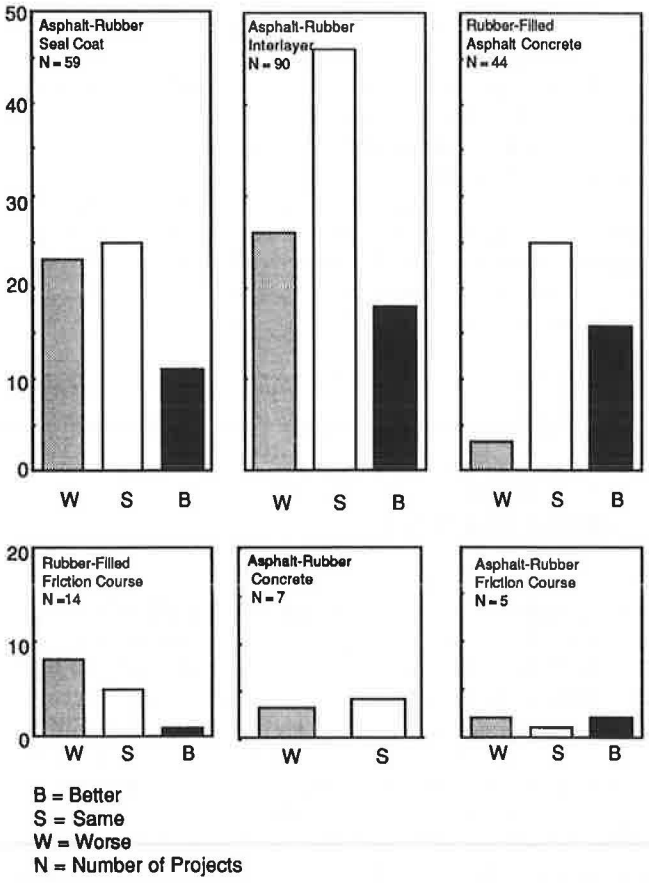

FIGURE 7 Project performance by application, in the national-pooled fund study on rubber-modified asphalt pavement tests.

climatic conditions may be of considerable importance in asphalt-rubber system performance.

MINING WASTES—COAL MINE REFUSE

Valley Forge Laboratories conducted a study, "Availability of Mining Wastes and Their Potential for Use as Highway Material" (*46–48*), to develop methods for using coal mine refuse in highway base course construction. A contract was executed to determine the potential for combining fly ash with coal refuse to form a base course material for highway construction. A survey was performed of existing information regarding the engineering properties and field testing of fly ash and coal mine refuse. Also, a nationwide survey was made to establish regions or areas of optimum use potential where the combination of economically available wastes and fly ash indicates attractive potential use of those waste materials in lieu of natural aggregates (*49*). Finally, an extensive laboratory testing program was established to study the physical and engineering properties of mixtures of coal mine refuse (CMR) and fly ash from 10 optimum use areas and a comparison of serviceability index and physical damage parameters based on the VESYS Predictive Design Procedure between crushed stone and CMR-fly ash compositions.

The major findings of the study were as follows (*50*):

1. CMR and fly ashes had physical, chemical, and engineering properties generally similar to those reported in the literature.
2. Several unstabilized CMR-fly ash compositions possessed good strengths but were not durable.
3. CMR-fly ash blends were successfully stabilized with each of the four stabilizing agents tested (portland cement, lime, asphalt cement, and emulsified asphalt).
4. Portland cement- and lime-stabilized CMR-fly ash base courses yielded thinner surface and base course layers than did crushed stone for the same loading, temperature, and subgrade conditions when evaluated by using the VESYS Predictive Design Procedure.
5. The predicted performance levels (serviceability index and physical damage parameters) of those thinner pavement layers are equal to and typically more favorable than those for crushed stone.
6. Unstabilized CMR-fly ash compositions appear to be unsuitable for highway base course application based on the results from the VESYS Predictive Design Procedure.

CONCLUDING REMARKS

The research and development efforts described in this paper were undertaken during the 1970s and early 1980s. During this period, even though there was beginning to be an increased awareness and concern regarding environmental problems, as evidenced by various pieces of legislation addressing resource recovery and hazardous materials, air and water pollution, etc., the thrust of FHWA's efforts was on the possible technical problems associated with use of wastes and by-products. Because much of the regulating legislation was in an embryonic stage in terms of implementation, the FHWA was able to develop design procedures and demonstrate the technical

viability and potential of many industrial/domestic/municipal/mining by-products without suffering unbearable regulation and delays. This is not to say that environmental impacts were not considered, just that in many cases they were not of primary concern. Thus, FHWA's efforts were not subjected to the severe scrutiny and constraints imposed by regulatory groups, environmental advocacy groups, and the general public, that are given by-product utilization today (Chesner, Warren G., *Work Plan for the Demonstration of the Utilization of Waste-to-Energy Combustion Residues as a Substitute Aggregate in Bituminous Paving Applications*, unpublished data).

Regardless of severe constraints exercised today with regard to the reuse of wastes and by-products, FHWA's past and present efforts in this area should provide valuable guidance to those wishing to ameliorate the waste problem by increased recycling (reuse). It is recognized that recycling is only part of the picture and that waste reduction at the source, incineration, and, last, limited landfilling will need to be carefully and fully integrated to prevent the world from being inundated in waste.

REFERENCES

1. R. H. Brink and W. J. Halstead. Studies Relating to the Testing of Fly Ash for Use in Concrete. *Bureau of Public Roads*, Vol. 29, No. 6, 1957, pp. 121–141.
2. A. G. Timms and W. E. Grieb. Use of Fly Ash in Concrete. *Bureau of Public Roads*, Vol. 29, No. 6, 1957, pp. 142–150.
3. R. H. Brink. Use of Waste Sulfate on Transpo '72 Parking Lot. *Proc., 3rd International Ash Utility Symposium*, March 13–14, 1973.
4. *Utilization of Waste Products in Highway Construction.* FHWA Demonstration Project 29, FHWA, U.S. Department of Transportation, 1972.
5. L. H. Minnick, C. L. Smith, and W. C. Webster. The Composition of Fly Ash and Lime Cement with Improved Hardening and Expansion Characteristics and the Process of its Manufacture. French patent 2,101,270, 1972.
6. L. M. Smith, A. Kawam, et al. *Technology for Using Sulfate Waste in Highway Construction.* Report FHWA-RD-76-31, FHWA, U.S. Department of Transportation, December 1975.
7. L. M. Smith and A. Kawam. *The Effect of Gypsum on Lime-Fly Ash Compositions: Literature Review and Annotated Bibliography.* Report FHWA-RD-76-84, Interim Report, FHWA, U.S. Department of Transportation, May 1976.
8. L. M. Smith and H. G. Larew. *Users' Manual for Sulfate Waste in Road Construction.* Report FHWA-RD-76-11, FHWA, U.S. Department of Transportation, Dec. 1975.
9. P. Andrieux and M. Colombel. Fly-Ash in Road Construction Techniques. *Bull. Liaison Labo. P. et Ch.*, Paris, No. 83, 1976, pp. 73–90.
10. J. W. Nebgen, et al. *Use of Waste Sulfate for Remedial Treatment of Soils*, Report FHWA-RD-76-143, FHWA, U.S. Department of Transportation, Aug. 1976.
11. J. W. Nebgen, et al. *Use of Waste Sulfate for Remedial Treatment of Soils*, Vol. 2: *Appendixes*, Report FHWA-RD-76-144, FHWA, U.S. Department of Transportation, Aug. 1976.
12. J. W. Nebgen, et al. *Evaluation of Sulfate-Bearing Waste Material from Fluidized Bed Combustion of Coal for Soil Stabilization.* Report FHWA-RD-77-136, FHWA, U.S. Department of Transportation, Sept. 1977.
13. R. J. Collins and J. J. Emery. *Kiln Dust-Fly Ash Systems for Highway Bases and Subbases*, Report FHWA/RD-82/167, FHWA, U.S. Department of Transportation, Sept. 1983.
14. W. A. Butte, E. M. Kohn, and E. G. Scheibel. *Highway Binder Materials from Cellulosic and Related Wastes.* Report FHWA/RD-130, FHWA, U.S. Department of Transportation, Dec. 1980.
15. R. L. Terrel, et al. *Evaluation of Wood Lignin as a Substitute or Extender of Asphalt.* Report FHWA/RD-80/125, FHWA, U.S. Department of Transportation, Oct. 1980.
16. K. Majidzadeh. *Users' Manual: Power Plant Bottom Ash in Black Base and Bituminous Surfacing: State-of-Art Report.* Report FHWA-RD-77-148, FHWA, U.S. Department of Transportation, Sept. 1979.
17. K. Majidzadeh. *Executive Summary: Power Plant Bottom Ash in Black Base and Bituminous Surfacing.* Report FHWA-RD-79-72, FHWA, U.S. Department of Transportation, September 1979.
18. J. F. Meyers, R. Pichumani, and B. S. Kapples. *Fly Ash as a Construction Material for Highways.* Report FHWA-IP-76-16, FHWA, U.S. Department of Transportation, May 1976.
19. *The Use of Fly Ash in Highway Construction.* FHWA Demonstration Project 59, FHWA, U.S. Department of Transportation, 1981.
20. W. F. Boles. *Fly Ash Facts for Engineers.* Report FHWA-DP-59-8, FHWA, U.S. Department of Transportation, 1986.
21. *The Resource Conservation and Recovery Act of 1976.* Sections 6002, 8002, and 8005, Public Law 94-580, October 21, 1976.
22. *Innovative Technologies.* Surface Transportation Assistance Act of 1982, Section 142 (a)(b)(c), HR report 97-987.
23. *Surface Transportation and Uniform Relocation Assistance Act of 1987.* Section 117(f), April 1987.
24. Guideline for Federal Procurement of Cement and Concrete Containing Fly Ash. *Federal Register*, Vol. 48, No. 20, Jan. 28, 1983, pp. 4230–4253.
25. *Use of Coal Ash.* FHWA Notice N-5080.109, FHWA, U.S. Department of Transportation, August 23, 1987.
26. *Use of Coal Ash in Embankments and Bases.* FHWA Technical Advisory T-5080.9, FHWA, U.S. Department of Transportation, May 1988.
27. *Dulles Access Highway Extension, Fairfax, Virginia.* Eastern Direct Federal Division, FHWA, U.S. Department of Transportation, Aug. 1982.
28. D. Pindzola and R. C. Chou. *Synthetic Aggregate from Incinerator Residue by a Continuous Fusion Process.* Report FHWA/RD-74/23, FHWA, U.S. Department of Transportation, 1974.
29. D. Pindzola. *Large-Scale Continuous Production of Fused Aggregate from Incinerator Residue.* Report FHWA/RD-76/115, FHWA, U.S. Department of Transportation, 1976.
30. R. R. Snyder. *Evaluation of Fused Incinerator Residue as a Paving Material.* Report FHWA-TS-88-229, FHWA, U.S. Department of Transportation, 1980.
31. R. J. Collins, R. H. Miller, S. K. Ciesielski, E. M. Wallo, M. J. Boyle, D. Pindzola, and J. Tropea. *Technology for Use of Incinerator Residue as Highway Material.* Report FHWA/RD-77/151, FHWA, U.S. Department of Transportation, Oct. 1976.
32. R. J. Collins, et al. *Guidelines for the Use of Incinerator Residue in Highway Construction.* Report FHWA-RD-77-72, FHWA, U.S. Department of Transportation, 1976.
33. J. Haynes and W. B. Ledbetter. *Incinerator Residue in Bituminous Base Construction.* Report FHWA/RD-76/12, FHWA, U.S. Department of Transportation, 1976.
34. D. J. Teague and W. B. Ledbetter. *Three Year Results on the Performance of Incinerator Residue in Bituminous Base.* Report FHWA/RD-78/144, FHWA, U.S. Department of Transportation, 1978.
35. J. Erdeley and W. B. Ledbetter. *Field Performance of Littercrete (Incinerator Residue) in Bituminous Base.* Report FHWA/RD-88/022, FHWA, U.S. Department of Transportation, September, 1981.
36. R. D. Pavlovich, H. J. Lentz, and W. C. Ormsby. Incinerator Residue as Aggregate for Hot-Mix Asphalt Base Course. In *Transportation Research Record 734*, TRB, National Research Council, Washington, D.C., 1979, pp. 38–44.
37. J. L. Griffith. *Summary Update of Research Projects with Incinerator Bottom Ash Residue.* Executive Office of Environmental Affairs, Department of Environmental Management, Bureau of Solid Waste Disposal, Boston, Mass., 1982.
38. M. D. Turo and A. M. Leonido. *Incinerator Residue as a Component of Bituminous Pavements.* Massachusetts Department of Public Works Report R-37-0, Boston, Mass., 1984.
39. W. C. Webster, et al. *Disposal Method and Use of Sewage Sludge.* Belgium Patent No. 822838, April 25, 1975.

40. A. Kawam, L. M. Smith, et al. *Feasibility of Using Sewage Sludge in Highway Embankment Construction.* Interim Report, FHWA Report No. RD-75-38, FHWA, U.S. Department of Transportation, Feb. 1975.
41. C. H. McDonald. Recollections of Early Asphalt-Rubber History. *Proc., National Seminar on Asphalt-Rubber*, San Antonio, Tex., Oct. 1981, pp. 23–39.
42. *Discarded Tires in Highway Construction.* FHWA Demonstration Project 37, FHWA, U.S. Department of Transportation, 1976.
43. D. J. Brown. Involvement of the FHWA's Demonstration Projects Division in the Development of Asphalt-Rubber Materials. *Proc., National Seminar on Asphalt-Rubber*, San Antonio, Tex., Oct. 1981, pp. 27–29.
44. T. S. Shuler, R. D. Pavlovich, J. A. Epps, and C. K. Adams. *Investigation of Materials and Structural Properties of Asphalt-Rubber Paving Mixtures*, Vol. 1, *Technical Report.* Report FHWA/RD-86/027, FHWA, U.S. Department of Transportation, Sept. 1986.
45. *Use of Scrap Automobile Tire Rubber in Highway Construction.* Special Report 85, New York State Department of Transportation, State Campus, Albany, May 1986.
46. R. J. Collins and R. H. Miller. *Availability of Mining Wastes and Their Potential for Use as Highway Material*, Vol. 1, *Classification and Technical and Environmental Analysis.* Report FHWA-RD-76-106, FHWA, U.S. Department of Transportation, May 1976.
47. R. J. Collins. *Availability of Mining Wastes and Their Potential for Use as Highway Material*, Vol. 2, *Location of Mining and Metallurgical Wastes and Mining Industry Trends.* Report FHWA-RD-76-107, FHWA, U.S. Department of Transportation, May 1976.
48. R. J. Collins. *Availability of Mining Wastes and Their Potential for Use as Highway Material.* Vol. 3, Report FHWA-RD-76-188, FHWA, U.S. Department of Transportation, May 1976.
49. P. V. McQuade, P. E. Glogowski, F. P. Toloser, and R. B. Anderson. *Investigation of the Use of Coal Refuse-Fly Ash Compositions as Highway Base Course Material: State of the Art and Optimum Use Area Determinations.* Report FHWA-RD-78-208, FHWA, U.S. Department of Transportation, Feb. 1980.
50. P. V. McQuade, W. J. Head, and R. B. Anderson. *Investigation of the Use of Coal Refuse-Fly Ash Compositions as Highway Base Course Material.* Report FHWA/RD-80/129, FHWA, U.S. Department of Transportation, 1980.

Publication of this paper sponsored by Committee on Soil-Portland Cement Stabilization.

Stabilization Characteristics of Class F Fly Ash

MUMTAZ A. USMEN AND JOHN J. BOWDERS, JR.

Stabilized fly ash is a mixture of fly ash and lime, or fly ash and cement, compacted at optimum moisture content and cured to form a product-like soil-lime or soil-cement. Limited past applications and engineering properties of stabilized class F fly ash are discussed. A research study was undertaken to establish the physical, chemical, compaction, strength, and durability characteristics of class F fly ash stabilized with lime, cement, or lime/cement combinations. Two ashes obtained from West Virginia power plants were included in the laboratory testing program. It was found that although the ashes are quite different in properties, both ashes can be successfully stabilized to produce pozzolanic mixtures of adequate strength and durability for use as base or liner, with the addition of a proper amount of stabilizer and by allowing the mixture to cure for a sufficiently long period. Cement stabilization, in general, produced better strength and durability than lime stabilization for a given stabilizer content for curing periods up to 56 days. Freeze-thaw cycles caused substantial strength losses, and wet-dry cycles resulted in strength gains. Vacuum saturation with water and an acetic acid solution produced intermediate effects. Very good correlations were found between freeze-thaw and water vacuum saturation tests.

Large quantities of fly ash continue to be generated by coal-burning power plants, and the disposal of this material in a safe, economical, and environmentally acceptable manner is becoming increasingly troublesome for the electric utility industry and becoming a public concern. The most desirable way of disposal is utilization, which provides economic benefits by reducing disposal costs and mitigates possible negative environmental effects through proper engineering controls. Fly ash has been used in many types of engineering applications because of its wide availability and desirable pozzolanic (and self-hardening) characteristics and has been used as an admixture in cement and concrete and as a stabilizing agent (in combination with lime or cement) for soils and aggregates in pavement subgrades, bases, and subbases. Fly ash also has been used as a fill material on a limited scale.

The use of fly ash in concrete and aggregate/soil stabilization applications has proven beneficial both technically and economically, but relatively small amounts of fly ash can be exploited in those types of projects because, in most cases, fly ash constitutes a small percentage of the total material composition. This suggests that, in view of the economic and environmental concerns mentioned, further benefits and incentives remain for establishing utilization schemes that will incorporate larger amounts of ash. One such scheme is "stabilized fly ash," defined here as a pozzolanic mixture of fly ash and lime or cement compacted at optimum moisture content to form a product-like soil-lime or soil-cement that can serve as a base or subbase course for pavements or as a low permeability liner or cut-off material when designed (proportioned) to meet pertinent performance criteria. Because this material does not contain any aggregate or soil, the use of fly ash is maximized per ton or cubic yard of base, subbase, or liner material constructed. Fly ash in such an application serves the dual role of pozzolan and aggregate.

Detailed technical information is not available on stabilized fly ash although an abundance of information exists on the technology for pozzolanic base courses employing mixtures of lime, fly ash, and aggregate (LFA); cement, fly ash, and aggregate (CFA); and lime, cement, fly ash, and aggregate (LCFA) (*1–3*), as well as the use of fly ash in soil stabilization (*3,4*). A research study was performed to review and document the limited existing information from the literature on material properties and applications and to produce new information on material properties through an organized laboratory study. Two class F (bituminous coal based) fly ashes from West Virginia were included in the laboratory study. Those ashes were first characterized by subjecting them to standard ASTM tests for pozzolans. Next, the ashes were mixed with hydrated lime and portland cement at varying stabilizer contents to investigate compaction characteristics (optimum moisture content and maximum dry density). Then, the specimens were fabricated, cured for different lengths of time, and tested for strength and durability. Findings of those investigations are reported in this paper. Permeability and leachate characteristics of the stabilized fly ash mixtures were also studied as part of this research project. However, relevant information and findings concerning those aspects are presented elsewhere (*5*) and are discussed by Bowders et al. in a companion paper in this Record.

PAST RESEARCH AND UTILIZATION

Material Properties

It is known that the most unique and outstanding characteristics of fly ash are pozzolanic reactivity and being self-hardening. Pozzolanic reactivity relates to the ability of fly ash to form cementitious products at ordinary temperatures when combined with alkali and alkaline earth hydroxides in the presence of moisture. The alkali and alkaline earth hydroxides needed to achieve pozzolanic reactions are provided by adding lime or cement to fly ash. If they are internally

M. A. Usmen, Department of Civil Engineering, Wayne State University, Detroit, Mich. 48202. J. J. Bowders, Jr., Department of Civil Engineering, West Virginia University, Morgantown, W. Va. 26506-6101.

present in sufficient amounts (e.g., as CaO or MgO), then the fly ash exhibits self-hardening behavior in addition to pozzolanicity. Fly ash is designated as class F or class C depending on the parent coal source. Class F ash is derived from bituminous or anthracite coals burned mostly in the eastern, midwestern, and southern United States. Class C ash comes from subbituminous or lignite coals predominantly mined in the western United States. It is almost always necessary to combine class F fly ash with lime or cement to produce pozzolanic reactions, but this may not be needed with class C ashes, which contain significant amounts of CaO. However, many class C ashes also produce better stabilization characteristics when lime or cement is added (*3,6*).

Pozzolanic reactions between lime and fly ash are complex. According to Minnick (*7*), those reactions involve various combinations of the hydrated calcium or magnesium in lime with the amorphous silica and alumina in fly ash or both. Reaction products may include tobermorite (calcium silicate hydrate), ettringite (high-sulfate calcium sulfoaluminate: $3CaO\ Al_2O_3\ CaSO_4\ 12H_2O$), and the low sulfate form of calcium sulfoaluminate ($3CaO\ Al_2O_3\ CaSO_4\ 12\ H_2O$). The extent and rate of the reactions will be affected by the fineness and chemical composition of fly ash, the type and amount of stabilizer, moisture content, temperature, and age. When cement is used in lieu of lime to stabilize fly ash, it hydrates relatively quickly on contact with moisture and produces its own cementitious compounds and also releases some free lime that can further react with fly ash in a pozzolanic manner. Consequently, cement enhances short-term strength.

Limited information has been reported in the literature on the strength characteristics of lime- and cement-stabilized fly ash (*6,8–10*). Evident from those studies for mixtures of lime and fly ash is that normal (70°–75°F) cured unconfined compressive strengths at 7 to 28 days range from 100 psi to 1200 psi and that longer curing periods (90 days and over) may yield strengths exceeding 2000 psi. Cement may produce two to three times higher strengths in the short term, but the differences largely disappear in the long term.

Durability data on stabilized fly ash are very limited. Gray and Lin (*9*) have found that both lime and cement stabilization drastically reduce the frost susceptibility of fly ash. Freeze-thaw durability evaluations by Joshi et al. (*10*) have revealed that mixtures of lime and fly ash have questionable durability in the short term and that mixtures of cement and fly ash produce satisfactory results.

Complete mix-design data for stabilized fly ash could not be found in the literature. Therefore, effects of stabilizer contents on mixture properties cannot be clearly assessed. Evidence exists that increased cement content will increase mixture strength (*11*). However, strength may increase with increasing lime content (*10,11*) or results may be varied (*9*).

According to GAI Consultants (*6*), the standard soil-cement wet-dry and freeze-thaw durability tests, using the brushing technique, are not suitable for cement-stabilized fly ash. Because wet-dry cycles apparently produce negligible effects on durability and freeze-thaw cycles are unduly abrasive, and because test results are dependent on sample preparation techniques, it is suggested that compressive strength tests can be used alone for ensuring adequate durability. For cement-stabilized fly ash, a 7-day normal cured strength between 400 and 800 psi has been specified, along with the requirement that the strength of the mix must increase with time. A minimum 28-day normal cured strength of 550 psi has been recommended for lime-stabilized ash, again with the additional stipulation that there must be strength increase with time. However, stabilized fly ash pavements subjected to extreme service conditions should be tested for durability by observing residual strength after a suitable number of freeze-thaw cycles or after vacuum saturation.

In general, a partial or full replacement of lime by cement in pozzolanic mixtures has been considered advantageous, although this has so far been tried only on pozzolan-aggregate mixes (*2*). In addition to better early strength, cement apparently also enhances durability. It has been suggested that the designer can have better control over the mixture quality (by adjusting cement content) and that nonspecification ashes not highly lime reactive may be effectively stabilized with cement.

Applications

Cement-stabilized fly ash has been successfully used as a base course material in England and France for many years and has been specified and accepted on both public roads and private projects (*4,6*). This type of application is relatively new in the United States but is expected to gain increased attention especially in locations where fly ash can economically compete with alternative aggregate materials. Field trials and demonstration projects have been undertaken in recent years to evaluate the performance of stabilized fly ash pavements (*4,10–13*). Three cases related to cement-stabilized class F fly ash mixes are briefly described here.

- In September 1975 a parking lot pavement consisting of an 8-in.-thick cement-stabilized fly ash base, which was topped by a 3-in. bituminous wearing surface, was constructed at Harrison Power Station in Haywood, West Virginia (*4*). The purpose of the project was to demonstrate cement-stabilized fly ash as an easily constructed and highly serviceable base course. Cement and fly ash were premixed with water in a pugmill at the rate of 83 lb of fly ash and 10 lb of cement per cubic foot of compacted mix. An average in-place density of 98.5 percent of the maximum Standard Proctor of 92.5 pcf was obtained at an optimum water content of 14 percent. Average unconfined compressive strengths of cores taken from the completed base course at 7 and 90 days were 566 and 869 psi, respectively. Strengths of cores taken after a period of 180 days, which encompassed a severe winter, indicated that the pavement had experienced no strength loss. The parking lot has continued to perform well.
- Cement-stabilized fly ash was used in the construction of a base course for a haul road near American Electric Power's Clinch River power plant in southwestern Virginia (*12*). The cement-stabilized fly-ash base course was designed by the procedures presented by GAI Consultants (*4,6*). The resulting pavement consisted of cement-treated fly ash base course 5.5 in. thick overlain by a 1.5-in.-thick emulsified asphalt-stabilized bottom ash surface course. A cement content of 14 percent of the dry weight of the fly ash and a water content of 17 percent were selected for the base-course mix. The haul road was subjected to a low traffic volume, although many of the vehicles were heavy trucks, and the road performed satisfactorily for several years.

• An experimental project, using a 10-in.-thick cement stabilized fly ash as the road base material, was conducted by the Oakland County Road Commission in Michigan in 1983 (*13*). The mix contained 10 percent cement and presented no unique problems during pugmilling and construction. Ease of construction was roughly comparable to the installation of a gravel or bituminous base. Traffic control was also similar, except for a recommendation that the traffic be kept off the completed base during the initial curing period (7 days). Cores taken at 7 and 28 days yielded unconfined compressive strength of 190 psi and 142 psi, respectively. However, early laboratory testing on a sample of fly ash from the plant indicated the design mix would produce a 7-day strength over 400 psi. This difference probably arose from discrepancies between laboratory testing conditions and in-place field conditions. This level of performance, however, was considered unsatisfactory, and this mixture was not recommended for use in the Detroit, Michigan, area.

RESULTS OF THE LABORATORY STUDY

The laboratory studies involved testing of fly ashes in unstabilized and stabilized form. The purpose of the study was to determine the specification conformity of the ashes, the compaction behavior and parameters of the ash-stabilizer mixtures in the freshly mixed condition, and the strength and durability characteristics of the same mixes after curing. All testing in the laboratory was performed on duplicate specimens to obtain average results. If the test results had significant variability, then additional tests were performed before averaging.

Materials

Two fly ashes were used in this study: Harrison, obtained from the Harrison Power Plant in Haywood, West Virginia, and Amos, acquired from the Amos Power Plant, in Nitro, West Virginia. The samples were collected from the dry hoppers in the power plants and were transported to the laboratory for testing. The hydrated lime used in this study was manufactured by the Greer Plant of Morgantown, West Virginia, and the Type I portland cement was produced in Armstrong, West Virginia. Both were bought in paper sacks from local suppliers.

Ash Properties

A variety of ASTM specification tests were performed on the fly ashes and included specific gravity (ASTM D854); fineness, as established by the amount retained when wet-sieved on No. 200 and No. 325 sieves (ASTM D422); pozzolanic activity index with portland cement and pozzolanic activity index with lime (ASTM C311); and lime-pozzolan strength development (ASTM C593). A summary of the test results is presented in Table 1, along with the related ASTM specification criteria. Data on the chemical analyses of the ashes shown in the table were provided by the utility companies, except for the loss on ignition values and CaO contents, which were determined in the laboratory.

The specific gravity values presented in Table 1 indicate that the Harrison ash is much heavier than the Amos because of its high Fe_2O_3 content. The Amos ash conversely has a higher total amount of glassy components (SiO_2, Al_2O_3, and Fe_2O_3) than does the Harrison and has a higher pozzolanic activity index with lime and a higher lime-pozzolan strength development value than does the Harrison. However, both ashes exhibit excellent pozzolanic reactivity with both cement and lime. The sieve analysis results indicate that the Harrison is somewhat finer than the Amos. The loss on ignition values are comparable for both ashes, with the Harrison slightly lower. The values presented in the table indicate that relatively small amounts of carbon and other combustible materials exist in the ashes. The CaO percentage for the Harrison is significantly higher than that for the Amos. Overall, both ashes, although quite different in properties, satisfy the ASTM specification criteria for class F fly ashes for use in cement and concrete and for lime-pozzolan stabilization.

Compaction Characteristics

Compaction characteristics of mixtures of fly ash and lime and of fly ash and cement were investigated by performing Standard Proctor tests (ASTM D698) on materials by using varying stabilizer contents. The maximum dry density (MDD) and optimum moisture content (OMC) were obtained on each mixture. Results are presented graphically in Figures 1 and 2 for Harrison lime (HL), Harrison cement (HC), Amos lime (AL), and Amos cement (AC) mixtures. Results for unstabilized mixtures (zero percent stabilizer) are also included. Some differences exist between the compaction characteristics of the two fly ashes. The Harrison with the higher specific gravity produces higher maximum dry densities when compared with the Amos. However, the Amos, being a lighter weight material, yields higher optimum moisture contents because of the larger surface area it has per unit mass.

The data for both ashes also indicate that increased lime content results in increased OMC and decreased MDD, which can be attributed to the fineness and light weight of lime. Conversely, increased cement content does not appear to produce any clear trends, or any significant variation, relative to OMC and MDD. The moisture-density relationships for individual mixtures were very straightforward to obtain, and the standard laboratory procedures posed no problems or anomalies.

Strength Development

The stabilized fly ash mixtures were first compacted in Proctor molds at their OMC. They were then extracted from the molds and placed in plastic closeable bags and cured in a moist room at 73°F and 100 percent relative humidity. The mixtures were then tested after specified curing periods for unconfined compressive strength in the unsoaked condition to assess the degree of stabilization through progressing pozzolanic reactions between the fly ashes and the stabilizers. The soaking procedure normally employed to determine design strength was omitted to avoid the possibility of negating effects that would obscure the results. (The soaking procedure, however, was

TABLE 1 PROPERTIES OF FLY ASHES

Property	Harrison Ash	Amos Ash	ASTM Specifications
Specific Gravity	2.81	2.25	---
%Retained #200 Sieve	4.4	8.9	ASTM C593 30.0 max.
Fineness, % retained on #325 Sieve	14.4	22.4	ASTM C618 34.0 max.
Moisture Content (%)	0.1	0.1	ASTM C618 3.0 max.
Pozzolanic Activity Index with cement (%)[a]	97.6	86.0	ASTM C618 75 min.
Pozzolanic Activity Index with lime (psi)[b]	944	1003	ASTM C618 800 min.
Lime-Pozzolan Strength Development (psi)[c]	644	979	ASTM C593 600 min.
Silicon Dioxide (SiO_2), %	34	58	---
Aluminum Oxide (Al_2O_3), %	21	30	---
Ferric Oxide (Fe^2O^3), %	24	4	---
Sum of SiO_2, Al_2O_3, and Fe_2O_3, %	79	92	ASTM C618
Loss on Ignition (%)	2.2	2.5	ASTM C618 12 max.
CaO (%)	6.8	1.4	---

[a] - Cured 1 day at 73 F plus 27 days at 100 F

[b] - Cured 1 day at 73 F plus 6 days at 130 F

[c] - Cured 7 days at 130 F

replaced by vacuum saturation, which is reported in the next section.)

The different ash-stabilizer combinations and curing periods employed in this phase of the study and the test results are presented in Table 2. Both ashes were stabilized with 3, 6, 9, 12, and 15 percent lime and with 3, 6, 9, 12, and 15 percent cement. In addition, the Harrison was stabilized with 9 percent cement and 3 percent lime, 6 percent cement and 6 percent lime, and 3 percent cement and 9 percent lime, to study the effects of using combined stabilizers on mixture strength development. The Amos mixtures were tested after 7 and 28 days of curing only, and the Harrison mixtures were tested after 7, 28, and 56 days to assess the effects of longer-term curing. Unconfined compressive strengths for unstabilized ashes (zero percent lime or cement) were also obtained to establish baseline values.

From the results presented in Table 2, increasing cement content causes considerable increases in the strength of both ashes for all curing periods. Increasing lime content, however, may increase or decrease strength. A slight decrease is observed with the Harrison, in general with increasing lime contents at 7 and 28 days. However, the trend reverses at 56 days. This may be caused by unfinished pozzolanic reactions between lime and fly ash in the short term. In the Amos lime mixtures, increased lime content causes negligible strength gain at 7 days, but extended curing effects a notable increase in strength.

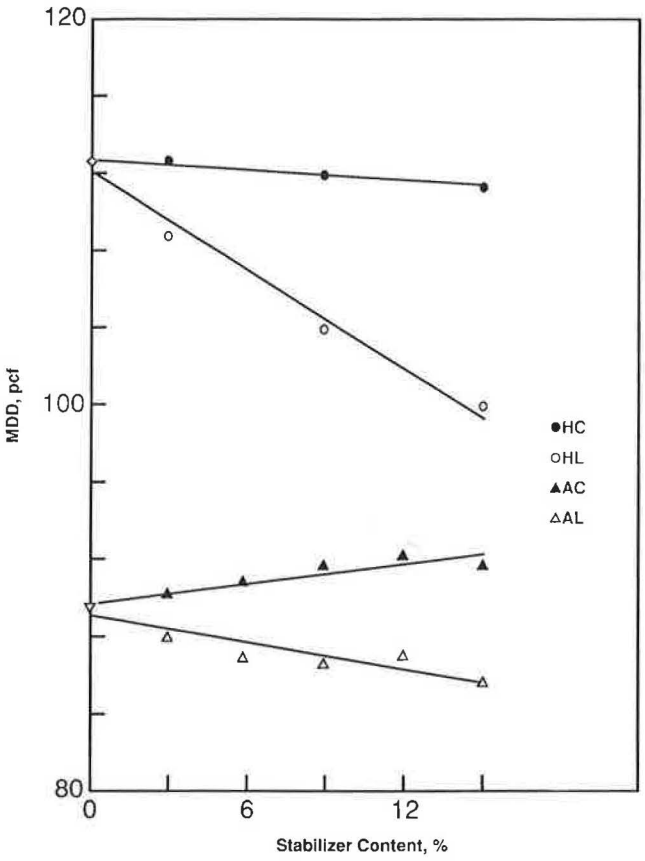

FIGURE 1 MDD versus stabilizer content for ash mixtures.

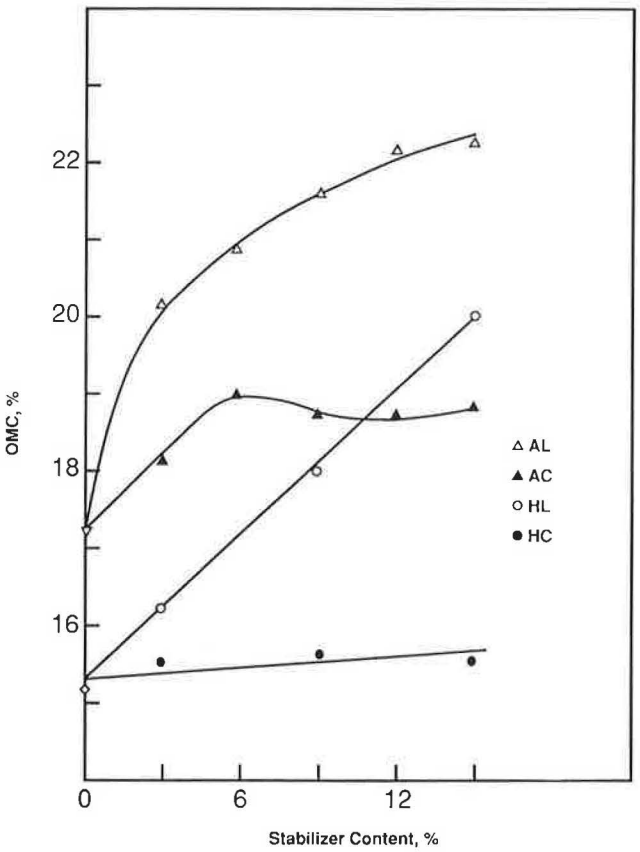

FIGURE 2 OMC versus stabilizer content for ash mixtures.

Overall, the results show that cement-stabilized ashes exhibit higher strengths than their lime-stabilized counterparts, regardless of the length of curing period. However, as the curing period gets longer the differences between the cement- and lime-stabilized fly ash mixes at a given stabilizer content become somewhat smaller.

When comparing the strengths of the two ashes, the Harrison has developed higher strengths for both lime and cement stabilization. This, unfortunately, cannot be readily predicted from the pozzolanic reactivity test results presented in Table 1, because the Amos appears to have higher pozzolanic reactivity with lime than does the Harrison. However, the test results presented in Table 1 are based on accelerated curing at high temperatures. Further, the high CaO content and the fineness of the Harrison can be important factors that contribute to high strength. The results in Table 2 indicate that the Harrison ash shows very satisfactory strength values with both lime and cement for all stabilizer contents and curing periods. The Amos exhibits relatively low strengths with lime in the short term, but extending curing results in appreciable strength gains and reaches satisfactory levels at higher lime contents, a favorable characteristic. The length of curing, actually, has a very dramatic effect on all mixtures. The longer the curing period, the higher the strengths.

Finally, the dominance of cement in the strength development of stabilized fly ash mixes is quite evident from the results given in Table 2 for the Harrison stabilized with combined lime and cement. As the cement/lime ratio increases in the combined stabilizer, the strength of the total mixture also tends to increase. The mixtures containing combined stabilizers indicate strengths much higher than those stabilized with lime only. When compared with cement-stabilized mixtures, the differences are much less and become quite insignificant at high cement/lime ratios.

Durability Evaluation

Durability of lime- and cement-stabilized fly ash mixtures was evaluated by obtaining the residual strength q_r of the cured specimens after subjecting them to different exposure conditions and then comparing this value to the original (pre-exposure) strength q_0. Three levels of stabilizer contents were used in the preparation of the mixes: 3, 9, and 15 percent. However, part of the Amos specimens was prepared only with 9 percent stabilizer to economize on time and materials. Two curing periods, 7 and 28 days, were selected for specimen preparation.

Five types of exposure conditions were chosen for durability evaluations. The first series of tests employed vacuum saturation with water and was performed in accordance with ASTM C593. The second series used a freeze-thaw cycles exposure and was performed as outlined in ASTM D560, except for employing 10 cycles instead of 12 and for substituting unconfined compressive strength testing at the end of the exposure period for the brushing and weighing procedures. A similar

TABLE 2 COMPRESSIVE STRENGTHS OF STABILIZED ASHES

Mixture	Compressive Strength (psi) 7-day	28-day	56-day
Unstabilized Harrison	80	95	----
Harrison + 3% Lime	559	909	1116
+ 6% Lime	543	780	1182
+ 9% Lime	439	761	1220
+12% Lime	394	895	1277
+15% Lime	372	758	1138
Harrison + 3% Cement	193	422	----
+ 6% Cement	442	756	792
+ 9% Cement	917	1209	1353
+12% Cement	1074	1675	1773
+15% Cement	1341	1803	2423
Harrison + 9% Lime and 3% Cement	694	1251	1695
Harrison + 6% Lime and 6% Cement	756	1361	1687
Harrison + 3% Lime and 9% Cement	959	1635	1928
Unstabilized Amos	40	40	
Amos + 3% Lime	104	148	
+ 6% Lime	116	239	
+ 9% Lime	126	360	
+12% Lime	130	482	
+15% Lime	142	669	
Amos + 3% Cement	217	251	
+ 6% Cement	307	508	
+ 9% Cement	488	764	
+12% Cement	637	1112	
+15% Cement	826	1492	

approach was adopted in the third series, which involved wet-dry cycles. In this case, the procedures specified in ASTM D559 were modified so as to include 10 cycles of wetting and drying rather than 12 and compressive strength testing instead of brushing and weighing. The fourth and fifth series of durability testing involved a vacuum saturation exposure, this time using an acetic acid solution (0.575 M with a *p*H of 2.5) instead of water. The vacuum saturation period was extended to 2 hours for both series to ensure better pervasion of the acid solution into the specimens. This procedure was devised to test the durability of the mixtures in an acidic environment (i.e., as a landfill liner).

Two sets of specimens were tested, one directly after vacuum saturation, another after 48 hours, to assess the effects of prolonged exposure while the specimens were sealed in plastic bags. The weights of all specimens were monitored throughout the durability testing program to study moisture changes and material loss owing to possible sample deterioration. Visual observations were also performed to supplement quantitative evaluations.

Durability test results for the mixtures and exposure conditions are summarized in Tables 3 and 4 for 7 and 28 day curing periods, respectively. Results are presented in terms of q_r values and q_r/q_0, which is the ratio of the residual strength and the original strength. The original strength values used in computing these ratios are those given in Table 2 for the same mixtures. A q_r/q_0 ratio of less than 1.0 indicates a strength decrease as a result of the exposure, and a q_r/q_0 ratio of greater than 1.0 signifies a strength increase as a result of the exposure. If any of those exposures and testing procedures are adopted for durability evaluations, then the particular criterion to be met by those parameters should be determined for the anticipated field conditions to which the pavement or liner material will be subjected. Low q_r values and q_r/q_0 ratios might indicate a need to critically evaluate the potential durability problems for the given case.

TABLE 3 DURABILITY TEST RESULTS FOR STABILIZED ASHES (7 DAYS)

Exposure Condition	Vac. Saturation with Water		Freeze-Thaw Cycles		Wet-Dry Cycles		Vac. Saturation with Acetic Acid Tested Immediately		Vac. Saturation with Acetic Acid Tested after 48 Hours	
Mixture	q_r [a] (psi)	q_r/q_o [b]	q_r (psi)	q_r/q_o	q_r (psi)	q_r/q_o	q_r (psi)	q_r/q_o	q_r (psi)	q_r/q_o
Harrison + 3% Lime	446	0.80	373	0.67	1540	2.75	394	0.70	400	0.72
+ 9% Lime	346	0.79	129	0.27	2666	6.07	359	0.82	320	0.73
+15% Lime	317	0.85	56	0.15	2845	7.67	276	0.74	283	0.76
Harrison + 3% Cement	169	0.88	295	1.53	812	4.21	241	1.25	103	1.05
+ 9% Cement	736	1.00	844	1.14	3462	4.69	1166	2.09	1096	1.96
+15% Cement	1069	1.03	1106	1.07	2348	2.26	977	1.33	858	1.17
Amos + 3% Lime	64	0.62	0	0	---	---	---[c]	---	---	---
+ 9% Lime	60	0.48	26	0.21	1313	10.42	64	0.51	58	0.46
+15% Lime	86	0.61	34	0.24	---	---	---	---	---	---
Amos + 3% Cement	155	0.71	54	0.25	---	---	---	---	---	---
+ 9% Cement	346	0.71	213	0.44	1393	2.85	201	0.41	243	0.50
+15% Cement	585	0.71	549	0.66	---	---	---	---	---	---

a - q_r = Residual compressive strength (post-exposure)

b - q_o = Original compressive strength (pre-exposure)

c - --- indicates that test was not performed

TABLE 4 DURABILITY TEST RESULTS FOR STABILIZED ASHES (28 DAYS)

Exposure Condition	Vac. Saturation with Water		Freeze-Thaw Cycles		Wet-Dry Cycles		Vac. Saturation with Acetic Acid Tested Immediately		Vac. Saturation with Acetic Acid Tested after 48 Hours	
Mixture	q_r [a] (psi)	q_r/q_o [b]	q_r (psi)	q_r/q_o	q_r (psi)	q_r/q_o	q_r (psi)	q_r/q_o	q_r (psi)	q_r/q_o
Harrison + 3% Lime	718	0.79	690	0.76	1791	1.97	527	0.58	495	0.54
+ 9% Lime	756	0.99	374	0.49	3084	4.05	541	0.71	549	0.72
+15% Lime	611	0.81	362	0.48	3064	4.04	543	0.72	573	0.76
Harrison + 3% Cement	291	0.69	304	0.72	1055	2.50	605	1.43	645	1.53
+ 9% Cement	798	0.66	614	0.51	2646	2.19	1717	1.42	1631	1.35
+15% Cement	1202	0.67	868	0.48	3870	2.15	1733	0.96	2171	1.20
Amos + 3% Lime	90	0.61	28	0.19	---	---	---[c]	---	---	---
+ 9% Lime	229	0.64	36	0.10	1811	5.03	201	0.56	185	0.51
+15% Lime	374	0.56	44	0.07	---	---	---	---	---	---
Amos + 3% Cement	183	0.73	121	0.48	---	---	---	---	---	---
+ 9% Cement	655	0.86	691	0.40	1353	1.77	584	0.76	603	0.79
+15% Cement	1212	0.81	1431	0.96	---	---	---	---	---	---

a - q_r = Residual compressive strength (post-exposure)

b - q_o = Original compressive strength (pre-exposure)

c - --- indicates that test was not performed

Several observations can be made from the data presented in Tables 3 and 4. First, stabilized mixtures of the Harrison ash have produced much better durability in most cases than the stabilized Amos mixtures. Residual strengths are invariably higher for the Harrison primarily because the original strengths were higher to start with and underscores the importance of obtaining sufficiently high strength in stabilized ash mixtures before their exposure to possible detrimental service environments. The Harrison has also produced higher q_r/q_0 ratios with few exceptions. Cement-stabilized Harrison, in particular, shows excellent durability with respect to all exposures, with an exception observed in the q_r/q_0 ratios for the freeze-thaw test. Cement-stabilized Amos may have done better than lime-stabilized Amos, producing satisfactory durabilities in many cases, particularly at relatively higher cement contents (greater than 9 percent) and longer curing periods (28 days). Lime-stabilized Amos also has performed better after the 28-day curing period when compared with the 7-day curing. This is true for most exposures. However, this mixture failed in freeze-thaw after both curing periods.

Overall, increased stabilizer contents and extended curing periods enhance the durability of the stabilized ash mixtures, and cement-stabilized mixtures perform better in most of the durability exposure conditions. The freeze-thaw cycles test produces the severest exposure and results in substantial strength losses in most cases. The wet-dry cycles test, however, invariably results in very high strength gains for the specimens, indicating that this type of exposure will not be critical in terms of the durability evaluation of stabilized fly ash.

Weight changes of 28-day cured specimens during the freeze-thaw and wet-dry cycles are presented graphically in Figures 3, 4, 5, and 6 to augment the results given in Table 4. The HL, HC, AL, and AC symbols used in those figures denote Harrison lime, Harrison cement, Amos lime, and Amos cement mixtures, respectively, and the numbers at the end of each symbol designate the stabilizer contents. Similar curves were obtained for 7-day curing. Evident from Figures 3 and 4 is that both lime- and cement-stabilized ashes have gained significant amounts of moisture after the first freeze-thaw cycle. Afterward, an approximately constant weight is maintained for cement-stabilized ashes, but moisture gains continue in varying degrees in the lime-stabilized ashes. Weight losses observed in the higher cycles indicate material loss owing to cracking, scaling, and spalling; and continued moisture gain is indicative of internal deterioration. Extreme deterioration was observed in specimens of 3 and 9 percent lime-stabilized Amos after the first few cycles, and the specimens were tested for strength without completing all the cycles. The curves in Figures 5 and 6 reveal that substantial moisture losses occur in all specimens during the first wet-dry cycle, followed by a more or less constant weight achieved through the next one or two cycles and maintained the rest of the way. Because the dry cycle involves the exposure of the specimens to an environment maintained at 160°F, accelerated curing

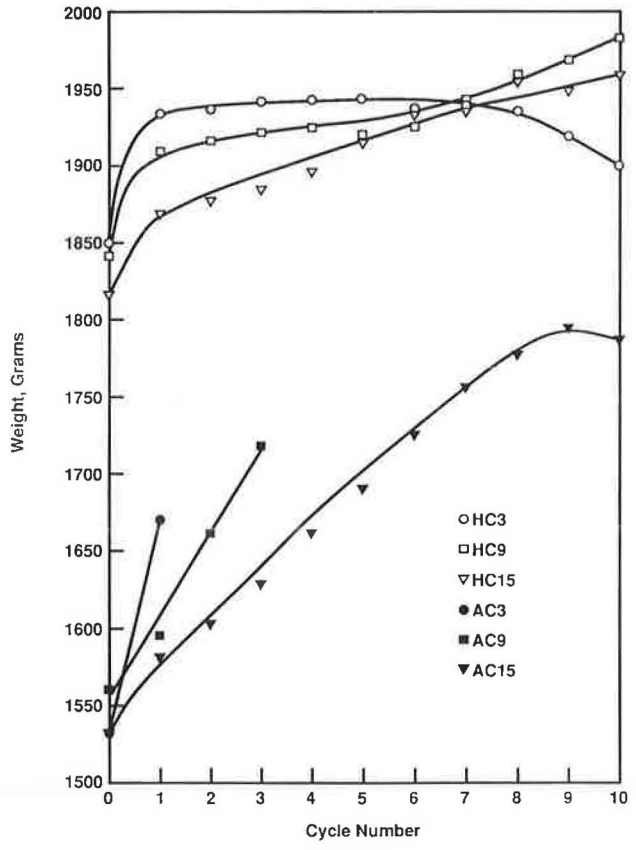

FIGURE 3 Weights of lime-stabilized ashes exposed to freeze-thaw cycles (28 days).

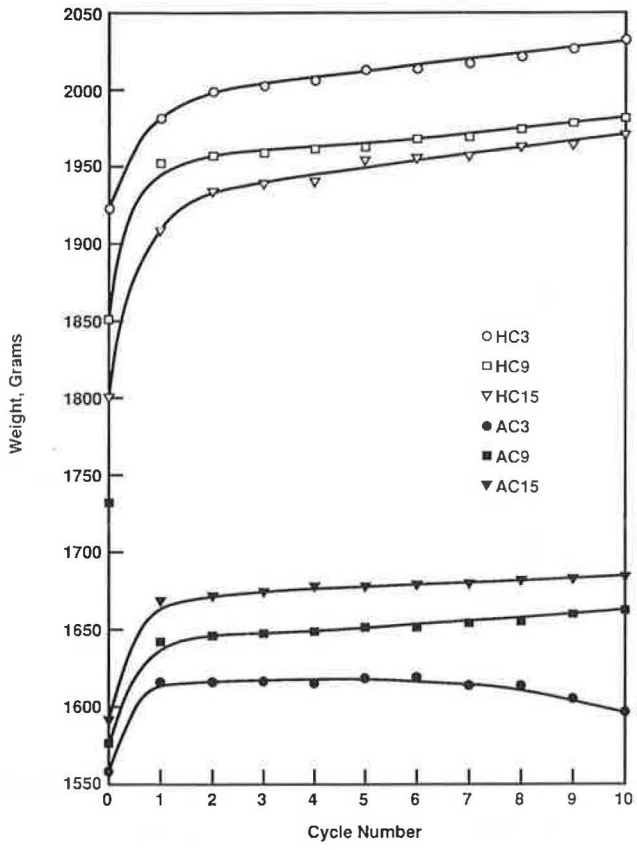

FIGURE 4 Weights of cement-stabilized ashes exposed to freeze-thaw cycles (28 days).

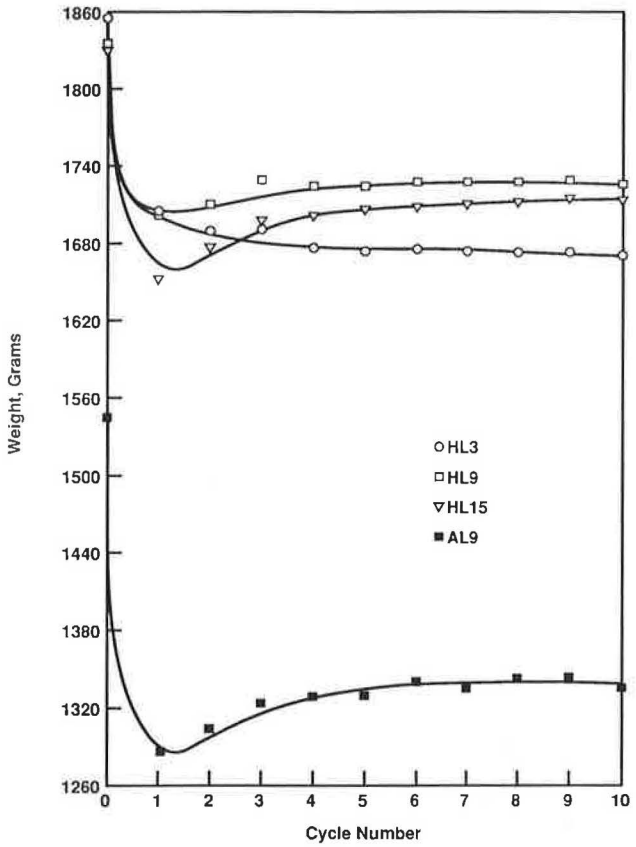

FIGURE 5 Weights of lime-stabilized ashes exposed to wet-dry cycles (28 days).

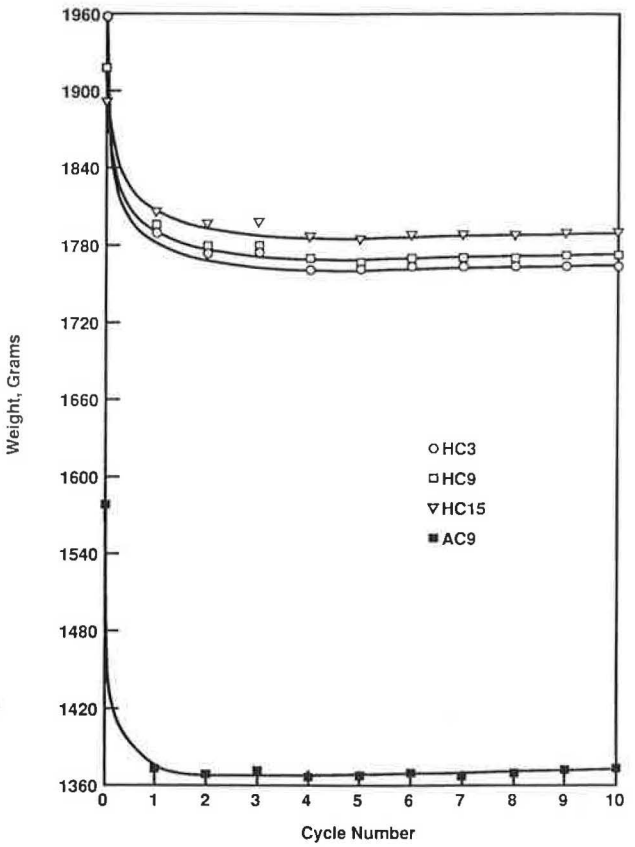

FIGURE 6 Weights of cement-stabilized ashes exposed to wet-dry cycles (28 days).

occurs in the stabilized mixtures, resulting in very high levels of strength gain. Visual observations of the specimens also indicated that none of the specimens experienced detectable shrinkage cracking.

Results shown in Tables 3 and 4 further indicate, with few exceptions, that the vacuum saturation test by using water produced minor to moderate strength losses. Good durability may be achieved with both lime- and cement-stabilized fly ash by adding a sufficient amount of stabilizer and by providing adequate curing. Interesting results have been obtained with the acetic acid vacuum saturation test. Exposure to acetic acid has caused higher strength losses in lime-stabilized mixtures than in cement-stabilized mixtures, but strength gains are observed with the cement-stabilized Harrison. This may be attributable to the formation of cement-like ionic compounds, such as ferric acetate, resulting from the dissolution of Fe_2O_3 present in the Harrison ash. The same favorable effect as a result of acetic acid exposure was also experienced with the cement-stabilized Harrison ash in the later phase of the testing program involving permeability evaluation. This was manifested as appreciable decreases in permeability (see Bowders et al., this Record).

Vacuum Saturation Versus Freeze-Thaw

The vacuum saturation method is frequently used to evaluate the freeze-thaw durability of the pozzolan-aggregate bases on the basis of the excellent correlations obtained between the results of the vacuum saturation (with water) and cyclic freeze-thaw tests (*14*). The data obtained in this study were used in correlation and linear regression analyses to assess whether this would hold true for stabilized fly ash mixtures. Results presented in Table 5 indicate that the correlations between the two tests are fairly good, as reflected by the relatively high correlation coefficients, and are excellent in the case of cement-stabilized ashes, where the correlation coefficient is 96.7 percent. The regression equations in Table 5 represent the statistical relationships between the residual strengths obtained after vacuum saturation and 10 freeze-thaw cycles. On the basis of these analyses, the vacuum saturation test can be used in lieu of the freeze-thaw test to predict the freeze-thaw durability of stabilized fly ash mixtures.

SUMMARY AND CONCLUSIONS

Limited applications and engineering properties related to the stabilization of class F fly ash were discussed. The findings of the studies lead to the following general observations and conclusions.

1. Class F fly ash can be successfully stabilized with lime, cement, or lime and cement combinations to produce a pozzolanic base course material that does not require the addition of aggregate or soil.

TABLE 5 CORRELATION AND LINEAR REGRESSION ANALYSIS OF FREEZE-THAW AND VACUUM SATURATION RESIDUAL STRENGTHS

Mixture	Curing Period (days)	Correlation Coefficient r	Regression Equation* $q_{FT} = b + aq_{VS}$
Lime-stabilized ashes	7	0.815	$q_{FT} = 118.8 + 0.995\ q_{VS}$
Cement-stabilized ashes	7	0.967	$q_{FT} = 72.3 + 0.858\ q_{VS}$
Lime-stabilized ashes	28	0.863	$q_{FT} = 237.6 + 0.882\ q_{VS}$
Cement-stabilized ashes	28	0.911	$q_{FT} = 141.8 + 0.866\ q_{VS}$
Stabilized Harrison ash	7	0.927	$q_{FT} = 172.7 + 0.733\ q_{VS}$
Stabilized Amos ash	7	0.983	$q_{FT} = 73.3 + 0.977\ q_{VS}$
Stabilized Harrison ash	28	0.844	$q_{FT} = 133.8 + 1.11\ q_{VS}$
Stabilized Amos ash	28	0.973	$q_{FT} = 176.7 + 0.716\ q_{VS}$

*q_{FT} = residual strength after freeze-thaw test

q_{VS} = residual strength after vacuum saturation test

a,b = intercept and shape of the regression equation; constants

2. The two fly ashes evaluated in this study exhibited high levels of pozzolanic reactivity and satisfied all the relevant ASTM specification criteria for pozzolans used in cement and concrete and in lime-pozzolan stabilization. However, considerable differences exist in the compaction, strength, and durability characteristics of the stabilized fly ash mixtures.

3. In standard Proctor compaction, addition of increasing percentages of lime to fly ash resulted in increased OMC and decreased MDD for the mixtures. Addition of increasing percentages of cement did not affect the OMC and MDD appreciably.

4. Studies indicated that adequate strength development and durability levels can be achieved with stabilized fly ash by incorporating sufficient amounts of lime or cement or both and allowing the mixture to cure for a sufficient period. Achieving adequate levels of strength before service exposure is important.

5. In general, cement stabilization produced better strengths than lime stabilization. For cement-stabilized fly ash, increasing cement contents and extended curing resulted in increased strength. For lime-stabilized fly ash, increasing lime content caused an increase or decrease in strength, depending on the stabilizer content and the length of curing. Extended curing, however, increased strength invariably. The difference between the strengths of lime- and cement-stabilized ash at a given stabilizer content diminished somewhat as the curing period got longer.

6. Cement showed a dominant effect in strength development in combined lime- and cement-stabilized fly ash mixtures. Addition of cement to partially replace lime markedly improved the early (7 days) and intermediate strengths (28 to 56 days).

7. Cement-stabilized fly ash mixtures, in general, exhibited better durability characteristics than did the lime-stabilized mixtures after being exposed to different environments. High original (pre-exposure) strengths resulted in relatively high residual strengths. With few exceptions, increased stabilizer content and longer curing period enhanced durability.

8. Freeze-thaw cycles exposure produced the severest effects on durability of both stabilized ashes and resulted in substantial strength losses. Wet-dry cycles, in contrast, did not have any detrimental effect on durability and produced significant strength gains without any shrinkage cracking. Intermediate effects were observed relative to vacuum saturation with water or acetic acid solution. Acetic acid had a positive effect (increased residual strength) on durability with one of the cement-stabilized ashes, indicating enhanced durability after exposure to an acidic environment.

9. Results of the standard vacuum saturation tests (using water) correlate very well with those of the cyclic freeze-thaw tests. Therefore, vacuum saturation can accurately predict the freeze-thaw durability of stabilized fly ash.

ACKNOWLEDGMENTS

The authors wish to thank Tareq Ashour and Peter Chou, graduate research assistants at West Virginia University, who performed the experimental work, and the Monongahela Power Company and American Electric Power Corporation, who supplied the fly ashes. Appreciation is also expressed to James S. Gidley for his valuable contributions to the research project described in the paper. This project was funded by the Energy and Water Research Center of West Virginia University. This support is gratefully acknowledged.

REFERENCES

1. Lime-Fly Ash Stabilized Bases and Subbases. National Cooperative Highway Research Program. *Synthesis of Highway Practice 14*, HRB, National Research Council, Washington, D.C., 1976.
2. E. J. Barenberg. Cement-Fly Ash Mixes for Pavements. *Proc., Seventh International Ash Utilization Symposium*, DOE/METC-85/6018, Vol. 1, May 1985, pp. 57–66.

3. R. L. Terrel et al. *Soil Stabilization in Pavement Structures: A User's Manual*, Vol. 2, *Mixture Design Considerations*. FHWA-IP-80.2, FHWA, U.S. Department of Transportation, Oct. 1979.
4. J. F. Meyers, R. Pichumani, and B. S. Kapples. *Fly Ash: A Highway Construction Material*. FHWA-IP-76-16, FHWA, U.S. Department of Transportation, June 1976.
5. M. A. Usmen, J. J. Bowders, and J. S. Gidley. Low Permeability Liners Incorporating Fly Ash. In *Disposal and Utilization of Electric Utility Wastes*, (M. A. Usmen, ed.) ASCE, May 1988, pp. 50–65.
6. *Fly Ash Design Manual for Road and Site Applications*, Vol. 1, *Dry and Conditioned Placement*. GAI Consultants, Inc., EPRI, Feb. 1986.
7. L. J. Minnick. Reactions of Hydrated Lime with Pulverized Fuel Ash. In *Proceedings, Fly Ash Utilization Symposium*, U.S. Bureau of Mines Information Circular 8348, 1967, 1967, pp. 287–315.
8. H. B. Sutherland, T. W. Finlay, and I. A. Cram, Engineering and Related Properties of Pulverized Fuel Ash. *Journal of the Institution of Highway Engineers*, Vol. 15, June 1968, pp. 19–35.
9. D. H. Gray and Y. K. Lin. Engineering Properties of Compacted Fly Ash. *Journal of the Soil Mechanics and Foundations Division*, ASCE, Vol. 98, No. SM4, April 1972, pp. 361–380.
10. R. C. Joshi, D. M. Duncan, and H. McMaster. New and Conventional Engineering Uses of Fly Ash. *Transportation Engineering Journal*, ASCE, Vol. 101, No. TE4, Nov. 1975, pp. 791–806.
11. D. C. Kraft et al. Ash Utilization in Bikeway Construction. *Proc., Fifth International Ash Utilization Symposium*, METC/SP-79/110, February 1979, pp. 694–712.
12. W. J. Head and R. K. Seals. Design of Experimental Haul Road and Parking Lot Facilities Utilizing Power Plant Ash. *Proc., Fifth International Ash Utilization Symposium*, METC/SP-79/10, Feb. 1979, pp. 679–693.
13. D. C. Oberst. Cement-Stabilized Fly Ash Road Base. *Proc., Seventh International Ash Utilization Symposium*, DOE/METC-85-6018, Vol. 2, May 1985, pp. 590–596.
14. B. J. Dempsey and M. R. Thompson. Vacuum Saturation Method for Predicting Freeze-Thaw Durability of Stabilized Materials. In *Highway Research Record 442*, HRB, National Research Council, Washington, D.C., 1973, pp. 44–57.

Publication of this paper sponsored by Committee on Soil-Portland Cement Stabilization.

Permeability and Leachate Characteristics of Stabilized Class F Fly Ash

JOHN J. BOWDERS, JR., JAMES S. GIDLEY, AND MUMTAZ A. USMEN

A 2-year laboratory investigation of the permeability and leachate characteristics of stabilized fly ash has been completed at West Virginia University. Two class F fly ashes from coal-fired power plants in West Virginia were amended with either lime, cement, or bentonite. Stabilized specimens were permeated in either rigid- or flexible-wall permeameters. Permeant liquids included distilled water, highly concentrated organic solutions, and acidic solutions. Effluents from the permeability tests were collected periodically during the tests and analyzed for toxic elements. Results from the study indicate, for the ashes tested, permeabilities near 1.0E-06 cm/s can readily be obtained when 15 percent (by weight) of lime or cement is added to the fly ash. Much lower permeabilities (1.0E-08 cm/sec) can be obtained by substituting bentonite in place of the lime or cement. Addition of lime or cement appears to stabilize the fly ash with respect to toxic elements being leached from the ash. Bentonite may not be as successful at fixing the elements onto the fly ash. In conclusion, difficulty in using fly ash as a liner material probably does not lie in the ability to obtain low permeability nor in fixing the toxic elements from leaching but rather in combining those two properties into one material. Permeability can be decreased to acceptable values through the addition of bentonite, but some ability to fix elements from leaching may be lost. In addition, ashes from different plants and from different operating periods, as found in this study, can have markedly different properties. To use a particular ash in a liner application, ash must be tested for its behavior to ensure that the correct properties are used in design of the particular liner.

Use of coal as a fuel for the production of power has increased owing to improved technology for burning coal cleanly, the increased cost of oil and gas, and the mounting problems in the nuclear industry. This increased burning of coal has resulted in the production of vast quantities of fly ash, which is the finely divided residue that results from the burning of coal and is composed of noncombustible mineral matter in the coal and any carbon remaining owing to incomplete combustion.

Disposal of fly ash on-site or in landfills can be a major concern for power plant owners. The principal environmental concern is the possibility of leaching heavy metals from the fly ash into the underlying groundwater. A method of stabilizing the fly ash and, if possible, incorporating it into a useful material will be of major benefit to the electric utility industry, the coal industry, and the supporting industries, including those that transport coal or fly ash.

Stabilization can result in reducing the permeability of the ash in addition to fixing the elements from being leached from the fly ash. The use for such a material in vast quantities already exists and is demonstrated in the waste disposal industry as liners for landfills (*1*,*2*). Current regulations require liner systems for waste impoundment facilities to be composed of one or more synthetic liners backed up, or underlain, by an earth material liner or a demonstrated substitute (*3*). Stabilized fly ash may provide an attractive alternative in areas where natural soils are insufficient or their supply inadequate. Indeed, stabilized fly ash may even provide a method of lining areas to contain the quantities of fly ash that must be disposed.

Findings of a comprehensive study involving the stabilization of fly ash are reported in this paper. Two class F fly ashes from West Virginia power plants were acquired and evaluated for permeability and leaching characteristics both in the stabilized and unstabilized form. Compaction, strength, and durability characteristics also were evaluated (*4*,*5*). Initially, stabilization was performed by adding lime or cement. Later, bentonite was added as an alternative admixture for some specimens. The admixture and stabilizer materials were acquired commercially. The hydrated lime and Type I portland cement were produced locally (West Virginia), and the bentonite was obtained from Black Hills, Wyoming.

MATERIAL PROPERTIES

The composition of fly ash can vary considerably depending on the nature of the coal burned and power plant operational characteristics. Two somewhat different ashes were selected for this study. However, both are typical of ashes produced in the eastern United States by electric utilities that burn bituminous coal.

The first ash, known as Harrison, was obtained from the Harrison Power Plant in West Virginia. The second ash, Amos, was acquired from the Amos Power Plant, also located in West Virginia. Both ashes were obtained from the hopper at a moisture content of 0.1 percent and were tested to determine their relevant material properties. Harrison ash was found to have a higher iron (Fe_2O_3) content and thus a higher specific gravity (2.81) when compared with Amos (2.25). Harrison, showing only 4.4 percent retained on the No. 200 sieve and 14.4 percent retained on the No. 325 sieve, was somewhat finer than the Amos, with 8.9 percent and 22.4 percent retained on the respective sieves. The Amos ash had a higher pozzolanic activity index with lime and a higher lime-pozzolan strength development than the Harrison ash and is likely owing to the Amos ash's higher total of glassy components.

Both ashes were mixed with 3 to 15 percent by weight of either lime or portland cement and compacted by using Standard Proctor procedures. Maximum dry densities (MDD)

J. J. Bowders, Jr., and J. S. Gidley, Department of Civil Engineering, West Virginia University, Morgantown, W. Va. 26506. M. A. Usmen, Department of Civil Engineering, Wayne State University, Detroit, Mich. 48202.

decreased with increasing lime content and remained about the same regardless of the cement content. Harrison ash unit weights ranged from 15.7 to 17.0 kN/m³ (100 to 108 pcf) for lime and 17.3 to 17.6 kN/m³ (110 to 112 pcf) for cement addition. Amos ash unit weights ranged from 13.3 to 13.8 kN/m³ (85 to 88 pcf) for lime addition and from 14.1 to 14.3 kN/m³ (90 to 91 pcf) for cement addition. Optimum moisture contents (OMC) for Harrison ash ranged from 16 percent *t* for a 3 percent lime addition to 20 percent for a 15 percent lime addition. The cement addition resulted in OMCs from 18 to 19 percent. OMCs ranged from 20 to 22 percent for 3 to 15 percent lime for the Amos ash, and from 18 to 19 percent for 3 to 15 percent cement. Because Harrison had a higher specific gravity than does Amos, the resulting MDDs were higher than for the Amos ash. Adequate strength and durability could be obtained on the fly ashes by adding sufficient quantities of lime or cement and by curing for a sufficient period. A detailed discussion of the material properties can be found elsewhere (*4*, Usmen and Bowders, this Record).

EXPERIMENTAL PROGRAM

The principal experiment was permeability testing of stabilized fly ash specimens. Effluent was collected during the permeability tests and analyzed for elements that might have leached from the ash. The majority of the permeability tests were performed in rigid-wall, double-ring compaction mold permeameters. However, a series of flexible-wall permeability tests was performed on specimens that had been allowed an extended curing period. Hydraulic gradients of 100 were used in the compaction mold permeability tests. The gradients varied in the flexible-wall tests but were generally higher than 100 to reduce the testing time for the specimens with the lowest permeabilities. Specimens were permeated until the permeability stabilized and until two pore volumes of flow had taken place.

Fly ashes were mixed with lime or cement, compacted by using standard Proctor compaction procedures, and allowed to moist cure for 7 or 28 days. One series of specimens was permitted longer curing times. The Amos ash was eliminated from further testing when the permeability to water results indicated that the ash would not meet typical landfill liner requirements.

Three different permeant liquids were used in the study: distilled-deionized water, a solution of 5 percent methanol in water, and a 3.2 percent solution of acetic acid. Water was used to obtain baseline permeabilities and was considered a nonreactive liquid. The methanol solution contained a high level of organic carbon (18,750 mg/l), representing the possible organic carbon content in a landfill leachate. The 3.2 percent acetic acid solution had a pH of 2.5, typical of some landfill leachates especially in the early years of leachate generation.

Permeabilities were calculated on the basis of the quantity of liquid that flowed into the specimens. A constant-head test was performed, and the hydraulic conductivities were calculated based on Darcy's law:

$$K = (Q/t)/(i\ A) \tag{1}$$

where Q is the quantity of inflow, t is the time during which the inflow was measured, A is the cross-sectional area of the specimen perpendicular to the flow, i is the hydraulic gradient (change in head divided by the length of flow through the specimen), and K is the permeability of the specimen.

Note that throughout the remainder of this paper, the term "permeability" will be used to refer to values of K, the hydraulic conductivity (or coefficient of permeability). This usage is traditional among highway engineers. The values given should not be confused with the intrinsic permeability k given by

$$k = (u/\rho)\ K, \tag{2}$$

where u is the dynamic viscosity and ρ the density of the permeant liquid.

Three samples of the effluent were collected during each permeability test. The first sample of each test was collected at the beginning of the test, the second at about one pore volume of flow, and the third at about two pore volumes of flow. Effluents were analyzed by using atomic absorption spectroscopy for cadmium, chromium, copper, lead, and mercury.

The fly ash itself was also chemically analyzed for major and trace constituents. The major constituents determined were aluminum, potassium, calcium, and iron, assumed to be present as oxides. The trace constituents determined were cadmium, copper, lead, mercury, manganese, and zinc. Ash samples were prepared for atomic absorption analysis by fusion at 1000°C with lithium metaborate as a flux and followed by dissolution in a nitric acid solution (ASTM D4503-86) (*5*).

PERMEABILITY TEST RESULTS

The permeability of the fly ash in liner applications is the property of principal concern. Assuming low hydraulic gradients, the permeability controls the flow volumes passing through the liner. If low permeabilities are maintained, then the total mass flux of the leachate constituents remains small and the liner will have been successful. Permeability tests on various configurations of stabilized fly ash were performed to ascertain the effectiveness of the stabilizers. Four different series of tests were performed on the specimens. The first three series were based on the type of permeating liquid, deionized-distilled water, methanol, and acetic acid. The fourth series of tests was based on the length and conditions of the curing period. The results of each series of tests are presented next.

Distilled-Deionized Water Series

The permeability results for the specimens permeated with distilled-deionized (DD) water are presented in Table 1. The reported values are generally the average of two tests. Three or four tests were conducted in a few cases for that particular mix design. Time constraints did not allow for a statistically valid number of tests for each mix design. As such, the conclusions drawn have not been statistically verified. The permeability of unstabilized Harrison, compacted at optimum moisture content, was 7.2E-06 cm/sec and for Amos was 1.9E-05 cm/sec. Both ashes showed a trend of decreasing permeability

TABLE 1 PERMEABILITIES OF FLY ASH SPECIMENS STABILIZED WITH LIME, CEMENT, OR BENTONITE AND PERMEATED WITH DISTILLED-DEIONIZED WATER (cm/sec)

Stabilizer (%)	Harrison				Amos			
	7-Day		28-Day		7-Day		28-Day	
	K_f	K_f/K_o	K_f	K_f/K_o	K_f	K_f/K_o	K_f	K_f/K_o
Lime								
0	7.2E-06	1.0	---	-----	1.9E-05	1.0	----	-----
3	2.8E-06	0.39	2.2E-06	0.31	8.1E-06	0.43	6.4E-06	0.34
9	2.2E-06	0.31	1.8E-06	0.25	3.7E-06	0.19	4.6E-06	0.24
15	1.6E-06	0.22	1.2E-06	0.17	4.4E-06	0.23	3.7E-06	0.19
Cement								
3	6.6E-06	0.92	5.6E-06	0.78	6.2E-06	0.33	1.1E-05	0.58
9	1.6E-06	0.31	1.4E-06	0.19	3.1E-06	0.16	3.7E-06	0.19
15	7.5E-07	0.10	1.1E-06	0.15	3.0E-06	0.16	2.1E-06	0.11
Bentonite								
0.5	3.5E-06	0.49	------		1.5E-05	0.08	------	
2	1.7E-06	0.24	------		8.6E-06	0.45	------	
5	2.2E-07	0.03	------		7.2E-07	0.04	------	
10	5.0E-08	0.01	------		1.5E-07	0.01	------	

K_o: Permeability of the unstabilized ash to water
K_f: Final permeability for the specimen.
K_f/K_o: Final permeability of the specimen divided by the permeability of the unstabilized ash.
$K_f/K_o < 1.0$ indicates that the stabilizer reduced the permeability of the ash.
7-Day: Seven day moist curing time.
28-Day: Twenty-eight day moist curing time.
------: No tests under these conditions

as the percentage of stabilizer increased. At 15 percent lime or cement (by dry weight), the decrease in permeability was slightly less than 1 order of magnitude. The increased curing times, from 7 to 28 days, resulted in a slight but insignificant decrease in the permeability. Lowest permeabilities were recorded for the specimens with the maximum stabilizer content. At the 7-day curing times and 15 percent stabilizer addition, Harrison had permeabilities of 1.6E-06 for lime and 7.5E-07 for cement additions. Amos showed permeabilities of 4.4E-06 cm/sec for lime and 3.0E-06 for cement at 15 percent replacement.

At this juncture it became obvious that to reduce the permeability of those fly ashes to meet landfill regulations for the soil component (*3*), an alternative additive would be necessary. To this end bentonite was added to the two fly ashes in an attempt to reach the 1.0E-07 cm/sec permeability typically required. Those results are also presented in Table 1. Harrison required 5 percent bentonite to produce a permeability near 1.0E-07 cm/sec, and Amos required 10 percent replacement to meet the same mark. This behavior might be expected because Amos had an unstabilized permeability about three times greater than did the Harrison ash.

In addition, bentonite was added to lime or cement stabilized fly ashes to see what effect it would have on the stabilized materials. Of special concern were the possible effects on the leaching characteristics (which are presented in a later section). Regarding permeability, results presented in Table 2 indicate that adding bentonite to either lime or cement stabilized fly ash does not result in as large a reduction in the permeability as when bentonite is the sole admixture. Reduction was generally less than a factor of one-half when compared with one or two orders-of-magnitude for the bentonite alone. The final permeability was actually greater than that for the ash stabilized with cement when 10 percent bentonite was added to fly ash containing nine percent cement. It is believed that the free calcium associated with either the lime or cement replaces some of the sodium cations in the bentonite, thus reducing its ability to swell and reduce the permeability of the fly ash.

Methanol Series

The results of the permeability tests where a 5 percent solution of methanol was used as the permeant liquid are presented in Table 3. The ratio of the permeability of the methanol compared with that of the same mixture to water is reported in the fifth column of the table. Values less than 1.0 indicate that the permeability of the ash decreased for the methanol relative to that for water.

As is indicated in Table 3, the permeabilities to methanol were highly varied. Specimens in which lime was used for stabilization showed decreases in the permeability to methanol. Cement-stabilized specimens indicated an increase in the permeability to methanol. The specimens in which bentonite was used as the sole additive indicated mixed permeability results. It might be suspected that the methanol reacted with the ash of stabilizer and resulted in the varied response seen in the permeabilities. However, similar work with soils (*6,7*) indicated that dilute organic liquids do not readily affect the permeability of the soil. This conclusion is considered to be applicable to the fly ash work, and the variances in the

TABLE 2 PERMEABILITIES OF HARRISON SPECIMENS STABILIZED WITH LIME OR CEMENT MIXED WITH BENTONITE AND PERMEATED WITH DISTILLED-DEIONIZED WATER (cm/sec)

Bentonite	3% Cement		3% Lime	
(%)	K_f	K_f/K_o	K_f	K_f/K_o
0	6.6E-06	1.0	2.8E-06	1.0
2.5	2.7E-06	0.41	1.2E-06	0.43
5	1.4E-06	0.21	2.6E-06	0.93
10	1.4E-06	0.21	2.6E-06	0.93
	9% Cement		9% Lime	
	K_f	K_f/K_o	K_f	K_f/K_o
0	1.6E-06	1.0	2.2E-06	1.0
2.5	1.6E-06	1.0	1.6E-06	0.73
5	6.2E-07	0.39	2.1E-06	0.95
10	2.4E-06	1.50	1.8E-06	0.82

K_o: Permeability of the Harrison ash with the noted lime or cement content, no bentonite (values from Table 1).

K_f: Permeability of the Harrison ash with the noted lime or cement, and bentonite contents.

K_f/K_o: Indicates the permeability of the stabilized specimen with a particular percentage of bentonite divided by the permeability of the stabilized ash without the bentonite addition.

TABLE 3 PERMEABILITY OF STABILIZED HARRISON SPECIMENS PERMEATED WITH A PERCENT SOLUTION OF METHANOL (cm/sec)

Material Composition	Specimen No.	K_f	K_w	K_f/K_w
15% Cement	1	1.2E-06	7.5E-07	1.60
	2	8.7E-06		11.6
15% Lime	1	2.2E-08	1.6E-06	0.01
	2	4.9E-07		0.31
5% Bentonite	1	5.2E-07	2.2E-07	2.36
		8.6E-09		0.04
10% Bentonite	1	1.9E-06	5.0E-08	38.0
	2	1.3E-08		0.26
5% Bent/ 9% Cement	1	1.9E-06	6.2E-07	3.1
	2	3.8E-06		6.2
5% Bent/ 9% Lime	1	4.0E-07	2.1E-07	0.19
	2	8.2E-08		0.04

K_w: Permeability of the mixture to distilled water (Tables 1 or 2).

K_f: Permeability of the mixture to methanol.

K_f/K_w: Final permeability using methanol divided by the permeability of the same material composition to water.

permeabilities are reasoned to be attributable to specimen variability than to complex chemical alteration. Indeed, this is an area that deserves considerably more attention.

Acetic Acid Series

The permeabilities of lime-, cement-, and bentonite-stabilized fly ash specimens permeated with a 3.2 percent solution of acetic acid are presented in Table 4. The acid solution had a pH of 2.5. An examination of the final permeabilities of the specimens indicates that permeation with the acid solution lowered the permeabilities when compared with values for permeation with water or the methanol solution and indicates that the acid might be responsible for increasing the degree to which a stabilized specimen cures while also increasing the rate of the curing process. Observations of the specimens after testing showed small crystal particles throughout the speci-

TABLE 4 PERMEABILITY OF STABILIZED HARRISON SPECIMENS PERMEATED WITH A SOLUTION OF ACETIC ACID (cm/sec)

Material Composition	Specimen No.	K_f	K_w	K_f/K_w
15% Cement	1	1.2E-08	7.5E-07	0.02
	2	4.3E-08		0.06
15% Lime	1	1.8E-08	1.6E-06	0.01
	2	-------		-----
5% Bentonite	1	8.1E-08	2.2E-07	0.37
	2	4.3E-08		0.20
10% Bentonite	1	8.2E-07	5.0E-08	16.1
	2	3.9E-07		7.8
5% Bent/ 9% Cement	1	1.9E-08	6.2E-08	0.03
	2	1.4E-08		0.02
10% Bent/ 9% Lime	1	8.2E-08	2.1E-06	0.04
	2	3.9E-08		0.02

K_w: Permeability of the mixture to distilled water (Tables 1 or 2).
K_f: Permeability of the mixture to acetic acid.
K_f/K_w: Final permeability using acetic acid divided by the permeability of the same material composition to water.

TABLE 5 EFFECT OF CURING CONDITIONS ON THE PERMEABILITY OF STABILIZED HARRISON PERMEATED WITH DISTILLED-DEIONIZED WATER (cm/sec)

No. of Days of Curing	9% Lime		9% Cement	
	K_f	K_f/K_7	K_f	K_f/K_7
7	1.7E-05	1.0	6.5E-06	1.0
28	1.5E-06	0.09	3.7E-06	0.57
56	8.1E-07	0.05	8.0E-06	1.23
128	3.2E-07	0.02	3.4E-06	0.52
256	2.7E-08	0.002	3.2E-07	0.05

All specimens were cured in a 100% humidity, 22C environment.
K_7: Permeability of the specimen cured for seven days.
K_f: Permeability of the specimen at the specified number of days.
K_f/K_7: Final permeability divided by the permeability of the specimen which was cured for seven days.

mens. No direct investigation was made. However, it is believed that those particles resulted from the interaction of the acid with the admixtures or the fly ash or both.

Specimens stabilized with bentonite alone exhibited permeabilities greater than when permeated with water. Specimens that included either lime or cement alone or with 5 percent bentonite exhibited the lowest values of permeability.

Findings indicate that the acid possibly has a beneficial effect on the lime- and cement-stabilized specimens and causes a decrease in the permeability as permeation proceeds. This is a positive note in light of the fact that many municipal waste landfill leachates are acidic in nature.

Curing Conditions Series

A set of specimens was prepared with 9 percent cement or lime and allowed to cure for up to 256 days in a constant temperature (21°C) and humidity (100 percent) environment to examine the effect of curing conditions on the permeability of the stabilized fly ash. Permeabilities of the specimens were measured at various times during the curing process. Results of the tests are presented in Table 5. Lime-stabilized specimens showed marked decreases in permeability as the curing times increased. The 256-day specimen exhibited a three order-of-magnitude decrease in permeability when compared with that of the 7-day specimen.

Cement-stabilized specimens showed little variation in permeability at extended curing times, except the 256-day specimen, which underwent about a two order-of-magnitude decrease in permeability.

Some shrinkage of the stabilized fly ash was expected during the curing process. In some instances, especially under dry curing, this shrinkage process has been considered as a contributing cause to cracking and increased permeability of the stabilized material. Thus, the effect of extended periods of

dry curing was also evaluated in a second set of specimens. A group of 11 specimens stabilized with 9 to 15 percent lime or cement was first moist cured for a period of 7 or 28 days. Specimens were then placed in a room environment where the temperature remained about 21°C. Humidity was low but varied slightly. The specimens remained in this environment until they were set up in permeameters and tested. This period ranged from 180 to 270 days.

Mean permeability of the specimens was 2.6E-05 cm/sec. The lowest permeability was 4.2E-06 cm/sec, and the highest was 8.6E-05 cm/sec. Those values are slightly greater than the values for specimens tested immediately following moist curing (Table 1). However, no evidence of significant shrinkage cracking appeared, as would be indicated by large increases in the permeability of the dry cured specimens. Visual inspection of the specimens before and after permeation did not detect any macro-cracks.

EFFLUENT ANALYSIS RESULTS

Not only does the stabilized fly ash have to contain the waste of the facility it is used to line but it must contain any toxic elements inherent within its own matrix. The chief concern here is the chance of certain constituents leaching into the groundwater at concentrations determined to be hazardous to health. Those constituents include metals such as cadmium, chromium, copper, lead, and mercury. In a study by Malik et al. (*8*), a class F fly ash was subjected to leaching experiments. The U.S. EPA's procedure for determining if a waste is to be considered hazardous was used. The researchers also devised a flow-through leaching system, in which simulated rain was used in a setting that much more closely approximated the actual leaching process. Both raw ash and ash stabilized with 7 percent Type I portland cement were subjected to leaching. It was concluded that the cement stabilization lowered the solubilities of most elements relative to the raw ash. Only sodium, released from the cement, exceeded the elements released from the raw ash. The stabilized ash was determined not to be a hazardous material.

In this project samples of fly ash were analyzed for their chemical composition to be characterized for comparison with other fly ashes and to assess the potential for their leaching of toxic elements. Concentrations of the major constituents in the fly ashes used in this study are presented in Table 6. Concentrations of selected trace elements in the fly ashes, stabilizers, and bentonite are presented in Table 7. Note that the trace element concentrations in the fly ashes are significantly greater than in the stabilizers or bentonite.

The Harrison ash has undergone the most extensive testing of the two ashes. Therefore, the discussion of the results of the effluent analyses will be limited to this ash. Effluent analyses were performed for copper, cadmium, chromium, and lead. Results from eight of the mixes are presented in Table 8. In general, the percentage of copper, cadmium, and lead leached from the fly ash mixtures within this study was less than 0.041 percent. The percentage of chromium leached was up to 0.427 percent. Of special note, as indicated in Table 8, is that the rate of leaching is much higher within the initial flows and subsequently decreases after one or two pore volumes of flow. The percent concentrations of those four metals is a function of the type and percent of stabilizer added. In general, the leachability of cadmium and lead decreased as the length of the curing period increased. The cadmium and chromium concentrations were reduced with the addition of cement or lime. Addition of bentonite to the cement-stabilized ash resulted in an increase in the copper and chromium concentrations in the effluent. Bentonite may inhibit the fixation of those elements by the cement.

TABLE 6 SELECTED MAJOR ELEMENTS IN THE FLY ASH COMPOSITION

Constituent	Concentrations (% as oxide)	
	Harrison	Amos
Al_2O_3	18.9	30.0
K_2O	1.76	2.91
CaO	6.76	1.41
Fe_2O_3	25.4	(9.98)

Parentheses indicate less reliable values.

TABLE 7 CONCENTRATION OF SELECTED TRACE ELEMENTS IN FLY ASH, STABILIZERS, AND BENTONITE

Element	Concentrations (mg/kg)				
	Harrison	Amos	Lime	Port Cement	Bentonite
Cadmium	25.3	24.7	18.3	20.8	230.8
Chromium	358	293	47.5	100.8	66.7
Copper	336	441	259.2	279.2	288.3
Lead	250	169	429.2	503.3	583.3
Manganese	409	340	--	--	--
Mercury	89	(13)	--	--	--
Zinc	93	103	--	--	--

Parentheses indicate less reliable values.

TABLE 8 SELECTED EFFLUENT ANALYSES INDICATING THE EFFECT OF STABILIZATION ON HARRISON ASH

	Effluent Concentrations* (mg/l)											
	Copper			Cadmium			Chromium			Lead		
Mixture	1	2	3	1	2	3	1	2	3	1	2	3
H-0-0	0.079	0.088	0.026	0.024	0.012	0.009	3.229	1.700	0.719	0.867	0.867	0.733
H-7-15C	1.131	0.270	0.190	0.016	0.006	0.005	1.381	0.500	0.090	2.067	0.733	0.867
H-28-15C	0.478	0.192	0.062	0.013	0.007	0.005	0.423	0.176	0.039	1.367	0.300	0.014
H-7-3L	0.943	0.178	0.706	0.026	0.014	0.009	1.116	0.988	0.176	0.867	0.467	0.733
H-28-3L	1.327	0.316	0.135	0.014	0.006	0.004	1.463	0.142	0.042	0.400	0.333	0.200
H-7-9L	0.713	0.496	0.414	0.014	0.012	0.012	1.762	0.765	0.158	0.555	0.400	0.289
H-7-9C +5B	0.333	0.212	0.128	0.013	0.011	0.008	7.859	4.995	3.303	0.200	0.078	0.100
H-7-9C +10B	0.303	0.166	0.116	0.010	0.007	0.006	7.076	2.331	1.189	0.200	0.200	0.200

H-0-0: Harrison Ash-Uncured-No Stabilizer
H-7-15C: Harrison Ash-7 Days Curing-15% Cement
H-28-15C: Harrison Ash-28 Days Curing-15% Cement
H-7-3L: Harrison Ash-7 Days Curing-3% Lime
H-28-3L: Harrison Ash-28 Days Curing-3% Lime
H-7-9L: Harrison Ash-7 Days Curing-9% Lime
H-7-9C+5B: Harrison Ash-7 Days Curing-9% Cement + 5% Bentonite
H-7-9C+10B: Harrison Ash-7 Days Curing-9% Cement + 10% Bentonite
*1: Initial Effluent Collection Period
2: Effluent Collected At About One Pore Volume of Flow
3: Effluent Collected At About Two Pore Volumes of Flow

CONCLUSIONS

Two fly ashes from West Virginia have been stabilized with lime and cement by using stabilizer contents ranging from 3 to 15 percent. The stabilized, compacted specimens have been tested for permeability and leaching characteristics by using different permeant liquids.

Permeability results indicate that cement- and lime-stabilization can reduce the permeabilities of the ashes to about 1.0E-06 cm/sec when either stabilizer (15 percent by dry weight) is added. Adding bentonite to the stabilized fly ash further reduces the permeability. However, when water is the permeating liquid, the lowest permeabilities are obtained for fly ash mixed solely with bentonite. The lime and cement impede the effectiveness of the bentonite in reducing the permeability when they are incorporated together.

Results of the permeability tests where a solution of methanol was used indicated there was no significant change in the permeability of the stabilized ash specimens. The high concentration of organic carbon in the solution, similar to what might exist in a landfill leachate, does not appear to cause the deterioration of the stabilized ash.

The acid-permeated specimens displayed a marked decrease in permeability, especially in the lime-stabilized specimens. The cement specimens underwent a small decrease in permeability, and the bentonite specimens exhibited an even smaller and almost negligible decrease in permeability. The effect of the acid may be one of enhancing the degree of curing and of speeding up the process in the lime- and cement-stabilized specimens.

Extended periods of curing had negligible effect on the permeability of dry-cured specimens. No evidence of significant shrinkage cracking was found, as demonstrated by consistently low permeabilities. Increased moist curing of lime-stabilized specimens resulted in up to a three order-of-magnitude decrease in the permeability for curing times of 256 days. Permeabilities of the moist-cured cement specimens were unaltered except for the 256-day specimen and is believed to be partially due to cement's initially rapid curing rate and subsequent decreased rate of curing at long periods.

Leaching tests indicate that much of the concentration of toxic elements is loosely bound on the surface of the ash. This concentration is washed from the ash during the initial flow of liquid. Subsequent flow indicates a marked decrease in the concentration of toxic elements. Addition of lime or cement appears to stabilize the fly ash with respect to some of the toxic elements being leached from it. However, ash stabilized with bentonite alone may not be as successful at immobilizing the elements monitored in this study.

The difficulty in using fly ash as a liner material probably does not lie in the ability to obtain a low permeability or in immobilizing the toxic elements from leaching but rather in

the variability in the ash itself. Ashes from different plants and from the same plants at different operating periods, as found in this investigation, can have dramatically different properties. Thus, to use a particular ash in a liner application, test that particular ash to determine its properties. Of course, the testing must continue long enough to determine the variability of the ash with time. A final note concerns the fact that the permeabilities reported here were measured in the laboratory. A trial fly ash liner in the field, constructed with the equipment designated for the actual liner, is recommended to determine field permeabilities.

In summary, given the need for a sufficient supply of adequate materials for use as liners for landfills, waste impoundments, and other disposal facilities coupled with the increasing supply of fly ash from electric power-generating facilities, a stabilized fly ash liner represents an attractive development. This high volume use of fly ash in an environmentally beneficial role can lead to enhanced economic returns for the electric power industry, the coal industry, and the transportation network serving both entities.

ACKNOWLEDGMENTS

The experimental work reported in this article was performed by Daniel Hamric, Terry Irwin, Chrystalla Stylianou, and Murthy Bhadriraju, graduate research assistants in the Department of Civil Engineering at West Virginia University. Their efforts are greatly appreciated. The fly ashes were donated by Monongahela Power Company and American Electric Power Corporation. The assistance of James Burnell of Monongahela Power and Joe Dalton of American Electric Power is especially appreciated. Funding for this project was through the Energy and Water Research Center at West Virginia University, Project WUR-16-86. This support and the encouragement of Carl Irwin of the Center are gratefully acknowledged.

REFERENCES

1. J. J. Bowders, Jr. Fly Ash Liners for Waste Disposal Facilities. *Geotechnical News*, Vol. 6, No. 4, Dec. 1988, pp. 26–29.
2. C. J. Moretti, C. A. Wentz, and K. W. Wiken. Development of Fly Ash Liners for Waste Disposal Sites. *Proc., Eighth International Ash Utilization Symp.*, Vol. 2, Washington, D.C., Oct. 1987.
3. *Solid Waste Management Regulations.* Title 47, Series 38, West Virginia Department of Natural Resources, Dec. 1988.
4. M. A. Usmen, J. J. Bowders, Jr., and J. S. Gidley. Low Permeability Liners Incorporating Fly Ash. *Proc., ASCE National Convention*, Nashville, Tenn., April 1988, pp. 50–65.
5. C. Stylianou. *The Leachability of Stabilized and Unstabilized Fly Ash.* Problem Report, Department of Civil Engineering, West Virginia University, Morgantown, W.Va., Jan. 1990.
6. D. E. Daniel and H. M. Liljestrand. *Effects of Landfill Leachates on Natural Liner Systems.* GR83-6, Geotechnical Engineering Center, Department of Civil Engineering, University of Texas, Austin, Jan. 1984.
7. J. J. Bowders, Jr. and D. E. Daniel. Hydraulic Conductivity of Compacted Clay to Dilute Organic Chemicals. *Journal of Geotechnical Engineering*, Vol. 103, Dec. 1987, pp. 1432–1448.
8. R. I. A. Malek, P. H. Licastro, and D. M. Roy. Short- and Long-Term Leaching Behavior of a Low-Calcium Fly Ash and Cement-Stabilized Fly Ash. *Proc., Materials Research Society Symposium*, Vol. 65, 1986, pp. 269–284.

Publication of this paper sponsored by Committee on Soil-Portland Cement Stabilization.

Characterization and Structural Design of Cement-Treated Base

K. P. GEORGE

Proper mix design, adequate thickness, and diligent construction and control techniques are prerequisites to the successful performance of a cement-treated base (CTB) layer and, in turn, the entire pavement structure. A critical review and verification of the structural design procedures are presented. Highlighted are the structural characteristics relevant to the design procedure and design criteria, including distress modeling. Structural characteristics paramount to the thickness design procedure are discussed. On the basis of those properties only the predominant failure modes of CTB and the governing failure criteria are discussed. A short description highlighting the failure criterion of various design methods, six in all, is also discussed. Those methods vary widely in their use of mechanistic principles: for example, three methods are strictly fatigue-based and two others rely on precedent and experience. The validity of each design procedure is assessed by performance history of pavements in service, which is compiled from the literature. A comparison of CTB pavements for a typical sun-belt area for a range of traffic—5×10^6, 1×10^6, 2×10^6, 5×10^6 18-kip ESAL—indicates that the structural thicknesses mandated by the six design procedures are different. The most conservative design is approximately 30 percent thicker than the least conservative design.

Cement-stabilized materials have been used extensively in the United States and other countries primarily as base and subbase in flexible pavements. More recently, those materials have been used as sub-bases to concrete pavings. All cement-treated base (CTB) pavements basically consist of a layer of CTB on a prepared sub-base/subgrade with an overlying surfacing of asphaltic materials. The surface type and thickness depend on traffic volume, availability of materials, cost, climatic conditions, and local practices. A common type of wearing surface for lightly trafficked pavements is a double bituminous surface treatment (DBST) about ¾ in. thick. Thicker hot mix asphaltic concrete surfacings are warranted as traffic volumes increase.

Proper consideration should be given to mix design, thickness design, and construction procedures when using soil-cement. The mix design determines the proper proportion of cement (and water) in the mixture to ensure that the soil-cement base will have the required strength for both load carrying capacity and durability. In the PCA method (*1*), for example, the trial mixtures of soil and cement used to determine the correct mix are subjected to tests to show both the compressive strength of the mixture and the durability. Structural design procedures, taking into consideration the traffic volume expected on the roadway in question and predicated on the assumption of adequate mix design, construction, and maintenance practices, is confined to the selection of the thickness of the various layers of the pavement structure.

Mix design procedures have been standardized: ASTM Test Designations D559-57 and D560-57. Those tests serve well in formalizing a mix design for soil-cement and for recycled soil-cement. However, the structural design methodology, to say the least, is not well accepted.

For example, the question of structural design of cement-treated layer is altogether deleted from the draft state-of-the-art report on soil-cement (*2*). Also, the procedures vary over a wide range in sophistication and required material characterization. Some agencies use empirical procedures, where thickness of CTB is chosen by relying on precedent (e.g., the Province of Alberta (*3*)). Occupying the other end of the spectrum is the PCA design procedure, which is based on fatigue failure in CTB and which can handle the effect of mixed traffic in computing the life of CTB pavement.

Much information has been acquired regarding factors influencing the compressive strength of cement-treated material. However, there is a growing awareness among researchers of the need to examine the structural properties that influence pavement response for bases designed for heavy traffic. This interest is prompted by theoretical studies that show that the use of a stiff base material, such as a cement aggregate mixture having a high value of resilient modulus when compared with that of an unbound material, greatly reduces the vertical subgrade pressure but at the same time attracts tensile stresses at the underside of the base. Therefore, insofar as stresses induced by wheel loads are concerned, a need for information regarding resilient modulus, tensile strength, and fatigue resistance of cement-stabilized materials exists, especially under repeated loading conditions or thermal (shrinkage) loading or both. A better understanding of the structural properties of cement-treated material (CTM) is paramount for engineers to predict with greater certainty the performance of roads under changing traffic conditions.

This paper is an investigation of the structural inputs warranted for thickness design and, most important, their role in the distress modeling. In addition, the current structural design methodologies are critiqued and the resulting solutions are compared.

In accordance with the objectives of the study, the discussions are presented under the following subtopics:

1. Basic structural characterization of CTM relevant to thickness design,
2. Distress manifestations in CTB, and
3. Structural design procedures with special reference to failure criteria.

Department of Civil Engineering, University of Mississippi, University, Miss. 38677.

STRUCTURAL CHARACTERIZATION OF CTM

Modulus of Rupture (M_R)

Because CTM cracking is associated with stress (fatigue-related or thermal/shrinkage) exceeding strength (modulus of rupture), the latter is crucial in assessing structural adequacy of CTM. Scott (*4*) reported the following relationship between 7-day compressive strength (f_c) and modulus of rupture:

$$f_c = 4.47\ M_R \tag{1}$$

Resilient Modulus of CTM

Resilient moduli of CTM satisfying a given mix design criterion are not unique. A cursory study of previous results (*4–6*) suggests that resilient modulus is a function of soil type. Mitchell and Shen (*5*) reported flexural resilient moduli of 0.39×10^6 psi (2.69×10^6 kPa) and 2.1×10^6 psi (14.48×10^6 kPa) for silty-clay cement and sand cement respectively. A Maryland study asserted that different relationships between resilient modulus and unconfined strength exist for the cement-treated dense graded aggregate (DGA) and soil-cement materials. Data for Figure 1 are compiled from the author's (*6*) study and from a Saskatchewan study (*4*). The graphical representation of unconfined compressive strength (4 in. diameter (100 mm) by 4.6 in. (117 mm) high Proctor specimens) versus resilient moduli of various soil-cement mixtures reveals a trend for the data's falling into three bands: the first group consists of A-1 soils; the second, A-2 and A-3 soils; and the third, A-4 and A-6 soils. For an unconfined compressive strength of 600 psi, which is the design value adopted, the moduli for the three categories are 1.9×10^6 psi (13.1×10^6 kPa), 1.4×10^6 psi (9.65×10^6 kPa), and 1×10^6 psi (6.89×10^6 kPa), respectively.

One significant aspect of modulus is that modulus in compression is different from that in tension. Their relative magnitudes still remain unresolved. For example, Bofinger (*7*) and Raad et al. (*8*) reported that the modulus in tension is lower than that in compression. But Wang and Huston (*9*) found the opposite to be true. Those conflicting results are of minor consequence only because Khanna and Kachroo (*10*) indicated that using nonequal moduli exerts little effect on tensile horizontal stresses. Raad (*11*) in a recent study concluded that the bimodular ratio (E_c/E_t) in bending ranges between 0.5 and 3 or 5 depending on soil type. His analytical studies indicate that the bimodular properties have a significant effect on the traffic-induced stresses and strains on the underside of the stabilized base and on fatigue cracking. Scott indicated that a lower tensile modulus will develop a lower stress that, when compared with a lower fatigue breaking stress, basically leads to no change in thickness of the CTB.

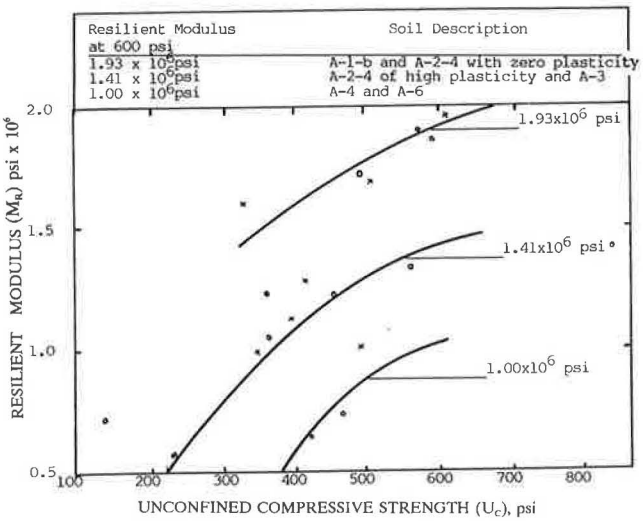

FIGURE 1 Resilient moduli of three classes of cement-treated soil. 1 psi = 6.89 kPa. [Adapted from George (*28*).]

Fatigue Behavior

Cement-treated soils are susceptible to fatigue failure after repeated applications of stresses greater than some limiting value. Fatigue in flexure is of interest because of its impact on pavement cracking. Nussbaum and Larsen (*12*) developed the earliest method of accounting for fatigue. In this analysis, the fatigue life is expressed in terms of a ratio involving the radius of curvature, R, under repeated load.

$$\frac{R_c}{R} = aN^{-b} \tag{2}$$

where

R_c = critical (failure) radius of curvature,
R = radius of curvature developed for a given load and number of load repetitions,
N = number of load repetitions, and
a, b = coefficients depending on soil type and specimen thickness.

By using flexural strain criterion, Pretoruis (*13*) indicated that excellent agreement occurs between Larsen's relationship and the results obtained from repeated flexural fatigue testing.

Some recent studies (*4,14*) advocate stress-related fatigue and strain fatigue (*13*) as well. One of the stress-fatigue relations (*4*) and the Pretoruis strain-fatigue relation will be referred to later; for ready reference, therefore, they are included here:

$$\%M_R = 94.4 - 4.71 \log N_f \tag{3}$$

$$\log N_f = 9.11 - 0.0578\ \varepsilon_t \tag{4}$$

where

$\%M_R$ = critical stress expressed as a percentage of modulus of rupture,
ε_t = initial tensile strain at the bottom fiber of the base, and
N_f = number of load (that induces stress of a specified magnitude) applications before fatigue failure occurs.

Additional results for allowable stress/strain to preclude excessive fatigue cracking are tabulated in Table 1. That there

TABLE 1 SUMMARY OF CRITICAL DESIGN VALUES OF CEMENT TREATED SOIL [ADAPTED FROM GEORGE (*28*)]

	Static		10^6 applications		10^7 applications		Unlimited applications
Source	Stress, psi	Strain, 10^{-6}in./in.	Stress, psi	Strain, 10^{-6}in./in.	Stress, psi	Strain, 10^{-6}in./in	Strain, 10^{-6}in./in.
Mitchell (5)		150	50 % of flexural strength	50[a]	-	65	
Scott (4)	95	-	66	-	62	-	60
Hadley et al. (15)	250	150-250	87.5	20			
Terrel et al. (30)	140		51				
Otte (31)				38 to 60			

[a]33% of the strain at failure in bending.

1 psi = 6.89 kPa, 1in. = 25.4 mm

is hardly any agreement on permissible value can be inferred from the summary data in the table. The fact that Hadley et al. (*15*) used indirect tensile test and others relied on flexural bending stress should explain the large discrepancy between those critical values. The critical design strain value of 20 × 10^{-6} in./in. proposed by Hadley et al. is considered overly conservative. Accordingly, critical stress and strain values of 60 psi (410 kPa) and 50 × 10^{-6} in./in., respectively, is recommended.

Distress Manifestations in CTB

In the past 2 decades, researchers have given increased attention to performance of soil-cement as a structural material, particularly its behavior in regard to fatigue. Equally damaging to CTB are the cracks that appear because of volume changes. The latter, known as shrinkage cracks, have been recognized as a major deterrent in the use of CTM in the base. Simply put, load-induced fatigue cracking and shrinkage cracking owing to volume change are the primary distresses that detract from performance. Despite the interest and concern of highway engineers regarding the overall problem of cracking, their opinions differ as to the gravity of each type of cracking (*16,17*). The following discussion calls attention to the cracking problem, especially how and when cracks are initiated, the sequence in which the two types appear, and methods to minimize the incidence of cracking in the CTB.

There is no general consensus regarding how and when cracks originate (occur). The popular view is that shrinkage cracks appear at the surface during the early life of CTB, as early as a few days to a few years after construction. Fatigue cracks, on the other hand, are initiated at the bottom of the base when fatigue consumption exceeds a certain magnitude (1, according to Miner's hypothesis). In either case, the crack initiated at the top or bottom face, depending on the load, propagates through the depth of the layer in a matter of a few weeks to a few years. Figure 2 is a schematic representation showing crack initiation and propagation in a finite series of steps owing to drying shrinkage alone. A thorough discussion as to how load-induced cracks—longitudinal and transverse—develop in cement-treated aggregate mixtures can be seen in Norling (*16*).

Chronologically, the first cracks in CTB occur during compaction. George (*17*), using theoretical calculations, indicated that slip planes, approximately perpendicular to the road surface and transverse to the direction of rolling, are induced in the CTB. Although those slip planes will be partially "healed" during curing, they present weak planes in the base. Because all cracks can be visualized as initiating at zones of weakness or flaws, those shear planes serve as the primary seat for further cracking. Perhaps, in recognition of these compaction cracks, Scott (*4*) asserted that CTM should be proportioned so that the young mix will not suffer fatigue cracking under construction traffic. If early cracking can be eliminated, then, according to Scott, CTM is likely to be fatigue resistant because it gains strength with time. Should the theory of early fatigue cracking prevail, shrinkage cracking can still occur at specific intervals because of tensile shrinkage/thermal stresses. It is reasonable to speculate that the fewer the compaction planes, the fewer (and perhaps narrower) the shrinkage cracks.

An experimental study conducted in Japan (*18*), and a complementary study in Switzerland (*19*), suggested opening the young soil-cement base to traffic, which induces many microcracks that enhance the performance of the base layer. On the surface this result appears to contradict the theory that heavy construction traffic should be avoided altogether for better performance. The difference seems to lie in the severity of induced cracks. Yamanouchi (*18*) recommended inducing microcracks under normal traffic, and Scott and others want to avoid larger cracks likely to occur under heavy construction traffic or smooth-wheeled rollers.

The question now arises as to how early trafficking minimizes cracking and improves performance of the cement base.

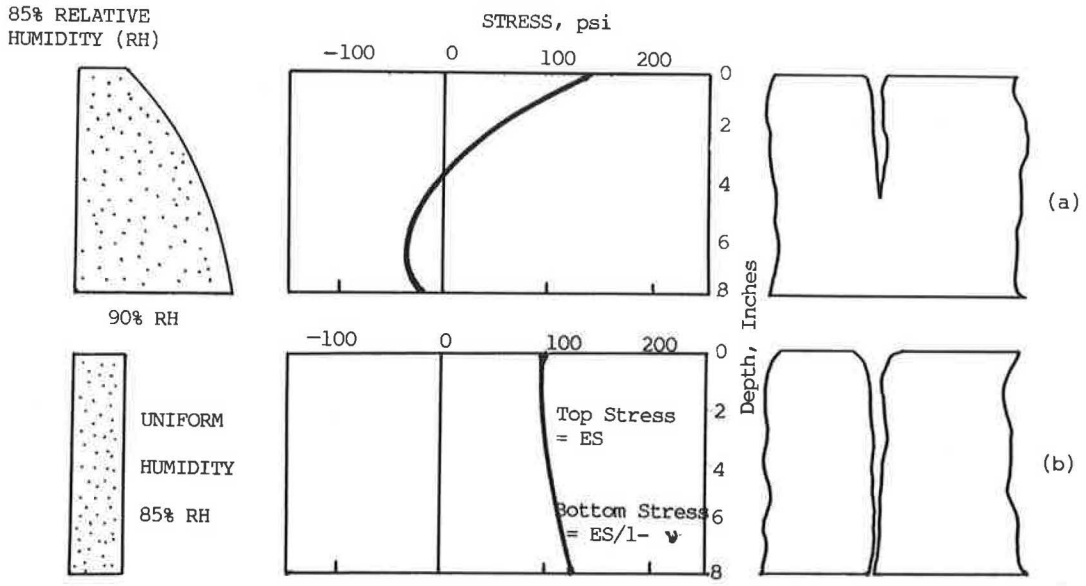

FIGURE 2 (a) Crack initiated owing to localized surface (tension) stress. (b) Crack propagated through owing to continued shrinkage (E = resilient modulus; S = free, unrestrained shrinkage, and ν = Poisson's ratio). 1 psi = 6.89 kPa. [Adapted from George (*17*).]

First, early trafficking helps to promote numerous fine cracks as opposed to fewer wide cracks. In addition, the young soil-cement can become denser on trafficking within a day or two of its placing. Healing of "compaction cracks" developed under rolling compaction can be another reason for superior performance. Fetz (*19*) speculated that a cement-treated layer with fine cracks induced in it will exhibit relatively low modulus and, in turn, attract lower wheel load stresses and thermal/shrinkage stresses.

Bofinger (*20*) appears to be more explicit in asserting what causes cracking in cement base. According to him, the characteristic cracking observed in soil-cement bases most often results from traffic loads rather than from shrinkage stresses. Controlling the spacing of cracks includes the early stressing of soil-cement base with rollers, a method claimed to be efficient for predetermining the crack size and spacing. A French study (*21*) is in general agreement with the predominance of load-related cracks in that cracking is attributed to load-induced tensile stresses and occurs at the base of the treated layer. The evidence is overwhelming that load-related cracking in CTB is more predominant than any other type (mostly shrinkage cracking).

Shrinkage Cracking

After the role of load-related fatigue cracking is understood, the significance of shrinkage cracking on the performance of CTM pavement can be investigated. Shrinkage cracking at times is considered a natural characteristic of soil-cement (*16*). Norling (*16*) asserts that such cracks are not the result of structural failure and, from an engineering standpoint, have not created a significant problem except in some very localized instances. Research and experience, however, suggest differently: for example, shrinkage cracks accelerate pavement deterioration. A Soviet study (*22*) indicates an increase in moisture content in the zone around and beneath the cracks with concomitant increase in deflection. Costigan and Thompson (*23*) assert that critical pavement response affecting performance occurs at transverse shrinkage cracks.

Shrinkage cracking is one of the unsatisfactory aspects of the overall behavior of soil-cement bases. At the time of occurrence it has relatively little effect on the riding quality of highway pavement. However, "secondary deterioration" effects, such as deflection and the resultant weakening of the subgrade, can be highly detrimental to the performance and useful life of the pavement structure.

Shrinkage cracking mechanism has been studied by George (*17*), who attributes the cracks to internally developed shrinkage-induced stresses. Through a step-by-step initiation and propagation, the base indeed undergoes cracking in a predictable configuration. George (*17,24*), in a series of papers, recommended reducing molding moisture, increasing compaction density, and carefully avoiding soils with montmorillonite clays as a means for reducing shrinkage and, in turn, shrinkage cracking. Fetz (*19*) asserted that limiting the degree of saturation to 70 percent can significantly reduce cracking. By using soil mechanics principles he showed that the liquid is in continuous phase when the saturation exceeds 70 percent. This situation is conducive to shrinkage and cracking, as schematically shown in Figure 3. When the saturation is less than 70 percent, no continuity of the liquid phase is evident. Only microfissures can occur, possibly reducing shrinkage stresses.

Undoubtedly, load-induced (fatigue) cracking constitutes the predominant pavement distress manifestation followed by shrinkage cracking.

STRUCTURAL DESIGN PROCEDURES

Structural design methods currently used are briefly described, highlighting (a) the failure criteria, if any, employed and (b)

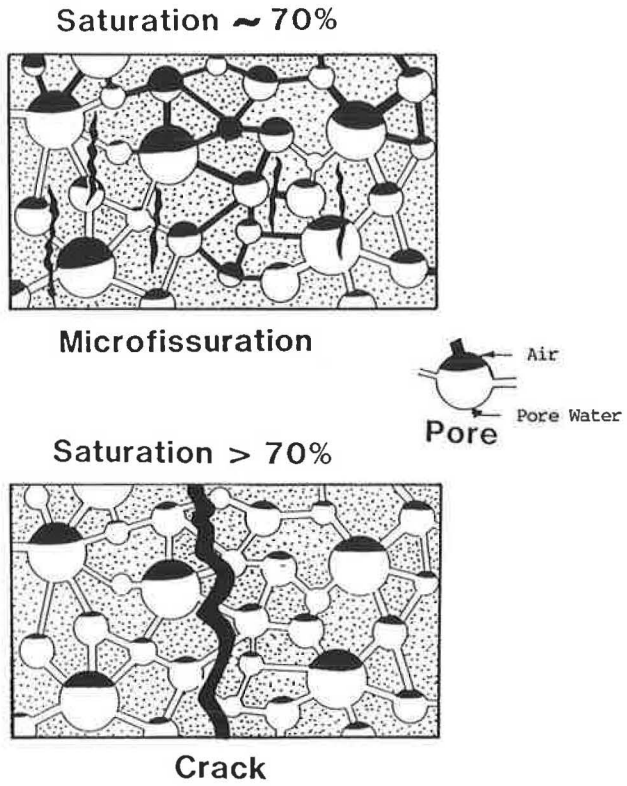

FIGURE 3 Degree of saturation influencing cracking in soil-cement. [Adapted from Fetz (*19*).]

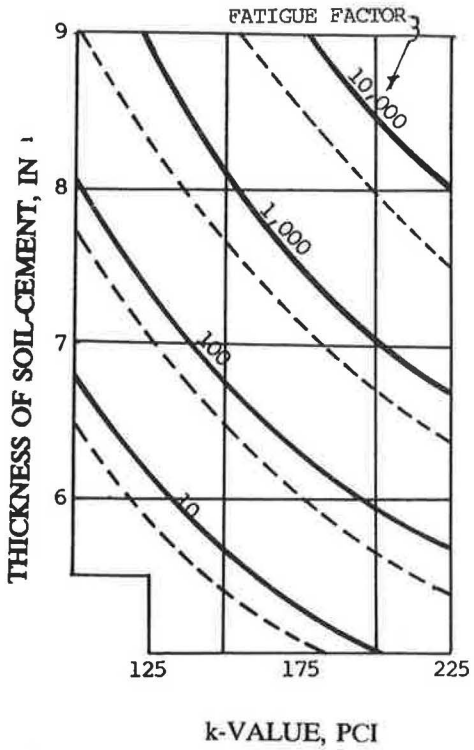

FIGURE 4 Thickness design chart for fine-grained soil-cement. [Adapted from *Thickness Design for Soil-Cement Pavements* (*26*).] 1 in. = 25.4 mm, 1 pci = 0.271 kPa/mm.

the predominant material characteristic(s) that supports the failure criterion. In all of the methods the structural design is often predicated on the assumption of a high standard of mix design, construction, and maintenance practices. Procedures currently practiced include the AASHTO method (*25*), the PCA method (*26*), stress/strain fatigue-based methods (*4,6*), and other thickness selection procedures that rely on precedent and experience (*3,27*).

AASHTO Method

The AASHTO flexible pavement design procedure—either 1972 Interim Guide or 1986 Revised Guide—in conjunction with such input values as traffic, subgrade strength, and environmental conditions, determines a structural number. The layer coefficients of component layers need to be determined in proportioning the thicknesses of various layers. AASHTO Guide has furnished layer coefficient value for CTM in relation to compressive strength or resilient modulus. George (*28*), in a recent study, employed a fatigue criterion (either in the CTM layer or in the overlying asphalt layer) to derive the layer coefficient of CTM. The layer coefficient value, 0.24, for soil-cement [7-day compressive strength no less than 600 psi (4094 kPa)] is in good agreement with those reported by other agencies including AASHTO.

The AASHO design procedure, especially the Revised Guide, includes several features that make it more realistic and site-specific. Nonetheless, the many physical limitations of the AASHO Road Test—its short duration (2 years), its single climate, its narrow range of materials and construction techniques, and the ad hoc approach used for mathematical modeling including the definition of layer coefficient—undermine the validity of the design procedure.

PCA Method

Soil-cement base course thickness is governed by fatigue consumption under repeated loads. Demonstrating that the strength of the pavement is more accurately assessed by the degree of bending, radius of curvature (see Equation 2) rather than deflection was used as a principal factor in evolving the design formulations. PCA research has shown that the ultimate "fatigue factor" of soil-cement can be described by a single equation, regardless of soil type and cement content, as long as the final product meets the criteria for fully hardened soil-cement. Two sets of fatigue consumption coefficients, one for granular soil-cement and the other for fine-grained soil-cement, are proposed by PCA researchers. Fatigue consumption factors are multiplied by the numbers (in thousands) of axles in each weight group and then summed to give a single value fatigue factor. When fatigue factor is known, engineers can select a soil-cement base course thickness by using nomographs provided (a typical nomograph for granular soil-cement is shown in Figure 4). Additional inputs required for the design include (a) subgrade strength, measured in terms of Westergaard modulus of subgrade reaction, k; (b) traffic, including volume

and distribution of axle weights; and (c) bituminous surface thickness (BST). Supported by research findings, PCA asserts that BSTs of under 2 in. (50 mm) do not appreciably add to the structural capacity of the soil-cement pavement.

Methods Based on Stress/Strain Fatigue

The first method [from Scott (*4*)] is based on the premise that if tensile stresses are limited to 60 percent of the modulus of rupture calculated by conventional elastic theory then no flexural fatigue will occur in soil-cement. Scott, from studying a few soils in Saskatchewan, derived the generalized relation (Equation 3).

The first step in the design procedure is to estimate the modulus of rupture and, in turn, resilient modulus. The latter also can be estimated either from compressive strength or from indirect tensile strength, both of which are relatively simple to determine. The limiting stress corresponding to number of load repetitions anticipated is obtained from Equation 3. When the resilient modulus is known, a layer analysis program (CHEV-5L) can be employed to estimate tensile stresses for various thicknesses of CTM and to choose an appropriate thickness for the design.

The fatigue relationship expressed by Equation 3 is perhaps the weak link in the design process because the $\%M_R$-N_f equation is derived based on samples tested in the laboratory. As far as is known, the design procedure has not been substantiated, either by field tests or by matching performance of as-built pavements.

The second method, proposed by George (*6*), basically using stress/strain fatigue in CTM, was developed for the purpose of designing flexible pavements and uses the concepts of limiting subgrade strain to control permanent deformation and limiting tensile strain in the asphalt layer (or limiting tensile stress/strain in the cement-treated layer, if applicable) to control fatigue cracking. Besides the fatigue relationships (Equations 3 and 4), resilient modulus of CTM is the other characteristic employed in the development of the design procedure. Typical resilient modulus values can be seen in Figure 1.

Applicable to stabilized and DGA bases, the design charts include design reliability as well. Because the method was originally intended for designing flexible pavements, the procedure includes asphalt grade selection criteria and a rational adjustment factor to account for the variation of asphalt mix stiffness from one climatic region to another. A typical design chart for 50 percent reliability is included in Figure 5.

Empirical Approach Based on Field Trials

Many highway agencies determined CTB thickness based on experience backed by proven field technique. Some adjustment to thickness, however, is generally made to account for traffic volume. A typical example is the design practice adopted by the Province of Alberta (*3*). That design is composed of a CTB layer overlaid with asphalt-stabilized granular base course (ASBC) layer and surfaced with an asphalt-concrete pavement (ACP). The thickness of the various layers is varied to give the required structure for different traffic and environmental conditions.

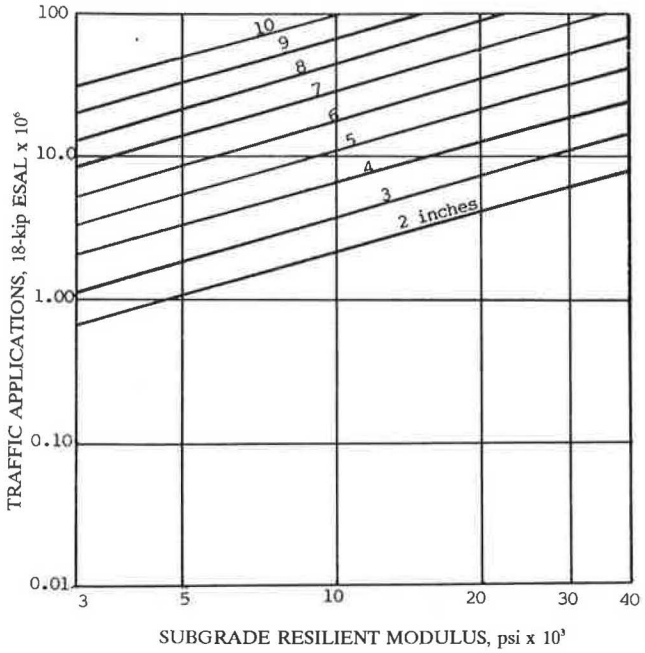

FIGURE 5 Design chart for CTB 8 in. thick. Fifty percent confidence level. 1 psi = 6.895 kPa; 1 kip = 4.448 kN; 1 inch = 25.4 mm. [Adapted from George (*6*).]

Road Note 29 (*27*) permits the use of two types of cement-stabilized materials, cement-bound granular material (CBGM) and soil-cement, both of which have grading requirements. CBGM should give minimum 7-day compressive strength (cube strength) of 500 psi (3445 kPa), and its use is limited to roads with a design life of less than 5 million standard axles. The load repetition limit stands at 1.5 million standard axles for soil-cement. In both of those mixes, it is commonly assumed that the frost resistance will be adequate if the compressive strength requirements have been met. The design chart in Figure 6 is reproduced from Road Note 29.

Adequacy of Design Procedures

Evaluating the performance of as-built pavements in which the design procedure in question was used is a technique often adopted for assessing the adequacy of design procedures. Many highway agencies, including Mississippi, have used the AASHTO method or slightly modified versions in designing CTM bases. Seventy one road sections with CTB, ranging in thickness from 4 to 10 in. (100 to 254 mm) with DBST or varying thicknesses of ACP, were investigated for their performance. All of those sections are in service in north Mississippi and have been overlaid once or more. With the tacit assumption that the useful life of the pavement is exhausted when an overlay is placed, the mean life of CTB pavements were computed and are presented in Table 2. The mean life increases slightly with ACP thickness but is independent of the CTB thickness. Traffic loading is poorly correlated to pavement life owing to either collinearity between loading and strength (consequent to design) or to dominant environmental effects. The fact the lives of CTM pavements average

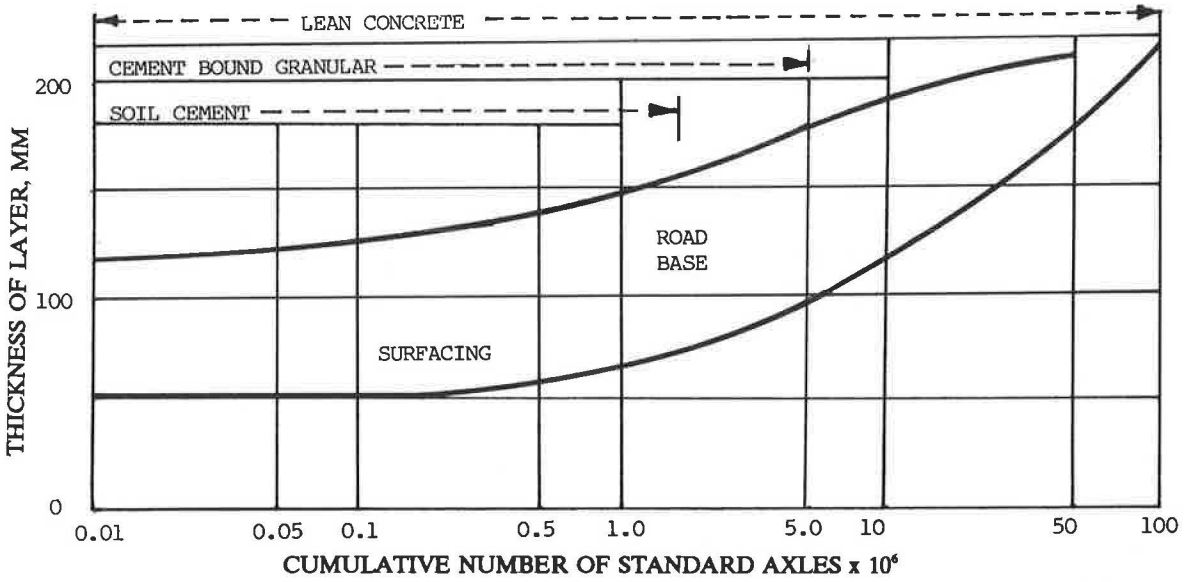

FIGURE 6 Lean concrete, soil-cement, and cement-bound granular road bases: minimum thickness of surfacing and road base. 1 in. = 25.4 mm. [Adapted from *A Guide to the Structural Design of Flexible and Rigid Pavements for New Roads* (27).]

TABLE 2 SUMMARY OF MEAN LIFE OF IN-SERVICE CEMENT-TREATED BASE PAVEMENTS IN NORTH MISSISSIPPI

Asphalt Surface Course Thickness, mm	Number of Sections in the Database	Mean Life, Years	Coefficient of Variation percent
19 (Double bituminous surface treatment)	42	16	35
50	3[a]	16.7	61
75	2[a]	23.5	15
100	15	18.9	17
200	9	19.6	2.7

[a]Too few sample points to be of significance

more than 15 years attests to the validity of the AASHTO design procedure. According to Scott (*4*), several hundred miles of cement-treated bases have been in place in Saskatchewan. To this author's knowledge, however, no performance evaluation of those roads has been reported. The structural design procedure (*3*) used in Alberta, although empirical in nature, has been successfully used for the construction of 1,800 mi (3000 km) of CTB roads. Engineers attribute the success to high standards of materials, mix design methods, construction, and maintenance practices used in the province. Inclusion of the 2-in. (50-mm) thick asphalt stabilized course has been very beneficial to the overall performance of the pavement and serves as a protective layer against reflective cracking. The performance evaluation of Alberta's CTB roads indicates that a useful service life of at least 15 years can be expected of CTB pavements built in the province provided the proper mix design, structural design, and construction and maintenance procedures are followed.

The British experience with soil-cement has been mixed at best. In the pavement design experiment at Alconbury Hill, six of the seven stabilized base sections with a single-sized sand mixed with 8 percent cement failed during the first 6 years. The poor performance is attributed to difficulty in compacting the soil-cement on site: the mean 7-day strength

achieved was only 140 psi (980 kPa). According to Wright (*29*), 164 lightly trafficked soil-cement roads in the United Kingdom that were 8 to 23 years old have performed well.

This author was unable to ascertain the field performance of roads constructed according to the PCA method and the reliability-based flexible pavement method. From limited comparisons, the authors of the two methods have demonstrated that they are valid.

Comparison of Structural Designs

Because data regarding field verification of the design procedures have been lacking, an alternative approach has been followed here for validating the design procedures. Employing the various design methods the CTB thickness to use in comparison has been computed (adopted in some cases). The input values for the pavement presumed to be located in the

TABLE 3 MATERIAL CHARACTERISTICS FOR SAMPLE PROBLEM

Description/Property	
Soil for Stabilization	SP sands (A-3) with 6-8 percent cement
Subgrade, A-4, (medium plasticity silty clay)	CBR = 8.0 percent Resilient modulus = 12000 psi (83,760 kPa) Modulus of subgrade reaction = 180 pci (0.049 N/mm^3)
Modulus of Rupture of CTM	108 psi (754 kPa)
Resilient Modulus of CTM	$1x10^6$ psi ($6.98x10^6$ kPa)
Resilient Modulus of ACP	$5x10^5$ psi ($3.50x10^6$ kPa)
Regional Factor	2.0
Traffic	varies (see Table 4)

TABLE 4 COMPARISON OF CTB THICKNESS REQUIREMENTS, MATERIAL PROPERTIES LISTED IN TABLE 3

Method	CTB Thickness /AC Surface Cumulative Equivalent (18-kip) Single Axles, ESALs			
	$5x10^6$	10^6	$2x10^6$	$5x10^6$
AASHTO Revised Guide[a] (25)	171mm/50mm	168/75	162/100	181/125
PCA Method (26)	158mm/50mm	167/50	171/63	182/63
Stress-Fatigue (Scott, 4)	228mm/50mm	222/75	207/75	191/125
Stress/Strain-Fatigue (George, 6)	152mm/40mm	203/40	203/57	203/95
Alberta (3)	150mm/50mm	175/-[b]	200/100	230/150
United Kingdom, Road Note 29 (27)	135mm/60mm	145/70	160[c]/75	

1 in. = 25.4 mm

[a] Terminal Serviceability level of 2.5

[b] Not available from reference

[c] Soil-cement bases recommended upto $1.5x10^6$ 18-kip; therefore, some extrapolation is required

sun belt are presented in Table 3. The subgrade soil is a medium plasticity silty clay, and the soil to be stabilized with cement is a poorly graded sand.

Despite the fact that an explicit comparison of thicknesses (because total thickness = CTB thickness + ACP thickness) between designs is not valid, some clear trends are evident. First, the PCA design and the Road Note 29 give lower overall thicknesses, and the Alberta design tends to be conservative, especially for heavily trafficked roads, not to mention the 2-in. (50 mm) ASB provided in conjunction with the CTB. Scott's stress-fatigue approach, though satisfactory for heavy trafficked roads, tends to overpredict the CTB thickness for light-trafficked roads. Second, the designs, from the thinnest (PCA design) to the thickest (Alberta method), vary by as much as 30 percent at the traffic level of 2×10^6 18-kip ESAL. This calculation assumes (a) 2:1 layer equivalency for ACP, CTM, and (b) the mean of all six methods estimates the required thickness.

CONCLUDING REMARKS

This review examines material characterization and failure criteria that spearhead structural design procedures of CTB. Modulus of rupture, resilient modulus, and fatigue behavior comprise the structural properties sought for in design. Load-induced fatigue cracking, followed by shrinkage cracking, constitutes the predominant distress manifestations in CTB. Six different structural design methods have been identified. Hypothetical designs employing those methods and compiled for a range of traffic reveal that the designs—from the thinnest to the thickest—vary as much as 30 percent. Therefore, a need exists for additional performance data regarding pavement in place to substantiate the validity of the design procedures.

Despite the fact that shrinkage cracking detracts from serviceability, only the Alberta design procedure includes provision for a 2-in. (50 mm) asphalt-stabilized granular base course, provided between the CTB and the asphalt concrete surfacing. This author believes that an open-graded, stabilized intermediate layer should be encouraged to minimize reflection cracking.

ACKNOWLEDGMENTS

The author's studies, some of which are reported in this paper, are sponsored by the Mississippi State Highway Department and Federal Highway Administration. The author acknowledges the support of those agencies and is also grateful to A. S. Rajagopal and L. K. Lim for reviewing the manuscript and making design calculations, respectively.

The opinions, funding, and conclusions expressed in this report are those of the author and not necessarily those of the Mississippi State Highway Department or the Federal Highway Administration. This report does not constitute a standard, specification, or regulation.

REFERENCES

1. *Soil-Cement Laboratory Handbook*. Portland Cement Association, 1971.
2. *State-of-the-Art Report on Soil-Cement*. Draft Report, ACI Committee 230, American Concrete Institute, 1988.
3. E. B. Owusu-Antwi and K. O. Anderson. *Cement-Treated Bases for Highways in Alberta*. Presented at the Sixty-Sixth Annual Meeting of the Transportation Research Board, Washington, D.C., 1987.
4. J. L. M. Scott. *Flexural Stress-Strain Characteristics of Saskatchewan Soil-Cements*. Technical Report 23, Saskatchewan Department of Highways, Saskatchewan, 1974.
5. J. K. Mitchell and C. K. Shen. Soil-Cement Properties Determined by Repeated Loading in Relation to Bases for Flexible Pavement. *Proc., International Conference on Structural Design of Asphalt Pavements*, University of Michigan, Ann Arbor, 1967.
6. K. P. George. *Overlay Design and Reflection Cracking Analysis for Flexible Pavements*. Final Report MSHD-RD-85-79, Department of Civil Engineering, University of Mississippi, 1985.
7. H. E. Bofinger. *The Measurement of Tensile Properties of Soil-Cement*. RRL Report LR 365, Road Research Laboratory, Crowthorne, Berkshire, England, 1970.
8. L. Raad, C. L. Monismith, and J. K. Mitchell. Tensile Strength Determinations of Cement-Treated Materials. In *Transportation Research Record 641*, TRB, National Research Council, Washington, D.C., 1977, pp. 48–51.
9. M. C. Wang and M. T. Huston. Direct Tensile Stress-Strain Property of Cement-Stabilized Soil. In *Highway Research Record 379*, HRB, National Research Council, 1972, pp. 19–24.
10. S. K. Khanna and P. N. Kachroo. Modification of Layered Theory for Pavement Design Analysis. *Journal of the Australian Road Research Board*, Third Conference, 1966.
11. L. Raad. Behavior of Cement-Treated Soils in Flexure. In *Transportation Research Record 1190*, TRB, National Research Council, Washington, D.C., 1988, pp. 1–12.
12. P. J. Nussbaum and T. J. Larsen. Load-Defection Characteristics of Soil-Cement Pavements. In *Highway Research Record 86*, HRB, National Research Council, Washington, D.C., 1965.
13. D. C. Pretoruis. *Design Considerations for Pavements Containing Soil-Cement Bases*. Ph.D. Dissertation, University of California, Berkeley, 1970.
14. L. Raad. A Mechanistic Model for Strength and Fatigue of Cement-Treated Soils. *ASTM Geotechnical Testing*, Vol. 4, No. 3, 1981.
15. W. O. Hadley et al. *A Comprehensive Structural Design for Stabilized Pavement Layers*. Research Report 98-12, CFHR, University of Texas, Austin, 1972.
16. L. T. Norling. Minimizing Reflective Cracks in Soil-Cement Pavements: A Status Report of Laboratory Studies. In *Highway Research Record 442*, HRB, National Research Council, Washington, D.C., 1973.
17. K. P. George. Mechanism of Shrinkage Cracking of Soil-Cement Bases. In *Highway Research Record 442*, HRB, National Research Council, Washington, D.C., 1973.
18. T. Yamanouchi. Some Studies of the Cracking of Soil-Cement in Japan. In *Highway Research Record 442*, HRB, National Research Council, Washington, D.C., 1973.
19. L. B. Fetz. *Soil-Cement: Mix Design, Structural Design and Research in Progress in Switzerland*. Presented at the Sixty-First Annual Meeting of the Transportation Research Board, Washington, D.C., 1982.
20. H. E. Bofinger. The Behavior of Soil-Cement Pavements with Special Reference to the Problem of Cracking. Proc., Fourth Asian Regional Conference.
21. K. Eyrolles. *Cement and Lime in Carriageway Stabilized Layers*. (in French). Paris, France.
22. O. A. Slavutskii. Characteristics in the Behavior of Soil-Cement in Eastern Siberia (in Russian), *Automobil Nye Dorogi*, Vol. 30, No. 3.
23. R. R. Costigan and M. R. Thompson. Response and Performance of Alternate Launch and Recovery Surfaces that Contain Layers of Stabilized Material. In *Transportation Research Record 1095*, TRB, National Research Council, Washington, D.C., 1986.
24. K. P. George. Shrinkage Characteristics of Soil-Cement Mixtures. In *Highway Research Record 255*, HRB, National Research Council, Washington, D.C., 1968.
25. *Revised Guide for Design of Pavement Structures*, AASHTO, Washington, D.C., 1986.

26. *Thickness Design for Soil-Cement Pavements*, Portland Cement Association, 1970.
27. *A Guide to the Structural Design of Flexible and Rigid Pavements for New Roads*. 3rd Edition, Road Note 29, Road Research Laboratory, H.M.S.O., London, 1970.
28. K. P. George. *Material Parameters for Pavement Design Using AASHTO Interim Guide*. Final Report MSHD-RD-81-66-1, Department of Civil Engineering, University of Mississippi, Mississippi, 1981.
29. M. J. Wright. *The Performance of Roads with Soil-Cement Bases*. Technical Report TRA 418, Cement and Concrete Association, London, 1969.
30. R. L. Terrell et al. *Soil Stabilization in Pavement Structures, A User's Manual: Mixture Design Considerations*. FHWA-IP-80-2, FHWA, U.S. Department of Transportation, Washington, D.C., 1979.
31. E. Otte. A Tentative Approach to the Design of Pavements Having Cement-Treated Layers. Presented at NIRR-PCI Symposium on Cement-Treated Crusher Run Bases, Johannesburg, South Africa, 1973.

Publication of this paper sponsored by Committee on Soil-Portland Cement Stabilization.

Expansive Behavior of Subgrade Soils in Arid Areas

NABIL F. ISMAEL, A. M. JERAGH, M. A. MOLLAH, AND O. AL-KHALIDI

Crushed cemented sand from arid areas has been used as a road base material in highway construction in Kuwait owing to the lack of good granular soils. Following several problems of pavement heave and cracking and of ground floor slabs placed on those soils, an extensive laboratory testing program was carried out on samples from six sites to examine the causes of those problems and to focus on suitable remedial measures. The program consisted of classification tests, chemical and mineralogical analysis, swelling tests in the consolidation apparatus, and CBR tests. The tests were performed on crushed or remolded soils and on the fines and coarse fractions separately. Test results indicated that several environmental factors have contributed to the high swell potential: the low natural moisture content, large placement density, soil disturbance owing to the breaking of cementation bonds, and the presence of large amounts of fines in the soil matrix. Swelling increased sharply as the percent of fines exceeded 35 percent, although the clay minerals were rather scarce in the fines and the plasticity index was below 20 for all soils. Hydrated lime was found to be effective as an additive in reducing the swelling potential of the local soils and in increasing their bearing capacity.

With the rapid development of arid areas in recent years, many construction projects have been completed including major highways, housing projects, and office buildings. Following completion of those projects, several problems associated with the collapse of the local surface soils of Kuwait (*1*,*2*) or the swelling of the underlying cemented sands have been observed. Cracking and damage occurred in highway pavements at some locations owing to the swelling of subgrade soils. Moreover, heave and cracking of groundfloor slabs of light buildings resting on compacted soils was observed. Because subgrade soils at many locations consist of calcareous silty sand with varying degrees of cementation (*3*), which is crushed prior to placement and compaction, it is surprising to observe swelling of those basically granular soils. Swelling of clays of high plasticity containing expansive clay minerals is known and has been examined in detail over the past 25 years. However, those soils differ in properties and basic characteristics from the subgrade soils in arid areas.

To examine the causes of swelling of those soils in Kuwait, an extensive laboratory testing program was performed over the past 2 years on samples recovered from six sites. The program consisted of tests for classification and physical properties, chemical and mineralogical composition, and oedometer and CBR tests. Several important environmental-related factors have been investigated, including the very low natural moisture content of the subgrade soils; the effect of initial cementation and subsequent soil disturbance resulting from breaking cementation bonds during excavation, placement, and compaction; and the influence of the amount and characteristics of the fines. The potential use of hydrated lime as a possible treatment technique has been examined by laboratory testing.

This paper presents and analyzes the results of this laboratory testing program to assess the relative importance of the various factors contributing to the observed expansive behavior of cemented sands when used as a base material or foundation course in Kuwait. Practical remedial measures are also discussed in light of test results and previous work on similar soils.

N. F. Ismael, Civil Engineering Department, Kuwait University, 13060 Safat, Kuwait. A. M. Jeragh, M. A. Mollah, and O. Al-Khalidi, Government Laboratories and Testing Station, Ministry of Public Works, Kuwait.

SOIL PROPERTIES AT THE TEST SITES

The soil profile at the sampling sites consists of a thin layer of wind-blown fine dune sand to a depth of up to 0.5 m, underlain by an extensive cemented calcareous sand deposit that extends to a great depth over limestone bedrock. The excess of evaporation over rainfall and the hot temperatures over the summer months lead to the precipitation of carbonates and other salts in the soil matrix and the formation of crusts of cemented sands, known locally as "gatch." Blocks of cemented sand were recovered from existing excavation pits at a depth of 1 m below ground level. The samples for classification tests were prepared by breaking the block samples by mortaring with a rubber pestle. Atterberg limit tests were conducted on fractions passing the No. 40 U.S. sieve. A summary of the physical properties and classification test results is given in Table 1 and reveals that after crushing and breaking the cementation bonds the soils can be classified as silty sand or as clayey sand mixtures. The amount of fines varies within a large range from 17.7 to 58.4 percent, with the clay size nearly 50 percent of the fines. All the soils tested had plasticity indices less than 20. The activity of the soil given in Table 1 is defined by

$$\text{activity} = A = \frac{\text{PI}}{C} \tag{1}$$

where PI is the Plasticity Index and C is the percentage of clay (particles < 0.002 mm) by weight.

The compaction characteristics of the test soils were determined by using the Modified Proctor test. The corresponding optimum moisture content varied within a narrow range of 8 to 12 percent.

TABLE 1 PHYSICAL PROPERTIES OF THE TEST SOILS

Property	Mirgab A	Dasmah B	Mishrif C	Shuwaikh D	Jabriya E	Andalus F
Sand %	81.2	66.4	54.6	82.3	73.3	41.6
Fines (Silt & Clay)%	18.8	33.6	45.4	17.7	26.7	58.4
Clay (<0.002 mm) %	8.5	13	20	11.4	14	30.9
Clay/Fines %	45.2	38.7	44	64.4	52.4	52.9
Liquid Limit - %	N.P	31	35	27	29	49
Plastic Limit - %	N.P	25	23	19	18	32
Plasticity Index - %	N.P	6	12	8	11	17
Shrinkage limit - %	-	-	19.6	18	17	17.3
Specific Gravity	2.69	2.72	2.74	2.66	2.7	2.63
Mean Diameter (mm)	0.18	0.15	0.10	0.33	0.26	0.07
Unified Soil Classification	SM	SM	SM-SC	SC	SM-SC	SM
AASHTO Classification	A-2-4	A-2-4	A-6	A-2-4	A-2-6	A-7-5
*Max Dry Unit Wt. (kN/m³)	19.81	18.83	19.71	20.10	19.81	18.24
*Optimum Moisture Content %	9	10	12	8	10	12
*Max Dry Unit Wt. with 5% lime	18.83	18.34	18.93	-	-	-
*Optimum Moisture with 5% lime	11	12	13.5	-	-	-
Activity of Soil	N.P	0.46	0.60	0.70	0.78	0.55
**Free Swell - %	0.3	2.5	11.2	4.56	10.9	27.3
**Swell Pressure KPa	20	60	210	92	164	686
**Free Swell-Soil-Lime Mix	Nil	Nil	1.2	-	-	-
**Swell pressure kPa soil-lime mix	10	40	170	-	-	-

* Based on ASTM D 1557-78 using 4.5 kg Rammer

** Samples prepared at maximum Modified Proctor dry density and optimum moisture content and tested as per ASTM D 3877-80.

\- Not measured

Chemical tests on selected samples from all sites and X ray mineralogical analysis of samples from four sites were carried out to gain a clear understanding of the factors affecting soil behavior. The results (summarized in Tables 2 and 3) reveal that the soils consist mainly of quartz with the clay minerals limited to a maximum of 10 percent of the soil composition at site F and a minimum of 2 percent at site E. Mineralogical analysis was not carried out for sites A and B. However, their clay mineral content, judging from the physical and chemical composition, is believed to be closer to the lower limit (2 percent) of the four tested soils.

It is clear that most of the clay size particles are not clay minerals when comparing the clay fraction from Table 1 with the clay mineral content of Table 3. The clay mineral content is only 25 percent, on average, of the clay size particles and is composed of chlorite and illite minerals. The remaining clay size particles include carbonates, salts, and other minerals in very fine form.

ENVIRONMENTAL FACTORS

Low Moisture Content

The surface and near-surface soils are in a relatively dry condition with natural moisture content below 2 percent within

TABLE 2 CHEMICAL ANALYSIS OF THE SOIL SAMPLES

Component	% Composition					
	Mirgab A	Dasmah B	Mishrif C	Shuwaikh D	Jabriya E	Andalus F
S_iO_2	80.5	80.0	87.47	91.74	76.4	82.51
AL_2O_3	3.5	7.4	5.23	2.71	2.25	7.6
Fe_2O_3	0.48	-	1.96	0.83	0.91	2.36
CaO	4.84	1.74	0.37	1.94	9.28	1.35
MgO	0.21	1.59	0.3	0.29	0.32	0.3
TiO_2	-	-	0.51	0.15	0.16	0.55
K_2O	-	-	1.64	1.14	0.82	1.58
Na_2O	-	-	1.20	0.55	0.12	1.06
SO_3	0.07	0.03	1.24	0.24	0.71	1.37

- Not measured

TABLE 3 SUMMARY OF MINERALOGICAL COMPOSITION OF THE TOTAL SAMPLES

Mishrif C	Mostly Quartz (~90%), very little feldspar Clay minerals: ~6% (chlorite, illite)
Shuwaikh D	Mostly Quartz (~90%), little feldspar, dolomite Clay minerals: ~3% (chlorite, illite)
Jabriya E	Mostly Quartz (~80%), dolomite (~12%) Clay minerals: ~2% (chlorite, illite)
Andalus F	Mostly Quartz (~90%), very little feldspar Clay minerals: ~10% (chlorite, illite)

the upper 1.5 m (*1*) for most of the year. The mean annual rainfall of about 100 mm occurs in several heavy showers during the winter season. The extremely hot weather during the summer months with temperatures exceeding 50°C and the lack of rain in the period from April to November leads to very low moisture content near ground level. To examine the effect of this low moisture content, samples from soils A, B, and C were compacted at different molding moisture contents to their maximum Modified Proctor dry density in a consolidation ring in accordance with ASTM D 3877-80. All specimens had a diameter of 73 mm and a thickness of 19 mm. Free swelling tests were performed after saturation under a seating pressure of 2.4 kPa for 48 hours. Identical tests were done on samples of the same soils mixed with 5 percent hydrated lime compacted to maximum modified dry density of the soil lime mix and cured for 28 days in humid conditions. Test results (see Figure 1) indicate the remarkable effect of the initial moisture content on the free swell. The free swell occurring at the natural moisture content of ~2 percent is nearly four to five times the corresponding value at optimum moisture content of each soil. The addition of lime results in a significant reduction of the free swell at all moisture contents.

Following those tests just described, samples of soils A, B, and C were tested in the consolidation apparatus at their natural moisture content (~2 percent), optimum moisture content, and optimum moisture content of the soil lime mixes containing 5 percent lime. All samples were compacted to their maximum modified dry density, and two series of tests were performed: (a) loaded and expanded, where the unsoaked specimen is saturated with water, loaded to prevent uplift,

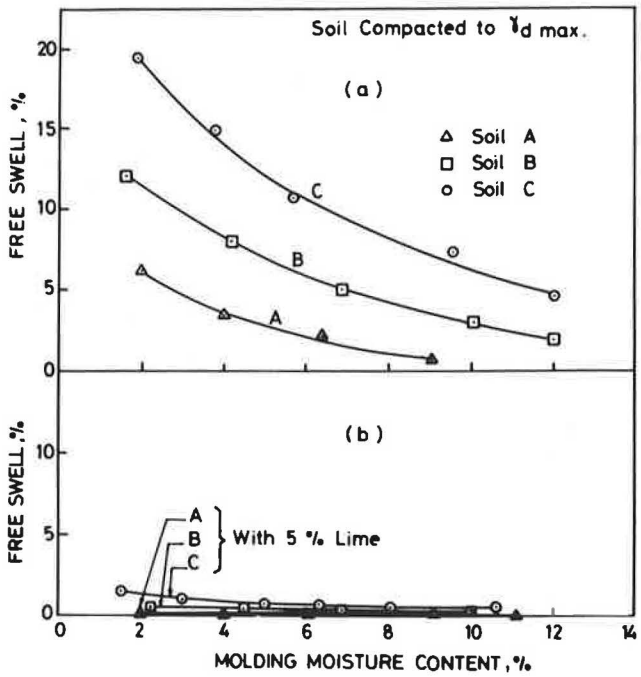

FIGURE 1 Free swell versus molding moisture content for compacted soils and soil-lime mixes.

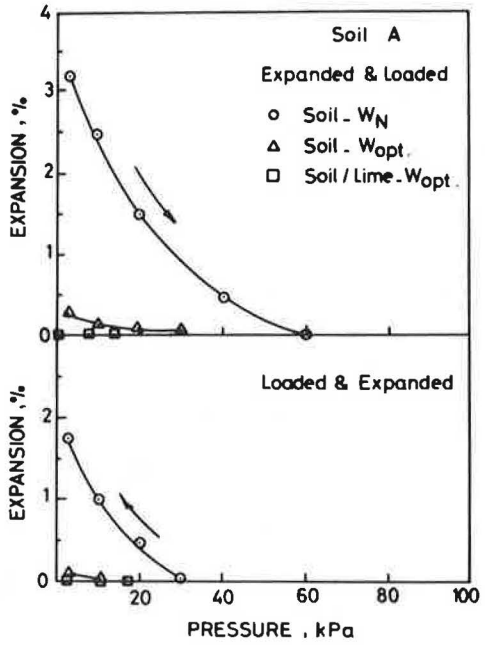

FIGURE 2 Load-expansion curves for soil A.

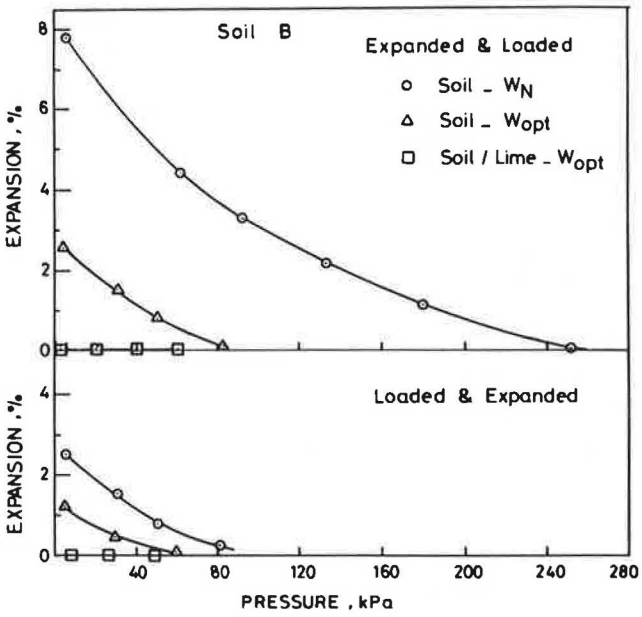

FIGURE 3 Load-expansion curves for soil B.

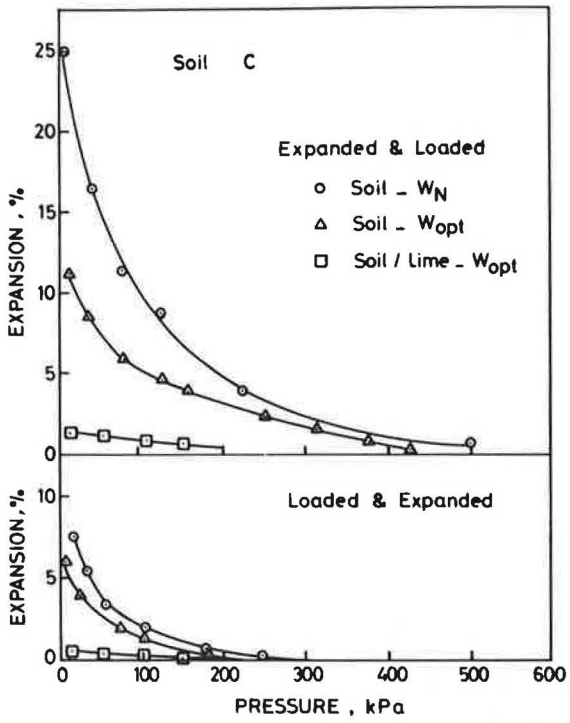

FIGURE 4 Load-expansion curves for soil C.

and then unloaded; and (b) expanded and loaded, where the specimen is saturated prior to loading under a seating load equal to a pressure of 2.4 kPa. The testing procedure for this and subsequent swelling tests followed ASTM Designation D 3877-80.

Test results are plotted in Figures 2–4 for soils A, B, and C, respectively. Expansion or swell is plotted against the applied pressure for samples expanded and loaded and for samples loaded and then expanded. Three curves are shown on each plot. The top curve is for the samples prepared at natural moisture content. The center curve is for samples prepared at the optimum moisture content. The bottom curve is for samples treated with lime at optimum moisture content and cured for 28 days prior to testing. The curves show that the

free swell and swelling pressure increased several times when the moisture content decreased from the optimum to the natural values.

The preceding results can be explained by moisture deficiency and large suction potential of the local soils. The soil reaches minimum volume as the moisture content drops well below the shrinkage limit. The soil absorbs water when it becomes available and increases in volume as the water content increases above the shrinkage limit toward an equilibrium value that depends on the gradation characteristics and the amount and properties of the fines in the soil matrix.

A comparison between the expansion versus applied pressure curves for samples of three soils prepared at natural moisture content is presented in Figure 5. Because the dry unit weight and molding moisture content are nearly the same for the three soils (see Table 1), the large difference in behavior is attributed to differences in the percent of fines in the soil matrix. Soil C, for example, has 1.35 times the fines and 4.5 times the free swell of soil B. The characteristics of the fines will be examined later.

CBR tests were performed on specimens of the three soils prepared according to AASHTO Designation T 193-63 by using three energies. The samples, soaked for 96 hours before testing, were prepared at natural moisture content, optimum moisture content, and mixed with 5 percent lime and optimum moisture content. Figure 6 indicates that a significant increase in strength was achieved by the addition of 5 percent lime and by curing for 28 days. CBR values for samples prepared at optimum moisture content are somewhat larger than the corresponding values for samples prepared at the natural moisture content, and this reduction in strength corresponding to dry conditions should be considered in pavement design.

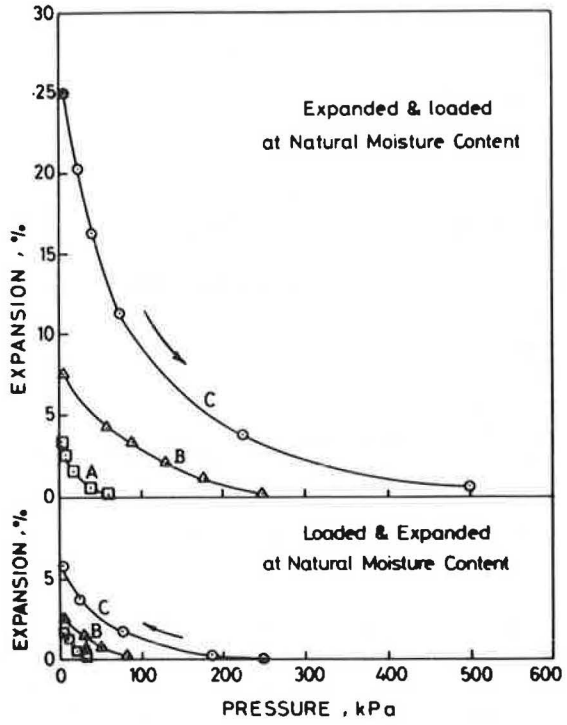

FIGURE 5 Comparison of the load expansion curves for specimens of soils A, B, and C molded at natural moisture content.

Loss of Cementation Bonds

Excavation of cemented sand leads to breaking the cementation bonds and disturbance of the soil fabric, and a new soil is formed on placement and compaction. Because of this disturbance, and of soil placement at high unit weight (γ_d max $\simeq$ 19.6 kN/m^3), additional swelling on saturation with water may happen. Undisturbed samples were trimmed from block samples taken from site E at a depth of 1.0 m to examine this factor. Both the expanded and loaded and the loaded and expanded tests were performed in the oedometer on undisturbed samples at in situ conditions and on samples remolded to the same moisture content and density. The results (plotted in Figure 7) reveal that the free swell and swell pressure are 6 percent and 50 kPa for undisturbed samples and 18 percent and 100 kPa for remolded samples. Thus, the free swell increased three times and the swell pressure increased twice owing to the crushing of cementation bonds and remolding. The moisture content increased from 1.6 percent at the beginning of the test to 20.7 at the end of the test for the undisturbed samples and to 26.7 percent for the remolded samples, thus reaching an equilibrium value above the plastic limit of 18 percent in both cases.

Although long-term monitoring of the moisture content with time following field compaction was not performed, it is possible to predict the direction of moisture changes throughout the year from the few measurements made so far. The moisture content drops from optimum (8 to 12 percent) to ~2 percent during the long summer season. Complete saturation and moisture content exceeding the optimum values are reached in the winter and following heavy rain. This, however, will last for short periods, and the preceding laboratory saturation of small samples is considered and is, therefore, severe when compared with field conditions. Thus, laboratory values will overestimate the actual swell under field conditions.

The results presented in Figure 7 point to the importance of soil disturbance as a factor aggravating or activating the expansive behavior of subgrade soils derived from cemented sands. Ratio of swelling of remolded to undisturbed cemented sand will depend on the degree of cementation and the type and amount of cementing agents present in the soil matrix. What caused the breaking of the cementation bonds to result in more swelling? It is evident that a large amount of fines is produced by breaking the cementation bonds (Table 1). The percent of fines is proportional to the degree of cementation (*3*), and most of the cementing agents break into fine sizes. Those fines that have a large surface area are moisture deficient. When densely packed, it has a high potential for absorbing water and for swelling freely when compared with the cemented sand matrix where the soft fine particles are welded to the larger size particles in a more stable soil fabric. Additional research is needed in this area that will involve testing soils of different degrees of cementation to assess the relative contribution of the different factors affecting this behavior.

Swell parameters determined from the preceding test methods may not be representative of many field conditions and should be considered as qualitative in nature. The lateral swell is not simulated, and swelling in the field depends on the availability of water while the specimen in the laboratory is inundated with distilled water. The chemical content of the

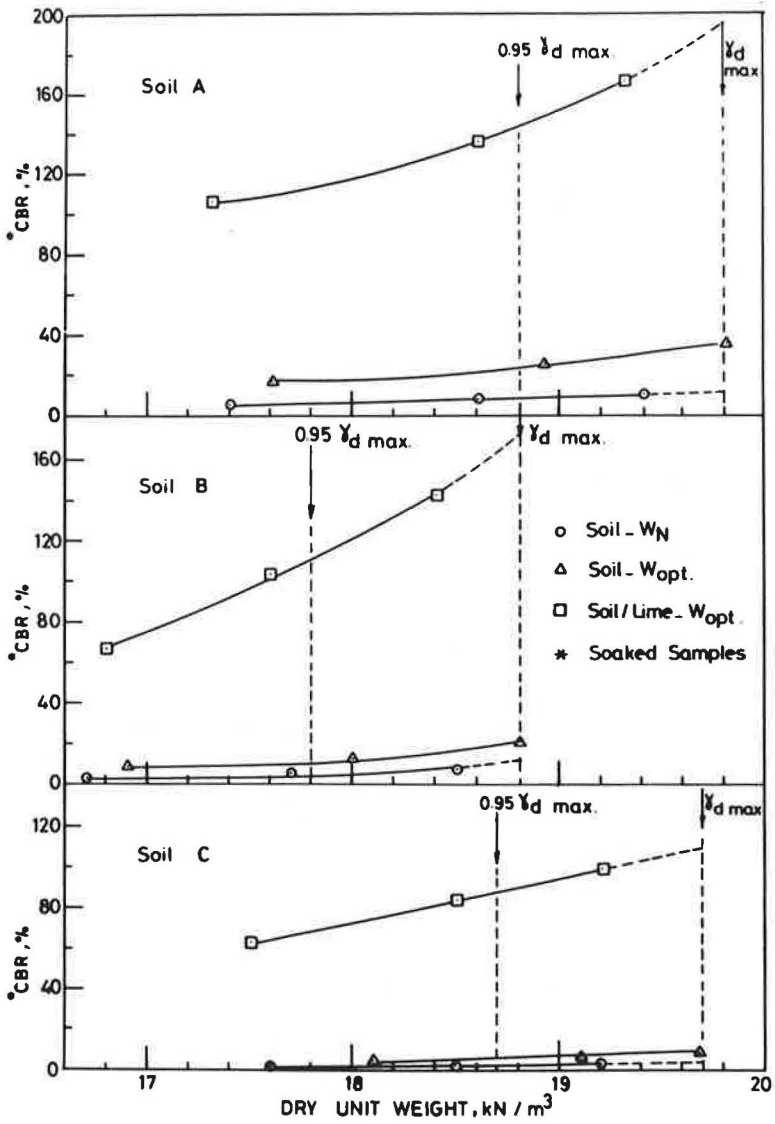

FIGURE 6 CBR versus dry unit weight for soils A, B, and C.

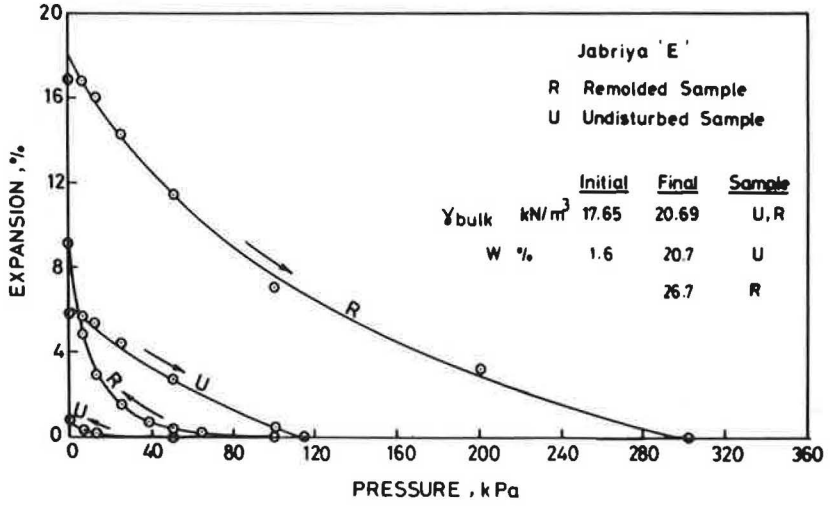

FIGURE 7 Load-expansion curves for undisturbed and remolded specimens from site E (depth = 1 m).

inundating water affects volume change and swell pressure in the field.

Characteristics of the Fines

Because of the important role of fines with respect to the swelling phenomenon, three samples were taken from sites D, E, and F and the fines fraction (< 0.075 mm) isolated from the coarse fraction. Free swelling tests were performed first on samples of the coarse fraction compacted to maximum dry density and optimum moisture content of the coarse fraction. Free swell was zero in all tests, indicating that swelling occurs entirely in the presence of fines. A summary of physical and engineering properties of the fines is presented in Table 4. Because of the limited number of fines available for testing, compaction tests on the fines were performed by using the Harvard Miniature Compactor apparatus, a proposed ASTM (1971) standard method of test.

Free swell and swell pressure values in Table 4 are for samples compacted to maximum dry density and optimum moisture content of the fines. Detailed chemical analysis of the fines is presented in Table 5 and indicates great similarity of the fines composition. Table 4 also confirms the similarity of the classification and compaction characteristics of the fines.

From Table 5 it can be seen that the fines contain approximately 30 percent of carbonates consisting of calcium and magnesium carbonates with a mineral hardness of 3 (compared with 7 for silica sand) (*4*). Because of its compressibility and soft structure, it is evident that it transforms to silt and clay size particles when breaking the cementation bonds and thus increases the amount of fines.

The results of the swelling tests are plotted in Figure 8. All samples were compacted to maximum dry density and optimum moisture content. Significant differences exist between the characteristics of the fines in the expanded and loaded tests and possibly is due to the disturbance caused by absorbing water at practically no restraint, which makes this particular test method unreliable for swelling or settlement calculation. However, the loaded and expanded tests indicate little difference in the behavior of the fines for the three soils (Figure 8).

Additional tests were conducted on the fines fraction only to determine the effect of molding moisture content on the expansive behavior of fines. Specimens for those tests were prepared at moisture contents of 15 to 35 percent with an interval of 5 percent to densities reflecting the compaction curves. The free swell in percent is plotted versus the molding moisture content in Figure 9, which also presents the compaction test results of the fines. The top and bottom envelopes of the data points indicate similar behavior of all fines especially considering the expected scatter of the test results. By examining Figure 9 one can see a significant reduction of the free swell when the moisture content is increased above the optimum values.

EXPANSIVE BEHAVIOR OF THE TEST SOILS

The expansive behavior for soils A, B, and C has been discussed in connection with the influence of the moisture content and the samples were prepared at natural moisture content and at optimum moisture content and maximum Modified Proctor dry density and were tested in the consolidation appa-

TABLE 4 PHYSICAL AND ENGINEERING PROPERTIES OF THE FINES

Property	Shuwaikh D	Jabriya E	Andalus F
Liquid Limit - %	59.5	72.8	65.0
Plastic Limit - %	32.2	36.7	35.8
Plasticity Index - %	27.3	36.1	29.2
Shrinkage Limit - %	13.6	19.0	15.2
Shrinkage Index - %	18.6	17.7	20.6
Specific Gravity	2.7	2.65	2.68
Unified Classification	MH	MH	MH
AASHTO Classification	A-7-5	A-7-5	A-7-5
*Maximum Dry Unit Wt. kN/m³	14.91	13.73	14.32
*Optimum Moisture Content %	22.5	29.8	27.5
Free Swell %	20.1	12.9	17.9
Swell Pressure - kPa	320	220	295

* Specimens were prepared in five layers and ten tamps per layer using Harvard Miniature Compaction Apparatus.

TABLE 5 SUMMARY OF THE CHEMICAL ANALYSIS OF THE FINES

Component Oxides	% Composition		
	Shuwaikh D	Jabriya E	Andalus F
SiO_2	43.46	45.40	43.1
AL_2O_3	14.18	15.08	13.92
Fe_2O_3	1.48	2.16	2.96
CaO	7.82	5.16	6.82
MgO	9.70	8.29	8.65
CO_2	16.7	14.88	13.75
CL^-	0.09	0.03	0.06
SO_3	0.71	0.75	2.91
Organic matter	4.95	6.43	7.18
Compounds	**% Composition**		
$CaCO_3$	13.96	9.21	12.18
$MgCO_3$	20.19	17.41	16.03
Total Carbonates	34.15	26.62	28.21
pH value	7.81	7.70	7.75

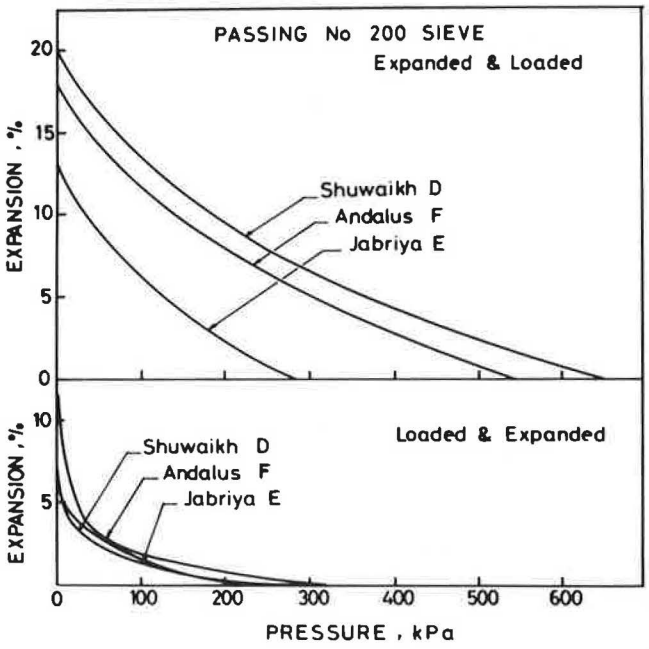

FIGURE 8 Load-expansion curves for the fines fraction of soils D, E, and F.

ratus. For soils D, E, and F, only samples compacted to maximum Modified Proctor dry density were tested. The results are depicted in Figure 10, and swell parameters are presented in Table 1. The significant influence of the presence of fines can be seen from the curves of soil F. Here, the free swell and swell pressure are 27.3 percent and 686 kPa, in comparison with soil D where the corresponding values were 4.56 percent and 92 kPa. Considering that the percent of fines in soil F is over three times greater than that of soil D, it is possible to relate this large difference in swell potential directly to the difference in the percent of fines in the two soils.

The relationships between the percent of fines, free swell, and swell pressure for the test soils are shown in Figure 11. When the percent fines exceeded about 35 percent, both the free swell and swell pressure increased rapidly to unacceptably large values. This means it is necessary to limit the amount of fines in those soils to a maximum of 35 percent if heave, cracking, and possible damage owing to expansive subgrade soils is to be avoided. This would place suitable local subgrade soils with respect to expansive behavior within the granular materials defined by the AASHTO soil classification system.

The preceding test results explain clearly the swelling behavior of subgrade soils in Kuwait. Swelling occurs in the presence of fines and increases as the percent of fines increases in the soil matrix. The characteristics of the fines are nearly the same

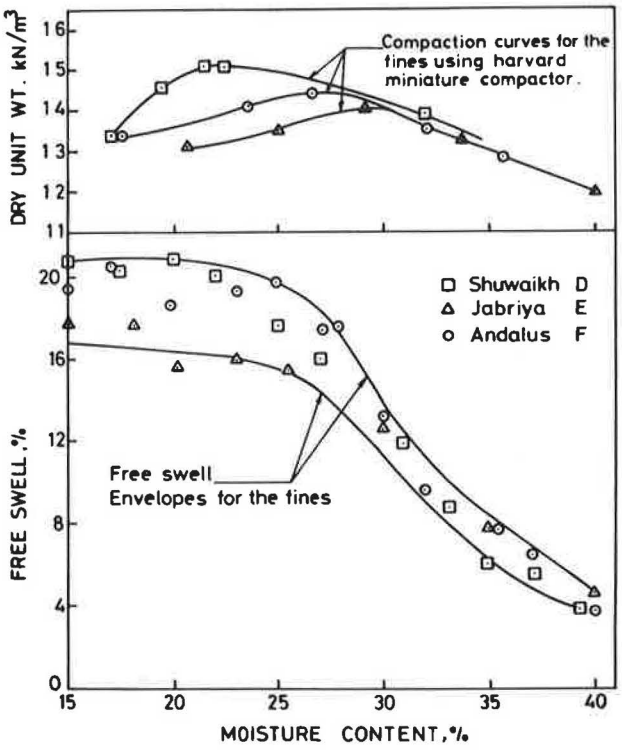

FIGURE 9 Free swell and dry unit weight versus molding moisture content for the fines of soils D, E, and F.

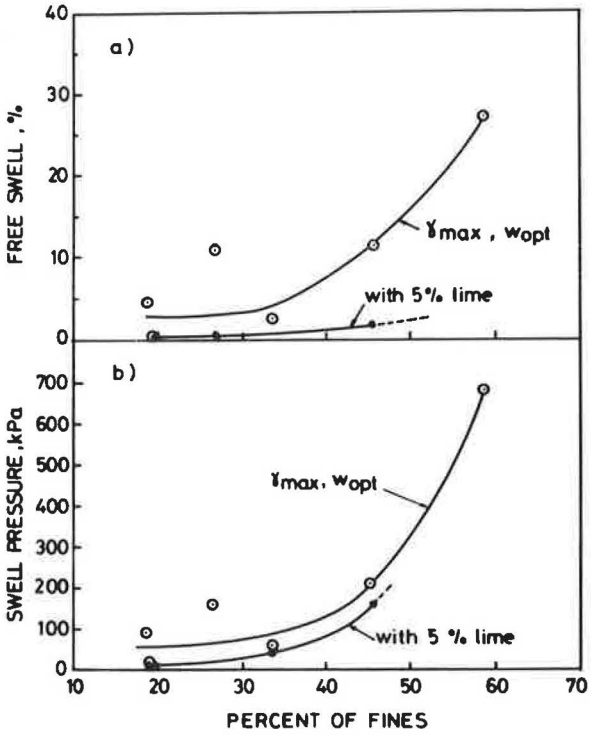

FIGURE 11 Free swell and swell pressure versus percent of fines for the test soils.

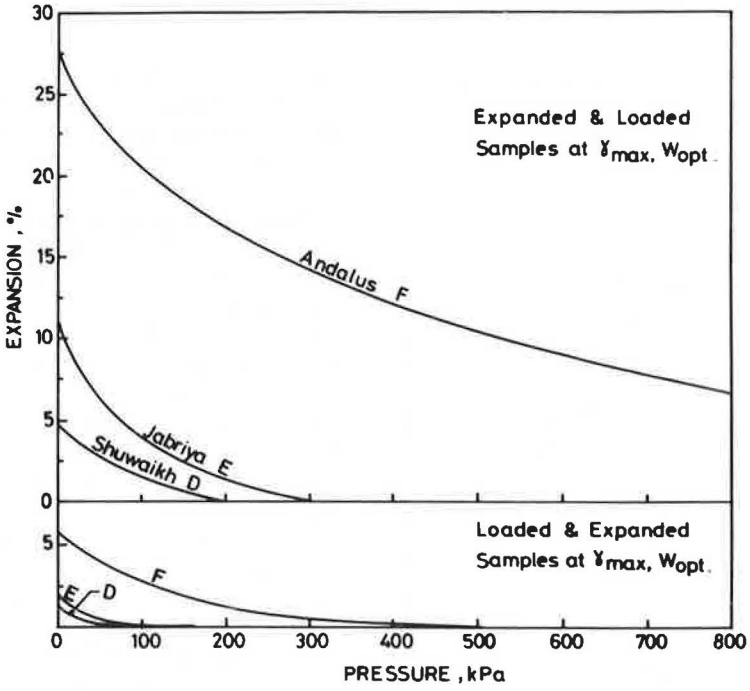

FIGURE 10 Load-expansion curves for soils D, E, and F.

at the test locations with the clay size nearly 50 percent of the fines. Approximately one-fourth of the clay size particles consist of clay minerals not considered highly expansive.

The presence of a large percentage of fines and the high placement density are aided by several environmental or climatic factors to cause unexpectedly intolerable swell and include the very low natural moisture content of the soil, which is well below the shrinkage limit and thus creates high soil suction. The presence of cementation bonds and the breaking of those bonds during excavation and compaction lead to disturbance of the soil fabric and high swelling. The precipitation of carbonates in the soil matrix during evaporation leads to an increase in the fines content as the cementation bonds are broken and causes more swell on saturation. Those factors combined lead to high potential for swell contrary to other soils with similar liquid limit and plasticity. On the basis of classification charts for swelling potential of cohesive soils that employ Atterberg limits (*5*,*6*), all the six test soils with liquid limit less than 50 and plasticity index below 20 will be classified as having low swell potential with the expected swell limited to 1 percent. However, problems of heave and cracking occurred in pavements and ground slabs that required costly maintenance and repair. Therefore, it is recommended to assess the swelling potential of the local soils in the oedometer by using an applied pressure equal to the overburden pressure plus the expected foundation pressure.

TREATMENT METHODS

Lime Stabilization

Because good granular materials are in short supply in Kuwait, it is necessary to use crushed cemented sand (gatch) as a road base material. If the percent of fines is excessive or if it is desired to limit volume changes to nearly zero, then the use of 5 percent hydrated lime as an additive appears to be an attractive option. Figures 1–4 and 6 present the effect of lime use on the swelling and bearing capacity of compacted gatch specimens. Because clay minerals are rather scarce in gatch [as shown here and in other studies (*7*)], gatch may not be suited for lime stabilization. However, with the present test results and the low cost of lime locally, lime is highly recommended because it reduces drastically the plasticity index and volume changes and improves the bearing capacity of compacted gatch soils.

Cement Stabilization

The use of ordinary portland cement as an additive has proven successful for local soils. The characteristics of the surface dune sand (*8*) and the underlying cemented sands can be improved significantly with the use of cement. Riedel and Simon (*7*) recommended for practical applications not less than 3 percent cement should be added to the gatch. However, cement is more costly than lime but will lead to higher strength.

Limiting the Percent of Fines

Because the amount of fines in the crushed cemented sand is a critical indicator of the possible swelling, limit the fines to a maximum of 30 to 35 percent of the composition of the fill. In many locations the local gatch will satisfy this requirement. However, if more fines are found, then isolate some of the fines by sieving to arrive at an acceptable ratio. This method may not be practical if a large amount of fill is employed.

Other Methods

Compaction to lower unit weight on the high side of optimum moisture content (3 to 4 percent above the optimum moisture content) is a method that may be applicable to local conditions (*9*). Compaction at moisture content above optimum leads to significant reduction of the free swell of the local soils and their fines (see Figure 1, soil B, and Figure 9). Prewetting may be used to achieve most of the heave before construction. After ponding, 5 percent of hydrated lime may be added to the top layer of soil to reduce its plasticity and swell potential (*10*). With time, moisture will be removed by gravity and evaporation. However, the presence of lime will restrain upward swell in case of sudden saturation by rain, broken pipes, or irrigation.

CONCLUSIONS AND RECOMMENDATIONS

An extensive laboratory testing program was performed on cemented sand samples obtained from six sites in Kuwait to examine the factors affecting the swelling potential of those soils and the practical treatment measures. On the basis of test results, the following conclusions and recommendations are reached:

1. Several environmental factors contribute to the swelling problem and include the very low moisture content of the near-surface soils and the high suction potential, loss of cementation bonds, and the presence of clay and silt size carbonates.
2. Swelling occurs owing to the presence of a large percent of fines in the soil matrix. The fines content should be limited to a maximum of 35 percent to avoid objectional swelling and heave.
3. Characteristics of the fines are nearly the same at the different test locations. Comparison of the physical and chemical composition of the fines and the free swell at different molding moisture content leads to this conclusion.
4. Clay fraction is nearly 50 percent of the fines for all soils. However, clay minerals are only one-fourth the clay fraction and consist of illite and chlorite.
5. Owing to its unique characteristics, and to the influence of environmental factors, the swelling of crushed cemented sands cannot be predicted by the charts employed for cohesive soils, which present low swelling potential in variance with reality. Laboratory and field swelling tests are recommended.

6. Compaction at moisture contents on the wet side of optimum leads to significant reduction of the free swell of the local subgrade soils and their fines.

7. The use of 5 percent of hydrated lime has proven effective in reducing or eliminating the swelling potential and in improving the bearing capacity of local soils.

REFERENCES

1. N. F. Ismael, O. Al-Khalidi, and M. A. Mollah, Saturation Effects on Calcareous Desert Sands. In *Transportation Research Record 1089*, TRB, National Research Council, Washington, D.C. 1986, pp. 39–48.
2. N. F. Ismael, A. M. Jeragh, M. A. Mollah, and O. Khalidi. Factors Affecting the Collapse Potential of Calcareous Desert Sands. *Proc., 9th Southeast Asian Geotechnical Conference*, Bangkok, Thailand, Dec. 1987, pp. 5.147–5.158.
3. N. F. Ismael, M. A. Mollah, and O. Al-Khalidi. Geotechnical Properties of Cemented Soils in Kuwait. *Australian Road Research Journal*, Vol. 16, June 1986, pp. 94–104.
4. B. McClelland. Design of Deep Penetration Piles for Ocean Structures. *Journal of the Geotechnical Engineering Division*, ASCE, Vol. 100, No. GT7, July 1974, pp. 709–747.
5. H. B. Seed, R. J. Woodward, and R. Lundgren. Prediction of Swelling Potential for Compacted Clays. *Journal of the Soil Mechanics and Foundations Division*, ASCE, Vol. 90, No. SM4, 1962, pp. 107–131.
6. M. W. O'Neill and N. Poormoayed. Methodology for Foundations on Expansive Clays. *Journal of the Geotechnical Engineering Division*, ASCE, Vol. 106, No. GT12, 1980, pp. 1345–1367.
7. G. Riedel and A. B. Simon. Geotechnical Properties of Kuwaiti "Gatch" and Their Improvement. *Journal of Engineering Geology*, No. 7, 1973, pp. 155–165.
8. N. F. Ismael. Cement Stabilization of Kuwaiti Soils. *Arab Gulf Journal of Scientific Research*, Vol. 2, No. 1, 1984, pp. 349–359.
9. B. M. Das. *Principles of Foundation Engineering*. PWS, Boston, Mass., 1984, pp. 485–486.
10. G. J. Gromko. Review of Expansive Soils. *Journal of the Geotechnical Engineering Division*, ASCE, Vol. 100, No. GT6, 1974, pp. 667–687.

Publication of this paper sponsored by Committee on Environmental Factors Except Frost.

Reinforced Soil Highway Slopes

RYAN R. BERG, RONALD P. ANDERSON, ROBERT J. RACE, AND VICKY E. CHOUERY-CURTIS

Reinforced soil highway slopes are an economical alternative to conventional grade separations within limited rights-of-way, such as flattened slopes, selected-fill embankments, or vertical retaining walls. Reinforced soil slopes are applied in six main areas of highway construction: steepened slopes, surficial reinforcement, compound slopes for road widening, repair of landslides, embankments over soft foundations, and vertical slopes or walls. Critical applications with a design life of 50 to 75 years and, therefore, grid geosynthetic reinforcement, are emphasized. Those applications are defined and illustrated and their relative economics are reviewed. Steepened embankment slopes are examined in detail. Economics are presented and compared with alternatives. Design of steepened slopes is reviewed with emphasis on stability analysis procedures and appurtenant features. Also, long-term reinforcement material property requirements and specification writing are evaluated. Brief case histories are presented to illustrate applicability, aesthetics, and construction of reinforced soil slopes in highway works, showing that reinforced soil slopes are a proven method of construction having broad applicability in highway construction. It is concluded that highway planners and route layout engineers should consider the reinforced soil slope alternative(s) when faced with grade separations that must fit within limited rights-of-way.

A better angle on highway grade separations is one that provides economic benefits while maintaining or improving safety and aesthetics. Traditionally, separations are created with embankment or vertical retaining wall structures as illustrated in Figures 1a and 1b. An embankment would be at an angle that would be stable against deep-seated and surficial slope failures. Also, embankment slopes are usually constructed flat enough (4H:1V to 2.5H:1V) to allow mowing of grass. Reinforced soil walls, or mechanically stabilized earth (MSE) embankments, have been used extensively in highway construction since the mid-1970s. Reinforced soil walls offer the advantages of precast concrete facing, structural flexibility, and lower cost than does traditional cast-in-place concrete construction. Most of those walls use steel strip or grid-reinforcing elements and a select granular backfill.

A better angle for grade separations is one that lies between the flatter 4H:1V (14 degrees) slope and the vertical (90 degrees) wall, as illustrated in Figure 1c. Aesthetically, the slope may have a vegetated face, which is often more acceptable to the public than are vertical concrete faces. Low-growth, maintenance-free vegetation is typically specified. A steepened, reinforced slope requires less fill and rights-of-way (ROW) than do flat slopes. Steepened slopes eliminate precast or cast-in-place concrete used for facings, thus saving material costs and construction time. The requirement of select granular backfill can also be waived when chemically resistant, structural polymer grid-reinforcing elements are used.

Geogrids, polymer-based grids specifically developed for long-term critical structures, were introduced into North America in the early 1980s (*1*) and typically differ from geotextiles in long-term load carrying definition and in soil interaction characteristics. Critical highway structures reinforced with geogrids are addressed next.

Since the early 1980s, reinforced slopes have typically been used by transportation agencies in problem areas but not as a routine construction alternative for grade separations. The goal of this paper is to familiarize route layout and structural highway engineers with where and how reinforced slopes may be used and with their economic and aesthetic benefits.

COMPONENTS OF REINFORCED SLOPES

The material components of a reinforced slope are labeled in Figure 2. Inclusions of tensile elements in the fill soil create a structurally stable composite mass. Tensile elements used with the reinforced fill to create the stable mass are termed primary reinforcement. Secondary, or surficial, reinforcing elements at the slope face are used to aid in compaction, for alignment control, and to minimize sloughing. The soil at the outer edge of the slope is also faced to prevent or minimize soil erosion. External and internal drainage provisions should also be included in the design.

The reinforcing element typically used is a polymer geogrid. Structural limitations, such as allowable tensile load and design life, are specific to polymer type and product manufacturing process. Extruded, uniplanar geogrids have been used for permanent, critical highway slope and retaining wall construction.

Additional components of reinforced slopes include design, specifications, installation, and inspection. The reinforcement, design, erosion protection, and installation assistance can all be specified to be supplied from one prequalified manufacturer. This is similar to the way "vertical slopes," or MSE walls, are now specified by most transportation agencies. An exception is the supplier should be responsible for all aspects of structural stability and not just internal stability. Alternatively, the specifying agency may provide its own design and specify reinforcing materials. Inspection is routinely conducted by the specifying agency.

R. R. Berg, R. P. Anderson, R. J. Race, Tensar Earth Technologies, Inc., 3000 Corporate Center Drive, Morrow, Ga. 30260. V. E. Chouery-Curtis, Tensar Environmental Systems, Inc., 1210 Citizens Parkway, Morrow, Ga. 30260. Current affiliation for R. R. Berg: Ryan R. Berg and Associates, 7501 S. 80th Street, Cottage Grove, Minn. 55016.

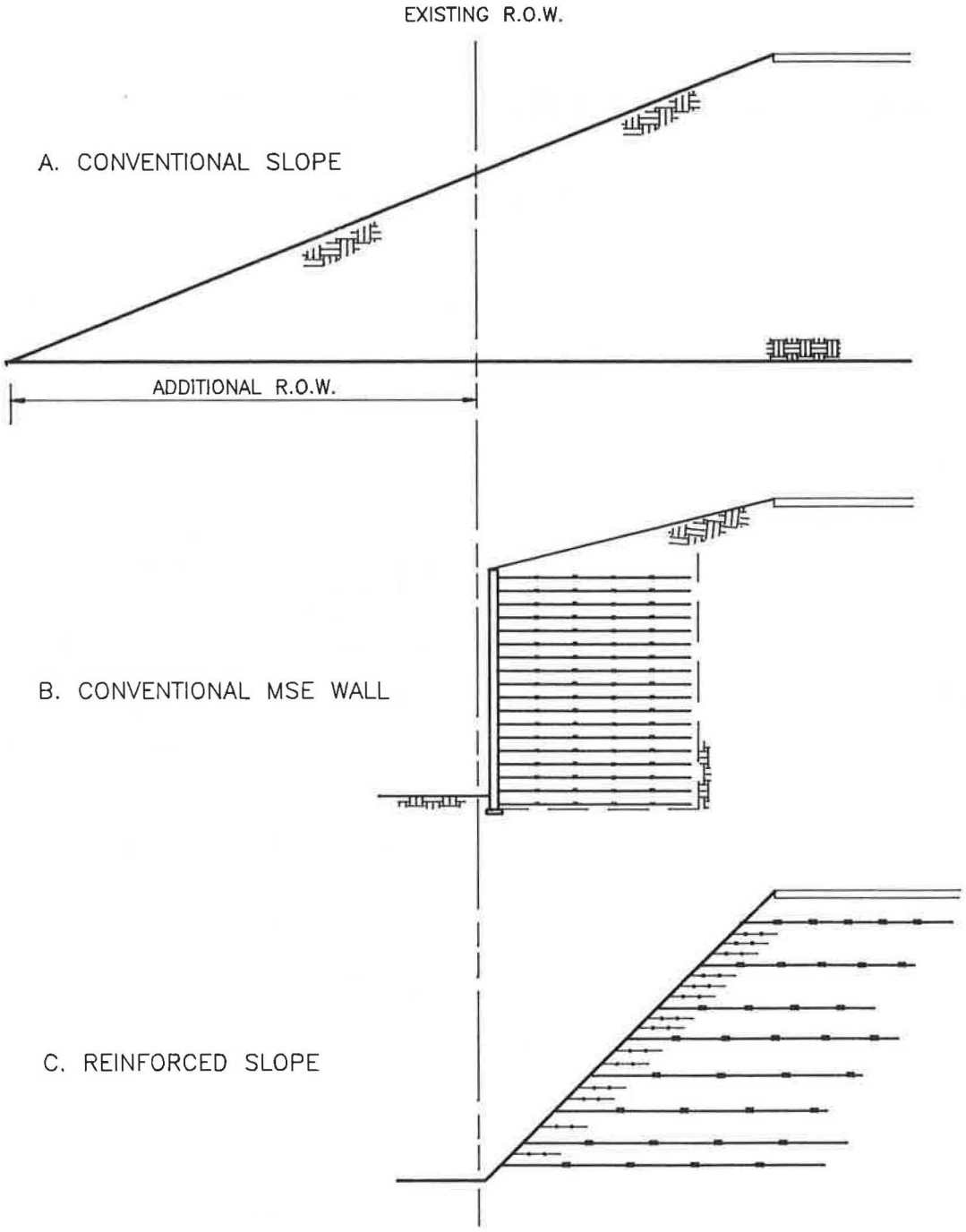

FIGURE 1 Grade separation options.

APPLICATIONS

The primary application of reinforced slopes in highway construction is steepened slopes. Related reinforced slope applications include surficial reinforcement, compound slope construction, landslide repair, and embankments over soft foundations and are briefly reviewed in this and in the Case Histories section.

Steepened Slopes

A steepened slope may be defined as a reinforced mass that would have a factor of safety against slope instability of less than 1 if it were unreinforced. A typical steepened slope is illustrated in Figure 2. On the basis of current design procedures, a structure with a slope angle up to 80 degrees can be classified as a steepened slope. A structure with a slope

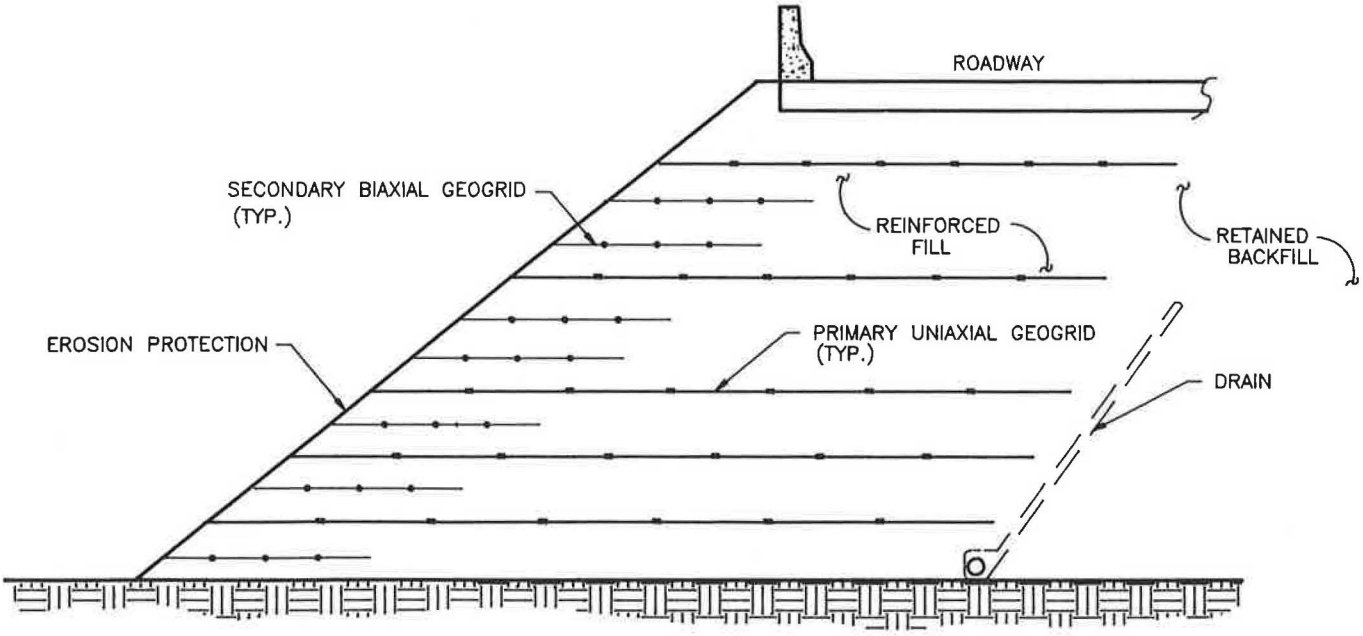

FIGURE 2 Components of a reinforced slope.

angle greater than 80 degrees will typically be classified as a retaining wall. Steepened slopes from 2 : 1 (26.6 degrees) to 0.35 : 1 (70 degrees) are routinely constructed. Construction details and erosion protection requirements vary between those extremes, as is illustrated in the Case Histories section.

Steepened slopes are used in lieu of flatter slopes to create more useable land on top of a slope or to minimize land take or ROW requirements at the bottom of a slope. Cost savings over retaining walls are realized by elimination of concrete facings and, in the case of steel-reinforced MSE walls, by use of on-site or nonselect fill. Aesthetically, a vegetated slope is usually more appealing than the vertical concrete facing.

Related Applications

Surficial Reinforcement

Shallow slope failures are not an uncommon sight along many roadways. Some of those slides can be attributed to lack of soil compaction near the edge of the slope, resulting in a weaker soil that more readily takes in surface water and further weakening the soil and leading to sloughing. Reinforcement allows soil compaction equipment to operate effectively on the slope edge (illustrated in Figure 3), thus achieving desired compaction and preventing future sloughing. Reinforcement for this application is typically 3- to 6-ft long and is spaced at 8- to 36-in. centers, vertically.

Compound Slope Construction

Compound slope construction refers to construction of a steepened reinforced slope into an existing stable, unreinforced slope and differs from the previous applications because analysis and construction details vary. Global stability of the overall system may be more difficult to assess.

FIGURE 3 Surficial reinforcement on a 1:1 fill.

The most prominent use of this application is in widening of existing roads (see Figure 10). In the near future, many of the nation's freeways and tollways need to be widened, which may either be in the direction of the median, space permitting, or along the exterior lanes. The exterior widening of tall embankments requires large amounts of fill and additional ROW if the new slope is constructed at the same angle as is the existing one. Stability of new fill may be questionable if compaction of the soil at the edge of the existing fill was not achieved during (or maintained since) original construction. The use of a reinforced compound slope to widen roadways facilitates the assurance of global stability, reduces fill requirements, eliminates additional ROW, and often speeds construction.

Landslide Repair

Landslides in soil cut or fill areas can be repaired with a reinforced gravity mass structure that must extend back beyond the slope failure plane and should incorporate drainage provisions. On-site soils are typically used in the reconstruction when tensile-reinforcing elements are incorporated into the reconstructed soil mass. Tensile reinforcement allows the reuse of "failed" soil and reconstruction of the slope to its original lines and grades.

Embankments Over Soft Foundations

Roadway embankment construction over soft soils and high water tables can pose several challenges to the design engineer and contractor. Geogrid reinforcement placed across soft soils increases load distribution and reduces contact pressures and enables the contractor to gain access to place an initial soil lift. Higher strength reinforcement designed to prevent global instability can then be placed on top of this lift. Side slopes of the embankment may also be steepened to reduce weight and therefore decrease consolidation settlements. This method of construction is more economical than dump and displace techniques or pile-supported systems. Soil reinforcement has also been used in conjunction with other techniques, such as deep dynamic compaction, stone columns, geotextiles, and wick drains, to create cost-effective systems.

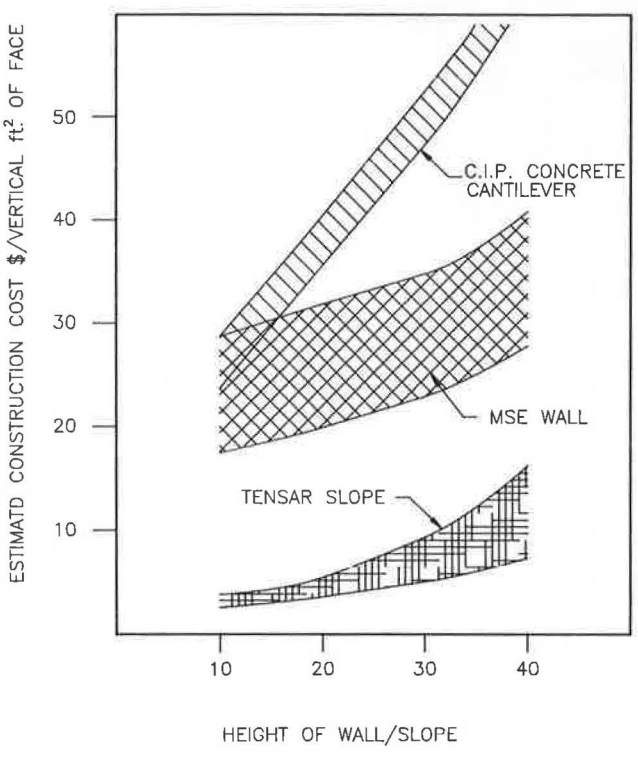

FIGURE 4 Estimated construction costs for grade separation structures.

ECONOMICS OF STEEPENED SLOPES

Steepened slopes are nearly always more economical than retaining wall alternatives and are often more economical than flatter slopes. Savings are realized both from material and construction time reductions and by reduced ROW requirements. Approximately 50 percent of the material cost of an MSE highway wall is in the precast concrete panel facing, which can be eliminated by use of a vegetated, reinforced slope.

Significant material savings over MSE walls in most areas also can be realized by use of local on-site fills. Geogrids were specifically developed to be used with fine or coarse grained soils or both (*1*). Clean, granular fills for use with metal-reinforced MSE walls typically range from $5.00 to $15.00 per cubic yard (in 1990). On-site fill can typically range from $2.00 to $5.00 per cubic yard. This differential will be slightly offset by the additional fill required by a slope, assuming the top of wall/slope is held constant. Therefore, steepened slopes options should be examined during the route layout and cut and fill balancing operations of a project to maximize cost savings.

The cost savings of a geogrid-reinforced steepened slope over other grade separation options is illustrated in Figure 4. The parameters used to develop this graph are listed next. Cost ranges shown for components are in-place costs. Although local economics will vary, it is clear that steepened slopes are a cost-effective alternative to retaining walls.

1. Steepened slope: $\phi' = 28$ to 34 degrees; $\beta = 26$ to 45 degrees; F.S. = 1.5.
   - Erosion protection: $1.25 to $4.00/yd²
   - On-site fill: $2.00 to $3.50/yd³
   - Reinforcement: $0.25 to $9.15/vertical sq. ft. face (no allowance for any additional R.O.W.)
2. MSE Wall: $\phi' = 34$ degrees; F.S. = 1.5; L/H = 0.75.
   - Select fill: $5.00 to $10.00/yd³
   - Facing panels, reinforcement, and design: $17.00 to $26.00/ft² face ($9.00 to $13.50 for materials and design and $8.00 to $13.00 for erection)
3. C.I.P. Concrete Cantilever: $\phi' = 34$ degrees; F.S. = 1.5.
   - On-site fill: $2.00 to $3.50/yd³
   - Reinforced concrete: $300.00 to $400.00/yd³

DESIGN OF STEEPENED SLOPES

As with any earthen structure, several aspects to design exist. Material properties of the different components of the soil structure must be assessed to ensure performance over the life of the structure. Stability analyses should then be performed and appurtenant features designed. Writing the specifications is the next step and is of crucial importance to ensure that the structure built meets the design requirements and functions as intended over the design life. Finally, inspection is required to ensure proper construction. A thorough sum-

mary of soil-reinforcement design with geosynthetics has been presented by Bonaparte et al. (*2*).

Material Properties

Soil

Fill soils may come from designated on-site sources or from undefined off-site borrow locations. In the first case (designated on-site sources), material parameters may be defined by standard geotechnical field exploration and laboratory testing practices before bid. Variabilities may be addressed by using conservative values in design or by parametrically investigating their affects on stability. Soils adjacent to a reinforced mass, which will remain in situ, and phreatic surfaces should also be defined by standard geotechnical practices. In the second case (undefined off-site borrow locations), a material specification for fill must be prepared.

Reinforcement

Two key reinforcement parameters used in design are (a) long-term design strength and (b) soil reinforcement interaction coefficients. Accurate definition of those parameters are required to ensure the slope structure will perform as intended over its entire design life. This is particularly true for critical highway structures.

Procedures for determining long-term design strength of geosynthetic reinforcement are being developed by the AASHTO-AGC-ARTBA Task Force 27 (*3*) and by the Geosynthetic Research Institute (*4*). (Both works were still in draft form and not publicly available when this paper was prepared, though final documents are pending from both organizations.) Other procedures have been presented by Bonaparte and Berg (*5*) and by Jewell and Greenwood (*6*). All procedures are similar and typically address creep of the polymer product, chemical degradation, biological degradation, damage during installation, strength of connections and junctions, and soil-reinforcement interaction characteristics.

Potential degradation of polymer reinforcement over the life of the structure, long-term creep, and long-term soil interaction mechanisms must be quantified. Those are areas that may be glossed over owing to their complexity. Reliance is typically heavily based on manufacturer's recommendations. Polymer materials may be subject to chemical or biological degradation or both in a soil environment. Product-specific studies should be conducted to determine durability reduction or safety factors for application to long-term design strength and to soil-interaction coefficients.

For time-dependent tensile characteristics the general rule in the plastics industry is not to extend creep predictions more than one order of magnitude beyond actual test data. Obviously, this is impractical for highway structures with a design life of 50 to 75 years, because tests of 5 to 7.5 years in duration would be required. Conservative approaches and techniques (*6–8*), such as time-temperature superposition, are used to extend 1.2-year creep data by two orders of magnitude to 120 years. Therefore, it is critical that an acceptable technique for extrapolation of long-term properties be specified and then be accurately documented.

Interaction coefficients between tensile elements and the soil it reinforces are functions of the soil type, soil density, overburden pressure, reinforcement geometry, and long-term load transfer mechanisms of the reinforcement. The geogrid-soil interaction consists of both frictional and passive components. Test procedures used for quantifying the interaction values must therefore account for long-term effects, such as creep and degradation on materials of the grid structure, that are transferring frictional and passive loads.

Analysis Techniques

Limit equilibrium methods are commonly used in analyses of reinforced soil slopes. The designer must be aware of the assumptions used in development of the implemented analysis procedures. Modified Bishop's procedure, Simplified Bishop's procedure, two-part wedge, and three-part wedge methodologies are commonly used in analysis of steepened reinforced slopes. Those methods were existing analysis techniques adapted to analyze reinforced soil structures. Therefore, it is also important to check the assumptions used in adaptation of those procedures, because versions of different design charts and computer programs vary. The reinforcing properties and soil/reinforcement interaction assumptions used also must be checked for validity to the case at hand.

Design charts, such as those presented by Jewell et al. (*9*), Tensar Corp. (*10*), Schmertmann et al. (*11*), and Christopher and Holtz (*12*) may be used for final design if all of the assumptions used in their development are met. It should be noted that those charts are based on specific soil-reinforcement interaction parameters and are especially useful for conceptual cost estimating and for checking reasonability of computerized slope analyses of more complicated slopes.

A computerized search for potential failure planes in steepened highway slope structures is recommended for structures that do not meet design chart assumptions. Some existing slope stability programs have been modified to incorporate tensile reinforcement elements, such as the STABGM (*13*) program modified from STABR. The failure plane search must directly incorporate the reinforcing effects into the factor of safety computation. Further, the search must examine compound type of failures (*14*) in addition to internal and external failures. Internal, external, and compound failure planes are illustrated in Figure 5.

Decisions to use a system such as a reinforced slope often are based on experience. Details such as constructability, construction movements, and site damage factors therefore are based on specifics of those prior projects. Soil type, analysis procedures, reinforcement product, and construction control variances from early projects can affect the performance of the proposed structure. The design and specification process should address possible variances and make allowances for or prevent variances from occurring.

Appurtenant Features

As with any earth structure the design does not end with the stability analyses. The structure must be constructible and must perform over its design life. The stability of the tem-

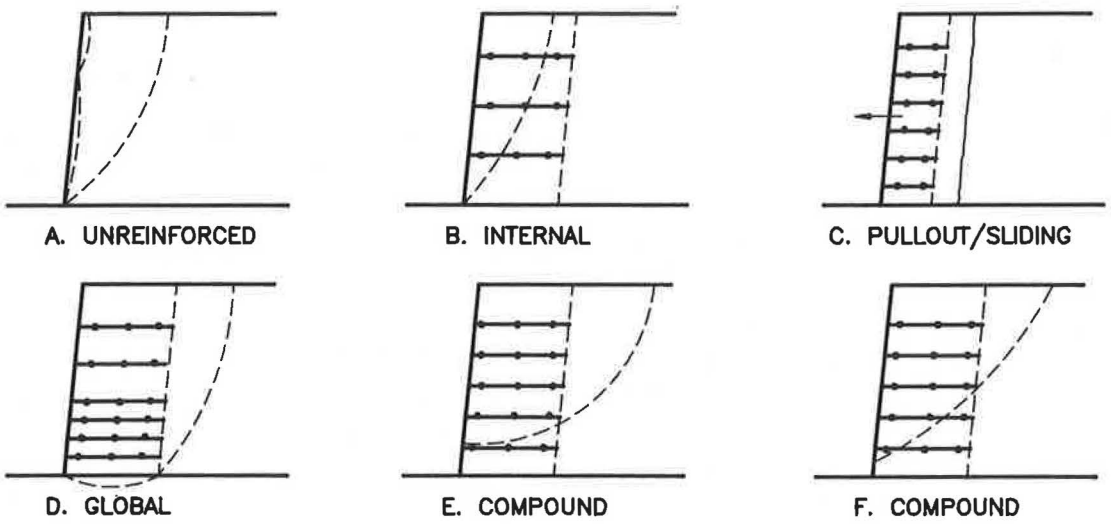

FIGURE 5 Reinforced steepened slope failure modes (*14*).

porary backcut must be assured for cut situations. Either the engineer specifies the maximum cut angle and accepts liability or the backcut stability is specified to be the contractor's responsibility. The backcut should also be benched to interlock the reinforced mass with the retained backfill soils and negate the potential formation of a linear failure plane.

Water or lack of proper drainage is a common culprit of soil structures failing or not performing as designed. Drainage both during construction and for the completed structure is an important detail that should not be overlooked during design. Surface water runoff should be diverted away from open construction cuts to minimize potential erosion and saturation of the reinforced fill soils. Partially completed fills should be sloped away from the face at the end of each work day to minimize water runoff across the slope face. Internal drains behind the reinforced mass should be installed if groundwater is, or may become, present. Often, drains are installed as an added degree of assurance even if groundwater is not anticipated.

Construction forming of some type is required for slopes steeper than about 45 to 50 degrees, depending on cohesiveness of the soil. Details of a forming system may be specified on the construction drawings or be left to the contractor's discretion. Experienced designers and contractors will know if forming is needed and, if so, which systems will work for a particular project.

Erosion control of the face of the finished slope must be considered in design. The authors recommend that a method of erosion protection be clearly specified by the designer and not be left to the discretion of the contractor or reinforcement supplier. Cost and performance of erosion control systems can vary significantly, and lack of tight specification can create a performance problem with the structure.

Specifications

As with MSE highway wall structures, two options exist in specifying reinforced slopes. One option is for the system to be preapproved by the agency and a line and grade approach be used. The system supplier will then be responsible for design, materials, and site assistance during construction. Design should include responsibility of global and compound failure modes (unlike the current MSE practice). The soil profiles and properties, required factors of safety, and analysis method should be supplied by the specifying agency. The other option is for the highway department to fully design the reinforced slope. This, of course, requires some experience of such structures. With this approach the written reinforcement specification is key to achieving desired results.

With either option, long-term design strength and long-term soil interaction characteristics of the reinforcement should be specified by using the proposed Task Force 27 Guidelines (*3*) or the Geosynthetic Research Institute Standard of Practice: GG4 (*4*) or both. The Task Force 27 guideline is specifically written for retaining walls but may be considered for slopes with minor revisions. Fill soil requirements should be modified to allow use of nonselect soils, erosion protection should be addressed, and stability factors of safety should be specified per slope application practice.

Construction Inspection

As with any earthwork construction the soil type, compaction, and moisture content should be monitored during construction. The other materials in a steepened slope (i.e., reinforcement and erosion protection) should also be inspected during construction. The grade of reinforcement, its length, and the elevations at which it is installed should be monitored by the owner's construction inspectors. Proper installation is key to satisfactory performance of an erosion control system and should therefore be closely inspected.

CASE HISTORIES

The following case histories are representative of where geogrid reinforced slopes have been used in highway construction to date. Steepened slope projects are emphasized because

they have the broadest applicability to highway construction. References to technical papers, when available, are provided for further information.

Project Name: Van Duzen, Peanut, California Forest Highway and Federal Lands, Highway 4-1(5)

- *Owner*: USDA Forest Service and Caltrans
- *Specifying agency*: U.S. Department of Transportation, Federal Highway Administration, Central Direct Federal Division
- *Designer*: U.S. DOT, FHWA, Central Federal Division
- *Slope heights*: Approximately 20 to 60 ft
- *Slope angle* (*H:V*): 1:1
- *Facing system*: Turf reinforced with a polymer mat
- *Alternative*: Retaining walls/flattened slopes
- *Reinforcement type*: TENSAR UX1600, UX1500, UX1400, BX1100 geogrids
- *Construction date*: Sept. 1987 to Nov. 1988

Five side-hill fills of a new federal roadway through scenic Redwood Forest of northern California were constructed with steepened slopes. The 1 : 1 slopes were constructed with polymer soil-reinforcing geogrids. The steepened embankments range from 100 to 400 ft long and are 20 to 60 ft high. A typical reinforcement layout is illustrated in Figure 6. The fill soils were cohesionless and could ravel during and after construction. Intermediate reinforcing geogrids were used to minimize raveling during construction. The finished slopes were faced with native grasses, which were seeded into a three-dimensional polymer turf-reinforcing mat to prevent post-construction raveling.

The Central Direct Division of the FHWA designed the geogrid-reinforced steepened slopes and administered construction, which was completed in fall 1988. Working in conjunction with the U.S. Forest Service and Caltrans, the FHWA selected geogrid-reinforced slopes over retaining walls for their economy, aesthetics, and safety in this mountainous terrain.

Project Name: Cannon Creek

- *Specifying agency/owner*: Arkansas State Highway and Transportation Department
- *Designer*: Raymond Technical Facilities
- *Slope height*: 76 ft
- *Slope angle* (*H:V*): 2:1
- *Facing system*: vegetation
- *Reinforcement type*: TENSAR UX1500 geogrid
- *Alternative*: new geometry and purchase of additional right-of-way
- *Cost savings*: $200,000

A large embankment was planned to carry State Highway 16 over Cannon Creek. The proposed 100,000-yd^3 embankment had a maximum height of 76 ft and was to be constructed with on-site clay soils and 2 : 1 side slopes. A cast-in-place concrete box culvert was first constructed to carry the creek under the embankment. Embankment construction started but was stopped quickly when several small slope failures occurred. It then became apparent that the embankment fill could not be safely constructed at 2 : 1 slopes.

With the box culvert in place there were two options for continuation of embankment construction. A gravelly soil could be used for embankment fill or on-site soils could be used with geogrid reinforcement. Both options were bid as alternatives, and the geogrid option, as illustrated in Figure 7, was used in construction. The geogrid reinforcement option was estimated to be $200,000 less expensive.

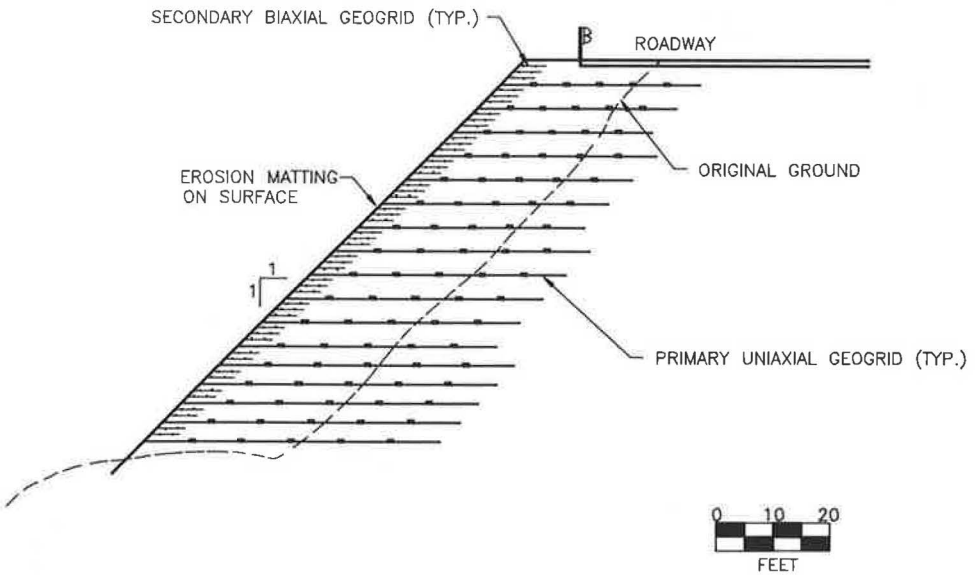

FIGURE 6 Van Duzen-Peanut cross section.

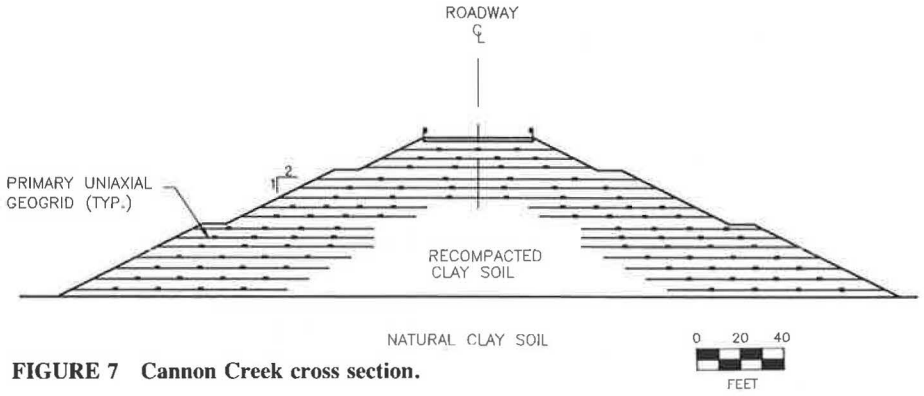

FIGURE 7 Cannon Creek cross section.

Project Name: Maryland Route 410

- *Specifying agency/owner*: Maryland Department of Transportation
- *Designer*: Tensar Engineering, Inc.
- *Slope height*: 48 ft
- *Slope angle* (H:V): 1.5:1
- *Facing system*: vegetation
- *Reinforcement type*: TENSAR UX 1400 and UX 1500
- *Alternative*: imported select fill or retaining walls
- *Construction date*: Summer 1989

A new interchange on U.S. Route 50 at MD Route 410 and MD Route 450 was designed by the Maryland Department of Transportation. Existing ROW were not wide enough to accommodate the new embankments. Embankments at slopes of 2.5 : 1 could be carried to the ROW limits and retaining walls constructed to contain the fill or additional ROW could be purchased. However, part of the existing embankment was an uncontrolled fill that could not be widened by building on top of it. It would need to be excavated and removed or recompacted.

Steepened geogrid-reinforced slopes were selected for construction. The 1.5H:1V slopes stayed within existing ROW limits and eliminated the need for retaining walls (see Figure 8). Some of the original uncontrolled fill was excavated and recompacted during installation of the stabilizing reinforcement. A view of the slope under construction is presented in Figure 9. Slopes were faced with native vegetation and did not require a permanent erosion mat system. Drains were installed behind the reinforced mass to intercept any possible groundwater.

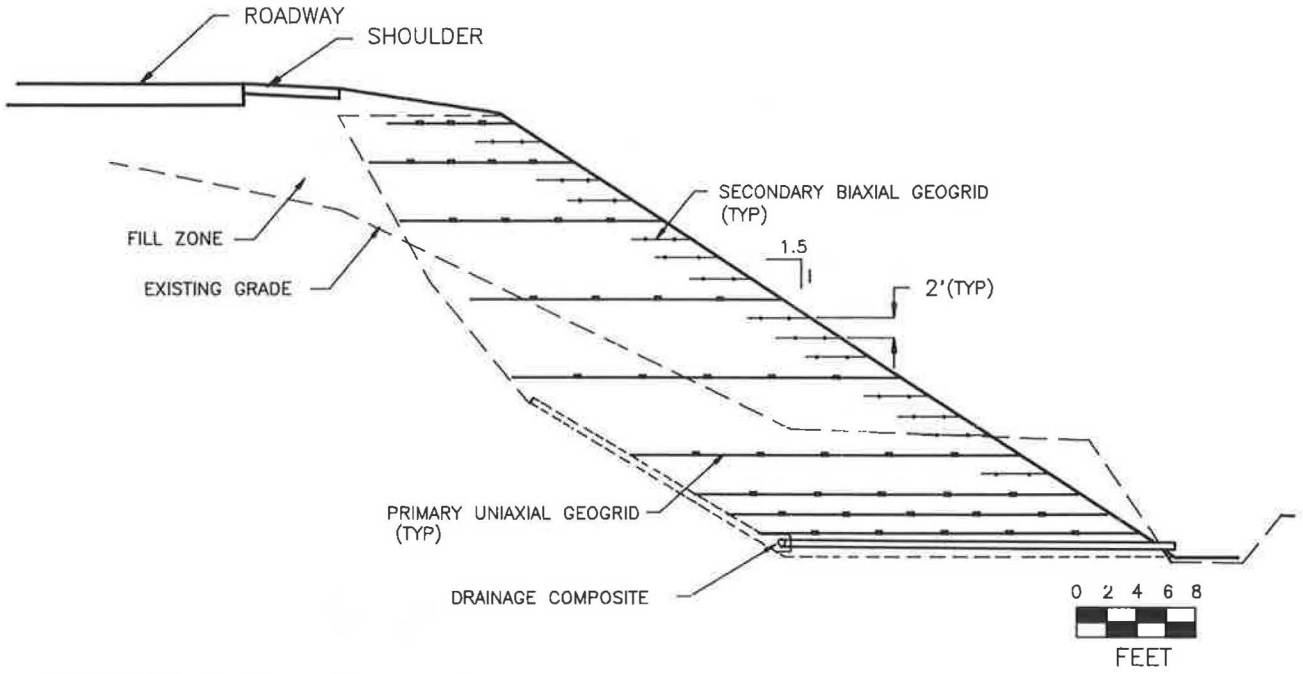

FIGURE 8 Maryland Route 410 cross section.

FIGURE 9 Maryland Route 410 project photo.

Project Name: Pennsylvania Turnpike-PTC 6902-86-628

- *Specifying agency/owner*: Pennsylvania Turnpike Authority
- *Designer*: Baker Engineers
- *Slope heights*: 13 ft reinforced; 35 ft total height
- *Slope angle (H:V)*: 1:1 on upper reinforced slope; maximum 1.5:1 on unreinforced slope below
- *Facing system*: geogrid wrap with vegetation
- *Reinforcement type*: TENSAR UX 1600, UX 1400, BX 1100 geogrids
- *Alternative*: retaining wall
- *Construction date*: Summer 1988

The Pennsylvania Turnpike Authority began widening the existing 50-year-old turnpike along the exterior lanes. On this project a geogrid-reinforced slope was used in existing fill sections to add a 10-ft-wide paved shoulder (as shown in Figure 10). A 1 : 1 backcut was used in construction, which allowed traffic to be maintained on the existing traffic lanes.

The reinforced slope option provided an estimated 25 percent cost savings over retaining walls and even a greater savings over a conventional slope. Soil borings from the original construction 50 years ago and performance of existing slopes were used to select soil parameters. This method of road widening has now become a standard procedure with the Pennsylvania Turnpike Authority.

CONCLUSIONS

1. Geogrid-reinforced slopes have broad applicability to highway construction and are (a) an economic alternative to conventional grade separation construction methods; (b) used to build steepened slopes, provide surficial reinforcement, build compound slopes for road widening, repair landslides, construct embankments over soft foundations, and build retaining walls; and (c) a proven method of construction used by a variety of transportation agencies and major design consultants.
2. Steepened slopes can cost up to 50 percent less than retaining walls.
3. Steepened, reinforced highway slopes may be specified as (a) packaged systems, where lines and grades are presented in the bid package and materials, design, and technical assistance are supplied by a single source or (b) designed in-house with the reinforced material a specified item.
4. Geogrid-reinforcement elements should be specified with consideration of installation damage, long-term soil inter-

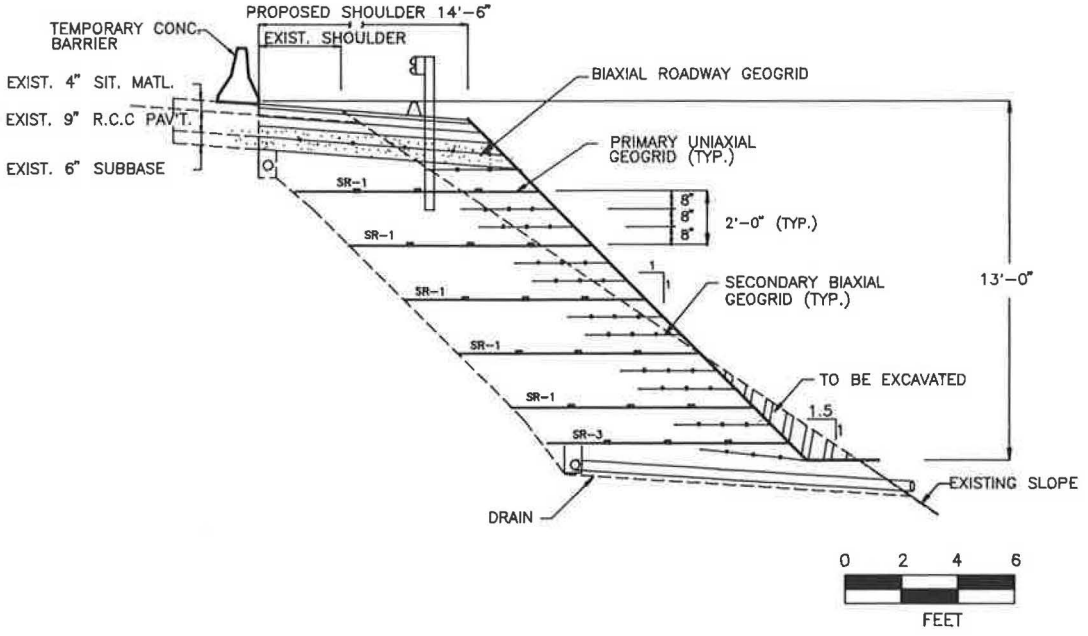

FIGURE 10 Pennsylvania Turnpike cross section.

action characteristics, long-term creep, and chemical and biological degradation potential over the design life of the structure.

5. Steepened, reinforcement slopes may be specified as an alternative grade separation method to retaining walls or flat slopes or both.

REFERENCES

1. F. B. Mercer. *Critical Aspects of Industrial and Academic Collaboration*. Netlon, Ltd., Blackburn, England, 1986.
2. R. Bonaparte, R. D. Holtz, and J. P. Giroud. Soil Reinforcement Design Using Geotextiles and Geogrids. In *Geotextile Testing and the Design Engineer*, ASTM STP 952 (J. E. Fluet, Jr. ed.), American Society for Testing and Materials, Philadelphia, Pa., 1987, pp. 69–116.
3. *Design Guidelines for Use of Extensible Reinforcements (Geosynthetic) for Mechanically Stabilized Earth Walls in Permanent Applications*, Part 2, Draft, Task Force 27, AASHTO-AGC-ARTBA Joint Committee, Feb. 1989.
4. *Determination of the Long-Term Design Strength of Geogrids*. Draft, Geosynthetic Research Institute, GRI Test Method GG4 Drexel University, Philadelphia, Pa., Nov. 1989.
5. R. Bonaparte and R. R. Berg. Long-Term Allowable Tension for Geosynthetic Reinforcement. *Proc., Geosynthetics '87*, Vol. 1, New Orleans, La., Feb. 1987, pp. 181–192.
6. R. A. Jewell and J. H. Greenwood. Long-Term Strength and Safety in Steep Soil Slopes Reinforced by Polymer Materials. *Geotextiles and Geomembranes*, Vol. 7, No. 1 and 2, 1988, pp. 81–118.
7. N. E. Wrigley. The Durability and Aging of Geogrids. *Proc., Durability and Aging of Geosynthetics*, Geosynthetic Research Institute, Drexel University, Philadelphia, Pa., Dec. 1988.
8. R. T. Murray and A. McGown. Assessment of the Time Dependent Behavior of Geotextiles for Reinforced Soil Applications. In *Durability of Geotextiles*, Chapman and Hall, New York, 1988, pp. 52–73.
9. R. A. Jewell, N. Paine, and R. I. Woods. Design Methods for Steep Reinforced Embankments. *Proc., Conference on Polymer Grid Reinforcement*, Thomas Telford, London, March 1984, pp. 70–81.
10. *Slope Reinforcement with TENSAR Geogrids: Design and Construction Guideline*. Tensar Technical Note SR1, Tensar Corporation, Morrow, Ga., May 1986.
11. G. R. Schmertmann, R. Bonaparte, V. C. Chouery, and R. J. Johnson. Design Charts for Geogrid Reinforced Slopes. *Proc., Geosynthetics '87*, Vol. 1, New Orleans, La., Feb. 1987, pp. 108–120.
12. B. R. Christopher and R. D. Holtz. *Geotextile Engineering Manual, Course Text*. FHWA, U.S. Department of Transportation, 1985.
13. J. M. Duncan and K. S. Wong. *STABGM: A Computer Program for Slope Stability Analysis With Circular Slip Surfaces and Geogrid Reinforcement: Users Manual*. Virginia Polytechnic Institute and State University, Blacksburg, Va., Dec. 1984.
14. R. B. Berg, V. E. Chouery-Curtis, and C. H. Watson, Critical Failure Planes in Analysis of Reinforced Slopes. *Proc., Geosynthetics '89*, Vol. 1, San Diego, Ca., Feb. 1989, pp. 269–278.

Publication of this paper sponsored by Committee on Geosynthetics.

Failure of a Geogrid-Reinforced Soil Wall

RICHARD J. BATHURST AND DANIEL J. BENJAMIN

The construction and testing of a large-scale reinforced soil wall 3 m high built within the Royal Military College Retaining Wall Test Facility is discussed. The wall was constructed to retain a sand fill and comprised full-height (propped) panel facings and four layers of a relatively weak geogrid. The weak geogrid was chosen so that the wall could be failed under surcharge. Following construction the wall was stage loaded by applying a series of increasing surcharge loads up to 80 kPa pressure. Each load was sustained for a minimum of 100 hr to observe creep in the composite system. The wall was heavily instrumented to record displacements along the grid layers, grid strains, connection loads, panel deformations, toe forces, and vertical earth pressures. Test results indicated that during the final surcharge increment a well-defined failure plane was generated through the reinforced soil mass and was followed some days later by (creep) rupture of the reinforcement. Large strains in the grid layers were observed in the vicinity of the connections that were comparable in magnitude to the peak strains recorded at the location of the observed failure plane in the reinforced soil mass. Finally, important implications are drawn concerning the design and construction of those systems.

A research program has been underway for several years at the Civil Engineering Department of the Royal Military College (RMC) of Canada that is concerned with monitoring full-scale geosynthetic-reinforced soil walls to acquire a comprehensive set of physical data from carefully constructed and monitored reinforced soil wall models. The data can be used to understand better the complex behavior of those systems and to guide the development of physically correct analytical methods for the design and construction of those generic structures.

To date, 10 full-scale model walls have been tested in the RMC Retaining Wall Test Facility. Variables between tests have included the facing treatment (i.e., incremental panels, propped panels, wrap around) and the geogrid reinforcement type (strong, weak). Results of several of those tests have been reported by the authors and coworkers in previous publications (*1–4*).

This paper reports the results of a recent test on a full-height (propped) panel wall that was heavily instrumented and then taken to failure under uniform surcharging. The scope is restricted to presentation of some of the test data and identifies qualitative features of model behavior of interest to those involved in the design and analysis of propped wall structures.

R. J. Bathurst, Civil Engineering Department, Royal Military College of Canada, Kingston, Ont., Canada K7K 5L0. D. J. Benjamin, Base Construction Engineer Officer, CFB Valcartier, Que., Canada.

RMC RETAINING WALL TEST FACILITY

Full-scale geosynthetic reinforced wall tests have been performed in the RMC Retaining Wall Test Facility located within the structures laboratory of the Civil Engineering Department. The principal structural components of the test facility are illustrated in Figure 1, and an overview of the test facility is presented in Figure 2. The test facility comprises six reinforced concrete counterfort wall segments used to confine a block of soil approximately 6.0 m long by 2.4 m wide by 3.6 m high. The modules are anchored to the structural floor of the laboratory by a series of anchor bolts that pass through the center of each counterfort. Those bolts also provide the reaction for cross beams that contain an air bag surcharging system used to apply a uniform vertical pressure to the surface of test configurations. This current surcharging arrangement allows a maximum uniform pressure of 100 kPa to be applied to the soil surface. The inside walls of the modules are lined with Plexiglas over plywood and covered by three sheets of lubricated polyethylene sheeting. The results of shearbox tests modeling the sidewall/sand interface give a fully mobilized friction angle of less than 15 degrees. Three-dimensional stability calculations indicate that the contribution of the test facility sidewalls to model stability is less than 15 percent of the total active force that would otherwise act in a true plane-strain condition (*5*).

Mechanical response of retaining walls reinforced with polymeric materials is dependent on a large number of variables related to soil properties, facing type, quality of construction, loading conditions, and environmental conditions (principally temperature). A major advantage of the RMC Retaining Wall Test Facility is that those variables can be controlled and, hence, the influence of specific variables (such as grid type and facing type) on wall performance can be isolated.

PROPPED WALL TEST CONFIGURATION

A full-height propped panel wall model was constructed in the RMC Retaining Wall Test Facility with the general arrangement indicated in Figure 3. The wall was supported by a series of external props until the soil behind the panels was placed to the full height of the wall (3.0 m). The wall facings comprised a central panel 1 m wide and two 0.7 m-wide edge panels. The central panel was manufactured from aluminum and was instrumented. The edge panels were constructed out of timber and were used to further isolate the

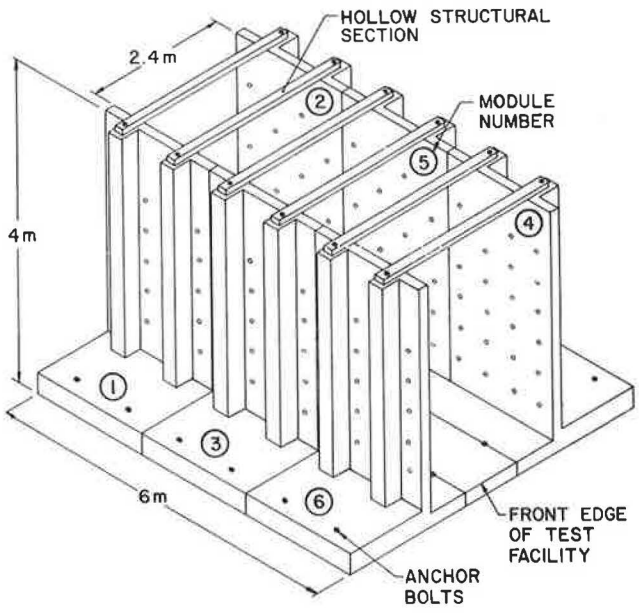

FIGURE 1 RMC retaining wall test facility.

central instrumented section of the model from the influence of sidewall friction.

The geosynthetic reinforcement comprised a Tensar Geogrid SS1 oriented in the weak direction. Grid geometry is illustrated in Figure 4, and some properties are listed in Table 1. The grid is a biaxial-oriented grid with polypropylene as the constituent material and is relatively weak and extensible and would not be used in a field installation. The choice of this grid was dictated by a desire to be able to fail the reinforced soil system with the surcharging capacity at hand. In some of the first model walls constructed at RMC, layers of Tensar Geogrid SR2 were used as the reinforcement. SR2 is relatively stiff and strong and is routinely specified by the manufacturer for this purpose. However, full-scale models constructed with SR2 reinforcement did not develop significant strain, and, consequently, wall behavior at incipient failure could not be studied (*1*).

The propped wall in the current investigation was constructed with four layers of SS1 spaced at 0.75-m intervals. The grid layers were trimmed to widths conforming to center and edge panel dimensions, and each layer extended 3 m into the retained soil. The grid spacing and lengths represent a standard geometry that has been adopted in all wall models constructed to date in the RMC facility. The initial grid arrangement has not been modified to make fair comparisons between tests with a variety of facing treatments and grid type.

The soil in all wall tests has been a uniformly graded washed sand with some fine gravel (Figure 5). The average bulk density as compacted is about 1.8 Mg/m^3 and is usually placed at a moisture content of 1 to 3 percent. The results of large-scale shearbox tests have indicated that the material has a peak (secant) friction angle that varies from $\phi = 56$ degrees at a confining pressure of about 10 kPa to $\phi = 43$ degrees at a normal stress of 120 kPa (*6*). The high strength of the sand is considered to be caused by the high angularity of the constituent sand particles. This material would be considered an ideal material in a field application owing to its high friction angle, permeability, and ease of compaction.

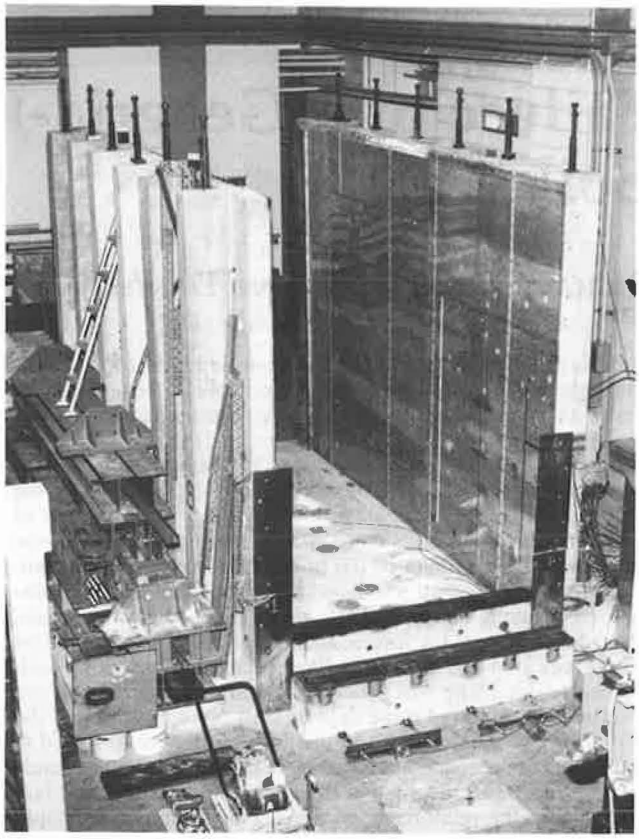

FIGURE 2 Overview of RMC retaining wall test facility.

CONSTRUCTION AND SURCHARGING

The central and edge panels were mounted on a leveling pad used to model the strip footing used in field applications to support and align the facing units. The panels were pinned at the base and supported by external props until the full depth of soil behind the wall was placed and compacted. The sand soil was placed and compacted in 125-mm lifts. Each grid was lightly pretensioned before placement to remove, as far as practical, any warps or slackness in the reinforcement. External props and facing units were not perfectly rigid, and approximately 6 mm of outward movement at the top of the wall was recorded as a result of sand placement and compaction before prop release.

A series of uniform surcharge pressure increments were applied to the retained soil following removal of the props. The fill placement history and surcharging schedule for the propped panel wall test is presented in Figure 6. Surcharge increments were typically left on for a period of 100 hr to observe creep in the wall structure and in the polymeric reinforcement. As is indicated on the figure there were two unplanned unload/load cycles during the final 80 kPa surcharging increment that were the result of power outages.

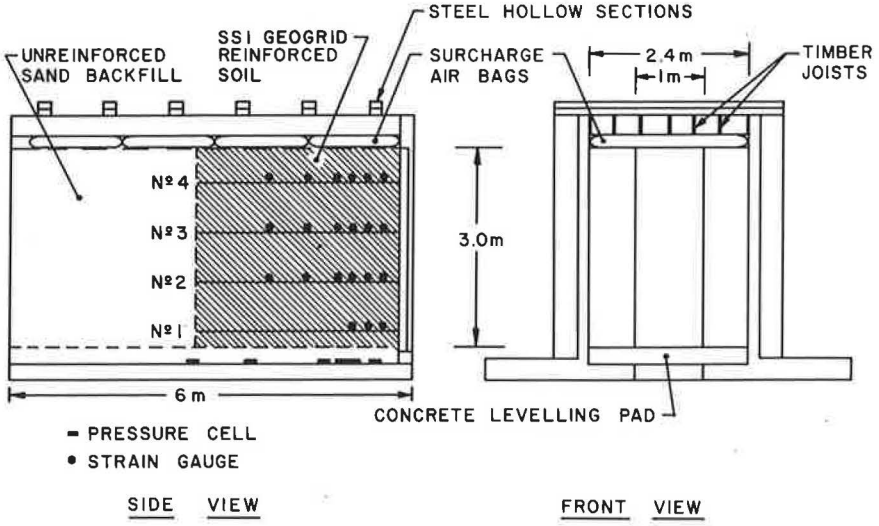

FIGURE 3 General arrangement for propped full-height panel wall test.

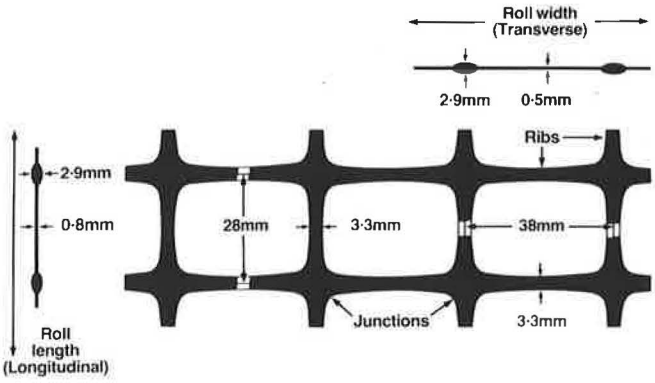

FIGURE 4 Tensar Geogrid SS1 (from Netlon Ltd. 1984).

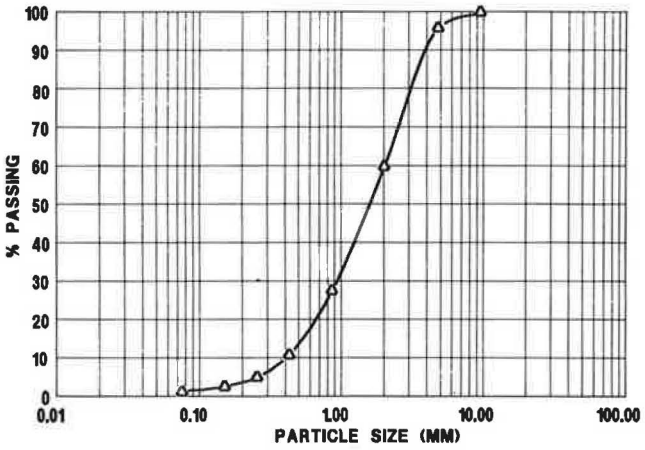

FIGURE 5 Grain size distribution for RMC sand.

TABLE 1 MECHANICAL PROPERTIES OF TENSAR SS1 GEOGRID REINFORCEMENT

Orientation	Stiffness (kN/m) (@ 2% strain)	Peak Load (kN/m)	Strain @ Peak Load (%)
transverse (strong)	292	20	14
longitudinal (weak)	204	12	14

*Manufacturers Literature/ ASTM D4595 Wide Width Strip Tensile/Elongation Test SS1 oriented in weak direction

INSTRUMENTATION

The following measurements were taken to monitor the performance of the propped wall during construction, surcharging, and at failure:

1. Horizontal movements of the instrumented central panel,
2. Reinforcement displacements and strains,
3. Loads at the toe of the wall and at panel/grid connections, and
4. Vertical earth pressures at the base of the reinforced soil mass and in the vicinity of selected grid layers.

Details of instrumentation, calibration, and interpretation of readings from many RMC trial walls are reported in a companion paper by the first author (7).

TEST RESULTS

General

Obvious signs of wall behavior can be associated with outward movements of the central monitored wall facing panel. In this test, outward wall movements were observed to match the application of each new load increment (see Figure 7). Further, as the magnitude of load level increased, the rate of time-dependent movement was observed to increase. Finally,

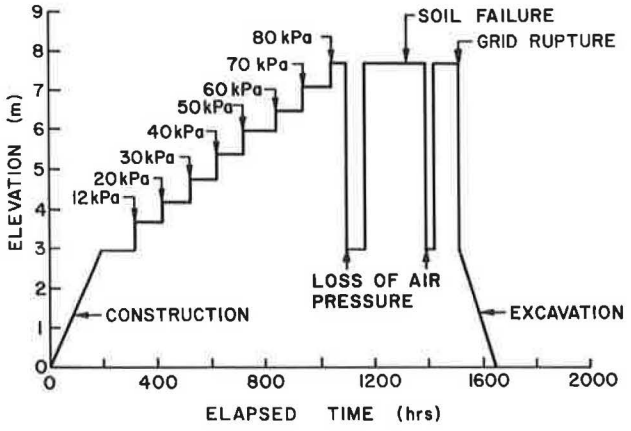

FIGURE 6 Construction and surcharging history.

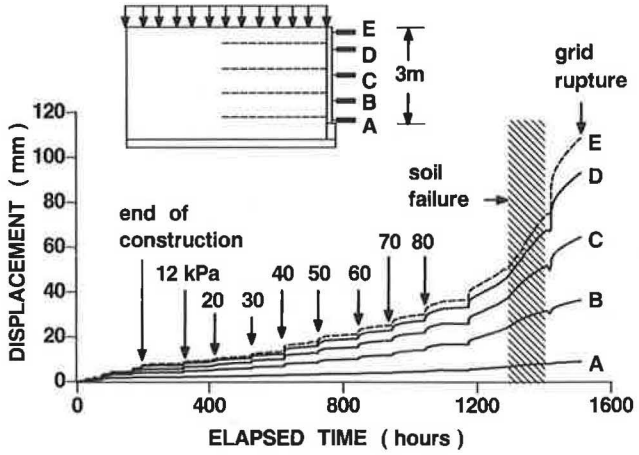

FIGURE 7 Panel displacements.

between the time of the two unload/load cycles during the final 80 kPa surcharge increment, evidence of a soil-to-soil failure through the reinforced soil mass occurred manifest as the simultaneous damage of several pieces of instrumentation embedded in the reinforced soil mass and accelerated deformation rates in displacement recording devices. Several days after the final 80 kPa reloading episode the sound of tearing grid could be heard over a period of 28 hr, signaling imminent collapse of the structure. At this point the surcharge was removed to protect the array of instrumentation at the wall face from damage. Removal of the surcharging system at the top of the model wall revealed a failure scarp at the surface of the reinforced soil mass approximately 1 m behind the panel wall. The surface of the slumped soil mass was observed to have dropped approximately 65 mm. Careful excavation of the soil behind the wall indicated that grid layer 4 was ruptured over about 80 percent of its width at the panel connection, indicating that collapse of the wall was likely minutes away when the test was terminated. Further excavation and removal of the facing panels revealed the internal failure surface (traced on Figure 8) and is believed to be that generated during the final 80 kPa surcharge increment. The failure surface has a geometry corresponding to a log-spiral shape, but, from prac-

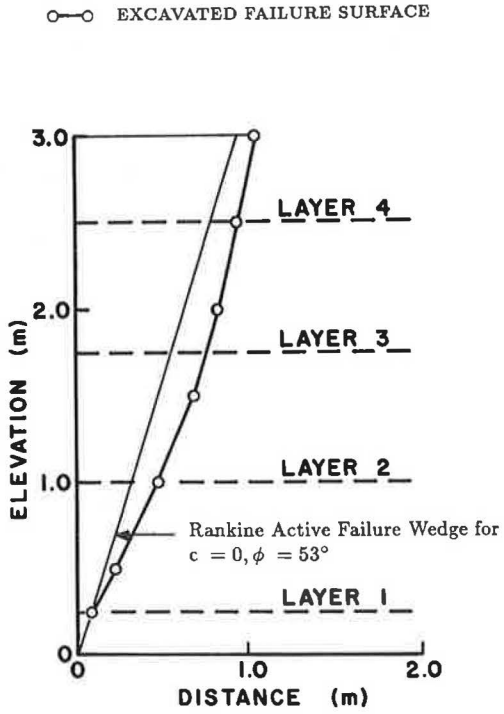

FIGURE 8 Excavated soil failure surface.

tical considerations, the volume of failed soil can be approximated by considering a Rankine wedge of soil commencing at the toe of the wall (based on representative soil strength parameters of $c = 0$ and $\phi = 53$ degrees). The geometry of the volume of failed soil is similar to that reported by the authors from the results of an unreinforced wall test used to calibrate the test facility for edge effects (*5*). Under the heavy surcharging conditions applied to this relatively short panel wall the initial failure mechanism can be represented by a wedge of soil as if the reinforcement was not present.

Panel and Grid Movements

The central facing panel profile at intervals during the propped wall test is presented in Figure 9. As was expected, the wall rotated outward from the pinned base of the panels as surcharging was applied. Relatively larger incremental deformations occurred during the 70 and 80 kPa surcharge stages. The lack of curvature at the top of the wall at the end of the test was considered to be due to the almost complete rupture of grid layer 4. The maximum vertical out-of-alignment at prop release was about 8 mm, about 14 percent of the movement recorded at soil failure.

Horizontal displacements recorded by extensometers on the grid layers and interpolated panel movements opposite the grid layers are summarized in Figure 10 for grid layer 4. The sensitivity of panel movements to surcharge loading can be seen in this figure for reinforcement layer 4 and was also apparent from similar data taken from the other grid layers. The figure also indicates a series of sudden minor jumps in grid displacements under constant surcharge load, suggesting a "stick-slip" type of load-transfer mechanism between grid and

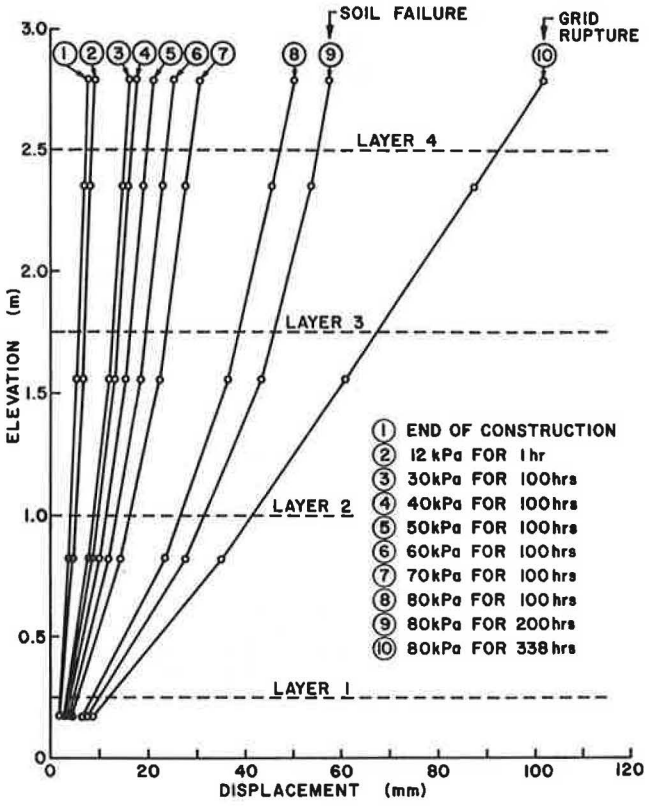

FIGURE 9 Panel displacement profiles.

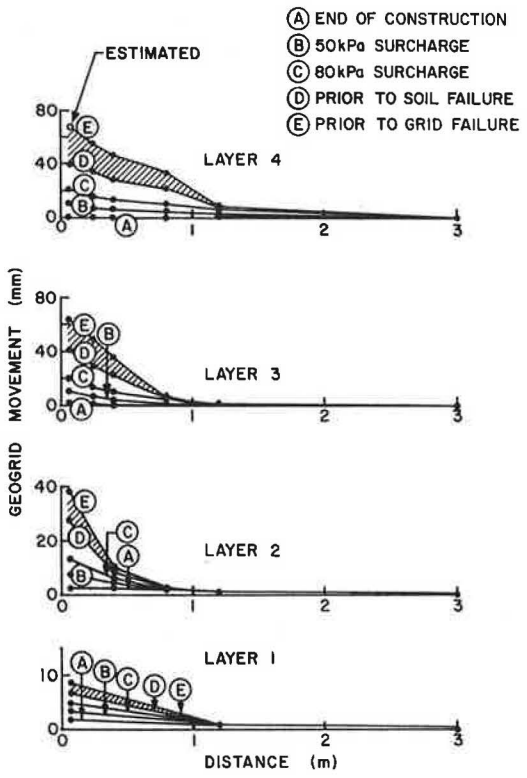

FIGURE 11 Summary of horizontal grid displacements.

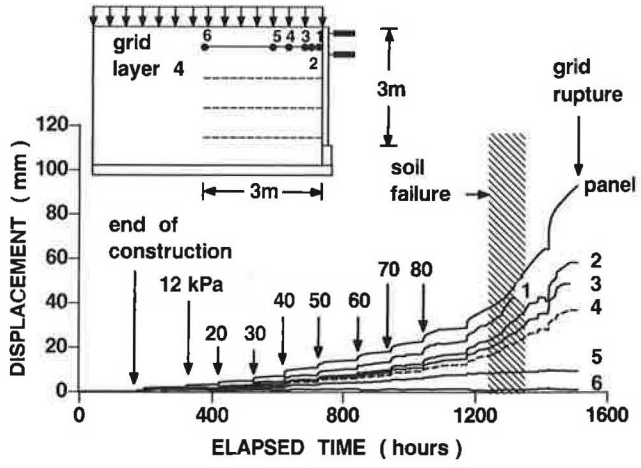

FIGURE 10 Example of grid displacements.

soil. The unload sequences were not planned but do indicate that the grid deformations (and panel movements) were irrecoverable and that elastic deformations in layer 4 were negligible when compared to the plastic deformations that had accumulated during the 80 kPa surcharge. Soil failure is believed to have occurred between the two 80 kPa surcharge reload episodes because during this period grid deformations were observed to accelerate and several pieces of equipment including extensometer 1 on grid layer 4 and a number of Bison inductance coils embedded in the soil were damaged. Grid deformations are summarized for all layers in Figure 11. The shaded portions in the figure represent the range of grid deformation in each layer during which soil failure is believed to have occurred. Extensometers attached to the free end of the grid layers did not record any displacements. In fact the figure shows that grid-to-soil load transfer in this test was restricted to less than 1.5 m into the reinforced soil mass. Consequently, the 3-m lengths employed in this model appear unnecessarily long for anchorage purposes.

Grid Strains

Grid strain profiles at selected times during the propped wall test are summarized in Figure 12. Strains in excess of 2 percent strain were calculated from the array of extensometers attached to the reinforcement and lower magnitudes of strain from strain gauges bonded directly to the grid (*7*). If the 50-kPa surcharge increment is considered to be a working load condition, then strains in the grid at working load levels are less than 2 percent and the largest strains occur at the connections. However, at incipient failure, strains were estimated to be as high as 10 to 12 percent at the connection in layer 4 (based on panel movement) and about 8 percent at similar locations on grids 2 and 3. The estimated strain at the connection for grid layer 4 is consistent with the rupture strain inferred from load-strain-time mechanical properties of virgin samples of the Tensar Geogrid SS1. However, a second region of locally

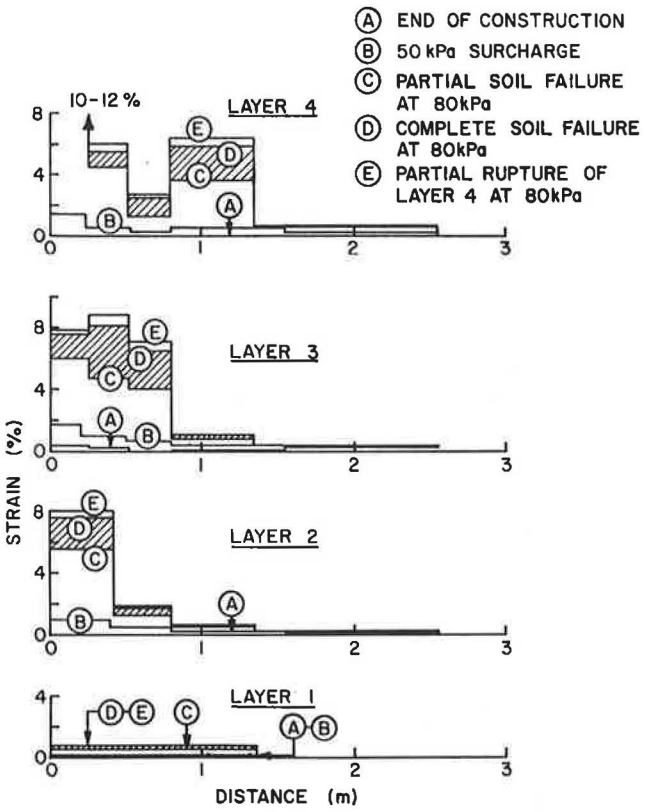

FIGURE 12 Summary of grid strains.

high strains (6 percent) was observed in layer 4 that matches the soil-to-soil failure plane revealed during excavation of the soil wall (Figure 8). The region of high strain in layer 3 extending to about 0.8 m into the reinforced soil mass can also be considered to be due to the combined effect of high connection strains and anchorage strains associated with a deep-seated failure surface that intersected grid layer 3 at about this location. The relatively short length of elevated grid strains suggests that under the given test conditions the grid anchorage length associated with lateral restraint of the failure wedge is very short (i.e., less than 0.5 m). The trend toward high grid strains at the panel connections has been observed in previous tests with propped panel construction performed by the authors and coworkers at RMC by using stiffer Tensar SR2 as the reinforcement (*1*,*7*) and is thought to be due to the reinforced soil mass behind the wall moving down relative to the panel, which is fixed in the vertical direction. This is particularly evident by the 65-mm drop in soil surface observed directly behind the panels at wall excavation. Consequently, a membrane effect is generated in the grid behind the wall where vertical earth pressures are transferred to the locally unsupported grid and then to the panel facing.

Panel Forces

The horizontal component of tensile grid forces transferred to the central monitored panel were recorded by using a series of proving rings. The proving rings were mounted on the face of the panels but were connected to the grid by stainless steel

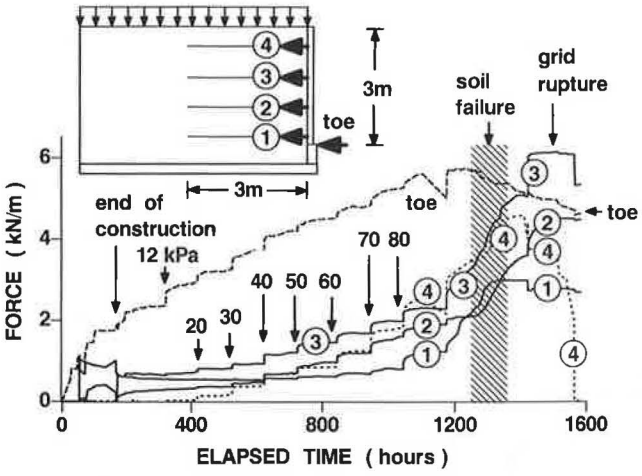

FIGURE 13 Grid connection forces.

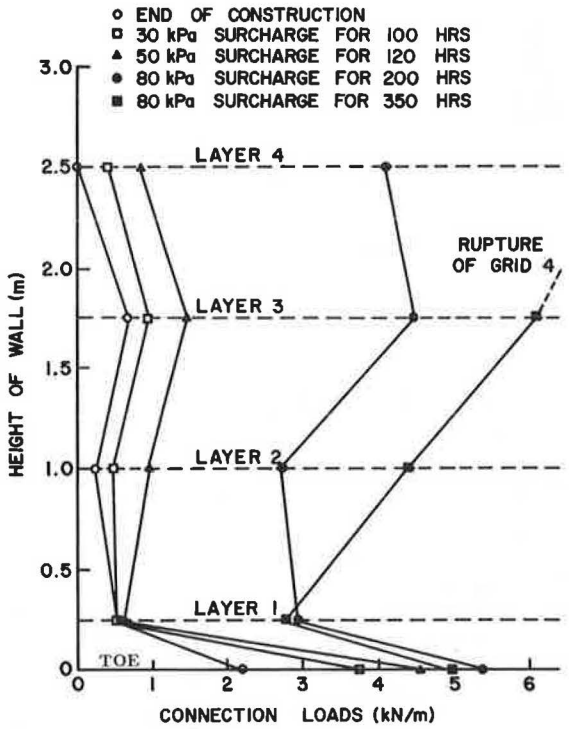

FIGURE 14 Summary of grid connection forces.

rods passing through a bushing arrangement built into the aluminum panels (*7*). The horizontal component of grid connection forces is presented in Figure 13. The data on the figure show that after soil failure there was evidence of load-shedding from grid 4 to grid layers 2 and 3 as the topmost layer was strained to rupture.

Horizontal connection forces are summarized on Figure 14 at selected times in the test program. At the end of the 50-kPa surcharge increment the grid connection forces were reasonably constant but the connection loads were increased in the two topmost layers as failure was approached. The data highlight the difficulty of simply scaling the magnitude of

lateral earth pressures determined at soil or wall collapse to arrive at the distribution and magnitude of pressures assumed to act under working load conditions as is routinely done in conventional limit-equilibrium-based methods of design. Also on Figures 13 and 14 is the measured horizontal toe force recorded at the base of the panel that was significant at all stages in the test program. The relatively stiff restraint offered by the pinned base of the wall may account for load attenuation in grid layers 1 and 2 at the latter stages of the test. Equivalent lateral earth pressures calculated from grid strains in the vicinity of the observed internal failure plane at incipient collapse of the wall are plotted on Figure 15. The horizontal toe force and the connection force in layer 1 have been added and the grid forces have been determined from isochronous load-strain-time data for the polymeric reinforcement. Superimposed on the figure are distributions based on active Rankine earth pressure theory ($c = 0, \phi = 53$ degrees). It is reasonable to say within experimental error that the trend of constant lateral earth pressures is evident in the measured data but the magnitude of earth pressures is overestimated by Rankine theory (even when sidewall friction is considered).

The vertical component of base force was determined from an array of load cells supporting the full height panels. The results of those measurements indicated that the vertical forces were about 25 kN/m in magnitude during the final surcharge increment, equivalent to about 30 percent of the surcharge load applied to the top of the failed wedge of soil. From a practical point of view, toe force measurements indicate that at working load levels and at incipient collapse the rigid leveling pad can be considered to be at least equal to a layer of grid for purposes of translational stability of the facing panel. In addition, a significant portion of the vertical force acting on the potential failure wedge under the heavy surcharging is taken by the base of the wall. The additional restraint offered to the reinforced soil mass at the base of the wall is not considered in conventional methods of design for those structures.

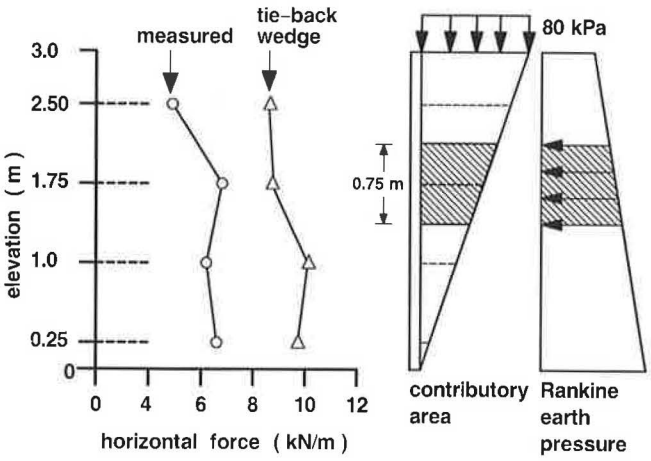

FIGURE 15 Apparent lateral earth pressures.

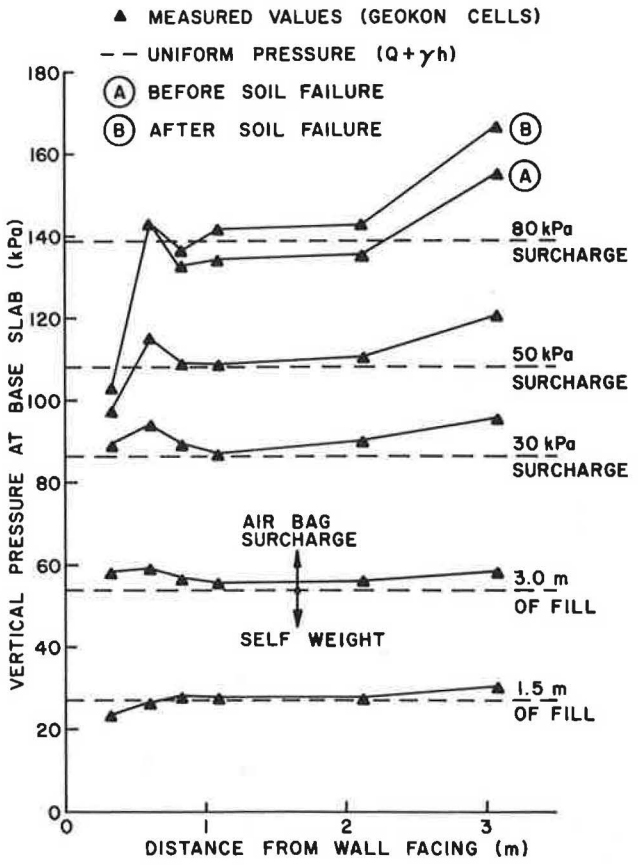

FIGURE 16 Vertical earth pressures at base of reinforced soil.

Vertical Earth Pressures

The magnitude of vertical earth pressures over the course of construction and surcharging was determined by using six earth pressure cells cast into the base of the test facility and Glotzl cells placed in the vicinity of grid layer 3. All earth pressure cells were calibrated in situ by determining the response of each cell based on the first meter of soil compacted in place over the instrument during construction of the wall. The results of base pressure measurements are summarized on Figure 16. In general, the vertical earth pressures are reasonably well estimated considering the self-weight of the retained soil, its height, and the magnitude of the applied surcharge. The important exception to this case occurs in the vicinity of the panel toe where significant stress reduction was observed at the end of the test within about 0.5 m of the leveling pad. This observation is consistent with the membrane effect identified earlier that leads to vertical stresses being passed to the panels through the constrained panel/grid connections. The reduction in vertical stress integrated over a 0.5-m width is roughly equivalent to the magnitude of vertical force recorded by load cells mounted at the base of the wall. A uniform pressure distribution is reasonable for those walls if vertical toe loads are considered in the manner just discussed.

The membrane effect was examined further by plotting earth pressures generated by Glotzl cells placed one lift (125 mm) below grid layer 3 (Figure 17) close to the back of the panel. The measured pressures are plotted with the uniform pressure distribution on the basis of depth and unit weight of the soil and surcharge magnitude. The same general trend in

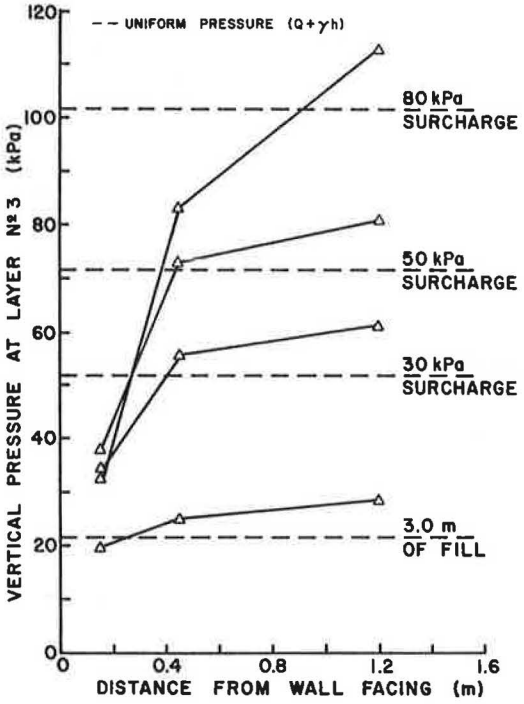

FIGURE 17 Vertical stresses below grid layer 3.

vertical stresses as recorded for the base pressure cells is apparent, but the losses are somewhat greater. The Glotzl cells were 125 mm below the grid and the base pressures cells were about 500 mm below grid layer 1.

CONCLUDING REMARKS

The distribution of strains and panel toe loads observed in this and other similar tests performed by the authors has important implications to tie-back wedge methods of analysis. In a previous test reported by the authors (*2*), using the same grid and surcharging arrangement but an incremental panel wall construction, the magnitude of grid strains in the vicinity of the internal soil failure surface at the end of the test were of similar magnitudes in layers 2, 3, and 4 (i.e., 4 to 6 percent). In the current test it can be argued that within the margins of experimental accuracy strains are also of a similar magnitude at the location of the internal failure surface during the last surcharging increment. Tensile grid forces in layers 2, 3, and 4 may be similar and the grids may attempt to equilibrate tensile loads. If the test geometry and surcharging conditions represent a field case, then from an analysis point of view it may be useful to combine the horizontal toe force with grid layer 1 and to assume that each grid layer carries equal horizontal load in restraining the potential internal failure wedge at incipient failure.

Test results have indicated that the vertical restraint offered by the wall toe is also significant and is consequently an additional restraining mechanism that assists in the stability of those systems. Nevertheless, vertical toe capacity is not routinely considered in limit-equilibrium methods of analysis.

The results of this test and previous similar tests reported by the authors and coworkers have highlighted the importance of connection forces in the grid at all stages up to failure in those walls. Propped panel walls are common for geosynthetic-reinforced soil retaining wall systems. However, the effect of relative panel/soil movements is not normally considered in the design of those structures even though the results of the tests have indicated that the highest grid loadings occur at the grid/panel connections and that consequently this is the likeliest location for grid rupture in a field installation. In the model wall tests reported here special attention was paid to minimize the size and extent of the void that is inevitably formed below the connection during fill placement and compaction. In several field installations the level of attention to this detail has been observed by the authors to be less and it can be expected that the potential for the highest grid forces to occur at the connections is even more certain as the grid acts as a (unsupported) membrane in the vicinity of connection.

ACKNOWLEDGMENTS

The authors would like to express their appreciation to P.M. Jarrett and J. Bell and J. DiPietrantonio who have assisted in the successful pursuit of this research program. The authors are also indebted to Tensar Corp. and Netlon Ltd. for provision of reinforcement materials. The funding for the work reported in the paper was provided by the Department of National Defence (Canada).

REFERENCES

1. R. J. Bathurst, W. Wawrychuk, and P. M. Jarrett. Laboratory Investigation of Two Large-scale Geogrid Reinforced Soil Walls, In *The Application of Polymeric Reinforcement in Soil Retaining Structures*, (P. M. Jarrett and A. McGown, eds.) NATO Advanced Study Institutes Series, Kluwer, 1987.
2. R. J. Bathurst, D. J. Benjamin, and P. M. Jarrett. Laboratory Study of Geogrid Reinforced Soil Walls. In *Geosynthetics for Soil Improvement*, (A. D. Holtz, ed.) ASCE Special Publication 18, 1988, pp. 178–192.
3. R. J. Bathurst, P. M. Jarrett, and S. R. Lescoutre. An Instrumented Wrap-Around Geogrid Reinforced Soil Wall. *Proc., 3rd Canadian Symposium on Geosynthetics*, Waterloo, Ontario, Oct. 4, 1988.
4. R. J. Bathurst, D. J. Benjamin, and P. M. Jarrett. An Instrumented Geogrid Reinforced Soil Wall. *Proc., 12th International Conference on Soil Mechanics and Foundation Engineering*, Rio de Janerio, Brazil, Aug. 1989.
5. R. J. Bathurst and D. J. Benjamin, Preliminary Assessment of Sidewall Friction on Large-Scale Models in the RMC Test Facility. In *The Application of Polymeric Reinforcement in Soil Retaining Structures*, (P. M. Jarrett and A. McGown, eds.) NATO Advanced Study Institutes Series, Kluwer, 1987.
6. R. A. Jewell. Analysis and Predicted Behaviour for the Royal Military College Trial Wall. In *The Application of Polymeric Reinforcement in Soil Retaining Structures*, (P. M. Jarrett and A. McGown, eds.) NATO Advanced Study Institutes Series, Kluwer, 1987.
7. R. J. Bathurst. Instrumentation of Geogrid-Reinforced Soil Walls. In *Transportation Research Record 1277*, TRB, National Research Council, Washington, D.C., (in press).

Publication of this paper sponsored by Committee on Geosynthetis.

Rockfall Hazard Analysis Using the Colorado Rockfall Simulation Program

TIMOTHY J. PFEIFFER AND JERRY D. HIGGINS

The Colorado Rockfall Simulation Program (CRSP) was developed to provide a statistical analysis of probable rockfall behavior at any given site and to be used as a tool to study the behavior of rockfalls, to determine the need for rockfall mitigation, and to aid in the design of rockfall mitigation. The basic theory behind CRSP is summarized, and the results of recent program modifications and calibration are discussed. CRSP uses numerical input values assigned to slope and rock properties to model rockfall behavior. The model applies equations of gravitational acceleration and conservation of energy to describe the motion of the rock. Empirically derived functions relating velocity, friction, and material properties are used to model the dynamic interaction of the rock and slope. The statistical variation among rockfalls is modeled by randomly varying the angle at which a rock impacts the slope within limits set by rock size and slope irregularities. The program provides estimates of probable velocity and bounce height at various locations on a slope. Experimental verification and calibration of CRSP was conducted by analyzing videotapes of rocks traveling down a slope. A comparison of rock velocity and bounce height obtained from the tapes with CRSP prediction indicates reasonable agreement. Also, an evaluation of the sensitivity of input parameters indicates that slope angle and surface roughness are the most important parameters on steep slopes. Design graphs are developed based on CRSP simulations by using surface roughness and slope angle to estimate rock velocity and bounce height on uniform slopes.

Rockfalls are a natural result of weathering on steep natural slopes or rock cuts. Rocks falling from steep slopes, natural cliffs, or rock cuts usually travel down the slope in a combination of free fall, bouncing, and rolling. In this paper, rockfall refers to rocks traveling in a combination of those modes. Rockfalls in this rapid down-slope motion present a common hazard to transportation and structures in steep mountainous terrain. Often, no protective measures are taken other than posting warning signs. The need for an understanding of rockfall behavior increases as more transportation routes and structures are placed in areas of rockfall hazards.

The construction of I-70 through Glenwood Canyon, Colorado, required rockfall mitigation measures to protect the highway structures and to improve safety to motorists. Conventional design of rockfall protection by using ditch-design criteria was often not applicable for the natural slopes or was aesthetically unacceptable considering the intense environmental pressure in Colorado and especially in Glenwood Canyon. A reasonable estimate of probable bounce height and velocity of rockfalls was needed input for the design of rockfall fences and alternative rockfall catch ditches in Glenwood Canyon. This information could best be provided by a rockfall simulation program for field office PC-compatible computers.

The Colorado Rockfall Simulation Program (CRSP) was developed to aid in the design of rockfall mitigation by supplying data on probable rockfall bounce height and velocities. The program uses easily identified parameters to produce a rockfall simulation on PC-compatible computers and has proven useful in designing rock cuts, ditches, and rockfall fences in Glenwood Canyon. CRSP simulates rockfalls at a site based on slope irregularities, slope materials, slope profile, and rock size. The final product is a reasonably easy-to-use rockfall simulation program.

The detailed development of the CRSP algorithm has been published previously (*1*,*2*). The purpose of this paper is to summarize briefly the basic theory behind the program and to discuss the results of recent work on program modifications and calibration and includes an evaluation of program sensitivity to input parameters, development of design charts for simple rockfall analyses, and presentation of field test results.

Experimental verification and calibration of CRSP was conducted in conjunction with the testing of rockfall fences at a site near Rifle, Colorado. The motion of rocks traveling down a slope and hitting the test fence was recorded on videotape. Researchers at the Colorado School of Mines added graphical data presentations to the program and analyzed the videotapes to aid the verification and calibration of the program (*1*).

LITERATURE REVIEW

The published literature contains abundant studies that deal with slope stability and rockfall mitigation measures, but there are few papers concerning the mechanics of rockfall motion (*2*). Because all rocks cannot be prevented from falling, an understanding of rockfall mechanics is important.

A rockfall study was conducted by Ritchie of the Washington Department of Transportation (*3*) in the 1960s. Ritchie observed the importance of angular momentum and bouncing ledges, or "ski jumps," in rockfalls by studying 16-mm films of rockfall. Criteria were developed from these observations for designing cut slopes and ditches, which are widely used today (*4*).

Several computer simulation models have been developed to describe rockfall dynamics in an effort to improve rockfall mitigation designs. Piteau and Associates (*5*) developed and tested a computer rockfall simulation program designed for a mainframe computer that produces velocity and bounce

Department of Geology and Geological Engineering, Colorado School of Mines, Golden, Colo. 80401. T. J. Pfeiffer, current affiliation, Geotechnical Resources, Inc., 7412 Southwest Beaverton-Hillsdale Highway, Portland, Oreg. 97225.

height probability distributions from the input coefficients, slope geometry, and probability of surface variations. During the relocation of I-40 in North Carolina, the North Carolina Department of Transportation produced the program ROCKSIM to simulate rockfall and to test the effectiveness of widening the roadway ditch to mitigate rockfall hazard (*4*,*6*). Hoek (*7*) in 1987 also developed a copyrighted computer program to model rockfall. The development of CRSP relied on many of the basic concepts used in some of those programs but with the idea of improving on the individual approaches.

A study conducted by Evans (*8*) at the University of Arizona compared and tested ROCKSIM, Hoek's program, and CRSP. The study incorporated data from 260 induced rockfall events with eight different slope geometries. Evans found CRSP to be the most consistent at predicting rockfall behavior and incorporated it into a program to aid in the design of rockfall catch benches.

GENERAL DESCRIPTION OF CRSP

CRSP provides estimates of probable rockfall bounce heights and velocities for rockfall on natural or cut slopes. Like any computer simulation model the accuracy of results produced by CRSP is determined by the accuracy of the input data, the applicability of the program to the field situation, and the accuracy of the model. Every effort has been made to make the model as accurate as possible, but the program user must decide on the quality of the data produced by CRSP.

CRSP requires the following input data:

- A slope profile, input as a series of straight line segments called cells, designated by the coordinates of the end points of each line;
- An estimation of the roughness of the slope surface within each cell;
- Estimated coefficients that quantify the frictional and elastic properties of the slope; and
- The size, shape, and starting location of rocks involved in the rockfalls.

CRSP uses this input data in a stochastic model to produce statistics on probable rockfall velocity and bounce height. The following data are produced by CRSP:

- Slope profile showing cell locations and the position of each simulation rock every tenth of a second as it travels down the slope;
- Maximum and average bounce heights at the end of each cell and for one selected location on the slope;
- Maximum and average velocities at the end of each cell and at the selected location on the slope;
- Maximum total kinetic energy of the falling rock at the selected location on the slope;
- Histograms of the distribution of velocities and bounce heights at the selected location on the slope; and
- Graphs of the maximum velocity and bounce height along the slope.

THEORY

The proper use of any computer engineering tool requires an understanding of the basis of the program that enables the user of the program to choose appropriate input data and recognize reasonable results. While CRSP adds objectivity to the otherwise subjective task of investigating rockfall, many aspects of using CRSP are dependent on the judgement of the investigator. The theory behind CRSP has been discussed in detail in previous papers (*1*,*2*). However, it is important to provide a general discussion of theory here for the reader who is unfamiliar with the earlier work.

Rockfall Parameters

The behavior of rockfalls is influenced by slope geometry, slope material properties, rock geometry, and rock material properties (*1*,*5*). Rockfalls originating from the same source location may behave very differently as a result of the interaction of those factors. Parameters that quantify the factors listed are used in CRSP to model rockfall behavior (Table 1).

TABLE 1 PARAMETERS DETERMINING BEHAVIOR OF ROCKFALLS (*2*)

Factor	Parameter
Slope Geometry	Slope Inclination Slope Length Surface Roughness
Slope Material Properties	Elastic Coefficients Frictional Coefficients
Rock Geometry	Rock Size Rock Shape
Rock Material Properties	Rock Durability Rock Mass Elastic Coefficients Frictional Coefficients

Slope inclination, slope length, and surface roughness are slope geometry parameters influencing the behavior of rockfalls. Slope inclination is critical because it defines zones of acceleration and deceleration of the rockfall. Slope length determines the distance over which the rock accelerates or decelerates. Slope inclination and length are input to CRSP by dividing the slope into straight-line segments (cells) and then by entering the beginning and ending coordinates of each segment.

Apart from slope inclination and length, interaction of surface irregularities with the rock is perhaps the most important factor in determining the behavior of rockfalls. Irregularities in the slope surface account for most of the variability observed among rockfalls originating from a single source location. Those irregularities, referred to in this paper as surface roughness, alter the angle at which the rock hits the surface. It is this impact angle that largely determines the character of the bounce (*4*). CRSP models the effects of surface roughness by randomly varying the slope angle between limits defined by the rock size and surface roughness. The surface roughness and maximum variation of the slope angle (Θmax) is defined in Figure 1.

The properties of slope material influence the behavior of a rock rebounding from the slope. Numerical representations of these properties are termed the normal coefficient of restitution (Rn) and the tangential coefficient of frictional resistance (Rt), where the normal direction is perpendicular to the surface and the tangential direction is parallel to the surface (*3*,*4*). The velocity components (Vn,Vt), coefficients (Rn,Rt), impact angle (α), and slope variation (Θ) are illustrated in Figure 2.

Separate normal and tangential coefficients are necessary owing to the different mechanisms involved in resisting motion normal and tangential to the slope to determine new velocity components for a rock following impact. When a rock bounces on a slope, kinetic energy is lost owing to inelastic components of the collision and friction. The primary mechanism in resisting motion parallel to the slope is sliding or rolling friction, but the elasticity of the slope determines the motion normal to the slope. Rn is a measure of elasticity in collisions normal to the slope, and Rt is a measure of friction parallel to the slope. Tables 2 and 3 present the suggested ranges of coefficients for use with CRSP developed by observation and literature review (*1*,*2*).

Assumptions

For a natural slope the 11 parameters in Table 1 typically have a wide range of values and would be difficult to analyze as independent variables. It is convenient to reduce the number of variables by means of the following simplifying assumptions:

- Lateral slope variability need not be considered because the slope profile follows the most probable rockfall path as established by field investigations.
- Coefficients assigned to the slope material can account for both the rock and slope properties because the rock type is constant for each analysis and the range of slope material properties is much greater than that of rock material properties.
- The worst-case scenario is generally that of the largest rock that remains intact while traveling down a slope. Therefore, it is assumed the rock does not break apart in its fall.
- Rock size and mass are assumed constant for analysis of rockfall from a given source. This is justified by the worst-case assumption.
- A sphere may be used to determine a rock's volume and inertia because a sphere yields a maximum volume for a given radius that will tend toward a worst case.

Algorithm

Kinetic energy is lost in any nonperfectly elastic collision. In the case of a rock hitting a slope, the component of kinetic energy parallel to the slope and the rotational energy are attenuated by friction along the slope and collisions with features perpendicular to the slope. Friction is a function of the slope material, quantified by the tangential coefficient (Rt)

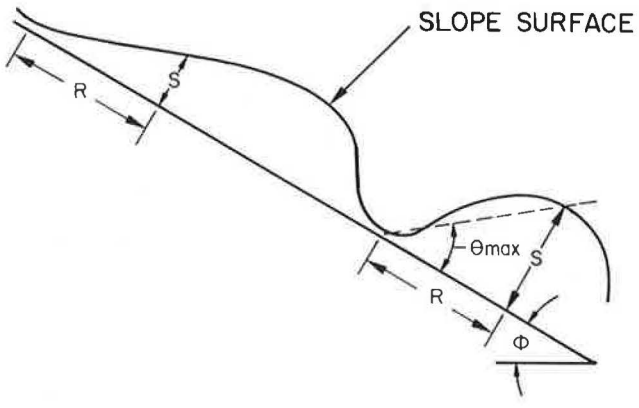

FIGURE 1 Surface roughness (S) established as the perpendicular variation within a slope distance equal to the radius of the rock (R). Maximum slope variation (Θmax) defined by S and R.

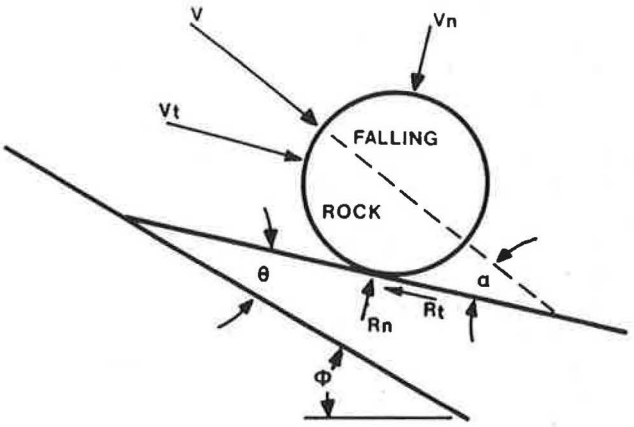

FIGURE 2 Impact angle (α) defined as a function of rock trajectory, slope angle (Φ), and slope variation (Θ). Vn, velocity normal to the slope; Vt, velocity tangential to the slope; Rt, coefficient of frictional resistance tangential to the slope; Rn, coefficient of restitution normal to the slope.

TABLE 2 SUGGESTED NORMAL COEFFICIENT INPUT VALUES

Normal Coefficient Rn	Description of slope
0.37 - 0.42	Smooth hard surfaces and paving.
0.33 - 0.37	Most bedrock and boulder fields.
0.30 - 0.33	Talus and firm soil slopes.
0.28 - 0.30	Soft soil slopes.

TABLE 3 SUGGESTED TANGENTIAL COEFFICIENT INPUT VALUES

Tangential Coefficient Rt	Description of slope
0.87 - 0.92	Smooth hard surfaces such as pavement or smooth bedrock surfaces.
0.83 - 0.87	Most bedrock surfaces and talus with no vegetation.
0.82 - 0.85	Most talus slopes with some low vegetation.
0.80 - 0.83	Vegetated talus slopes and soil slopes with sparse vegetation.
0.78 - 0.82	Brush covered soil slope.

and whether the rock is initially rolling over or sliding on the surface. A friction function is used to adjust the tangential coefficient according to the difference between the velocity at the surface of the rock relative to the ground at the start of the impact (*2*).

The velocity normal to the slope is another major influence on the loss of kinetic energy tangential to the slope. An increase in velocity normal to the surface results in a greater normal force during impact. A scaling factor is incorporated to adjust for the increased frictional resistances owing to an increase in the normal force. CRSP considers angular momentum by allowing rotational energy to be converted to tangential energy or by allowing tangential energy to be converted to rotational energy (*1*,*2*).

The normal coefficient of restitution (Rn) and a velocity-dependent scaling factor are used to determine a new normal velocity. A normal scaling factor adjusts for the decrease in normal coefficient of restitution as the impact velocity increases (*2*). This factor represents a transition from a more elastic rebound at low velocities to a much less elastic rebound caused by increased fracturing of the rock and cratering of the slope surface at higher impact velocities (*2*,*9*).

An iteration is used after each bounce to find the time elapsed until the next bounce. Elapsed time is calculated from the x, y velocities, gravitational acceleration, and the slope profile. The next bounce is calculated as before after a new impact position is established. If the distance the rock travels between bounces is less than its radius, then the rock is considered to be rolling and is given a new x, y position equal to a distance of one radius from its previous position. This models a rolling rock as a series of short bounces, much like an irregular rock rolls on an irregular surface (*2*).

Sensitivity to Input Parameters

With so many parameters affecting the simulation results in different ways it becomes difficult to understand just how each parameter affects the results. The effects of the input parameters on both bounce height and velocity predictions often vary because of changes in other input parameters. For example, the effects of surface roughness and slope material coefficients decrease on steep slopes because the rock bounces less often.

As is expected, slope angle is an important factor in determining the behavior of rockfalls. Rockfalls will increase in velocity up to an equilibrium velocity where the energy lost in the bounce equals the energy gained since the previous bounce. The relationship between slope angle and equilibrium velocity for various surface roughness conditions is presented in Figure 3. The average rockfall equilibrium velocity from Figure 3 is the average velocity predicted by CRSP after the

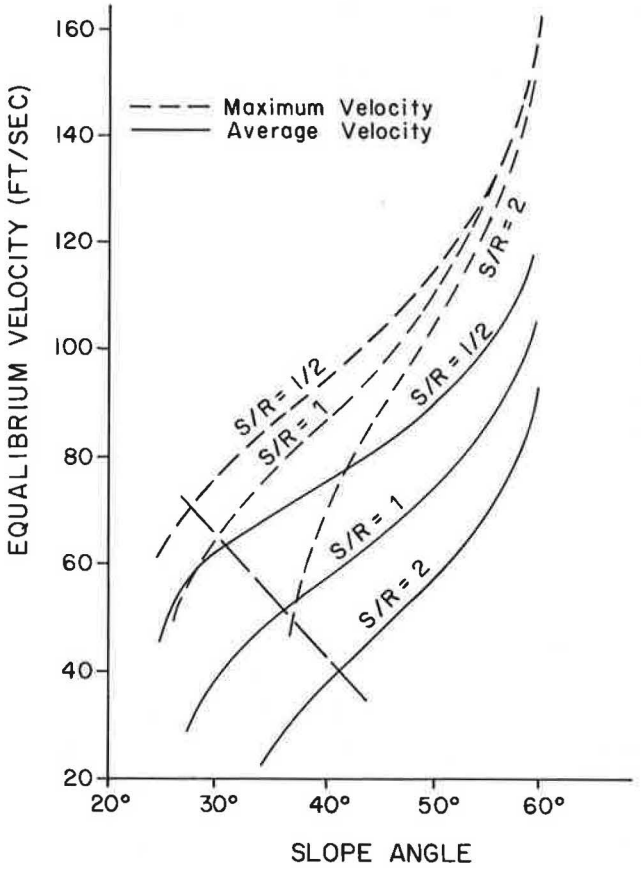

FIGURE 3 Maximum and average equilibrium velocity versus slope angle for uniform slopes.

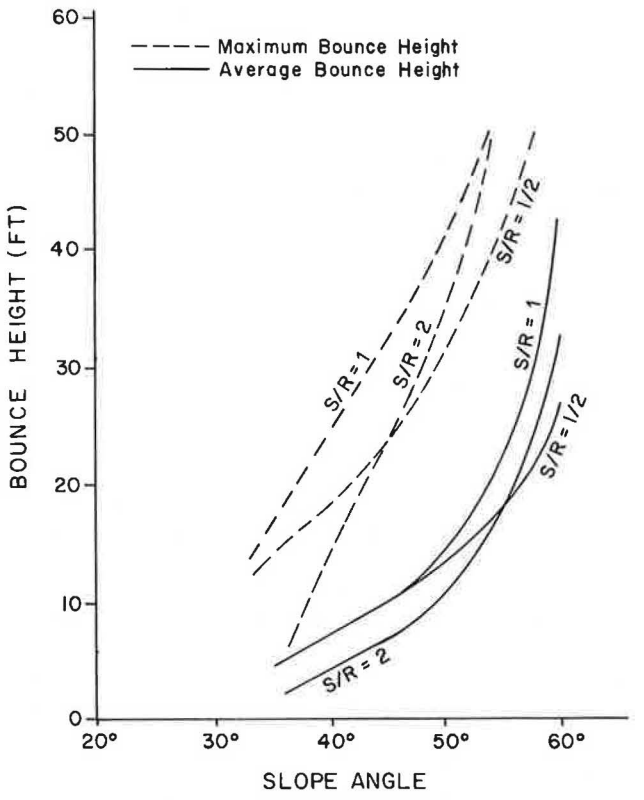

FIGURE 4 Maximum and average equilibrium bounce heights versus slope angle.

equilibrium condition is reached. The maximum equilibrium velocity predicted is the velocity of the fastest rock.

Bounce height will also tend to reach an equilibrium height on long slopes. The relationship between slope angle and bounce height is presented in Figure 4.

Also important in determining rockfall behavior is surface roughness. The ratio of the surface roughness to rock size (S/R) is used to determine the maximum variation in the slope. Therefore, the effect of surface roughness may be studied by investigating the effect of S/R (defined in Figure 1). Figures 3 and 4 indicate that an increase in the S/R ratio will generally result in a decrease in velocity and an increase in bounce height on slopes over 45 degrees. However, on shallower slopes the decrease in velocity with increasing S/R ratio results in a decrease in bounce height.

Material coefficients affect rockfall behavior by controlling the amount of energy absorbed during impact. Higher coefficient values correspond to less energy loss during impact. The effect of material coefficients on bounce height and velocity depends on the number of impacts or bounces. On steep slopes, where rocks hit the slope with less frequency, the effect of material coefficients on rockfall behavior becomes negligible. The effect of the coefficients on rockfall behavior is greatest for gradual slopes, where the rockfall velocity is decreasing. On most slopes, changes in material coefficients, within reasonable limits for a specific slope material, will not produce a significant change in results (*1*).

To summarize, several factors act to reduce the effect of slope material on rockfall behavior. First, the effect of slope angle and surface roughness is so much greater than the effect of material properties that the angle and roughness obscure the effects of variations in material coefficients. Second, the coefficients are modified by scaling factors and the friction function, which tend to further obscure the results of changes in coefficients. Third, and most important, is that the velocity normal to the slope at impact depends on the impact angle, which is determined by the slope angle, rock radius, and surface roughness. For those reasons the effect of variations in material coefficients depends largely on the slope configuration.

Figures 3 and 4 provide a basis for developing a conceptual understanding of the relationships between the input parameters and may also be used to make estimates of probable rockfall bounce heights and velocities for uniform slopes. However, cases with variable slope angles are too complex for estimates by using those graphs.

Figures 3 and 4 are limited to slopes between 30 and 60 degrees. The energy lost during the bounce will always be less than the energy gained between bounces on slopes greater than about 60 degrees, and the velocity will decrease until the rock comes to rest on slopes of less than about 30 degrees. Figure 3 was developed for hard, rocky slopes. The equilibrium velocity for soil slopes of less than about 40 degrees will be about 15 percent less than that predicted by the graph. The effect of surface material will be negligible on slopes steeper than 50 degrees.

Figure 3 gives the average and maximum equilibrium velocities. The rockfall may not reach the equilibrium condition for slopes shorter than 300 to 500 ft. In this case the average and maximum velocities may be obtained by multiplying the velocity from Figure 3 by the distance factor obtained for the slope length and angle in Figure 5. Similarly, the bounce height values obtained from the graph in Figure 4 may be corrected for slope length by multiplying by the distance factor obtained from Figure 5. Those products are an estimate of the velocities and bounce heights that would be predicted by CRSP for uniform slopes (*1*).

CRSP FIELD TESTING

Rocks were rolled down a 300-ft-high hillside near Rifle, Colorado, to test rockfall fence designs and to collect data on rockfalls for verification and calibration of CRSP. The test hillside consisted of thin desert soil with rocky ledges (Figure 6). The sparse vegetation visibly had little effect on the behavior of the rockfalls. All of the rockfalls were initiated from the same point, but the topography of the upper slope resulted in a wide dispersion. Data could only be obtained for the rocks that traveled down the most direct path to the gully on the lower part of the slope. Figure 7 presents the slope profile of the test site.

The time for each rock to travel through two zones of the hillside, the number of bounces in each zone, and the bounce height at the analysis point were collected from viewing videotapes of the rockfalls. Those data were compared with data generated by CRSP. The program required modification to present the travel time data (*1*). Material coefficients were chosen according to the guidelines presented in Tables 2 and 3.

Figure 8 presents a graphical representation for the simulation at the West Rifle test site. Dots that represent the position of the simulation rock every tenth of a second occur in characteristic parabolic arcs above the slope profile. This visual aid can be helpful to determine the most likely locations for and types of mitigative measures that can be taken.

Figure 9 presents the distribution of simulated rock velocities and bounce heights produced for the analysis point near the base of the slope and maximum bounce heights and velocities along the slope profile. Those results provide estimates of parameters required for the location and design of fences, ditches, or other types of structures at the selected analysis point.

Table 4 compares the field tests with CRSP results. Because CRSP attempts to represent worst-case situations, only data from the fastest 50 percent of the rocks rolled were used in the comparison. The comparison in Table 4 indicates that CRSP was able to provide reasonable predictions of rockfall behavior.

CRSP Application in Glenwood Canyon

CRSP has been used extensively to aid in the design of rockfall mitigation for I-70 in scenic Glenwood Canyon where aesthetic values were an important concern. The steep canyon slopes above the road lead to frequent rockfalls in the 15-mi-long canyon. Rockfalls may originate both high on the steep canyon slopes and from rock cuts and natural cliffs near the roadway. Rockfall hazards from high on the canyon slopes may be reduced by using catch fences designed with the aid of CRSP. Rockfall hazards associated with rock slopes closer to the highway may require other mitigative measures such as benches or ditches.

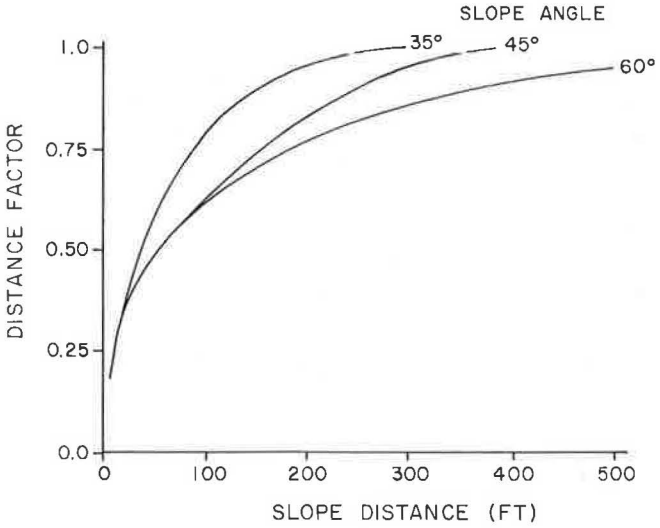

FIGURE 5 Distance factor indicating the proportion of the equilibrium velocity achieved versus horizontal slope distance.

FIGURE 6 Slope used for CRSP testing near Rifle, Colo.

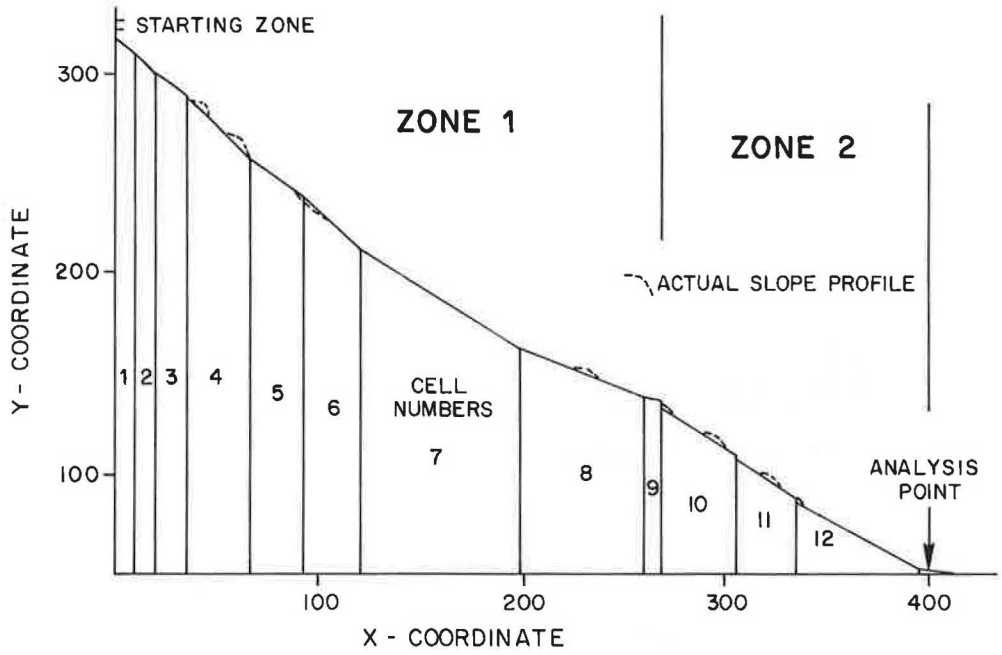

FIGURE 7 Slope profile of West Rifle test site.

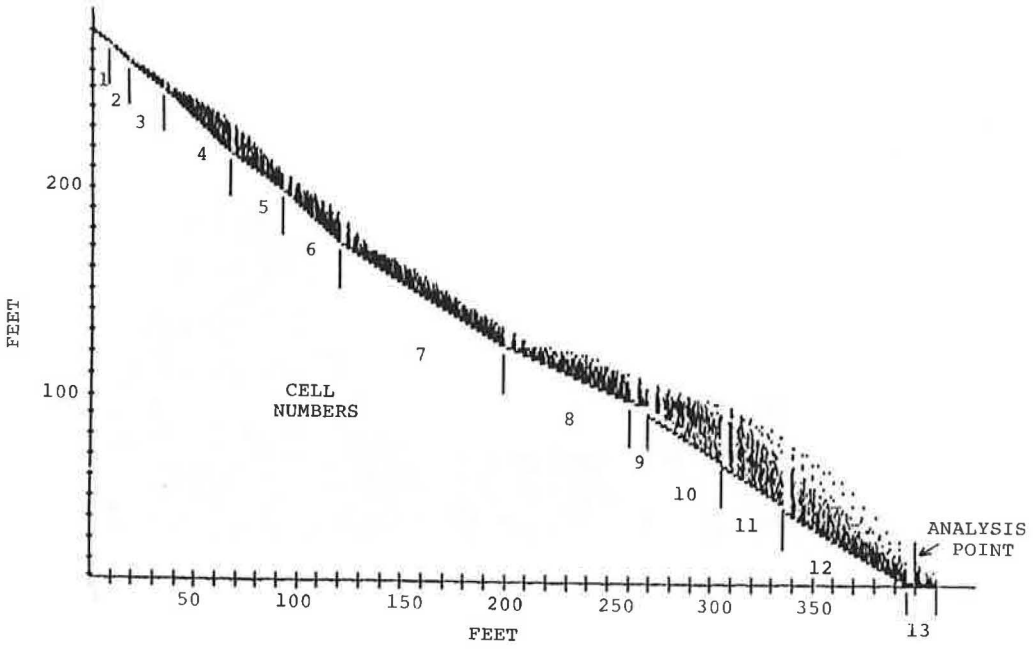

FIGURE 8 CRSP graphical representation of rockfalls at the West Rifle test site.

The concern for aesthetics was the driving force behind the design philosophy to minimize disturbance to natural slopes and to construct rock cuts to look natural. Therefore, rock cuts were constructed with irregular cut faces and minimal planted ditches or benches. However, those construction methods could result in a greater rockfall hazard than that associated with traditional rock slope design considerations that call for even, presplit slopes and large ditches. Few practical methods were available to assess the rockfall hazard associated with irregular slopes before the development of CRSP.

CRSP use allows compromises between the landscape architect's aesthetic concerns and concerns for rockfall safety. Safe rock cuts could be designed and constructed while still incorporating planted benches and the irregular shape needed to have the appearance of a natural rock slope. The "ski

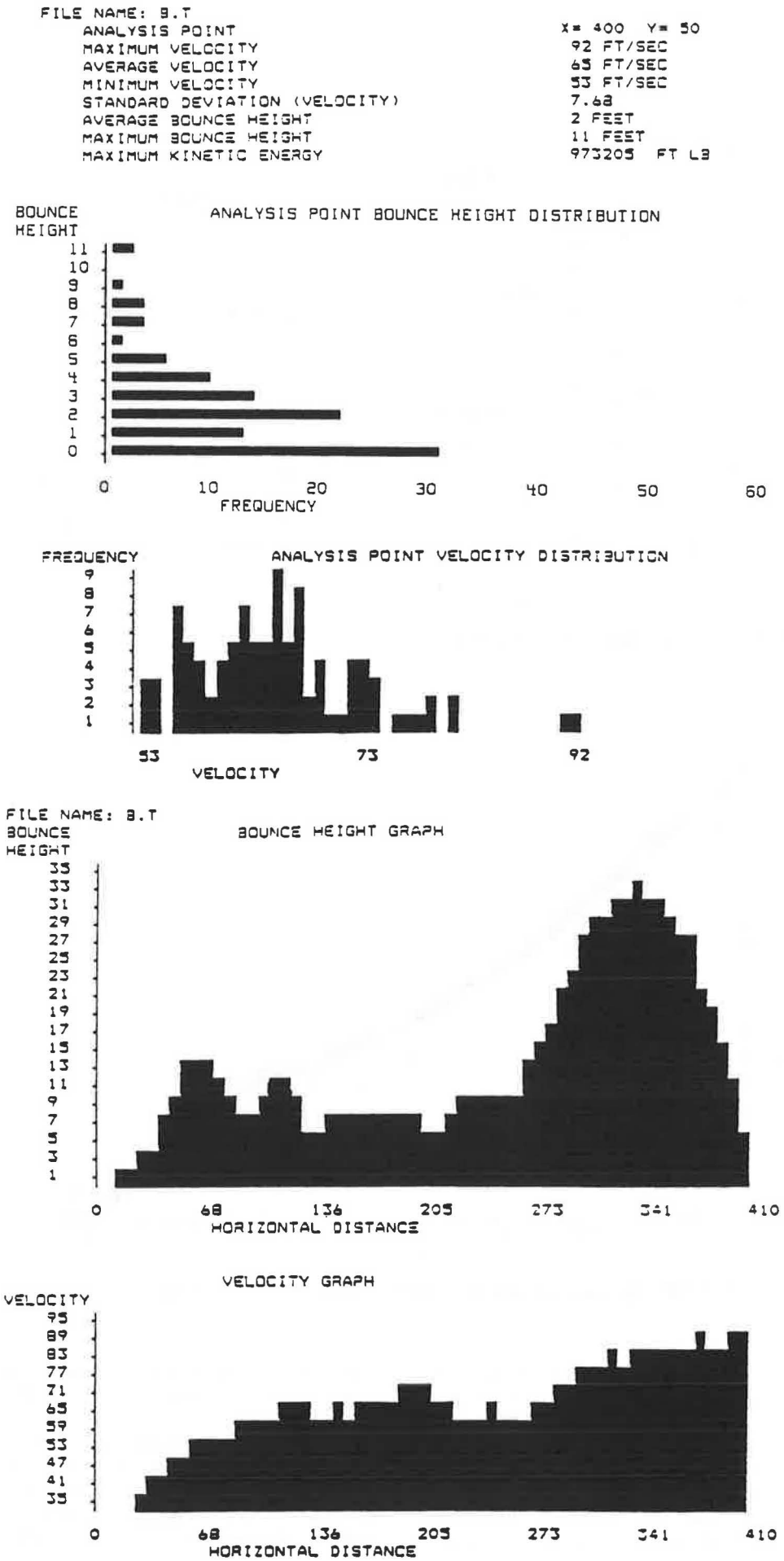

FIGURE 9 CRSP output of the distribution of rockfall simulations by (a) bounce height and velocity for the analysis point and (b) maximum bounce heights and velocities along the slope profile at the West Rifle test site.

TABLE 4 COMPARISON OF FIELD DATA FROM THE WEST RIFLE TEST SITE WITH DATA GENERATED BY CRSP

	ZONE 1		ZONE 2		ANALYSIS POINT
	TIME SEC.	# OF BOUNCES	TIME SEC.	# OF BOUNCES	BOUNCE HEIGHT (FT)
FIELD DATA					
SAMPLE SIZE	(23)	(21)	(19)	(18)	(17)
AVERAGE	8.72	12.6	2.58	2.0	2.52
RANGE	7.8-9.8	10-16	2.2-2.9	1-4	0-11
STANDARD DEVIATION	0.61	1.43	0.23	0.88	3.36
CRSP DATA					
AVERAGE	8.4	12.6	2.62	1.5	2.45
RANGE	7.8-10.5	10-16	2.2-3.4	1-3	0-11
STANDARD DEVIATION	0.95	1.85	0.38	0.64	2.43

jump" effect of proposed bench locations and size was modeled, allowing adjustment of location and size to reduce the likelihood of launching rocks into the roadway.

CRSP results often aided in reaching a compromise on ditch configurations. Wider ditches were acceptable to the landscape plan if some variety could be incorporated into the visible area of the ditch. Rock ledges and irregular-shaped slopes within the ditch area could be modeled with CRSP and located so as not to create a rockfall hazard. Usually this required several feet of backslope and no features over a specified height in the ditch. The addition of the graphics display to the program proved to be a useful visual aid to convince landscape architects that design changes were needed to reduce rockfall hazard.

At some locations, CRSP would indicate that rockfalls could present a hazard to the roadway, but wider ditches or reshaping of the slope did not present a practical solution. CRSP was used to evaluate alternative methods of rockfall mitigation located above the roadway in those cases.

CONCLUSIONS

CRSP is used in Glenwood Canyon on a daily basis as part of a comprehensive rockfall program. Simulation results help determine rockfall hazard severity and determine necessary rockfall fence capacities. Also, CRSP is used to help plan rock cut and ditch configurations both safe and aesthetically acceptable. The use of CRSP in Glenwood Canyon provides an objective means to help evaluate rockfall hazards.

Even though determining input values and using the output data requires judgment, the computer analysis adds objectivity to an otherwise largely subjective investigation of rockfall hazard. Because this computer program provides a site-specific analysis of rockfall, the program may help identify areas where roadside ditches can be narrowed or where alternate rockfall mitigation measures should be considered. Rockfall simulation may also note applications in open pit mines and hillside property development.

Computer analysis of a site is rapid, inexpensive, and allows for consideration of numerous alternatives. Increased use of computer analyses for rockfall studies can improve the state-of-the-art in rockfall hazard investigation and mitigation.

The CRSP method of rockfall analysis has been in use on the Glenwood Canyon project and at the Rifle, Colorado, test site. Also, it has been tested by using field data from the technical literature and data provided by practitioners. However, CRSP is still in the field-testing and development stages. The program will need industry-wide use in a variety of situations to ensure the validity of the program output and to identify any limitations of the program.

ACKNOWLEDGMENTS

The work on which this paper is based was supported in part by the Colorado Department of Highways and the U.S. Department of Transportation, Federal Highway Administration. The authors would like to thank Bob Barrett of the Colorado Department of Highways and Tim Bowen of the Colorado Geological Survey for their continued support of rockfall research in Glenwood Canyon. The authors also wish to thank Roger Pihl, Amy Pfeiffer, and Michael Byle for their valuable input.

The contents of this paper reflect the views of the authors and do not necessarily reflect the official views or policies of CDH or FHWA.

CRSP is available from the Research Section, Colorado Department of Highways, 4201 East Arkansas Avenue, Denver, Colo. 80222, (303) 757-9506.

REFERENCES

1. T. J. Pfeiffer. *Rockfall Hazard Analysis Using Computer Simulation of Rockfalls*. Masters thesis. Colorado School of Mines, Golden, Colo., May 1989.
2. T. J. Pfeiffer and T. D. Bowen. Computer Simulation of Rockfalls. *Bulletin of the Association of Engineering Geologists*, Vol. 26, No. 1, Feb. 1989, pp. 135–146.
3. A. M. Ritchie. The Evaluation of Rockfall and its Control. In *Highway Research Record 17*, HRB, National Research Council, Washington, D.C. 1963, pp. 13–28.
4. M. R. Nichol and R. J. Watters. Comparison and Effectiveness of Rockfall Mitigation Techniques Applied by States in the USA and Canada. *Proc., 20th Annual Engineering Geology and Soils Engineering Symposium*, Boise, Idaho, 1983, pp. 123–142.
5. Piteau and Associates Ltd. Slope Stability Analysis for Rockfall Problems: The Computer Rockfall Model for Simulating Rockfall Distributions, Part D. In *Rock Slope Engineering*, Reference Manual FHWA-TS-79-208, FHWA, Department of Transportation, 1980, pp. 62–68.
6. S.-S. Wu. Rockfall Evaluation by Computer Simulation. *Transportation Research Record 1031*, TRB, National Research Council, Washington, D.C., 1984, pp. 1–5.
7. E. Hoek. *Rockfall: A Program in Basic for the Analysis of Rockfalls From Slopes*. Golder Associates, Vancouver, B.C., 1987.
8. C. L. Evans. *The Design of Bench Geometry in Surface Mines to Control Rockfall*. Masters thesis. University of Arizona, Tucson, 1989.
9. P. Habib. Note Sur Le Rebondissement Des Blocs Rocheux, Instituto Sperimentale Modolli E Structture. *Proc., Rockfall Dynamics and Protective Works*, Bergamo, Italia, 1976, pp. 123–125.

Publication of this paper sponsored by Committee on Engineering Geology.

Minimum Cover Heights for Corrugated Plastic Pipe Under Vehicle Loading

MICHAEL G. KATONA

The minimum soil cover requirements are provided for corrugated plastic pipe (high density polyethylene) to safely withstand vehicular loading when the pipe is installed under roadways such as in culvert applications. Pipe diameters ranging from 12 to 36 in. and all pipe wall corrugations currently produced are also included. Design criteria are adopted from AASHTO specifications, and it is discussed that the allowable deflection criterion, 7.5 percent of the pipe diameter, controls the minimum soil cover requirement. It is also discussed that by increasing the corrugation's moment of inertia or improving the quality of the soil or both the minimum soil cover requirement can be reduced. Design solutions are obtained with aid of CANDE, the plane strain computer program. A new methodology is introduced to account for the three-dimensional effects of tire loads (H-trucks) in the context of a plane strain analysis. The design/analysis methodology is shown to compare favorably with field data for shallow buried plastic pipes with simulated H-20 truck loadings. As a final result, design tables and guidelines are presented that specify the minimum required soil cover as a function of pipe diameter, H-truck loading, corrugation section properties, and soil type and percent compaction. Also, the results are extended to railroad loadings.

The objective is to establish minimum soil height requirements for high density polyethylene (HDPE) corrugated plastic pipe to safely withstand loadings from roadway vehicles (H-trucks). The final results are tabulated in easy-to-use charts and guidelines that give the minimum cover height as a function of pipe diameter and flexural stiffness, soil type and percent compaction, and H-truck loading.

BACKGROUND

A previously completed companion study (*1*) provides maximum allowable fill heights for the same class of HDPE corrugated plastic pipes that are considered in this study for minimum cover. The major source of loading for deeply buried pipes is the gravity weight of soil as opposed to the additional soil stresses from vehicle surface loads that disperse rapidly with depth. The loads on the pipe for minimum cover primarily are due to the surface loading. A minimum amount of soil cover is needed to spread the surface loading and to create a more favorable soil pressure distribution around the pipe. With too little soil cover the pipe will experience high pressure concentrations at the crown and cause collapse.

Vehicular loadings, unlike well-defined gravity loads, vary widely in load magnitude and distribution owing to the wide variety of vehicle types. Other difficulties associated with defining vehicular loading include impact, cyclic frequency, load shift, and wind. Also, construction equipment used during the placement of the pipe can cause greater loads on the pipe than the vehicular loads for which the pipe has been designed. Thus, the minimum cover requirement is a more challenging design problem than the maximum fill height.

Currently, the tentative guideline for minimum cover of plastic pipe, as suggested by the AASHTO Flexible Culvert Committee, is taken directly from the metal culvert industry, the American Iron and Steel Institute (AISI) (*2*). The AISI specification for corrugated metal culverts requires a minimum of 12 in. of soil cover for all pipe diameters up to 96 in. Paving material, if any, is not permitted to be included in the 12-in. minimum cover owing to the concern of construction loads prior to paving. This requirement is based on long-time observations by the corrugated steel pipe industry of structural performance under live loads.

Corrugated plastic pipes are considerably more flexible in ovaling deformation than are typical corrugated steel pipes of the same diameter. Consequently, it is natural to ask if the minimum 12-in. cover is adequate for plastic pipe, and, if not, what is the requirement and what does it depend on. Herein lies the motivation behind the stated objective.

APPROACH AND SCOPE

The finite-element program CANDE (*3*), a proven methodology for soil-structure interaction analyses of buried conduits, is used with established design criteria to achieve the design objective, which are the minimum cover requirements for corrugated plastic pipe. Experimental data are used to verify the analytical assumptions.

The following step-by-step procedure outlines the approach and scope presented in this paper.

1. **Establish H-truck loadings:** Five loading cases are considered based on AASHTO truck definitions: H-10, H-15, H-20, H-25, and H-30. Conservative assumptions are employed to define contact area and pressure magnitude for each truck's tire footprint.
2. **Identify plastic pipe properties:** Six pipe sizes are considered: 12, 15, 18, 24, 30, and 36 in. diameter pipe. Cross-sectional properties are defined for each pipe size, and material properties for short-term loading are identified.

Headquarters, Air Force Engineering and Services Center, Tyndall Air Force Base, Fla. 32403-6001.

3. **Introduce design/analysis methodology:** The CANDE plane strain computer program is reviewed along with the soil modeling assumptions. A new technique for modeling the tire loads is presented and followed by the design criteria for plastic pipe.

4. **Perform parametric studies:** The influence of design variables (cross-section properties, quality of soil, and cover height) are examined in conjunction with the design criteria to establish the controlling criterion.

5. **Compare analysis with experimental data:** The design/analysis procedure is verified with experimental field data, and conservatism is demonstrated.

6. **Present final design results:** Minimum cover height tables are given for each pipe size as a function of H-truck loading, pipe stiffness, and soil quality. Interpolation schemes and design examples are also given.

The final section, containing the design results, is self-contained so the reader may make use of this section without referring to previous sections.

H-TRUCK LOADINGS

H-Truck Definition

The H-truck loading, as defined by AASHTO and presented in Figure 1 is designated by the symbol H-x where x is one half of the total gross weight of the truck expressed in kips. The H-truck loading has two axles: 80 percent of the total gross weight is assigned to the rear axle and the remaining 20 percent is assigned to the front axle. Tires (single or dual) carry one-half the axle load. For example, the H-20 truck has a total gross weight of 40 kips, a rear axle load of 32 kips, and a rear tire load of 16 kips.

The H-truck loading definition does not necessarily represent a real truck. Rather, it is a reference design vehicle developed by U.S. bridge engineers to serve as a worst case or umbrella loading for all vehicles whose actual load distributions (e.g., axial loads or spacing or both) are less severe to bridge design than the H-truck loading.

Tire Load Distribution

The tire contact area on the roadway surface must be known in addition to the tire load to determine the minimim soil cover requirements for culverts. For any given tire loading (e.g., 16 kips for the rear tire of an H-20 truck) the air pressure in the tire is a close approximation to the average contact pressure between the tire and roadway surface. Accordingly, the tire contact area (or tire footprint) may be computed by dividing the tire loading by the tire air pressure.

A high-pressure tire induces more structural distress in a shallow buried culvert than does an equally loaded low-pressure tire because the low-pressure tire distributes the load over a larger area. The tire air pressure of interstate trucks ranges from 65 to 100 psi. Because the AASHTO H-truck loading definition does not include specifications of tire air pressure, conservative assumptions are presented next based on a tire pressure of 100 psi.

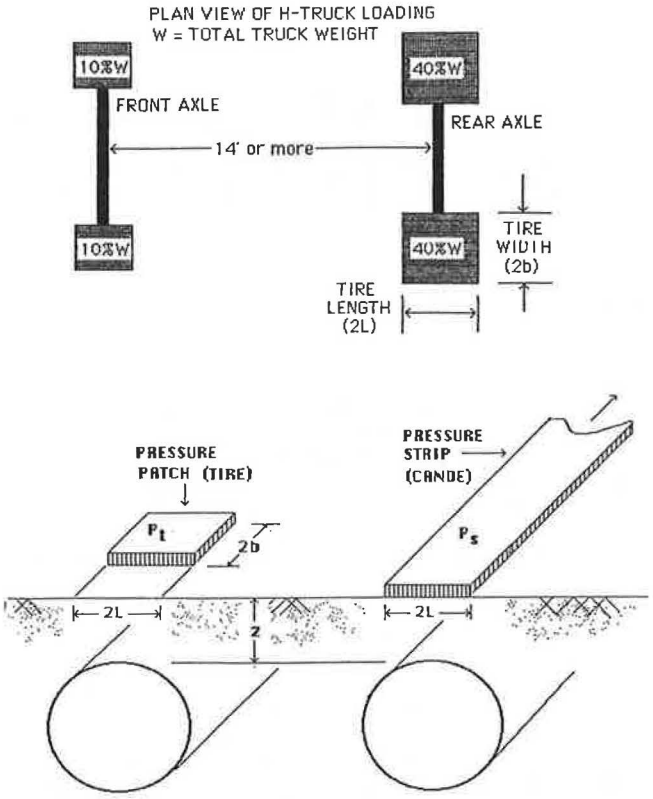

FIGURE 1 H-truck loading and tire pressure distribution.

TABLE 1 H-TRUCK LOADING ON REAR TIRE

Truck Type	Gross Wt. (kips)	Rear Tire Wt. (kips)	Tire length (inches)	Tire width (inches)
H10	20	8	10	8
H15	30	12	10	12
H20	40	16	10	16
H25	50	20	10	20
H30	60	24	10	24

Tire (single or dual) pressure = 100 psi

Tire Loading Assumptions For Culvert Analysis

Table 1 supplies the five H-truck loadings as defined by AASHTO along with the assumed dimensions of a rectangular-shaped footprint for the rear tire. In each case the tire pressure is taken as 100 psi, which is an upper-bound value for actual tire pressures. The footprint length, in the direction of travel, is taken as 10 in., which is a nominal average of actual footprint lengths. With the tire pressure and footprint length so defined, the footprint width becomes a function of the H-truck rear wheel loading and is easily determined by force

equilibrium. The implication is that as the H-truck series increases the additional load is accommodated by wider tires or the use of dual tires or both, thereby distributing the load along the rear axle. This method of distributing the rear wheel load presents a worse loading condition on a buried culvert than if the load were distributed in the direction of travel (e.g., increased footprint lengths or tandem axles or both).

No further load enhancements (wind, impact, load shift, etc.) appear justifiable in view of all the conservative assumptions employed in defining the tire loads and the pressure distributions. Thus, H-loading defined in Table 1 will constitute the net live load for subsequent design process.

CORRUGATED PLASTIC PIPE PROPERTIES

Section Properties

Corrugated plastic pipes are referenced by the inside diameter (also called the pipe size, e.g., 24-inch pipe). Unlike the corrugated metal pipe industry, the manufacturers of corrugated plastic pipe do not employ a standardized set of corrugated shapes for each pipe diameter. Rather, a typical plastic pipe manufacturer makes only one corrugation size per pipe size. However, the corrugated shape made by one manufacturer and that of another differs somewhat in material thickness and in shape and height of the corrugation. As a consequence, the key sectional properties, cross-sectional area per unit length, and moment of inertia per unit length vary from manufacturer to manufacturer. This variation of section properties is accommodated in the design process.

In general, the robustness of a corrugated pipe can be assessed by the hoop stiffness, which is proportional to the corrugated section area, and by the flexural (ovaling) stiffness, which is proportional to the corrugation moment of inertia. The moment of inertia is the key section property that controls the minimum cover height for shallow buried pipes subject to vehicular loading because deflection by ovaling is almost always the controlling design criterion. Conversely, the cross-sectional area does not influence the minimum cover height as long as its value is greater than a certain minimum value that precludes thrust stress from controlling the design. The validity of those statements is amply demonstrated later in this study.

The following geometrical relationships, based on a previous survey study of corrugated section properties produced by five of the largest plastic pipe manufacturers (*1*), are noted for pipe sizes 12, 15, 18, 24, 30, and 36 in.:

1. The average cross-sectional corrugated area A is related to the inside pipe diameter ID (inches) by the empirical expression

$$A = (ID + 4.5)/10 \quad (\text{in.}^2/\text{in.}) \quad (1)$$

2. The average corrugation height (i.e., one-half of the distance between outside and inside diameter) is related to ID by the expression

$$h = ID/11 \quad (2)$$

3. The upper- and lower-bound moment of inertia that comfortably brackets all actual data is given by the dimensionally correct expressions

$$I_{max} = Ah^2/5 \quad (3a)$$

$$I_{min} = Ah^2/10 \quad (3b)$$

The moment of inertia will be treated as a design variable varying between the limits I_{min} and I_{max}, and the cross-sectional area and corrugation height will be assigned their average values.

Pipe Material

Polyethylene exhibits significant creep behavior under long-term constant loading (*4*). Thus, the effective short-term modulus is considerably higher than the long-term modulus. Table 2 summarizes the AASHTO M294 specification and indicates that the recommended modulus for the short term is five times more than long term (50 years).

Strength behavior is not as well studied or understood as stiffness. The AASHTO specifications, as presented in Table 2, are based on tensile stress-strain experiments, which exhibit nearly unlimited ductility without rupture. Those strength values are assumed to hold for compression and tension and are generally considered to be conservative.

Although the duration of the short-term loading period is not explicitly defined by AASHTO, the short-term plastic properties are considered appropriate for shallow buried pipe subject to vehicular loads. The validity of this assumption is demonstrated with experimental field data later in this study.

METHOD OF ANALYSIS/DESIGN

CANDE Analysis

CANDE, an acronym for culvert analysis and design, is a well-known and well-accepted finite-element computer program developed especially for the structural design and analysis of buried conduits (*3*,*5*,*6*). Both the pipe and the surrounding soil envelope are incorporated into an incremental, static, plane strain formulation. The pipe is modeled with a connected sequence of beam-column elements, and the soil is modeled with continuum elements by using a revised Duncan hyperbolic soil model (*5*). The fundamental analysis assumptions are small deformation theory, linear elastic polyethylene properties (short term), and a bonded pipe-soil interface.

TABLE 2 POLYETHYLENE MATERIAL PROPERTIES

Time Period (rel.)	Young's Modulus (psi)	Design Strength (psi)
Short term	110,000	3,000
Long term	22,000	900

The gravity loading of the soil is applied in the first load step for the analysis of each pipe-soil system with a specified minimum cover. Next, the H-truck rear wheel loading, as defined in Table 1, is simulated by applying increments of pressure to the soil surface over a 10-in. segment (i.e., footprint length) centered directly above the pipe. Note only one rear wheel of the H-truck vehicle need be considered because the other wheels are too far away to add to the local deformation of the pipe under the wheel being considered. The method of analyzing the effects of various footprint widths (out-of-plane) is discussed next.

H-Truck Load Representation

Because CANDE is a two-dimensional plane strain formulation, the footprint length $2L$ in Figure 1 can be modeled exactly. However, plane strain analysis infers that the footprint width is infinitely deep, as is illustrated on the right side of Figure 1. To reasonably simulate a finite footprint width as pictured in the left side of Figure 1, the plane strain pressure P_s should be appropriately reduced from that of the actual tire footprint pressure P_t, that is,

$$P_s = r\,P_t \tag{4}$$

where r is a reduction factor (less than 1.0). This reduction is required because the soil stress associated with P_t diminishes more rapidly with depth than does the soil stress associated with P_s (i.e., two-dimensional load spreading versus one-dimensional load spreading).

To compute the reduction factor, use is made of an exact elasticity solution for a homogenous half space (no pipe) loaded by the pressure P_t acting on a rectangular footing with dimensions $2L$ by $2b$ (7). The solution for vertical soil stress as a function of depth z beneath the center of pressure is given by

$$S_t = 2\,P_t\{\arctan(B/Z\,R3) + BZ[1/(R1\,R1\,R3) + 1/(R2\,R2\,R3)]\}/\pi \tag{5}$$

where

$B = b/L$,
$Z = z/L$,
$R1 = \sqrt{(1 + ZZ)}$,
$R2 = \sqrt{(BB + ZZ)}$,
$R3 = \sqrt{(1 + BB + ZZ)}$, and
$\pi = 3.14$

Similarly, the vertical soil stress for the pressure P_s acting on an infinite strip of dimension $2L$ (i.e., width $2b$ is infinite) is given by

$$S_s = 2\,P_s\{\arctan(1/Z) + Z/(R1\,R1)\}/\pi \tag{6}$$

By equating $S_t = S_s$ from Equations 5 and 6 and solving for the reduction factor ($r = P_s/P_t$),

$$r = \frac{\arctan(B/ZR3) + BZ/[1/(R1\,R1\,R3) + 1/(R2\,R2\,R3)]}{\arctan(1/Z) + Z/(R1\,R1)} \tag{7}$$

The reduction factor is a function of the footprint dimensions ($2b$ by $2L$) and the depth at which the soil stress equality is desired. This depth, which is nondimensionally expressed as $Z = z/L$, is, for the moment, unspecified.

Table 3 supplies the reduction factors as a function of Z for each of the H-truck footprint dimensions defined in Table 1. Note that the reduction factor decreases with depth and increases tire loading (footprint width).

A reasonable depth to establish "soil stress equivalence" is somewhere between the crown and springline elevation. For this study the depth is taken midway between the crown and springline elevations, which are based on comparisons with experimental data (shown later). Thus, the nondimensional depth Z is taken as

$$Z = [H + ID/4]/L \tag{8}$$

where H is the soil cover height above crown and L is one-half the footprint length (5 in. for all H-Trucks).

To illustrate the use of Table 3 together with Equation 8, suppose a plane strain analysis (e.g., CANDE) is performed for a 24-in. pipe under 12 in. of soil cover and loaded by an H-20 truck tire (100 psi). From Equation 8 $Z = 18/5 = 3.6$, and from Table 3 $r = 0.57$. Therefore, in accordance with Equation 4, the "equivalent pressure" to be used in plane strain analysis is $P_s = 57$ psi.

Soil Model

All design cases are analyzed for two soil conditions generically called "fair" and "good" quality soil. Specifically, those two cases are represented by the Duncan soil models for silty clayey sand at 85 percent compaction (fair = SC 85) and silty clayey sand at 100 percent compaction (good = SC 100). Table 4 supplies the Duncan model parameters for those two soil conditions. More general interpretations for those two "bracketing" cases are given in the last section, allowing the solutions to be interpolated over a range of soil types and percent compaction.

TABLE 3 REDUCTION FACTOR FOR STRIP PRESSURE

Depth Ratio Z = z/L	H-Truck designation and ratio (b/L) H10 (0.8)	H15 (1.2)	H20 (1.6)	H25 (2.0)	H30 (2.4)
1.2	.72	.86	.93	.96	.98
1.8	.56	.73	.84	.90	.94
2.4	.45	.62	.74	.82	.88
3.0	.37	.52	.65	.74	.81
3.6	.32	.45	.57	.67	.74
4.2	.28	.40	.51	.60	.68
4.8	.24	.35	.46	.55	.62
5.4	.22	.32	.41	.50	.57
6.0	.20	.29	.38	.46	.53
6.6	.18	.27	.35	.42	.49
7.2	.16	.24	.32	.39	.46
7.8	.15	.23	.30	.36	.43

TABLE 4 STANDARD HYPERBOLIC PARAMETER (7)

Soil Type	ϕ (deg)	$d\phi$ (deg)	C (psf)	K -	n -	Rf -	Kb -	m -
(SC-85)	33.0	0.0	200.	100.	0.6	0.7	50.0	0.5
(SC-100)	33.0	0.0	500.	400.	0.6	0.7	200.0	0.5

TABLE 5 DESIGN CRITERIA FOR POLYETHYLENE PIPE

Distress Measure	Allowable Limit
(1) Thrust stress	1/2 Design strength*
(2) Flexural strain	5.0% in outer fiber
(3) Relative deflection	7.5% of ID (vertical)
(4) Buckling pressure	1/2 Critical pressure**

* From Table 2, Design strength = 3000 psi (short term).
** Critical buckling pressure from Chelapati-Allgood (4).

Design Criteria

The design criteria are a set of maximum allowable structural responses for which the pipe is considered structurally safe against various modes of distress. Table 5 explicitly lists the four design criteria where the measures of pipe distress are thrust stress, relative deflection, flexural strain, and buckling pressure. Those criteria satisfy the AASHTO requirements for Service Load Design and are regarded as reasonably conservative. As is indicated in the next section, the relative deflection criterion (7.5 percent of pipe diameter) controls the design for minimum cover height in all cases.

ANALYTICAL RESULTS AND COMPARISONS

Parametric Studies

A parametric study is presented to demonstrate how the predicted responses for the design criteria are influenced by the key system variables: corrugated section area, moment of inertia, soil quality, height of soil cover, and pavement overlay. Figure 2 illustrates a baseline system composed of a 24-in. plastic pipe with 12 in. of fair quality soil cover without a pavement overlay. Table 6 supplies the baseline values for each of the key variables along with two parametric variations per variable. CANDE solutions are obtained for each individual variation, inferring 10 separate solutions in addition to the baseline solution. Each CANDE solution is obtained by first applying the gravity loading followed by increments of live load pressure up to 120 psi.

Figure 3 presents the parametric influence of the corrugated section area where the analytical predictions for thrust stress, flexural strain, relative deflection, and buckling pressure are presented as a function of live load pressure. Those responses are given as ratios to the corresponding allowable design criterion previously defined in Table 5. For example, the deflection ratio is the predicted deflection divided by 7.5 percent of the diameter, the thrust ratio is the predicted thrust stress divided by one-half the yield stress, and so on. The allowable

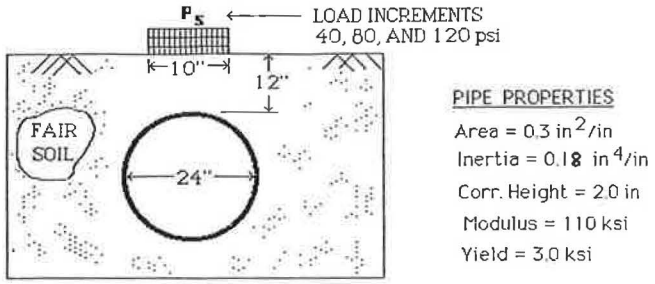

FIGURE 2 Baseline problem for parametric study.

TABLE 6 KEY PARAMETER VALUES AND VARIATIONS

Variable name	Baseline value	Variation #1 value	Variation #2 value
Section Area (in^2/in)	0.30	0.25	0.35
Mom Inertia (in^4/in)	0.18	0.12	0.24
Cover Height (in)	12.	24.	36.
Soil Quality	Fair (SC 85)	Medium (SC 95)	Good (SC 100)
Pavement Overlay	None	Asphalt (6 inches)	Concrete (6 inches)

pressure loading has been reached when a response ratio reaches the value of 1.0.

Figures 4–7 are presented in an identical format to Figure 3 and indicate the parametric influence of the remaining key variables supplied in Table 6. The following observations can be made from those figures:

1. Deflection is the controlling design criterion in all cases. That is, the deflection ratio reaches the value of 1.0 at a lower live load pressure than do the other corresponding response ratios (Figures 3–7).
2. The corrugated section area has negligible influence on the deflection, whereas increases in the moment of inertia help to reduce the deflection (Figures 3 and 4).
3. Improving the soil quality or increasing the cover height or both significantly reduces the deflection (Figures 5 and 6).
4. Paving material (asphalt or concrete) greatly reduces all structural distress including deflections (Figure 7). However, as is discussed earlier, it is not usually possible to take design advantage of the paving material because the pipe must support construction loads prior to placement of paving material.
5. The results in Figures 3–7 may be correlated to H-truck loading by computing the nondimensional reference depth given by Equation 8 and then referring to Table 3 to get the equivalent surface pressure. For example, the equivalent pressure for an H-20 truck is 57 psi for cover heights of 12 in.

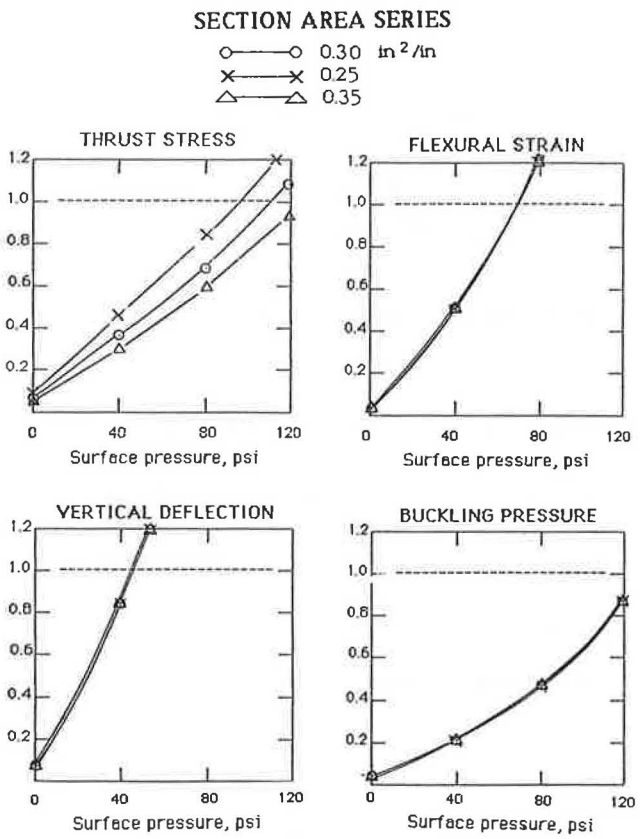

FIGURE 3 Influence of corrugated section area on design criteria.

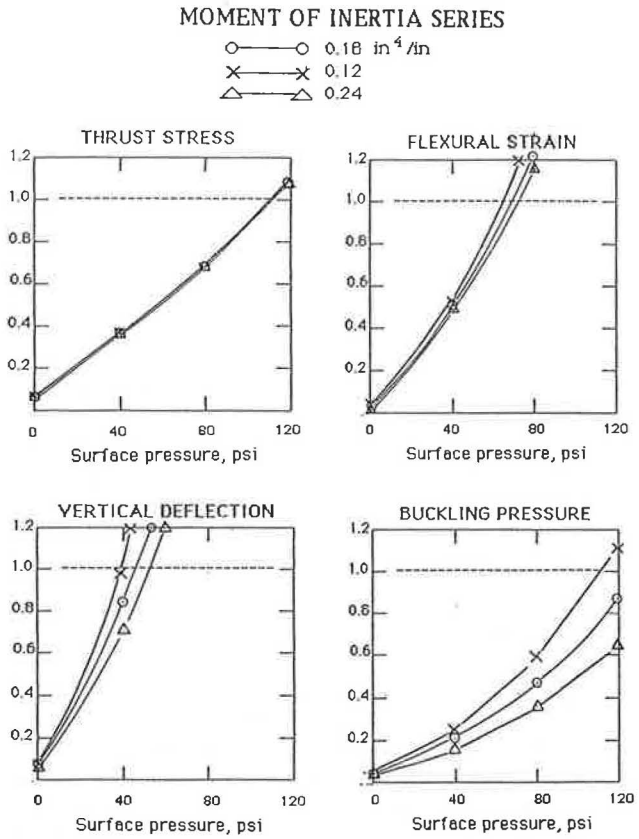

FIGURE 4 Influence of moment of inertia on design criteria.

Comparison with Experimental Data

Watkins and Reeve (*8*) in 1982 completed a comprehensive experimental test program to determine the live load deflection of plastic pipe as a function of soil cover and soil compaction. They investigated the response of a 24-in. corrugated plastic pipe subjected to an H-20 truck loading, simulated by a John Deere tractor (16 kips per wheel) as illustrated in Figure 8.

A sequence of tests was performed where the backfill soil, described as a sandy clayey silt, was compacted to densities ranging from 75 to 95 percent AASHTO standard. The soil cover height was varied for each soil density from 12 to 36 in., and the deflections were measured at 10 locations for each test. Statistical curves were derived to give deflections as a function of fill height at a confidence level of 95 percent (i.e., the curves are conservative because 95 percent of the deflection data falls below the curves). Figure 9, taken directly from Watkins and Reeve (*8*), presents two such curves for soil densities of 75 and 95 percent.

Also presented in Figure 9 are the CANDE deflection predictions for both fair and good quality soil. The predictions are based on the previously established methodology, that is, short-term polyethylene properties and H-20 truck tire representation. The corrugated section properties, supplied in Figure 8, are taken as reported by the pipe supplier (*1*).

The analytical predictions for fair soil and good quality soil track well, but conservatively, with the experimental curves for 75 and 95 percent soil density, respectively. Those results

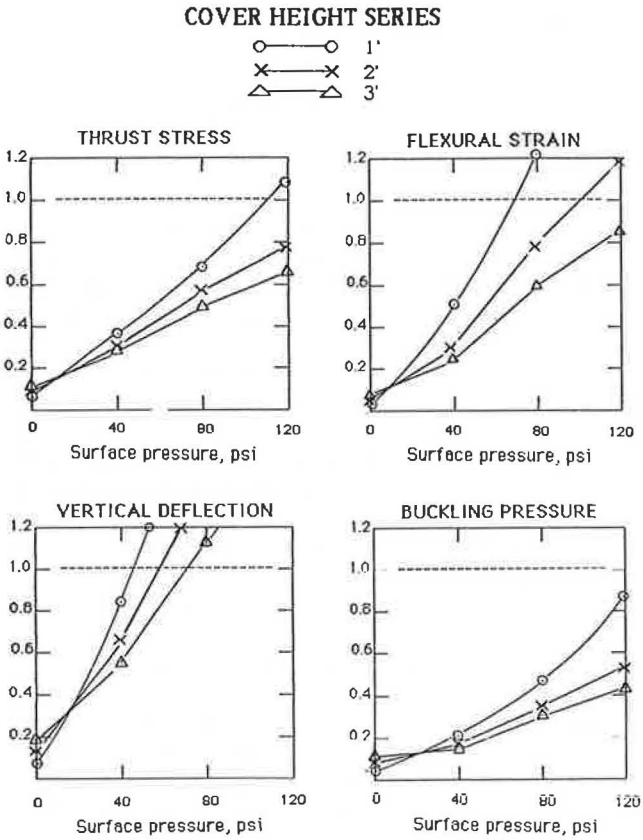

FIGURE 5 Influence of soil cover height on design criteria.

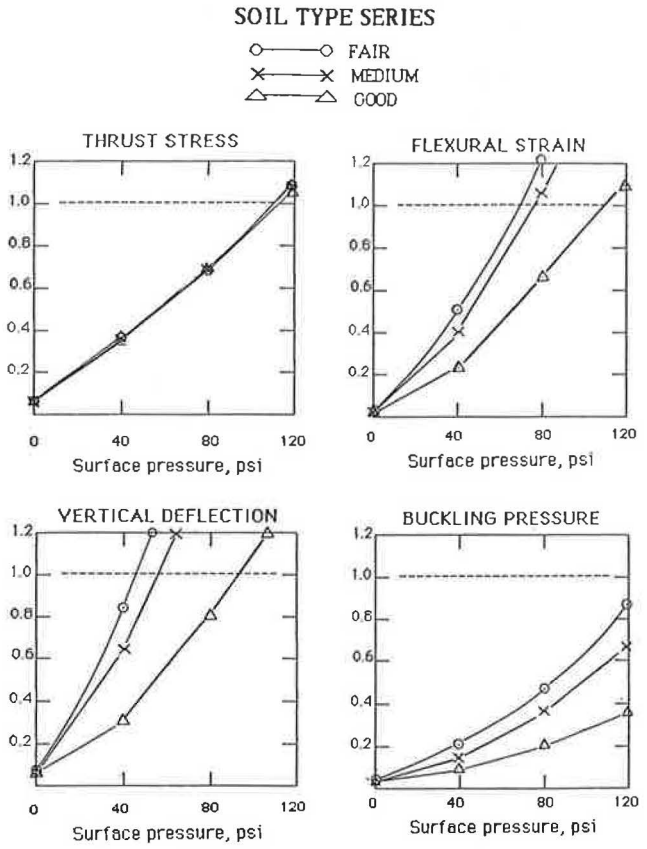

FIGURE 6 Influence of soil type on design criteria.

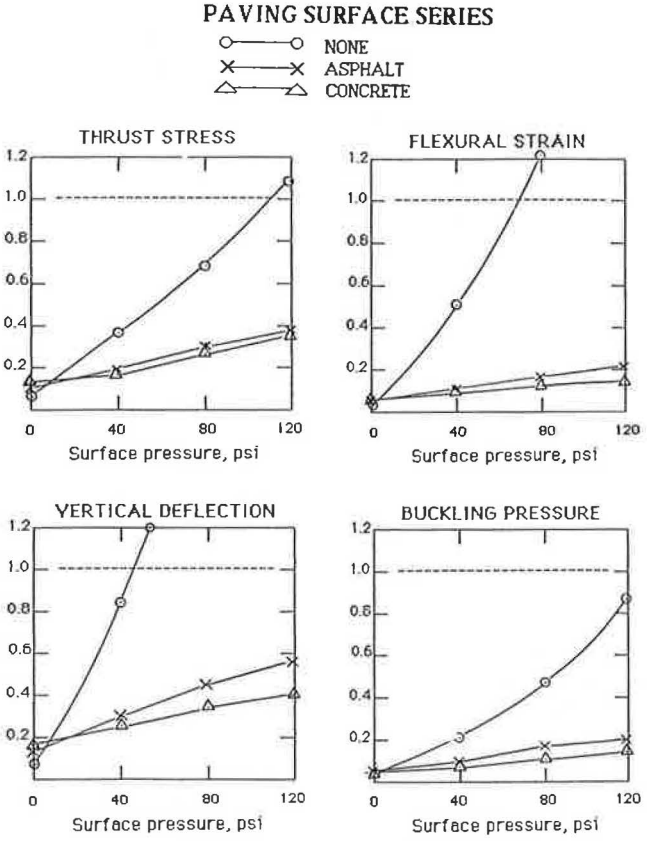

FIGURE 7 Influence of pavement overlay on design criteria.

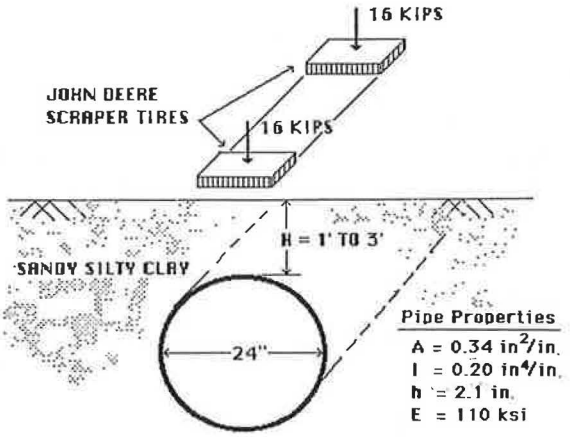

FIGURE 8 Watkins-Reeve experiment simulating H-20 truck.

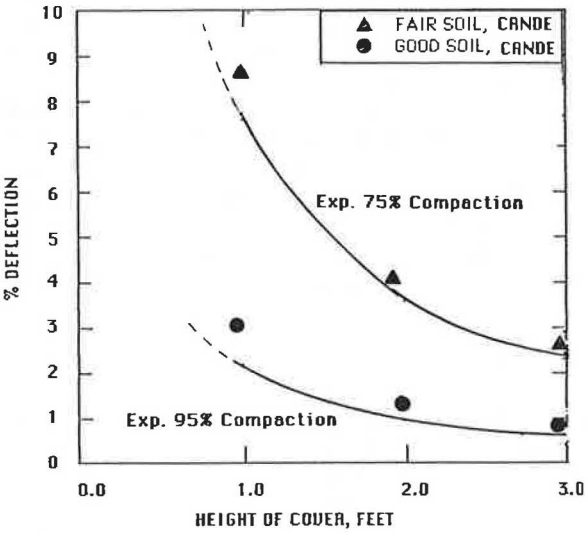

FIGURE 9 Comparison of experimental data with CANDE.

lend credence to the foregoing methodology and the following design solutions for minimum cover.

DESIGN RESULTS FOR MINIMUM COVER

Minimum Cover Tables

Table 7 gives the computed minimum soil cover requirements for pipe diameters ranging from 12 to 36 in. as a function of H-truck loading. The cover depths are tabulated for two soil conditions, fair and good. For the fair soil condition the cover depths are given for the lower bound moment of inertia (I_{min}) and the upper-bound moment of inertia (I_{max}), which brackets the range of corrugated cross sections produced by plastic pipe manufacturers. Those values are supplied in Table 8 as computed by Equations 3a and 3b. Design guidelines are given subsequently to determine the required soil cover height for intermediate values of the moment of inertia and various soil conditions.

Table 7 was developed by the following procedure. For each pipe diameter, four CANDE models were established on the basis of the four combinations arising from two soil conditions and two moments of inertia. Each CANDE model was solved for three different soil cover heights (12, 24, and 36 in.) with three increments of live load pressure (40, 80, and 120 psi) applied to the surface of each cover height. The relative displacements predicted by CANDE were recorded in a 3 × 3 matrix for each model (i.e., relative displacements as a function of cover height and surface pressure). The pressure level corresponding to each of the five H-truck loads was determined by using this matrix as a data base in accordance with Table 3, and a special interpolation/extrapolation scheme was devised to determine the required cover height for which the predicted displacement would match the allowable displacement (7.5 percent of the diameter).

If the computed cover height requirement was less than 12 in., then the absolute minimum requirement of 12 in. was enforced. The absolute minimum requirement always governed for good soil so that cover height was 12 in. for any moment of inertia greater or equal to the lower bound, I_{min}. The other design criteria supplied in Table 5 were checked, but in all cases the deflection criterion or the 12-in. minimum requirement controlled.

It may be somewhat surprising to note that the larger diameter pipes generally required less cover depth than that of a smaller diameter pipe with the same loading. This is because pipe manufacturers make larger pipes more robust than smaller pipes, as demonstrated by the average flexibility factor listed in the last column of Table 8 (i.e., the flexibility factor decreases with increasing pipe diameter).

Design Guidelines

A quick and conservative estimate of the minimum required soil cover can be read directly from Table 7 by assuming a pipe's corrugation provides only a minimum moment of inertia and the soil quality is only fair. Under those assumptions, for example, Table 7 indicates that an 18-in. pipe for H-20 loading requires 18 in. of soil cover.

If, however, the pipe's actual moment of inertia is known, say, I^*, or the actual quality of the soil is known (i.e., soil type and percent compaction), or both, then the minimum required soil cover, called H^* can be accurately determined by the following interpolation scheme:

$$H^* = H1(1 - q)(1 - r) + H2(q)(1 - r) + 12(r) \quad (9)$$

where

$H1$ = cover height for fair soil and I_{min} (column 1 of Table 7),
$H2$ = cover height for fair soil and I_{max} (column 2 of Table 7),
r = a ratio from 0 to 1 depending on soil quality (Table 9), and
$q = (I^* - I_{min})/(I_{max} - I_{min})$ (a computed ratio using Table 8).

The soil quality ratio r was developed in a previous study (*1*) and is presented in Table 9 as a function of soil type and percent of standard compaction.

TABLE 7 MINIMUM COVER HEIGHT IN INCHES

ID (in)	H-truck (H-x)	Fair Soil Imin	Fair Soil Imax	Good Soil Imin
12	H-10	12	12	12
	H-15	16	12	12
	H-20	19	15	12
	H-25	21	17	12
	H-30	23	19	12
15	H-10	12	12	12
	H-15	14	12	12
	H-20	18	14	12
	H-25	21	16	12
	H-30	23	18	12
18	H-10	12	12	12
	H-15	14	12	12
	H-20	18	13	12
	H-25	20	16	12
	H-30	23	18	12
24	H-10	12	12	12
	H-15	12	12	12
	H-20	15	12	12
	H-25	18	12	12
	H-30	20	14	12
30	H-10	12	12	12
	H-15	12	12	12
	H-20	12	12	12
	H-25	15	12	12
	H-30	18	12	12
36	H-10	12	12	12
	H-15	12	12	12
	H-20	12	12	12
	H-25	12	12	12
	H-30	15	12	12

TABLE 8 MAXIMUM AND MINIMUM MOMENT OF INERTIA AND FLEXIBILITY FACTOR

ID (in)	Imin (in^4/in)	Imax (in^4/in)	D=ID+h (in)	FF=D^2/EIavg (1/lb/in)
12	.02	.04	13.1	.052
15	.04	.08	16.4	.041
18	.06	.12	19.6	.039
24	.15	.30	26.2	.028
30	.26	.52	32.7	.025
36	.44	.88	39.3	.021

As an example of the above, suppose an 18-in. pipe has a moment of inertia, $I^* = 0.08$ in.^{4}/in, and that it is installed in a silty sand (SM) compacted to 85 percent standard density. The required minimum soil cover for an H-20 loading is computed as follows. First, the moment of inertia ratio is computed with the aid of Table 8 as $q = (0.08 - 0.06)/(0.12 - 0.06) = 0.333$. Second, from Table 9 the soil quality ratio is found to be $r = 0.5$, and from Table 7 the reference cover heights are found as $H1 = 18$ in. and $H2 = 13$ in. By using

TABLE 9 SOIL QUALITY RATIO FOR SOIL TYPES AND PERCENT COMPACTION

Soil quality ratio r	Granular SM %	Mixed SC %	Cohesive CL %
0.0 (Fair)	80	85	90
0.25	82	87	95
0.50	85	90	100
0.75	90	95	NA
1.0 (Good)	95	100	NA

SM = Silty sand, well graded
SC = Silty clayey sand
CL = Clay (no organic)

those values in Equation 9 the required minimum soil cover is determined as $H^* = 18(1 - 0.333)(1 - 0.5) + 13(0.333)(1 - 0.5) + 12(0.5) = 14.2$ in. Thus, rounding to the nearest inch the required minimum soil cover is 14 in.

Pavement Overlays

Demonstrated in a previous section was that pavements, asphalt or concrete, are extremely effective in reducing the live load distress on a shallow buried plastic pipe. Nonetheless, the pavement thickness is customarily not included as part of the minimum soil cover requirement because the pipe must be protected by a certain minimum soil cover to withstand the construction loads prior to the placement of the pavement. Thus, in keeping with the metal culvert industry (AISI), the general recommendation offered here is to assume that the thickness of the pavement overlay plays no role in the minimum soil cover requirement.

Conversely, special situations may exist where the engineer is confident that construction loads prior to the placement of pavement will be minimal. An example of such a special situation might be the case of installing a pipe under an existing pavement by tunneling, jacking, or trenching. In this and similar cases the inclusion of the pavement thickness into the required soil cover is justifiable.

Minimum Soil Cover Under Railroads

The required minimum soil cover for plastic pipes under railroad tracks is the same as that required by an H-30 truck. This equivalence is based on standard railroad design practices (*10*).

The maximum allowable load for a statically loaded train wheel is 33 kips. By using an impact factor of 1.3, the maximum dynamic load is 43 kips. Up to 60 percent of this dynamic load (26 kips) is transmitted to the tie directly beneath the wheel, and the remainder of the load is transmitted by the rail to the neighboring ties, typically spaced at 21 in. on center. The 26 kip tie load is distributed to the ballast beneath the tie over a contact area of approximately 300 in.^{2} [i.e., one-third of the tie length (⅓ of 102 in.) times the tie width (9 in.)]. Thus, the local contact pressure of the tie on the ballast is 87 psi.

In comparison with the preceding, the 26 kip tie load is very nearly equal to the 24 kip rear tire load of the H-30 truck. Also, the 87-psi contact pressure of the tie is only slightly less than the 100 psi truck tire pressure, and the width of the tie is comparable to the tire footprint length. Thus, having demonstrated the equivalence between H-30 truck loading and railroad loading it is recommended that the soil cover height requirements for railroad loading follow the requirements for an H-30 truck loading, as was previously presented. Ballast depth should not be included as part of the minimum soil cover requirement for the same reason pavements are usually excluded.

CONCLUDING REMARKS

The minimum soil cover requirements presented here are applicable to all corrugated plastic pipe where material and cross-sectional properties conform to AASHTO specifications. Further, the backfill soil must be compacted to the design specification and be placed uniformly around the pipe without hard inclusions of soft voids in the soil envelope. Within those restrictions the minimum cover heights presented in Table 7 along with the design guidelines may be used with conservative confidence.

ACKNOWLEDGMENTS

Thanks are extended to the Corrugated Plastic Tubing Association for their support of this study and a special thanks to William Altermatt of Hancor, Inc., for his unwavering support and technical guidance.

REFERENCES

1. M. G. Katona. Allowable Fill Heights for Corrugated Polyethylene Pipe. In *Transportation Research Record 1191*, TRB, National Research Council, Washington, D.C., 1988, pp. 30–38.
2. *Handbook of Steel Drainage and Highway Construction Products*. 3rd Edition, American Iron and Steel Institute, Washington, D.C., 1983.
3. M. G. Katona. *CANDE: A Modern Approach for the Structural Design and Analysis of Buried Culverts*. Report FHWA-RD-77-5, FHWA, Department of Transportation, Oct. 1976.
4. L.-E. Janson. Investigation of the Long-Term Creep Modulus for Buried Polyethylene Pipes Subjected to Constant Deflection. *Proc., Advances in Underground Pipeline Engineering*, Pipeline Division, ASCE, Madison, Wisc., Aug. 1985.
5. M. G. Katona. *CANDE, 1980: Box Culverts and Soil Models*. Report FHWA-RD-172, FHWA, Department of Transportation, May 1981.
6. M. G. Katona and A. Y. Akl. Structural Design of Buried Culverts with Slotted Joints. In *Transportation Research Record 1129*, TRB, National Research Council, Washington, D.C., 1988, pp. 39–54.
7. H. G. Poulos and E. H. Davis. *Elastic Solutions for Soil and Rock Mechanics*. John Wiley, New York, 1980.
8. R. K. Watkins and R. C. Reeve. Effect of Heavy Loads on Buried Corrugated Polyethylene Pipe. Report, Advanced Drainage Systems, Inc., Columbus, Ohio, 1982.
9. R. K. Watkins, J. M. Dwiggins, and W. E. Altermatt. Structural Design of Buried Corrugated Polyethylene Pipes. In *Transportation Research Record 1129*, TRB, National Research Council, Washington, D.C., 1987, pp. 12–20.
10. W. G. Hay. *Railroad Engineering*. 2nd ed., John Wiley, New York, 1982.

Publication of this paper sponsored by Committee on Subsurface Soil-Structure Interaction.

Live Load Distribution on Concrete Box Culverts

A. M. Abdel-Karim, M. K. Tadros, and J. V. Benak

The effects of wheel loading on concrete box culverts is discussed. Distributions of wheel loads through pavement, embankment soil, and culvert top slab are considered separately. Description of full-scale testing of a functional cast-in-place concrete box culvert is provided. Load dispersion through soil is also discussed, and the relevant AASHTO provisions are reviewed and compared with field measurements and with theoretically predicted values by using the Boussinesq elasticity solution. Similar load distribution characteristics were observed in the transverse and longitudinal directions. It was further observed that AASHTO's 1.75 distribution factor can be safely applied for fill heights below 2 ft and above 8 ft. Distributions through rigid pavements and culvert top slab are also discussed, and empirical procedures for incorporating their effect in the design are presented.

In addition to the pressures induced by soil weight on reinforced concrete box culverts (RCBC), pressures owing to the wheel loads of moving vehicles (live loads) are often an important consideration in their design. The live load contribution to the total pressure on RCBC becomes increasingly important as the depth of cover decreases. To take the live loads (LL) into account when designing RCBC, a reasonably accurate yet practical procedure is needed to predict the effect of those loads.

The problem of LL effects on box culverts may be divided into three separate problems: (a) the distribution of live load through fill; (b) the distribution of live load owing to the rigidity of the roadway pavement, if any; and (c) the distribution of concentrated loads through the top slab itself.

With regard to the first problem, AASHTO currently specifies what follows for single spans:

- When the depth of fill is less than 2 ft, the wheel load shall be distributed as in exposed slabs with concentrated loads.
- When the depth of fill is 2 ft or more, concentrated loads shall be distributed over a square with sides equal to 1.75 times the depth of fill.
- When the depth of fill is more than 8 ft, and exceeds the span length for single spans or exceeds the distance between the faces of end supports or abutments for multiple span culverts, the effect of live load may be neglected.

This treatment is attractive in its simplicity. However, it can result in some inconsistencies at transition heights. For example, use of the AASHTO specification can require an RCBC covered with 8 ft of fill to have thicker walls and more reinforcement than one with 9 ft of fill (the latter being designed with LL fully ignored). The Nebraska Department of Roads, for this reason currently uses a slightly modified version of the AASHTO procedures.

This study deals primarily with this problem of wheel load distribution through soil and attempts to develop theoretical and experimental data for comparison with the current AASHTO specifications and to provide a smooth transition for the entire range of effective fill heights.

The second problem, pertaining to load distribution through pavement, is not explicitly taken into account by AASHTO. The third problem, pertaining to concentrated load distribution owing to the top slab influence, is considered for exposed slabs only (*1*). The second and third problems are briefly discussed in this paper, and their significance is examined. Final recommendations regarding those two problems require further analysis and will be reported at a later date.

BACKGROUND

Very little experimental research has been done on the subject of LL distribution through fill on RCBC structures. A major research program was performed by Texas A & M University (*2*). The research project included construction and instrumentation of a full-scale 8-ft by 8-ft reinforced concrete box culvert. Pressure measurements were recorded at 2-ft fill increments up to a total of 8 ft above the top slab level. A test vehicle representing the AASHTO alternate interstate design loading (two 24,000-lb axles spaced 4 ft apart) was positioned at various loading stations at each level of fill and pressure measurements recorded. A nonlinear regression analysis was later performed on the data to arrive at an empirical equation that best fit the experimental results. The authors concluded that this empirically determined function agreed well with the data up to 2 ft of fill. A modified form of the Boussinesq equation based on concentrated loads was recommended at fill heights equal to or greater than 4 ft. No specific recommendations were reported for fill heights between 2 and 4 ft.

While the idea of curve-fitting, suggested in James and Brown (*2*), may be attractive from the standpoint of accuracy, the resulting nonlinear pressure distribution highly complicates the analysis and design processes. Further, increased accuracy may not be justified considering the variability of both the magnitude and the distribution of soil pressures under field conditions of mixed traffic and variable axle configuration.

Department of Civil Engineering, University of Nebraska, Omaha, Neb. 68182.

THEORETICAL DISTRIBUTIONS

Theoretical distribution of wheel loads through fill is a problem that has been investigated by a number of researchers (*3–5,8*). As a result, two general solutions are available: closed form and numerical. The characteristics of each approach will be discussed briefly.

Closed-Form Solutions

Closed-form solutions treat soil as a continuum, and the solution is given anywhere in the domain of the problem in equation form. This type of solution is very difficult to obtain for all types of loading and boundary conditions without considerably simplifying the assumptions that can decrease their accuracy appreciably. Assumptions commonly made are pertinent to the stress-strain relations and directional properties of soil. Additionally, assumptions regarding the geometry of the problem domain are also required.

Usually, a closed-form solution is first determined for a single point loading. The principle of superposition is then used to extend this solution to other forms of loading, such as rectangular or circular. The effect of the form of loading on vertical soil pressures was investigated in part in this study, and it was found possible to approximate conservatively standard rectangular wheel loads as point loads whenever the distance to the point of pressure calculation exceeded 5 ft. Beyond this limit the pressures owing to both types of loading were virtually the same (*7*).

The rigidity caused by the culvert itself in the soil medium was investigated in this study by assuming that the elastic layer, representing the soil cover, was underlain by a rigid base. The calculated pressures were based on charts and tables that account for the three-dimensional distribution effects (*5,6*) and were graphically represented in three-dimensional plots. Sections were passed through the center of the loaded area and resulted in two-dimensional plots. The pressures thus obtained were compared with those calculated by using an elastic half space [Boussinesq, a three-dimensional solution based on the chart given in Figure 3.30 of Poulous and Davis (*6*, pp. 57)] solution, which ignores the culvert rigidity, and with experimentally determined pressures, as indicated in the example in Figure 1. On the basis of this comparison the Boussinesq solution exhibited better agreement with the experimental data, especially at the higher fill heights. This is probably because of the deflection of the culvert top slab and the overall settlement of the structure, which rests on a granular base (yielding foundation). However, this may not be the case had the foundation been of the nonyielding type. The Boussinesq solution is used throughout this paper and is referred to hereinafter as the theoretical solution.

Numerical Solutions

A notable deficiency in closed-form solutions is their inability to account for material and boundary nonlinearities. However, it is possible to incorporate such nonlinearities into a finite-element formulation with little effort. The key issue is

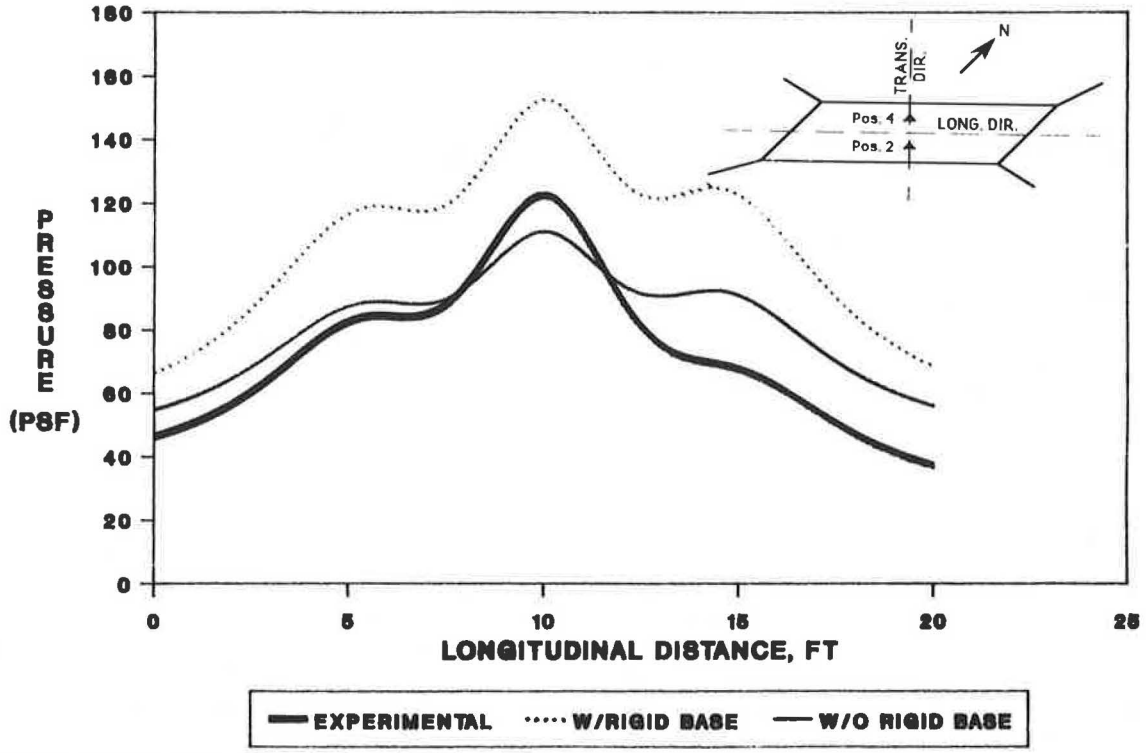

FIGURE 1 Longitudinal pressure distribution at position 2.

the creation of an accurate soil model that can adequately describe the soil behavior at all levels of stress and deformation. The correctness of any particular model is best verified through comparison with measured data, and this explains the urgent need for additional full-scale testing of culverts.

DESCRIPTION OF THE EXPERIMENTAL PHASE

Culvert Construction and Instrumentation

The culvert selected for the experimental phase of this study is a double cell cast-in-place reinforced concrete box structure, located on the outskirts of Omaha in Sarpy County, Nebraska. The inside dimensions of each cell are 12 ft × 12 ft. The culvert occurs at a 35 degree skew angle with respect to the roadway. The permanent fill height is 8.5 ft over the top slab but was temporarily raised to 12 ft for testing purposes. The fill consisted of compacted silty clay (loess) with a liquid limit of about 40 and a plasticity index of about 16. Compaction water content was in the range of 21 to 25 percent. Dry densities ranged from 95 to 103 pcf. This exceeded 90 percent of the maximum dry density determined by AASHTO method T-99. Undrained triaxial compression tests of thin-wall tube samples taken from the fill indicated that the undrained secant modulus of deformation (determined at one-half maximum deviator stress) was in the range of 250,000 psf to 300,000 psf.

Several types of instrumentation were used for the project including earth pressure cells, strain gauges, piezometers, settlement plates, and deflection measurements. The earth-pressure cells used to measure the normal pressure on the surface of the structure were the most important instruments. Research (*8*) indicated that it is very difficult to obtain data from earth-pressure cell measurements, realistically ± 20 to 40 percent. A careful selection of the most suitable cell was vital to the success of this project.

The following features were identified as the selection criteria (*9*): (a) the readings should be environmentally stable; (b) the cell should be very robust; (c) the hysteresis effect should be low to allow for repeated application of loading; (d) the minimum diameter-to-grain size ratio should be 50; and (e) economy, so that a large number could be used. The cell selected was a contact pressure cell manufactured by Geonor (*10*) that operates on the vibrating wire principle. The reading accuracy reported by the manufacturer is 0.02 kg/cm² (41 psf). The layout of the top slab pressure cells is presented in Figure 2.

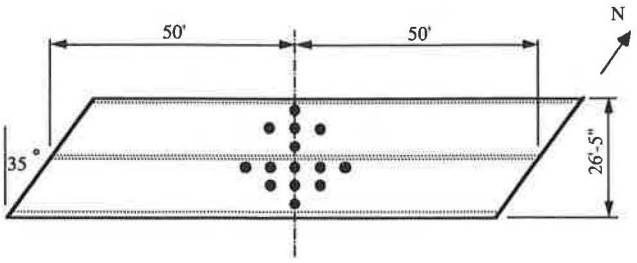

Top Slab Plan View

FIGURE 2 Layout of pressure cells.

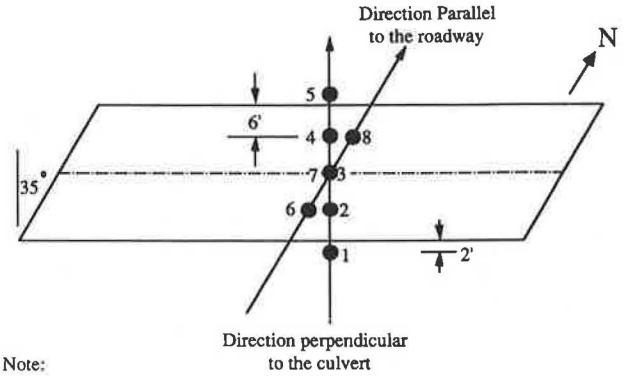

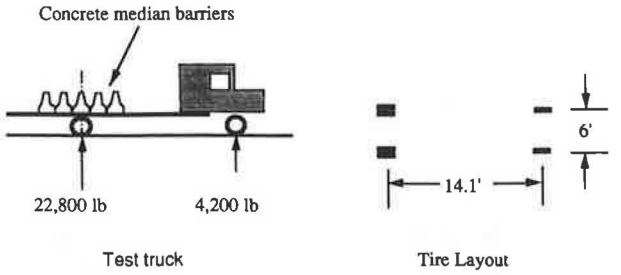

FIGURE 3 Live load positions and test truck.

Live Load Tests

Eight LL test stations were selected. Five stations were established perpendicular to the longitudinal centerline of the culvert and three stations parallel to the roadway (Figure 3). Two LL tests were performed: wheel (axle) loads and concentration loads. In the wheel load tests, the rear axle of the test truck (Figure 3) was centered over each of the positions indicated in the figure, and then the instruments were read. In the concentrated load tests, a point load was simulated by using a hydraulic jack to transfer the entire axle load through a single 1-ft² bearing plate. Wheel load tests were performed at fill increments of about 2 ft, and concentrated load tests were run at increments of 4 ft.

A zero reading, indicating the pressures owing to soil only, was taken at all stages of backfill prior to LL testing. The so-called zero LL pressures were subtracted from pressures recorded with the LL in place. The resulting pressures are the net pressures produced by the LL and are referred to hereinafter as LL pressures.

EXPERIMENTAL RESULTS AND COMPARISONS

The layout of pressure cells on the top slab of the culvert allowed for a three-dimensional graphical representation of the measured pressures. These plots served as a useful means for identifying the extent and pattern of the interaction between different axles and between wheels of the same axle. Most of the LL data were put into this form for the purpose of analysis. Examples of the three-dimensional plots are presented in Figures 4–6. The following descriptive observations are based on those plots:

1. At low fill heights the pressure distributions were characterized by high isolated peaks at the points of load application, surrounded by regions of reduced pressure (i.e., pressures below those owing to soil only), and followed by fairly uniform distributions. This pattern indicates little or no interaction between pressures owing to different wheels.
2. Lower peaks and smaller pressure reductions were observed as the fill height increased. Wheel loads became distributed over increasingly large areas. Relatively high pressures were noticed in the regions where those areas overlapped (Figure 6). The value of the pressure under the center of the rear axle exceeded those directly under the wheels at a fill height of 8 ft.
3. Little interaction was observed between the wheels of the front and rear axles. Such interaction started to form at a fill height of about 10 ft, where considerable dispersion of the load had already occurred. Because the effect of the front axle was largely isolated, and that the load it carried was small in comparison with that carried by the rear axle, its effect can be neglected in the analysis without appreciable loss of accuracy.
4. Concentrated load tests have indicated that the rate of load dispersion is virtually the same in the longitudinal and transverse directions. It is therefore recommended that the load continue to be distributed over a square area, contrary to what was previously concluded in relation to flexible culverts (*11*). Rigid culverts have comparable stiffnesses in both the tranverse and longitudinal directions resulting in similar distribution characteristics in those directions.

Cross sections were taken from the three-dimensional plots to obtain the variation of pressure in a single direction. Figure 7 presents the pressure distribution along the longitudinal axis of the culvert for various fill heights and indicates a high rate of pressure decay as the fill height was increased. The only exception occurred at 2 ft of fill, where the measured pressures were less than those recorded at 3.5 ft of fill. The wheel load is spread over a small area at such shallow depths

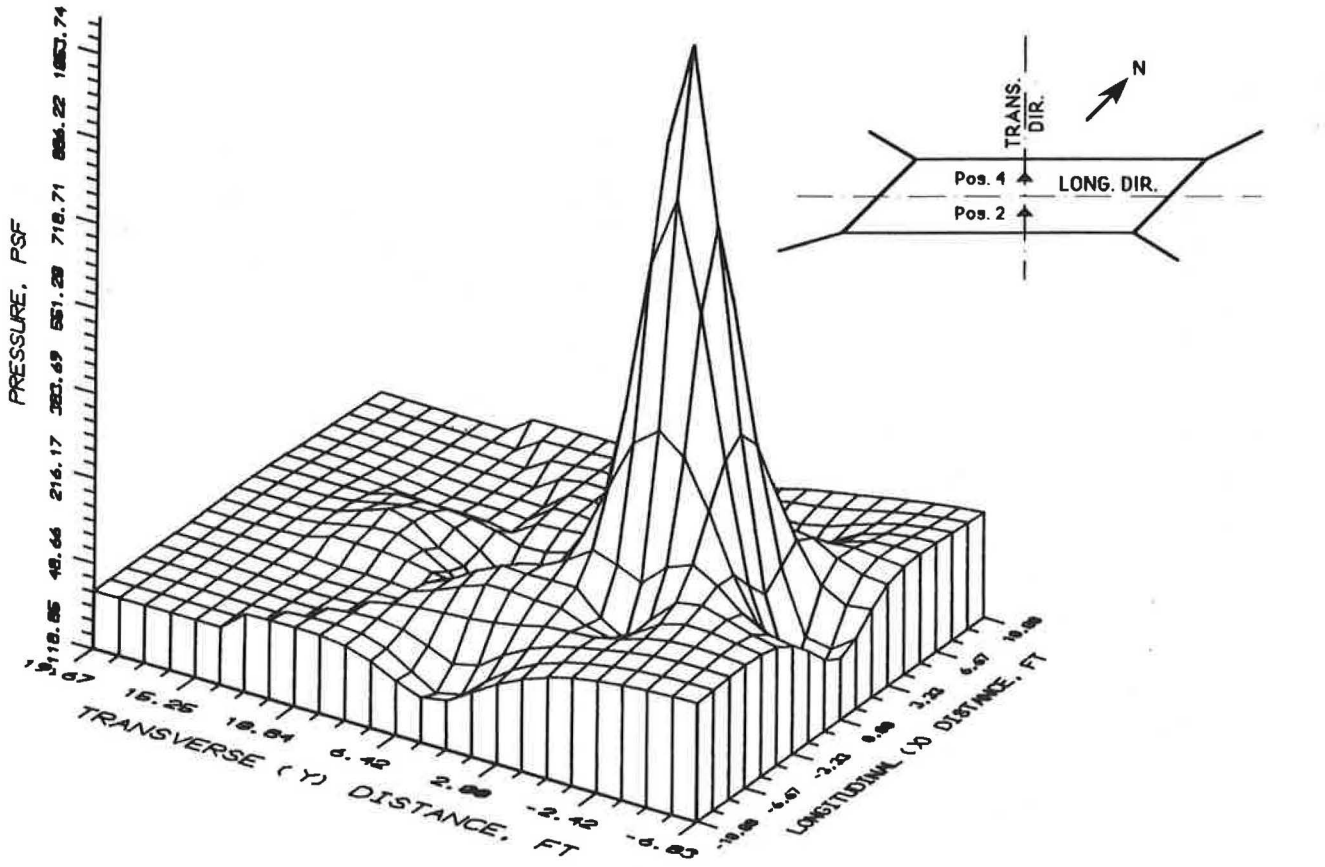

FIGURE 4 Measured pressure distribution owing to point loading at 3.5 ft, position 2.

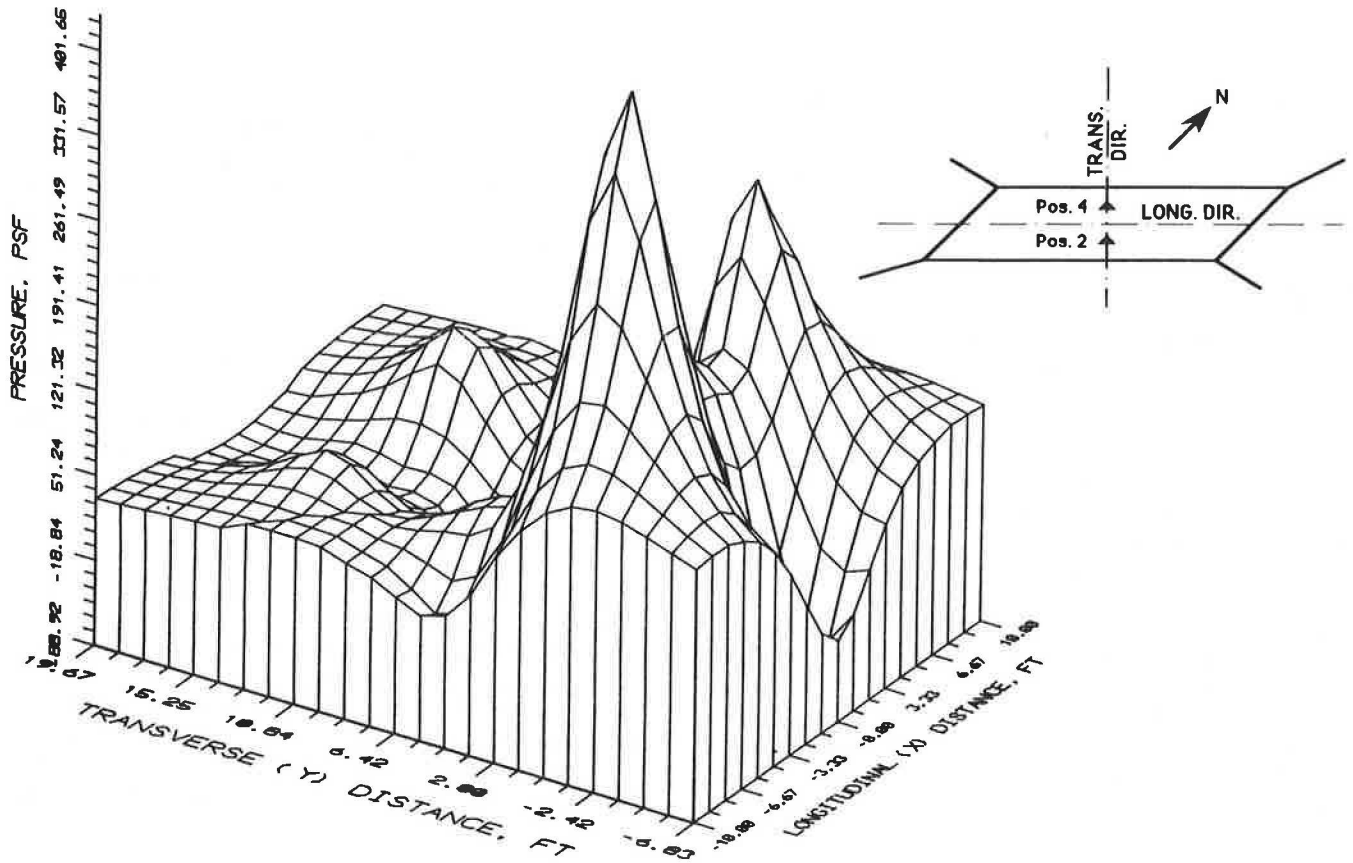

FIGURE 5 Measured pressure distribution owing to axle loading at 3.5 ft, position 2.

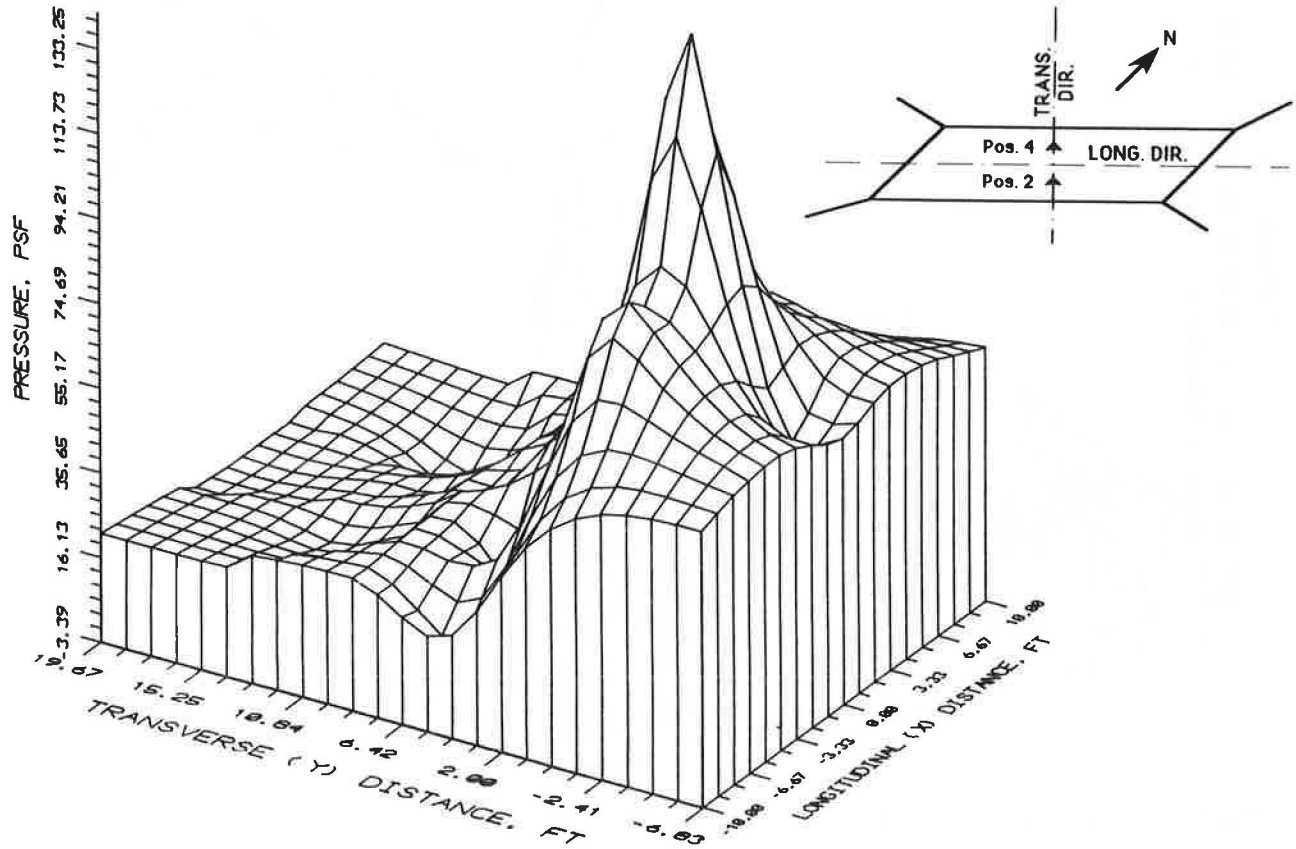

FIGURE 6 Measured pressure distribution owing to axle loading at 8 ft, position 2.

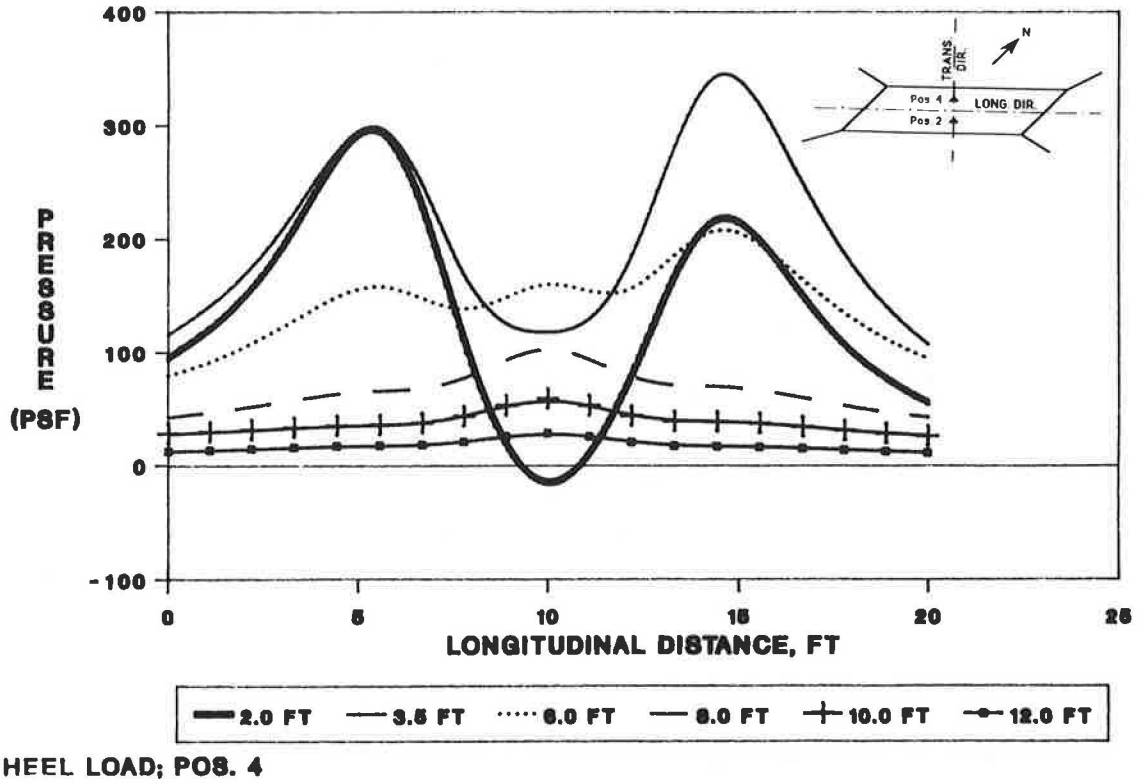

FIGURE 7 Longitudinal pressure distribution at position 4.

of cover, and its effect diminishes quickly away from the center of the load. The discrepancy is likely to be caused by a slight error in positioning the rear axle of the truck over the desired station, causing considerable reduction in the measured pressures.

The amount and nature of the interaction between wheels is also a function of the fill height. A nearly uniform pressure distribution was obtained at 8 ft of fill (see Figure 7). The measured peak pressure at this height was about 8 percent of the soil pressure. Gilliland (*1*) suggested that the LL load pressures be neglected if their magnitudes are equal to or less than 10 percent of the corresponding values owing to soil load only.

The theoretical and AASHTO pressures are compared with field measurements in Figures 8–11. The theoretical and measured pressures decrease in both horizontal directions and result in a three-dimensional bell-shaped curve for each load. Conversely, the AASHTO distribution is uniform in both directions, corresponding to a truncated pyramid shape. Thus, even though the measured pressures contain higher peaks, AASHTO pressures still conservatively correspond to a larger total load. Also, the difference between the theoretical and measured pressure distributions is within the accuracy of the pressure cells, making the theoretical distribution practically acceptable (see Figures 10 and 11).

Figures 12 and 13 present the transverse and longitudinal pressure distributions owing to point loads. Comparison of the two figures indicates similar distribution patterns in both directions. The smaller peak to the right in Figure 12 corresponds to a residual pressure effect caused by a preceding concentrated load test at position 2. Figure 14 compares the theoretical and AASHTO pressures with field measurements. Although the measured peak pressure is approximately twice as large as the AASHTO values, both distributions seem to be equal to the same total load. This observation is an indication as the validity of the field measurements.

The experimental results in this project indicated that the LL effect beyond 8 ft of fill diminished considerably. Thus, AASHTO's distinction between single- and multi-cell culverts seems to be unnecessary. More important, the data seem to indicate that the use of AASHTO's 1.75 distribution factor is valid regardless of the fill height. The cutoff limit for ignoring the LL pressures should be at a level at which the structural engineer feels that the LL effect is less than, say, 5 percent of the total load effect (shear, moment, etc.).

The measured moments owing to the effect of LL only are compared in Figures 15–18 with those obtained by three different prediction methods by using the FE program CANDE (*12,13*). In the first method (known as the strip or AASHTO method), the wheel loads are distributed through the soil by using AASHTO's 1.75 factor. The culvert frame is then subjected to two loading stages: the first representing soil load only and the second representing the combined effects of soil and LL. This two-stage loading is necessary owing to the nonlinearities of concrete caused by cracking and other factors. The moments owing to LL only are obtained by subtracting the moments obtained in stage 1 from those of stage 2. The second and third methods are based on an equivalent line load applied to the full mesh representing the entire soil-structure system and boundary conditions (*12*). In the second method an equivalent line load is found (from the Boussinesq solution) that produces a vertical pressure at the culvert sur-

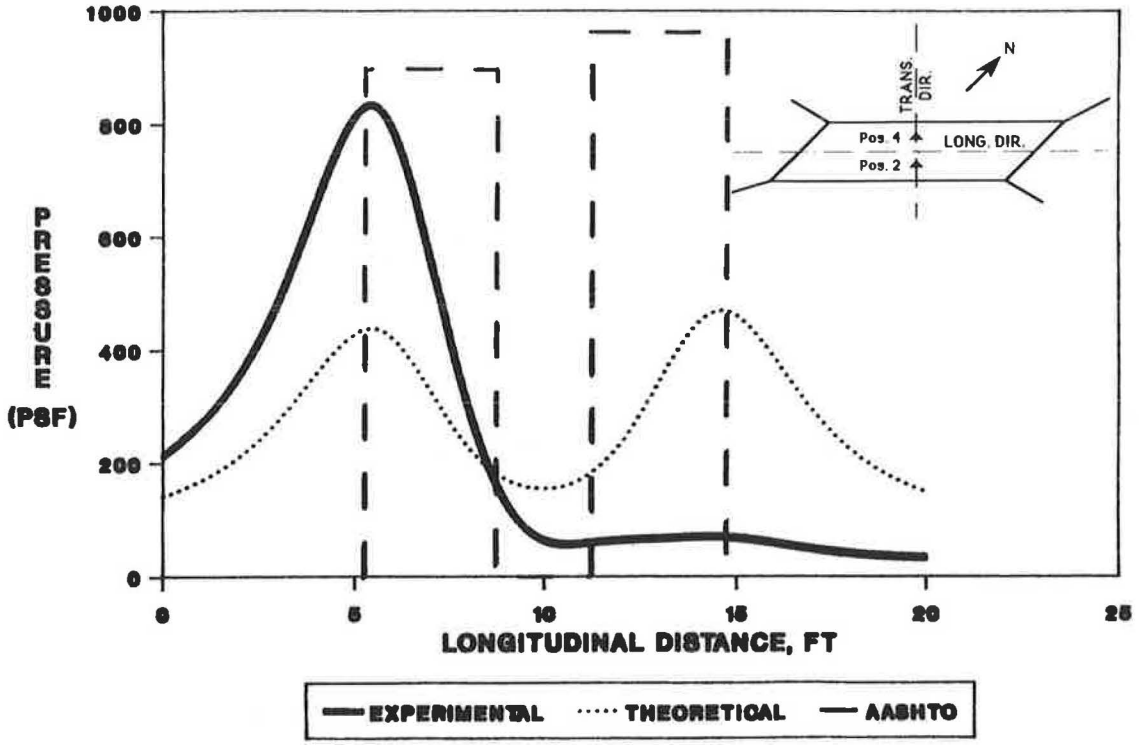

FIGURE 8 Longitudinal pressure distribution at 2 ft of fill owing to axle load, position 2.

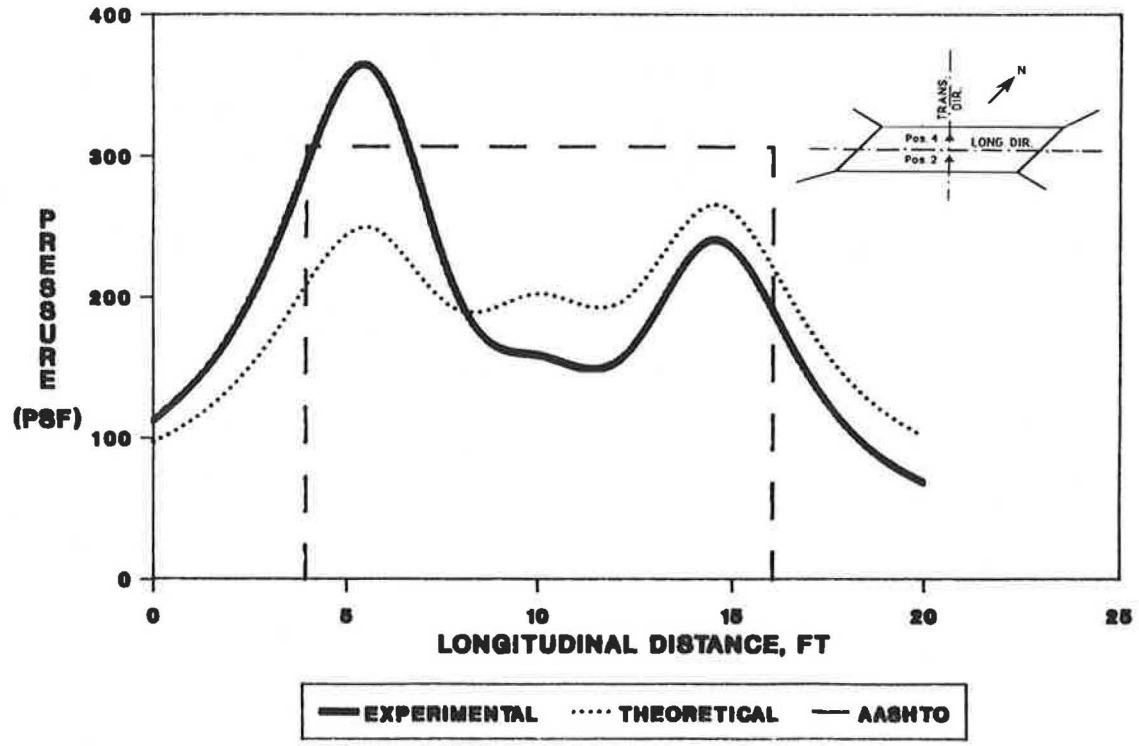

FIGURE 9 Longitudinal pressure distribution at 3.5 ft of fill owing to axle load, position 2.

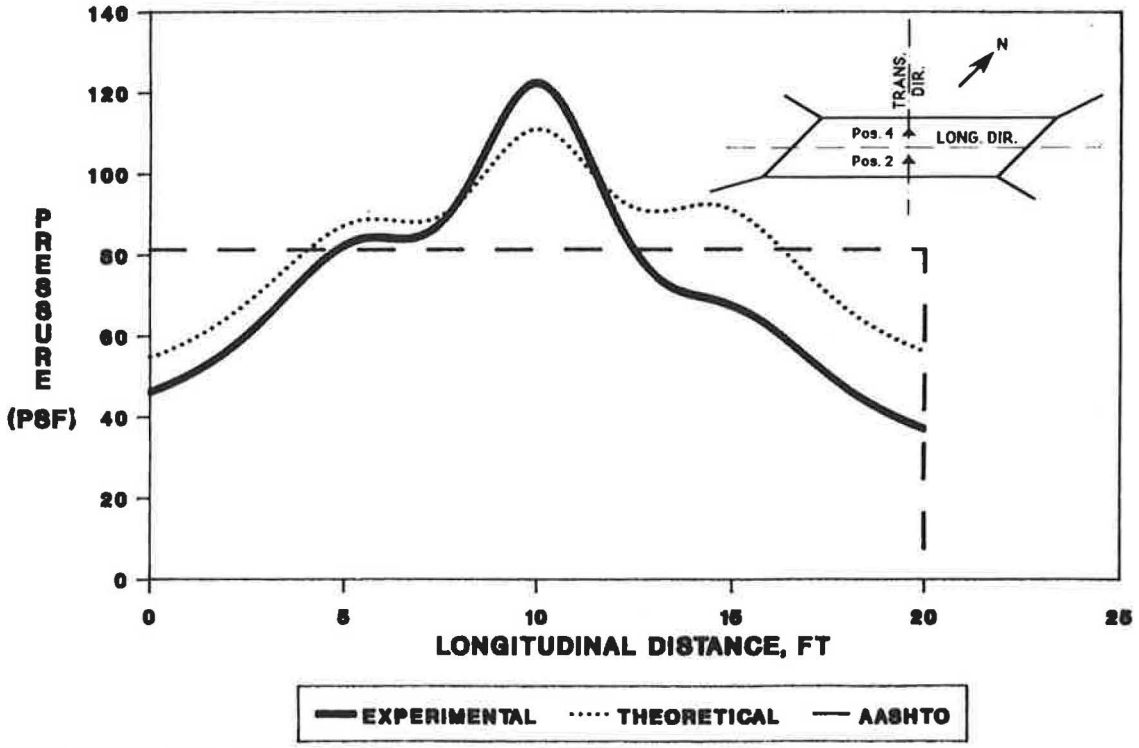

WHEEL LOAD; FILL HT. = 8.0 FT; POS. 2

FIGURE 10 Longitudinal pressure distribution at 8 ft of fill owing to axle load, position 2.

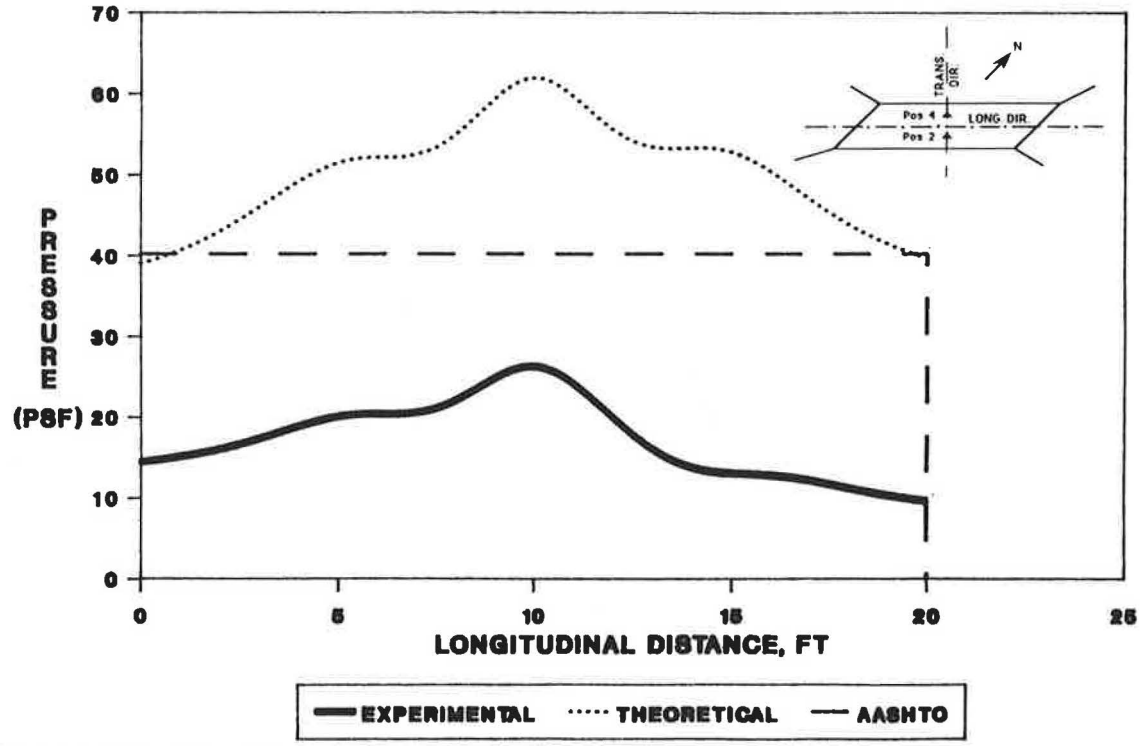

WHEEL LOAD; FILL HT. = 12.0 FT; POS. 2

FIGURE 11 Longitudinal pressure distribution at 12 ft of fill owing to axle load, position 2.

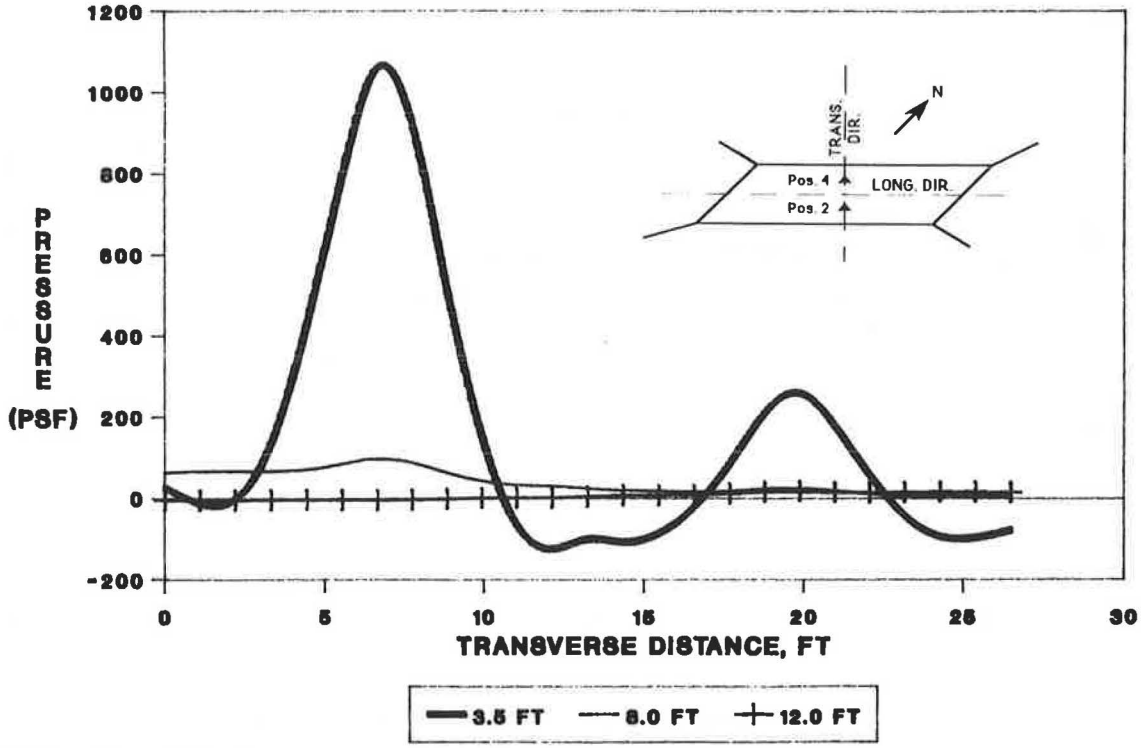

FIGURE 12 Transverse pressure distribution owing to point loading at position 4.

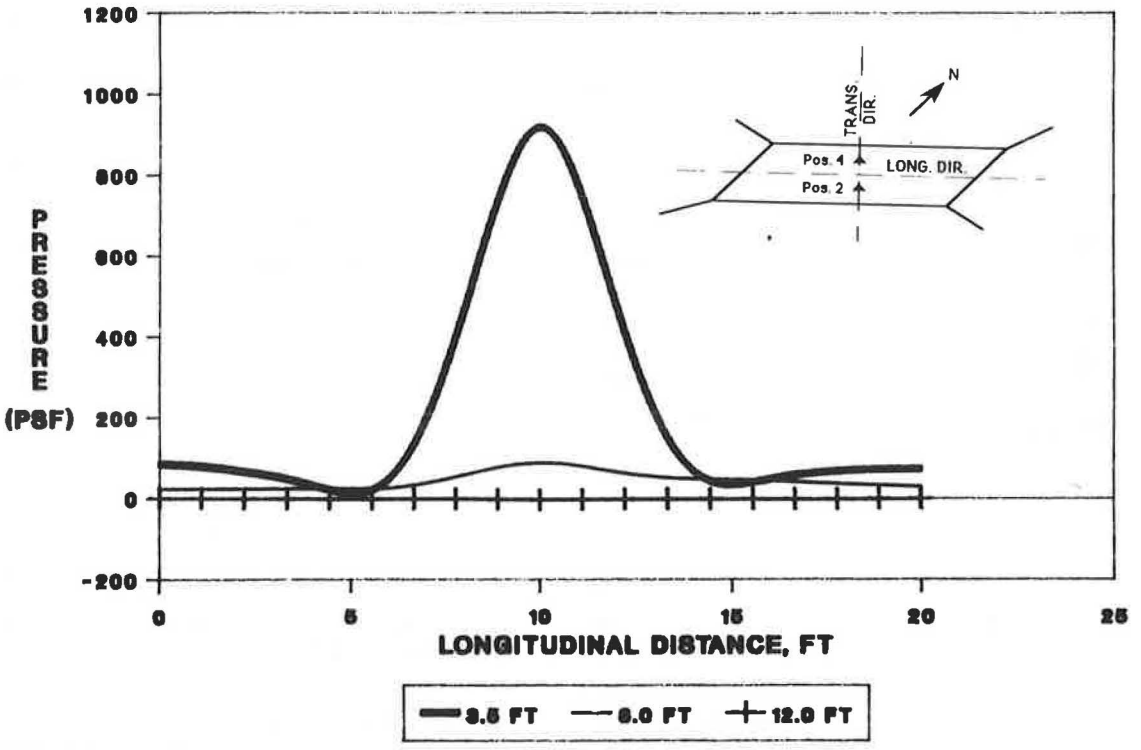

FIGURE 13 Longitudinal pressure distribution owing to axle load at position 4.

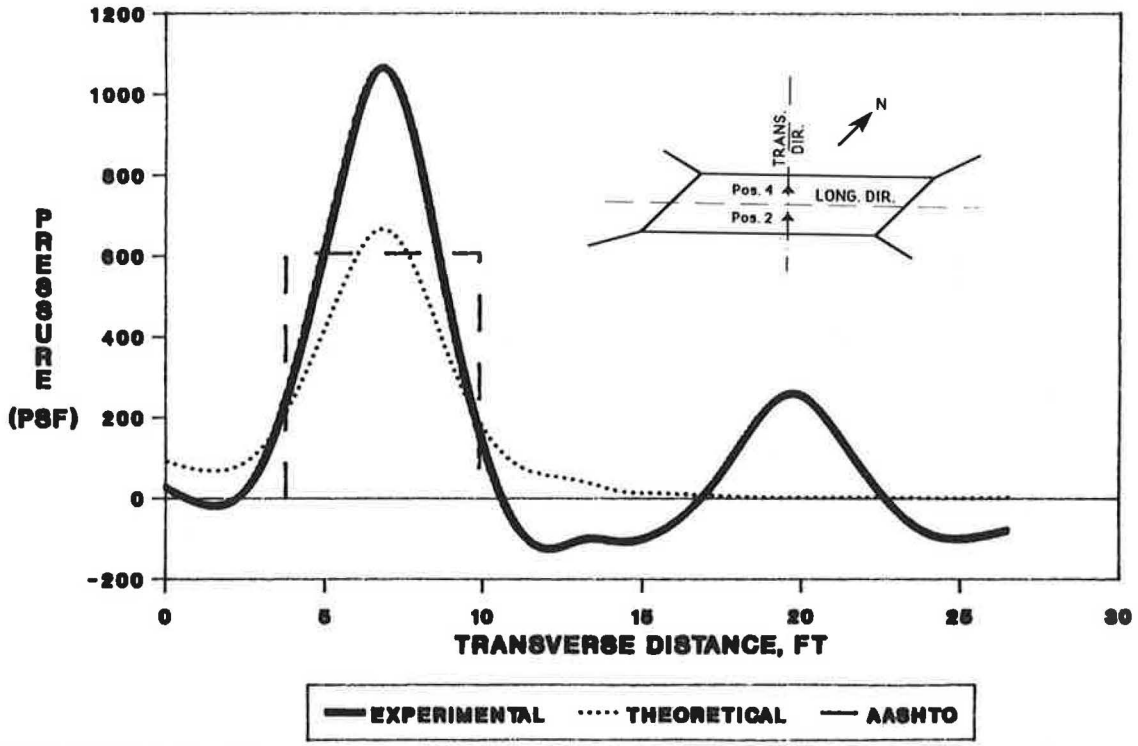

FIGURE 14 Transverse pressure distribution owing to point loading at position 4.

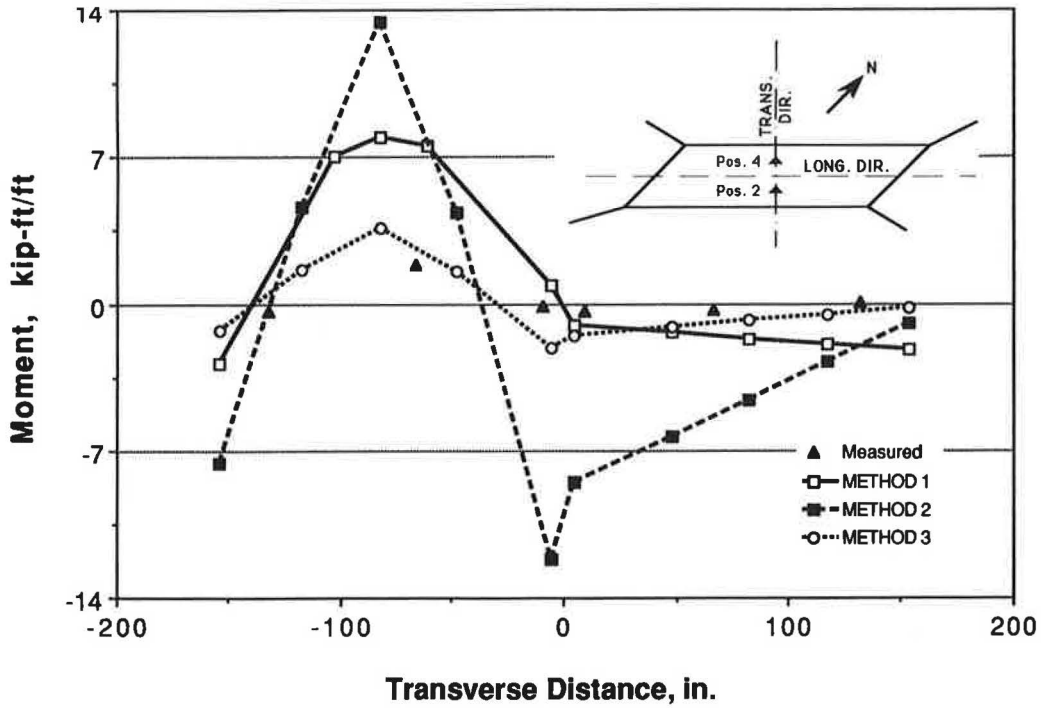

FIGURE 15 Measured versus predicted live load moments at 2 ft of fill, position 4.

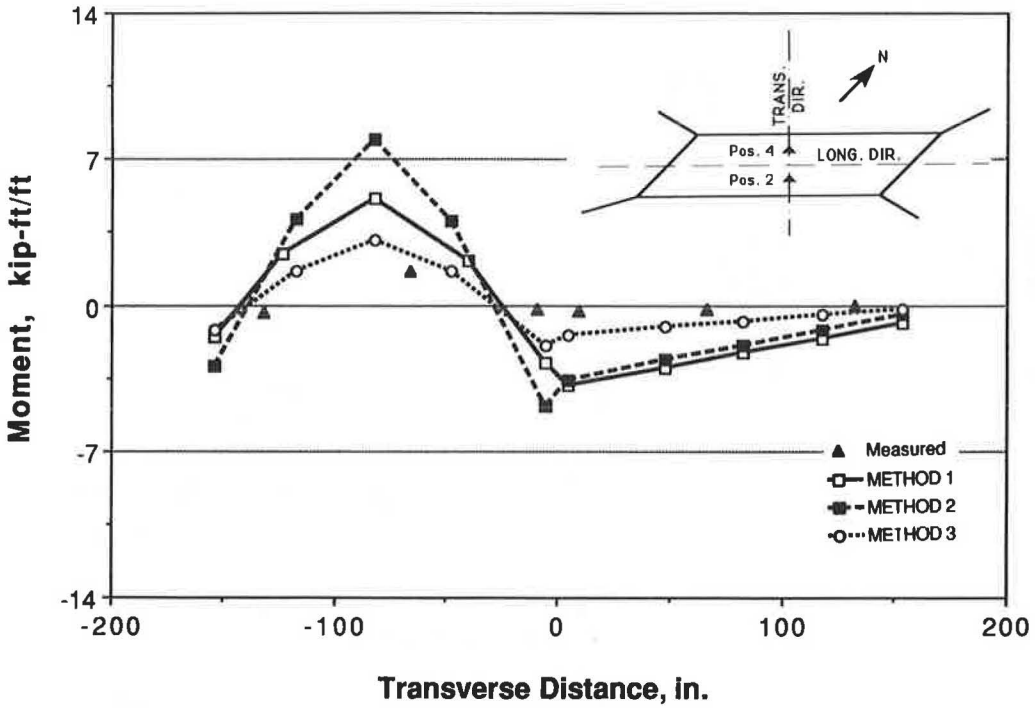

FIGURE 16 Measured versus predicted live load moments at 3.5 ft of fill, position 4.

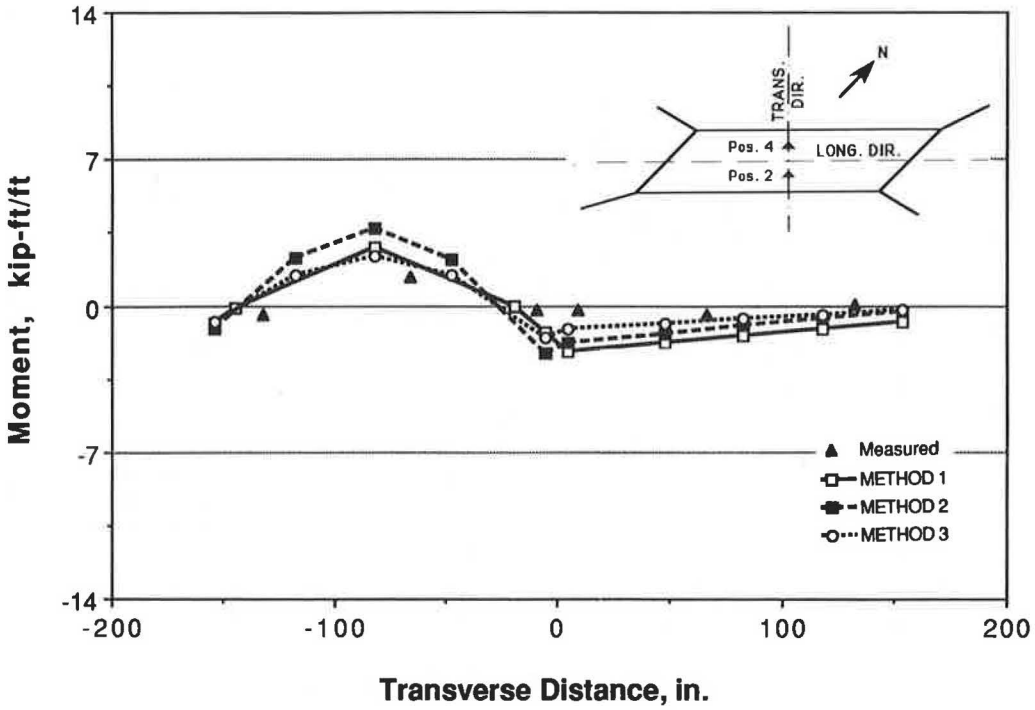

FIGURE 17 Measured versus predicted live load moments at 6 ft of fill, position 4.

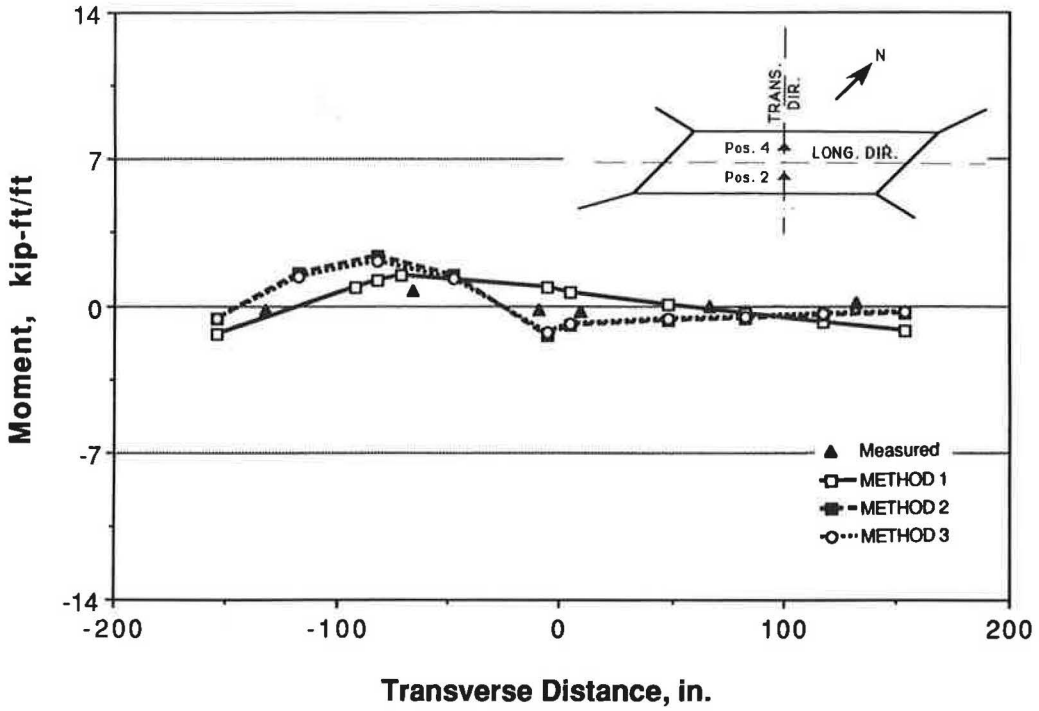

FIGURE 18 Measured versus predicted live load moments at 8 ft of fill, position 4.

face, directly under the load, equal to the pressure caused by the original load. In the third method (*13*) the line load is assumed to be equal to the wheel load divided by the axle length (independent of the depth of cover). A comparison of the moments in the figures tends to favor the third method.

WHEEL LOAD DISTRIBUTION THROUGH PAVEMENT

Pavement, when present, can have a substantial effect on the design of RCBs. The importance attached to the pavement is attributed to its ability to distribute the traffic-induced loads. However, the method and the extent of load distribution are largely dependent on the type of pavement provided. Pavements in general can be classified as either rigid or flexible. Rigid pavements usually consist of a thin layer of high modulus of elasticity material such as portland cement concrete that distributes the load owing to the flexural rigidity of the slab. Flexible pavements consist of one or more layers of a relatively low modulus of elasticity material such as asphalt concrete with or without a stabilized granular base course that distributes the load to the subgrade.

A flexible pavement can reasonably and conservatively be considered as additional fill, ignoring the effect of its higher modulus of elasticity. A rigid pavement can cause considerable spreading of the load owing to its stiffness. Gilliland (*1*) introduces a simplified procedure to account for this effect. According to this method an equivalent depth of fill is determined that provides approximately the same amount of distribution as does the rigid pavement and the accompanying actual fill. This procedure takes into account the difference in slab and fill properties by using the factor L, referred to as the radius of relative stiffness, given by

$$L = \sqrt[4]{\frac{Eh^3}{12(1 - \mu)k}} \tag{1}$$

where

E = modulus of elasticity of the pavement (psi),
h = thickness of the pavement (in.),
μ = Poisson's ratio of the pavement, and
k = modulus of subgrade reaction (pci).

An extension of the Boussinesq solution was then employed to calculate the pressures owing to a circular load of radius L. The resulting pressures are fairly sensitive to the values of E, h, and k. As a consequence the equivalent fill heights derived for a specific case should be applied only to that case.

As an example, consider a 9-in.-thick concrete pavement (E = 4,000,000 psi, μ = 0.15) overlaying a subgrade fill material (k = 300 psi). The radius of stiffness from Equation 1 is found to be approximately 30 in. The resulting pressures were plotted in Figure 19 with a solid curve for a single 16,000-lb point load and the fill height indicated. Then, by inspection, the fill height that produced a conservative but similar pressure distribution for a single 16,000-lb point load with no pavement was determined and superimposed on the figure with dashed lines. As expected, the pavement causes the pressure distribution curve to be of a relatively flat shape when compared with the bell-shaped distribution with no pavement, the latter being more conservative because it produces higher maximums.

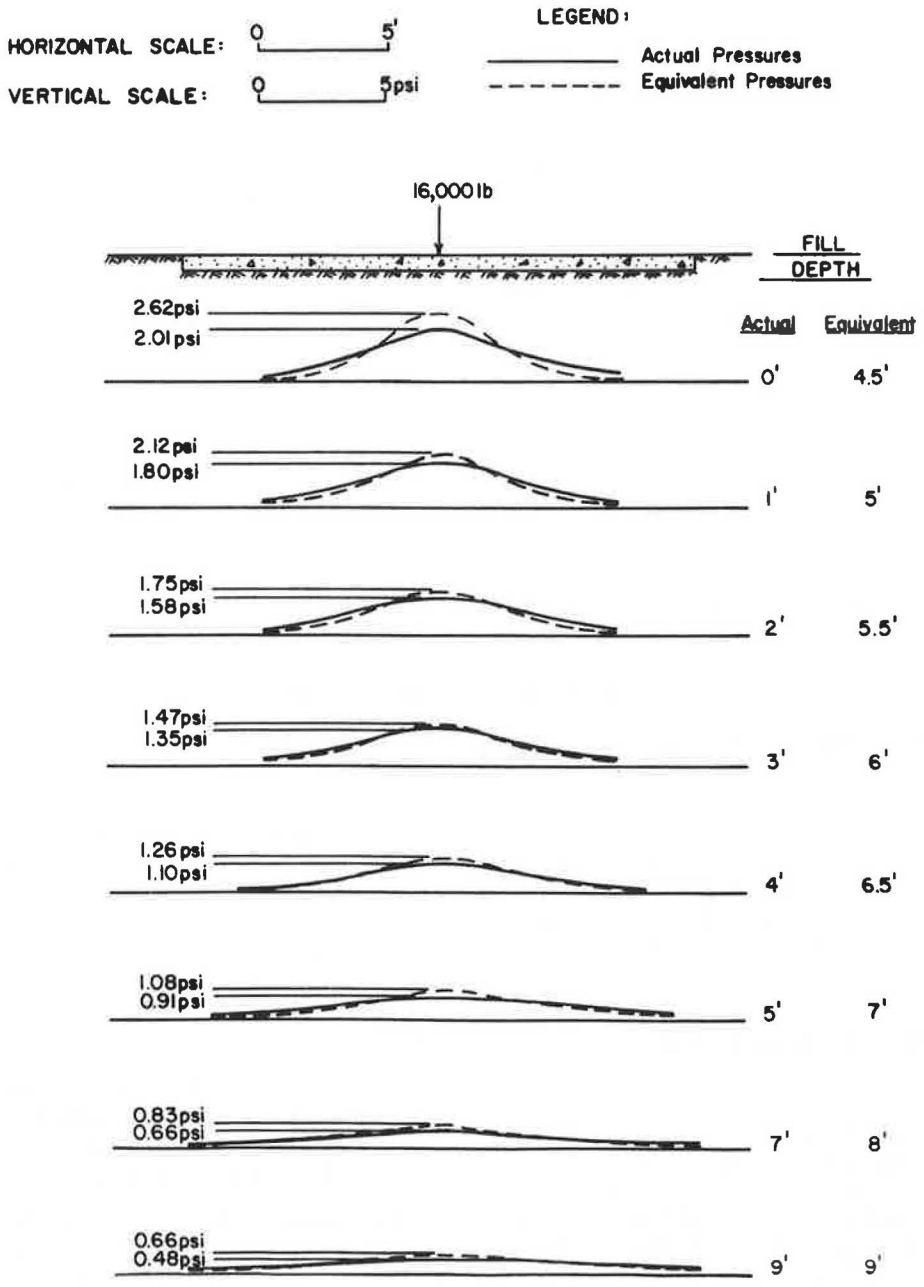

FIGURE 19 Equivalent fill depths for rigid pavements (*1*).

The distribution for pavement for this specific set of values corresponds approximately to the distribution owing to 4.5 ft of fill alone. Also, the effect of pavement is more pronounced at lower fill heights and eventually dissipates at approximately 9.0 ft of fill. An approximately linear relationship exists between 4.5 and 9.0 ft, resulting in the following relation:

$$ED = 4.5 + 0.5 \times H \quad \leq H \tag{2}$$

where ED and H are the equivalent and actual depths of fill in feet, respectively. This equation is applicable up to an actual fill depth of 9 ft.

Similar analysis can be made for other situations that involve different pavement thicknesses and material properties. The results can be tabulated in a suitable form and be made available for design purposes. In all cases, however, judgment on the part of the designer is required to determine if the geometry of the culvert-roadway intersection is such that the distribution owing to pavement can be depended on.

BENDING MOMENTS IN SLABS OWING TO PARTIAL LOADING

In addition to the distribution of wheel loads owing to pavement and fill, the top slab of the culvert provides additional distribution owing to its flexural stiffness along the length of the culvert. The current AASHTO specifications address this

type of distribution only when the culvert has less than 2 ft of cover. The top slab is designed for this situation as a concrete slab bending with the wheel load assumed to be distributed over a width E given by (*14*):

$$E = 4 + 0.06 \times S \qquad \leq 7 \text{ ft} \tag{3}$$

where E is the effective distribution width (ft) and S is the span (ft). This equation is intended for exposed slabs subjected to wheel loads because it is independent of the area occupied by the load.

AASHTO specifications indicate that from zero to less than 2 ft of fill, the distribution owing to the slab is predominant and that the distribution owing to the fill is negligible. The same E is recommended by AASHTO for fills not greater than 2 ft. For 2 ft or more of fill the distribution of wheel loads owing to fill is predominant and the distribution owing to the slab is negligible. While those assumptions simplify the problem of determining the design moments, the transition at 2 ft of fill results in design discrepancies.

The suggested extension of AASHTO's 1.75 factor to fill heights less than 2 ft would result in a uniformly loaded square area, or partial loading, corresponding to each wheel load on the slab. This proposal was made to aid in eliminating the design discrepancies through varying fill heights. Because equation 3 is applicable for point loads only, a similar relation for partial loads is needed if the proposed extensions are to be adopted. Figure 20 presents the top slab of a box culvert subjected to a uniformly distributed load p over a square area ($b \times b$). Currently, for fill heights of 2 ft or more, a unit width is passed through the partial loading to calculate the design moment and is referred to as the strip method and completely ignores the distribution owing to the slab and thus overestimates the design moment. This moment, which will be referred to as M_{strip}, is distributed through a width of b. The actual transverse moment distribution m is given and has a maximum value equal to M_{max}. This is the true design moment for which the slab should be designed, provided that M_{max} is obtained from the worst loading condition. M_{strip} is greater than M_{max} and would result in over design. Also shown in the figure is the moment produced by spreading the load over an effective distribution width E' that produces a design moment equal to M_{max}.

Gilliland (*1*) used a simplified analysis procedure to determine the magnitude of the distribution owing to the top slab. Ratios of M_{max}/M_{strip} were determined for several culvert sizes and boundary conditions for both positive and negative moments. The analysis was repeated for various fill heights and support conditions, and the results are plotted in Figure 21. Gilliland proposed the following relation between M_{max} and M_{strip}:

$$C = 0.10 + 0.45 \times H \qquad H < 2 \text{ ft}$$

$$C = 1.0 \qquad H \geq 2 \text{ ft} \tag{4}$$

where C is moment coefficient, M_{max}/M_{strip} and H is the fill height (ft). This equation is similar to Equation 3, proposed by AASHTO for point loads, but is valid for batch loading generated from dispersion through fill of point or other loads. The coefficient C can be thought of as the inverse of the equivalent width. LL moments based on the strip and suggested methods are compared with the measured values in Figure 22, for 0-ft fill height. The figure clearly indicates the advantage of using the suggested method.

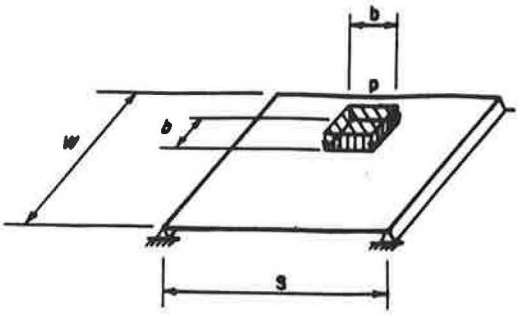

(a) Partially Loaded One-Way Slab

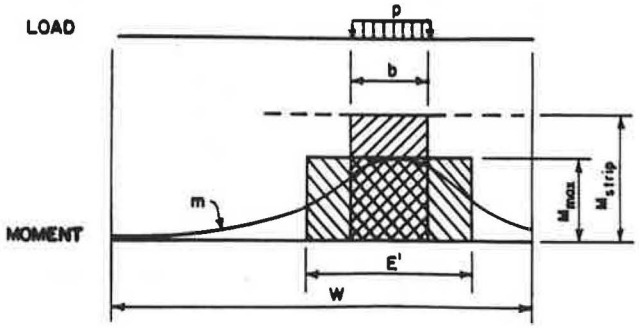

(b) Transverse Distribution of Moment Due to Partial Loading

FIGURE 20 Bending moments in slabs owing to partial loading.

CONCLUSIONS

1. The Boussinesq (three-dimensional) elasticity solution has been shown to give reasonable predictions of the measured soil pressures owing to wheel loads. While this method provides a powerful analytical tool, its use for everyday design is not convenient. A simple uniform distribution such as that suggested by AASHTO can be used without appreciable loss of accuracy.

2. The AASHTO 1.75 distribution factor can be safely used for fill heights less than 2 ft and more than 8 ft.

3. The measured LL pressures at fill heights of 8 ft or more may become exceedingly small when compared with the soil-induced pressures. However, the cutoff limit beyond which LL pressures can be safely ignored should be determined by the structural designer on the basis of the pressure contribution to the total load effects. A suggested criterion for neglecting LL effects (shear, moment, etc.) is when those effects contribute less than 5 percent of the total load effects.

4. Similar load distributions were observed in the longitudinal and transverse directions. It is therefore recommended

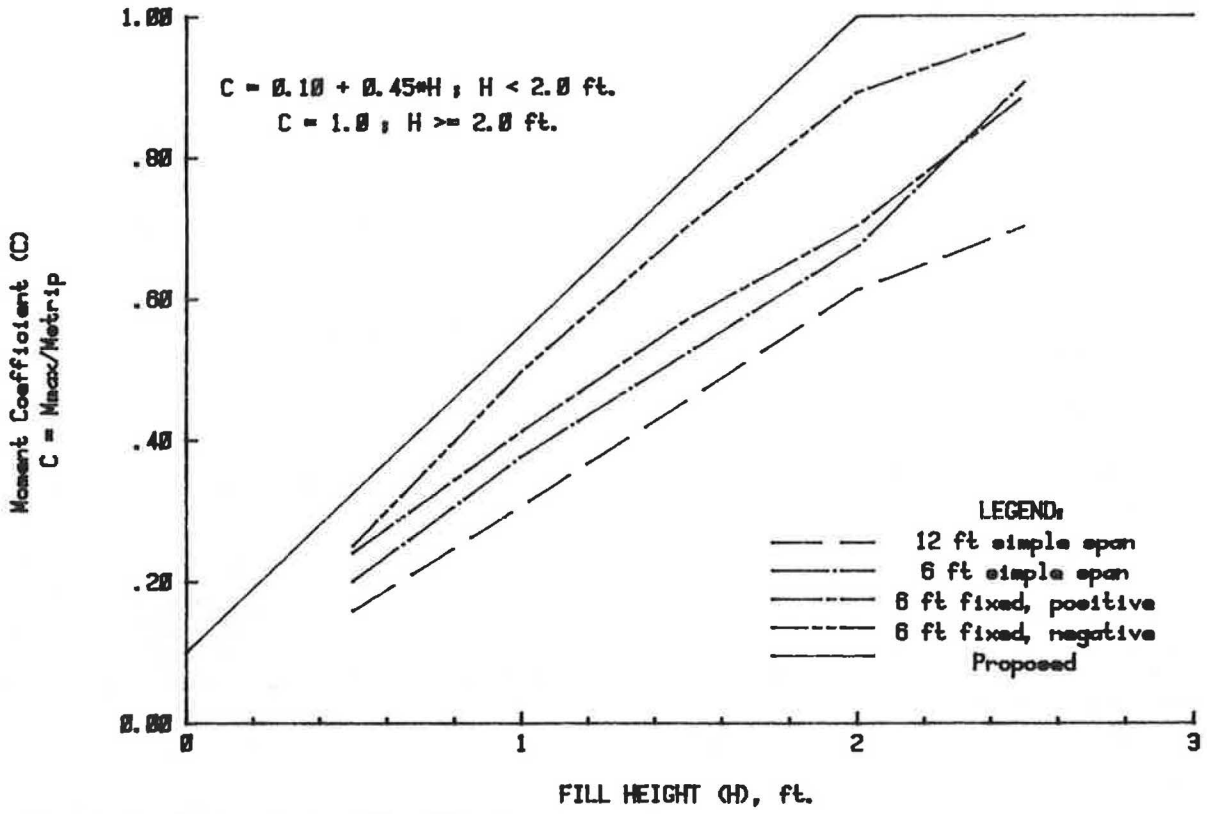

FIGURE 21 Moment coefficients versus fill heights (*I*).

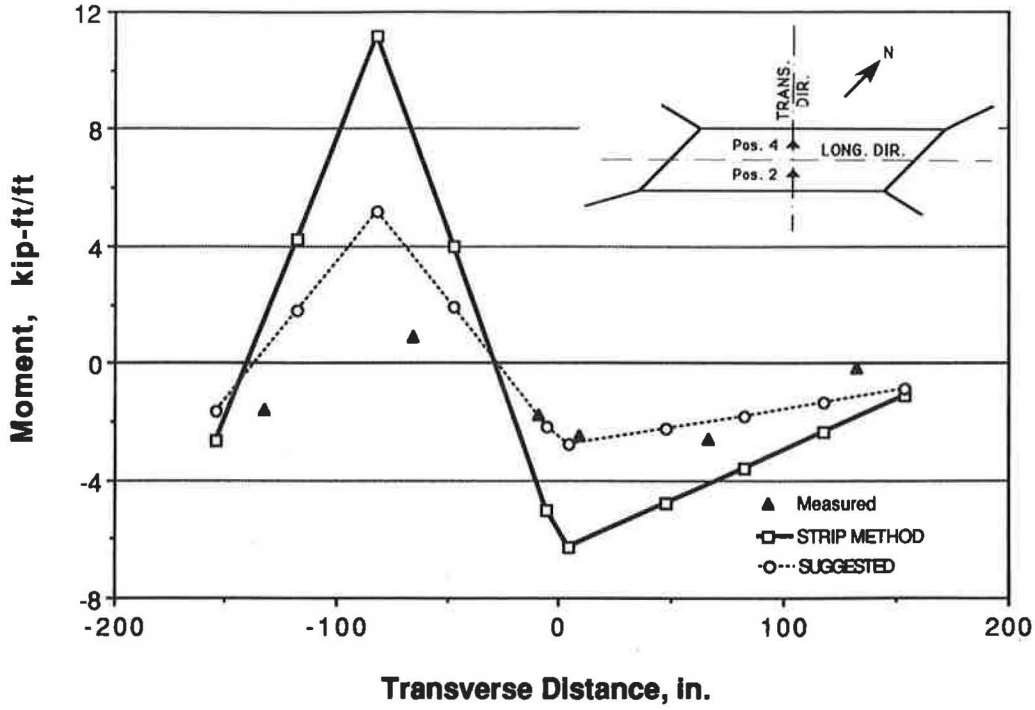

FIGURE 22 Comparison of strip and suggested live load moments with field measurements.

that the distribution of the load over a square area be continued.

5. Two other factors, besides soil fill, aid in dispersing wheel load effects through the culvert: pavement and distribution through the two-way action of the culvert top slab itself.

6. Rigid pavements can help distribute wheel loads considerably, especially when soil fill height is relatively small. A procedure is outlined to determine equivalent fill height to pavements of certain properties.

7. AASHTO recognizes the ability of exposed slabs to distribute wheel loads by means of an equivalent width E. This study extends the equivalent width concept for slabs covered with soil to provide for a smooth transition of wheel load effects for various soil fill heights.

ACKNOWLEDGMENTS

Sponsors of the project are the FHWA, Nebraska Department of Roads (NDOR), and the University of Nebraska-Lincoln. Many individuals have contributed to the various phases of this project. Special thanks are due to George Schmid, Paul Koenig, Dalyce Ronnau, Wayne Horn, Tom Goodbarn, and Jerry Koloen, all of NDOR; to Ron Rystrom, Sarpy County Engineer; and to Dallas Meyer, Karen Bexten, and Say-Gunn Low.

REFERENCES

1. M. K. Gilliland, *Cost-Effective Concrete Box Culvert Design*. Masters thesis. University of Nebraska-Lincoln, 1986.
2. Ray W. James and Dale E. Brown. Wheel-Load-Induced Earth Pressures on Box Culverts. In *Transportation Research Record 1129*, TRB, National Research Council, Washington, D.C., 1987, pp. 55–62.
3. M. G. Spangler and R. L. Handy. *Soil Engineering*, 4th ed., Harper and Row, New York, 1982.
4. E. J. Yoder and M. H. Witczak. *Principles of Pavement Design*, John Wiley, New York, pp. 13–28.
5. D. M. Burmister. Stress and Displacement Characteristics of a Two-Layer Rigid Base Soil System: Influence Diagram and Practical Applications. *HRB Proc.*, Vol. 35, 1956, pp. 773–813.
6. H. G. Poulos and E. H. Davis. *Elastic Solutions for Soil and Rock Mechanics*, John Wiley, New York, 1974.
7. M. K. Tadros and J. V. Benak. *Load Distribution on Box Culverts*, Research Report, Nebraska Department of Roads, Aug. 1989.
8. R. E. Davis, F. M. Semans, D. W. Spannagel, and A. E. Bacher. *Rigid Pipe Proof Testing Under Excess Overfills With Varying Backfill Parameters, 1, Introduction, Historical Background, Project Discussion, and Instrumentation*, California Department of Transportation, FHWA/CA/SD-78/02, FHWA, Department of Transportation, 1978.
9. D. W. Meyer. *Instrumentation and Analysis of A Full-Scale Concrete Box Culvert*. Masters thesis. University of Nebraska-Lincoln, 1987.
10. *Product Literature*, Geonor-USA, Clifton, N.J., 1986.
11. G. Abdel-Sayed and B. Bakht. Analysis of Live-Load Effects in Soil-Steel Structures, *Transportation Research Record 878*, TRB, National Research Council, Washington, D.C., 1982, pp. 49–55.
12. M. G. Katona, and J. M. Smith, *CANDE User Manual*. Report FHWA-RD-77-6, FHWA, Department of Transportation, Oct. 1976.
13. M. G. Katona et al. *CANDE-1980: Box Culverts and Soil Models*. Report FHWA/RD-80/172, FHWA, Department of Transportation, May 1981.
14. H. M. Westergaard, Computation of Stresses in Bridge Slabs Due to Wheel Loads. *Public Roads*, Vol. 2, No. 1, March 1930.

Publication of this paper sponsored by Committee on Subsurface Soil-Structure Interaction.

Analysis of Retaining Structures With Skew Reinforcement

S. BANG AND H. YEON

A method of analyzing earth-retaining structures with skew reinforcement based on the principle of generalized plane-strain finite-element analysis is presented and it can calculate quasi-three-dimensional responses of the soil and the structural elements without resorting to a fully three-dimensional finite-element analysis. A significant reduction in computational effort with little loss in accuracy has been obtained. The developed method of analysis has been applied to investigate the effect of reinforcement skew angle associated with the Reinforced Earth retaining wall and the conventional tie-back concrete retaining wall.

Many earth-retaining structures use some kind of reinforcing technique to increase stability, including the Reinforced Earth wall (*1*), the Retained Earth wall (*2*), soil nailing (*3*), anchored bulkhead, and conventional retaining wall with tie-backs. All those methods use internal reinforced members installed within the backfill. However, a deviation from the standard method of construction is sometimes inevitable when those structures are used as bridge abutments. For instance, many bridge abutments are skew (i.e., the abutments are not perpendicular to the alignment of the bridge owing to the constraint imposed by the geometric conditions). Therefore, it is necessary under such circumstances to use skew-reinforcing members so that adequate friction develops along the length of the reinforcement or sufficient passive resistance develops in front of the deadman.

A truly three-dimensional analysis may have to be performed to analyze such skew retaining structures. However, if the reinforcements are parallel with one another and have the same geometric and material properties, then the analysis can be simplified to quasi-three dimensional (*4*). This paper summarizes one method and illustrates how the method can be applied to analyze earth-retaining structures with skew reinforcement.

METHOD OF ANALYSIS

The detailed behavior of the soil, the retaining structure, and the reinforcement must be taken into account in formulating a method of analysis. Those factors that greatly influence the performance of the earth-retaining structures generally favor the use of the finite-element method of analysis.

A generalized plane-strain condition (*5*) has been assumed to study the behavior of earth-retaining structures with skew reinforcement. The generalized plane-strain approach simply dictates that the plane-strain directional strain ε_z remains zero instead of the plane-strain directional displacement w being zero, as is commonly adopted in the conventional plane-strain approach. Therefore, the approach includes three nonzero displacement components u, v, and w along the x, y, and z coordinates, none of which is dependent on the out-of-plane coordinate, z. This approach was chosen mainly because the conventional two-dimensional plane-strain approach cannot effectively represent the out-of-plane behavior of the skew reinforcement. Conversely, a truly three-dimensional analysis is prohibitively complicated and time consuming. The main advantage of the generalized plane-strain approach is that it can calculate the three-dimensional stresses and displacements while the finite-element grid remains in two dimensions.

The generalized plane-strain approach can calculate the approximate three-dimensional response of the system with minimal effort.

The total virtual work in the finite-element formulation is described as

$$\delta V = \sum_{e=1}^{N} \delta V_e = \sum_{e=1}^{N} [\delta U_e - \delta W_e] = 0 \quad (1)$$

where

N = total number of elements,
δV_e = virtual work of element,
δU_e = element virtual internal energy, and
δW_e = element virtual external work.

The incremental material constitutive relationship is

$$\{\Delta\sigma\} = [C]\{\Delta\varepsilon\} \quad (2)$$

where

$\{\Delta\sigma\}$ = changes in stress vector,
$\{\Delta\varepsilon\}$ = changes in strain vector, and
$[C]$ = constitutive matrix.

Note that the constitutive matrix $[C]$ in incremental analysis depends on current stress state and its history. The element virtual internal energy expression can be written incrementally as

$$\delta\Delta U_e = \int_{V_e} \{\delta\varepsilon\}^T \{\Delta\sigma\}\, dV_e \quad (3)$$

Department of Civil Engineering, South Dakota School of Mines and Technology, Rapid City, S. Dak. 57701.

where

$\delta\Delta U_e$ = incremental element virtual internal energy,
V_e = volume of the element, and
$\{\delta\varepsilon\}^T$ = incremental strain vector transpose.

Substitution of Equation 2 into Equation 3 yields

$$\delta\Delta U_e = \int_{V_e} \{\delta\varepsilon\}^T [C] \{\Delta\varepsilon\} \, dV_e \tag{4}$$

The three-dimensional displacements in generalized plane-strain approach are independent of the out-of-plane z coordinate; that is,

$$\begin{aligned} u &= u(x, y) \\ v &= v(x, y) \\ w &= w(x, y) \end{aligned} \tag{5}$$

From the definition of strains in three dimensions,

$$\{\varepsilon\} = \{\varepsilon_x, \varepsilon_y, \varepsilon_z, \gamma_{xy}, \gamma_{xz}, \gamma_{yz}\}^T = \begin{bmatrix} \dfrac{\partial u}{\partial x} \\ \dfrac{\partial y}{\partial y} \\ \dfrac{\partial w}{\partial z} \\ \dfrac{\partial u}{\partial y} + \dfrac{\partial y}{\partial x} \\ \dfrac{\partial u}{\partial z} + \dfrac{\partial w}{\partial x} \\ \dfrac{\partial v}{\partial z} + \dfrac{\partial w}{\partial y} \end{bmatrix} \tag{6}$$

where ε equals normal strain and γ equals shear strain.

It is evident that the strain components in generalized plane strain are

$$\{\varepsilon\} = \begin{bmatrix} \dfrac{\partial u}{\partial x} \\ \dfrac{\partial v}{\partial y} \\ 0 \\ \dfrac{\partial u}{\partial y} + \dfrac{\partial v}{\partial x} \\ \dfrac{\partial w}{\partial x} \\ \dfrac{\partial w}{\partial y} \end{bmatrix} \tag{7}$$

By using a linear approximation for displacements, the three displacements at each node of the isoparametric quadrilateral continuum element can be approximated as

$$\begin{aligned} u &= \sum_{i=1}^{4} N_i \, u_i \\ v &= \sum_{i=1}^{4} N_i \, v_i \\ w &= \sum_{i=1}^{4} N_i \, w_i \end{aligned} \tag{8}$$

where u_i, v_i, w_i equals the approximate ith nodal displacements and N_i equals first-order shape function.

Substituting Equation 8 into Equation 7 yields

$$\begin{aligned} \varepsilon_x &= \frac{\partial u}{\partial x} \\ &= \frac{\partial}{\partial x}\left[\sum_{i=1}^{4} N_i \, u_i\right] \\ &= \sum_{i=1}^{4} F_i \, u_i \\ \varepsilon_y &= \frac{\partial v}{\partial y} \\ &= \frac{\partial}{\partial y}\left[\sum_{i=1}^{4} N_i \, v_i\right] \\ &= \sum_{i=1}^{4} G_i \, v_i \\ \gamma_{xy} &= \frac{\partial u}{\partial y} + \frac{\partial y}{\partial x} \\ &= \frac{\partial}{\partial y}\left[\sum_{i=1}^{4} N_i \, u_i\right] + \frac{\partial}{\partial x}\left[\sum_{i=1}^{4} N_i \, v_i\right] \\ &= \sum_{i=1}^{4} \left[G_i \, u_i + F_i \, v_i\right] \\ \gamma_{xz} &= \frac{\partial w}{\partial x} \\ &= \sum_{i=1}^{4} F_i \, w_i \\ \gamma_{yz} &= \frac{\partial w}{\partial y} \\ &= \sum_{i=1}^{4} G_i \, w_i \end{aligned} \tag{9}$$

where

$$F_i = \frac{\partial N_i}{\partial x}$$

$$G_i = \frac{\partial N_i}{\partial y}$$

The incremental strain-displacement relationships are

$$\{\Delta\varepsilon\}_e = [B]\{\Delta u\}_e \tag{10}$$

where

$\{\Delta\varepsilon\}_e$ = element incremental strain vector,
$\{\Delta u\}_e$ = element incremental displacement vector
$= \{\Delta u_1, \Delta u_2, \Delta u_3, \Delta u_4, \Delta v_1, \Delta v_2, \Delta v_3, \Delta v_4, \Delta w_1, \Delta w_2, \Delta w_3, \Delta w_4\}^T$,

$$[B] = \begin{bmatrix} \{F\}^T & \{0\}^T & \{0\}^T \\ \{0\}^T & \{G\}^T & \{0\}^T \\ \{0\}^T & \{0\}^T & \{0\}^T \\ \{G\}^T & \{F\}^T & \{0\}^T \\ \{0\}^T & \{0\}^T & \{F\}^T \\ \{0\}^T & \{0\}^T & \{G\}^T \end{bmatrix} 6 \times 12,$$

$\{F\}^T = \{F_1, F_2, F_3, F_4\}$,
$\{G\}^T = \{G_1, G_2, G_3, G_4\}$, and
$\{0\}^T$ = null vector transpose.

Substitution of Equation 10 into Equation 4 yields

$$\delta\Delta U_e = \int_{V_e} \{[B]\{\delta u\}_e\}^T [C] \{[B]\{\Delta u\}_e\}\, dV_e$$

$$= \{\delta u\}_e^T [EK] \{\Delta u\}_e \tag{11}$$

where

$[EK]$ = element tangent stiffness matrix with a dimension of 12 × 12
$= \int_{V_e} [B]^T [C] [B]\, dV_e$ and
$[C]$ = incremental constitutive matrix.

The coefficients of matrix $[C]$ can be obtained from the stress-strain relationship.

If a nonlinear soil characterization is used, then the soil tangent modulus depends on the current stress state and its history. Therefore, the correct value of soil tangent modulus and the matrices $[C]$ and $[EK]$ must be determined from an iteration process.

Once the element tangent stiffness matrices are determined for each element, they are assembled to obtain a global system stiffness matrix based on the element-node arrangement. Meanwhile, the element load vectors, resulting from gravity loading and traction, are assembled separately to produce a global system load vector. Finally, a set of simultaneous equations satisfying the boundary conditions is obtained and the equations are solved to obtain the global nodal displacements. The obtained nodal displacements are then used to calculate the strains and the stresses. The calculated stresses are used to estimate a set of new soil tangent modulus values for the next iteration when nonlinear soil properties are considered.

The special characteristics of the generalized plane-strain finite-element analysis must be reiterated. Conventional two-dimensional plane-strain finite-element analysis requires the size of element stiffness matrix, $[EK]$, to be 8 × 8 (i.e., two displacements along x and y coordinates at each of the four nodes of a linear isoparametric quadrilateral element). Conversely, truly three-dimensional finite-element analysis requires an element stiffness matrix $[EK]$ of 24 × 24 for a linear isoparametric brick element because three displacements exist at each of eight nodes. The generalized plane-strain finite-element analysis requires an element stiffness matrix $[EK]$ of 12 × 12 (i.e., three displacements at each of four nodes of a linear isoparametric quadrilateral element). A smaller element stiffness matrix is always desirable because the majority of the computational effort in finite-element analysis comes from the solution of simultaneous equations.

COMPARISON WITH THREE-DIMENSIONAL SOLUTIONS

A comparison has been made with the results obtained from a truly three-dimensional analysis (*6*) to illustrate the effectiveness of the generalized plane-strain finite-element method of analysis. Figure 1 presents a schematic description of the problem considered for the comparison and it includes an L-shaped bridge abutment reinforced with tie-rods and drilled-in concrete anchors. The tie-rods are made of steel with a yield strength of 90,000 lb/in.^{2}, a diameter of 1.5 in., and a skew angle of 11.31 degrees to the plane perpendicular to the abutment. The drilled-in concrete anchors are 2.5 ft in diameter with a length of 5 ft. The abutment stem and base have uniform thickness of 1 ft. It rests on top of linear elastic soil with Poisson's ratio of 0.3, tangent modulus of 3,500 lb/in.^{2}, and unit weight of 120 lb/ft^3.

The tie-rods and drilled-in concrete anchors are simulated by the beam-column elements in both the generalized plane-

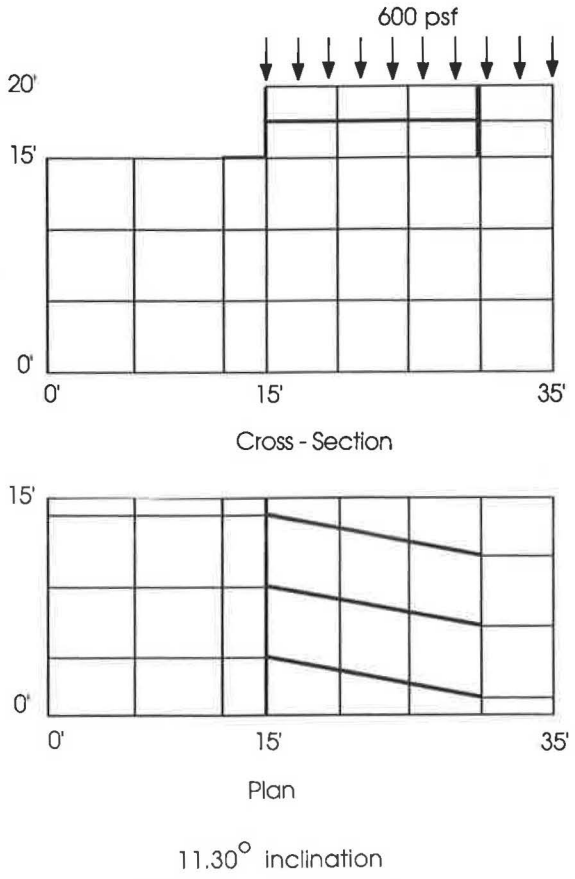

FIGURE 1 Schematics of tie-back wall.

strain and the truly three-dimensional finite-element analysis. The generalized plane-strain finite-element approach, by virtue of its two-dimensional finite-element grid, allows beam-column elements to model the abutment. However, plate elements are needed in the truly three-dimensional finite-element analysis (*7*).

A total of 42 nodes, 29 isoparametric quadrilateral continuum elements, and 8 beam-column elements are used in the generalized plane-strain finite-element analysis, whereas the three-dimensional analysis requires a total of 210 nodes, 116 brick elements to model the continuum, 9 beam-column elements for the tie-rods, 6 beam-column elements for the drilled-in concrete anchors, and 12 plate elements for the abutment. It required a CDC Cyber-180 mainframe computer approximately 8.5 and 182.5 sec of CPU time, to complete the generalized plane-strain finite-element analysis and the truly three-dimensional finite element analysis, respectively, resulting in a ratio of 21.5 in computational time.

Tables 1 and 2 present comparisons of three-dimensional displacements at selected nodes and the responses of the structural members. The differences are virtually negligible. Thus, the generalized plane-strain finite-element method of analysis can effectively capture most of the significant three-dimensional response of the skew retaining structures without significant error but with a remarkable reduction in computational effort.

EFFECT OF SKEW ANGLE

A Reinforced Earth retaining wall has been analyzed (*8*) to develop an understanding of the effect of skew angle. The wall has reinforcing strips installed horizontally with equal spacing and skew angle. The soil considered is silty sand with a friction angle of 32 degrees and no cohesion and is modeled by the nonlinear hyperbolic soil characterization proposed by Duncan et al. (*9*).

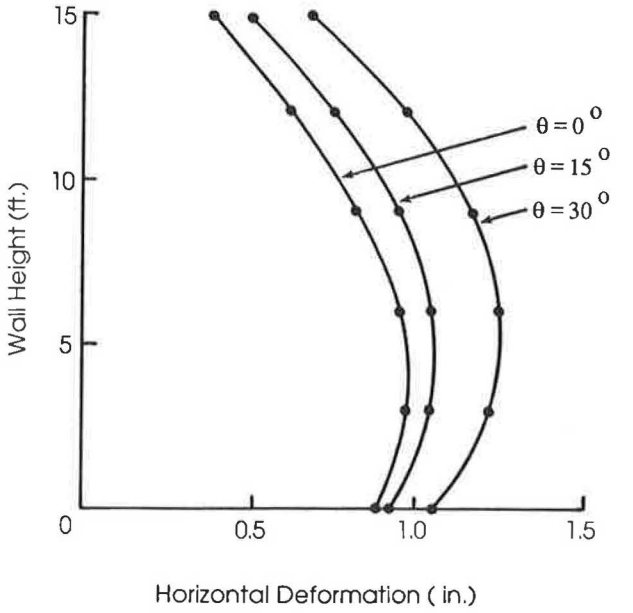

FIGURE 2 Horizontal deformation of Reinforced Earth wall.

The main variable considered in the study is the skew angle of the reinforcing strips, which varies from 0 to 30 degrees. The reinforcing members are made of metal strips 2.5 in. in width, ⅛ in. in thickness, 15 ft in length, and a spacing of 3 ft both horizontally and vertically. The height of the wall remains as 18 ft.

Figure 2 presents the calculated deformations of the retaining walls with different skew angles. As the skew angle increases, the larger outward movements result. For instance, maximum outward movement of 0.96 in. occurs with no skew angle, whereas 1.24 in. of maximum outward movement is expected with 30 degree skew angle, resulting in an increase of approximately 29 percent. However, the pattern of outward bulge

TABLE 1 COMPARISON OF DISPLACEMENTS AT NODES ALONG THE MIDDLE TIE-BACK

Nodal Distance from Abutment	u (ft.)		v (ft.)		w (ft.)	
	GPS	3-D	GPS	3-D	GPS	3-D
0 ft.	0.015	0.014	- 0.390	- 0.391	- 0.006	- 0.000
5 ft.	0.011	0.010	- 0.552	- 0.556	0.003	0.003
10 ft.	0.012	0.012	- 0.617	- 0.622	- 0.002	- 0.002
15 ft.	0.008	0.008	- 0.618	- 0.622	0.004	0.002

TABLE 2 COMPARISON OF FORCES AND MOMENTS

	Axial Force (lbs.)		Shear (lbs.)		Bending Moment (ft.-lbs.)	
	GPS	3-D	GPS	3-D	GPS	3-D
Concrete Anchor	12,360	11,030	977	952	29,243	28,544
Tie-Rod	390	401				

of the wall becomes slightly different as the skew angle increases. Maximum outward deformation occurs toward the toe of the wall when the skew angle is zero or relatively small, with a gradual upward shift as the skew angle increases. The out-of-plane directional displacements, as presented in Figure 3, indicate a similar pattern. As was expected, the out-of-plane displacements become larger as the skew angle increases. The conventional plane-strain approach is not capable of calculating this out-of-plane displacement directly.

The same formulation has been applied to analyze an L-shaped concrete bridge abutment reinforced with skew tie-backs (*8*). The abutment has dimensions of 8 ft in height and 1 ft in stem thickness with a 5-ft wide and 2.5-ft thick base and is supported by 40-ft-long and 1-ft-diameter friction timber piles, which are installed in two rows. The front row consists of one pile per group and the rear row of two piles per group. The spacings of the pile group and the tie-backs are both 12.73 ft. The external loads include a surcharge of 650 psf and a bridge girder support reaction of 6,800 lb/ft acting on the base of the abutment. The backfill material consists of crushed limestone, and the foundation soil consists of silty clay. The strength and the hyperbolic soil properties are presented in Table 3. The tie-rods have a diameter of 1⅜ in. and a length of 35 ft and are embedded at a depth of 2.67 ft from the ground surface and are tied to 2.5 ft diameter drilled-in concrete anchors.

Figure 4 presents the variations of tie-rod axial force and abutment bending moment as a function of skew angle and indicates that the axial force within the tie-rod decreases as the skew angle increases. However, the pattern of bending moment developed within the abutment is the opposite. However, the rate of bending moment increase is very small. For instance, increasing the skew angle from zero degrees to 45 degrees results in an increase of bending moment of a mere 3.5 percent.

The out-of-plane displacement at the top of the abutment indicates an almost identical pattern to that of the Reinforced Earth wall, increasing rapidly from zero (with no skew angle) as the skew angle increases. However, the out-of-plane displacement remains more or less the same beyond a skew angle of approximately 30 degrees (Figure 5).

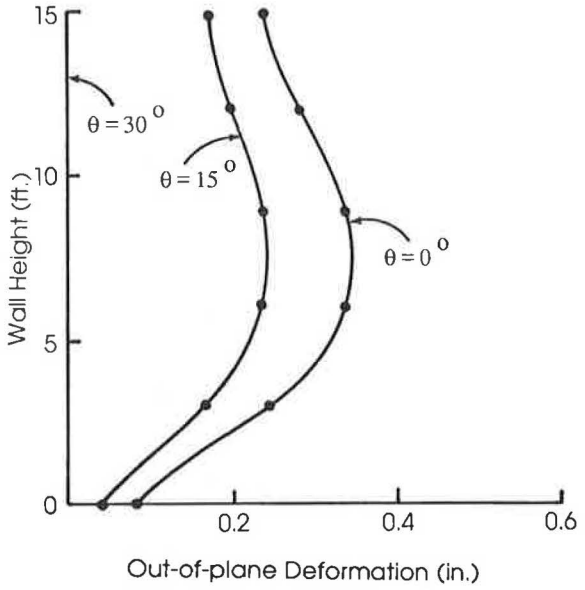

FIGURE 3 Out-of-plane deformation of Reinforced Earth wall.

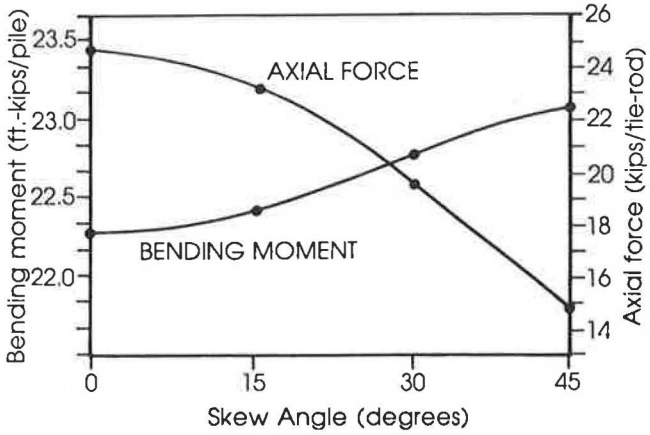

FIGURE 4 Axial force and bending moment of tie-back wall.

TABLE 3 SOIL PARAMETERS

	Crushed Limestone	Silty Clay
Unit Weight (lb/ft^3)	103.5	136
Cohesion (psf)	0	1,100
Friction Angle (deg)	50	35
Loading Modulus	700	215
Modulus Exponent	0.85	0.41
Failure Ratio	0.74	0.60
Poisson's Ratio	0.3	0.3

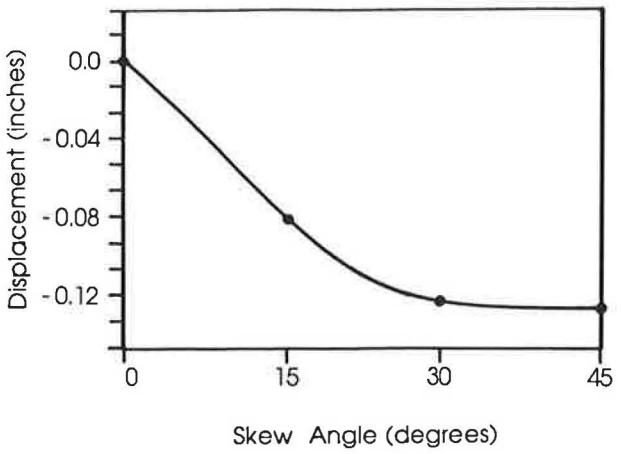

FIGURE 5 Out-of-plane deformation of tie-back wall.

CONCLUSION

Development of a finite-element method of analysis based on the generalized plane-strain approach is briefly described and has been applied to compare the results with those obtained from a truly three-dimensional analysis. The comparison indicates that the generalized plane-strain method of analysis is very effective and efficient in calculating the three-dimensional response of earth-retaining structures with skew reinforcement without a significant loss in accuracy.

A study is also included of the effect of skew angle associated with retaining structures by using the generalized plane-strain method of analysis. Considered in the analysis are the Reinforced Earth retaining wall reinforced with skew metal strips and the conventional reinforced concrete abutment reinforced with skew tie-backs.

The generalized plane strain method of analysis is intended to capture the most essential characteristics involved in earth-retaining structures with skew reinforcement without resorting to a fully three-dimensional analysis. Though the study shows a promising capability of the developed method analysis, a more detailed study must be conducted to verify the validity of the formulation further.

ACKNOWLEDGMENT

The author is grateful for the financial and technical support provided by the Federal Highway Administration and the South Dakota Department of Transportation.

REFERENCES

1. H. Vidal. The Principle of Reinforced Earth. In *Highway Research Record 282*, HRB, National Research Council, Washington, D.C., 1969.
2. J. K. Mitchell and W. C. B. Villet. *NCHRP Report 290: Reinforcement of Earth Slopes and Embankments*. TRB, National Research Council, Washington, D.C., June 1987.
3. C. K. Shen, S. Bang, and L. R. Herrmann. Ground Movement Analysis of Earth Support System. *Journal of the Geotechnical Engineering Division*, ASCE, GT12, Dec. 1981.
4. S. Bang. *Design and Analysis of Reinforcing Distressed Bridge Abutments*. Final Report, South Dakota Department of Transportation, Oct. 1988.
5. S. Bang and C. K. Shen. *Soil Reinforcement in Soft Ground Tunneling*. Report DOT/RSPA/DMA-50/83/15, U.S. Department of Transportation, Jan. 1983.
6. K. J. Bathe, E. L. Wilson, and F. E. Peterson. *SAPIV: A Structural Analysis Program for Static and Dynamic Response of Linear Systems*. Report EERC73-11, University of California, Berkeley, April 1974.
7. S. Bang and S. Schelske. Bridge Abutments Reinforced with Skew Tie-Backs. Presented at 3rd International Conference on Numerical Models in Geomechanics, Niagara Falls, Canada, May 1989.
8. S. Bang and S. I. Hwang. Analysis of Skew Reinforcement System. Presented at 24th Annual Engineering Geology and Soils Engineering Symposium, Coeur d'Alene, Idaho, March 1988.
9. J. M. Duncan, P. Byrne, K. S. Wong, and P. Mabry. *Strength, Stress-Strain and Bulk Modulus Parameters for Finite Element Analysis of Stresses and Movements in Soil Masses*. Report UBC/GT/80-01, Department of Civil Engineering, University of California, Berkeley, Aug. 1980.

Publication of this paper sponsored by Committee on Foundations of Bridges and Other Structures.

Sound Barrier Wall Foundations in Granular Material

ALIREZA BOGHRAT

Sound barrier walls are necessary for highways when alignments cross residential areas. Drilled shafts (caissons) are simple foundations for sound barrier walls. Four different design methods for drilled shafts are discussed and compared. All methods result in comparable capacities for shafts up to certain embedment depths, as is indicated by the analysis. Two of the methods, which originally were developed only for level ground, are modified to accommodate sloped ground surfaces.

Sound barrier walls are frequently used for new highway construction. The design and construction of sound barriers are essential when a proposed highway alignment passes residential areas that have no natural noise reduction features. A short drilled shaft is an economical and reliable foundation for sound barrier walls. Shafts are constructed by drilling a hole with the required diameter to the appropriate depth, placing the reinforcing cage in the hole, and filling the hole with concrete. One of the most important characteristics of the concrete (placed by tremie or pumping) is high workability; that is, having a slump of 6 in. or more (*1*).

Short-drilled shafts may be designed as short piles (piles with a length-to-diameter ratio less than or equal to 10). Short piles unrestrained against rotation fail when lateral soil resistance is exceeded and when rigid-body rotation occurs. Various methods of approach to the problem exist, and four different design methods for cohesionless soils are discussed and compared here. These four methods are very simple to use because one is computerized and three are in chart/table form. Two of the presented methods (originally prepared only for level ground surfaces) when modified are also adequate for sloped ground surfaces.

TRR 616 METHOD

The TRR 616 method was developed by Davidson et al. (*2*). The solution is in graph form and is very simple to use. Figure 1 presents the actual and assumed soil resistance distribution at failure. The method does not assume a fixed point of rotation. The study by Davidson et al. (*2*) demonstrated that the rotation point changed from some point below the middle of the shaft embedment distance for light loads to beyond the three-quarter point for failure loads.

Pennsylvania Department of Transportation, Geotechnical Section, Harrisburg, Penn. 17120.

If the principles of statics are applied to the assumed soil pressure distribution, then the following equations can be determined (*2*):

$$S = (\alpha/2)(2X^2 - D^2) \quad (1)$$

$$M = (-\alpha/3)(2X^3 - D^3) \quad (2)$$

where

S = applied lateral load,
M = applied bending moment,
X = unknown distance to the point of rotation,
α = slope of the soil resistance diagram, and
D = embedment depth.

The value of (α) is the same as the one assumed by Broms (*3*) (i.e., passive pressure will act over a width equal to three times the shaft diameter). The only difference is that a soil strength reduction factor (μ) is added to account for the accuracy of the soil strength parameters (*2*).

$$\alpha = 3\gamma B \tan^2(45 \text{ degrees} + \phi/2) \quad (3)$$

where

B = diameter of the drilled shaft,
γ = effective unit weight of the soil, and
ϕ = angle of internal friction.

The value of (μ) can be determined from Table 1. To present the solution in chart form, Davidson et al. used another variable (K), which is the ratio of X to D. Therefore, Equations 1 and 2 were modified to a nondimensional form (*2*).

$$S/\alpha D^2 = K^2 - \frac{1}{2} \quad (4)$$

$$(S/\alpha D^2)(H/D) = \left(-\frac{2}{3}\right)K^3 + \frac{1}{3} \quad (5)$$

where H is a distance that begins at the application point of lateral load to the ground surface.

A graph relates the ($S/\alpha D^2$) to the (H/D) values. The procedure for determining needed resistance is choosing D and determining Su (ultimate capacity) by using Figure 2. Davidson et al. made a comparison of ultimate capacity determined from Figure 2 and from the actual capacity determined from the model and full-scale drilled-shaft tests. Results indicate that the observed mean value of Su is 1.64 times the theo-

retical mean value (*2*) and that a factor of safety equal to 1.64 is already built into the solution and, on the average, the actual *Su* would be 1.64 times the calculated *Su* from the chart.

The design procedure presented in TRR 616 is for level ground, but, with a simple modification, it can be used to determine the actual ultimate value of soil resistance for sloped ground in front of the pile or shaft.

MODIFICATION OF TRR 616 FOR SLOPED GROUND

If the ground surface in front of the sound barrier wall is sloped, then an approximate procedure is to consider only the resistance in the passive zone in front of the drilled shaft or caisson. The assumption is that the soil in the triangle (KLM, Figure 3) does not exist and that only the passive resistance below KL should be used. In reality, the soil in triangle (KLM) will produce some resistance. However, to be more conservative, this resistance is neglected. The value of A would be determined from Equation 6.

$$A = (D \tan \theta \times \tan \beta)/(\tan \theta \times \tan \beta + 1) \quad (6)$$

where θ is the slope angle and $\beta = 45 + \phi/2$.

To use this procedure, a trial D is assumed. Then, by using the H/D ratio and α, Su can be determined from Figure 2. The actual ultimate lateral load would be the determined Su times 1.64. Trial D should result in an acceptable factor of safety. Of course, the actual embedment of the caisson or pile would be $(D + A)$. The necessary steps to determine ultimate lateral strength by using TRR 616 follow.

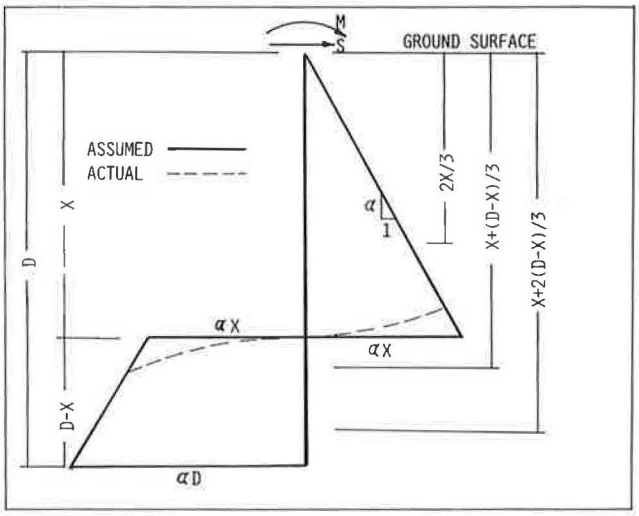

FIGURE 1 Ultimate soil resistance for cohesionless soil (*2*).

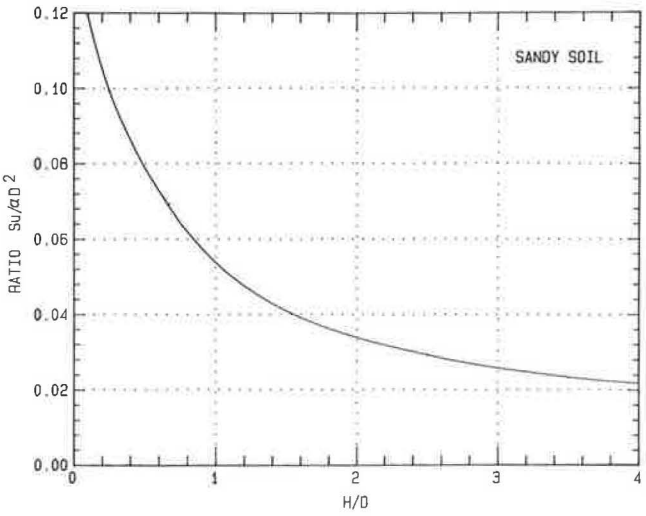

FIGURE 2 Design chart for cohesionless soil (*2*).

TABLE 1 VALUES OF μ FOR DIFFERENT TESTS (*2*)

μ	Quality of Soil Information
0.5	Good visual description possibly supplemented by standard penetration testing in general area.
0.7	Standard penetration testing or other in situ testing at location of structure.
0.9	Laboratory testing at location of structure.

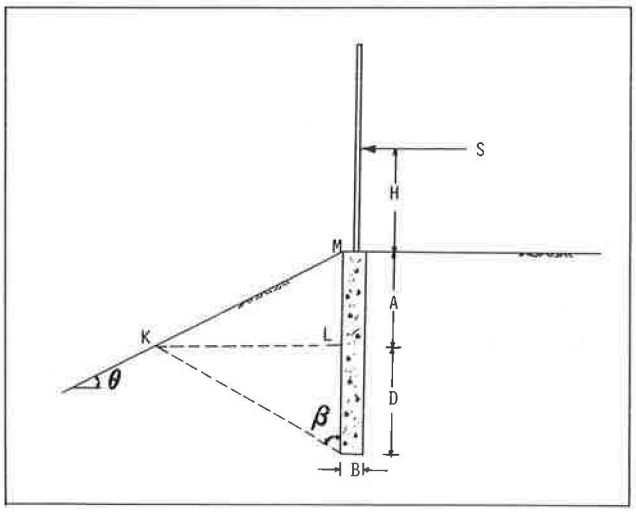

FIGURE 3 Geometry of modification in TRR 616 method for sloped ground.

Level Ground

The same geometry is used as is presented in Figure 10.

Step 1

$Su/\alpha D^2 = 0.049$ (from Figure 2 for $H/D = 1.14$)

Step 2

$\alpha = 3\gamma B \tan^2(45 + \phi/2)\mu$ (use $\mu = 0.8$)

$\alpha = 3(120)(2.0)\tan^2(45 + 30/2)0.8 = 1728$ psf

Step 3

$Su = (0.049(1728)(7)^2 = 4149$ lb

Step 4

Su (actual) $= 4149 \times 1.64 = 6{,}800$ lb

$= 6.80$ kips

Sloped Ground

Assume $D = 3$ ft for first trial and $\mu = 0.8$. (See Figure 4.)
Step 1

$\beta = 45 + 30/2 = 60$ degrees

$\theta = 26.6$ degrees (for 2 : 1 slope)

Step 2

A = (3 tan 26.6 degrees tan 60 degrees)/
(tan 26.6 degrees tan 60 degrees + 1)
= 1.39 ft (use $A = 1.5$ ft)

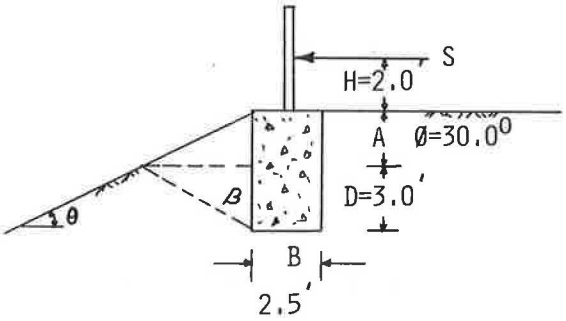

FIGURE 4 Geometry used for TRR 616 method for sloped ground.

Step 3

$Su/\alpha D^2 = 0.07$ (from Figure 2 for $H/D = 0.67$)

Step 4

$\alpha = 3(125)(2.5)\tan^2(45 + 30/2)0.8 = 2250$ psf

Step 5

$Su = (0.07)(2250)(3)^2 = 1420$ lb

Step 6

Su (actual) $= 1420 \times 1.64 = 2{,}330$ lb

$= 2.33$ kips

WOODWARD AND GARDNER METHOD

The ultimate lateral resistance for a drilled shaft or pile with a free-headed condition in cohesionless soil can be determined by using Brom's assumption that the soil passive resistance acts on three times pile diameter (*4*):

$$Su = \left(\frac{1}{2} \times B \times D^3 \times K_p \times \gamma\right)/(H + D) \quad (7)$$

where

$K_p = \tan^2(45 + \phi/2)$

Su from Equation 7 is the actual ultimate resistance. This equation is based only on the passive soil pressure, so the active pressure effect is neglected. If active pressure is also considered from static equilibrium equations, then the value of Su would be

$$Su = \gamma \times B \times D^3\left(\frac{1}{2} \times K_p - \frac{1}{6} \times K_a\right)/(H + D) \quad (8)$$

where

$K_a = \tan^2(45 - \phi/2)$

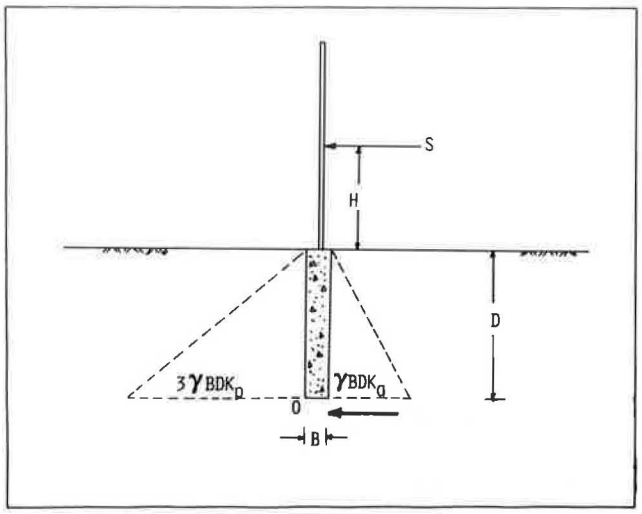

FIGURE 5 Geometry of modification in Woodward and Gardner method for level ground.

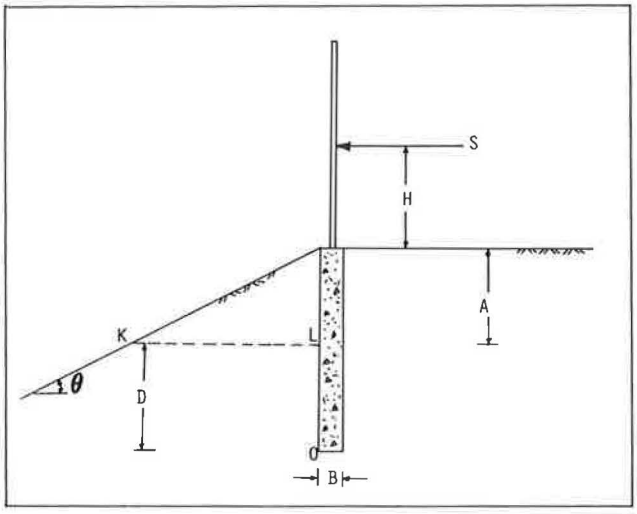

FIGURE 6 Geometry of modification in Woodward and Gardner method for sloped ground.

The calculated *Su* by using Equation 8 would be about 5 percent less than by using Equation 7. Figure 5 presents the geometry of the wall and the pile. High pressures may exist near the toe of the laterally loaded pile. For the purpose of analysis it is assumed that this pressure can be substituted by a concentrated load in Figure 5 (*3*). It also is assumed that active pressure acts only on the width of the pile or caisson. If the ground surface on the front of the wall is sloped, then the following method is proposed as a solution to achieve ultimate lateral capacity.

MODIFICATION OF WOODWARD AND GARDNER METHOD FOR SLOPED GROUND

Equation 6 also can be used to determine the section that is assumed not to contribute to passive resistance. Therefore, the actual depth of embedment would be $(D + A)$. It also is assumed that active soil pressure will act on the entire length of the pile [embedment depth, $(D + A)$] and its diameter and that passive soil pressure will act on (D) and three times the pile diameter. *Su* can be determined by using the equation of equilibrium. Figure 6 shows the geometry of the condition. It should be noted that the unit weight used is the effective unit weight of the material in the affected area.

$$P_a = \frac{1}{2} \times \gamma \times B \times (D + A)^2 K_a \tag{9}$$

$$P_p = \frac{3}{2} \times \gamma \times B \times D^2 \times K_p \tag{10}$$

By taking moments about point 0,

$$Su = \left(\frac{1}{2} \times \gamma \times B \times D^3 K_p - \frac{1}{6} \times \gamma \times B \times (D + A)^3 K_a\right)/(H + D) \tag{11}$$

It is assumed that the material above (KL) does not provide any resistance. Therefore, its effect on calculating passive force is ignored.

This method is also a trial-and-error process. A depth (D) will be assumed, and then *Su* should result in an adequate factor of safety. Again, the actual embedment for the pile would be $(D + A)$.

NEW YORK DEPARTMENT OF TRANSPORTATION METHOD

The New York Department of Transportation method was prepared to design free-headed vertical piles to resist static lateral loads (*5*). The method assumes that the structure rotates as a rigid mass at some depth below the ground surface.

This method considers level and sloped ground surfaces. The solution is in graph and table form. The geometry of the drilled shaft is first drawn. Then, the required values can be determined from related tables and graphs and can be input into the following equation to calculate the *Su* value (*5*).

$$Su = RKYGBD^2 \tag{12}$$

where

- R = resistance coefficient dependent on (H/D) and soil type,
- K = soil strength coefficient dependent on (D/B) and ϕ angle,
- Y = groundwater coefficient dependent on (Z/D) and soil type where Z is the depth to the water table, and
- G = ground slope coefficient dependent on the direction of the wind load.

B and D values are diameter (or width) and depth of the drilled shaft, respectively. Graphs and tables used in determining different coefficients are presented in Figures 7–9 and Table 2.

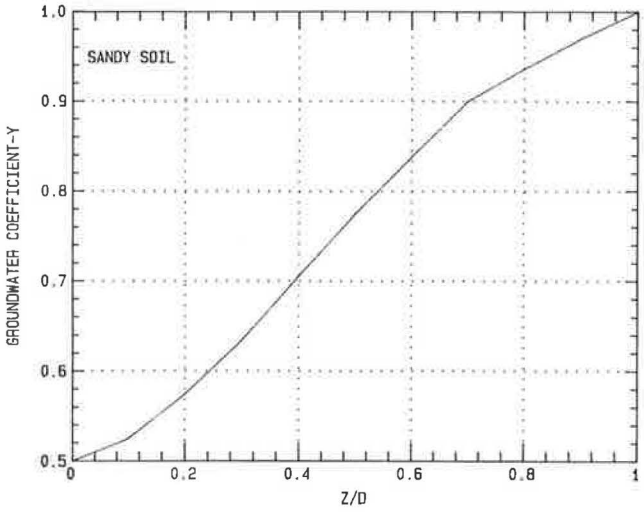

FIGURE 7 Ground water coefficient (*Y*) for use in the New York method (*5*).

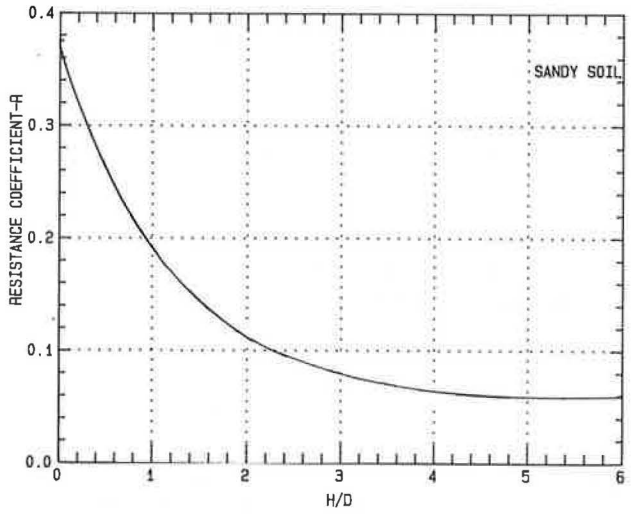

FIGURE 8 Resistance coefficient (*R*) for use in the New York method (*5*).

Some of the tables and plots are presented in this paper. However, for design purposes, the actual report that covers different soil types, effect of wall and pile weight, and other loading conditions should be used. A step-by-step solution, using this method, follows.

Level Ground

See Figure 10 for geometry.

Here, $m = n =$ level.

Step 1

$H/D = 8/7 = 1.14$ and $D/B = 7/2 = 3.5$

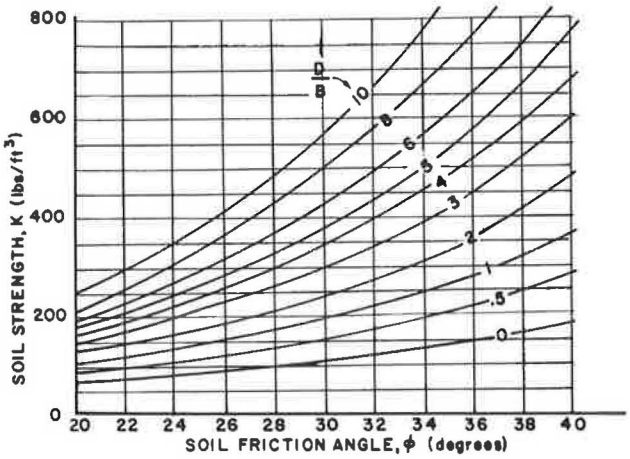

FIGURE 9 Soil strength coefficient (*K*) for use in the New York method (*5*).

Step 2

$G = 1$ (from Table 2 for $m = n =$ level)

Step 3

$Y = 1$ (from Figure 7 for $Z/D = 1$)

Step 4

$R = 0.18$ (from Figure 8 for $H/D = 1.14$)

Step 5

$K = 325$ (from Figure 9 for $D/B = 3.5$ and $\phi = 30$ degrees)

Step 6

$$Su = RKYGBD^2$$
$$= (0.18)(325)(1)(1)(2)(7)^2$$
$$= 5733 \text{ lb}$$
$$= 5.73 \text{ kips}$$

where

H = from top of pile to the actual point of loading,
D = embedment depth,
B = pile width or diameter,
m = average ground slope for a distance of $2D$ in front of pile loading,
n = average ground slope for a distance of $2D$ behind pile loading, and
Z = depth to water table.

TABLE 2 GROUND SLOPE COEFFICIENT, G, USED IN NEW YORK METHOD (5)

M \ N	-2	-3	-4	LEVEL	+4	+3	+2
-2	0.37	0.42	0.45	0.48	0.53	0.56	0.60
-3	0.46	0.55	0.58	0.60	0.66	0.70	0.75
-4	0.52	0.60	0.64	0.70	0.75	0.78	0.83
LEVEL	0.63	0.77	0.85	1.00	1.10	1.14	1.16
+4	0.73	0.90	1.10	1.27	1.55	1.64	1.67
+3	0.80	1.05	1.15	1.37	1.69	1.80	1.92
+2	1.00	1.10	1.20	1.50	2.00	2.15	2.46

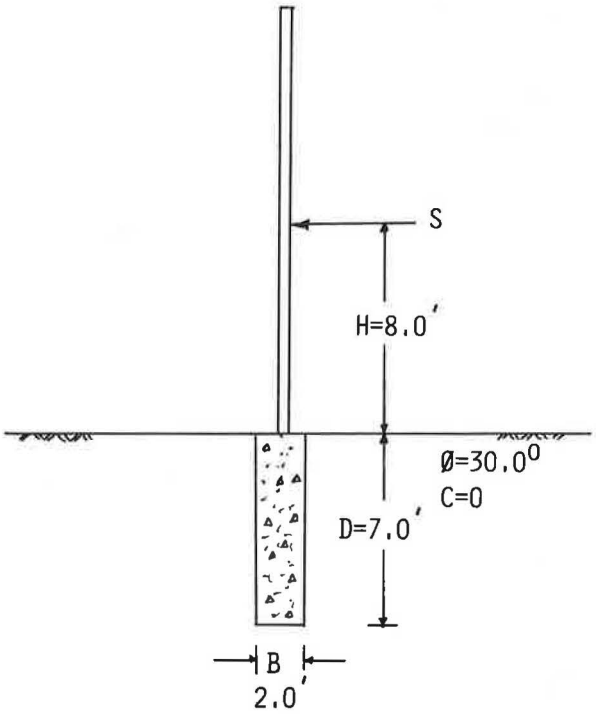

FIGURE 10 Geometry used for New York method for level ground.

Sloped Ground

See Figure 11 for geometry.
Step 1

$H/D = 2/4.5 = 0.44$ and $D/B = 4.5/2.5 = 1.8$

Step 2

$G = 0.48$ (from Table 2 for $m = -2$ and $n =$ level)

Step 3

$Y = 1.0$ (from Figure 7 for $Z/D = 0$)

Step 4

$R = 0.27$ (from Figure 8 for $H/D = 0.44$)

Step 5

$K = 240$ (from Figure 9 for $D/B = 3.5$ and $\phi = 30$ degrees)

Step 6

$$Su = RKYGBD^2$$
$$= (0.27)(240)(1)(0.48)(2.5)(4.5)^2$$
$$= 1575 \text{ lb}$$
$$= 1.58 \text{ kips}$$

where

$m = -2$ (− indicates sloping downward) (+ indicates sloping upward) and
$n =$ level.

NORTH CAROLINA METHOD

The North Carolina method was prepared for FHWA by Roy H. Borden and M. Gabr of North Carolina State University (6). They studied the base resistance contribution to the ultimate load capacity of the drilled pile or shaft. For D/B ratios greater than 4, the base resistance accounts for less than a 15 percent increase in capacity. But, the importance of the base resistance increases as the D/B ratio decreases. Borden and Gabr determined that for a D/B ratio of 2.5 the capacity could be underpredicted by as much as 25 percent if the base

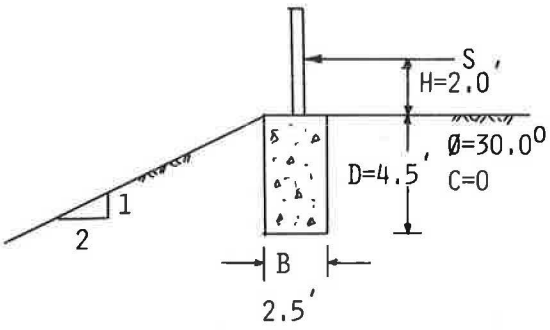

FIGURE 11 Geometry used for New York method for sloped ground.

resistance is not included (*6*). The method is computerized, and the software is called LTBASE (Lateral Pier Analysis Including Base and Slope Effect). The method uses a three-dimensional force equilibrium model to determine the ultimate lateral capacity of the piles in both cohesionless and cohesive soils.

The program is user friendly. The input data include job description and location, loading conditions, piles dimensions, soil properties, and slope effect. After the data are executed, the results are directed to three output files (*6*):

- OUTPUT PRN: Presents information about critical input data and output results for all loading increments used in the analysis.
- SUMMARY PRN: Presents a summary of applied loads, input soil properties, and pile dimensions. The computed factor of safety that depends on the predicted capacity is printed when appropriate.
- PLOT PRN: Presents special information for using output results in association with any graphic software package to produce a load-deflection plot.

This method was used to determine ultimate load capacity of piles with different embedment depths and widths in granular material. The Borden and Gabr report contains the assumption used in reaching the design procedure, modeling and equations, plus step-by-step directions for using the computer program.

WIND PRESSURE

The wind pressure can be determined by using the following equation (*7*).

$$Pw = (.003)V^2 \tag{13}$$

where Pw is the wind pressure in pounds per square foot and V is the wind velocity in miles per hour.

Wind pressure, which is assumed to act horizontally, is calculated for the entire area of the sound barrier wall. The area of a sound barrier panel is the spacing between two drilled shafts multiplied by the height of the wall. Wind moment is calculated with respect to the top of the drilled shaft.

A 25-psf wind pressure, which corresponds to a 90-mph wind (a wind velocity of not less than 75 mph is ordinarily used by designers), is usually used as the maximum wind pressure. If the local wind pressure is larger than this value, then the actual maximum wind pressure should be used in calculating wind load on the sound barrier wall. A reliable factor of safety against foundation failure of sound barrier walls is 2.0.

COMPARISON OF THE FOUR DESIGN METHODS FOR LEVEL SURFACE

The four methods were used to evaluate the capacity of some rigid piles. Also, the factor of safety for an applied wind load was determined for each procedure. In Table 3, A means New York Method (NYM); B, modified for slope or regular TRR 616 method (TRRM); C, modified for slope or regular Woodward and Gardner method (MWGM); and D, North Carolina method (NCM).

As can be seen from Table 3, NCM predicts the smallest capacities and MWGM predicts the largest values. The table indicates that MWGM values are about 25 percent larger

TABLE 3 COMPARISON OF FOUR DIFFERENT METHODS FOR LEVEL GROUND

			PILE CAPACITY Su - (KIPS)				FACTOR OF SAFETY			
EMBEDMENT DEPTH D-FT	PILE WIDTH B-FT	WIND LOAD (KIPS)	A	B	C	D	A	B	C	D
7.0	2.0	7.0	5.73	6.80	7.39	5.81	0.82	0.97	1.13	0.83
10.0	2.0	7.0	14.44	17.56	19.27	13.86	2.06	2.51	2.75	1.98
12.0	2.0	7.0	26.00	28.57	29.96	22.19	3.71	4.08	4.28	3.17

when compared with other methods. Therefore, the NYM, TRRM, and NCM methods are compatible when designing rigid pile foundations for sound barrier walls on level ground in cohesionless soils.

The results are also presented in graph form in Figure 12. All those methods follow the same trend, but MWGM values are always larger than all other values. The calculated values of the ultimate capacity load are graphically closer for smaller embedment depths. However, they become farther apart as depths increase.

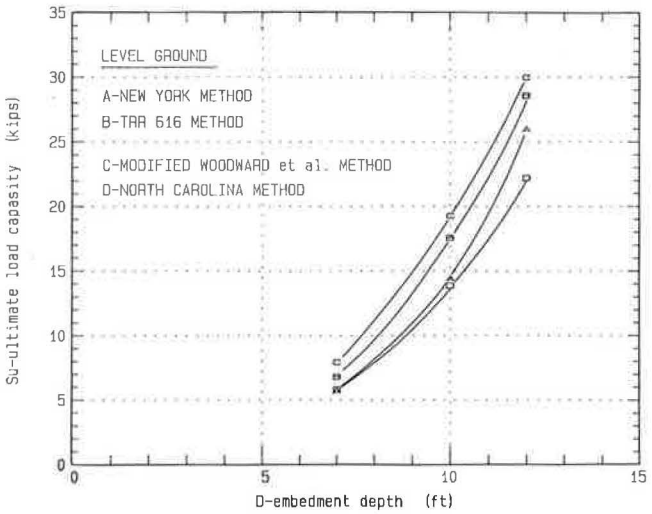

FIGURE 12 Plot of ultimate load capacity versus depth for different design methods (level ground).

COMPARISON OF THE FOUR DESIGN METHODS FOR A 2 : 1 SLOPE

The NYM and NCM are suitable for level and sloped ground. As was previously mentioned, TRR 616 and Woodward and Gardner methods were modified to handle sloped surfaces in front of sound barrier walls. The four methods were used to calculate ultimate load capacity for different drilled shaft embedment depths where the front of the wall is sloped 2 : 1 (θ = 26.6 degrees). The results are presented in Table 4.

The value of actual embedment (D) is plotted versus ultimate load capacity (Su) in Figure 13. The predicted values of Su from all four methods are very close for embedments up to 15 ft.

Su values from NYM are smaller than those from all other methods for embedment depths up to 9 ft. For embedments larger than 15 ft, the NYM-predicted Su values become much larger than those from the other three methods. It could be concluded that Su from the four methods are comparable for embedments up to 15 ft. However, for larger D values, NYM overestimates the ultimate load capacity. For embedment depths larger than 15 ft, the other three methods would result in similar values.

COMPARISON OF THE FOUR DESIGN METHODS FOR A 3 : 1 SLOPE

Ultimate load capacity was also determined from those four methods for a 3 : 1 slope (θ = 18.43 degrees). The results are presented in Table 5. Moreover, the actual embedment

TABLE 4 COMPARISON OF FOUR DIFFERENT METHODS FOR A 2 : 1 SLOPE

ACTUAL EMBEDMENT (D+A) - FT	D FT	PILE WIDTH B-FT	WIND LOAD (KIPS)	PILE CAPACITY Su - (KIPS) A	B	C	D	FACTOR OF SAFETY A	B	C	D
4.5	3.0	2.5	1.20	1.57	2.33	1.85	2.69	1.31	1.94	1.85	2.24
6.0	4.0	2.5	1.80	2.70	3.90	3.76	2.77	1.50	2.16	2.09	1.54
7.5	5.0	2.5	2.70	4.66	5.54	5.40	6.05	1.73	2.05	2.00	2.24
12.0	8.0	2.5	4.80	14.26	13.22	13.14	13.92	2.97	2.76	2.74	2.90
15.0	10.0	2.0	7.0	22.80	18.14	17.53	21.28	3.26	2.59	2.50	3.04
18.0	12.0	2.0	7.0	42.86	28.57	27.26	31.57	6.12	4.08	3.89	4.51
21.0	14.0	2.0	7.0	68.60	42.21	39.35	42.77	9.80	6.03	5.62	6.11

depth values are plotted versus the ultimate load capacity and presented in Figure 14.

Results indicate that NYM values are again smaller for embedments up to 9 ft. Also, *Su* values are very close for embedments up to 15 ft. Again, when *D/B* ratios become close to 10, NYM values become much larger than the others. Overall, the values from TRRM, MWGM, and NCM remain close.

The same results are concluded for a 3 : 1 slope for embedment depths up to 15 ft; that is, all four methods result in comparable values. But NYM overestimates the ultimate capacity for depths above 15 ft.

It should be noted that only TRRM considers a reduction factor (μ) to account for reliability of soil strength parameters. Therefore, when using the other three methods the reliability of soil parameters should be considered by using a larger factor of safety. A simple procedure is to divide the appropriate factor of safety by (μ) from Table 1 to determine the required factor of safety.

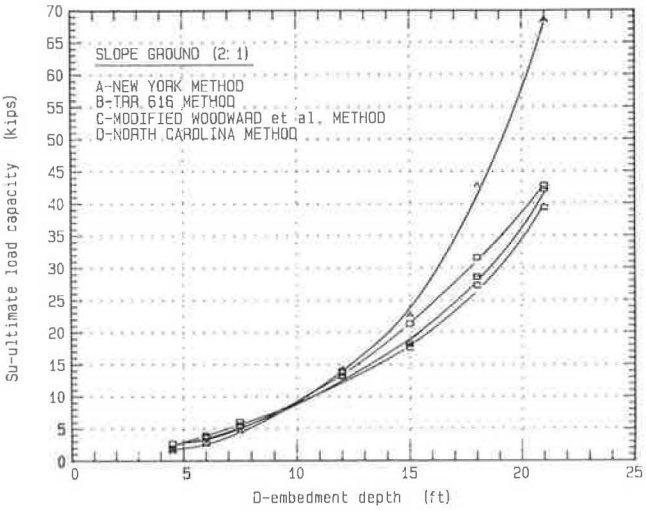

FIGURE 13 Plot of ultimate load capacity versus depth for different design methods (2 : 1 slope).

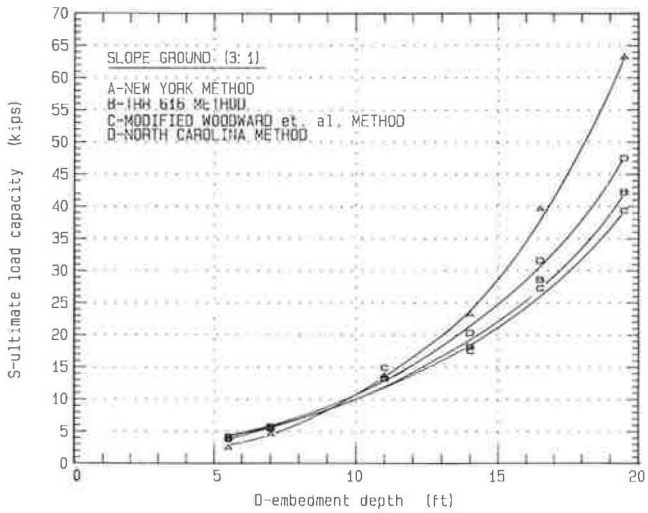

FIGURE 14 Plot of ultimate load capacity versus depth for different design methods (3 : 1 slope).

TABLE 5 COMPARISON OF FOUR DIFFERENT METHODS FOR A 3 : 1 SLOPE

				PILE CAPACITY				FACTOR OF SAFETY			
ACTUAL EMBEDMENT (D+A) - FT	D FT	PILE WIDTH B - FT	WIND LOAD (KIPS)	Su - (KIPS) A	B	C	D	A	B	C	D
5.5	4.0	2.5	1.8	2.51	3.90	3.76	4.16	1.40	2.16	2.09	2.31
7.0	5.0	2.5	2.7	4.63	5.54	5.40	5.70	1.72	2.05	2.00	2.11
11.0	8.0	2.5	4.8	13.72	13.22	14.90	13.30	2.86	2.76	3.11	2.77
14.0	10.0	2.0	7.0	23.26	18.14	17.53	20.30	3.32	2.59	2.50	2.90
16.5	12.0	2.0	7.0	39.67	28.57	27.26	31.57	5.67	4.08	3.89	4.51
19.5	14.0	2.0	7.0	63.31	42.21	39.35	47.46	9.04	6.03	5.62	6.78

CONCLUSIONS

1. The four design procedures result in close values of ultimate soil resistance for drilled piles supporting sound barrier walls constructed on level ground.
2. The TRR 616 and Woodward and Gardner methods were originally prepared for level ground surfaces but, with some modification, can also be used to determine *Su* for sloped ground surfaces.
3. All four methods result in relatively close *Su* values for embedment depths of up to 15 ft in sloped ground.
4. For embedment depths larger than 15 ft, the New York method estimates higher ultimate soil resistance than the other three methods.
5. If the embedment depth is larger than 15 ft, then the predicted value of *Su* from TRRM, MWGM, and NCM are very close.
6. The same soil parameters and reliability on those parameters should be used when comparing the four methods.

ACKNOWLEDGMENT

The author thanks the Pennsylvania Department of Transportation for providing the opportunity to conduct this study.

REFERENCES

1. *Drilled Shafts*. FHWA-HI-88-042, FHWA, Department of Transportation, 1988.
2. J. L. Davidson, C. O. Hays, and E. M. Hagan. Design of Drilled Shafts Supporting Highway Signs. In *Transportation Research Record 616*, TRB, National Research Council, Washington, D.C., 1976, pp. 62–66.
3. B. B. Broms. Lateral Resistance of Piles in Cohesionless Soils. *Journal of Soil Mechanics and Foundation Division*, ASCE, Vol. 90, No. SM3, 1964, pp. 123–156.
4. R. J. Woodward, W. S. Gardner, and D. M. Greer. *Drilled Pier Foundation*. McGraw-Hill, New York, 1972.
5. R. P. Ungerer. *Procedures for Analyzing Pole Foundations to Resist Horizontal Loads*. Report FHWA/NY/SR/86/86, New York Department of Transportation, Albany, N.Y., 1986.
6. R. H. Borden and M. A. Gabr. *Computer Program for Laterally Loaded Pier Analysis Including Base and Slope Effects*. Report FHWA/NC/87-001, FHWA, North Carolina Department of Transportation, Raleigh, N.C. 1987.
7. F. D. Henry. *The Design and Construction of Engineering Foundation*. McGraw-Hill, New York, 1956.

Publication of this paper sponsored by Committee on Foundations of Bridges and Other Structures.

Value Engineering Approach to Geologic Hazard Risk Management

JEFFREY R. KEATON AND DAVID W. ECKHOFF

Decision makers and planners need answers to four basic questions to deal responsibly with geologic and other hazards: (a) When will the hazard occur? (b) What will happen when the hazard occurs? (c) What area will be affected? (d) What can be done to reduce the risk? A perspective for evaluating in comparable terms all hazards at a site and a means for intelligent decision making based on the evaluation is the purpose here. The value engineering approach to geologic hazard risk management (*1*) is a creative effort concerned with eliminating or modifying those aspects of a system that add costs without reducing risk. The model for risk management, and the risk-based framework, permit estimation of risk costs initially for the existing conditions and subsequently for the variety of alternative responses. Selection of the optimum response to a hazard usually will be based on the least cost at some acceptable level of risk. Absolute safety is not possible, and the costs of approaching absolute safety increase exponentially. Risk costs can be considered to be expected values. Investment decisions are often based on the present worth of the expected values, on the basis of annual discount or interest rates over the design life of a facility or system. Calculation of present worth values for the variety of possible risk reduction measures permits a systematic assessment of alternatives in comparable terms to facilitate decision making. The value engineering component of this approach to geologic and other hazard risk management requires an integrated, multidisciplinary effort among geologists, engineers, seismologists, meteorologists, and socioeconomists working closely with the decision makers.

The purpose of this paper is to provide a perspective for evaluating in comparable terms all hazards at a site and a means for intelligent decision making. Value engineering (VE), an appropriate hazard management approach, is an objective, systematic method of optimizing the total cost of a facility or system for a specific number of years.

Total cost means ultimate costs to construct, operate, maintain, and replace a facility or system during its design life. The VE approach is a creative effort directed toward the analysis of functions and is concerned with eliminating or modifying those aspects that add cost without adding function or, in the case of hazards, without reducing risk.

In this context a hazard is a naturally occurring or human-induced process that has the potential to cause damage to property or injury to people. Risk is exposure of something of value to a hazard. Strong earthquake shaking is an example of a natural hazard. Citizens and facilities in the cities of San Francisco, Salt Lake City, and Memphis are at risk of injury and damage owing to shaking during a future earthquake. An earthquake occurring in an uninhabited region of the world, such as the Dasht-e-Namak in east-central Iran, certainly would be regarded as a hazard. However, no facilities would be near enough to be at risk of damage. Similarly, rocks falling from steep slopes are clearly hazardous, and a substantial population can be at risk of injury on roads next to steep-cut slopes. However, in areas where no population is exposed to potential injury, no risk would be associated with the rockfall hazard.

Systematic evaluation of hazards and risks permits assessment of the costs associated with alternative responses that provide an acceptable level of risk of damage. Figure 1 is a model of geologic hazard risk management. The initial phase in the assessment is recognition of the hazard, and failing to recognize or ignoring hazards may lead to liability for damage caused by the hazards. Once hazards are recognized, they may be evaluated in terms of the frequency or probability of damage intensities. Risks may be evaluated in terms of the extent of exposure and consequence of damage. Selection of an acceptable level of risk can be very difficult and, in many cases, is a public policy issue.

Five alternative responses exist and should be assessed sequentially (see Figure 2). A segment of highway subjected to rockfall hazards provides a useful example of the five alternative responses. The first possible response is to continue current practices, and this is the so-called "do nothing" alternative. In the context of the rockfall example, continuing current practices would constitute removing rock debris from the roadway and repairing damaged pavement on an as-needed basis. It could also include settling legal claims for damage to cars or personal injury. If continuing current practices meet the risk acceptability criteria, then present-worth costs are estimated and stored for comparative purposes. If the risk acceptability criteria are not met, then the costs need not be estimated.

The second response is to modify the hazard. In the context of the rockfall example, modifying the hazard could include measures to prevent rocks from falling from the slope or to prevent rocks from falling onto the roadway. Engineering measures to accomplish such prevention could consist of bolting or strapping rocks on the slope or draping wire mesh on the slope.

The third response is to modify the system at risk. In the context of the rockfall example, modifying the system at risk could include constructing a rock deflection shed to protect the roadway from falling rocks or placing Jersey walls along the shoulder of the road to prevent rocks from rolling onto the roadway.

The fourth response is to modify system operation. In the context of the rockfall example, modifying system operation could include placing signs warning of the rockfall hazard in

J. R. Keaton, Sergent, Hauskins and Beckwith Engineers, 4030 S. 500 W., Salt Lake City, Utah 84123. D. W. Eckhoff, Eckhoff, Watson and Preator Engineering, 1121 E. 3900 S., Salt Lake City, Utah 84121.

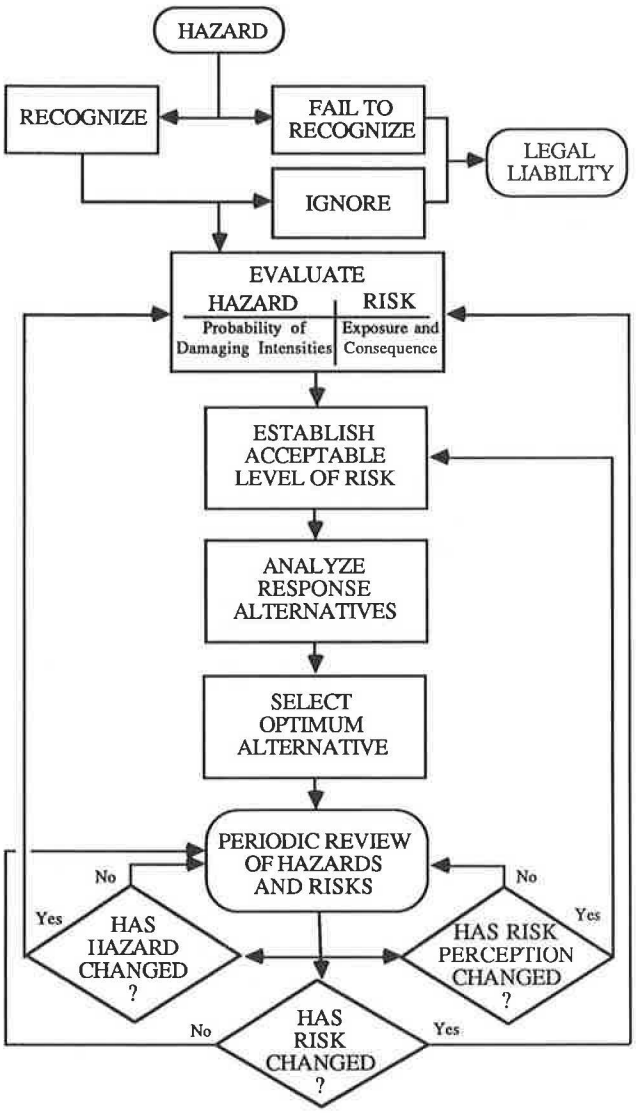

FIGURE 1 A model for geologic hazard risk management [Adapted from Keaton (*1*, p. 238).]

an attempt to get motorists to be more cautious and alert and to limit legal liability in the event of damage or injury resulting from rockfall.

If the risk acceptability criteria are not met by any of the four responses, then the acceptable level of risk may be so small that it approaches absolute safety. The fifth alternative response is to avoid the hazard regardless of the cost. In the context of the rockfall example, avoiding the hazard would require relocating an existing road or abandoning a possible alignment of a proposed road. Deciding to avoid a hazard can be particularly difficult for existing facilities that may have to be abandoned. Risk management is an iterative process with continuous checking for changes in the hazards or in the risks or the perception of acceptable risk (see Figure 1).

DECISION MAKER'S QUESTIONS

Decision makers and planners need answers to four basic questions to deal responsibly with geologic hazards.

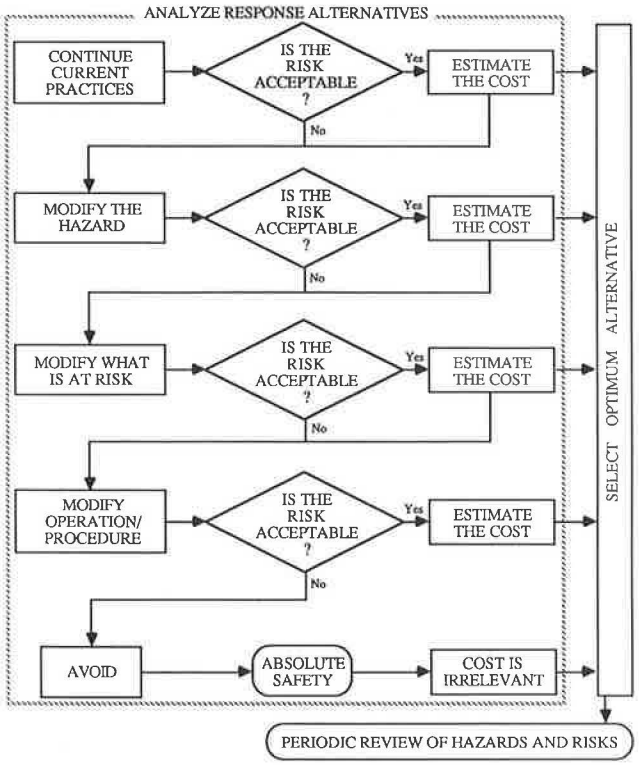

FIGURE 2 Alternative responses to geologic hazards. [Adapted from Keaton (*1*, p. 240).]

When Will the Hazard Occur?

This is a difficult question for two reasons. First, hazards are natural processes that occur at potentially damaging intensities. Second, precisely predicting the occurrence of a hazard is not presently possible. Microearthquakes and runoff from gentle rains occur frequently with no resulting damage. Major earthquakes and flooding from very heavy rains occur less frequently with some resulting damage. Intensities ranging from "no damage" to "total damage" are possible depending on the quality of construction and the character of the hazard.

Weather forecasting provides a good example of the predictability of natural processes. The traditional question "Will it rain tomorrow?" really is not the correct question for hazard analysis. A better question would be "Will a damaging flood occur tomorrow?" or "Will crops or property be damaged by a hailstorm?" Weather forecasting is based on regional weather data over the past 24 to 48 hours and on a previously developed understanding of regional weather patterns. Thus, weather forecasting is relatively easy to understand, and, in most cases, if the forecast is wrong, then no one is injured to the extent that lawsuits are filed against the forecaster. Further, weather forecasts are put in terms of probabilities (e.g., a 20 percent chance of rain tomorrow in the forecast area). The chance of rain anywhere on earth approaches 100 percent almost all the time. Such a forecast is not meaningful to most people. For example, more meaningful forecasts would describe the chance of rain along the Atlantic seaboard or, more specifically, in Washington, D.C.

Forecasting earthquakes is much more troublesome. The real question to be answered is, "When will damage occur in

St. Louis, Missouri, owing to earthquake shaking?" This question is directed at the issue of local moderate earthquakes and of distant major earthquakes. Clearly, major earthquakes in California will be too far away to cause damage in St. Louis. An adequate analysis of earthquake hazards in St. Louis needs to focus on earthquake sources within about 200 miles of the city. Earthquake hazards are evaluated by assessing historical earthquake patterns (historical seismicity) and by evaluating geologic features (faults) capable of generating earthquakes (paleoseismicity).

One of the fundamental laws of geology is called the Law of Uniformitarianism and states that processes operate today in more or less the same way as they acted throughout geologic time; that is, the present is the key to the past. This law helped early geologists interpret rock formations of sandstone and conglomerate as ancient stream channels.

The Law of Uniformitarianism needs to be amended for application to hazard analysis. The engineering geology corollary is, "The recent past is the key to the near future." Thus, for hazards such as earthquakes and landslides the geologic record must be examined for evidence that such processes occurred in the recent past (the most recent 10,000 years or more, depending on the nature of the facility). If such evidence exists, then the magnitude and frequency of such occurrences must be estimated to predict the probability that future events will occur. Those probabilities can be annualized or averaged over project lifetimes. Annual probabilities are needed by actuaries who set insurance premiums. Project life probabilities are more useful for those who make decisions about engineering design and site selection.

What Will Happen When the Hazard Occurs?

The assessment of the effects of a hazard usually is based on two other questions: (a) What has happened in similar events in the immediate area and elsewhere? (b) How fragile is the feature or structure at risk? An important issue in the context of those questions is the contrast between planned new facilities and existing old facilities. Planned facilities can be designed to accommodate the forces of infrequent hazards, but significant uncertainty commonly is associated with many design details of existing facilities.

Structural damage and damage to building components and contents are easy to visualize and to understand. An issue commonly overlooked is business interruption or loss of function. Critical facilities—those needed during and immediately following natural disasters—clearly have a smaller tolerance for interruption than do noncritical facilities. Some critical facilities are hospitals, fire stations, police stations, and schools.

What Area Will be Affected?

Damage usually is greatest close to the "center" of a hazard and diminishes with increasing distance. Flood damage usually is concentrated along the margins of stream channels. Landslide damage usually is confined to the landslide itself.

A notable exception to this generalization is the Thistle landslide, which occurred in central Utah in 1983. The landslide disrupted the ground over which a major highway and a major railroad crossed. No facilities were built on the slide mass itself. Thus, immediate damage caused by the moving earth of the landslide was restricted to a highway and a railroad. Secondary damage was caused by a lake that formed behind the landslide and dammed the Spanish Fork river. The lake inundated the small community of Thistle. The threat of tertiary damage owing to catastrophic release of water in the event the landslide dam failed was great. Thus, much money and effort were used to reinforce the landslide dam and to drain the lake. Also, the Denver and Rio Grande Western Railroad was losing approximately $1 million each day they could not use their tracks past the landslide. Coal miners in central Utah were furloughed until coal could be shipped by rail to Wasatch Front markets. Travelers were forced to go hundreds of miles out of their way because the landslide blocked the only transportation route across the northern Wasatch Plateau to central Utah. Thus, although the damage owing to primary and secondary hazards was significant, losses owing to business interruption and travel inconvenience probably were greater.

The example of the Thistle landslide clearly demonstrates that assessing the area that could be affected by a hazard is complicated, particularly when potential business interruption is included.

What Can Be Done to Reduce Risk?

The answer to the question of what can be done to reduce risk depends on the specific characteristics of the hazard, and the reader is referred to the discussion of alternative responses to hazards (Figures 1 and 2). Proposed facilities, for relatively little additional cost, can be designed to resist the forces of infrequent hazards or be located to avoid them. Conversely, existing facilities require significant additional cost to be upgraded and strengthened to resist larger forces than was originally anticipated. Further, business interruption costs can be substantial while upgrading is done. The costs of alternative responses must be compared to the probability of occurrence of hazards and the potential losses (dollar-value damage, personal injury, and business interruption). An innovative method of addressing this complicated issue is value engineering in a risk-based framework.

RISK-BASED FRAMEWORK

A risk-based method for assessing possible improvements for dam safety was developed by Bowles et al. (*2*) and consists of four elements: risk identification, risk estimation, risk aversion, and risk acceptance. Those elements, modified to reflect sedimentation hazards on arid region alluvial fans, are presented in Figure 3. The risk identification element involves listing the various factors that could contribute to potential losses and then organizing those into logical event sequences that cover all expected events and responses. Such event sequences commonly are configured into event trees that serve as risk models for evaluating existing conditions and the effectiveness of proposed mitigation or aversion alternatives. The risk estimation element involves assigning probabilities to each branch of the event tree model and then assessing the con-

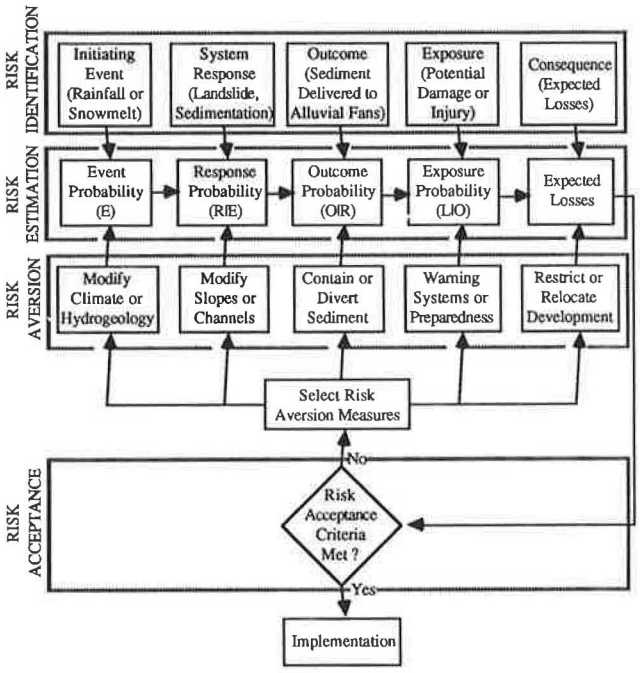

FIGURE 3 Risk-based method for assessing hazards and responses. From Keaton (*1*, p. 174) after Bowles et al. (*2*).

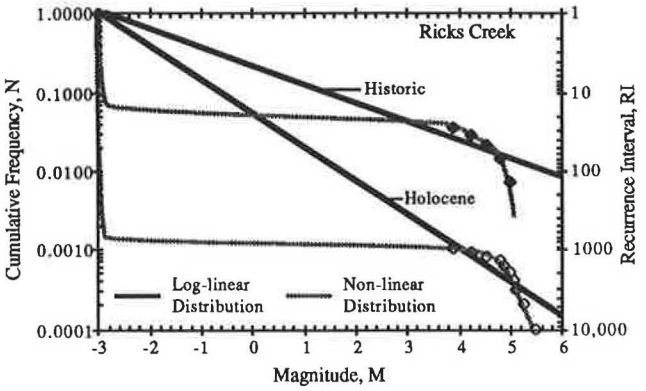

FIGURE 4 Annual frequency of sedimentation events as a function of event magnitude. Modified from Keaton (*1*, p. 394).

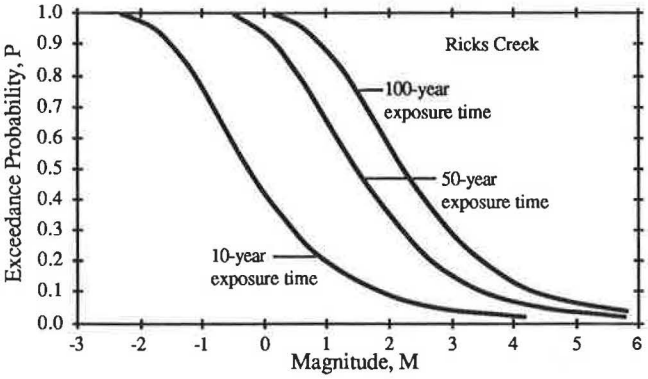

FIGURE 5 Exceedance probability curves for sedimentation events. Based on an average of the magnitude-frequency relationships shown on Figure 4. From Keaton (*1*, p. 223).

sequences of each event and response along separate pathways in the event tree. If the expected losses (damage or injury or both) are unacceptable under existing conditions, then some form of risk aversion may be desired to reduce the probability associated with an initiating event, a system response, or an outcome or to reduce the exposure to the hazard. (Alternative responses for dealing with hazards were described earlier and are shown in Figure 2.) The risk acceptance element is involved with deciding what degree of safety is appropriate or what residual risk will be accepted.

A complete hazard evaluation of potentially damaging processes consists of (a) identifying locations, (b) estimating frequencies, (c) estimating magnitudes, (d) estimating the rates at which they occur, (e) estimating durations, (f) estimating the certainty with which they can be forecast, and (g) estimating possible effects. Those seven components of hazard evaluation must be addressed in a quantitative way to answer the four questions just discussed.

A relationship appears to exist between frequency and magnitude. Large magnitude events (earthquakes, floods, sediment delivery) appear to occur less frequently than do small magnitude events. This relationship for sedimentation events is presented in Figure 4 in terms of annualized frequency versus event magnitude. Two types of relationships are indicated on this figure: a straight line (linear) relationship and an irregular line (nonlinear) relationship. Because the annual frequency is represented as a logarithm, the straight line relationship is actually a log-linear relationship. (Mathematical expressions can be developed to describe those relationships, but the discussion of the expressions is beyond the scope of this conceptual paper.) The important issue displayed by Figure 4 is that small events occur relatively frequently and that large events are rare. For example, an annual frequency of 1.0 (shown on the left side of Figure 4) means that events of the size corresponding to that frequency occur (or recur) on average every year (shown on the right side of Figure 4).

Magnitude-frequency relationships may be transformed into exceedance probabilities, as presented for sedimentation events in Figure 5. The same procedure is commonly used for earthquake or flood risk assessment. Exceedance probabilities may be developed for normal (evenly distributed about a mean value) and extreme-value (skewed about a mean value) distributions of event magnitudes. Detailed discussion of those distributions of event magnitudes is beyond the scope of this paper, but a brief description is presented in the Appendix. However, knowledge of those distributions is needed for quantitative estimation of probabilities needed in risk evaluation.

The risk estimation element of the method developed by Bowles et al. (*2*) (see Figure 3) is expressed in terms of the probabilities of events, responses, and outcomes. Their risk model is in the form of an event tree with a number of pathways that represent an outcome associated with a response to an event. For an event tree with n possible mutually exclusive pathways, Bowles et al. (*2*, p. 216) report that the pathway probability for the ith pathway is

$$P(Pi) = P(E)P(R|E)P(O|R) \quad (1)$$

where $P(Pi)$ is the pathway probability for the ith pathway, $P(E)$ is the probability that event E will occur, $P(R|E)$ is the conditional probability that response R will occur given that event E occurs, and $P(O|R)$ is the conditional probability that outcome O will occur given that response R occurs. The partial risk cost for the ith pathway is

$$C(Pi) = P(Pi) \cdot Le \tag{2}$$

where Le is the possible economic loss. The total risk cost (C) is obtained by summing the partial risk costs over all n mutually exclusive pathways in the event tree or

$$C = \sum_{i=1}^{n} C \cdot (Pi) \tag{3}$$

For a population at risk (PAR), the magnitude of life loss (Ll) owing to events along the ith pathway is given by

$$\text{Ll} = P(L|O) \cdot \text{PAR} \tag{4}$$

where $P(L|O)$ is the conditional probability of life loss L given that outcome O occurs.

An example of a hypothetical event tree for earthquake-induced rockfall damage to a highway is presented in Figure 6. The initiating event (see Figure 3) is an earthquake subdivided into three magnitude ranges. The event probabilities [$P(E)$], annualized in this example, are developed from analyses similar to those shown in Figures 4 and 5. In this simplified example, each of the three event magnitude ranges has five possible system responses, resulting in 15 possible pathways. However, only those five pathways related to the middle event magnitude are presented in Figure 6. The annualized conditional probabilities for system response given the initiating event [$P(R|E)$] are estimated on the basis of past performance of, in this example, the slope above the highway. The occurrence of a rockfall or slope failure does not necessarily imply damage to a system or a facility at risk. Therefore, each of the 15 possible system response pathways has five possible outcome pathways, resulting in 75 possible pathways. However, only those five pathways related to the middle response are presented in Figure 6. The annualized conditional probabilities for outcome given the system response [$P(O|R)$] are estimated on the basis of the geometry and past performance of the slope, the location of the highway, and the possibly seasonal aspect of slope performance (e.g., an earthquake occurring during or shortly following the rainy season).

Annualized pathway probabilities [$P(Pi)$] are the product of the individual annualized probabilities just described. Possible economic loss [Le] in this example is restricted to capital cost of reopening the road and repairing damage. Many other costs, much more difficult to estimate than repair costs (e.g., business interruption costs), would be considered in an actual probabilistic evaluation of the risk of damage to a highway. The partial annualized risk costs [$C(Pi)$] are the product of the possible economic losses and the pathway probabilities. The total annualized risk cost is the sum of the partial risk costs for all 75 mutually exclusive pathways in this simplified example.

PROBABILISTIC EVALUATION

The probabilistic analysis to this point has focused on the probabilities and costs of individual components of potential hazard occurrences. Similar event trees as those presented in Figure 6 would be developed for the variety of possible hazards (nonearthquake landslides, flooding, hail storms, wind storms). Decisions must be made about dealing with the hazards, and probabilistic methods provide the basis for such decisions.

Earthquake and flood hazards commonly are evaluated on the basis of the probability that a certain size of event will be equalled or exceeded in a specified period of time, known as exceedance probability. The specified period of time represents an exposure time and commonly is called a "design life" or an "economic life" for the facility or feature under consideration. Earthquake engineering commonly employs two levels of "design" earthquake events: a lower-level event (LLE) and an upper-level event (ULE). The LLE is an event that has a relatively high probability of occurring during the design life, and the ULE has a relatively low probability. Consequently, the LLE has a smaller magnitude (hence, lower level) than does the ULE (hence, upper level). Typical design lives range from as little as 10 years to as much as 100 years or more, depending on the critical or noncritical nature of the facility. Commonly accepted probabilities for design range

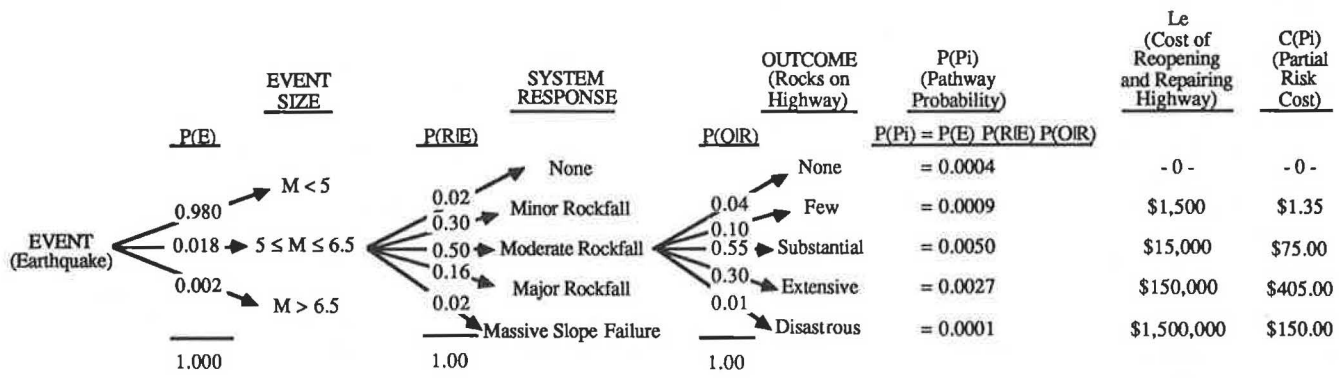

FIGURE 6 Part of a hypothetical event tree for earthquake-induced rockfall damage to a highway.

from 50 to 10 percent. For example, the LLE usually is taken as the earthquake acceleration that has a 50 percent probability of being equalled or exceeded during a 50-year period, and the ULE has a 10 percent probability in the same 50 years. Urban flood hazards commonly are evaluated in the context of the "100-year" floodplain, which is that area with an annual probability of 0.01 that it will be inundated by flood waters. A "100-year" flood has a probability of 0.63 of occurring during a 100-year design period or 0.39 of occurring during a 50-year design period.

It is at this point that a most difficult question must be addressed: How safe is safe enough? This question commonly is not addressed uniformly with respect to a variety of hazards. Usually only those hazards regulated (e.g., floods and earthquakes) are considered. Consequently, a de facto acceptance of risk, even if the risk is unacceptable, results for those hazards not considered specifically. Therefore, systematic assessment of all hazards and alternative responses promotes intelligent decision making.

VALUE ENGINEERING APPROACH

The value engineering approach to geologic hazard risk management described by Keaton and Eckhoff (*3*) is a creative effort concerned with eliminating or modifying those aspects of a system that add cost without reducing risk. The model for risk management (Figures 1 and 2) and the risk-based framework (Figure 3) permit estimation of risk costs initially for the existing conditions and subsequently for the variety of alternative responses. Selection of the optimum response to a hazard normally will be based on the least risk at the least cost. Absolute safety is not possible, and the cost of approaching absolute safety increases exponentially. (This concept is portrayed schematically in Figure 7.) The annualized risk cost is optimized for a hazardous event that has a moderate probability of occurring and a moderate cost of potential losses. This is true because higher costs of potential losses correspond to low probabilities of occurrence, and higher probabilities correspond to low potential costs. This can be seen in the partial risk cost column in Figure 6.

The risk costs can be considered to be expected values. Investment decisions usually are based on the present worth of the expected values. Present worth (PW) is calculated on the basis of annual discount or interest rates (i) over the period of time of interest or the design life of a facility or system (t) in the following way:

$$\mathrm{PW} = \sum_{n=1}^{t} (\mathrm{CEV}) \cdot (1 + i)^{-n} \tag{5}$$

where CEV is the annualized expected value of the risk cost and n is incremented 1 year at a time for the total facility life. Calculation of present worth values for the variety of possible risk reduction measures permits a systematic assessment of alternatives in like terms that can facilitate decision making. Similar calculations can be made for the present worth of future operating and maintenance costs.

The value engineering approach to geologic hazard risk management requires an integrated multidisciplinary effort among geologists, engineers, seismologists, meteorologists, and socioeconomists working closely with decision makers.

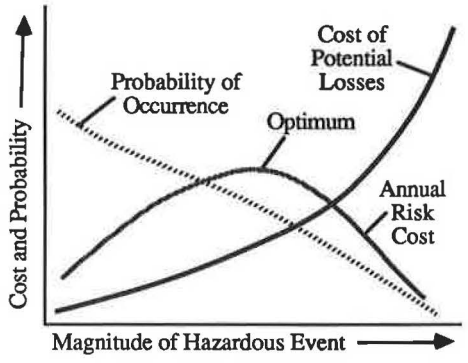

FIGURE 7 Schematic diagram showing optimization of annualized risk cost.

APPENDIX

The annual frequency of sedimentation events at Ricks Creek, Davis County, Utah, presented on Figure 4, was calculated on the basis of observations of the number and size of the events deduced from geomorphic expression and stratigraphy of the alluvial-fan deposits. Two distributions are shown on Figure 4 for two time frames. The two distributions are log-linear and non-linear. The two time frames are historic (the past 140 years in this part of the Wasatch Front in north-central Utah) and Holocene (approximately the past 10,000 years, or post-Lake Bonneville time). The sediment discharge events shown on Figure 4 are listed in Table A1.

Cumulative frequencies, NPR, were calculated by the Weibull plotting position formula:

$$\mathrm{NPR} = \frac{\mathrm{Re}}{(\mathrm{PR} + 1)} \tag{A1}$$

where Re is the event rank and PR is the period of record. The sediment event volume was converted to an event magnitude by defining magnitude M as a dimensionless parameter:

$$M \equiv \log \frac{V}{Vo} \tag{A2}$$

where V is the event volume in m^3 and Vo is 1 m^3. The mean log-linear relationship for the historic data at Ricks Creek is

$$\log N_{\mathrm{PR}} = -0.674 - 0.236 \cdot M \qquad (n = 6;\ r^2 = 0.951) \tag{A3}$$

and for the Holocene data is

$$\log N_{\mathrm{PR}} = -1.255 - 0.432 \cdot M \qquad (n = 11;\ r^2 = 0.975) \tag{A4}$$

The nonlinear relationship is manipulated with extreme-value statistics (*4*) and is based on the mean and standard deviation of the sample population along with reduced extreme-

TABLE A1 SUMMARY OF SEDIMENT DELIVERY EVENTS AT RICKS CREEK FAN, DAVIS COUNTY, UTAH

Year	Volume (m^3)	Magnitude ($\log \frac{V}{V_o}$)
Prehistoric	315,000	5.50
Prehistoric	183,000	5.26
Prehistoric	132,000	5.12
Prehistoric	118,000	5.07
Prehistoric	80,000	4.90
1923	72,000	4.86
1930	100,000	5.00
1932	34,000	4.53
1934	22,000	4.34
1983	8,000	3.90

value mean and standard deviation. All years during the 140-year historic period in Davis County without documented sediment delivery were assumed to have actually experienced 0.001 m^3 of sediment ($M = -3$). The historical mean magnitude at Ricks Creek was calculated to be -2.731 with a standard deviation of 1.404. Gumbel's (*4*, p. 228) reduced extreme-value mean for $n = 140$ is 0.56369 with a standard deviation of 1.22157.

Exceedance probabilities were evaluated with binomial and Poisson statistics for the Holocene period and with extreme-value statistics for the historical period. The results of those two methods of analysis were averaged and presented in Figure 5. The different methods of analysis were believed to better represent reality, as described by Keaton (*1*). The binomial and Poisson methods gave results that were not statistically different. The binomial exceedance probability relationship is

$$P(e \geq M, t) = 1 - (1 - N_{PR,M})^t \quad \text{(A5)}$$

where $P(e \geq M, t)$ is the exceedance probability that an event e will equal or exceed a magnitude M in a period of time t, and $N_{PR,M}$ is the annual frequency of events of magnitude M in a period of record PR. Thus, Equation A4 can be solved for N_{PR} as a function of M:

$$N_{PR} = 10^{(-1.225 - 0.432M)} \quad \text{(A6)}$$

The extreme-value exceedance probability relationship is

$$P(e \geq M, t) = 1 - e^{-te^{-A(M-U)}} \quad \text{(A7)}$$

where

$$A = \left(\frac{\sigma_G}{\sigma_M}\right) \quad \text{(A8)}$$

$$U = \mu_M - \left(\frac{\mu_G}{A}\right) \quad \text{(A9)}$$

where μ_G and σ_G are the mean and standard deviation of the reduced extreme value for the period of record and μ_M and σ_M are the mean and standard deviation of the observations that are reported for Ricks Creek.

REFERENCES

1. J. R. Keaton. *A Probabilistic Model for Hazards Related to Sedimentation Processes on Alluvial Fans in Davis County, Utah*. Ph.D. thesis. Texas A&M University, College Station, 1988.
2. D. S. Bowles, L. R. Anderson, and T. R. Glover. Design Level Risk Assessment for Dams. In *Dynamics of Structures* (J. M. Roesset, ed.), ASCE, New York, 1987, pp. 210–225.
3. J. R. Keaton and D. W. Eckhoff. A Value Engineering Approach to Geologic Hazard Risk Management [abstract]. *Association of Engineering Geologists Abstracts and Program*, Kansas City, 1988.
4. E. J. Gumbel. *Statistics of Extremes*. Columbia University Press, New York, 1958.

Publication of this paper sponsored by Committee on Exploration and Classification of Earth Materials.

Predictive Modeling of Roadway Costs in Northeastern Nigeria

JOSEPH O. AKINYEDE, A. KEITH TURNER, AND NIEK RENGERS

Road investments often exceed 20 percent of the development budget in most developing countries, such as Nigeria. Fast-growing population and economic development require an expanded road network. Application of probabilistic analysis methods during the early planning, or pre-engineering, phases allows for the prediction of probable construction and maintenance costs. Satellite remote sensor imagery can supply quantified descriptions of terrain conditions. When this information is digitized and stored in a Geographic Information System, a data base is created that can be queried to produce appropriate predictive models for roadway construction and maintenance costs. Those can, in turn, create a series of predictive economic roadway development models that reflect alternative design scenarios. Definition of the most economical routes that satisfy the constraints can be automatically produced by optimization algorithms based on linear programming techniques. The results are summarized of a study conducted over the past 3 years at the International Institute for Aerospace Survey and Earth Sciences (ITC), in Enschede, The Netherlands, which developed and tested those methods for road planning in northeastern Nigeria.

Investment on roads accounts for a substantial proportion, often in excess of 20 percent, of the development budget in most developing countries, such as Nigeria. Fast-growing population and economic development require an expanded road network. Previously, the identification of routes with the lowest construction and maintenance costs had been based mainly on scanty information from small-scale geological maps and from often inadequate topographic data. As a consequence, unforeseen geotechnical problems frequently were encountered at the time of detailed final ground surveys or during construction and, because the problems could affect a considerable length of road, led to greatly increased construction or maintenance costs.

A number of researchers in the 1970s began to quantify road construction and maintenance costs. The MIT Highway Cost Model (*1*) and the subsequent Road Transport Investment Model developed by the British Transport and Road Research Laboratory (*2*) were used to study the design and operation of specified roadway links in developing countries. Those models required a detailed specification of the alignment and were suitable for engineering design support, the evaluation of alternatives, and similar activities in the preconstruction phase. Those models do not address the selection of the general transportation corridor or route.

J. O. Akinyede, and I. N. Rengers, Department of Earth Resource Surveys, International Institute for Aerospace Survey and Earth Sciences (ITC), 7500 AA Enschede, The Netherlands. A. K. Turner, Department of Geology and Geological Engineering, Colorado School of Mines, Golden, Colo. 80401.

Application of similar, but more generalized, probabilistic analysis methods during the earlier planning, or pre-engineering, phase should allow the prediction of probable construction and maintenance costs. The use of satellite remote sensor imagery, supplemented by aerial photography when available, can supply quantified descriptions of terrain conditions. Those data sources greatly improve the information available to the road system planners. When this information is digitized and stored in a Geographic Information System (GIS), a data base is created that can be queried to produce appropriate predictive models for roadway construction and maintenance costs and can, in turn, create a series of predictive economic roadway development models that reflect alternative design scenarios. Definition of the most economical routes that satisfy the constraints can be automatically produced by optimization algorithms based on linear programming techniques. The feasibility of those techniques has been studied by Akinyede (*3*) during the past 3 years at the International Institute for Aerospace Survey and Earth Sciences (ITC), in Enschede, The Netherlands.

DEVELOPMENT OF THE TERRAIN DATA BASE

An initial test area, covering about 25,000 km^2 in northeastern Nigeria, was selected for study in cooperation with the Nigerian Federal Ministry of Works. Following extensive regional terrain analysis by using a variety of satellite remote sensor systems, two smaller test areas, 4500 and 600 km^2, were selected for detailed study.

Description of the Test Area

Northeastern Nigeria includes a geological rift zone, the Benue Trough, created when South America separated from Africa. As a consequence the area is variable both topographically and geologically. The terrain is characterized by rugged hilly regions underlain by granite and sandstone, sedimentary and volcanic plateaux, isolated steep volcanic plugs, and low swampy plains. These features combine to form some of the most variable and attractive scenery in Nigeria.

A Precambrian basement complex, dominated by granites and gneisses, underlies considerable areas. The rocks are overlain by Cretaceous sedimentary rocks, predominantly sandstones and shales of both marine and continental origin. The older sedimentary rocks are complexly folded and create long ridges. The younger rocks are more gently folded. All are faulted. Younger Quaternary sediments are found in the

northern portions of the area and to the south are volcanic flows and vents. The geology has been mapped and described in detail (*4*, *5*).

This variety of conditions creates potential problems and opportunities for road construction. Some regions have abundant high quality sources of aggregates and others have few or none. Highly plastic "black cotton" clay soils are found in areas of basalt flows. Laterite soils are common in many areas and are especially persistent in the north.

Definition of the Land Systems Mapping Units

Terrain information was developed by applying techniques of land systems classification. The terrain is assessed on the basis of certain geologic, geomorphic, and geotechnical characteristics spatially related to the ground by defining areas (land systems and land facets), each of which is characterized by essentially uniform characteristics.

The method is hierarchical. Over broad regions, and at small scales of mapping, major land systems are defined on the basis of similar landforms, rocks, and soils. At a more detailed level, land facets may be defined that have uniform slopes, soils, and hydrologic conditions. The land systems classification has gained wide acceptance as a highway planning methodology in many developing countries, including Nigeria (*6–8*).

Initial land systems were defined in this project by applying standard visual photointerpretation methods to Landsat Thematic Mapper (TM) satellite imagery and to Side Looking Airborne Radar (SLAR) imagery. Subsequently, two more detailed test areas (the Ngamdu and Gongola areas) were selected and further evaluated by using SPOT satellite images and some aerial photography. Those studies developed 8 major land system units, 19 major sub-units, and 30 detailed Land System Mapping Units (LSMUs) within the two test areas.

Geographic Information System

The outlines of those LSMUs were digitized and stored, along with their attributes, in a GIS relational data base. An IBM-PC-based software system was used. The system, called ILWIS, was developed at the ITC for use in developing countries (*9*). Figure 1 presents the basic system.

ILWIS includes a spatially oriented image data base and an associated nonspatial attribute data base as is shown by Figure 2. The image data base contains a digital representation of the study area map, defined as a series of lines (arcs) and points (nodes), that combine to form a sequence of map units (polygons). Each LSMU (the ILWIS developers prefer the term Terrain Mapping Unit or TMU) is defined by one or several polygons in the image data base.

The associated attribute data for each LSMU use a commercial relational data base product called ORACLE. A series of numerical models can be created, according to specified algebraic and logical rules defined by the ILWIS user. The composition and structures of those data bases are described by Akinyede (*3*). The following sections describe the concepts underlying the predictive roadway cost models developed by using ILWIS capabilities.

FIGURE 1 Typical ILWIS hardware installation.

DEVELOPMENT OF PREDICTIVE COST MODELS

A series of predictive cost models was developed that use the available terrain data elements to estimate probable roadway construction or maintenance costs. Construction costs are estimated in terms of grading costs, pavement costs, and drainage structure costs.

Grading Cost Prediction Model

Grading costs are calculated by using estimates of cut and fill operations developed from data defining the terrain roughness and material excavation characteristics. Typical grading costs for a specified length of roadway may be predicted by multiplying the volumes of cut and fill required by the unit costs of excavation, handling, and placement of those materials.

Determining Cut or Fill Volumes

A roadway, of width L, crossing a typical symmetrical V-shaped valley, may be supported by a fill volume having a maximum fill height of h, a side slope gradient of g, and a length of fill D (see Figure 3). After examining Figure 3 it is obvious that such a fill volume can be subdivided into two identical wedges (A and B) and four identical triangular side pyramids, (*1*, *2*, *3*, and *4*). The volume of each wedge is $D \times h \times L/4$. The volume of a right pyramid can be computed as (base-area $\times$ height)/3 so that the volume of each side pyramid is $D \times g \times h \times h/12$.

The volume of a cut through a hill can be approximated in an identical fashion, although the side-slope gradients in a rock cut will be much steeper than in a fill. The volumes of benched rock cuts can be satisfactorily estimated by using an average side-slope gradient for purposes of predictive cost modeling. Thus,

$$\text{total volume of a fill (or cut)} = \left(\frac{hL}{2} + \frac{100h^2}{3g}\right)D$$

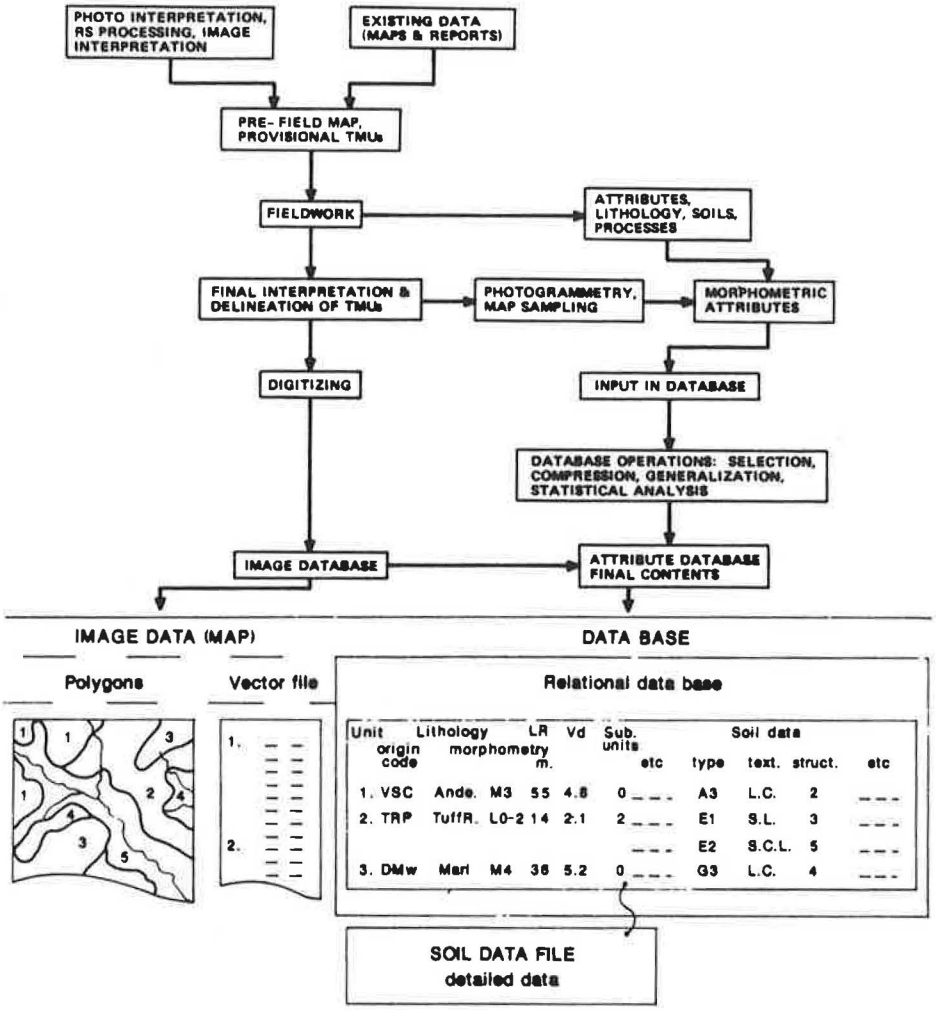

FIGURE 2 Procedures for creating the GIS data base.

where

D = typical length of fill (or cut),
h = typical maximum height of fill (or cut),
L = roadway width, and
g = side slope gradient in percent (for either fill or cut).

The values of roadway width (L) and fill side-slope gradients are defined by Nigerian road design standards for all road classes. The values for g in cuts are related to the local soil or rock conditions and thus can be defined for each LSMU. The values of D and h can be related to terrain roughness conditions, for each LSMU, by the methods and assumptions defined in the following four steps.

1. Defining characteristic terrain roughness: The terrain roughness was defined for each LSMU by the frequency of valley crossings along four directions (north-south, east-west, northeast-southwest, and northwest-southeast) and by the local relief and were estimated by placing a circular template, with a diameter of 8.3 cm, on 1 : 25000 scale aerial photographs or topographic maps or both and estimating the frequencies of valley crossings and the local relief. The valley frequency count was estimated in terms of fractional valleys per circle diameter. From such frequency counts it is possible to compute a typical valley width W (in meters) according to the formula

$$\text{typical valley width} = W \text{ (meters)} = \frac{\text{circle diameter (cm)} \times \text{map scale denominator}}{100 \times \text{frequency count}}$$

At least eight different sampling locations were chosen within each LSMU so that means and standard deviations of the typical valley widths for each of the four directions, and the minimum and maximum local relief values, a total of 10 descriptors, were computed for each LSMU.

2. Estimating typical cut/fill lengths (D): In a regularly undulating terrain, with a typical valley width W, the desire to balance cuts and fills will cause the road grade to move from cut to fill and back against at approximately the midpoint of each slope, regardless of the chosen ruling gradient. Under these circumstances the typical cut or fill length (D) will be about one-half the typical valley width (W). Admittedly, such

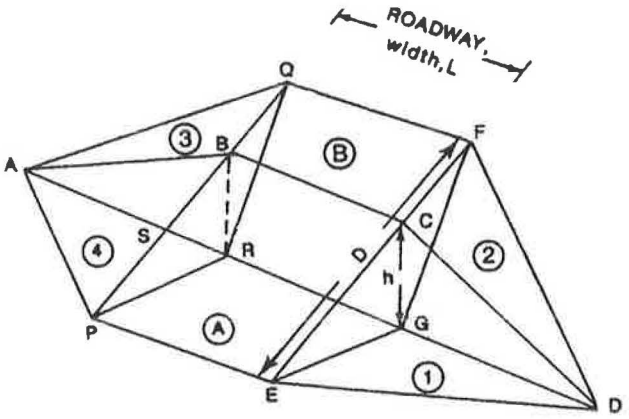

FIGURE 3 Geometrical representation of an idealized roadway fill.

a relationship includes a number of simplying assumptions that include (a) roughly equal side-slope gradients in cuts and fills, (b) local mass-balance equalities can be readily achieved, (c) material bulking and shrinkage ratios are either very small or offsetting and can be neglected, and (d) the amount of excavated material unsuitable for placement in fills, and thus must be wasted, is small and can be neglected. A correction factor is used to account for the necessary "wastage" of material excavated in a cut but unsuitable for a fill. Each LSMU is supplied with an estimate of the fraction of such unsuitable material that is likely to be encountered, and the total volume of material is increased by this amount. Adjustments can also correct for volume imbalances owing to other reasons, including differences in cut and fill side-slopes (*3*).

3. Estimating the maximum cut/fill height (h): The final value required by the volume formula is the estimated maximum height (h) of the cut and fill. This value is related to the terrain roughness estimates. For any desired principal direction a valley side-slope gradient (VSG) can be computed from the typical valley width and local relief data (see Figure 4). The VSG value can be compared to the maximum allowable longitudinal roadway gradient (rg), which is defined by Nigerian authorities. As is indicated by Figure 4 the maximum cut/fill height (h) can vary between a maximum value $h$max and a minimum value $h$min, where

$$h\text{max} = (\text{local relief})/2 = z/2$$

$$h\text{min} = h\text{max} - \Delta h$$

$$\Delta h = \frac{(\text{rg}) \times (W/4)}{100} = \frac{(\text{rg}) \times W}{400}$$

$$\text{average typical } h = h\text{max} - \Delta h/2 = \frac{z}{2} - \frac{(\text{rg}) \times W}{800}$$

where

z = local relief,
h = typical maximum height of fill (or cut),
$h$max = largest maximum height of fill (or cut),
$h$min = smallest maximum height of fill (or cut),
rg = ruling longitudinal roadway gradient, and
W = typical valley width.

4. Estimated grading volumes for smooth terrain: That formula will not give satisfactory values when the VSG is less than the allowable longitudinal roadway gradient (rg). Under such condition, the road profile can follow the terrain without any cutting or filling. Such terrain can be considered "smooth." However, road construction will require some minimum volume of fill to raise it above the general terrain and allow for drainage. In the areas studied, Nigerian practice includes the construction of subgrades between 1 and 3 m high, depending on local soil conditions. Accordingly, the volume estimation step includes an initial comparison of the VSG and rg values. When "smooth" terrain is thus defined, a minimum subgrade height, defined for the LSMU, is used to calculate default values of grading volumes.

Defining Unit Costs for Materials Excavation, Handling, and Placement

All unit cost values for grading costs were obtained by examining bills of quantity from recent road construction contracts in this area or in nearby areas (see Table 1). Insufficient information exists within the recent road construction bills of quantities to establish relationships between excavation costs and anticipated rock strengths and jointing patterns. The current Nigerian road costing practice is to classify all rippable rocks, including most of the sedimentary rocks in this area, as soils. All hard rocks, including most basalts and granites in this area, that require blasting are classed as rock for excavation.

The haul distance was assumed equal to the typical length of the cut or fill (D) and was compared to the 500 m haul distance criteria in Table 1 and the appropriate cost, for either soil or rock, was selected. Those include the entire costs for excavation, handling, and placement of the materials.

Creation of the Grading (Earthwork) Cost Model

A series of four different grading cost models, one for each of the primary geographic orientations (north-south, east-west, northwest-southeast, and northeast-southwest), were developed for the test areas. Those four cost models are most similar in regions that are relatively smooth. In those regions the grading costs are related to the requirement of raising the roadbed above the surrounding terrain to ensure adequate drainage and are little affected by ridge or valley orientations. Some directional differences can be seen in regions with more pronounced relief. Higher grading costs are associated with roadway directions that traverse frequent ridges or valleys. Figure 5 presents a simplified map example of the earthwork cost model for the Gongola test area, which was computed for east-west oriented routes.

Pavement Construction Cost Prediction Model

The cost of constructing the pavement for a given length of road can be computed by multiplying the required volumes of different pavement materials by their unit costs when delivered to the construction site.

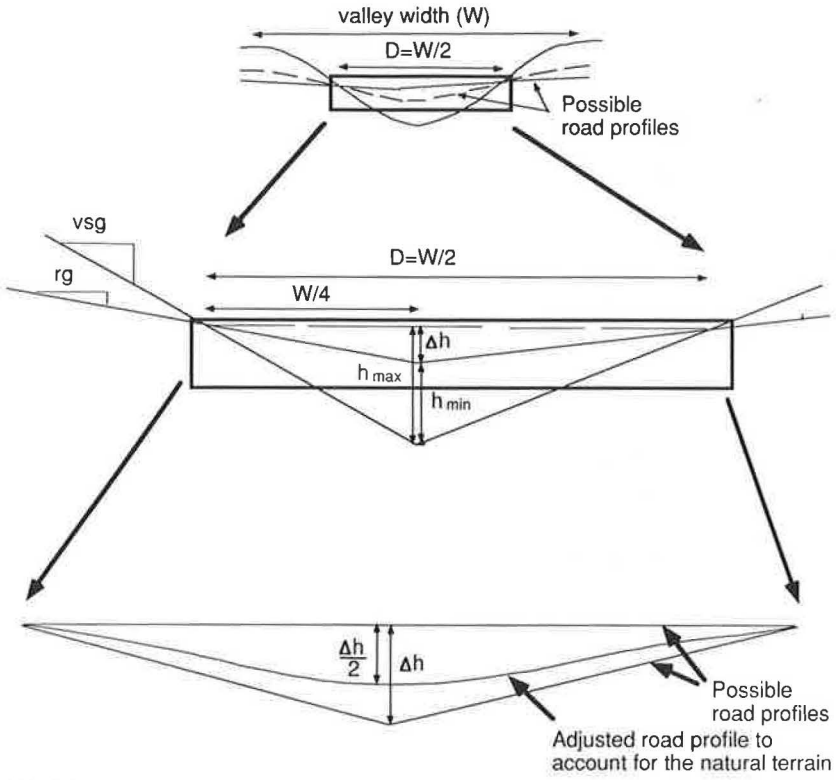

FIGURE 4 Sketches indicating idealized geometrical relationships between valley side gradient (vsg), allowable longitudinal road gradient (rg), and typical fill parameters length of fill ($D = W/2$) and fill height (h).

TABLE 1 COST OF HAULAGE AND EARTHWORK OPERATIONS DETERMINED FROM BILLS OF QUANTITIES FOR RECENT NIGERIAN ROAD CONTRACT AWARDS

Item Number	Item Evaluated	Distance Involved	Unit Cost N/m³	Source of Information
1a	Haulage cost for fills, including spreading & compaction	less than, equal to 500m	2.65	Cedaconsult 1978 (6)
1b	ditto	over 500m	3.50	
2a	Haulage cost for granular base material from borrow pit, including laying and compaction	less than, equal to 500m	4.00	Aggarwal & Jafri 1985 (16)
2b	Extra haul cost	over 500m	0.38/km	
3a	Excavation or ripping in soil or soft rock to any depth in cutting & ditches & hauling suitable material to fill site, including laying, compaction and disposal of unsuitable material.	less than, equal to 500m	2.30	Cedaconsult 1978 (6)
3b	ditto	over 500m	3.40	
4a	Excavation in rock, including secondary crushing	less than, equal to 500m	10.75	Cedaconsult 1978 (6)
4b	ditto	over 500m	11.85	

NOTE: Costs of materials are expressed in the Nigerian currency, Naira per cubic meter.

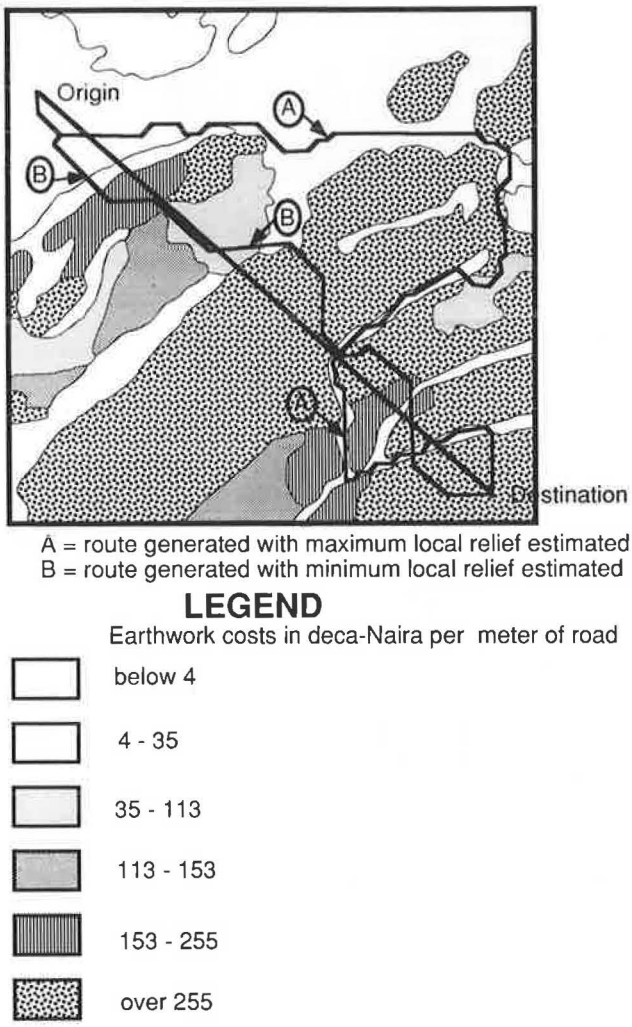

FIGURE 5 Example of earthwork cost map and generated routes.

Computation of Required Volumes

Standard Nigerian bituminous pavement road design includes a 5-cm-thick bituminous surface, a base course 15-cm thick, and a variable thickness of sub-base according to different subgrade strengths as measured by CBR values. Pavement and base course widths are specified according to road type and local terrain conditions, with higher classes of road and smoother terrains given wider dimensions. The volumes of bituminous pavement, base course, and sub-base materials required for a given length of roadway (in this case a roadway length of 40 m was used for estimation purposes) can be computed from those specifications and from a knowledge of local terrain characteristics and subgrade CBR values. This information was readily available within the ILWIS attribute data base.

Computation of Delivered Unit Costs

The unit costs for materials, delivered to a given location, can be estimated by summing the unit costs of production at the source and the haul costs. The estimation of those values involves five steps.

1. Estimation of unit haul costs: Haul costs for moving materials from pit or quarry sources to the construction site are computed according to general relationships. For short distances a fixed unit charge has to be made to cover equipment and materials handling costs. Beyond this distance costs increase linearly with distance. Finally, at some larger distance the haulage costs become prohibitively large, and a region of "marginal haul" can be identified.

2. Identification of "source-sheds": At many construction locations a number of competing sources, each with different materials quality and haul distance, may be found closer than the marginal haul distance and are potential sources. Source areas are defined by examining the LSMU attributes to identify those containing adequate quantities of suitable materials. The selection of the most economical source involves the concept of "source-sheds." Just as the surface of the earth is divided into a series of watersheds, the region of interest can be conceived as being covered with a "cost-surface" containing a series of hollows that correspond to the materials sources. The elevation of each hollow is related to the unit cost of producing the material. The surrounding areas are covered by sloping surfaces with gradients corresponding to the haul costs that will intersect to form "divides," which define a series of polygonal source-sheds. A source-shed is thus defined as a region where it is cheapest to obtain material from a single source. Figure 6 defines this basic concept. This basic concept needs to be modified to allow for more realistic simulations in many actual situations.

3. Adjustment for local trafficability and terrain conditions: Straight-line or cross-country haulage routes may be feasible in areas characterized by relatively flat terrain and surficial materials with good trafficability characteristics. The source-sheds can be computed with radial distances from the limits of source areas defining the haul costs. The source-sheds then approximate a series of intersecting-conics. Such conditions were true in the northern Ngamdu test area, which has relatively smooth lateritic terrain covered by shallow eolian sands. The definition of source-sheds must take into account the distribution of existing roads and the trafficability of all other regions in areas where soils and topography potentially interfere with cross-country travel. Rugged areas, or areas underlain by weak soils, for example, must be treated as barriers. The southern Gongola test area is characterized by those conditions. Consequently, the source-sheds in this region are much more complex and the resulting cost maps are much less regular.

4. Incorporation of materials quality considerations: A strict selection of materials sources based only on delivered price to the construction site may not always be the preferred solution. For example, a source having a higher quality may perform much better in service than an alternate lower-quality source. Its higher quality may bring a premium price at the source, however, owing either to higher production costs or to perceived market values. Under the basic procedure defined, such higher-priced premium-quality sources will not develop very extensive source-sheds in competition with lower quality materials. An extra step must be added to the development of the delivered unit cost model to allow for the higher-quality

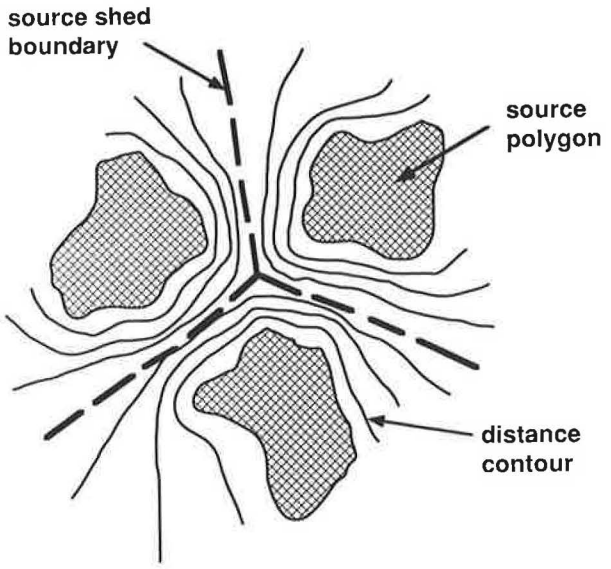

FIGURE 6 Definition of source sheds.

sources to be more frequently identified and selected. If the production prices of the higher-quality materials are artificially reduced, or those of the lower-quality materials are raised, then the source-sheds of the higher-quality materials will expand relative to those of lower quality. Essentially, the solution involves the use of "shadow prices," which incorporate not just economic factors but also judgment values.

5. Computation of delivered materials costs: Once the source-sheds are identified according to this modified pricing procedure, the true unit production costs are combined with the defined source-sheds and contain the unit haul costs to compute the delivered materials unit costs.

Computation of Overall Pavement Cost Model

The procedures outlined permit the development of cost models for each element of the pavement (bituminous surface, base course, and sub-base). Again, recent road construction experience data (Table 1) were reviewed to supply appropriate cost factors. The individual cost models were then summed to create a pavement construction cost model.

Prediction of Drainage Structure Costs

Drainage structure costs may be estimated from terrain and watershed hydrology data by using simple hydrologic estimation techniques to determine peak flows. A separate study of drainage crossing prediction was conducted over part of the Gongola test area, in a region characterized by rugged terrain and a fairly dense drainage network.

The selected test area included 58 watersheds, which were digitized and stored within ILWIS. The Rational method for small watersheds (less than 25 km^2) and the Talbott formula for larger watersheds, relationships between peak discharge and catchment area, were developed for each major terrain type by using standard hydrologic estimation procedures. Existing roadway engineering reports for northeastern Nigeria yielded relationships between peak discharge and culvert size for small drainages and between catchment area and length of bridge. It is possible to estimate approximate drainage structure costs along previously defined routes with this information. For example, routes selected to minimize grading and pavement costs can then be subjected to drainage structure cost analysis.

Integration of drainage structure costs into the selection of routes requires the development of a directionally related drainage structure cost predictive model, analogous to the predictive grading cost model described previously. The characteristic terrain roughness data, according to directional orientation, do supply valley frequency information. However, additional data concerning the size of the tributary being crossed, catchment area, or peak runoff value cannot be obtained from those data. Accordingly, additional analyses were undertaken to develop predictive relationships between stream order (a measure of size) and anticipated peak runoff for major LSMUs. With such data it may be possible to relate some relevant drainage structure design parameters, and therefore costs, to the various LSMUs. Some limitations can be foreseen. For example, many site-specific concerns exist at any crossing site that involve factors such as scour and bridge footing conditions. Work is continuing on this model.

Maintenance Cost Prediction Model

Maintenance costs may be developed on the basis of pavement maintenance and other right-of-way maintenance costs and can be estimated by using basic terrain and local materials durability factors and assumed baseline traffic volumes. A common rule-of-thumb suggests that 60 to 70 percent of the maintenance costs are related to pavement repairs.

General right-of-way maintenance activities include the clearing of vegetation, removal of debris from ditches and culverts, and the repair of side-slopes (either in cut or fill) subjected to erosion. In addition there may be occasional catastrophic failures, such as landslides or "washouts" at drainage crossings. All of those conditions can be related to local terrain and soil or rock erodability characteristics within a relatively uniform climate. Some factors, concerning the erosion of side-slopes, also will be affected by the amount of cut and fill related to topographic roughness.

Similarly, it should be expected that pavement deterioration will be related to subgrade conditions under specified traffic loadings. With such relationships it is possible to estimate annual pavement maintenance expenditures, useful pavement life, and similar factors to mapped data elements within each LSMU.

Accordingly, a maintenance cost model can be constructed that relates the terrain roughness and materials characteristics for each LSMU to an expected annual maintenance level. However, this requires some empirical relationships, based on experience in the region, that can predict anticipated annual maintenance efforts, or costs, according to such terrain characteristics. Unfortunately, such data are lacking for this part of Nigeria at present. The development of empirical relationships will allow the further application of the LSMU concept by including maintenance cost predictions to road planning and management in Nigeria.

ROUTE SELECTION METHODS BASED ON MINIMUM TOTAL COST CRITERIA

Those predictive cost models can be analyzed further to generate possible routes that best satisfy selected design criteria. Linear programming techniques have been applied to combinations of predictive cost models to identify routes (*10–13*). More recently, Linden (*14*) applied those methods to investigate the framework for planning support during highway location studies in Holland.

A new algorithm, GROUTES, was implemented for this study (*15*). Like its predecessors the algorithm determines the route, between any desired pair of termini, having the lowest total cost and takes into account both the distance traveled and the cost of movement per unit of distance. Those costs can be compared with the cost of the shortest (straight-line) alternative.

The GIS capabilities and the predictive cost models described earlier supplied the necessary cost matrices to the GROUTES algorithm. A number of analyses was made by using combinations of earthwork cost, pavement cost, and drainage crossing cost models. Figure 5 shows a typical result.

Generally, the generated routes were much cheaper than the straight-line routes, although they were longer. Costs for the cheapest routes ranged from 6 to 15 percent of the direct route costs. Lengths ranged up to double the straight-line distance.

Earthwork and drainage crossing costs dominated in determining the routes. Pavement costs were rather insignificant. The route selection and cost estimates appear most sensitive to the accurate determination of local topographic relief values, a parameter only indirectly estimated from most satellite imagery.

CONCLUSIONS

A series of procedures has been developed that allow the creation of predictive cost models that can support roadway planning in regions with limited terrain data. The use of remote sensing image interpretation techniques, in conjunction with GIS computer techniques, allows for the creation of a suitable data base. The predictive modeling techniques create numerical models that define roadway cost factors by accessing such a data base. Display of those factors as maps can be helpful in regional planning.

The cost models were analyzed further to generate possible routes that best satisfy Nigerian road design criteria. The cost of the cheapest route was found to be much less than that of the most direct route. Thus, the combination of predictive cost models and route identification may stimulate the development of more roads, even in areas with rugged terrain conditions.

Field visits in Nigeria and existing road construction reports were used to check several of the parameters used in the predictive models, but it has not yet been possible to compare the estimated route costs with those actually experienced. The concepts have been developed with examples from northeastern Nigeria, but similar procedures can be applied to other areas in Nigeria and in many other developing countries.

The route selection model is relatively simple to use, and its application and data requirements are well within the capabilities of potential users. The model is a decision making tool for transport planners and a cost-saving method that will be effective for the management of the economy in the road sector.

REFERENCES

1. F. Moavenzadeh. *Investment Strategies for Developing Areas: Analytic Model for Choice of Strategies in Highway Transportation*. Research Report 72-62, MIT Department of Civil Engineering, Cambridge, Mass., 1972.
2. R. Robinson, H. Hide, J. W. Hodges, J. Rolt, and S. W. Abaynayaka. *A Road Transport Investment Model for Developing Countries*. Transport and Road Research Laboratory Report 674, Department of the Environment, Crowthorne, Berkshire, England, 1975.
3. J. O. Akinyede. *Highway Cost Modelling and Route Selection Using a Geotechnical Information System*. PhD thesis. Faculty of Mining and Petroleum Engineering, Technical University, Delft, The Netherlands, 1990.
4. J. D. Carter, W. Barber, and E. A. Tait. The Geology of Parts of Adamana, Bauchi, and Bornu Provinces in Northeastern Nigeria. *Geological Survey of Nigeria Bulletin*, No. 30, 1963.
5. C. A. Kogbe. Attempt to Correlate the Stratigraphic Sequence in the Middle Benue with those of Anambra and Upper Benue. *Earth Evolution Science*, 1981. pp. 144–148.
6. Cedaconsult Nigeria Ltd. *Soils, Materials, and Pavement Design for Kwanga-Kusari-Shani Road*. Preliminary Road Engineering Report, Vols. 1 and 2, Borno State Ministry of Works, Nigeria, 1978.
7. J. W. P. Dowling. The Classification of Terrain for Road Engineering Purposes. *Proc., Conference on Civil Engineering Problems Overseas*, Institute Civil Engineers, London, 1968, pp. 209–236.
8. J. N. Bulman and C. J. Lawrence. The Use of Satellite Imagery in Highway Engineering in Africa. Presented at IRF IVth African Highway Conference, Nairobi, Kenya, 1980.
9. A. M. J. Meijerink, C. R. Valenzuela, and A. Stewart. *The Integrated Land and Watershed Management Information System: ILWIS*. ITC Publication 7, International Institute for Aerospace Survey and Earth Sciences, Enschede, The Netherlands, 1988.
10. A. K. Turner and R. D. Miles. The GCARS System: A Computer-Assisted Method of Regional Route Location. In *Highway Research Record 348*, HRB, National Research Council, Washington, D.C., 1971, pp. 1–15.
11. A. K. Turner and I. Hausmanis. *Special Report 138: Computer-Aided Transportation Corridor Selection in the Guelph-Dundas Area of Ontario*. HRB, National Research Council, Washington, D.C., 1973, pp. 55–70.
12. A. K. Turner. A Decade of Experience in Computer Aided Route Selection. *Photogrammetric Engineering*, Vol 44, No. 12, 1978, pp. 1561–1576.
13. A. K. Turner. Interactive and Graphic Techniques for Computer-Aided Route Selection. In *Transportation Research Record 729*, TRB, National Research Council, Washington, D.C., 1979.
14. G. Linden. *Highway Location: Towards a Framework for Planning Support*. Geo Pers, Groningen, The Netherlands, 1989.
15. M. C. Ellis. *General Route Selection Program Documentation*, ITC Internal Publication, ITC, Enschede, The Netherlands, 1989.
16. H. R. Aggarwal and R. H. Jafri. A Preliminary Study to Modify Material Specifications for Base Laterites for Secondary Roads. In *Geotechnical Practice in Nigeria*, (A. O. Madedor and J. O. Jackson, eds.), R.O.C., Surulere, Lagos, Nigeria, 1985, pp. 109–131.

Publication of this paper sponsored by Committee on Exploration and Classification of Earth Materials.

Methods for Developing Defensible Subjective Probability Assessments

WILLIAM J. ROBERDS

Typically, some degree of uncertainty exists in the value of geotechnical parameters at any site (e.g., owing to insufficient data, natural spatial variability, or possible changes with time). Often, this uncertainty must be quantified (e.g., in terms of probability distributions that express the relative likelihood of any value). Because of inevitable data base deficiencies, those probability distributions must be based to some degree on subjective assessments, reflecting personal opinions and judgment, consistent with all available information (site-specific and generic), and recognizing the entire range of possible values. Subjectively derived probability distributions can represent the opinions of individuals or of groups. There are problems associated with either, which, if uncorrected, render the results suspect and difficult to defend. Various techniques have been developed to conduct subjective probability assessments with varying effort and success in mitigating such problems. Thus, the appropriate technique is that which provides the desired level of defensibility at least cost.

Geotechnical parameters are often complex, varying spatially and, in some cases, with time, as a function of scale and possibly other factors. The values of those parameters must often be estimated (e.g., for analysis and design). However, data bases regarding those parameters in many cases will contain a small number of samples and inexact representation of the true conditions because of the cost involved in gathering representative data. Parameter values cannot be determined accurately in such cases where the data base is statistically insufficient. Instead, the parameter values must be estimated on the basis of whatever information is available, including generic as well as site-specific data. Those estimates, depending on their application, may represent conservative assumptions (e.g., to demonstrate compliance with some criteria) or best guesses (e.g., to predict actual performance of alternatives as input to decision making). Such estimates must necessarily incorporate interpretations and judgments regarding the data base, which are subjective and in many cases nonunique, and thus may be open to controversy. Controversy can significantly delay a project and cause unnecessary expense, especially if an ultra-conservative assumption results. Hence, the objective is to produce cost effectively appropriately defensible estimates of parameter values where significant uncertainty exists and must be subjectively assessed.

Many examples of such uncertainty analyses exist (*1*). This paper is derived from a detailed manual developed by the author specifically for conducting subjective probability assessments (*2*).

Golder Associates, Inc., 4101 148th Avenue, N.E., Redmond, Wash. 98052

UNCERTAINTY/PROBABILITY CONCEPTS

Variables can represent (a) the state at a particular place and time or (b) where the state may vary spatially or temporally or both, a group statistic (e.g., mean or variance of the population). The variables, in either case, would have a unique value. Moreover, such variables may be "continuous" (i.e., it may have an infinite number of possible states) or may be "discrete" (i.e., it may have a finite number of possible states).

Often, the state of a variable has not been directly and accurately observed, and there will generally be some uncertainty as to what the state of that variable actually is, was, or will be. The possible sources of this uncertainty can be summarized as follows (*2*):

- Statistically insufficient data: In direct observations of a variable state, measurement errors (random or systematic) and accuracy limitations may exist. Where the state has not been directly observed, it must be inferred (e.g., interpolated, extrapolated, or analytically derived) from other information. In analytically deriving a variable state from other site- and time-specific measurements, there may be imperfect understanding regarding the processes involved and approximations and simplifications in the analytical procedure. The applicability of indirect observations in the inference of the variable state must be considered. In assessing group statistics there may not be enough data to be statistically significant or the data may not accurately represent the population (i.e., biased sampling).
- Natural spatial or temporal variability or both: The variable state may vary spatially or temporally (i.e., change with time) or both. For example, the space may not be homogeneous and uniform and may instead have heterogeneities or the variable state may be affected by future events that cannot be predicted with certainty. In interpolating or extrapolating from observations (direct or indirect) elsewhere or at other times or both, this spatial or temporal variability and the effects of heterogeneities and of events and processes (both past and future) must be considered.

The uncertainty in the actual state of a variable can be quantitatively expressed in various related ways (e.g., ranges, accuracy measures, confidence levels, or probability distributions) (*3*). As is illustrated in Figure 1, probability distributions can be defined for

- Discrete variables (Figure 1a), in terms of a probability mass function (pmf), which expresses the probability of each possible variable state;

- Continuous variables (Figure 1b), in terms of (a) probability density function (pdf), which expresses the relative likelihood of each possible variable state, (b) cumulative distribution function (cdf), which expresses the probability that the variable state will be less than or equal to each possible variable state;
- Group statistics (Figure 1c), in terms of pdfs or cdfs or both for the mean (μ_x, first moment about zero), variance (σ_x^2, second moment about the mean), standard deviation (σ_x, square root of the variance), or other higher moments of a distribution; and
- Multiple variables (Figure 1d), in terms of (a) joint pmf/pdf, which expresses the probability or relative likelihood of each possible combination of discrete or continuous variable states actually occurring, (b) marginal pmf/pdf, which expresses the probability or relative likelihood of each possible state of one variable actually occurring, regardless of the state of the other variable, (c) conditional pmf/pdf, which expresses the probability or relative likelihood of each possible state of one variable actually occurring given the state of another variable and (d) covariance function/correlation coefficient, which expresses the relationship of the state of one variable to the state of another variable (including spatial and temporal correlation).

INDIVIDUAL PROBABILITY ASSESSMENT TECHNIQUES

Potential problems associated with a single individual subjectively developing probability assessments include the following ones (*2*):

1. Poor quantification of uncertainty: The assessor might not express uncertainty in a self-consistent or proper fashion. It has been shown (*4*) that people not trained in probabilistic analysis typically have problems in quantifying their uncertainty accurately. For example, if someone expresses a 90 percent probability or level of confidence that something will happen, it should happen nine out of 10 times on the average. Typically when verified, however, the event happens much less than nine (more like five) out of 10 times.
2. Poor problem definition: The parameter where the value is to be assessed might have been ambiguously defined so that the basis of the assessment might not be correct. For example, in assessing the value for shear strength within a specific slope, with respect to slope stability, the scale (large-scale average over the entire failure surface versus small-scale laboratory values) might not have been specified.
3. Unspecified assumptions: The assessor might not specify (or even be aware of) the assumptions that underlie this assessment so that the conditional nature of the assessment might not be apparent. For example, the assessor may have assumed circular arc failure through the rock mass rather than considering wedge failures along intersecting fractures in assessing the value for shear strength within a specific slope with respect to slope stability.
4. Uncorrected biases: The assessor might not specify (or even be aware of) biases that underlie the assessment so that the assessment does not accurately reflect the assessor's knowledge. Biases fall within various categories:

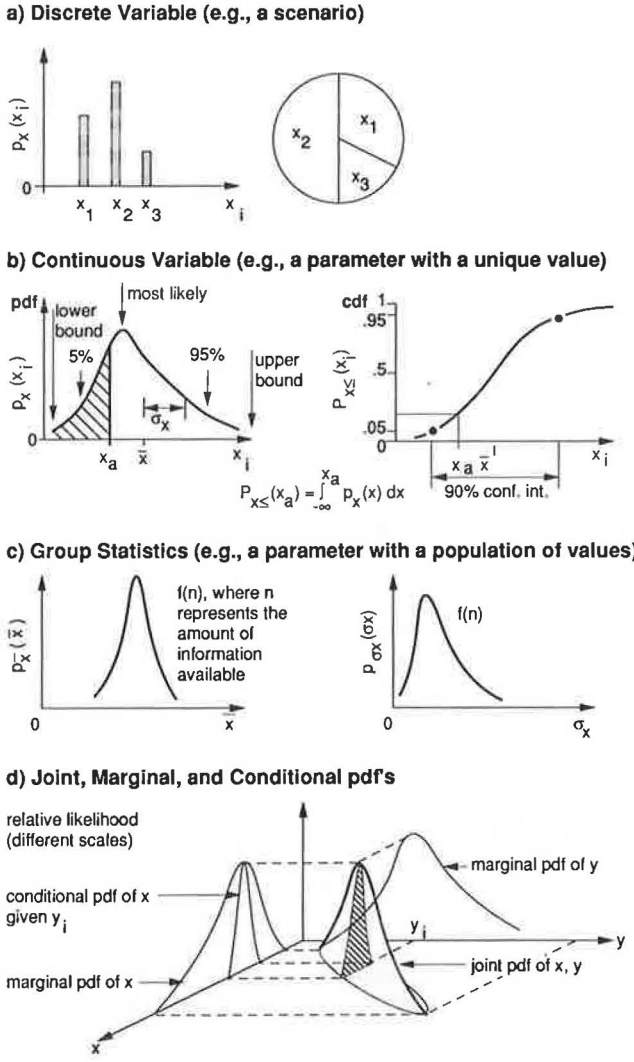

FIGURE 1 Probability distributions.

a. "Motivational," where the assessor's statements and conscious beliefs are inconsistent. Motivational biases, in turn, can be categorized as follows:
   (1) "Management" bias refers to the assessor's possible view of an uncertain variable (e.g., as an objective rather than an uncertainty). For example, if the objective is to achieve a high factor of safety with respect to slope stability, then the shear strengths may be overstated.
   (2) "Expert" bias refers to a possible reaction that the assessor may have to being considered as an expert. The assessor may feel that experts are expected to be certain of things. This bias tends to promote central bias (i.e., a tendency for the assessor to understate uncertainty). For example, the assessor may understate the range in the shear strength within a specific slope.
   (3) "Conflict" bias refers to a reward structure that might encourage the assessor to bias the estimates high or low. For example, an unethical assessor might overstate the value of a significant param-

eter (e.g., shear strengths) if it were personally beneficial (e.g., to make a project appear feasible).
(4) "Conservative" bias refers to the assessor's desire to err on the safe side. For example, if an event has an adverse impact, then the assessor may want to avoid underestimating the probability of that event (e.g., by consciously overstating its probability), thereby bounding the assessment rather than truthfully estimating it.

b. "Cognitive," where the assessor's conscious beliefs do not reflect the available information. Cognitive biases, in turn, can be categorized as follows:
(1) "Anchoring" refers to the tendency of individuals to produce estimates by starting with an initial value (suggested perhaps by the formulation of the problem) and then by adjusting the initial value to yield the final answer. The adjustment is typically insufficient. For example, the assessor might estimate the most likely value first and then the range in possible values where this estimated range would probably be larger if assessed first.
(2) "Availability" (or incompleteness) bias refers to the fact that if it is easy to recall instances of an event's occurrence (e.g., the event had some personal significance to the subject) then that event tends to be incorrectly assigned a higher probability. For example, if the assessor had been involved previously with a slope failure, then the resulting assessment of the shear strength would tend to be lower than without this experience.
(3) "Base rate" bias (or lack of moderation, law of small numbers) refers to the tendency of the assessor to focus only on specific information. Empirical evidence indicates that assessors often tend to attach less importance to general information. For example, if the specific information is some recent data (e.g., the results of recent field tests), then the importance of that information might be overrated in the assessor's mind.
(4) "Coherence and conjunctive distortions" refer to the tendency of an assessor to not account for and combine all of the components of a problem properly. For example, in assessing slope stability where various parameters (e.g., shear strength, pore pressures, ground accelerations) must all be within specific bounds for the slope to be stable, people seem especially prone to overestimate the probability that the slope will be stable.
(5) "Representativeness" refers to the tendency of an assessor to treat all information equally even though it may not be statistically representative. For example, intact rock (with high shear strengths) may be more easily sampled than highly weathered rock (with low shear strengths) so that there is a larger percentage of high shear strengths in the data base than there is in reality. If this sampling bias were not recognized, then the value of the parameter might be overestimated.
(6) "Overconfidence" refers to the tendency of an assessor to underestimate the uncertainty about the value of a parameter. For example, the assessor might not recognize and properly account for other possible values of the parameter.

5. Imprecision: The assessor may be indifferent over a specific range of values so that some "fuzziness" exists in the assessments. For example, an assessment of 20 to 30 percent probability that something will happen should be able to be refined further with additional consideration.

6. Lack of credibility: If the assessor cannot be considered an expert in the technical field, then the assessment (regardless of the other limitations) may lack credibility. Such an assessment would not be defensible to other experts or to the public. For example, a recent graduate engineer with little experience should not be making critical assessments alone.

As is summarized in Table 1, the techniques available for eliminating or mitigating the potential problems associated with developing individual subjective probability assessments include the following ones (*2*):

1. Self-assessment: The simplest approach to developing an individual subjective probability assessment is "self-assessment" (*5,6*) where the analyst interprets the available information and then quantifies an assessment of the likely value and its uncertainty. The rationale behind the assessment should be well documented, including a description of the available information and an evaluation of that information, to enhance defensibility of such subjective probability assessments. Although attractive because of its obvious simplicity, this method has significant limitations: (a) poor quantification of uncertainty; (b) uncorrected biases or unspecified assumptions or both, possibly in spite of documentation; (c) imprecision; and (d) lack of credibility if the analyst cannot be considered an expert in the technical field.

2. Informal solicitation of expert opinion: One of the most common methods of developing an individual subjective probability assessment consists of "informal solicitation of expert opinion" (*7,8*) where the analyst asks an "expert" to interpret the available information and quantify an assessment of the likely value of a parameter and its uncertainty. The defensibility of such assessments is increased over self-assessment techniques owing primarily to the increased credibility of the expert involved. As for self-assessment, the expert's rationale for the assessment should be well documented, including a description of the information available to the expert and the expert's evaluation of that information, to enhance defensibility of subjective assessments further. Although generally an improvement over self-assessment techniques, owing to increased credibility, informal solicitation of expert opinion has similar significant limitations and increased cost and potentially poor problem definition.

3. Calibrated assessment: A systematic approach to developing an individual subjective probability assessment is through the use of "calibrated assessments" (*9–11*) where the assessor's biases are identified and calibrated and the assessments are adjusted to correct for such biases. Hence, two sets of assessments are required: (a) the assessor's assessment (e.g., through the informal solicitation of expert opinion) and (b) an assessment of the assessor's biases. The assessment of the assessor's biases can be done either subjectively by peers (i.e.,

TABLE 1 EVALUATION OF SUBJECTIVE ASSESSMENT TECHNIQUES

TECHNIQUE	POTENTIAL PROBLEMS: Poor Quantification of Uncertainty	Poor Problem Definition	Uncorrected Biases/ Unspecified Assumptions	Imprecision	Lack of Credibility	Group Dynamics	Expense
INDIVIDUAL							
Self Assessment	●	○	●	●	●	NA	○
Informal Solicitation of Expert Opinion	●	●	●	●	◑	NA	◑
Calibrated Assessment	◑	●	◑	●	◑	NA	◑
Probability Encoding	○	○	○	◑	◑	NA	◑
GROUP (BEHAVIORAL)							
Open Forum	●	◑	●	●	◑	●	●
Delphi Panel	●	◑	◑	●	◑	○	●
Group Probability Encoding	○	○	○	◑	◑	◑	●
Formal Group Evaluation	○	○	○	◑	◑	◑	●

● Technique does not significantly mitigate potential problem

◑ Technique partially mitigates potential problem

○ Technique effectively mitigates potential problem

in the same way as other subjective assessments) or objectively through a set of experiments or questionnaires. The objective approach typically consists of asking the assessor a series of questions for which the true answer is available but unknown to the assessor. For example, the assessor may be given a set of relevant data that do not include the direct measurement of the parameter of interest even though such a measurement exists, the assessor estimates the parameter value based on the available data, the assessor's estimate is compared with the true value as given by the measurement, and a correction or calibration factor is determined for the assessor that when applied to the assessor's estimate results in the true value. In this way, the assessor's identified biases can be corrected. Although a general improvement over self-assessment or informal solicitation of expert opinion techniques exists, owing to the mitigation of some biases, calibrated assessments entail similar significant limitations (even after calibration) and increased costs and inherent difficulties in objectively determining calibration factors for many of the parameters of interest, because direct measurements might never be available for verification and the calibration factor may not be constant in any case.

4. Probability encoding: The most systematic and defensible approach to developing individual subjective probability assessments, but also the most expensive, is "probability encoding" (*1,12–15*). In probability encoding, analysts trained in probability theory elicit in a proper and self-consistent manner a technical expert's assessment of the pdf of a parameter value, which expresses that expert's uncertainty in the value in quantified terms. This is done in a formalized way (*2*) in five stages (i.e., motivating, structuring, conditioning, encoding, and verifying), during which the analyst attempts to (a) train the subject to properly quantify uncertainty, (b) identify and minimize the subject's bias tendencies, (c) define (and document) the item to be assessed in an unambiguous manner, (d) elicit and document the subject's rationale (including the available information) for assessment, (e) elicit (directly or indirectly) and document the subject's quantitative assessment of uncertainty and check for self-consistency, and (f) verify the assessment with the subject and repeating the process if necessary. As is illustrated by the example given in Figure 2, the subject's quantitative assessment of uncertainty can be elicited indirectly by determining the probability of various states through comparison with familiar reference events (e.g., poker hands) or by choosing between two lotteries (e.g., probability wheel or intervals, Figure 2a and b) until indifference is achieved. A cdf can then be defined, consistent with the various assessments (Figure 2c). Although a general improvement over other available methods (owing to mitigation of most of the potential problems), some imprecision may remain and probability encoding is relatively costly because it is labor intensive.

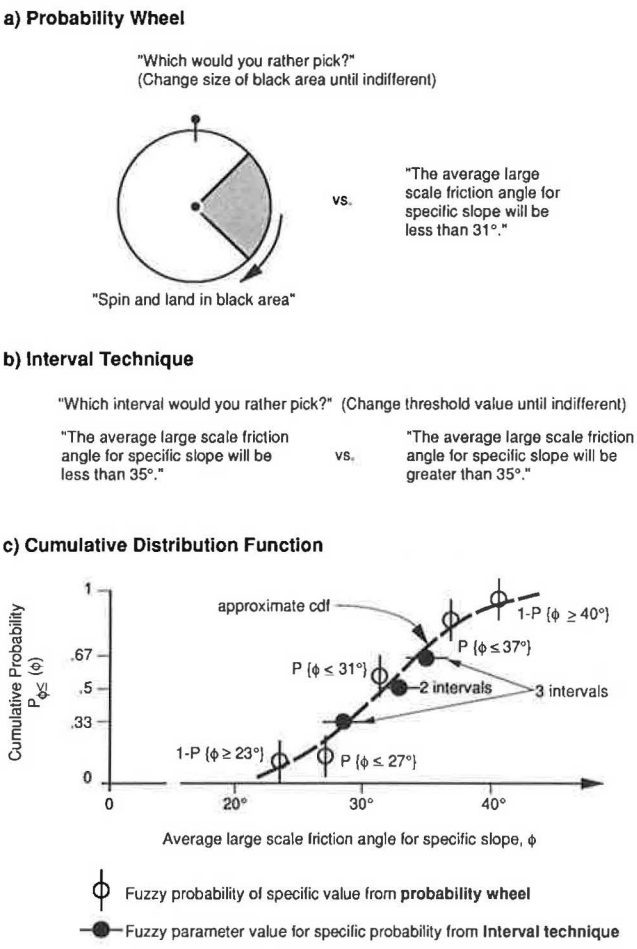

FIGURE 2 Probability encoding examples.

CONSENSUS PROBABILITY ASSESSMENT TECHNIQUES

Differences may exist in the assessment of individuals comprising a group that may arise from a number of sources (*2*):

- Disagreement on the assumptions or definitions that underlie assessments: Individual assessments are based on specific assumptions and definitions. If those assumptions or definitions differ between individuals, then the individual assessments may differ. For example, one individual may have ruled out a specific case that another individual assumes likely or one individual may have defined the parameter of interest at a different scale than did another individual.
- Failure to overcome assessment errors and biases: In conducting the individual assessments a key objective is to eliminate anchoring, availability, overconfidence, and other common distortions. Training individuals and then allowing them to practice making probability judgments prior to the individual assessment help to overcome biases, but such errors may persist. For example, overconfidence may have been mitigated to a large extent in an individual's assessment but not in another's so that although the means of their probability distributions may be similar the variances may be significantly different.
- Judgments based on differing information sources: Both specific data and general knowledge are relevant to the encoding process. Such knowledge varies even among highly specialized experts. Specific information may vary in quantity and quality and general information may vary owing to differences in training and experience. For example, an individual may have based an assessment on a specific data set in conjunction with general experience and another individual may have used a different specific data set in conjunction with different general experience.
- Disagreement on how to interpret available information: The available information must be interpreted by the individuals. For example, individuals may, in this interpretation, disagree on the methods used to obtain data, the relevance of such data to the quantity being assessed, or on the appropriateness of a particular theory or model. For example, individuals may disagree on how to interpret triaxial test results and their validity to assessing such large-scale shear strengths in assessing shear strengths within a slope with respect to slope stability.
- Different opinions or beliefs about the quantity of concern: Even after agreeing on the basis for the assessment, the information available, and how to interpret this information, individuals may still have a difference of opinion. For example, individuals may arrive at different pdfs for shear strength even after agreeing on all the preliminary aspects.

It is typically desirable to attempt to resolve those differences of opinion with the following possible outcomes:

- Convergence: A single assessment is determined that expresses the common belief of all individuals in the group as expressly agreed to by the group members.
- Consensus: A single assessment is determined, although the assessment may not reflect the beliefs of each individual. The consensus assessment may be derived from the individual assessments without the express agreement of the individuals (forced) or it may be expressly agreed to by the group for a particular purpose (agreed).
- Disagreement: Multiple assessments are determined where convergence or consensus on a single assessment is not possible (e.g., owing to major differences of opinion).

In general, convergence is generally desirable, as it is defensible, but may be difficult to achieve. Agreed consensus (i.e., with the concurrence of the group) is slightly less defensible but also less difficult to achieve. Forced consensus, without concurrence of the group, may be difficult to defend but is very simple. Disagreement may be difficult to use, because it is nonunique but is defensible.

Techniques available for resolving differences of opinion among a group of individual assessors can be categorized in terms of "mechanical aggregation" and "behavioral procedures."

Mechanical aggregation of individual assessments is a relatively simple approach to achieve at least forced consensus and involves applying a mathematical formula or procedure to combine the various individual probability distributions (*16,17*). If the individuals in the group agree to the resulting distribution, then agreed consensus (and possibly convergence) can be achieved. In general, mechanical aggregation

techniques are useful when the means, rather than the variances, of the individual probability distributions differ. Also, mechanical aggregation techniques can be used when a single distribution is required, but the parameter in question is not significant enough to warrant large amounts of effort to achieve convergence or agreed consensus.

The various forms of mechanical aggregation include the following ones (*2*):

- Averaging, the simplest mechanical aggregation technique, involves simply averaging the individuals' probabilities for each possible value. Several empirical studies (*18,19*) have indicated that averaged probabilities are often superior to individual assessments. As an example, if an individual assessed an 80 percent probability of the average large-scale friction angle for a cohesionless soil within a slope as being less than 35 degrees and the other individual in the group assessed a 60 percent probability, then the group average would be a 70 percent probability.
- Group statistics, a somewhat more rigorous treatment, involves determining the group's distribution of opinions regarding the probability for each value, thereby developing a "fuzzy" assessment or an assessment that corresponds to a given level of conservatism for the group. More complete statistical methods are available that incorporate dependence among variables and experts (*9*) and least squares or partitioning methods (*20*). As an example, the statistics of the group member opinions of the probability of the friction angle as being less than 35 degrees could be determined and used.
- Weighting methods, elaborations on either averaging or group statistics, involve the weighting of individual assessments by an external procedure to incorporate biases or differing levels of expertise among the individual assessors, similar to individual calibrated assessments. There are essentially two weighting procedures: (a) "calibration exercise," where the natural biases and tendencies of the individual assessors are evaluated and mitigated through the administration of a series of general questions to determine each assessor's ability to make correct assessments and the determination and application of weighting factors for each assessor to reflect that assessor's ability (relative to the other assessors) to make correct assessments, and (b) "peer ratings," where each of the individual assessor's relative ability to make correct assessments is assessed subjectively by peers, although such a subjective assessment may itself introduce additional biases.

Behavioral procedures can be used to attempt to develop convergence or at least agreed consensus and involve interaction among the individuals in the group and allows for the explicit identification and resolution of differences of opinion. Although evidence exists that such interaction results in better assessments (*21,22*) and that the results are generally more defensible because the group agrees on a given distribution, behavioral procedures tend to entail significantly more effort because the various individual assessors must be involved. Such behavioral procedures are necessary when at least agreed consensus (or disagreement) is required (i.e., for significant parameters) and are especially useful when the differences between the individual assessments are large.

As is summarized in Table 1, the various forms of behavioral procedures include the following ones (*2*):

- Open forum is a very informal means of achieving consensus and does not require prior individual assessments. The group attempts to achieve convergence or agreed consensus by open discussion of whatever each individual deems important to resolving the problem. However, the result can be distorted by the dynamics of the group, such as domination by an individual because of status or personality (*23*). For example, the persuasiveness of a vocal individual or the desire of some individuals to avoid dissension may distort the results. Other potential limitations to this method are the same as for the development of individual assessments through the informal solicitation of expert opinion (i.e., poor quantification of uncertainty, uncorrected biases, unspecified assumptions, and poor problem definition). The method is also limited by the credibility of the group members.
- Delphi panel is a systematic and iterative approach to achieve consensus and has been shown to generally produce results reasonably reproducible across independent groups (*22,24–27*). Each individual in a well-defined group is provided with the same set of background information and is asked to conduct and document (in writing) a self-assessment. Those assessments are then provided anonymously to each of the other assessors, who are encouraged to adjust their assessments in light of the peer assessments. Typically, the individual assessments tend to converge. Such iterations are continued until either consensus is achieved or the results stabilize otherwise (i.e., disagreement). Because the Delphi technique maintains anonymity and independence of thought through physical separation of the panelists, it precludes the possibility that any one member of the panel may unduly influence any other owing to actual or perceived personality dominance. Otherwise, it tends to have limitations similar to those for open forum.
- Group probability encoding is a formal process where a single probability distribution is assessed directly from a group of individuals, such as for the development of individual assessments by probability encoding (*1*). However, this requires the group to reach agreement on each question posed during the encoding process and would be a difficult and tiresome procedure. As is for the open forum, face-to-face interaction among participants can create destructive pressures within the group and distort the results.
- Formal group evaluation is a formal process of resolving differences between previously developed individual assessments (*1*). This process is similar to probability encoding in that it is a joint undertaking between a trained analyst and, in this case, a group that has completed individual assessments. It consists of six steps [motivating, identifying differences in the individual assessments, discussing the basis for each individual assessment, discussing information sources and interpretations, re-encoding (if warranted), and reconciling differences] where the analyst fulfills an essential role in questioning and probing the group, helping the group understand the differences, and guiding the group through the resolution process, often conducting group reassessments. This sharing of knowledge tends to produce a commonality (i.e., in definitions, assumptions, information bases, and interpretations) that is a key step in reducing the differences between individual assessments. As is for open forums, face-to-face interaction among participants can create destructive pressures within the group and distort the results. However,

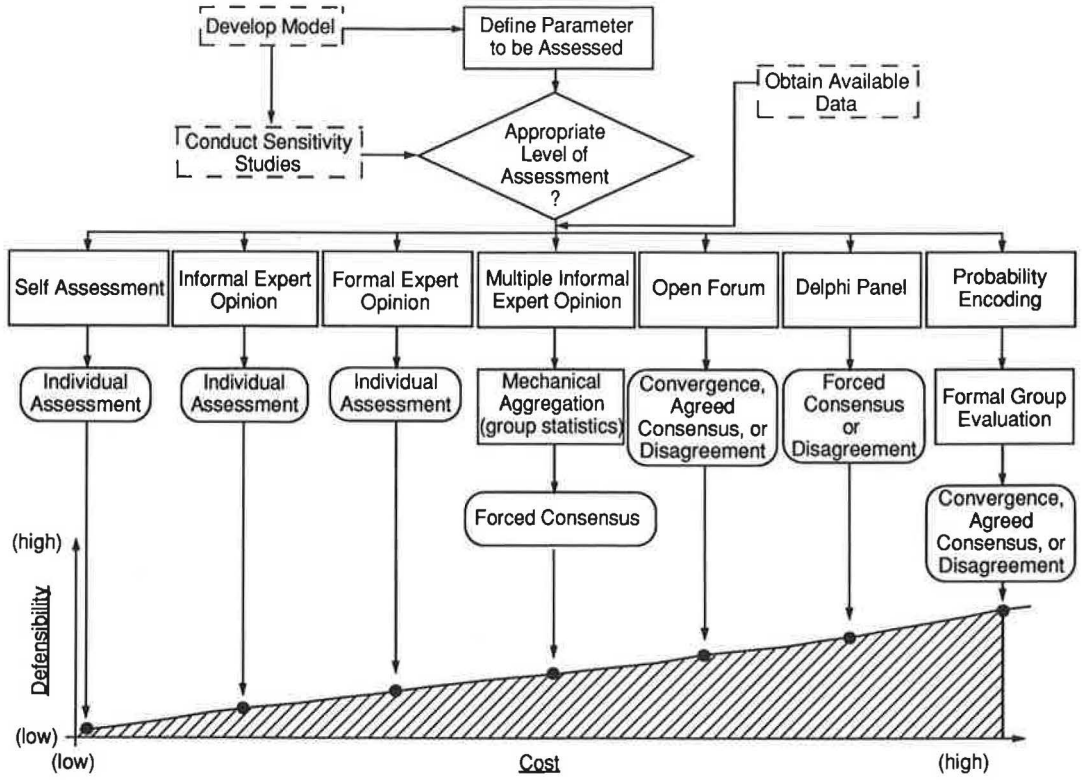

FIGURE 3 Procedure for selecting technique.

the analyst can be alert to such pressures and mitigate the effects to a large extent.

RECOMMENDED PROCEDURES

As is summarized in Figure 3, the recommended procedure for selecting the appropriate subjective probability assessment technique consists of the following steps (*2*):

1. Before conducting subjective probability assessments, (a) develop the model(s) for the system of interest (for example, a model would be needed to determine the factor of safety with respect to slope instability), (b) conduct sensitivity studies to determine the relative significance of each of the model parameters (for example, sensitivity studies on the model might indicate that slope instability is very sensitive to the average large-scale shear strength within the slope), and (c) obtain the available data regarding the various parameters, where the relative significance of the parameter will determine the appropriate level of effort in gathering data (for example, the data on shear strength might be limited to inference from measured physical properties and from generic information).
2. Each parameter to be assessed, on the basis of the model, must be defined unambiguously (considering temporal and spatial variability and conditional factors such as scale). Also, it may be useful to decompose a parameter into more elemental variables for assessment. For example, shear strength might be defined as being large scale (i.e., averaged over tens of meters), recognizing that the value may vary spatially within one geologic unit and within the time frame of interest (i.e., tens of years). Shear strength could be defined separately for the rock mass (e.g., for circular arc analyses) or for joints (e.g., for wedge analyses). Shear strength could be decomposed into cohesion and friction angle.
3. The appropriate level of assessment must be determined on the basis of relative significance of each parameter to be assessed (from sensitivity studies). For example, if a parameter is relatively insignificant (e.g., density), then a low level assessment (with corresponding low costs and low defensibility) will be appropriate. However, if a parameter is relatively significant (e.g., shear strength), a high level assessment (with corresponding high costs and high defensibility) will be appropriate. For cost efficiency, high level assessments should only be used for the most significant parameters where high defensibility is required, thus justifying their high costs.
4. The most cost-effective assessment technique is chosen (Figure 3) on the basis of necessary level of assessment and, in conjunction with the data base, implemented for each parameter [e.g., by using specific procedures (*2*)].

SUMMARY AND CONCLUSIONS

Subjective probability assessments must often be made (e.g., to predict performance accurately or to make decisions among alternatives or both) wherever the data are not statistically sufficient to make objective assessments. Such subjective probability assessments must be defensible enough to resolve potential controversies adequately. The required defensibility of such assessments is proportional to the significance of each

parameter that is assessed (e.g., as determined by sensitivity studies).

Potential problems have been identified that are associated with developing individual subjective probability assessments and with developing consensus subjective probability assessments among a group that if uncorrected can affect defensibility of the results. The available techniques for addressing those potential problems, with varying success and effort, have been presented. Procedures for cost-effectively conducting appropriately defensible subjective probability assessments have been developed.

ACKNOWLEDGMENT

The author is indebted to L. Merkhofer and R. Schwartz of Applied Decision Analysis, Menlo Park, Calif., for their significant contributions on past projects, from which some of the concepts presented in this paper have evolved.

REFERENCES

1. Golder Associates, *Groundwater and Methane Inflow Study for the BWIP ESF at Hanford, Washington*. SD-BWI-DER-001, Rev. 0, in conjunction with Applied Decision Analysis, Inc., Basalt Waste Isolation Project, Westinghouse Hanford Company, Richland, Wash., 1987.
2. W. J. Roberds. *Manual for Conducting Subjective Probability Assessments*. Draft report, Golder Associates Inc., Redmond, Wash., 1988.
3. A. Ang and W. H. Tang. *Probability Concepts in Engineering Planning and Design, 2, Decision, Risk, and Reliability*. John Wiley, New York, 1984.
4. E. C. Capen. The Difficulty of Assessing Uncertainty. *Journal of Petroleum Technology*, Vol. 28, 1976, pp. 843–849.
5. I. J. Good. *The Estimation of Probabilities*. Research Monograph 30, The M.I.T. Press, Cambridge, Mass., 1965.
6. C.-A. S. von Holstein. *Assessment and Evaluation of Subjective Probability Distributions*. Economic Research Institute, Stockholm, Sweden, 1970.
7. M. G. Morgan, M. Hennion, and S. C. Morris. *Expert Judgments for Policy Analysis*. BNL 51358, Brookhaven National Laboratory, Upton, N.Y., 1979.
8. D. L. Bernreuter. *Seismic Hazard Analysis: Solicitation of Expert Opinion*. NUREG/CR-1582, TERA Corp., Berkeley, Calif., 1980.
9. C. E. Agnew. Multiple Probability Assessments by Dependent Experts. *Journal of the American Statistical Society*, Vol. 80, No. 390, 1985, pp. 343–347.
10. A. P. Dawid. The Well Calibrated Bayesian. *Journal of the American Statistical Association*, Vol. 77, No. 379, Sept. 1982, pp. 605–613.
11. R. L. Winkler. Scoring Rules and the Evaluation of Probability Assessors. *Journal of the American Statistical Association*, Vol. 64, 1969, pp. 1071–1078.
12. C. S. Spetzler and C.-A. S. von Holstein. Probability Encoding in Decision Analysis. In *Example of a Probability Encoding Technique*. K-258802, Stanford Research Institute, ORSA-TIMS-AIEEE Joint National Meeting, Atlantic City, N.J., 1972.
13. R. M. Zamora. *ONR Probability Encoding Task*. Working paper, SRI Project 4030, Office of Naval Research, Operational Decision Aids Project, Stanford Research Institute, Menlo Park, Calif., 1975.
14. C.-A. S. von Holstein and J. E. Matheson. *A Manual for Encoding Probability Distributions*. Final Report, SRI International, Menlo Park, Calif., 1979.
15. M. W. Merkhofer and P. McNamee. *The SRI Probability Encoding Process: Experiences and Insights*. Technical report, SRI International, Menlo Park, Calif., 1982.
16. A. J. Harman and S. J. Press. *Collecting and Analyzing Expert Group Judgement Data*. The Rand Corporation, Santa Monica, Calif., 1975.
17. H. A. Ashton and R. H. Ashton. Aggregating Subjective Forecasts: Some Empirical Results. *Management Science*, Vol. 31, No. 12, 1985, pp. 1499–1508.
18. C.-A. S. von Holstein. Probabilistic Forecasting: An Experiment Related to the Stock Market. *Organizational Behavior and Human Performance*, Vol. 8, 1972, pp. 139–158.
19. R. V. Brown. *An Experiment in Probabilistic Forecasting*. R-944-ARPA, The Rand Corporation, Santa Monica, Calif., 1973.
20. D. V. Lindley, A. Tversky, and R. V. Brown. On the Reconciliation of Probability Assessments. *Journal of the Royal Statistical Society A*, Vol. 142, 1979, pp. 146–180.
21. D. A. Seaver. *Assessment of Group Preferences and Group Uncertainty for Decision Making*. SSRI 76-4, Social Science Research Institute, University of Southern California, Los Angeles, 1976.
22. J. Rohrbaugh. Improving the Quality of Group Judgement: Social Judgment Analysis and the Delphi Technique. *Organizational Behavior and Human Performance*, Vol. 24, 1979, pp. 73–92.
23. A. Delbecq, A. Van de Ven, and D. Gustafson. *Group Techniques for Program Planning*, Scott-Foresman, Glenview, Ill., 1975.
24. N. Dalkey and O. Helmer. *An Experimental Application of the Delphi Method to the Use of Experts*. AD A081 351, Memorandum RM-727-PR (Abridged), The Rand Corporation, Santa Monica, Calif., 1962.
25. O. Helmer. *The Delphi Method for Systematizing Judgments About the Future*. MR-61, University of California at Los Angeles, Los Angeles, 1966.
26. O. Helmer. *Systematic Use of Expert Opinions*. Technical paper, The Rand Corporation, Santa Monica, Calif., 1967.
27. H. A. Linstone and M. Truoff, eds., *The Delphi Method: Techniques and Applications*, Addison-Wesley, Reading, Mass., 1975.

Publication of this paper sponsored by Committee on Exploration and Classification of Earth Materials.

Implementation of a Bearing Capacity Design Procedure for Railway Subgrades: A Case Study

PAMELA SATTLER, D. G. FREDLUND, L. W. LAM, A. WAYNE CLIFTON, AND M. J. KLASSEN

Application of a bearing capacity design approach to evaluating railway subgrades is illustrated. The bearing capacity design approach was developed as part of an overall research program to assess the stability of track subgrades. The development of the design procedure was published earlier. The additional strength of the subgrade soil resulting from matric suction was incorporated into the bearing-capacity design procedure. The bearing-capacity design procedure was used as a complementary tool in conjunction with stress analyses and slope stability analyses for the Canadian Pacific Railways Floodway Trackage, Emerson Subdivision, Winnipeg, Manitoba, Canada. Stresses in the subgrade were predicted by using the GEOTRACK computer program. The ultimate bearing capacity was determined by using bearing-capacity theories modified to accommodate layered track systems and the additional strength of the soil resulting from soil suction. Slope stability modeling of the embankment slopes completed the analyses. Results of the complementary analyses were used to select appropriate design alternatives.

A bearing-capacity approach to railway design was developed at the University of Saskatchewan, Saskatoon, Canada, as part of an ongoing investigation into the stability of track subgrades (*1,2*). The design approach combines a computer stress analysis, using the computer program GEOTRACK, with conventional bearing capacity modified for layered systems and the influence of soil suction. Comparison of subgrade stress with subgrade strength (i.e., bearing capacity) provides a measure of the factor of safety against failure. Development of the design procedure has been documented earlier (*1,2*).

The objective in the development of the bearing capacity design procedure was to incorporate the soil suction term into a bearing-capacity approach to subgrade design. Soil suction, or matric suction, is a fundamental stress state variable defined as negative pore-water pressure u_w referenced to pore-air pressure u_a (*3*). Incorporation of soil suction into the bearing capacity design procedure permits the design procedure to use the additional strength of the soil that results from subgrade soil suction. Changes in subgrade strength owing to ponding or long-term evaporation may be quantified through the use of the soil suction term.

P. Sattler, D. G. Fredlund, and L. W. Lam, Department of Civil Engineering, University of Saskatchewan, Saskatoon, Sask., Canada S7N 0W0. A. W. Clifton, Clifton Associates Ltd., Regina, Sask., Canada S4N 5Y5. M. J. Klassen, CP Rail Ltd., Chief Engineer's Office, Montreal, Que., Canada H3C 3E4.

The bearing-capacity design procedure, incorporating subgrade soil suction, was used in the analysis of a railway embankment near Winnipeg, Manitoba, for Canadian Pacific Railways Ltd.

Winnipeg, which is situated on a highly plastic lacustrine clay of glacial Lake Agassiz at the confluence of the Red and Assiniboine rivers, has been plagued by intermittent flooding since 1826 (*4*). The Red River Floodway was constructed in the late 1960s to divert the floodwaters of the Red River around the Greater Winnipeg Area (Figure 1). The Canadian Pacific (CP) rail trackage was relocated in 1966 and 1967 (*5*) as part of the floodway project. The level of the track was raised approximately 3 m and a bridge was constructed across the floodway channel to cross the floodway. The floodway trackage embankment was designed with a 6.7-m top and 4:1 side slopes and was constructed of locally available highly plastic clay (*5*).

Maintenance was required to alleviate subgrade problems within a year of construction. Slope indicators installed in 1969 recorded movements of 22 mm/yr for 4 years before they were destroyed. Both shallow and deep-seated slip surfaces have been identified, and water has been observed to pond in depressions below the ballast. French drains and berms have been used over the years to attempt to stabilize the subgrade. Increased train loads and traffic volumes have aggravated embankment instability problems. Daily track lifting and realignment during wet periods were required on the floodway trackage, resulting in costly maintenance and the danger of derailment (*5*).

Analyses indicate that within the immediate vicinity of the floodway bridge the subgrade soil has been sheared past its peak strength and only a low residual strength is being mobilized. Figure 2 illustrates the severity of both bearing capacity and slope stability failures through the embankments near the floodway bridge.

FIELD AND LABORATORY INVESTIGATIONS

Eight testholes were drilled adjacent to the floodway bridge in 1980 (*5*). Samples were collected for Atterberg limits, density measurements, consolidation tests, direct shear tests, and triaxial repeated loading tests. Analyses were performed and remedial measures were suggested but never adopted owing to financial constraints.

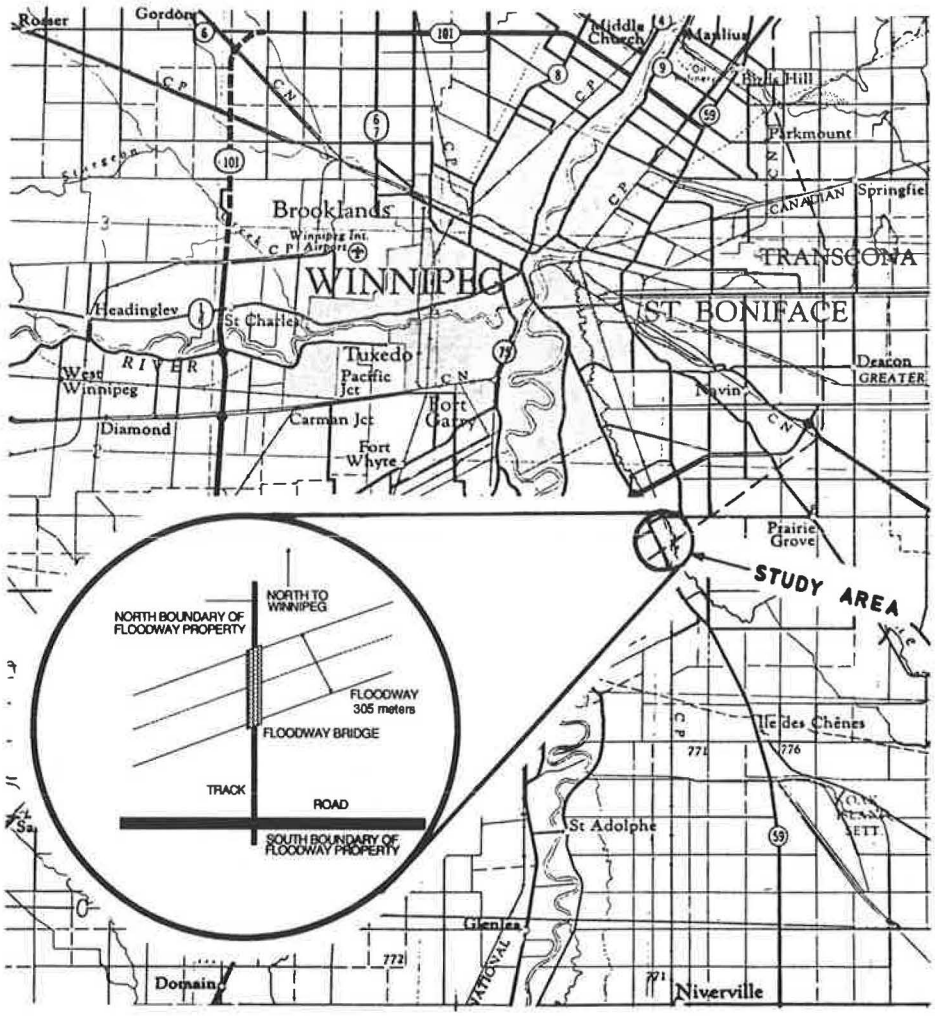

FIGURE 1 Location map of the study area.

FIGURE 2 Photograph of failures at the site.

Liquid limits ranged from 63 to 90 percent, and plastic limits varied from 18 to 29 percent. The average density was 1.95 g/cm^3. The swelling pressure, as measured from two consolidation tests, was about 275 kPa. The corrected swelling pressure was about 325 kPa. Results of five direct shear tests performed on the subgrade clay indicated a residual effective friction angle between 5.5 and 10.5 degrees with a cohesion intercept ranging from 5.5 to 20.0 kPa. Results of the triaxial repeated loading tests indicated an extreme variation in the resilient modulus value of 44.8 MPa to 177.8 MPa (*5*).

Subsurface conditions were again studied in March 1988 (*6*). The drilling program included 12 specified holes, plus 2 additional test holes and 6 holes for follow-up samples. The stratigraphic cross section interpreted from the test holes is presented in Figure 3. The ballast consisted of gravel ranging in size from 12 to 50 mm diameter, with an increasing sand fraction with depth. Thickness of the ballast varied from 0.20 to 0.45 m, averaging 0.30 m. Sub-ballast consisted of fine-to-medium sand with some gravel and a trace of silt. The sub-ballast thickness ranged from 0.45 to 1.55 m and averaged 1.15 m. Clay fill consisted of stiff to very stiff, highly plastic, mottled dark gray-green-to-black clay. Slicken-sided planes were abundant. Construction layering was also evident in some samples. A mixed zone between the clay fill and the sub-ballast was observed and consisted of a mixture of sub-ballast materials and softened clay fill. The natural strata consisted of an upper clay layer, a layered silt, a silty clay layer, and a highly plastic clay. The water table was identified approximately 5.5 m below the top of the ballast (*6*).

Fifty-two undisturbed Shelby tube samples and two bag samples were tested at the University of Saskatchewan. Index

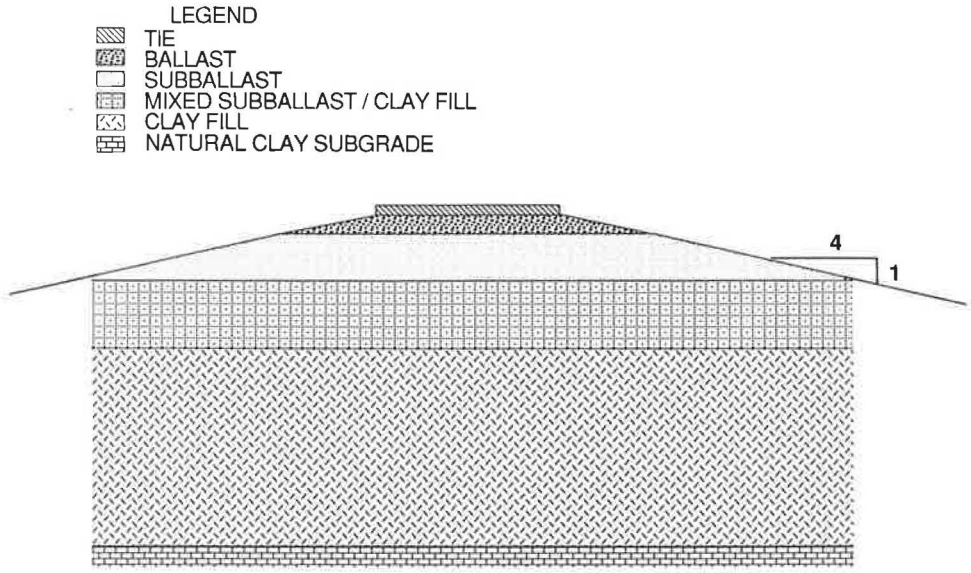

FIGURE 3 Stratigraphical cross section of embankment.

tests, matric suction measurements, and shear strength tests were performed.

The natural water contents varied between 23.3 and 52.6 percent with an average of 33.3 percent. Liquid limits varied between 65 and 98 percent with an average of 76 percent. Plastic limits varied between 21 and 29 percent with an average of 23 percent. The average plasticity index was determined to be 52 percent. The average specific gravity was measured and recorded as 2.71 (*7*).

Soil suction was measured in the laboratory on Shelby tube samples by using thermal conductivity sensors. A 125-mm (5-in.) long portion from the center of each Shelby tube sample was double wrapped in plastic film, confined with a layer of masking tape, and double wrapped in aluminum foil to prevent moisture loss during suction measurements (*8*). A thermal conductivity sensor, calibrated to measure soil suction (*9*), was installed into each sample (see Figure 4). Additional details on the use of thermal conductivity sensors to measure matric suction in the laboratory have been described by Sattler and Fredlund (*8*).

Measured negative pore-water pressures are illustrated in Figure 5. Measured values varied from 0 to 280 kPa. A tendency exists for the sample to expand in all directions when Shelby tube samples are released from the confinement of the Shelby tube. Expansion of the sample results in an increase in matric suction. The overburden pressure was subtracted from each measurement to compensate for this expansion, assuming a coefficient of lateral earth pressure at rest K_0 equal to 1 and a B pore pressure parameter equal to 1 (*8*). The resulting negative pore-water pressures are plotted in Figure 6. The measurements from all the test holes have been plotted on the same graph so the variability does not reflect the changes in any one test hole. The hydrostatic pore-water pressure line is illustrated in Figure 6 to aid interpretation.

Direct shear measurements were conducted to determine the rate of increase in shear strength for increasing soil suction ϕ^b. The angle measured in the laboratory was 25 degrees, which is slightly higher than the peak effective friction angle for the material. Interpretation of the results suggests that

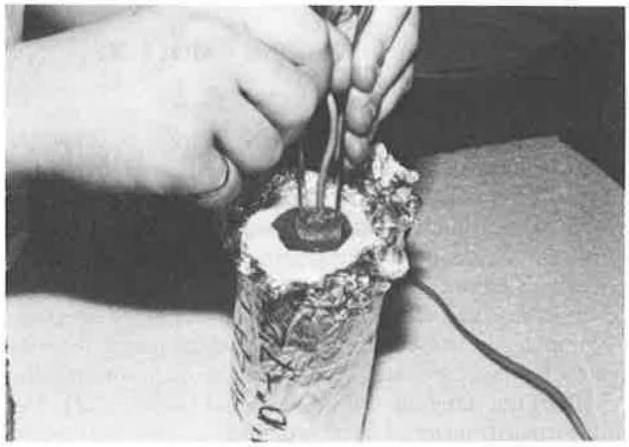

FIGURE 4 The installation of a thermal conductivity sensor.

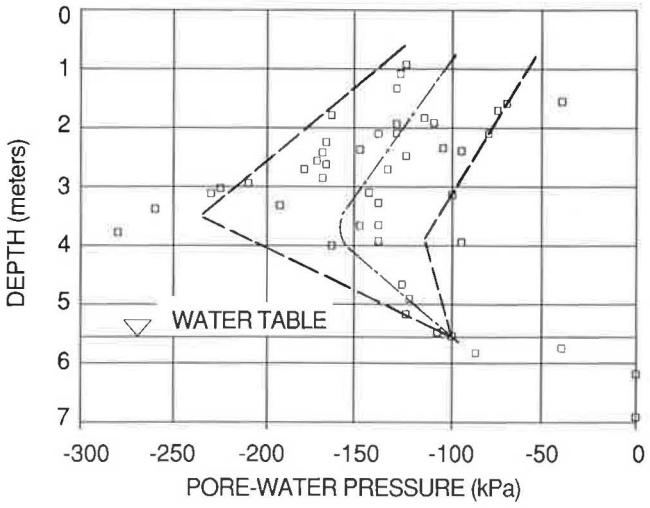

FIGURE 5 Measured negative pore-water pressures, using thermal conductivity sensors.

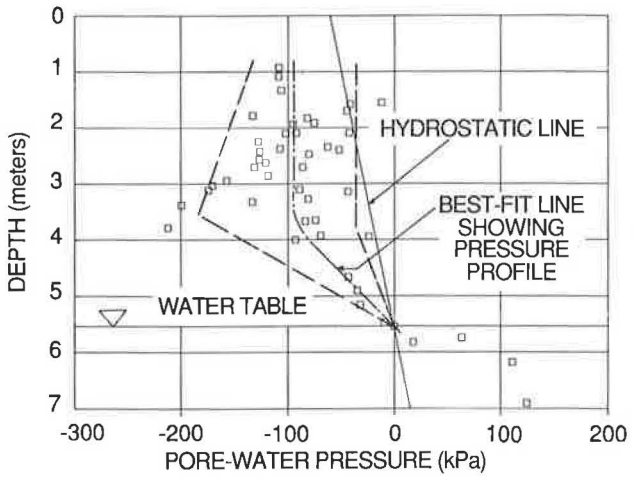

FIGURE 6 Negative pore-water pressures adjusted for overburden.

essentially the peak ϕ^b angle had been measured because research into appropriate values for ϕ^b suggest that ϕ^b should not exceed ϕ' (*7,10*).

STRESS ANALYSES AND BEARING CAPACITY ANALYSES

Railway design has been based on the concept of allowable stresses in the rails, ties, and subgrade. Most of the design aspects are quite empirical. The bearing capacity approach provides a measure against which subgrade stresses can be compared. The computer program GEOTRACK, documented by Chang et al. (*11*), was used for the prediction of stresses in the subgrade. The bearing capacity of the subgrade was computed by using conventional bearing capacity theories adapted for layered systems and then by incorporating the strength of the subgrade soil owing to soil suction (*1,2*). The bearing capacity factor of safety is defined as subgrade bearing capacity divided by subgrade stress, providing a comparative tool for analysis.

Input parameters required for the GEOTRACK model include the repeated loading moduli for the ballast, sub-ballast, and subgrade materials and for the two design materials, roller-compacted concrete and hot-mix asphalt. Reasonable values chosen to represent the ballast and subballast moduli were 241 MPa and 138 MPa, respectively (*11,12*). A design modulus value of 52 MPa was chosen to represent the softened upper layer of clay subgrade, and the lower stiffer layer was modeled with a modulus of 96 MPa on the basis of measurements conducted in 1980 (*5*). A value of 24,800 MPa was chosen for a repeated loading modulus for roller-compacted concrete (*13*), and a modulus of 8300 MPa was used for hot-mix asphalt (*14*). The GEOTRACK computer program, using those parameters, computed stresses at the subgrade surface for each of the design alternatives.

The conventional bearing capacity equation was used to compute subgrade bearing capacity q_u with the incorporation of soil suction as shown:

$$q_u = cN_c + \frac{1}{2}\gamma BN_\gamma + q_0N_q \quad (1)$$

where

$$c = c' + (u_a - u_w)\tan\phi^b \quad (2)$$

where

c = total cohesion,
c' = effective cohesion,
$(u_a - u_w)$ = soil suction or matric suction,
ϕ^b = rate of increase in shear strength with respect to soil suction,
γ = total unit weight,
B = bearing width,
q_0 = surcharge loading, and
N_c, N_γ, N_q = bearing capacity factors.

The effect of the ballast and sub-ballast layers were accommodated by using the concept proposed by Broms (*15,1,2*).

The parameters required for computing the subgrade bearing capacity include c', ϕ', ϕ^b and the design soil suction. Changes in pore-water pressure owing to train loading are considered to be insignificant relative to changes in pore-water pressure owing to the environment for an unsaturated soil where the pore-water pressures are negative. A design soil suction value was chosen to reflect the near-minimum suction expected over a period of several years. The design soil suction value for the subgrade was selected as the mean in situ suction minus 1 standard deviation. The selected value was equal to 55 kPa (see Figure 6).

A cohesion intercept of 2.5 kPa was selected along with an effective friction angle of 10 degrees on the basis of results of the direct shear measurements and modeling experience. An appropriate design value for ϕ^b was presumed to be on the order of 15 degrees (*10*). Experimental research studies indicate that ϕ^b should not be greater than the ϕ'. Therefore, a value of 10 degrees was selected for ϕ^b (*7*).

Design charts were developed for four alternatives:

- Alternative 1. Increased sub-ballast thickness (Figure 7);
- Alternative 2. Increased sub-ballast thickness with impermeable membrane (Figure 8);
- Alternative 3. Hot-mix asphalt layer (Figure 9); and
- Alternative 4. Roller-compacted concrete layer (Figure 10).

Four stress analyses were conducted to produce the four alternatives presented. Four suction values were selected for computing four bearing capacities for each alternative. Each chart indicates the relative increase in bearing capacity factor of safety for increased depth of granular material. The four values for bearing capacity are represented as four contours of soil suction on each chart to indicate the relative increase in factor of safety for increasing soil suction.

The increased sub-ballast alternative will serve to reduce stresses transmitted to the subgrade and therefore will increase the bearing capacity factor of safety. Alternative 2 with increased sub-ballast and impermeable membrane reduces stresses transmitted to the subgrade and also increases watershed capabilities of the subgrade so that a larger design suction value may be used. The hot-mix asphalt and roller-compacted concrete alternatives significantly reduce stresses transmitted to the subgrade and also provide for increased watershed

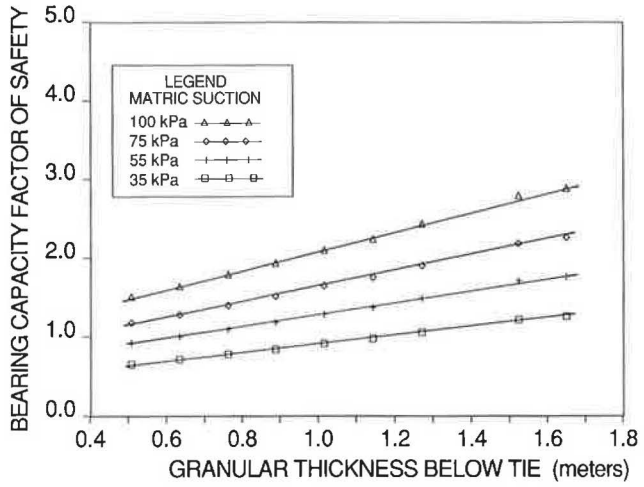

FIGURE 7 Bearing capacity factor of safety versus granular thickness below the tie for Alternative 1, increased sub-ballast.

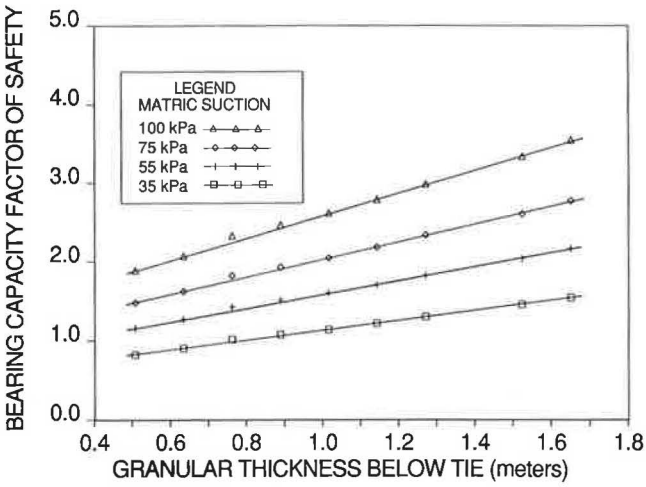

FIGURE 9 Bearing capacity factor of safety versus granular thickness below the tie for Alternative 3, hot-mix asphalt.

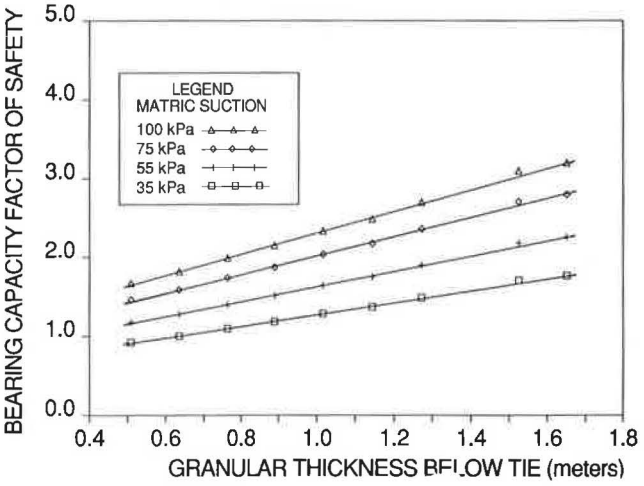

FIGURE 8 Bearing capacity factor of safety versus granular thickness below the tie for Alternative 2, increased sub-ballast with impermeable membrane.

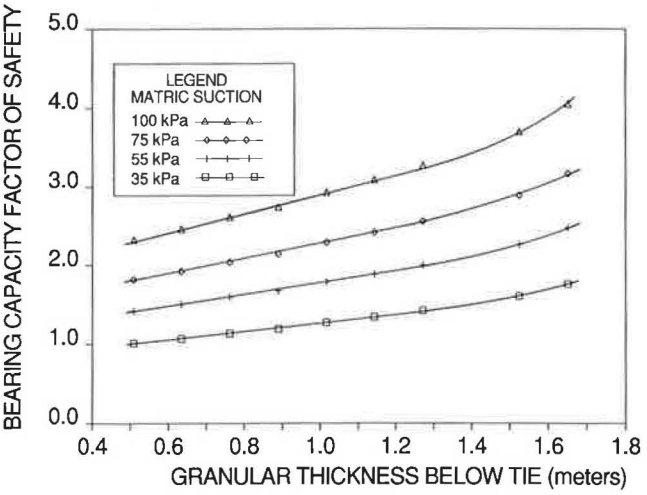

FIGURE 10 Bearing capacity factor of safety versus granular thickness below the tie for Alternative 4, roller-compacted concrete.

capabilities of the subgrade. For comparison purposes it was assumed that 75 kPa of suction could be maintained within the subgrade embankment for Alternatives 2, 3, and 4 (*7*).

For a bearing-capacity factor of safety equal to 2.0 and the assumed soil suction, the relative depths of granular material required beneath the tie for each of the alternatives are increased sub-ballast (55 kPa suction), 1.91 m; increased sub-ballast with impermeable membrane (75 kPa suction maintained), 1.40 m; hot-mix asphalt (75 kPa suction maintained), 1.02 m; and roller-compacted concrete (75 kPa suction maintained), 0.71 m. The corresponding thicknesses for a bearing-capacity factor of safety equal to 2.5 are 2.57, 1.83, 1.40, and 1.22 m, respectively.

The figures indicate relative depths of granular required to prevent bearing capacity failures. However, the site investigation revealed that the ultimate design must provide protection against both bearing capacity and slope-stability failures.

SLOPE-STABILITY ANALYSES

Slope-stability analyses were conducted by using the PC-SLOPE computer program (*16*). Two stabilizing berms were studied to increase the factor of safety of the embankment slope: a gravel berm with 4:1 side slopes and a clay berm with 5:1 side slopes. The effects of berm width and soil suction in the subgrade were investigated by using Bishop's Simplified method (*7*).

The water table was assumed to remain at 5.5 m below the top of the ballast. Zero suction was assumed for the ballast and sub-ballast layers. Constant suctions, somewhat greater than hydrostatic negative pore-water pressures, were assumed in the clay fill and upper natural subgrade strata, whereas hydrostatic pore-water pressures were assumed below the water table. Train loading was increased by 50 percent to simulate dynamic loading and was applied as a surcharge load to the top of the ballast (*7*).

Existing conditions, before remedial work, were used to calibrate the model for an appropriate matric suction value. With zero matric suction the factor of safety was computed at 0.684 with the train load applied and 0.884 without the train load. At the preceding two factor of safety values the embankment would have failed. Therefore, the incorporation of soil suction was justified. The factor of safety was computed at 0.926 with the train load and 1.205 without the train load by using the design matric suction value of 55 kPa (7). The fact that the existing embankment had been failing under train load suggested that the factor of safety with respect to slope stability was close to 1.0. The analysis of the existing condition developed an appreciation for the significance of the matric suction component of shear strength.

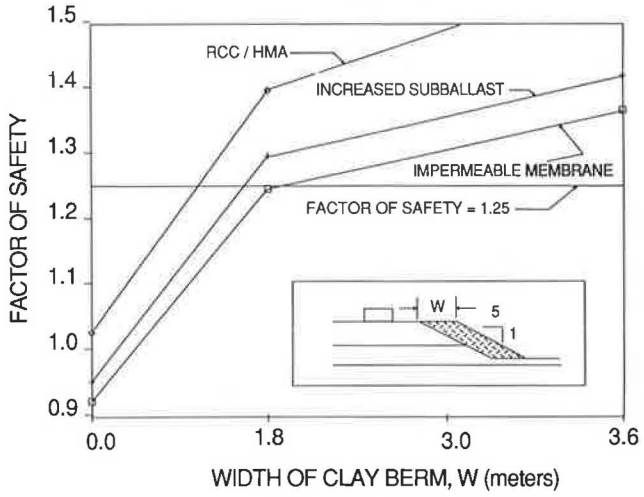

FIGURE 11 Slope stability factor of safety versus width of clay berm.

The four alternatives discussed earlier were analyzed for slope stability for each of the two berm designs. The clay berm produced a higher factor of safety than the gravel berm for the same width of berm and was due to the flatter slope selected for the clay berm. Therefore, only the clay berm is illustrated in Figure 11, which presents the factors of safety with respect to slope stability for each of the four alternatives. Without berming (i.e., berm width equal to zero) the factor of safety with respect to slope stability of the embankment slope ranges from 0.92 to 1.02, indicating a stabilizing berm was required for each design alternative considered. The roller-compacted concrete and the hot-mix asphalt produced similar results from a slope stability perspective. For the same berm width, roller-compacted concrete and hot-mix asphalt produced higher factors of safety than either increased sub-ballast alone or increased sub-ballast with an impermeable membrane.

COMPARATIVE DESIGN ALTERNATIVES

Analyses identified four equivalent design alternatives for remedial work on the floodway trackage railway embankment. A bearing capacity factor of safety equal to 2.0 and a factor of safety with respect to slope stability of 1.25 were suggested for design. The four recommended alternatives are illustrated in Figure 12.

Alternative 1 (increased sub-ballast thickness) consists of 229 mm of ballast and 1.68 m of sub-ballast (i.e., 1.91 m total), requiring the removal of existing ballast, sub-ballast, and approximately 1 m of original clay fill. A clay berm with 5:1 side slopes and 1.6 m top width is required for slope stability.

Alternative 2 (increased sub-ballast with impermeable membrane) consists of 229 mm of ballast, 1.17 m of sub-ballast, the removal of material to the bottom of the mixed

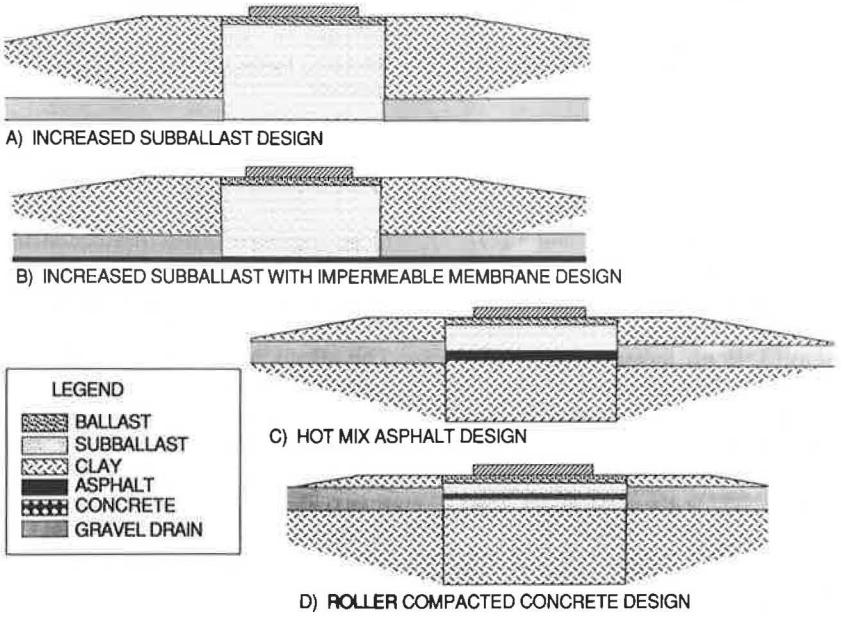

FIGURE 12 Comparison of the four design alternatives.

zone, and the recompaction of 127 mm of clay fill below the impermeable liner. A 1.9-m-wide clay berm is required.

Alternative 3 (hot-mix asphalt) is constructed of 229 mm of ballast, 0.79 m of sub-ballast, 229 mm of hot-mix asphalt, and 330 mm of compacted clay fill required to replace the mixed zone. The width of clay berm required is 1.14 m.

Alternative 4 (roller-compacted concrete) requires the same berm width as Alternative 3 but should be constructed from 229 mm of ballast, 330 mm of sub-ballast, and 203 mm of roller-compacted concrete. An additional 152 mm of sub-ballast is required below the concrete to resist sulphate attack from the clay subgrade. Removal of the mixed zone requires recompaction of an additional 635 mm above the natural clay subgrade.

The remedial design implemented consisted of removal of material to the bottom of the mixed zone. The embankment was constructed by using an increased thickness of glacial till as sub-ballast and a clay berm with a gravel drainage layer connected to the sub-ballast beneath the track. The glacial till material was locally available at considerable saving. The concepts presented by the design report facilitated the choice of material and design thicknesses.

CONCLUSIONS

The case study illustrates the complementary nature of the bearing-capacity design procedure in analyzing railway subgrade problems. Computation of subgrade bearing capacity provides a measure against which subgrade stresses can be compared. Traditionally, railway subgrade design has been based on limiting the subgrade stress to some value that is based on experience. The bearing capacity procedure accounts for the fact that subgrades may accommodate differing levels of stress, depending on material properties and environmental influences.

The investigation revealed the significance of using matric suction in the computation of shear strength for both slope stability and bearing-capacity problems.

ACKNOWLEDGMENTS

The authors wish to thank Canadian Pacific Railways Ltd. for the opportunity to be involved in this interesting project. The subsurface investigation carried out by the KGS Group, Winnipeg, Manitoba, under the direction of J. Bert Smith is acknowledged. The authors also wish to acknowledge the Transportation Development Center, Canadian Pacific Railways and Canadian National Railways for their financial contributions toward the development of the bearing-capacity procedure under a separate contract.

REFERENCES

1. P. J. Sattler, D. G. Fredlund, M. J. Klassen, and W. G. Rowan. Bearing Capacity Approach to Railway Design Utilizing Subgrade Matric Suction. In *Transportation Research Record 1241*, TRB, National Research Council, Washington, D.C., 1989, pp. 27–33.
2. P. J. Sattler and D. G. Fredlund. *The Development of Bearing Capacity Design Charts for Track Systems*. Final Report, Transport Canada Publication TP9521E, Transportation Development Center, Montreal, Quebec, 1988.
3. D. G. Fredlund. Appropriate Concepts and Technology for Unsaturated Soils. *Canadian Geotechnical Journal*, Vol. 16, No. 1, 1979, pp. 121–139.
4. J. Mishtak. Soil Mechanics Aspects of the Red River Floodway. *Canadian Geotechnical Journal*, Vol. 1, No. 3, 1964, pp. 133–146.
5. A. W. Clifton and J. Krahn. *Geotechnical Investigation and Analysis, Embankment Instability, Mile 7 to 9, Emerson Subdivision, Winnipeg, Manitoba*. Report R148. Clifton Associates Ltd., Regina, Saskatchewan, Sept. 1980.
6. J. B. Smith. *Report on Soils Investigation Phase I and Phase II, CP Rail Floodway Trackage, Emerson Subdivision*. Kontzamanis, Graumann and Smith, Inc., Winnipeg, Manitoba, 1988.
7. A. W. Clifton, L. W. Lam, and P. J. Sattler. *Embankment Instability, Investigation and Analysis, Emerson Subdivision, Winnipeg, Manitoba*, Clifton Associates Ltd., Regina, Saskatchewan, and the University of Saskatchewan Geotechnical Group, Saskatoon, Saskatchewan, July 1988.
8. P. J. Sattler and D. G. Fredlund. Use of Thermal Conductivity Sensors to Measure Matric Suction in the Laboratory. *Canadian Geotechnical Journal*, Vol. 26, No. 3, 1989, pp. 491–498.
9. D. G. Fredlund and D. K. H. Wong. Calibration of Thermal Conductivity Sensors for Measuring Soil Suction. *ASTM Geotechnical Journal*, Vol. 12, No. 3, 1989, pp. 188–194.
10. D. G. Fredlund, H. Rahardjo, and J. K. M. Gan. Non-Linearity of Strength Envelope for Unsaturated Soils. Presented at Sixth International Conference on Expansive Soils, New Delhi, India, Dec. 1987.
11. C. S. Chang, C. W. Adegoke, and E. T. Selig. GEOTRACK Model for Railroad Track Performance. *Journal of the Geotechnical Engineering Division*, ASCE, Vol. 106, 1980, pp. 1201–1218.
12. H. E. Stewart and E. T. Selig. Predicted and Measured Resilient Response of Track. *Journal of the Geotechnical Engineering Division*, ASCE, Vol. 108, No. GT11, 1982, pp. 1423–1442.
13. *Structural Design of Roller-Compacted Concrete for Industrial Pavements*. Portland Cement Association, Stokie, Ill., 1987.
14. J. G. Rose. Hot-Mix Asphalt Trackbeds: The U.S. Experience. *Proc., 32nd Annual Conference Canadian Technical Asphalt Association*, Toronto, Ontario, Vol. 32, Nov. 1987.
15. B. B. Broms. Effect of Degree of Saturation on Bearing Capacity of Flexible Pavements. Presented at the 43rd Annual Meeting of the Committee on Flexible Pavement Design, Ithaca, N.Y., 1965.
16. D. G. Fredlund. *PC-SLOPE User's Manual S-30*. GEO-SLOPE Programming Ltd., Calgary, Alberta, Canada, 1985.

Publication of this paper sponsored by Committee on Railroad Track Structure System Design.